

# New advances in the biology and pathogenesis of free-living amoebae

**Edited by**

Isabel Marcelino, Ascel Samba-Louaka and  
Christopher A. Rice

**Published in**

Frontiers in Microbiology  
Frontiers in Public Health



## FRONTIERS EBOOK COPYRIGHT STATEMENT

The copyright in the text of individual articles in this ebook is the property of their respective authors or their respective institutions or funders. The copyright in graphics and images within each article may be subject to copyright of other parties. In both cases this is subject to a license granted to Frontiers.

The compilation of articles constituting this ebook is the property of Frontiers.

Each article within this ebook, and the ebook itself, are published under the most recent version of the Creative Commons CC-BY licence. The version current at the date of publication of this ebook is CC-BY 4.0. If the CC-BY licence is updated, the licence granted by Frontiers is automatically updated to the new version.

When exercising any right under the CC-BY licence, Frontiers must be attributed as the original publisher of the article or ebook, as applicable.

Authors have the responsibility of ensuring that any graphics or other materials which are the property of others may be included in the CC-BY licence, but this should be checked before relying on the CC-BY licence to reproduce those materials. Any copyright notices relating to those materials must be complied with.

Copyright and source acknowledgement notices may not be removed and must be displayed in any copy, derivative work or partial copy which includes the elements in question.

All copyright, and all rights therein, are protected by national and international copyright laws. The above represents a summary only. For further information please read Frontiers' Conditions for Website Use and Copyright Statement, and the applicable CC-BY licence.

ISSN 1664-8714  
ISBN 978-2-8325-4886-8  
DOI 10.3389/978-2-8325-4886-8

## About Frontiers

Frontiers is more than just an open access publisher of scholarly articles: it is a pioneering approach to the world of academia, radically improving the way scholarly research is managed. The grand vision of Frontiers is a world where all people have an equal opportunity to seek, share and generate knowledge. Frontiers provides immediate and permanent online open access to all its publications, but this alone is not enough to realize our grand goals.

## Frontiers journal series

The Frontiers journal series is a multi-tier and interdisciplinary set of open-access, online journals, promising a paradigm shift from the current review, selection and dissemination processes in academic publishing. All Frontiers journals are driven by researchers for researchers; therefore, they constitute a service to the scholarly community. At the same time, the *Frontiers journal series* operates on a revolutionary invention, the tiered publishing system, initially addressing specific communities of scholars, and gradually climbing up to broader public understanding, thus serving the interests of the lay society, too.

## Dedication to quality

Each Frontiers article is a landmark of the highest quality, thanks to genuinely collaborative interactions between authors and review editors, who include some of the world's best academicians. Research must be certified by peers before entering a stream of knowledge that may eventually reach the public - and shape society; therefore, Frontiers only applies the most rigorous and unbiased reviews. Frontiers revolutionizes research publishing by freely delivering the most outstanding research, evaluated with no bias from both the academic and social point of view. By applying the most advanced information technologies, Frontiers is catapulting scholarly publishing into a new generation.

## What are Frontiers Research Topics?

Frontiers Research Topics are very popular trademarks of the *Frontiers journals series*: they are collections of at least ten articles, all centered on a particular subject. With their unique mix of varied contributions from Original Research to Review Articles, Frontiers Research Topics unify the most influential researchers, the latest key findings and historical advances in a hot research area.

Find out more on how to host your own Frontiers Research Topic or contribute to one as an author by contacting the Frontiers editorial office: [frontiersin.org/about/contact](https://frontiersin.org/about/contact)



# New advances in the biology and pathogenesis of free-living amoebae

## Topic editors

Isabel Marcelino — Institut Pasteur de la Guadeloupe, Guadeloupe

Ascel Samba-Louaka — University of Poitiers, France

Christopher A. Rice — Purdue University, United States

## Citation

Marcelino, I., Samba-Louaka, A., Rice, C. A., eds. (2024). *New advances in the biology and pathogenesis of free-living amoebae*. Lausanne: Frontiers Media SA. doi: 10.3389/978-2-8325-4886-8

## Table of contents

- 05 **Editorial: New advances in the biology and pathogenesis of free-living amoebae**  
Isabel Marcelino, Ascel Samba-Louaka and Christopher A. Rice
- 08 ***Acanthamoeba* spp. aggregate and encyst on contact lens material increasing resistance to disinfection**  
Allison Campolo, Reed Pifer, Rhonda Walters, Megan Thomas, Elise Miller, Valerie Harris, Jamie King, Christopher A. Rice, Paul Shannon, Brian Patterson and Monica Crary
- 30 ***Naegleria* genus pangenome reveals new structural and functional insights into the versatility of these free-living amoebae**  
Alexis Dereeper, Nina Allouch, Vincent Guerlais, Maëlle Garnier, Laurence Ma, Johan F. De Jonckheere, Sandeep J. Joseph, Ibne Karim M. Ali, Antoine Talarmin and Isabel Marcelino
- 56 **Biological characteristics and pathogenicity of *Acanthamoeba***  
Yuehua Wang, Linzhe Jiang, Yitong Zhao, Xiaohong Ju, Le Wang, Liang Jin, Ryan D. Fine and Mingguang Li
- 79 **Assessing *Acanthamoeba* cytotoxicity: comparison of common cell viability assays**  
Alvie Loufouma Mbouaka, Iwona Lesiak-Markowicz, Irene Heredero-Bermejo, Rounik Mazumdar, Julia Walochnik and Tania Martín-Pérez
- 89 **Mitochondrial genome diversity of *Balamuthia mandrillaris* revealed by a fatal case of granulomatous amoebic encephalitis**  
Cherie Tsz-Yiu Law, Thirapa Nivesvivat, Qing Xiong, Kasem Kulkeaw, Ling Shi, Pichet Ruenchit, Detchvijitr Suwanpakdee, Piradee Suwanpakdee, Nongnat Tongkrajang, Patsharaporn T. Sarasombath and Stephen Kwok-Wing Tsui
- 99 **Identification of novel anti-amoebic pharmacophores from kinase inhibitor chemotypes**  
Lori Ferrins, Melissa J. Buskes, Madison M. Kapteyn, Hannah N. Engels, Suzanne E. Enos, Chenyang Lu, Dana M. Klug, Baljinder Singh, Antonio Quotadamo, Kelly Bachovchin, Westley F. Tear, Andrew E. Spaulding, Katherine C. Forbes, Seema Bag, Mitch Rivers, Catherine LeBlanc, Erin Burchfield, Jeremy R. Armand, Rosario Diaz-Gonzalez, Gloria Ceballos-Perez, Raquel García-Hernández, Guiomar Pérez-Moreno, Cristina Bosch-Navarrete, Claudia Gómez-Liñán, Luis Miguel Ruiz-Pérez, Francisco Gamarro, Dolores González-Pacanowska, Miguel Navarro, Kojo Mensa-Wilmot, Michael P. Pollastri, Dennis E. Kyle and Christopher A. Rice

- 124 **Corrigendum: Identification of novel anti-amoebic pharmacophores from kinase inhibitor chemotypes**  
Lori Ferrins, Melissa J. Buskes, Madison M. Kapteyn, Hannah N. Engels, Suzanne E. Enos, Chenyang Lu, Dana M. Klug, Baljinder Singh, Antonio Quotadamo, Kelly Bachovchin, Westley F. Tear, Andrew E. Spaulding, Katherine C. Forbes, Seema Bag, Mitch Rivers, Catherine LeBlanc, Erin Burchfield, Jeremy R. Armand, Rosario Diaz-Gonzalez, Gloria Ceballos-Perez, Raquel García-Hernández, Guiomar Pérez-Moreno, Cristina Bosch-Navarrete, Claudia Gómez-Liñán, Luis Miguel Ruiz-Pérez, Francisco Gamarro, Dolores González-Pacanowska, Miguel Navarro, Kojo Mensa-Wilmot, Michael P. Pollastri, Dennis E. Kyle and Christopher A. Rice
- 126 **Phenotypic assay for cytotoxicity assessment of *Balamuthia mandrillaris* against human neurospheroids**  
Narisara Whangviboonkij, Worakamol Pengsart, Zhenzhong Chen, Seokgyu Han, Sungsu Park and Kasem Kulkeaw
- 137 **Characterization of the extracellular vesicles, ultrastructural morphology, and intercellular interactions of multiple clinical isolates of the brain-eating amoeba, *Naegleria fowleri***  
A. Cassiopeia Russell, Peter Bush, Gabriela Grigorean and Dennis E. Kyle
- 155 ***Naegleria fowleri* outbreak in Pakistan: unveiling the crisis and path to recovery**  
Abdullah Nadeem, Inshal Arshad Malik, Eesha Khan Afridi and Fariha Shariq
- 168 **Characterization of *Rosculus vilicus* sp. nov., a rhizarian amoeba interacting with *Mycobacterium avium* subsp. *paratuberculosis***  
Amélie Jessu, Vincent Delafont, Jean-Louis Moyen, Franck Biet, Ascel Samba-Louaka and Yann Héchard
- 178 **Providing an *in vitro* depiction of microglial cells challenged with immunostimulatory extracellular vesicles of *Naegleria fowleri***  
Lissette Retana Moreira, Alberto Cornet-Gomez, M. Rosario Sepulveda, Silvia Molina-Castro, Johan Alvarado-Ocampo, Frida Chaves Monge, Mariana Jara Rojas, Antonio Osuna and Elizabeth Abrahams Sandí



## OPEN ACCESS

## EDITED AND REVIEWED BY

Axel Cloeckaert,  
Institut National de recherche pour  
l'agriculture, l'alimentation et l'environnement  
(INRAE), France

## \*CORRESPONDENCE

Isabel Marcelino  
✉ IMarcelino@pasteur-guadeloupe.fr  
Ascel Samba-Louaka  
✉ ascel.samba@univ-poitiers.fr  
Christopher A. Rice  
✉ carice@purdue.edu

RECEIVED 14 March 2024

ACCEPTED 09 April 2024

PUBLISHED 29 April 2024

## CITATION

Marcelino I, Samba-Louaka A and Rice CA  
(2024) Editorial: New advances in the biology  
and pathogenesis of free-living amoebae.  
*Front. Microbiol.* 15:1401217.  
doi: 10.3389/fmicb.2024.1401217

## COPYRIGHT

© 2024 Marcelino, Samba-Louaka and Rice.  
This is an open-access article distributed  
under the terms of the [Creative Commons  
Attribution License \(CC BY\)](#). The use,  
distribution or reproduction in other forums is  
permitted, provided the original author(s) and  
the copyright owner(s) are credited and that  
the original publication in this journal is cited,  
in accordance with accepted academic  
practice. No use, distribution or reproduction  
is permitted which does not comply with  
these terms.

# Editorial: New advances in the biology and pathogenesis of free-living amoebae

Isabel Marcelino<sup>1\*</sup>, Ascel Samba-Louaka<sup>2\*</sup> and  
Christopher A. Rice<sup>3,4,5\*</sup>

<sup>1</sup>Institut Pasteur de la Guadeloupe, Les Abymes, Guadeloupe, France, <sup>2</sup>Laboratoire Ecologie et Biologie des Interactions, Université de Poitiers, Unité Mixte de Recherche (UMR) Centre national de la recherche scientifique (CNRS) 7267, Poitiers, France, <sup>3</sup>Department of Comparative Pathobiology, College of Veterinary Medicine, Purdue University, West Lafayette, IN, United States, <sup>4</sup>Purdue Institute for Drug Discovery (PIDD), Purdue University, West Lafayette, IN, United States, <sup>5</sup>Purdue Institute of Inflammation, Immunology and Infectious Disease (PI4D), Purdue University, West Lafayette, IN, United States

## KEYWORDS

free-living amoebae, pathogenesis, FLAM 2023, *Naegleria*, *Acanthamoeba*, *Balamuthia*, reviews, novel methods

## Editorial on the Research Topic

### New advances in the biology and pathogenesis of free-living amoebae

## Introduction

Free-living amoebae (FLA) are fascinating unicellular eukaryotic microorganisms found worldwide in aquatic and soil habitats. They have an important role in the ecosystems, actively feeding mainly on bacteria and other microorganisms. FLA life cycle is mainly composed of two stages: the trophozoite (the metabolically and replicative form of the amoeba) and the persistent cyst (which is highly resistant to various adverse conditions such as water disinfection processes and therapeutic treatments). While being mainly non-pathogenic, some FLA (namely *Acanthamoeba* and *Naegleria fowleri*) are currently considered emerging opportunistic pathogens (Bartrand et al., 2014; Sente et al., 2016). FLA are also well-known reservoirs of amoeba-resistant bacteria (ARB), possibly contributing to the spread of pathogenic ARB (such as *Legionella*), which constitutes a potential threat to water quality and human health (Samba-Louaka et al., 2019; Chaúque et al., 2022). It is therefore crucial to increase awareness of these neglected waterborne pathogens and related diseases. This Research Topic presents recent research on several FLA topics and includes studies presented by participants who attended the 19th International Free-Living Amoebae Meeting (FLAM) held in Poitiers, France, in June 2023.

## Summarizing the papers accepted

In this Research Topic, *Naegleria fowleri* extracellular vesicles (EVs) have garnered great interest in our community, with two papers by independent lab groups being published. Russell et al. and Retana Moreira et al. have both investigated EV characterization and their effect on various clinical isolates of *Naegleria fowleri*, as well as on host cells such as B103 neuroblastoma or primary cultures of mouse cell microglia,



using SEM methods. Staying on the theme of *N. fowleri*, Nadeem et al. highlight the emerging threat and “outbreak” of *N. fowleri* in Pakistan. This review highlights the need for improved awareness, public health measures, and water surveillance. Dereeper et al. contributed six new high-quality *Naegleria* genomes to establish the *Naegleria* genus pangenome with a near-to-complete repertoire of core and accessory genes, highlighting new architecture and functional features in *Naegleria*.

Excitingly, there was a description of one new putative host species of mycobacteria, *Rosculus vilicus*, within the environment that was published by Jessu et al. This may pose as a potential host and transmission route for John’s disease and should be kept a close eye on in the future.

A review from Wang et al. describes the characteristics of *Acanthamoeba* infection, including biological characteristics, classification, disease, and pathogenic mechanism, in order to provide a scientific basis for the diagnosis, treatment, and prevention of *Acanthamoeba* infection.

Loufouma Mbouaka et al. used Realtime-Glo as a novel two-dimensional (2D) cytotoxicity viability assay, being able to monitor the cell health and the pathobiology of *Acanthamoeba* on feeder cells. This assay could be adapted for *Balamuthia* pathogenicity models as well, but because *Naegleria* can also metabolize the propriety reagent, it may be difficult to differentiate between the pathogen or host response in that model.

One study assessed the phylogenetic diversity of the mitochondrial genome ribosomal protein S3 (rps3) over 10 strains of *B. mandrillaris*. Law et al. proposed that due to the copy-number variations (CNVs) and highly variable sequences of the protein tandem repeats of rps3, this could be a perfect target for a clinical genotyping assay for *B. mandrillaris*.

Whangviboonkij et al. presented a three-dimensional (3D) human neurospheroid model to assess the cytotoxicity and pathobiology response of *B. mandrillaris*. Using 3D models that mimic the human central nervous system (CNS) can provide a more physiologically relevant environment than traditional 2D cell culture for studying the pathogenicity of amoeba. These models are particularly useful for reducing the need for experiments using animal models.

Sticking to the theme of 3D models, Campolo et al. describe the aggregation and encystment of *Acanthamoeba*’s response on various contact lens materials under the same conditions. They found that some lenses will promote this aggregation phenotype, which will induce rapid encystment of some *Acanthamoeba* cells within a few hours to fully mature cysts, which they believe helps *Acanthamoeba* to withstand the disinfection process of contact lens care solutions.

Finally, to bring all the amoebae together, Ferrins et al. describe novel chemical pharmacophores that have various inhibitory activities against *Acanthamoeba* sp., *Naegleria fowleri*, or *Balamuthia mandrillaris*, which have been shown to cross the blood–brain barrier. This exciting physiological property is much needed for the development of any future anti-amoebic therapeutics for CNS disease. We cannot just stop at showing the amoeba inhibitory activity and stating that *in vivo* pharmacokinetic/pharmacodynamic or *in vivo* efficacy models are necessary to “validate the compounds future potential.”

## Conclusion

In conclusion, this Research Topic brings together diverse examples of the ongoing research on FLA regarding (i) FLA biology and pathogenesis (such as *Naegleria* pangenome or *Balamuthia mandrillaris*’ mitochondrial heterogeneity), the role of extracellular vesicles in *N. fowleri*–host interaction, (ii) FLA as hosts of zoonotic bacteria, (iii) drug development against FLA (namely brain permeable therapeutics against *Acanthamoeba*, *Naegleria*, or *Balamuthia*), various newly described 2D and 3D pathobiological models for brain organoid, cytotoxicity, or *Acanthamoeba* aggregation models, and (iv) FLA epidemiology. While this surely represents a glimpse of the ongoing research worldwide, we believe that increased research in disease, epidemiology, diagnostics, and treatment of pathogenic FLA species and the characterization of other emerging FLA should be encouraged, namely within the One Health concept.

Furthermore, we expect the emergence of the use of artificial intelligence (AI) in amoebae research. Indeed, the development and application of machine learning (ML) in the field of infectious diseases have gained massive attention in recent years, including other protozoans such as *Plasmodium* and *Trypanosoma* (Hu et al., 2022). We caught a glimpse of machine learning with Dr. Rice’s (unpublished data) and Dr. Debnath’s (Shing et al., 2022) novel *Acanthamoeba* cysticidal methodologies at the recent FLAM 2023 conference. Although the European Parliament and the US administration are trying to impose obligations for general-purpose AI to mitigate possible risks to health, fundamental rights, and democracy, we are assisting in the boost of AI in research and innovation. How AI will impact research in free-living amoebae is worth investigating. Beyond the identification of trophozoites or cysts, will AI be able to predict genera of amoebae present within the water or soil during sampling campaigns? Regarding the virulence factors identified in some pathogenic amoebae, will AI suggest human outcomes or some area to investigate, interrogate, and suggest optimal patient-specific treatment options? How deep will this rapidly advancing generative AI turn our field upside down? The next FLAM to be held in Mexico City, Mexico, in 2025, could be a place for an exchange around the impact of AI on the study of amoebae.

## Author contributions

IM: Writing—original draft, Writing—review & editing. AS-L: Writing—original draft, Writing—review & editing. CR: Writing—original draft, Writing—review & editing.

## Funding

The author(s) declare financial support was received for the research, authorship, and/or publication of this article. This study was partially funded by the EU project FEDER-Une Santé (IM).

## Acknowledgments

We thank the authors of this Research Topic for their valuable contributions. We also thank all the reviewers who have given up

their precious time to diligently peer-review and make impactful suggestions to the contributing authors.

## Conflict of interest

The authors declare that the research was conducted in the absence of any commercial or financial relationships that could be construed as a potential conflict of interest.

## Publisher's note

All claims expressed in this article are solely those of the authors and do not necessarily represent those of their affiliated organizations, or those of the publisher, the editors and the reviewers. Any product that may be evaluated in this article, or claim that may be made by its manufacturer, is not guaranteed or endorsed by the publisher.

## References

- Bartrand, T. A., Causey, J. J., and Clancy, J. L. (2014). *Naegleria fowleri*: An emerging drinking water pathogen. *J. Am. Water Works Assoc.* 106, E418–E432. doi: 10.5942/jawwa.2014.106.0140
- Cháuque, B. J. M., dos Santos, D. L., Anvari, D., and Rott, M. B. (2022). Prevalence of free-living amoebae in swimming pools and recreational waters, a systematic review and meta-analysis. *Parasitol. Res.* 121, 3033–3050. doi: 10.1007/s00436-022-07631-3
- Hu, R. S., Hesham, A. E. L., and Zou, Q. (2022). Machine learning and its applications for protozoal pathogens and protozoal infectious diseases. *Front. Cell. Infect. Microbiol.* 12:882995. doi: 10.3389/fcimb.2022.882995
- Samba-Louaka, A., Delafont, V., Rodier, M. H., Cateau, E., and Héchard, Y. (2019). Free-living amoebae and squatters in the wild: ecological and molecular features. *FEMS Microbiol. Rev.* 43, 415–434. doi: 10.1093/femsre/fuz011
- Sente, C., Erume, J., Naigaga, I., Magambo, P. K., Ochwo, S., Mulindwa, J., et al. (2016). Occurrence and genetic characterisation of *Acanthamoeba* spp. from environmental and domestic water sources in Queen Elizabeth Protected Area, Uganda. *Parasit. Vectors* 9:127. doi: 10.1186/s13071-016-1411-y
- Shing, B., Balen, M., Fenical, W., and Debnath, A. (2022). Development of a machine learning-based cysticidal assay and identification of an amebicidal and cysticidal marine microbial metabolite against *acanthamoeba*. *Microbiol. Spectr.* 10:e0007722. doi: 10.1128/spectrum.00077-22



## OPEN ACCESS

## EDITED BY

David Leitsch,  
Medical University of Vienna, Austria

## REVIEWED BY

Martina Köhler,  
Medical University of Vienna, Austria  
Nicole Carnt,  
University of New South Wales, Australia

## \*CORRESPONDENCE

Monica Cray  
monica.cray@alcon.com

<sup>†</sup>These authors have contributed equally to this work and share first authorship

<sup>†</sup>These authors have contributed equally to this work and share last authorship

## SPECIALTY SECTION

This article was submitted to  
Infectious Agents and Disease,  
a section of the journal  
Frontiers in Microbiology

RECEIVED 03 November 2022

ACCEPTED 28 November 2022

PUBLISHED 19 December 2022

## CITATION

Campolo A, Pifer R, Walters R, Thomas M, Miller E, Harris V, King J, Rice CA, Shannon P, Patterson B and Cray M (2022) *Acanthamoeba* spp. aggregate and encyst on contact lens material increasing resistance to disinfection. *Front. Microbiol.* 13:1089092. doi: 10.3389/fmicb.2022.1089092

## COPYRIGHT

© 2022 Campolo, Pifer, Walters, Thomas, Miller, Harris, King, Rice, Shannon, Patterson and Cray. This is an open-access article distributed under the terms of the [Creative Commons Attribution License \(CC BY\)](https://creativecommons.org/licenses/by/4.0/). The use, distribution or reproduction in other forums is permitted, provided the original author(s) and the copyright owner(s) are credited and that the original publication in this journal is cited, in accordance with accepted academic practice. No use, distribution or reproduction is permitted which does not comply with these terms.

# *Acanthamoeba* spp. aggregate and encyst on contact lens material increasing resistance to disinfection

Allison Campolo<sup>1†</sup>, Reed Pifer<sup>1†</sup>, Rhonda Walters<sup>1</sup>, Megan Thomas<sup>1</sup>, Elise Miller<sup>1</sup>, Valerie Harris<sup>1</sup>, Jamie King<sup>1</sup>, Christopher A. Rice<sup>2,3,4</sup>, Paul Shannon<sup>1</sup>, Brian Patterson<sup>1†</sup> and Monica Cray<sup>1†\*</sup>

<sup>1</sup>Alcon Research, LLC, Fort Worth, TX, United States, <sup>2</sup>Department of Comparative Pathobiology, College of Veterinary Medicine, Purdue University, West Lafayette, IN, United States, <sup>3</sup>Purdue Institute for Drug Discovery (PIDD), Purdue University, West Lafayette, IN, United States, <sup>4</sup>Purdue Institute of Inflammation, Immunology and Infectious Disease (PI4D), Purdue University, West Lafayette, IN, United States

**Introduction:** *Acanthamoeba* keratitis is often caused when *Acanthamoeba* contaminate contact lenses and infect the cornea. *Acanthamoeba* is pervasive in the environment as a motile, foraging trophozoite or biocide-resistant and persistent cyst. As contact lens contamination is a potential first step in infection, we studied *Acanthamoeba*'s behavior and interactions on different contact lens materials. We hypothesized that contact lenses may induce aggregation, which is a precursor to encystment, and that aggregated encystment would be more difficult to disinfect than motile trophozoites.

**Methods:** Six clinically and/or scientifically relevant strains of *Acanthamoeba* (ATCC 30010, ATCC 30461, ATCC 50370, ATCC 50702, ATCC 50703, and ATCC PRA-115) were investigated on seven different common silicone hydrogel contact lenses, and a no-lens control, for aggregation and encystment for 72h. Cell count and size were used to determine aggregation, and fluorescent staining was used to understand encystment. RNA seq was performed to describe the genome of *Acanthamoeba* which was individually motile or aggregated on different lens materials. Disinfection efficacy using three common multi-purpose solutions was calculated to describe the potential disinfection resistance of trophozoites, individual cysts, or spheroids.

**Results:** *Acanthamoeba* trophozoites of all strains examined demonstrated significantly more aggregation on specific contact lens materials than others, or the no-lens control. Fluorescent staining demonstrated encystment in as little as 4hours on contact lens materials, which is substantially faster than previously reported in natural or laboratory settings. Gene expression profiles corroborated encystment, with significantly differentially expressed pathways involving actin arrangement and membrane complexes. High disinfection resistance of cysts and spheroids with multi-purpose solutions was observed.

**Discussion:** Aggregation/encystment is a protective mechanism which may enable *Acanthamoeba* to be more disinfection resistant than individual trophozoites. This study demonstrates that some contact lens materials

promote *Acanthamoeba* aggregation and encystment, and *Acanthamoeba* spheroids obstruct multi-purpose solutions from disinfecting *Acanthamoeba*.

#### KEYWORDS

*Acanthamoeba*, aggregate, spheroid, cyst, contact lens, contact lens solution

## Introduction

*Acanthamoeba* keratitis (AK) is a serious ocular infection that is extremely difficult to treat and can lead to blindness (Siddiqui and Khan, 2012; Szentmary et al., 2019). Currently, AKANTIOR® (polyhexanide; PHMB) at 0.08% concentration is the only drug approved by the FDA (as an orphan drug designation) for *Acanthamoeba* keratitis (Pharma Boardroom, 2022). *Acanthamoeba* is a free-living protist that is pervasive in the environment, and often found in soil and water. Critically, this amoeba is not only commonly found in tap water specifically, but transmission *via* tap water and contact lens association has been linked to the leading causes of AK in Western countries (Carnt et al., 2018, 2020). There are significant education campaigns to inform contact lens wearers of the importance of avoiding water on their contact lenses at all times (Arshad et al., 2019, 2021; British Contact Lens Association, 2021). This amoeba is frequently introduced into the eye *via* contact lenses (Siddiqui and Khan, 2012; Randag et al., 2019), either as the result of inadequate contact lens hygiene habits or due to an ineffective multi-purpose solution (MPS; Verani et al., 2009; Tu and Joslin, 2010; Brown et al., 2018; Carnt et al., 2018). Data indicates that AK cases are increasing, including recent outbreaks in Western countries (Antonelli et al., 2018; Carnt et al., 2018; Randag et al., 2019) which were generally found to be the result of product-specific low *Acanthamoeba* MPS disinfection efficacy (Verani et al., 2009; Yoder et al., 2012). These outbreaks and the incidence rate of AK associated with contact lens users highlight the critical importance of adequate MPS disinfection efficacy against *Acanthamoeba*. While poor MPS disinfection efficacy is often blamed for *Acanthamoeba* infections, it is possible that contact lens materials themselves play an important role in the potential of *Acanthamoeba* to infect the eye. While *Acanthamoeba* trophozoites and cysts will bind to a wide variety of polymeric surfaces (Kilvington and Larkin, 1990; Beattie et al., 2011), the differences in silicone hydrogel contact lens materials have not been considered as playing a role in *Acanthamoeba* pathogenesis. Thus, contact lenses may have inappropriately avoided blame by being recognized as a mere vector in the path to *Acanthamoeba* keratitis infection, as opposed to having an impact on the potential for a corneal infection.

*Acanthamoeba* exists either in the motile, infective trophozoite form or as the more resistant, persistent cyst form, which can remain viable for years (Mazur et al., 1995; Siddiqui and Khan, 2012). Cysts are notoriously difficult to eradicate versus the trophozoite form, and have been shown to be impervious to most

disinfection methods that do not involve hydrogen peroxide or povidone iodine (Johnston et al., 2009; Coulon et al., 2010; Ahearn et al., 2012; Walters et al., 2022). While not generally considered a social amoebae like *Dictyostelium*, which can become a multicellular structure during their lifecycle, *Acanthamoeba* has been shown in the literature as forming clumps of cysts. This social behavior has not been studied significantly though *Acanthamoeba* aggregation has been observed during viral infection of the amoeba (Oliveira et al., 2019) as well as a precursor to encystment (Coulon et al., 2010). Both mechanisms suggest a protective action similar to that seen in *Dictyostelium* where the multicellular structure differentiates with some amoeba becoming cysts and others sacrificing themselves to form the protective fruiting body (Kilvington et al., 2009; Schaap, 2011; Kilvington and Lam, 2013; Oliveira et al., 2019). *Acanthamoeba* aggregation as a precursor to encystment has an evolutionary advantage that would allow protection of interior trophozoites from the environmental trigger promoting encystment. However, *Acanthamoeba* aggregation has not been studied outside of viral infection and many *Acanthamoeba* investigations identify that *Acanthamoeba* cysts are observed as clumps or spheroids but provide no hypothesis on the biological mechanisms occurring. Spheroids can be made of either trophozoites or cysts (Griffiths, 1969; Coulon et al., 2010; Ahearn et al., 2012) and it is currently unknown how aggregation affects cyst adherence to contact lenses. The underlying genes associated with aggregation remain largely unknown and the cellular pathways involved in encystment are still being described (Rolland et al., 2020). Encystment occurs when *Acanthamoeba* identifies the environment as unfavorable but any number of triggers from temperature, osmolarity, or nutrient availability, have been associated with encystment (Lloyd, 2014; Mahboob et al., 2016).

Encystment is a patient safety risk as *Acanthamoeba* cysts are difficult to kill both when they are on contact lenses and when they are in the cornea (Rayamajhee et al., 2021). One *Acanthamoeba* keratitis outbreak was specifically associated with a multi-purpose solution that induced encystment of *Acanthamoeba* trophozoites and failed to effectively kill *Acanthamoeba* cysts (Verani et al., 2009). This allowed *Acanthamoeba* to be transferred to the eye *via* contact lenses where *Acanthamoeba* then excysted and became pathogenic. Previous research on *Acanthamoeba*'s interaction with contact lenses has focused on its rate of adherence and the number of *Acanthamoeba* that can form strong bonds to the surface of contact lenses (Kilvington and Larkin, 1990; Ibrahim et al., 2009; Lee et al., 2018). Unfortunately, many of the published results in



this field are contradictory and little consensus can be found in the literature on which contact lenses demonstrate the most abundant *Acanthamoeba* adherence (John et al., 1989; Kilvington, 1993; Seal et al., 1995; Lee et al., 2016). Meanwhile, the contact lens industry continues to expand with new materials and surface chemistries (Musgrave and Fang, 2019). Here, we developed new methods to observe and quantify the behavior of six different potentially keratitis-causing *Acanthamoeba* strains on contact lens materials to determine if the *Acanthamoeba* response to different materials could possibly play a role in *Acanthamoeba* transmission to the eye. We observed that *Acanthamoeba* aggregates and encysts in response to some lens materials, independent of MPS exposure. To understand the mechanisms by which contact lenses contribute to aggregation, we evaluated the altered gene expression of *Acanthamoeba* when in contact with different lens materials and identified genes which may be critical to this material-specific aggregation process. Finally, we evaluated resistance to multi-purpose solution disinfection when *Acanthamoeba* are aggregated. Thus, we show here not only an extremely robust investigation into the behavior and motility of this pervasive pathogenic amoeba, but we also show for the first time that contact lens materials may play a critical role in increasing the risk of *Acanthamoeba* keratitis and affecting patient safety through disinfection resistance.

## Materials and methods

### *Acanthamoeba* culturing

*Acanthamoeba* strains were obtained from ATCC (American Type Culture Collection, Manassas, VA). Strains used and their information can be found in Table 1.

As previously described (Walters et al., 2022), trophozoites were axenically cultured in AC6 media (axenic culture medium, containing 20 g biosate peptone, 5 g glucose, 0.3 g  $\text{KH}_2\text{PO}_4$ , 10  $\mu\text{g}$  vitamin B12, and 15 mg L-methionine per liter of distilled deionized water). Media was adjusted to a pH of 6.6–6.95 with 1 M NaOH and autoclaved at 121°C for 20 min before storing at room temperature for use within 3 months.  $\frac{1}{4}$  Ringer's solution was used to harvest organisms. To create a homogenous population of *Acanthamoeba* trophozoites, *Acanthamoeba* were scaled up in fresh AC6 media 24 h to testing. Cells were then collected and centrifuged at 500 g for 5 minutes, followed by a wash and resuspension using  $\frac{1}{4}$  Ringer's solution. Count seeding was confirmed *via* manual counting using a hemocytometer.

### Contact lenses and multi-purpose solutions used

Information about contact lenses and multi-purpose solutions used and their details can be found in Table 1. Multi-purpose solutions tested were chosen by their representation of popular multi-purpose solutions and are identified by biocide throughout

the manuscript: PAPB/PQ [polyaminopropyl biguanide (0.00013%), polyquaternium (0.0001%)], PAPB/PQ/AD [polyaminopropyl biguanide (0.00013%), polyquaternium (0.0001%), alexidine dihydrochloride (0.00016%)], and PAPB [polyaminopropyl biguanide (0.00013%)]. Lenses were always paired by power for each replicate of an experiment (that is, for each replicate, every lens would be of the same power to reduce variability). Lenses were acquired based on market availability. For aggregation quantification, −12 power lenses were used. For RNA collection, −12 and −6 power lenses were used. For confocal experiments, −3 power lenses were used. All lenses used were recorded visually during the experimental procedure to ensure similar behavioral patterns – power was not observed to impact aggregation.

### *Acanthamoeba* observation and quantification of count and particle size on contact lens materials

Contact lenses were trimmed to 12 mm utilizing a biopsy punch. In a 48-well plate, a silicone O-ring was placed at the bottom of each well (Figure 1A). The contact lenses were placed on top of the silicone O-ring, then an additional O-ring was placed on top of the contact lens. This allowed the contact lens to maintain its normal curvature but prevented lens floating during extended timelapse observation. 500  $\mu\text{l}$  of  $\frac{1}{4}$  Ringer's was added to the top of the contact lenses. ~3,000 trophozoites were added to each well containing a contact lens. Amoeba occasionally demonstrated a ring pattern due to a slight wrinkle in the bottom of the lens caused by the round lens being sat on a flat well. A no-lens control (containing both O-rings) was also executed in the same polystyrene plate. The 48-well plate was transferred to a Nikon microscope with motorized stage. *Acanthamoeba* were allowed to settle for 10 min and then each well was imaged using a 2×2 stitched large image (NIS Elements AR 3.2) at 4× magnification for a continuous period of 12 h, with each well being imaged every 3 min. Later timepoints at 24, 48, and 72 h were also conducted for 30 min of continuous imaging with each well being imaged every 3 min. All videos were concatenated such that each contact lens had a single video file containing 274 images representing the entire 72-h period of observation. Seven contact lenses plus a no lens control were executed for each replicate. Six replicates were conducted for each strain of *Acanthamoeba* and six strains of *Acanthamoeba* were utilized.

Timelapse videos were recorded in grayscale using bright-field microscopy. Using ImageJ (version 1.53q), videos were converted into a high-contrast, binary format for analysis (Figure 1B). Briefly, image thresholding as determined by ImageJ was used to convert grayscale images into binary. Non-amoebic artifacts were removed utilizing fill and clear functions within ImageJ as needed. Particle analysis was conducted on the binary images, which included count and size of all particles (amoeba) within a frame. Individual images were created by duplicating frames within the timelapse video into new image files as needed. The size and count of each contact lens/replicate/strain were evaluated independently. For each timelapse

TABLE 1 Description of the strains of *Acanthamoeba* used (de Lacerda and Lira, 2021) contact lens material tested, and multi-purpose solutions used.

<i>Acanthamoeba</i>	Genotype	Strain	Keratitis-causing genotype	Original source
ATCC 50702	T3	TIO:H37	Yes (Sawyer, 1971; Chelkha et al., 2020)	Keratitis
ATCC 30461	T4	Eye	Yes ( <i>Acanthamoeba polyphaga</i> (Pushkarew), 2019; Pushkarew, 1913)	Keratitis
ATCC 50370	T4	Ma	Yes (Douglas, 1930; Gatti et al., 1998)	Keratitis
ATCC 30010	T4	Neff	Yes (Neff, 1957; Chelkha et al., 2020)	Environment
ATCC 50703	T5	45	Yes (Molet and Ermolieff, 1976; Cruz and Rivera, 2014)	Human Nose
ATCC PRA-115	T11	4RE	Yes (Sawyer et al., 1977; Gast, 2001)	Lens case
Contact lens material	Brand name	Manufacturer	Group/Water content	
omafilcon B	ProClear	CooperVision, San Ramon, CA, USA	2	
comfilcon A	Biofinity	CooperVision, San Ramon, CA, USA	5C/48%	
fanfilcon A	Avaira Vitality	CooperVision, San Ramon, CA, USA	5B /55%	
samfilcon A	Ultra	Bausch + Lomb* Rochester, NY, USA	5C/46%	
etafilcon A	Acuvue 2	Johnson & Johnson Vision Care, Jacksonville, FL, USA	4	
senofilcon A	Acuvue Oasys	Johnson & Johnson Vision Care, Jacksonville, FL, USA	5C/38%	
lehfilcon A	TOTAL30	Alcon* Fort Worth, TX, USA	5B/55%	
Multi-purpose solution biocide composition		Brand name	Manufacturer	Disinfection time
Polyaminopropyl biguanide (0.00013%), (PAPB)		Lite	CooperVision, San Ramon, CA, USA	6 h
Polyaminopropyl Biguanide Hydrochloride (0.00013%), polyquaternium (0.0001%) (PAPB/PQ)		Biotrue*	Bausch + Lomb* Rochester, NY, USA	4 h
Polyaminopropyl biguanide (0.00013%), polyquaternium (0.0001%), alexidine dihydrochloride (0.00016%) (PAPB/PQ/AD)		Biotrue* Hydration Plus	Bausch + Lomb* Rochester, NY, USA	4 h

video, 30-min (10 frame) sections were averaged for size and count across the 72 h. Size counts were normalized such that 100% represented a single individual trophozoite size, and anything over 100% indicates a spheroid of more than one trophozoite combined. This was conducted independently for each video as the image field had slight differences in plane, resulting in variable trophozoite size depending on if the microscope was focused on the top, middle or bottom of the cell. The size and count across the six replicates for a specific contact lens/no lens control were averaged for each strain of *Acanthamoeba*. Count and normalized particle size were graphed as a function of time for each strain.

To allow the amoeba to settle onto the lens and compensate for size differences observed between strains, the size of each strain-lens condition was normalized to its own 0.5–1.0 h reference time (Campolo et al., 2021). Additionally, due to the count difference of the no lens control, which was not confined to a smaller field of view by the bowl of the contact lens, the individual particle count of the no lens control was not included in the statistical analysis. Amoeba size and count within each timepoint within each replicate of each strain and lens combination were averaged, and standard deviation was calculated to identify outliers. Replicates ( $n=6$ ) of identical conditions were then averaged by timepoint, and standard error of the mean calculated. Normality was assessed using a Shapiro–Wilk test, and size and count (between conditions (lens

material) at any timepoint, and within each condition over time) were analyzed *via* two-way repeat measure ANOVA with a post-hoc Tukey's multiple comparisons test (GraphPad Prism 9.2.0). An alpha of 0.05 was used to assess significance in all comparisons.

## Standard curve spheroid generation

*Acanthamoeba* ATCC 30461 trophozoites were seeded into Biofloat plates (faCellitate, Mannheim, Germany) at a density of 8, 16, 32, 125, 250, 500, 1,000, or 2,000 cells/well in replicates of 8 per plate. The experiment was conducted across 4 independent 96-well plates per time period. Timelapse images were taken of each spheroid every 5 min for 3 h, then every 15 min for the subsequent 6 h, and then every 30 min from hours 9 through 24. Each well made one spheroid and the timelapse videos were converted to binary images in the same fashion as the contact lens videos. Each spheroid video was analyzed to determine the number of trophozoites per spheroid, as well as the area of each spheroid as a function of time. A standard curve was generated as a function of trophozoite count vs. spheroid size over time using spheroid area (Supplementary Figure S1). To validate standard curve cell count estimation method, count estimates using the standard curve were compared against traditional hemocytometer

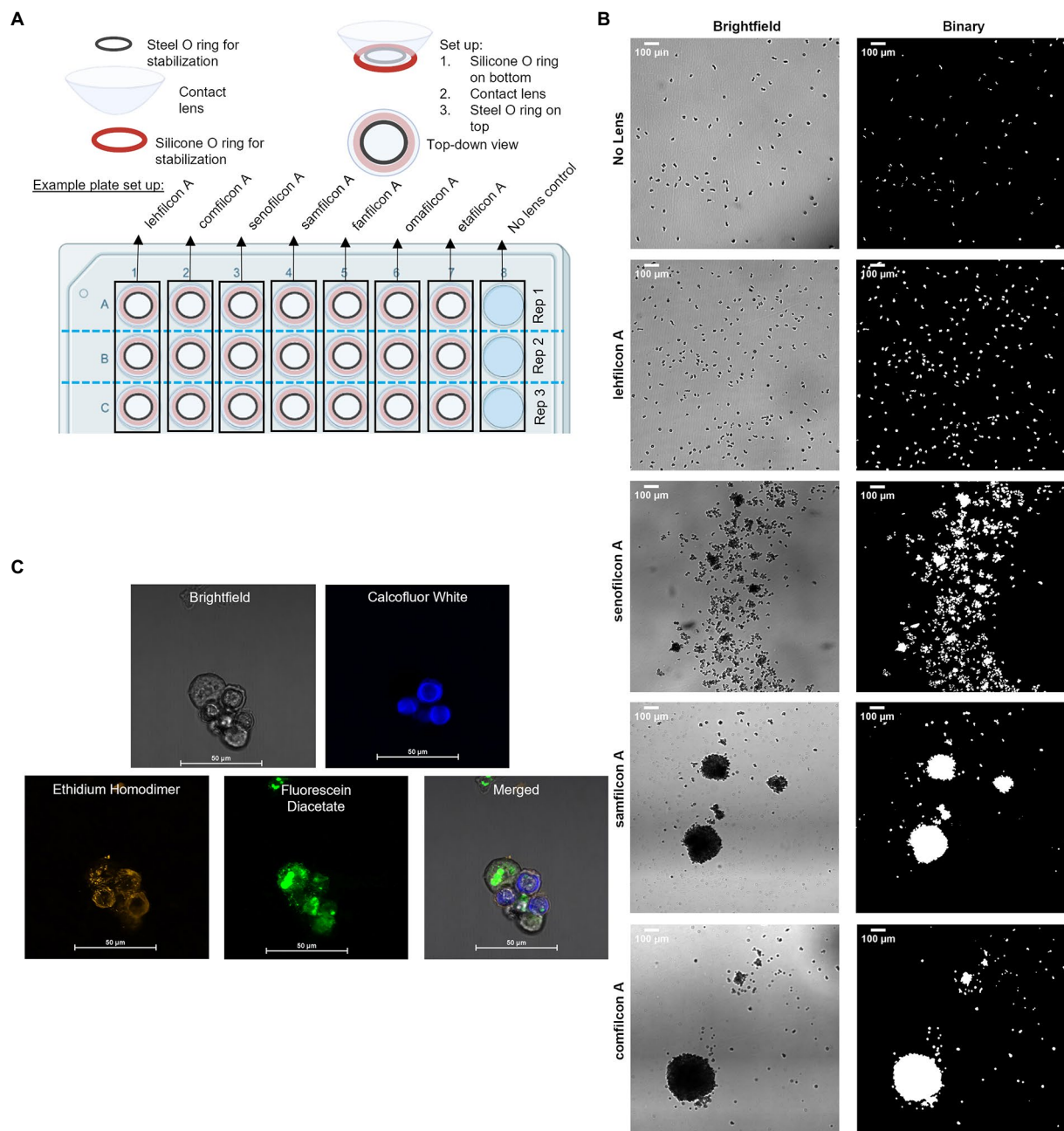


FIGURE 1

Methodological representations. (A) Plate set up for time lapse count and strain analysis of *Acanthamoeba* aggregation on contact lens materials. (B) Representative large images taken at 4x magnification in brightfield, and then as they appear in binary which is used for count and size analysis (scale bar=100  $\mu$ m). (C) Representative large images of fluorescent confocal microscopy images, taken in brightfield, with three different filters, and merged (please refer to Figure 7 for details; scale bar=50  $\mu$ m) depicting encystment at 6 h using a Biofloat spheroid plate.

method (Buck and Rosenthal, 1996) and validated across a range of 100–1,500 cells per spheroid.

## Confocal imaging of spheroids

Spheroids were generated on Biofloat (faCellitate, Mannheim, Germany) plates or contact lenses as described above (Figure 1C).

Spheroid age was between 2 and 72 h depending on the images. Prior to aggregation experiments, control trophozoites and cysts [pre-generated separately *via* starvation (Walters et al., 2022)] were stained to verify stain response to cells. No control cells were added to aggregation experiments. To investigate spheroid formation, trophozoites on normal tissue culture plates were incubated for the same time period as spheroids as a control. Following spheroid generation, spheroids were stained using calcofluor white (Millipore

Sigma, Darmstadt, Germany, Catalog #F1303), ethidium homodimer (ThermoFisher Scientific, Massachusetts, USA, Catalog #E1169), and fluorescein diacetate (ThermoFisher, Catalog #F1303). Spheroids were stained with calcofluor white (blue color) which binds to the cellulose of cell walls and is only present in cysts (Magistrado-Coxen et al., 2019). Ethidium homodimer (orange staining) binds to nucleic acids and indicates a compromised cell wall (cell death) or the formation of an extracellular matrix. Fluorescein diacetate (green color) is a dye that can penetrate cell walls and indicates ongoing enzymatic activity as only living cells will convert the nonfluorescent dye into the green fluorescent compound fluorescein.

## Acanthamoeba DNA sequencing

Crude DNA extracts were prepared from ATCC 30461 with a cetyl trimethylammonium bromide-based procedure using Carlson Lysis Buffer (CLB; Bioworld, Dublin, OH, USA, # 10450002; Vaillancourt and Buell, 2019). Briefly, *Acanthamoeba* trophozoites were passaged and collected to create a pellet of  $2 \times 10^7$  cells. Pellets were resuspended in CLB containing 0.25% 2-mercaptoethanol and 0.7 mg/ml RNase A and incubated at 54°C–56°C for 60 min at 1200 RPM in an Eppendorf Thermomixer R. Proteinase K was added to 7 U/ml and incubated with shaking for an additional 20 min. Two sequential chloroform:isoamyl alcohol extractions were performed, followed by an isopropanol precipitation. Crude extracts were dissolved at 54–56°C in Qiagen G2 buffer containing 0.2 mg/ml RNase A and 15 U/ml Proteinase K and further purified by through a 20/G genomic tip according to the manufacturer's instructions. DNA purity was assessed by agarose gel electrophoresis and quantified using a Take3 Micro-Volume Plate with a Synergy H4 plate reader and Gen5 Software (Biotek, Winooski, VT, USA). Illumina sequencing, Oxford Nanopore sequencing, and analysis were performed by Seqcenter (Pittsburgh, PA, USA). Quality control and adapter trimming was performed with *bcl-convert* (2021) and *rrwick/Porechop*, Github. Com (2017) for Illumina and ONT sequencing, respectively. Long read assembly with ONT reads was performed with Flye (Lin et al., 2016). The long read assembly was polished with Pilon (Walker et al., 2014). To reduce erroneous assembly artifacts caused by low quality nanopore reads, long read contigs with an average short read coverage of 15x or less were removed from the assembly. Assembly statistics were recorded with QUAST (Gurevich et al., 2013). Assembly annotation was performed with Funannotate (Jon and Jason, 2019).

## Acanthamoeba RNA harvesting and sequencing

In a 24-well plate, contact lenses were placed concave side up in each well. 100 µl of ¼ Ringer's solution was placed below the lens to keep it supported and moist, and the lid was secured to the plate to prevent drying. 75 µl of ¼ Ringer's suspending  $5 \times 10^4$

*Acanthamoeba* was placed onto the upward-facing concave side. Wells were imaged continuously at one image every 24 s while amoeba were on the lens to ensure that lenses were centered, amoeba were on top of the lens, and amoeba exhibited similar behavior as seen in *Acanthamoeba* quantification experiments. At the end of the specified time period, amoeba were harvested without disturbing the lenses by pipetting amoeba off and pipette-washing the lens with 50 µl ¼ Ringer's. All wells within a technical replicate were combined in a singular sample collection tube for a total minimum of  $5 \times 10^5$  cells per sample. Lenses and wells were examined *via* microscope after harvesting to ensure all amoeba were collected and none remained in the well. *Acanthamoeba castellanii* (ATCC 30461) samples were collected from the lenses directly into TRIzol (ThermoFisher, Waltham, MA, USA, #15596026) and RNA was isolated immediately using the PureLink RNA Micro Scale Kit (ThermoFisher, #12183016). RNA integrity was assessed by agarose gel electrophoresis and quantified using a Take3 Micro-Volume Plate with a Synergy H4 plate reader and Gen5 Software. For each condition and time point, six independent replicates were prepared on separate days. RNA sequencing and analysis was performed by Seqcenter. Samples were then DNase treated with Invitrogen DNase (RNase free). Library preparation was performed using Illumina's Stranded Total RNA Prep Ligation with Ribo-Zero Plus kit and 10bp IDT for Illumina indices. Sequencing was done on a NextSeq2000 giving 2x50bp reads. Quality control and adapter trimming was performed with *bcl-convert v3.9.3* (2021). Read mapping was performed *via* STAR (Dobin et al., 2012) using the previously sequenced genome of ATCC 30461 as reference. Feature quantification was performed using RSEM (Li and Dewey, 2011). Read counts loaded into R and were normalized using edgeR's (Robinson et al., 2009) Trimmed Mean of M values (TMM) algorithm. Subsequent values were then converted to counts per million (cpm). Differential expression analysis was performed using edgeR's Quasi-Linear F-Test (qlfTest) functionality against treatment groups. Differentially expressed genes were considered those with  $|\log_2FC| > 1$  and  $p < 0.05$ .

Affinity Propagation clustering (17218491) of RNA sequencing results was performed in Python version 3.8.8 using scikit-learn version 0.24.1. Parameters used were 0.5 damping, a maximum of 200 iterations, 15 unchanged iterations until convergence. The dimensional inputs for Euclidean distance-based affinity propagation were composed of the following gene expression comparisons: lehficon A vs. polystyrene control at 4, 12, or 24 h, samfilcon A vs. polystyrene control at 4, 12, or 24 h, and comfilcon A vs. polystyrene control at 4, 12, or 24 h. The average log2 fold changes in gene expression from six RNA sequencing replicates were used as value inputs for each dimension. Only significantly differentially expressed genes were included in analysis. The resulting gene clusters were further reduced into phenotypic clusters by correlational distance-based affinity propagation on the median expression change of all genes included in each primary cluster. Heatmaps of the resulting gene subsets were constructed in GraphPad Prism 9.2.0.



Locus tags from the genomic database created by DNA sequencing (of the ATCC 30461 strain, internal identifiers from these datasets are FUN\_\*) and the associated information with each tag was used to identify homologs and inferred gene function based on the known function of the ATCC 30010 strain. The amino acid sequence of each ATCC 30461 gene was used to search NCBI's BLAST (National Center for Biotechnology Information, Basic Local Alignment Search Tool) to determine percent homology with known genes of all species. As homology with ATCC 30010 was most prevalent, this and the associated Neff strain locus tag were used to estimate gene function. Neff strain locus tags (ACA1\_\*) were searched in the AmoebaDB informatics resource repository to define the GO (Gene Ontology) terms for each gene. Neff strain locus tags were also used to identify the associated protein ID in either the UniProt or KEGG (Kyoto Encyclopedia of Genes and Genomes) databases, and significant common pathways were identified using STRING (Search Tool for the Retrieval of Interacting Genes/Proteins; false discovery rate < 0.05 using the Benjamini-Hochberg procedure).

## Disinfection efficacy

The disinfection efficacy of individual trophozoites, spheroids, and cysts were evaluated in a disinfection study. The disinfection study was conducted concurrently across conditions with three independent inoculums of *Acanthamoeba* ATCC 30461.

**Spheroids:** The wells of a 96-well Biofloat plate (faCellitate, Mannheim, Germany) were seeded with a serial dilution of *Acanthamoeba* trophozoites such that wells contained either 100, 375, or 1,000 cells per well.

**Cysts:** Cysts were generated by starvation on non-nutrient agar plates. Briefly, trophozoites were harvested into ¼ Ringer's and plated on non-nutrient agar plates and incubated at 28°C for a minimum of 10 days. After incubation, cysts were rinsed from plates using ¼ Ringers and stored at 4°C until testing.

**Trophozoites and cysts:** The wells off a 96-well flat bottom tissue culture plate were seeded with a serial dilution of *Acanthamoeba* cells such that wells contained either 100, 375, or 1,000 cells per well.

**Spheroids, trophozoites, and cysts:** Eight replicates of each concentration were conducted per multi-purpose solution and independent inoculum. Cells were incubated in the wells for either 12 or 24 h prior to being exposed to multi-purpose solutions. Excess ¼ Ringer's was removed from each well, and 200 µl of the designated multi-purpose solution was added to the well. At disinfection time (4 or 6 h), the MPS was removed and 25 µl of Lethen broth was added to each well to neutralize any remaining biocide. The total contents of each well were transferred to a 48-well plate containing 500 µl of non-nutrient agar. Heat-killed *Escherichia coli* was added to each well and the 48-well plates taped and incubated for 21 days at 28°C.

After 21 days, all plates were scored for growth. Each multi-purpose solution/cell type/incubation length/inoculum was quantified as a % outgrowth for a particular condition.

Comparisons between cell type, incubation length and multi-purpose solutions were conducted and analyzed via 2-way ANOVA, with *post hoc* Tukey's test (GraphPad Prism 9.2.0). Significance was set at 0.05.

## Results

### *Acanthamoeba* behavior on lens materials

To understand the differences in *Acanthamoeba* behavior on popular lens materials, we investigated six different potentially keratitis-causing strains of *Acanthamoeba* for 72 h on seven different lens materials, as well as a polystyrene no lens control in which *Acanthamoeba* appeared to move independently and consistently similar to previously examined surfaces (Campolo et al., 2021; Figures 2–5; Supplementary Figures S2–S4). An experimental timeline was designed to allowed us to observe and quantify aggregation both in the clinically normal periods of when a contact lens might be stored individually in a contact lens case overnight, as well as longer periods to determine if any behavior was transient (de-aggregation of *Acanthamoeba* on their own without conditions otherwise changing). To quantify behavior, we determined both the particle count (the number of individual amoeba or spheroids identifiable in the field of view) and the particle size. As spheroids form, an inverse relationship between particle count and average size is observed (i.e., as counts decrease, size increases).

When data from all strains were combined (Figures 2A,B; Supplementary Figure S2), we found that all lens materials tested demonstrated a significantly lower particle count than lehfilcon A ( $p < 0.05$ ) from timepoints 1.5–2.0 h to 9.0–9.5 h, with comfilcon A, senofilcon A, samfilcon A, fanfilcon A, and omafilcon A being significantly lower through at least 12 h. Similarly, with all strains data combined, all lens materials except etafilcon A demonstrated a significantly higher particle size from at least 3.0–3.5 h through 72 h than lehfilcon A ( $p < 0.05$ ). In this analysis, etafilcon A demonstrated a significantly higher particle size than lehfilcon A from 6.0–6.5 h through 11.5–12 h. All lens materials were also analyzed for their change compared to their baseline (0.5–1.0 h) in both particle count and particle size. When all strains were combined it was noted that lehfilcon A, omafilcon A, and etafilcon A did not demonstrate a significant change compared to their particle count baseline, while comfilcon A, senofilcon A, samfilcon A, and fanfilcon A did, beginning by 1.5–2.0 h to 2.0–2.5 h ( $p < 0.05$ ). Some lens materials (comfilcon A, fanfilcon A) maintained this difference through 72 h, while others (senofilcon A, samfilcon A) demonstrated a relative return to their baseline before the end of the experiment. Overall, when combining the data from all six *Acanthamoeba* strains examined (Figures 2A,B), this demonstrated that the lehfilcon A material specifically allowed significantly lower aggregation versus all

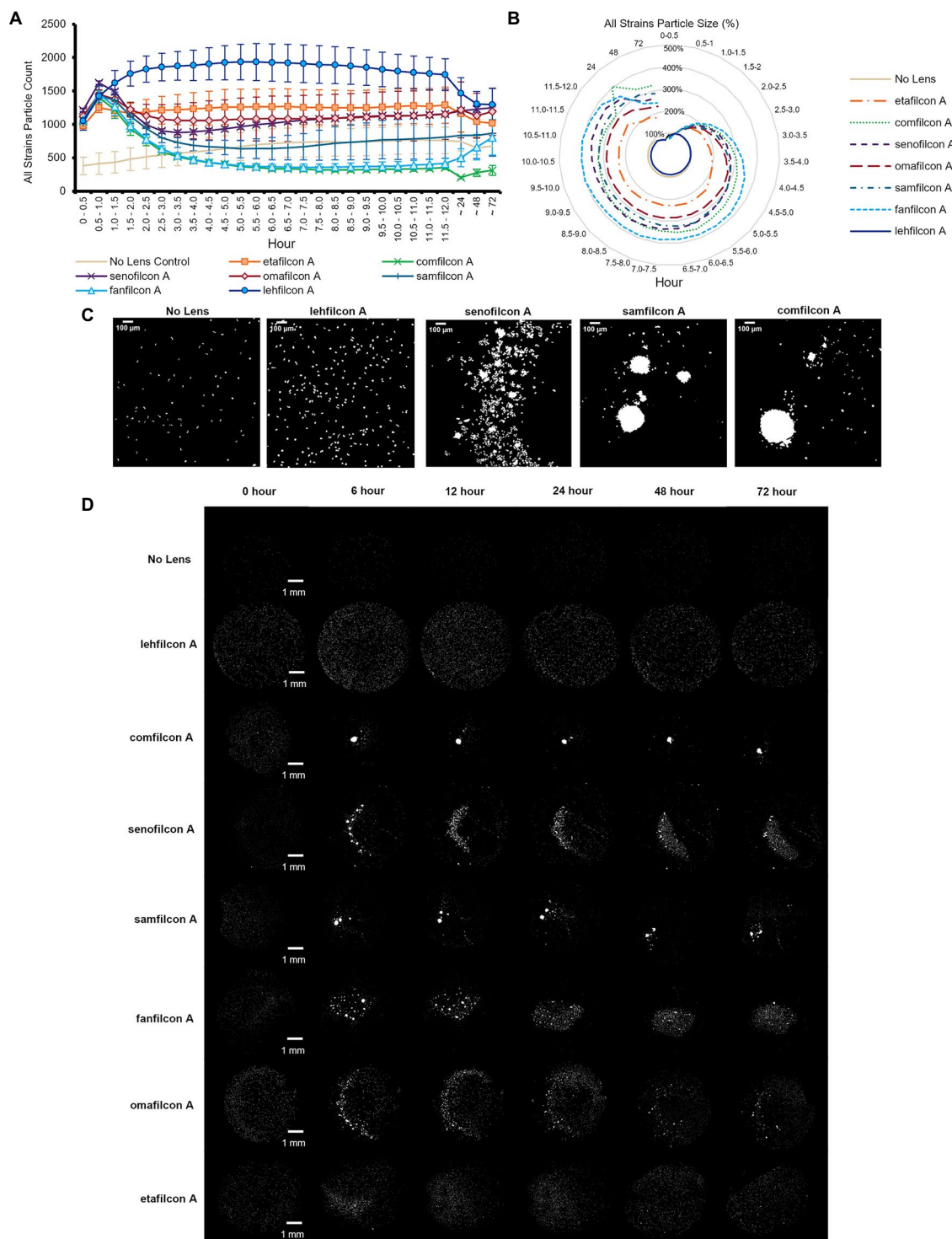


FIGURE 2

*Acanthamoeba* demonstrated significantly less aggregation on lehfilcon A lenses compared to other materials. Mean  $\pm$  SE of (A) all strains (ATCC 30010, 30461, 50370, 50702, 50703, and PRA-115) count (number of individual particles), (B) all strains normalized particle size. (C) Enlarged representative binary images of amoeba (ATCC 30461) on contact lenses at 12 h timepoint (scale bar=100 µm), (D) Representative binary images of amoeba (ATCC 30461) on all materials tested (scale bar=1 mm). Size is normalized to the baselines obtained in the 0.5–1.0 h. Statistical comparisons for subpanels (A) and (B) noted in [Supplementary Figure S2](#).  $n=6$  per group.

other materials tested. Visually, the no lens control and lehfilcon A showed individual trophozoites moving freely as individuals across the surface while other materials demonstrated

aggregation to various degrees across the course of the experiment ([Figures 2C,D](#); [Supplementary Videos S1–S6](#)). [Supplementary Videos S1](#): ATCC 30010, [S2](#): ATCC 30461, [S3](#):

ATCC 50370, [S4](#): ATCC 50702, [S5](#): ATCC 50703, [S6](#): ATCC PRA-115.

Additionally, despite being seeded with the same number of cells in the same plate at the same time, the no lens control in most strains tested demonstrated a lower particle count in the field of view than all lenses tested. This was due to amoeba having a larger available space (flat-bottomed well vs. bowl of a contact lens), although they were consistently observed to be evenly dispersed throughout the well both in this study and in previous ones ([Campolo et al., 2021](#)). Further, it is a noticeable phenomenon that count increases in all lens materials and in all strains from time 0–0.5 h to 0.5–1.0 h. This is due not only to amoeba settling onto the lens, but also to their inclination to walk down to the bottom of the bowl of the lens upon adherence to the lens, thereby coming into the field of view and being counted. When observed, aggregation into spheroids is most often seen at the 0.5–1.0 h time point (demonstrated by the marked decrease in count), while non-aggregation results in consistently higher particle counts.

When examined individually ([Figures 3–5](#); [Supplementary Figures S3, S4](#)), most strains demonstrated the similar trend of lehfilcon A maintaining a statistically higher cell count than other lens materials at most time points ( $p < 0.05$ ). The exceptions to this were etafilcon A, which demonstrated little aggregation in ATCC 30010 or ATCC 50703. The ATCC 50703 strain was the only strain tested where cell count continued to increase over time for senofilcon A, samfilcon A, and omafilcon A. Senofilcon A produced the highest particle size (i.e., largest spheroid size) in ATCC 30010 and ATCC 30461, while fanfilcon A and/or comfilcon produced the largest spheroid size in ATCC 50370, ATCC 50703, and ATCC PRA-115, and omafilcon A produced the largest spheroid size in ATCC 50702. The particle size of the no lens control and lehfilcon A were not statistically different from each other at any time point in any strain tested. It is noted that some strain-material combinations produced a pronounced peak in spheroid size in later timepoints, which may be slightly reduced before 72 h (such as ATCC 50703 comfilcon A) or may continue to grow through the 72 h timepoint (such as ATCC 30461 comfilcon A), while the majority of other strain-material combinations demonstrated a more consistent particle size from at least 3.0–3.5 h onwards. To note, ATCC 50703 had the least stable spheroids of all strains, with several lens materials showing substantial early aggregation followed by deaggregation at later timepoints.

## Cell counts within aggregated spheroids

Each spheroid (defined as more than four cells touching at once) was analyzed to determine the number of cells it contained from baseline (0.5 h) through hour 24 ([Figure 6](#)). Each lens material was noted to have unique aggregation profiles: the No Lens Control and lehfilcon A maintained no significant aggregation through all 24 h. Etafilcon A did not demonstrate aggregation at hours 0.5, 6, or 12, but did have significantly more aggregation vs. its own baseline and vs. the

No Lens Control at hour 24 ( $p < 0.05$ ). Comfilcon A, senofilcon A, samfilcon A, and fanfilcon A maintained significantly larger spheroids than the No Lens Control and lehfilcon A at hours 6, 12, and 24. Omafilcon A showed significant aggregation at hours 6 and 12, with a moderate dispersal of the spheroids by hour 24. Comfilcon A also demonstrated the largest spheroids by size ( $>1,500$  cells per spheroid at multiple time points) while aggregating materials such as senofilcon A and samfilcon A were more likely to produce several spheroids of more moderate size (between 100 and 1,500 cells per spheroid).

## Visualization of encystment within *Acanthamoeba* spheroids

To understand the formation of *Acanthamoeba* cysts within spheroids and evaluate if aggregation was a similar process regardless of material trigger, we utilized fluorescent confocal microscopy and three different spheroid-forming conditions: a BIOFLOAT™ spheroid plate, senofilcon A, and comfilcon A ([Figure 7](#)). Results were highly similar between all three materials tested, indicating that spheroids made on Biofloat spheroid plates were structurally similar to those made on contact lens materials. As early as 4 h, Calcofluor-white-positive cysts were observed on contact lens materials. Likewise, ethidium homodimer staining became evident in the vicinity of newly formed cysts, indicating the general building of an extracellular matrix, while still demonstrating some enzymatic activity *via* fluorescein diacetate staining. Notably, the ethidium homodimer staining outlining cell shapes (but not often filling a cell cytoplasm) indicates for the first time that *Acanthamoeba* spheroids may be forming an extracellular matrix as they age. Fluorescein diacetate was noted in spheroids at all timepoints and in both trophozoites and cysts, although it was more prominent in older spheroids, indicating mature spheroids are still viable, metabolically active, infectious cells ([Garajová et al., 2019](#)).

## Genomic analysis of *Acanthamoeba* on lens materials

Following the observation of material-dependent *Acanthamoeba* behavior leading to either independently motile trophozoites or enmeshed spheroids, we analyzed the transcriptome of *Acanthamoeba* ATCC 30461 (a commonly utilized strain) on lehfilcon A, comfilcon A, samfilcon A, and the no lens control ([Figures 8–10](#), online repository for complete data set). This study was undertaken to identify which genes or potential pathways may be contributing to the aggregation or may be contributing to the persistence of a spheroid (when it does not dissociate over time), and downstream cellular changes in *Acanthamoeba* as a result of



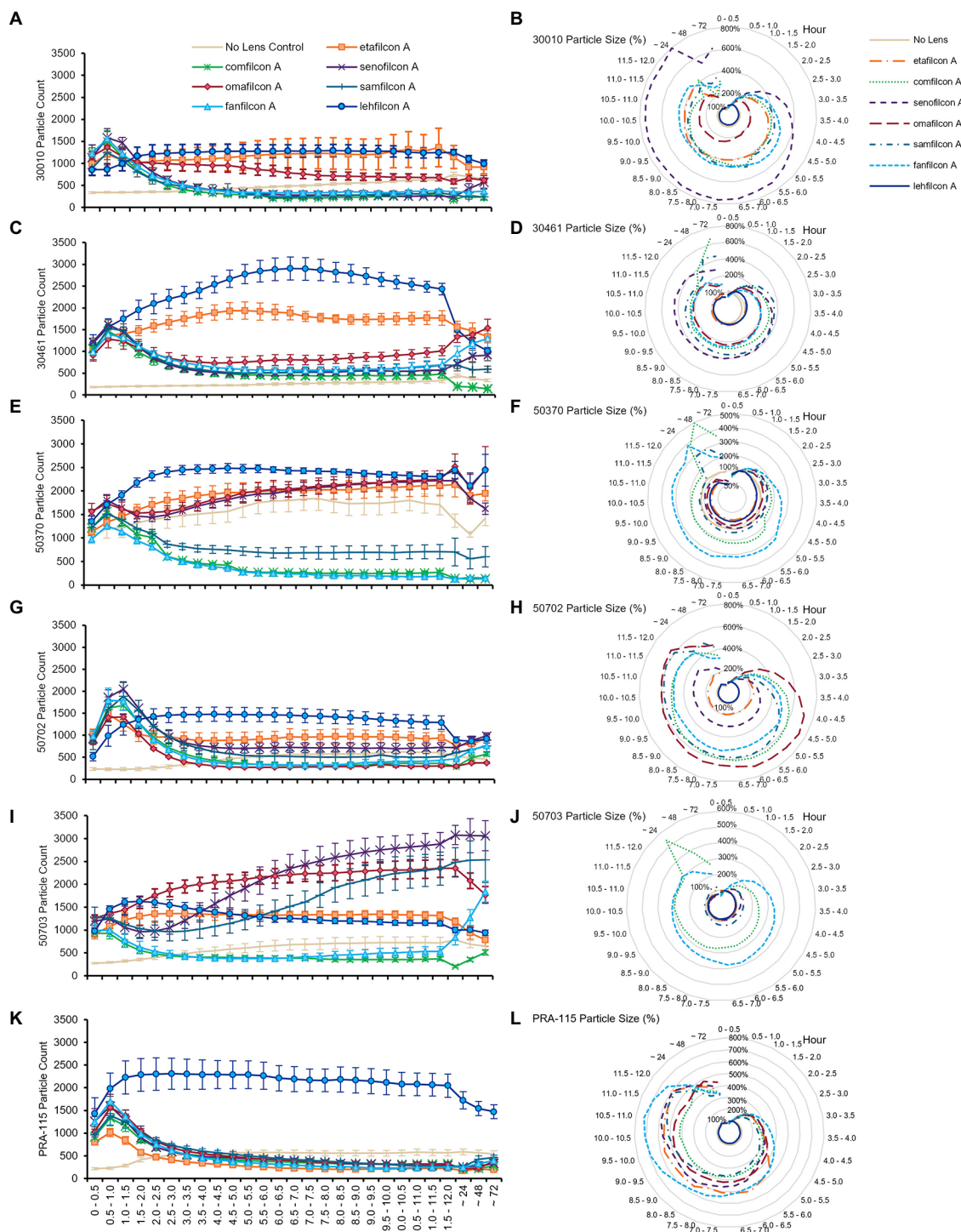


FIGURE 3

*Acanthamoeba* demonstrated significantly less aggregation on lehfilcon A lenses compared to other lens materials. Mean  $\pm$  SE of (A) ATCC 30010 count, (B) ATCC 30010 particle size, (C) ATCC 30461 count, (D) ATCC 30461 particle size, (E) ATCC 50370 count, (F) ATCC 50370 particle size, (G) ATCC 50702 count, (H) ATCC 50702 particle size, (I) ATCC 50703 count, (J) ATCC 50703 particle size, (K) ATCC PRA-115 count, (L) ATCC PRA-115 particle size. Size is normalized to the baselines obtained in the 0.5–1.0 h. Statistical comparisons noted in [Supplementary Figures S3 and S4](#). Matching representative images presented in [Figures 4 and 5](#).  $n=6$  per group.

being part of a spheroid. Lehfilcon A was again consistently noted as a non-aggregating lens. While both comfilcon A and samfilcon A dependably demonstrated aggregation, more

significantly differentially expressed genes were found at all time points in lehfilcon A vs. samfilcon A than lehfilcon A vs. comfilcon A.



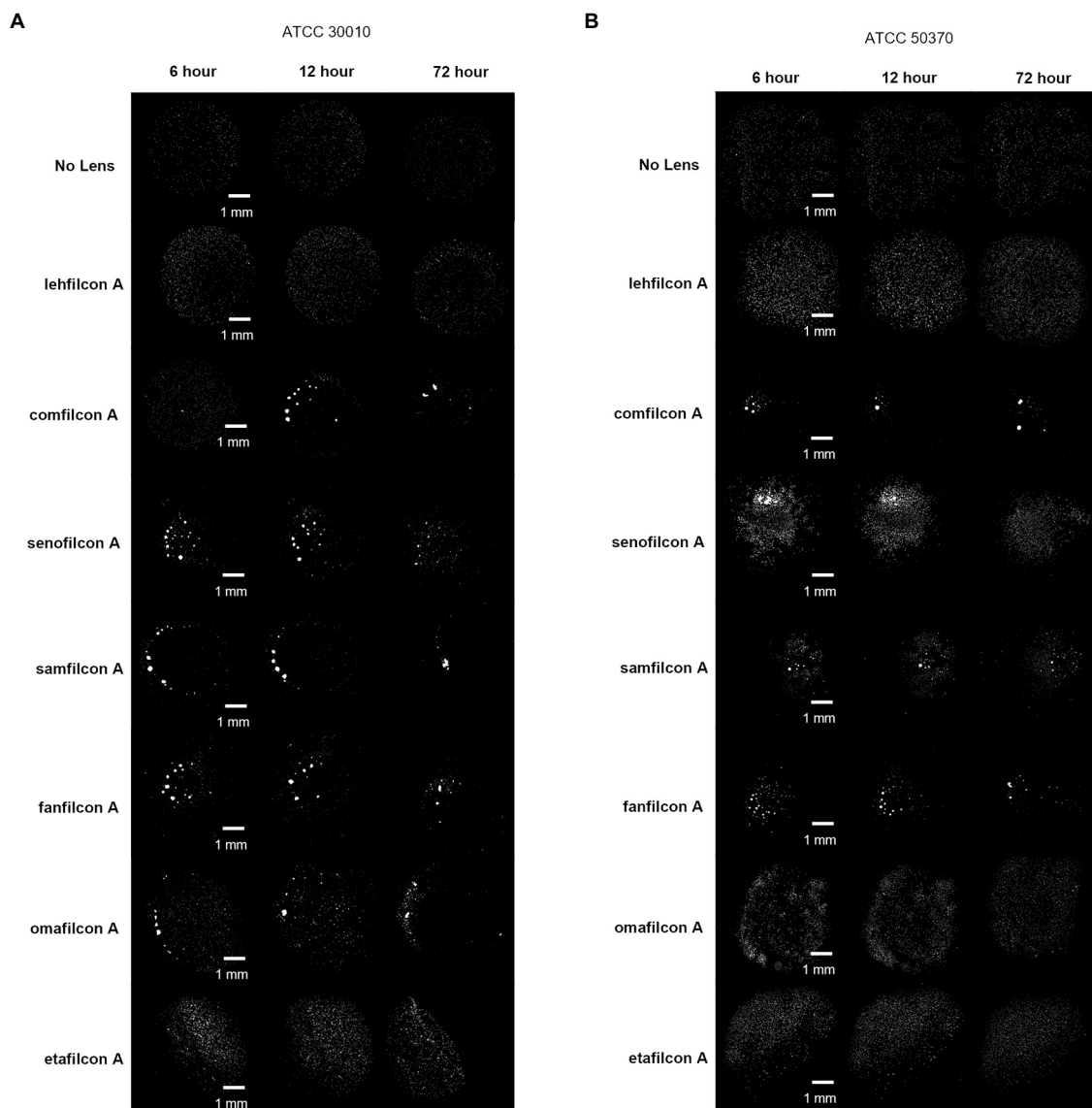


**FIGURE 4**  
Representative images of *Acanthamoeba* on contact lens materials at 6, 12, and 72 h. (A) ATCC 30010, (B) ATCC 50370. Mean  $\pm$  SE representation in Figure 3.  $n=6$  per group.

Twenty three genes were significantly differentially expressed at all timepoints (4, 12 and 24 h) in lehfilcon A vs. comfilcon A and samfilcon A, including two tRNA genes that were removed from the detailed analysis. The resulting 21 genes were visualized *via* heatmap and the homologous genes from ATCC 30010 (Neff strain) were identified (Figure 8D). All 21 genes demonstrated some degree of homology with ATCC 30010, and the majority demonstrated over 75% homology, although not all genes have inferred functions; 6 of the 21 genes are currently unknown. Further, all 21 genes possessed a similar differential expression profile between lehfilcon A vs. comfilcon A and lehfilcon A vs. samfilcon A (that is, if a gene was downregulated in one, it was downregulated in the other, and

so on). Overall, as indicated by the white coloration in the heatmap, the genes that were significantly differentially expressed between the aggregating lenses and the non-aggregating lens demonstrated very little difference when the two aggregating lenses were compared to each other, thus further signifying that these genes are involved in highly similar behavioral responses to lens materials. Protein–protein interactions and the significantly differentially expressed pathways were further identified (Figure 8E) and alterations were noted in pathways involving the actin cytoskeleton, intracellular vesicle formation, and metabolic activity. Further visualizations along with Neff strain homology and GO term descriptions can be found in Figures 9, 10.

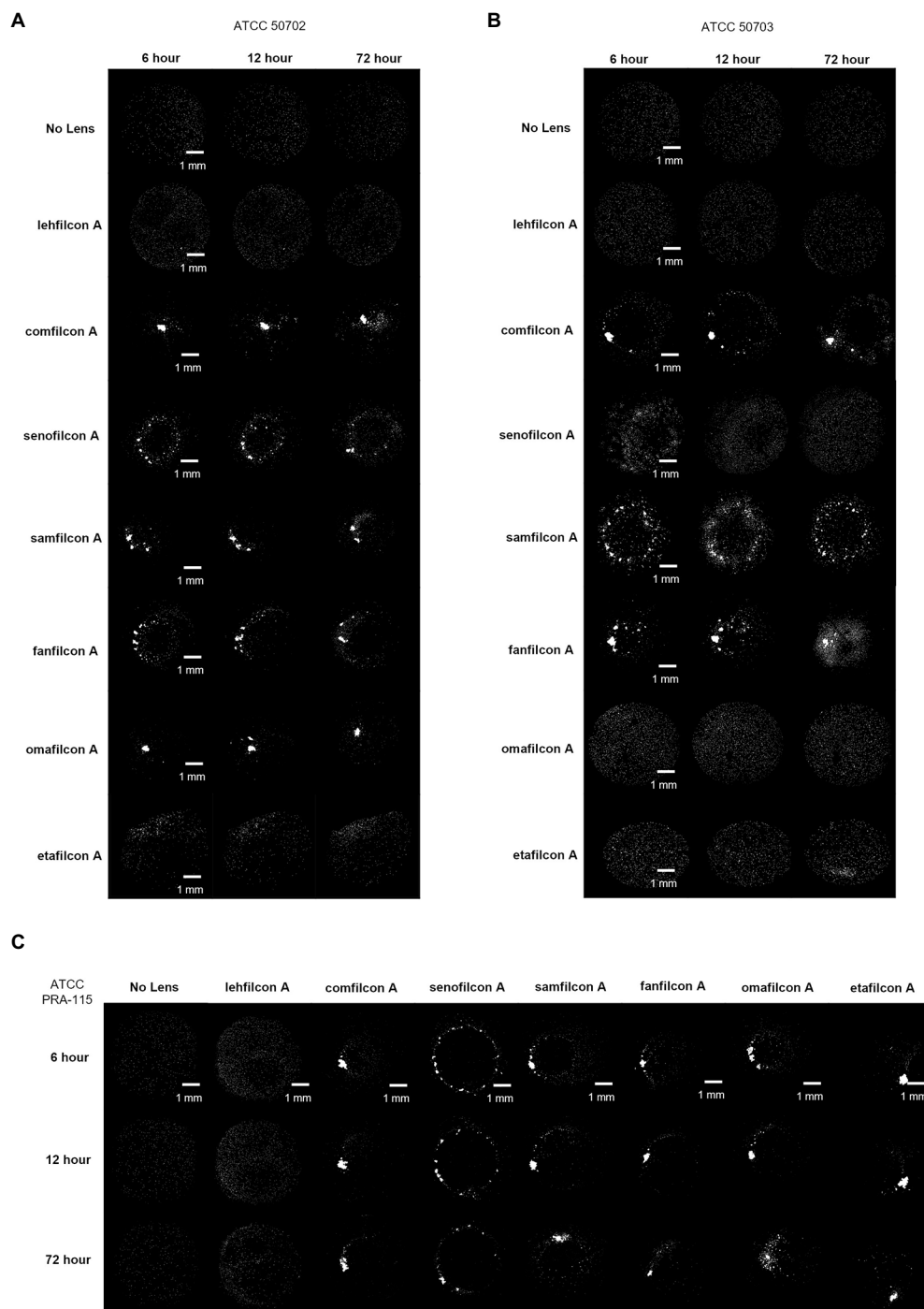


**FIGURE 5**  
Representative images of *Acanthamoeba* on contact lens materials at 6, 12, and 72 h. (A) ATCC 50702, (B) ATCC 50703, (C) ATCC PRA-115. Mean  $\pm$  SE representation in Figure 3.  $n=6$  per group.

## Aggregated *Acanthamoeba* impedes disinfection efficacy

To determine MPS disinfection efficacy of *Acanthamoeba* in different cellular formations (Figure 7), *Acanthamoeba* were assessed for biocide resistance in either trophozoite, cyst, or

spheroid forms after cells had been allowed to adhere (or aggregate) in plates for 12 or 24 h (Figure 11). Consistent with published findings (Gabriel et al., 2019; Walters et al., 2022), cells in the trophozoite form were the most susceptible to MPS biocides while cysts were significantly more challenging to disinfect. PAPB/PQ showed little ability to kill any form, with 100% survival for

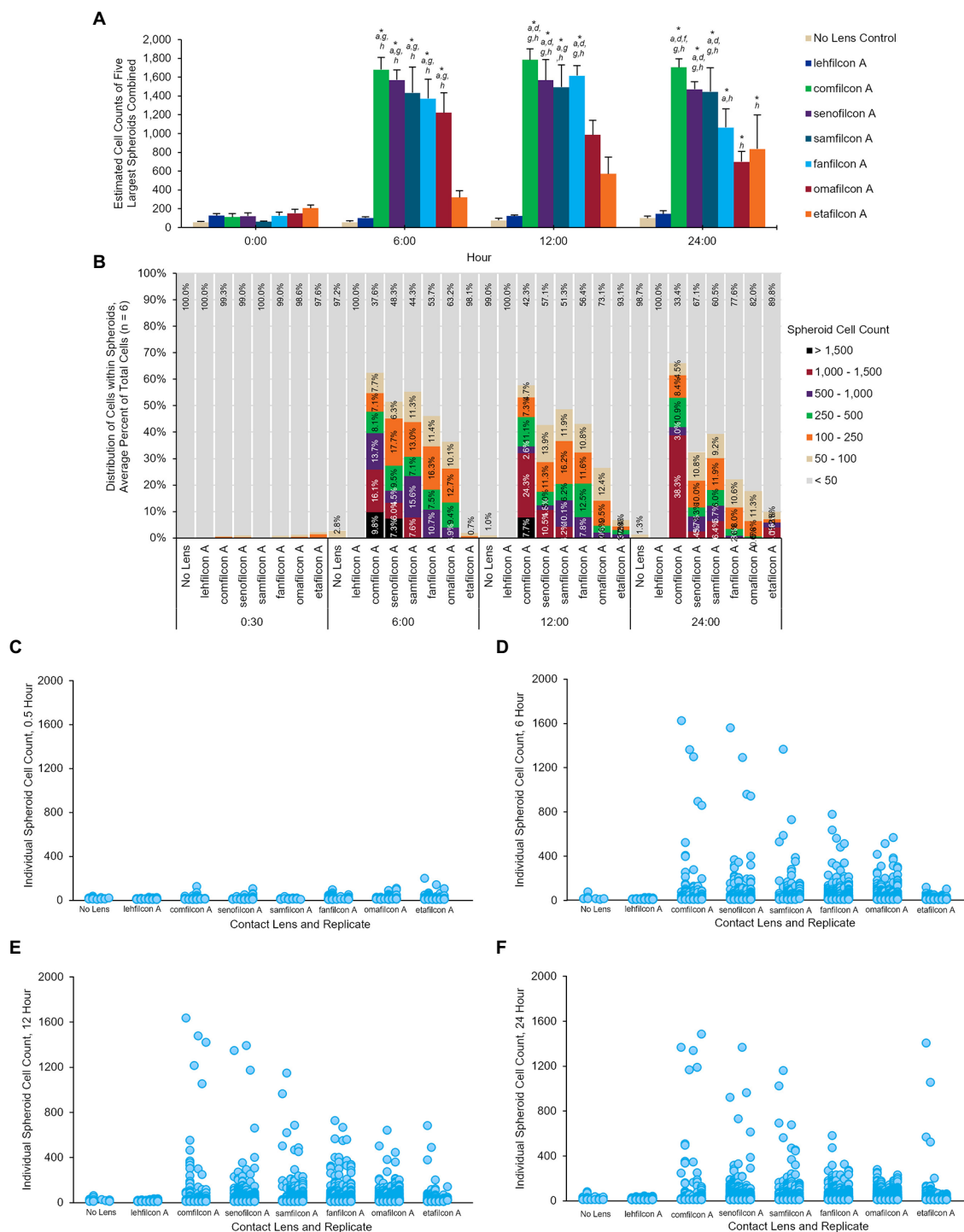
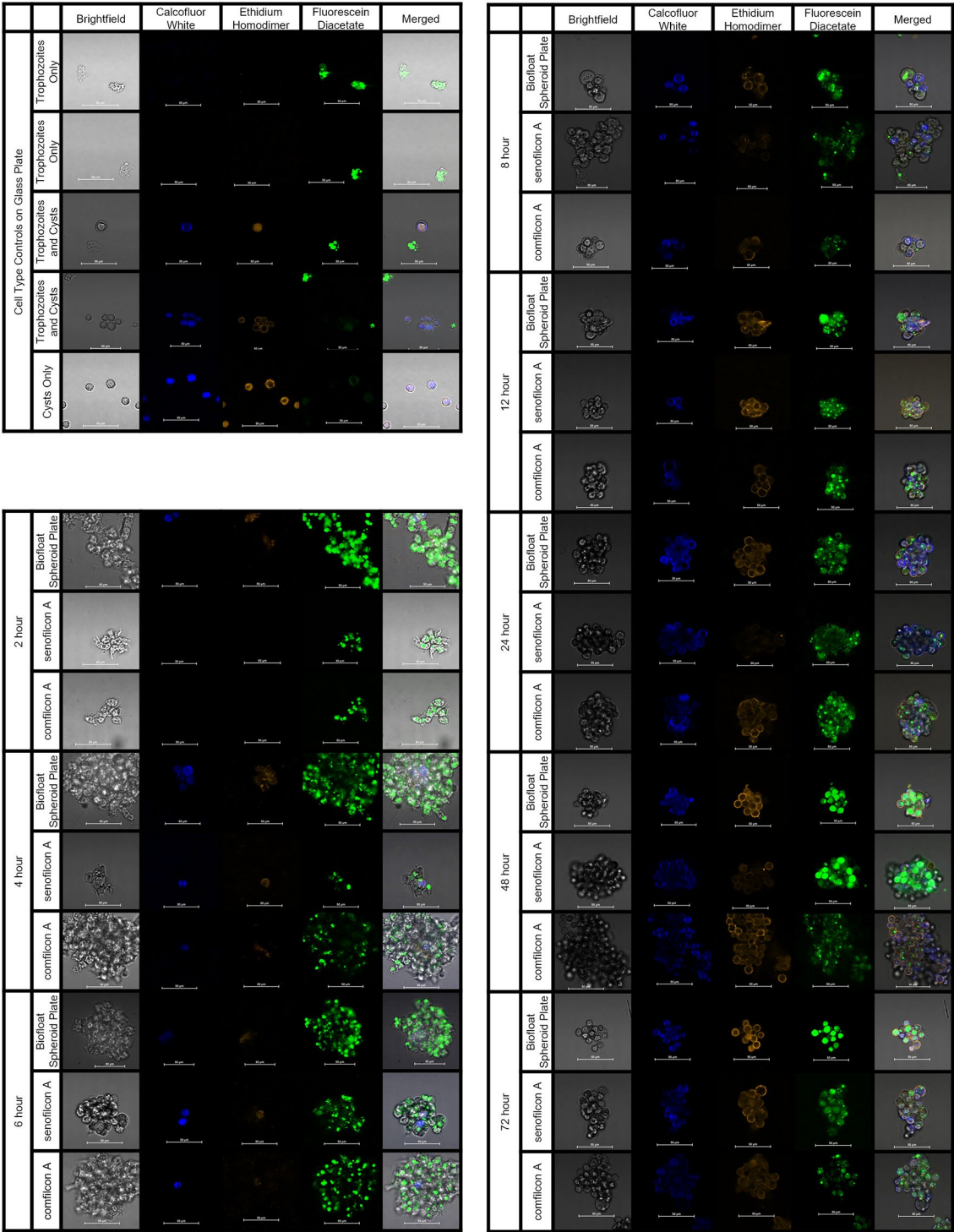


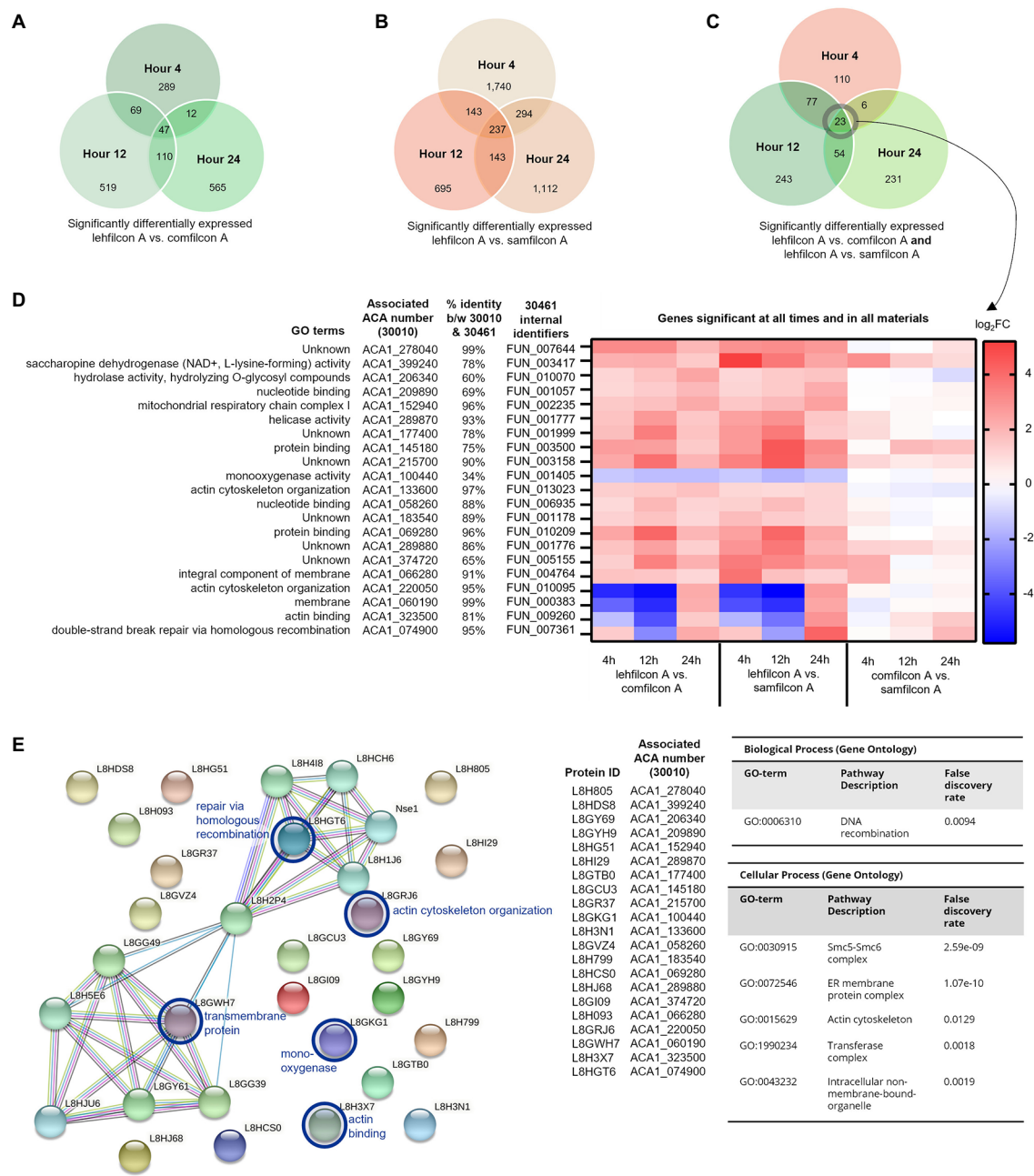
FIGURE 6

Once aggregated, cell counts of *Acanthamoeba polyphaga* (ATCC 30461) spheroids are maintained through 24 h. **(A)** Cell count of five largest spheroids on any one lens combined, calculated per lens type and presented at mean  $\pm$  SE among 6 replicates. **(B)** Percentage of cells that are maintained in spheroids of various sizes over time, delineated by color for each spheroid size. Percentages are an average from 6 replicates per lens material. **(C–F)** Individual spheroid cell counts at the 0.5 h, 6 h, 12 h, and 24 h timepoints. Each individual spheroid on any lens, replicate, and timepoint is represented by a dot corresponding to its cell count. Replicates are visualized from left to right for each lens material ( $n=6$ ). Time 0 baseline is calculated from the 0.5 h to allow cells to adhere to the material. Analyzed via two-way repeat measure ANOVA. Within a given timepoint: (a)  $p < 0.05$  vs. lehficon A, (b)  $p < 0.05$  vs. comfilcon A, (c)  $p < 0.05$  vs. senofilcon A, (d)  $p < 0.05$  vs. omafilcon A, (e)  $p < 0.05$  vs. samfilcon A, (f)  $p < 0.05$  vs. fanfilcon A, (g)  $p < 0.05$  vs. etafilcon A, (h)  $p < 0.05$  vs. No Lens Control. Within a given lens type, \* $p < 0.05$  baseline (0.5 h).



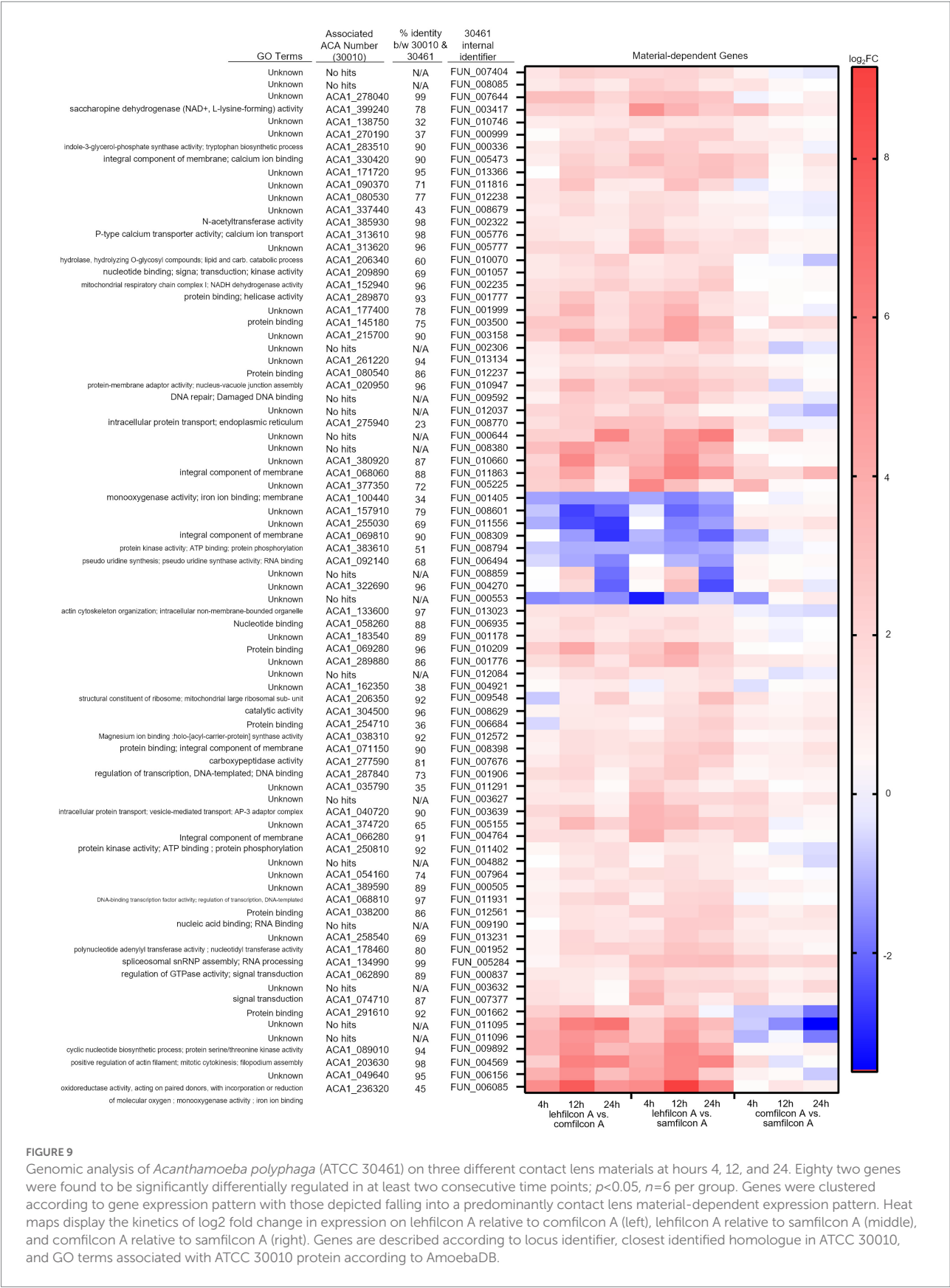
**FIGURE 7**  
*Acanthamoeba polyphaga* (ATCC 30461) demonstrated encystment at 4h on all three materials tested, and maintained encystment through 72 h. Controls: Control cells (trophozoites, and cysts pre-made *via* starvation) were imaged on a glass slide to indicate stain response prior to aggregation experiments. Aggregation: Representative images of fluorescently stained *Acanthamoeba* spheroids on a spheroid-producing Biofloat plate, senofilcon A, or comfilcon A, without other encystment-inducing substrates. Calcofluor white staining (DAPI filter, blue color) binds to the cellulose of cell walls and indicates cysts. Ethidium homodimer staining (TRITC filter, orange color) binds to nucleic acids and indicates compromised cells or cell death (able to be penetrated by stain and bind to nucleic acids) or presence of extracellular matrix. Fluorescein diacetate (FITC filter, green color) is a dye that can penetrate trophozoite cell walls and indicates enzymatic activity. All scale bars equal 50 μm. Eight spheroids were created and imaged for each condition in separate wells and representative images were chosen at random.

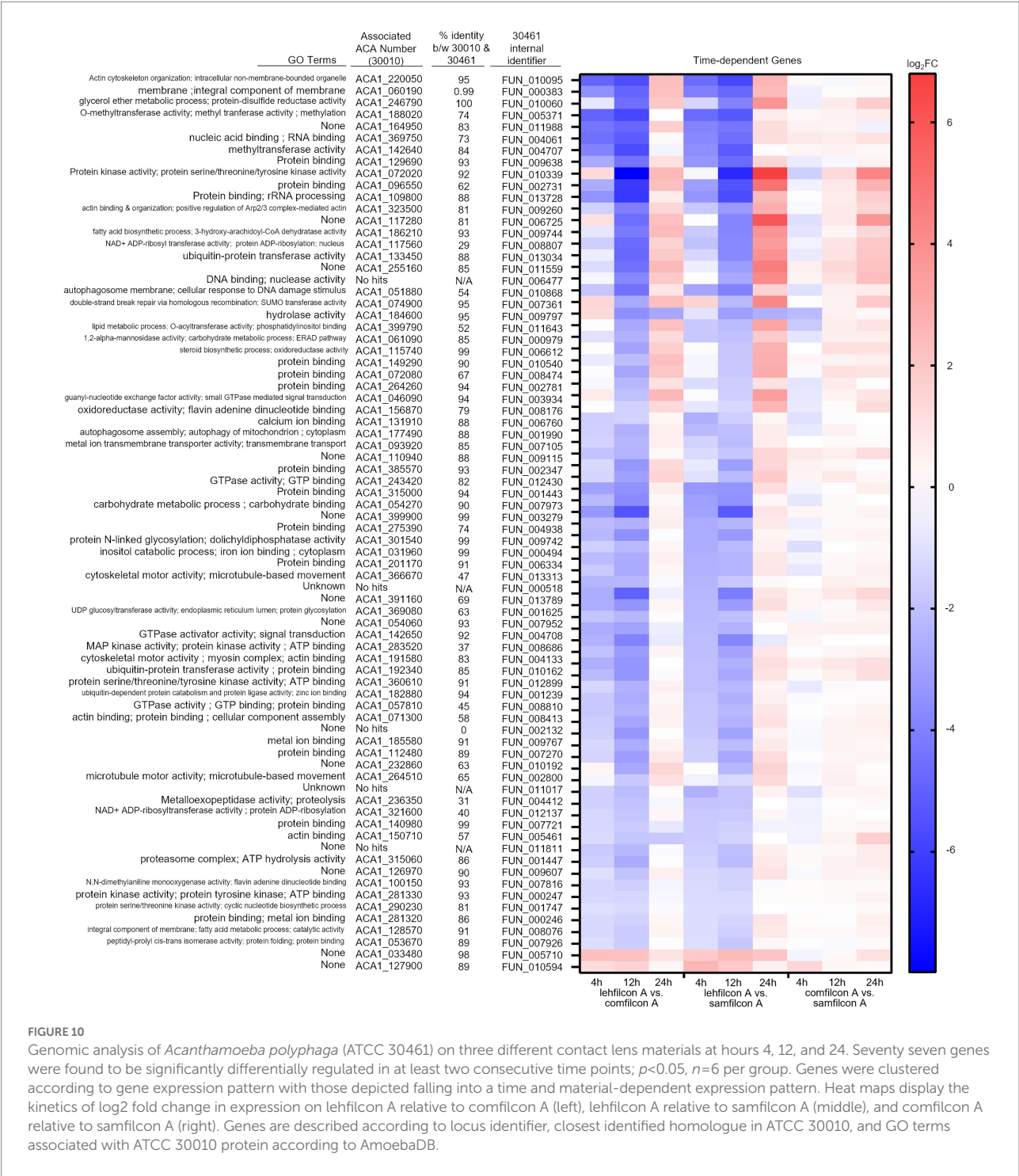




**FIGURE 8**  
Genomic analysis of *Acanthamoeba polyphaga* (ATCC 30461) on three different contact lens materials at hours 4, 12, and 24. **(A)** Venn diagram of overlapping genes that were significantly different between lehfilcon A vs. comfilcon A, by hour, **(B)** Venn diagram of overlapping genes that were significantly different between lehfilcon A vs. samfilcon A, by hour, and **(C)** Venn diagram of overlapping genes that were significantly different between lehfilcon A vs. comfilcon A and lehfilcon A vs. samfilcon A, by hour. **(D)** 23 genes were significantly differentially expressed between lehfilcon A and both other materials, and in all three time points;  $p < 0.05$ ,  $n = 6$  per group. Genes are described according to locus identifier, closest identified homologue in ATCC 30010, and GO terms associated with ATCC 30010 protein according to AmoebaDB. **(E)** All 21 genes are visualized as proteins and their protein-protein interactions are identified via STRING: significant pathways are identified using a false discovery rate of  $< 0.05$ . Proteins that were significantly upregulated in aggregating lenses at any timepoint are indicated in the protein-protein interaction map with a blue circle. All other proteins visualized were significantly downregulated in aggregating lenses compared to the non-aggregating lens. Further visualizations of other significant genes presented in Figures 9 and 10.

spheroids and cysts across all cell concentrations. Likewise, PAPB had no ability to disinfect cysts though some efficacy was observed against trophozoites. The increased survivability for trophozoites with PAPB over time may be due to individual cysts forming by 24h that PAPB has no ability to kill. PAPB demonstrated less efficacy against spheroids compared to individual trophozoites at





all concentrations and time periods despite the cells originating from the same stock. PAPB/PQ/AD demonstrated nearly complete kill of trophozoites for all concentrations and time points with limited survivors at the highest concentration of trophozoites at 24 h, again likely due to the development of individual cysts within the population. PAPB/PQ/AD also had the best efficacy against cysts due to the activity of alexidine where only 50% of the 375

cysts/well condition survived. In contrast, 100% of the spheroid wells survived disinfection with PAPB/PQ/AD for both timepoints at the two highest cell concentrations, and 50% spheroid survival at the lowest concentration, highlighting how the physical barrier of aggregated cells and subpopulations of cysts presented a substantial challenge for MPS disinfection compared to individual trophozoites and cysts at the same concentration.



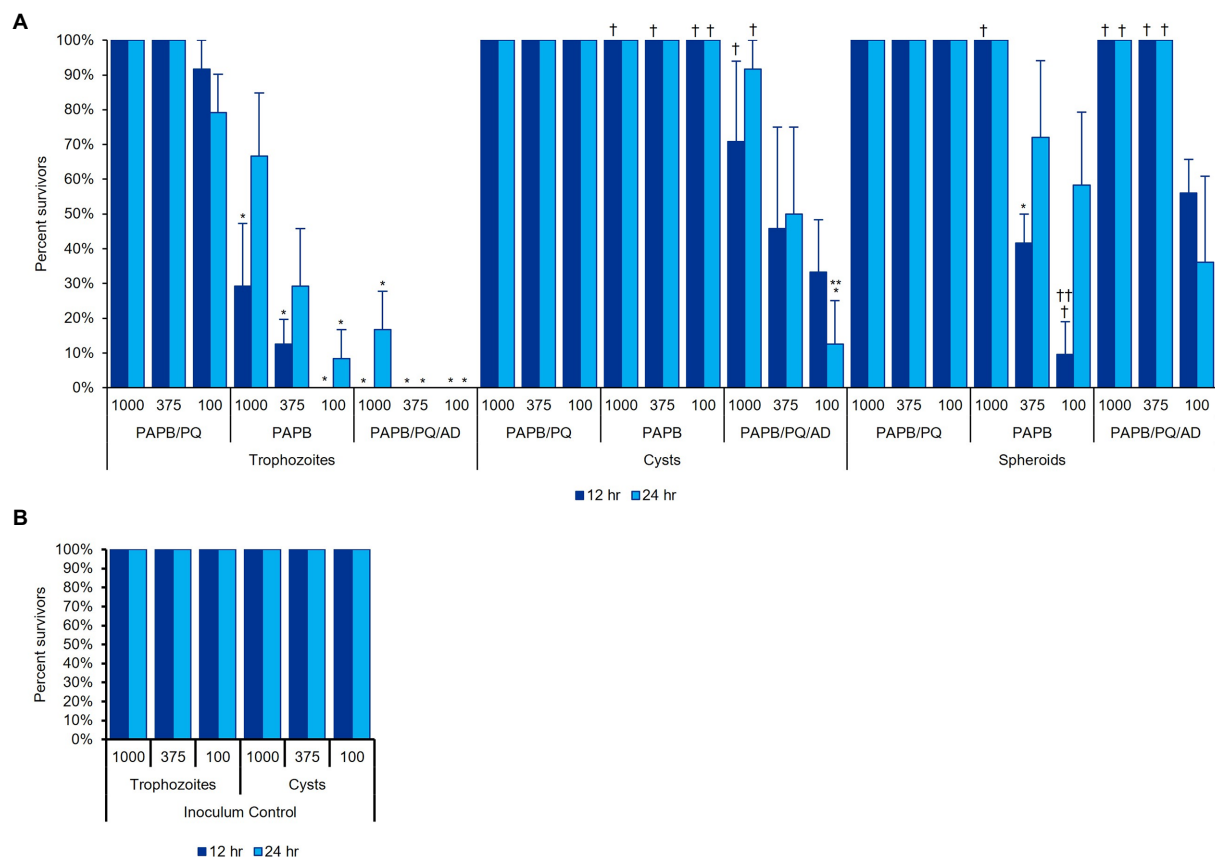


FIGURE 11

*Acanthamoeba polyphaga* (ATCC 30461) in three different cell concentrations (1,000, 375, or 100 cells per 100  $\mu$ l) was used to examine MPS disinfection efficacy against (A) trophozoites, cysts, and spheroids, after cells had adhered to the plate for 12 or 24 h. (B) An inoculum control was run concurrently with the same cultures used in (A). Each bar represents a mean  $\pm$  SE of 3 replicates, each replicate being composed of 8 wells from which percent survivorship was calculated. Statistical analysis via 2-way ANOVA: comparisons versus a MPS within the same cell condition and same time, \* $p$ <0.05 vs. PAPB/PQ, \*\* $p$ <0.05 vs. PAPB; comparisons versus a cell condition within the same MPS and same time, † $p$ <0.05 vs. trophozoites, †† $p$ <0.05 vs. cysts.

## Discussion

*Acanthamoeba* and its risk to contact lens users remains at the forefront of ophthalmology and optometry due the devastating consequences of infections and limited options for treatment (Siddiqui and Khan, 2012; Szentmary et al., 2019). While studied for decades, *Acanthamoeba* research has only recently expanded to utilize robust -omic methods to understand more about this amoeba's dynamic lifecycle (Bernard et al., 2022). Even now, limited genome annotation and no stable methods for impacting gene expression have significantly hampered *Acanthamoeba* research where the pathogenesis of other ocular microorganisms like *Pseudomonas* are well-described and the risk factors for infection clearly delineated (Gu et al., 2022). Equally, the infrequent diagnosis of *Acanthamoeba* keratitis' has prevented significant investment in treatment development and infection prevention, despite devastating outcomes for those affected (Siddiqui and Khan, 2012; Szentmary et al., 2019). Most outreach and publicity stems from survivors, though education of contact lens users and, equally, their

optometrists, is being pioneered by experts around the globe. Currently, the sole defense for contact lens users beyond water avoidance is the disinfecting solutions utilized to clean contact lenses (Arshad et al., 2019, 2021; British Contact Lens Association, 2021). Most disinfecting solutions were developed to reduce the bacterial and lipid/protein deposit load on a lens as opposed to engineering a lens or lens solution with a more challenging organism like *Acanthamoeba* in mind (although, the reduction of bacteria binding to a lens could limit the nutrient source and proliferation for *Acanthamoeba*). The regulatory requirements for *Acanthamoeba* multi-purpose solution disinfection efficacy continue to lag despite calls for action (Jobson Medical Information, LLC, 2009; Primary Care Optometry News, 2014). However, no multi-purpose solutions have a requirement to disinfect *Acanthamoeba* (ISO 14729:2001/A1:2010, 2010) and effective chemicals available against *Acanthamoeba* are unable to be utilized at sufficient concentrations due to toxicity to the cornea. Equally, the most effective products against all types of *Acanthamoeba* are hydrogen peroxide based (Walters et al., 2022). However, many

consumers avoid hydrogen peroxide use because of the risk of accidentally burning the corneal surface through misuse, despite the disinfection benefits, as well as the slightly more complicated user instructions. Here, we have shown it is most important to keep *Acanthamoeba* in their most susceptible state (trophozoites) where most multi-purpose solutions offer some level of disinfecting ability.

Contact lenses have evolved significantly from the polymethyl methacrylate and original rigid gas permeable lenses. Contact lens manufacturers must continue to evolve new materials to increase oxygen permeability and wettability to combat user discomfort that can cause patients to revert to glasses. For *Acanthamoeba* keratitis with small outbreaks associated with poor MPS efficacy, little examination has been done to evaluate the role of the contact lens in *Acanthamoeba* pathogenesis. Here, we have described a novel finding that many strains of *Acanthamoeba* will aggregate in response to specific contact lens materials. This is a significant potential risk to patients as *Acanthamoeba* aggregation is a precursor to encystment (Coulon et al., 2010; Bernard et al., 2022). As part of its natural life cycle, *Acanthamoeba* will aggregate into small clusters to encyst. Likely a protective measure, aggregation in response to a newly toxic environment makes evolutionary sense where even if the entire population fails to encyst, at least some individuals, potentially at the center of an spheroid, may survive the unfavorable environment (Coulon et al., 2010). To our knowledge, this is the first time this aggregation and encystment phenomenon has been observed in this short duration where issues like food availability and chemical induction were not at play. Trophozoites were induced to aggregate and encyst by the material they were in contact with, versus a change in chemical or nutrient availability commonly used in other studies (Coulon et al., 2010, 2012; Bernard et al., 2022). Gene expression evaluation indicated alterations in encystment pathways where actin cytoskeleton rearrangement is critical to the aggregation pathways as well as changes in metabolic activity and intracellular vesicles. Fluorescent confocal microscopy confirmed the presence of cysts as early as four hours after introduction to a contact lens surface. This demonstrates a significantly faster aggregation than has been observed in chemical induction such as Neff's encystment media (>24 h) or starvation (7–14 days; Aqeel et al., 2013). The contact lens surface demonstrated such a significant risk that *Acanthamoeba* actively initiated a terminal differentiation resulting in cysts far earlier than normal nutrient unavailability would stimulate. Other contact lens-associated risks were apparent as well, including the upregulation of autophagy and ubiquitination in the aggregating lenses versus lehilcon A. Interestingly, spheroids removed from contact lens materials can de-aggregate on polystyrene or lehilcon A though cysts within the spheroid remain cysts without a food source (Supplementary Video S7). For polystyrene controls and lehilcon A, there was no indication that any binary fission occurred based on cell count, and eventually individual trophozoites encysted though active trophozoites were visible through the 72 h despite no nutrient source. This supports previous work that shows

trophozoites will maintain motility through 24 h with no decrease in activity even without nutrients (Campolo et al., 2021). Here, *Acanthamoeba* trophozoites show a remarkable response to a surface they identified as inhospitable, responding quickly (<1 h) to many contact lens materials, aggregating and initiating encystment (< 4 h) despite no chemical induction beyond the contact lens surface. No nutrients are provided on the lens but this is not a long enough time period to be considered starvation. The properties of the aggregation-inducing contact lens materials that trigger this response are unknown and would require future investigation, but this response could potentially be due to diminished water content or surface topography of the contact lens materials. *Acanthamoeba* prefers to exist at the interfaces between soil and water, and surfaces indicating a strong water-aversion (Liang et al., 2022; Wesley et al., 2022) may trigger the protective response.

The risk of aggregation and encystment for *Acanthamoeba* and its potential to cause human disease has so far been dependent on the ability to kill *Acanthamoeba* before patient contact. For contact lenses, the creation of spheroids and cysts could significantly hamper multi-purpose solutions from adequately disinfecting *Acanthamoeba* from lenses. Here, we demonstrated that spheroids can resist disinfection in clinically relevant, low cell concentrations (Li et al., 2020). Seeding a well at a concentration of ~100 trophozoites/well was equivalent to a low inoculum concentration of  $5.0 \times 10^2$  cells/mL. Most microbial efficacy standards require inoculation at  $10^5$ – $10^6$  cells/mL for a microorganism, and a resulting 3-log disinfection efficacy for the solution being tested (ISO 14729:2001/A1:2010, 2010). Here, we demonstrated that spheroids could survive disinfection at far lower densities than any standard is currently evaluating. The resistance of the spheroid is two-fold: the spheroid itself provides a protective layer preventing penetration of biocides to interior cells, and the rapid formation of cysts at the center of spheroids offers cells with a naturally high biocide resistance. Interestingly, even biocides like alexidine known to be capable of killing cysts were less effective against spheroids despite showing efficacy against individual trophozoites and cysts.

This data indicates the need for continued research into *Acanthamoeba*'s interactions with contact lenses. For instance, the timeline of encystment noted in the observations here, as amoeba appear to encyst on contact lenses much faster than they do *via* starvation or *via* encystment media, should be further studied as the transcriptome analysis did not show differentially expressed genes from known encystment genes (Dudley et al., 2009; Rolland et al., 2020; Bernard et al., 2022). We attribute this to the speed at which encystment is being induced which is significantly faster than other studies that used chemical induction of encystment. Further, the observations made here regarding disinfection efficacy should be followed up with *in vivo* examinations to determine the risk that aggregating lenses may pose to patients. Similarly, to our knowledge, there are no meta-analyses relating

contact lenses themselves to *Acanthamoeba* keratitis cases or prevalence, and this would be a critical investigation to supplement the information presented here. Finally, while we did observe variability between strains, with ATCC 50703 being the most divergent from the group, we do note that when all strains are combined the results are consistently statistically significant regarding which lenses do and do not promote aggregation. We thought it important to show the differences between genotypes even when some strains did not show the strong aggregation behaviors found in others. These divergent strains or behaviors merit future investigation.

Together, this study demonstrates that *Acanthamoeba* behavior can be significantly altered by different polymeric surface properties, particularly those found in contact lens materials. That behavior, which results in a protective mechanism that promotes *Acanthamoeba* encystment far faster than natural stressors like starvation, may contribute to the pathogenesis of this organism by making it resistant to available disinfection methods. *Acanthamoeba* spheroids and the underlying surface properties that lead to their formation represent an under-investigated field of research. While promotion of proper disinfection of lenses is critical to patient safety, now it becomes equally important to impress on patients that their contact lenses should never come in contact with any water source that may contain *Acanthamoeba*. With contact lens materials continuing to diversify, *Acanthamoeba*'s response to contact lenses must be further studied to understand the complete implications to patient safety.

## Data availability statement

The data presented in the study are deposited in the NCBI BioProject repository, accession numbers PRJNA903937 (<https://www.ncbi.nlm.nih.gov/bioproject/PRJNA903937>) and PRJNA905484 (<https://www.ncbi.nlm.nih.gov/bioproject/PRJNA905484>).

## Author contributions

AC, RP, RW, JK, CR, PS, BP, and MC were involved in conceptualization. AC, RP, RW, MT, EM, VH, JK, BP, and MC were involved in data curation and methodology. AC, RP, CR, BP, and MC were responsible for formal analysis. AC, RP, VH, JK, BP,

and MC were involved in validation. AC, RP, RW, MT, EM, CR, BP, and MC conducted visualization. PS and MC were responsible for project administration, resources, and supervision. AC and MC conducted writing of the original draft. All authors participated in manuscript review and editing. All authors had full access to all the data in the study and had final responsibility for the decision to submit for publication. All authors contributed to the article and approved the submitted version.

## Funding

This research was funded by Alcon, which provided all financial support. CR reports grants from Purdue University, outside of the scope of the submitted work.

## Conflict of interest

The funder was not involved in the study design, collection, analysis, interpretation of data, or the writing of this article. The funder approved the decision to submit for publication. All authors except CR are employees of Alcon Research.

The remaining author declares that the research was conducted in the absence of any commercial or financial relationships that could be construed as a potential conflict of interest.

## Publisher's note

All claims expressed in this article are solely those of the authors and do not necessarily represent those of their affiliated organizations, or those of the publisher, the editors and the reviewers. Any product that may be evaluated in this article, or claim that may be made by its manufacturer, is not guaranteed or endorsed by the publisher.

## Supplementary material

The Supplementary material for this article can be found online at: <https://www.frontiersin.org/articles/10.3389/fmicb.2022.1089092/full#supplementary-material>

## References

- Acanthamoeba* polyphaga (Pushkarew). (2019). Encyclopedia of life. Available at: <https://eol.org/pages/593787> (Accessed October 6, 2022).
- Ahearn, D. G., Simmons, R. B., Ward, M. A., and Stulting, R. D. (2012). Potential resistant Morphotypes of *Acanthamoeba castellanii* expressed in multipurpose contact lens disinfection systems. *Eye Contact Lens* 38, 400–405. doi: 10.1097/ICL.0b013e318261ab1f
- Antonelli, A., Favuzza, E., Galano, A., Montalbano Di Filippo, M., Ciccone, N., Berrilli, F., et al. (2018). Regional spread of contact lens-related *Acanthamoeba* keratitis in Italy. *New Microbiol.* 41, 83–85. PMID: 29505068
- Aqeel, Y., Siddiqui, R., Ifikhar, H., and Khan, N. A. (2013). The effect of different environmental conditions on the encystation of *Acanthamoeba castellanii* belonging to the T4 genotype. *Exp. Parasitol.* 135, 30–35. doi: 10.1016/j.exppara.2013.05.017
- Arshad, M., Carnt, N., Tan, J., Ekkeshis, I., and Stapleton, F. (2019). Water exposure and the risk of contact lens-related disease. *Cornea* 38, 791–797. doi: 10.1097/ICO.0000000000001898
- Arshad, M., Carnt, N., Tan, J., and Stapleton, F. (2021). Compliance behaviour change in contact lens wearers: a randomised controlled trial. *Eye (Lond.)* 35, 988–995. doi: 10.1038/s41433-020-1015-9

- bcl-convert (2021). A proprietary Illumina software for the conversion of bcl files to basecalls. [https://support-docs.illumina.com/SW/BCL\\_Convert/Content/SW/FrontPages/BCL\\_Convert.htm](https://support-docs.illumina.com/SW/BCL_Convert/Content/SW/FrontPages/BCL_Convert.htm) (Accessed November 30, 2022).
- Beattie, T. K., Tomlinson, A., Seal, D. V., and McFadyen, A. K. (2011). Salicylate inhibition of acanthamoeba attachment to contact lenses. *Optom. Vis. Sci.* 88, 1422–1432. doi: 10.1097/OPX.0b013e318230f574
- Bernard, C., Locard-Paulet, M., Noël, C., Duchateau, M., Gai, Gianetto, Q., Moumen, B., et al. (2022). A time-resolved multi-omics atlas of *Acanthamoeba castellanii* encystment. *Nat. Commun.* 13:4104. doi: 10.1038/s41467-022-31832-0
- British Contact Lens Association (2021). Raising public awareness of no water and *Acanthamoeba* keratitis. Available at: <https://anchor.fm/bcla/episodes/Raising-public-awareness-of-nowater-and-AK-es7l9b/> (Accessed February 4, 2022).
- Brown, A. C., Ross, J., Jones, D. B., Collier, S. A., Ayers, T. L., Hoekstra, R. M., et al. (2018). Risk factors for *Acanthamoeba* keratitis—a multistate case-control study, 2008–2011. *Eye Contact Lens* 44, S173–S178. doi: 10.1097/ICL.0000000000000365
- Buck, S. L., and Rosenthal, R. A. (1996). A quantitative method to evaluate neutralizer toxicity against *Acanthamoeba castellanii*. *Appl. Environ. Microbiol.* 62, 3521–3526. doi: 10.1128/aem.62.9.3521-3526.1996
- Campolo, A., Harris, V., Walters, R., Miller, E., Patterson, B., and Crary, M. (2021). Continuous real-time motility analysis of *Acanthamoeba* reveals sustained movement in absence of nutrients. *Pathogens* 10:995. doi: 10.3390/pathogens10080995
- Carnt, N., Hoffman, J. M., Verma, S., Hau, S., Radford, C. F., Minassian, D. C., et al. (2018). *Acanthamoeba* keratitis: confirmation of the UK outbreak and a prospective case-control study identifying contributing risk factors. *Br. J. Ophthalmol.* 102, 1621–1628. doi: 10.1136/bjophthalmol-2018-312544
- Carnt, N. A., Subedi, D., Connor, S., and Kilvington, S. (2020). The relationship between environmental sources and the susceptibility of *Acanthamoeba* keratitis in the United Kingdom. *PLoS One* 15:e0229681. doi: 10.1371/journal.pone.0229681
- Chelkha, N., Jardot, P., Moussaoui, I., Levasseur, A., La Scola, B., and Colson, P. (2020). Core gene-based molecular detection and identification of *Acanthamoeba* species. *Sci. Rep.* 10:1583. doi: 10.1038/s41598-020-57998-5
- Coulon, C., Collignon, A., McDonnell, G., and Thomas, V. (2010). Resistance of *Acanthamoeba* cysts to disinfection treatments used in health care settings. *J. Clin. Microbiol.* 48, 2689–2697. doi: 10.1128/JCM.00309-10
- Coulon, C., Dechamps, N., Meylheuc, T., Collignon, A., McDonnell, G., and Thomas, V. (2012). The effect of in vitro growth conditions on the resistance of *Acanthamoeba* cysts. *J. Eukaryot. Microbiol.* 59, 198–205. doi: 10.1111/j.1550-7408.2012.00612.x
- Cruz, A. R. S., and Rivera, W. L. (2014). Genotype analysis of *Acanthamoeba* isolated from human nasal swabs in the Philippines. *Asian Pac. J. Trop. Med.* 7, S74–S78. doi: 10.1016/S1995-7645(14)62066-6
- de Lacerda, A. G., and Lira, M. (2021). *Acanthamoeba* keratitis: a review of biology, pathophysiology and epidemiology. *Ophthalmic Physiol. Opt.* 41, 116–135. doi: 10.1111/opo.12752
- Dobin, A., Davis, C. A., Schlesinger, F., Drenkow, J., Zaleski, C., Jha, S., et al. (2012). STAR: ultrafast universal RNA-seq aligner. *Bioinformatics* 29, 15–21. doi: 10.1093/bioinformatics/bts635
- Douglas, M. (1930). Notes on the calssification of the amoeba found by Castellani in cultures of a yeast-like fungus. *J. Trop. Med. Lond.* 33, 258–259.
- Dudley, R., Jarroll, E. L., and Khan, N. A. (2009). Carbohydrate analysis of *Acanthamoeba castellanii*. *Exp. Parasitol.* 122, 338–343. doi: 10.1016/j.exppara.2009.04.009
- Gabriel, M. M., McAnally, C., Bartell, J., Walters, R., Clark, L., Crary, M., et al. (2019). Biocidal efficacy of a hydrogen peroxide lens care solution incorporating a novel wetting agent. *Eye Contact Lens* 45, 164–170. doi: 10.1097/ICL.0000000000000549
- Garajová, M., Mrva, M., Vašková, N., Martinka, M., Melicharová, J., and Valigurová, A. (2019). Cellulose fibrils formation and organisation of cytoskeleton during encystment are essential for *Acanthamoeba* cyst wall architecture. *Sci. Rep.* 9:4466. doi: 10.1038/s41598-019-41084-6
- Gast, R. J. (2001). Development of an *Acanthamoeba*-specific reverse dot-blot and the discovery of a new ribotype. *J. Eukaryot. Microbiol.* 48, 609–615. doi: 10.1111/j.1550-7408.2001.tb00199.x
- Gatti, S., Cevini, C., Bruno, A., Penso, G., Rama, P., and Scaglia, M. (1998). In vitro effectiveness of povidone-iodine on *Acanthamoeba* isolates from human cornea. *Antimicrob. Agents Chemother.* 42, 2232–2234. doi: 10.1128/AAC.42.9.2232
- Griffiths, A. J. (1969). “Encystment in amoebae” in *Advances in Microbial Physiology*. eds. A. H. Rose and J. F. Wilkinson (Cambridge, MA: Academic Press), 105–129.
- Gu, X., Lu, X., Lin, S., Shi, X., Shen, Y., Lu, Q., et al. (2022). A comparative genomic approach to determine the virulence factors and horizontal gene transfer events of clinical *Acanthamoeba* isolates. *Microbiol. Spectr.* 10:e0002522. doi: 10.1128/spectrum.00025-22
- Gurevich, A., Saveliev, V., Vyahhi, N., and Tesler, G. (2013). QUAST: quality assessment tool for genome assemblies. *Bioinformatics* 29, 1072–1075. doi: 10.1093/bioinformatics/btt086
- Ibrahim, Y. W., Boase, D. L., and Cree, I. A. (2009). How could contact lens wearers be at risk of *Acanthamoeba* infection? A Review. *J. Optom.* 2, 6–60. doi: 10.3921/joptom.2009.60
- ISO 14729:2001/A1:2010 (2010). *Ophthalmic Optics—Contact Lens Care Products—Microbiological Requirements and Test Methods for Products and Regimens for Hygienic Management of Contact Lenses*; International Organization for Standardization: Geneva, Switzerland.
- John, T., Desai, D., and Sahm, D. (1989). Adherence of *Acanthamoeba castellanii* cysts and trophozoites to unworn soft contact lenses. *Am. J. Ophthalmol.* 108, 658–664. doi: 10.1016/0002-9394(89)90857-X
- Johnston, S. P., Sriram, R., Qvarnstrom, Y., Roy, S., Verani, J., Yoder, J., et al. (2009). Resistance of *Acanthamoeba* cysts to disinfection in multiple contact lens solutions. *J. Clin. Microbiol.* 47, 2040–2045. doi: 10.1128/JCM.00575-09
- Jon, P., and Jason, S. (2019). nextgenusf/unannotate: unannotate v1.5.3 (1.5.3). *Zenodo*. doi: 10.5281/zenodo.2604804
- Kilvington, S. (1993). *Acanthamoeba* trophozoite and cyst adherence to four types of soft contact lens and removal by cleaning agents. *Eye* 7, 535–538. doi: 10.1038/eye.1993.116
- Kilvington, S., Heaselgrave, W., Powell, H., and Lally, J. (2009). Physiological response of *Acanthamoeba* trophozoites to multipurpose contact lens solutions: aggregation and resistance to disinfection. *Invest. Ophthalmol. Vis. Sci.* 50:6360.
- Kilvington, S., and Lam, A. (2013). Development of standardized methods for assessing biocidal efficacy of contact lens care solutions against *Acanthamoeba* trophozoites and cysts. *Invest. Ophthalmol. Vis. Sci.* 54, 4527–4537. doi: 10.1167/iov.13-11927
- Kilvington, S., and Larkin, D. F. (1990). *Acanthamoeba* adherence to contact lenses and removal by cleaning agents. *Eye (Lond.)* 4, 589–593. doi: 10.1038/eye.1990.82
- Lee, S. M., Lee, J. E., Lee, D. I., and Yu, H. S. (2018). Adhesion of *Acanthamoeba* on cosmetic contact lenses. *J. Korean Med. Sci.* 33:e26. doi: 10.3346/jkms.2018.33.e26
- Lee, G.-H., Lee, J.-E., Park, M.-K., and Yu, H.-S. (2016). Adhesion of *Acanthamoeba* on silicone hydrogel contact lenses. *Cornea* 35, 663–668. doi: 10.1097/ICO.0000000000000788
- Li, S., Bian, J., Wang, Y., Wang, S., Wang, X., and Shi, W. (2020). Clinical features and serial changes of *Acanthamoeba* keratitis: an in vivo confocal microscopy study. *Eye* 34, 327–334. doi: 10.1038/s41433-019-0482-3
- Li, B., and Dewey, C. N. (2011). RSEM: accurate transcript quantification from RNA-Seq data with or without a reference genome. *BMC Bioinformatics* 12:323. doi: 10.1186/1471-2105-12-323
- Liang, S., Shows, A., Dunbar, D., Sharma, V., Shi, C. X., and Wu, J. (2022). Antifouling surfaces of Lehfilcon a silicone hydrogel contact lens. *Invest. Ophthalmol. Vis. Sci.* 63:532-A0230
- Lin, Y., Yuan, J., Kolmogorov, M., Shen, M. W., Chaisson, M., and Pevzner, P. A. (2016). Assembly of long error-prone reads using de Bruijn graphs. *Proc. Natl. Acad. Sci. U. S. A.* 113, E8396–E8405. doi: 10.1073/pnas.1604560113
- Lloyd, D. (2014). Encystment in *Acanthamoeba castellanii*: a review. *Exp. Parasitol.* 145, S20–S27. doi: 10.1016/j.exppara.2014.03.026
- Magistrado-Coxen, P., Aqeel, Y., Lopez, A., Haserick, J. R., Urbanowicz, B. R., Costello, C. E., et al. (2019). The most abundant cyst wall proteins of *Acanthamoeba castellanii* are lectins that bind cellulose and localize to distinct structures in developing and mature cyst walls. *PLoS Negl. Trop. Dis.* 13:e0007352. doi: 10.1371/journal.pntd.0007352
- Mahboob, T., Azlan, A.-M., Tan, T.-C., Samudi, C., Sekaran, S. D., Nissapatorn, V., et al. (2016). Anti-encystment and amoebicidal activity of *Lonicera japonica* Thunb. and its major constituent chlorogenic acid in vitro. *Asian Pac. J. Trop. Med.* 9, 866–871. doi: 10.1016/j.apjtm.2016.07.008
- Mazur, T., Hadas, E., and Iwanicka, I. (1995). The duration of the cyst stage and the viability and virulence of *Acanthamoeba* isolates. *Trop. Med. Parasitol.* 46, 106–108. PMID: 8525280
- Molet, B., and Ermoliev, B. G. (1976). Description d'yne amibe d'eau douce: *Acanthamoeba* Lenticulata, Sp. Nov. (Amoebida). *Protistologica* 12, 571–576.
- Musgrave, C. S. A., and Fang, F. (2019). Contact lens materials: a materials science perspective. *Materials (Basel)*. 12:261. doi: 10.3390/ma12020261
- Neff, R. J. (1957). Purification, axenic cultivation, and description of a soil amoeba, *Acanthamoeba* sp. *J. Protozool.* 4, 176–182. doi: 10.1111/j.1550-7408.1957.tb02505.x
- Oliveira, G., Silva, L., Leão, T., Mougari, S., da Fonseca, F. G., Kroon, E. G., et al. (2019). Tupanvirus-infected amoebas are induced to aggregate with uninfected cells promoting viral dissemination. *Sci. Rep.* 9:183. doi: 10.1038/s41598-018-36552-4



- Pharma Boardroom. Eyes on the prize: from Sicilian roots to FDA approval. Available at: <https://pharmaboardroom.com/articles/eyes-on-the-prize-from-sicilian-roots-to-fda-approval/> (Accessed November 22).
- Primary Care Optometry News (2014). Experts agree on need to standardize testing for contact lens products. Available at: [https://www.healio.com/news/optometry/20150420/j722\\_1911\\_1\\_news\\_print\\_1](https://www.healio.com/news/optometry/20150420/j722_1911_1_news_print_1) (Accessed September 21, 2022).
- Pushkarew, B. M. (1913). Über die Verbreitung der Süßwasser-Protozoen durch die Luft. *Arch. Protistenkd.* 23, 323–326.
- Randag, A. C., van Rooij, J., van Goor, A. T., Verkerk, S., Wisse, R. P. L., Saelens, I. E. Y., et al. (2019). The rising incidence of *Acanthamoeba* keratitis: a 7-year nationwide survey and clinical assessment of risk factors and functional outcomes. *PLoS One* 14:e0222092. doi: 10.1371/journal.pone.0222092
- Rayamajhee, B., Willcox, M. D., Henriquez, F. L., Petsoglou, C., and Carnt, N. (2021). *Acanthamoeba* keratitis: an increasingly common infectious disease of the cornea. *Lancet Microbe* 2, e345–e346. doi: 10.1016/S2666-5247(21)00093-8
- Robinson, M. D., McCarthy, D. J., and Smyth, G. K. (2009). edgeR: a Bioconductor package for differential expression analysis of digital gene expression data. *Bioinformatics* 26, 139–140. doi: 10.1093/bioinformatics/btp616
- Rolland, S., Mengue, L., Noël, C., Crapart, S., Mercier, A., Aucher, W., et al. (2020). Encystment induces Down-regulation of an acetyltransferase-like gene in *Acanthamoeba castellanii*. *Pathogens* 9:321. doi: 10.3390/pathogens9050321
- rrwick/Porechop, Github.Com (2017). Available at: <https://github.com/rrwick/Porechop> (Accessed September 26, 2022).
- Sawyer, T. K. (1971). *Acanthamoeba griffini*, a new species of marine amoeba. *J. Protozool.* 18, 650–654. doi: 10.1111/j.1550-7408.1971.tb03391.x
- Sawyer, T. K., Visvesvara, G. S., and Harke, B. A. (1977). Pathogenic amoebas from brackish and ocean sediments, with a description of *Acanthamoeba hatchetti*, n. sp. *Science* 196, 1324–1325. doi: 10.1126/science.867031
- Schaap, P. (2011). Evolutionary crossroads in developmental biology: *Dictyostelium discoideum*. *Development* 138, 387–396. doi: 10.1242/dev.048934
- Seal, D. V., Bennett, E. S., McFadyen, A. K., Todd, E., and Tomlinson, A. (1995). Differential adherence of *Acanthamoeba* to contact lenses: effects of material characteristics. *Optometry Vision Sci.* 72, 23–28. doi: 10.1097/00006324-199501000-00005
- Siddiqui, R., and Khan, N. A. (2012). Biology and pathogenesis of *Acanthamoeba*. *Parasit. Vectors* 5:6. doi: 10.1186/1756-3305-5-6
- Szentmary, N., Daas, L., Shi, L., Laurik, K. L., Lepper, S., Milioti, G., et al. (2019). *Acanthamoeba* keratitis - clinical signs, differential diagnosis and treatment. *J. Curr. Ophthalmol.* 31, 16–23. doi: 10.1016/j.joco.2018.09.008
- Shovlin, J. P. (2009). "Testing efficacy against *Acanthamoeba*: the FDA should take into consideration the strength of the strain to be used as a standard, as well as how to make the testing scenario relevant" in Review of Optometry. Vol. 146. p. 113. Available at: [https://galeapps.gale.com/apps/auth?userGroupName=tel\\_oweb&sid=googleScholar&da=true&origURL=https%3A%2F%2Fgo.gale.com%2Fps%2Fi.do%3Fid%3DGALE%257CA197442753%26sid%3DgoogleScholar%26%3D2.1%26it%3Dr%26linkaccess%3Dfulltext%26issn%3D1930160X%26p%3DAONE%26sw%3Dw&prodId=AONE](https://galeapps.gale.com/apps/auth?userGroupName=tel_oweb&sid=googleScholar&da=true&origURL=https%3A%2F%2Fgo.gale.com%2Fps%2Fi.do%3Fid%3DGALE%257CA197442753%26sid%3DgoogleScholar%26%3D2.1%26it%3Dr%26linkaccess%3Dfulltext%26issn%3D1930160X%26p%3DAONE%26sw%3Dw&prodId=AONE) (Accessed November 30, 2022).
- Tu, E. Y., and Joslin, C. E. (2010). Recent outbreaks of atypical contact lens-related keratitis: what have we learned? *Am J. Ophthalmol.* 150, 602–608.e2. doi: 10.1016/j.ajo.2010.06.045
- Vaillancourt, B., and Buell, C. R. (2019). High molecular weight DNA isolation method from diverse plant species for use with Oxford Nanopore sequencing. *bioRxiv [Preprint]*. doi: 10.1101/783159
- Verani, J. R., Lorick, S. A., Yoder, J. S., Beach, M. J., Braden, C. R., Roberts, J. M., et al. (2009). National outbreak of *Acanthamoeba* keratitis associated with use of a contact lens solution, United States. *Emerg. Infect. Dis.* 15, 1236–1242. doi: 10.3201/eid1508.090225
- Walker, B. J., Abeel, T., Shea, T., Priest, M., Abouelliel, A., Sakthikumar, S., et al. (2014). Pilon: an integrated tool for comprehensive microbial variant detection and genome assembly improvement. *PLoS One* 9:e112963. doi: 10.1371/journal.pone.0112963
- Walters, R., Campolo, A., Miller, E., McAnally, C., Gabriel, M., Shannon, P., et al. (2022). Differential antimicrobial efficacy of preservative-free contact lens disinfection systems against common ocular pathogens. *Microbiol. Spectr.* 10:e0213821. doi: 10.1128/spectrum.02138-21
- Wesley, G., Giedd, B., Hines, B., Bickle, K., Pearson, C., and Lorentz, H. (2022). Safety and efficacy of a new water gradient biomimetic monthly replacement spherical contact lens material (Lehfilcon a). *Clin. Ophthalmol.* 16, 2873–2884. doi: 10.2147/OPTH.S362926
- Yoder, J. S., Verani, J., Heidman, N., Hoppe-Bauer, J., Alfonso, E. C., Miller, D., et al. (2012). *Acanthamoeba* keratitis: the persistence of cases following a multistate outbreak. *Ophthalm. Epidemiol.* 19, 221–225. doi: 10.3109/09286586.2012.681336





## OPEN ACCESS

## EDITED BY

Carlos Robello,  
Universidad de la República, Uruguay

## REVIEWED BY

Gonzalo Greif,  
Institut Pasteur de Montevideo, Uruguay  
Tomas Panek,  
University of Ostrava, Czechia

## \*CORRESPONDENCE

Isabel Marcelino  
✉ IMarcelino@pasteur-guadeloupe.fr

## SPECIALTY SECTION

This article was submitted to  
Infectious Agents and Disease,  
a section of the journal  
Frontiers in Microbiology

RECEIVED 28 September 2022

ACCEPTED 21 December 2022

PUBLISHED 01 February 2023

## CITATION

Dereeper A, Allouch N, Guerlais V,  
Garnier M, Ma L, De Jonckheere JF,  
Joseph SJ, Ali IKM, Talarmin A and  
Marcelino I (2023) *Naegleria* genus  
pangenome reveals new structural and  
functional insights into the versatility of  
these free-living amoebae.  
*Front. Microbiol.* 13:1056418.  
doi: 10.3389/fmicb.2022.1056418

## COPYRIGHT

© 2023 Dereeper, Allouch, Guerlais,  
Garnier, Ma, De Jonckheere, Joseph, Ali,  
Talarmin and Marcelino. This is an open-  
access article distributed under the terms  
of the [Creative Commons Attribution  
License \(CC BY\)](https://creativecommons.org/licenses/by/4.0/). The use, distribution or  
reproduction in other forums is permitted,  
provided the original author(s) and the  
copyright owner(s) are credited and that  
the original publication in this journal is  
cited, in accordance with accepted  
academic practice. No use, distribution or  
reproduction is permitted which does not  
comply with these terms.

# *Naegleria* genus pangenome reveals new structural and functional insights into the versatility of these free-living amoebae

Alexis Dereeper<sup>1</sup>, Nina Allouch<sup>1</sup>, Vincent Guerlais<sup>1</sup>,  
Maëlle Garnier<sup>1</sup>, Laurence Ma<sup>2</sup>, Johan F. De Jonckheere<sup>3</sup>,  
Sandeep J. Joseph<sup>4</sup>, Ibne Karim M. Ali<sup>4</sup>, Antoine Talarmin<sup>1</sup> and  
Isabel Marcelino<sup>1\*</sup>

<sup>1</sup>Institut Pasteur de la Guadeloupe, Unité TReD-Path, Les Abymes, Guadeloupe, France, <sup>2</sup>Institut Pasteur de Paris, Biomix, Paris, France, <sup>3</sup>Scientific Institute of Public Health, Brussels, Belgium, <sup>4</sup>Centers for Disease Control and Prevention (CDC), Atlanta, GA, United States

**Introduction:** Free-living amoebae of the *Naegleria* genus belong to the major protist clade Heterolobosea and are ubiquitously distributed in soil and freshwater habitats. Of the 47 *Naegleria* species described, *N. fowleri* is the only one being pathogenic to humans, causing a rare but fulminant primary amoebic meningoencephalitis. Some *Naegleria* genome sequences are publicly available, but the genetic basis for *Naegleria* diversity and ability to thrive in diverse environments (including human brain) remains unclear.

**Methods:** Herein, we constructed a high-quality *Naegleria* genus pangenome to obtain a comprehensive catalog of genes encoded by these amoebae. For this, we first sequenced, assembled, and annotated six new *Naegleria* genomes.

**Results and Discussion:** Genome architecture analyses revealed that *Naegleria* may use genome plasticity features such as ploidy/aneuploidy to modulate their behavior in different environments. When comparing 14 near-to-complete genome sequences, our results estimated the theoretical *Naegleria* pangenome as a closed genome, with 13,943 genes, including 3,563 core and 10,380 accessory genes. The functional annotations revealed that a large fraction of *Naegleria* genes show significant sequence similarity with those already described in other kingdoms, namely Animalia and Plantae. Comparative analyses highlighted a remarkable genomic heterogeneity, even for closely related strains and demonstrate that *Naegleria* harbors extensive genome variability, reflected in different metabolic repertoires. If *Naegleria* core genome was enriched in conserved genes essential for metabolic, regulatory and survival processes, the accessory genome revealed the presence of genes involved in stress response, macromolecule modifications, cell signaling and immune response. Commonly reported *N. fowleri* virulence-associated genes were present in both core and accessory genomes, suggesting that *N. fowleri*'s ability to infect human brain could be related to its unique species-specific

genes (mostly of unknown function) and/or to differential gene expression. The construction of *Naegleria* first pangenome allowed us to move away from a single reference genome (that does not necessarily represent each species as a whole) and to identify essential and dispensable genes in *Naegleria* evolution, diversity and biology, paving the way for further genomic and post-genomic studies.

#### KEYWORDS

free-living amoebae, *Naegleria*, whole genome sequencing, genome plasticity, pangenome, core genome, species-specific genes, *Naegleria fowleri* virulence-associated genes

## 1. Introduction

Members of the *Naegleria* genus belong to the major eukaryotic lineage Heterolobosea, that deviated from other eukaryotic lineages over a billion years ago (Fritz-Laylin et al., 2010). They are ubiquitous in soils and freshwater habitats and are important predators of cyano- and eubacteria, hereby regulating bacterial populations in lakes and rivers (De Jonckheere, 2011). Some species can naturally grow at 37°C, and others can grow up to 45°C (De Jonckheere, 2014). *Naegleria* usually has two developmental stages: the trophozoite (which is the metabolically active form in which they can move, feed and multiply) and the cysts (the dormant and resistant form); some species can transform into flagellates, allowing the amoeba to rapidly move around and look for more favorable conditions (Fritz-Laylin et al., 2010; De Jonckheere, 2014). The *Naegleria* genus currently contains 47 recognized species (De Jonckheere, 2011) but only *N. fowleri* (also popularly known as “brain-eating amoeba”) is a confirmed human pathogen, causing primary amoebic meningoencephalitis (PAM).

PAM is a rare but fatal disease (with a 95% mortality rate), affecting mainly healthy children or young adults (Sarink et al., 2022). Infection occurs when contaminated water enters the nose, *N. fowleri* (specially trophozoites) follows the olfactory nerve to the brain through the cribriform plate. There, it induces phagocytosis of brain material, provoking tissue damage and hemorrhagic necrosis causing a fatal brain infection. The disease progresses rapidly leading to death within 7–12 days (Moseman, 2020). Combined with its low incidence (Trabelsi et al., 2012; Siddiqui et al., 2016), early diagnosis is difficult as the PAM symptoms closely resembled bacterial meningitis (Jahangeer et al., 2020); the link with *Naegleria* is usually made post-mortem by microscopic examination of the cerebral spinal fluid or by conventional or real-time PCR. In recent years, an increased number of PAM cases have been reported worldwide, in particular in temperate regions and developing countries; this is probably due to global warming, global overpopulation and increased industrial activities (Kemble et al., 2012; Siddiqui et al., 2016; Maciver et al., 2020). In the Caribbean region, the first fatal case

of *N. fowleri* was reported in a geothermal bath in Guadeloupe in 2008 (Nicolas et al., 2010). Despite successful treatment in a very few cases with miltefosine and other antimicrobial medication (Debnath, 2021), the same antibiotic regime failed in other cases, suggesting the need to find effective therapies (Khan et al., 2021). Several studies have shown that *N. fowleri* pathogenesis involves both contact-dependent interaction with the host (through brain damaging, sucker-like surface structure called “food cup” which enables *N. fowleri* to interact with the host extracellular matrix (ECM) through a process of adhesion, invasion and degradation of ECM and nerve cell) and contact independent interaction (through the release of different proteases with proteolytic function and hydrolysing activity, that in central nervous system, cause further destruction of nerves; Jamerson et al., 2012; Herman et al., 2021; Rodriguez-Anaya et al., 2021; Sarink et al., 2022). Despite such work, the pathogenic factors of *N. fowleri* are still unclear.

At the moment, over 60 *Naegleria* genome sequences are publicly available (with different levels of completeness and using different sequencing methodologies) for the non-pathogenic species *N. gruberi* (Fritz-Laylin et al., 2010) and *N. lovaniensis* (Liechti et al., 2018; Joseph et al., 2021), and for the pathogenic *N. fowleri* (Zysset-Burri et al., 2014; Ali et al., 2021; Herman et al., 2021; Joseph et al., 2021). Comparative genomic studies were already performed within *N. fowleri* species (Joseph et al., 2021) and between *Naegleria* species (Liechti et al., 2018; Herman et al., 2021) but they do not describe the complete gene landscape of a *Naegleria* species or genus because of the large numbers of variations between accessions.

To better understand *Naegleria* genome evolution, phenotypic diversity and versatility, we aimed to construct the first high-quality genus pangenome for *Naegleria* that would list the core genes (involved in housekeeping and conserved survival processes) and dispensable genes that are present only in a subset of species (being responsible for phenotypic differences between isolates and may be involved in pathogenesis). For this, we first sequenced and annotated three new *N. fowleri* strains (NF\_AR12 from United States, NF\_PA34 from Australia and NF\_NF1 from Guadeloupe, with different genotypes and all being environmental

isolates) and three new *N. lovaniensis* strains: NL\_F9 (from Belgium), NL\_Lova6 and NL\_Lova7 (both isolated in Guadeloupe). Afterwards, we compared these 6 new genomes to available genomic data with different levels of completeness, from different *Naegleria* species (and strains) isolated from distinct geographical regions and environments (water, soil, human).

## 2. Materials and methods

### 2.1. Amoebae samples

The biological samples used for Illumina sequencing are presented in Table 1. DNA samples originated from *N. fowleri* AR12 and PA34, and *N. lovaniensis* F9 were kindly provided by Professor J. F. De Jonckheere and produced as described elsewhere (De Jonckheere, 1998); the others 3 strains (1 *N. fowleri* and 2 *N. lovaniensis*) were obtained as described in the following section. For pangenome and comparative genomics analyses, we also included 8 assembled and annotated whole-genome sequences of *Naegleria* genus published (Table 1). At the time of writing this paper, 49 draft genome sequences of *N. fowleri* species (from clinical and environmental origin; Joseph et al., 2021) were also available in the NCBI's Sequence Read Archive (SRA). These sequences (Supplementary Table S1) were downloaded and used for whole-genome SNPs phylogenetic analysis (as described in Section 2.7.1).

#### 2.1.1. Amoebae isolation and identification (Guadeloupean strains)

Water samples (1 L) were collected from 3 geothermal baths in Guadeloupe: Curé (Bouillante), Dolé (Gourbeyre) and La Lise (Bouillante) and treated as previously described (Moussa et al., 2013, 2020). Amoebae cultivated in NNA-*E. coli* were recovered by scrapping the agar plate with 800  $\mu$ L of T1 Lysis Buffer (from the kit NucleoSpin Tissue, Macherey Nagel, Germany). Afterwards, the samples went through a DNA extraction protocol (NucleoSpin<sup>®</sup> Tissue DNA extraction kit, Macherey-Nagel), following the manufacturer's recommendations. DNA was stored at  $-20^{\circ}\text{C}$  until use. Amoebae identification was performed by PCR using ITS primers, as described elsewhere (Moussa et al., 2013). ITS amplicons Sanger sequencing was performed at Eurofins Genomics (Germany). A homology search was performed with BLAST software from the National Center for Biotechnology Information homepage.<sup>1</sup> The sequence data obtained were aligned by ClustalW software<sup>2</sup> with the sequences of *Naegleria* species are presented in Supplementary Table S2 and were also deposited in GenBank.<sup>3</sup>

For whole genome sequencing purposes, NF\_NF1 (5 biological replicates), NL\_Lova6 and NL\_Lova7 were cultured in axenic culture during at least 5 passages in tissue culture flasks using the SCGYEM conditions (De Jonckheere, 1977). Trophozoites ( $1 \times 10^6$  *Naegleria* per strain) cultivated in axenic culture conditions were scraped from T-flasks and centrifuged at 1,000g for 10 min at room temperature; after supernatant removal, 200  $\mu$ L of T1 buffer was added. "T1-cell suspension" was kept at  $-20^{\circ}\text{C}$  until further use. For genome Illumina sequencing, we included a RNase step during the extraction protocol, following the manufacturer's recommendations.

### 2.2. Whole genome sequencing

DNA samples were used for library preparation using TruSeq DNA PCR-free library prep kit (following fragmentation into 350 bp-long fragments) and TruSeq DNA UD Indexes (Illumina). Paired-end sequencing was performed on a MiSeq system with a nano v2 flowcell and reagents for  $2 \times 151$  cycles (Illumina). Whole genome Illumina sequencing was performed at the Biomics Core Facility (Institut Pasteur, Paris, France). Number of reads by experiment or replicate are presented in Supplementary Table S3.

### 2.3. Bioinformatics analyses

#### 2.3.1. Whole-genome SNP-based phylogenetic analysis

A whole-genome phylogenetic analysis based on SNPs was performed for *N. fowleri* and *N. lovaniensis*. For the comparison of *N. fowleri* strains, we compiled our 11 samples (including the 5 biological replicates of NF\_NF1) with the published raw data publicly available from SRA ( $N=49$ ; Supplementary Table S1; Joseph et al., 2021). For *N. lovaniensis*, we used our 3 samples plus the reads from the sequencing projects of the strains NL\_ATCC 30569 (Liechti et al., 2018) and NL\_76-15-250 (Joseph et al., 2021). After a cleaning of raw reads using Cutadapt, Illumina raw reads were first mapped either against the *N. fowleri* TY "close-to-complete" genome (Ali et al., 2021) or the *N. lovaniensis* ATCC 30569, using BWA-MEM (version 0.7.17-r1188) software (Li, 2013). BAM mapping files were then converted to pileup format using SAMtools (Danecek et al., 2021) and SNP calling was performed using VarScan (Koboldt et al., 2012) for each sample, using a minimum read coverage of 8X with a Phred quality score of at least 15. Genetic variations and alleles were then compiled into a global SNP matrix file (VCF file), using a home-made script. SNP-based phylogenetic tree was then generated using the SNIPlay web application (Dereeper et al., 2015). Finally, the phylogenetic tree was displayed using the iTOL v6 online application (Letunic and Bork, 2021). In addition, *N. fowleri* samples were assigned to internal transcribed space (ITS) genotype, using a home-made script searching for ITS genotyping loci directly from raw reads.

<sup>1</sup> <http://www.ncbi.nlm.nih.gov/>

<sup>2</sup> <http://www.nig.ac.jp>

<sup>3</sup> <http://www.ncbi.nlm.nih.gov/>

TABLE 1 Genome assemble and annotation statistics of published and newly sequenced genomes of *Naegleria* sp.

Species	<i>N. gruberi</i>	<i>N. fowleri</i>								<i>N. lovaniensis</i>				
Strain	NEG-M ATCC 30224	NF_ ATCC 30894 (Lee)	NF_ATCC 30863 (Carter)	NF_V212	NF_986	NF_TY* (ATCC 30107)	NF_NF1	NF_AR12	NF_PA34	NL_ ATCC 30569	NL_76– 15-250	NL_F9	NL_ Lova6	NL_ Lova7
Genotype	–	3	2	2	5	3	3	2	5	n/a	n/a	n/a	n/a	n/a
Origin	Environ. (soil)	Clinical			Environ. (water)	Clinical	Environmental (water)			Environmental (water)				
Geographical location	United States	United States			Australia	United States	Guadeloupe	United States	Australia	United States	Belgium	Belgium	Guadeloupe	
Year of origin	1969	1968	1978	1990	–	1969	2018	1976	1972	1970	1976	1980	2018	2018
Sequencing technology	Sanger	Nanopore	Illumina/Roche 454	Illumina/Roche 454	Illumina	Illumina/PacBio	Illumina	Illumina	Illumina	PacBio	PacBio	Illumina	Illumina	Illumina
Genome size (Mbp)	40.9	29.5	29.6	27.7	27.5	27.9	27.6	27.3	27.3	30.8	30.8	27.7	26.9	26.5
GC content (%)	35	36.9	35	36	36	36.9	36.9	36.9	36.9	37	36.3	36.9	37	37
Number of scaffolds (anchored in N chromosomes)	1,977	90	2,530	1962	1919	37	500 (37)	656 (37)	534 (37)	111	199	754 (37)	1,959 (37)	2,384 (37)
N50 of scaffolds (bp)	159,679	717,491	38,800	86,051	45,674	756,811	125,650	81,421	112,144	657,933	455,122	78,479	26,705	17,708
Number of predicted genes (ORFs)	16,620	13,925	11,499	12,677	11,599	9,405	9,336	9,441	11,036	15,195	11,305	9,481	9,578	9,305
Average gene length (bp)	1,677	–	1984	1785	1955	–	3,003	2,946	2,284	–	–	3,283	3,010	3,034
Coding (%)	57.8	–	70.79	71.35	73.01	68	59.4	58.5	68.5	–	65	57.5	60	61.5
Repeat content (%)	5.1	6	2.5	–	–	5.3	5	3.3	1.4	3.5	10.8	2.7	2.4	2.4
Complete BUSCOs (%)	85.7	86.5	87.8	88.3	87.9	84.3	82.0	84.8	87.2	85.5	78.8	88.3	87.2	86.0
Fragmented BUSCOs	1.3	2.3	2.7	2.4	3.1	2.8	6.7	4.1	2.9	2.6	5.1	4.7	3.5	4.1
BUSCO Missing	13	11.2	9.5	9.3	9.0	12.9	11.3	11.1	9.9	11.9	16.1	7.0	9.3	9.9
Reference	<a href="#">Herman et al. (2021)</a>	<a href="#">Liechti et al. (2019)</a>	<a href="#">Herman et al. (2021)</a>			<a href="#">Ali et al. (2021)</a> and <a href="#">Joseph et al. (2021)</a>	This work			<a href="#">Liechti et al. (2018)</a>	<a href="#">Joseph et al. (2021)</a>	This work		

“–” stands for not-available while “n/a” stands for non-applicable.\*Out of 52 *N. fowleri* genomes sequenced and presented by [Joseph et al. \(2021\)](#), we only shown only for the “close-to-complete” genome of the *N. fowleri* TY isolate.

### 2.3.2. Genome assembly

In order to estimate the conservation of scaffolds between genomes from different species, we first aligned the published scaffolds of *N. lovaniensis* (ATCC 30569) (Liechti et al., 2018) against the recently published genome of *N. fowleri* TY (Ali et al., 2021), which consists of 37 well defined pseudo-chromosomes. For this, we used the D-genies online application (Cabanettes and Klopp, 2018), taking advantage of minimap2 alignment software (Li, 2018). Except for minor rearrangements detected in only one pseudo-chromosome, a good collinearity was observed between *N. lovaniensis* scaffolds and *N. fowleri* pseudo-chromosomes (Supplementary Figure S1), suggesting that scaffolds from the 2 species can be simply ordered according to their matching positions in pseudo-chromosomes. This data manipulation prevents the generation of heterogeneous outputs for the different genomes and will facilitate thereafter the comparison of genomes and their graphical representation, notably for synteny analysis. The 6 new *Naegleria* genomes were assembled using the same strategy. Briefly, after a cleaning step by cutadapt, filtered reads were de-novo assembled using SPAdes (Prjibelski et al., 2020), to generate scaffolds independently of the respective reference genome and ensure subsequent microsynteny analysis. In a second step, scaffolds were anchored, ordered and oriented, using the 37 chromosomes of *N. fowleri* TY by running the RaGOO program (Alonge et al., 2019).

### 2.3.3. Ploidy and heterozygosity analyses based on SNPs

An estimate of ploidy level was performed for each of the newly sequenced genomes, based on the ratio of alleles of SNPs. For this purpose, cleaned reads were mapped back against the corresponding assembly of the genome with BWA mem, and SNPs were called with the same approach as previously with the combination SAMtools mpileup/VarScan. A home-made script was developed for evaluating the level of heterozygosity, and for extracting the information of allele depth ratio (i.e., between reference and alternate allele) at each heterozygous position. Allele ratios were then reported along the chromosomes using Circos visualization (Krzywinski et al., 2009) and the distribution of ratios was calculated for each genome. This technique allows to evaluate the global level of ploidy as well as its variation along the chromosomes and thus to detect potential abnormality in specific chromosomes or genomic regions.

### 2.3.4. Gene prediction and annotation

A complete Galaxy annotation workflow based on iterative runs of MAKER2 annotation pipeline (Holt and Yandell, 2011) was constructed and implemented on Galaxy KaruBioNet (Couvin et al., 2022) and applied for the annotation of each new genome, independently. The protein-coding gene annotation by MAKER2 combines homology prediction, *ab initio* prediction [using SNAP (Korf, 2004) and AUGUSTUS (Hoff and Stanke, 2013)], and full-length transcriptome prediction based on NGS sequencing. Transcriptomic

resources were prepared separately for *N. fowleri* and *N. lovaniensis* genomes, from public RNASeq datasets downloaded from European Nucleotide Archive (ENA), PRJNA642022 project, using, respectively, samples NF\_Nelson\_medium with NF\_PYNH\_medium (3 replicates each) and NL\_Nelson\_medium with NL\_PYNH\_medium (3 replicates each; Zysset-Burri et al., 2014; Supplementary Table S1). For each, RNASeq raw reads were cleaned using Cutadapt (Martin, 2011), mapped against the genome using MapSplice (Wang et al., 2010) and a genome-guided de-novo transcriptome assembly was constructed by Trinity (trinityrnaseq; Grabherr et al., 2011) using the `-genome_guided_bam` option. Assemblies were then gathered and concatenated by species to be subsequently provided as EST evidence for gene prediction; herein, we used 183,318 and 97,050 ESTs for *N. fowleri* and *N. lovaniensis*, respectively. In this work, 3 rounds of MAKER2 were performed. At each round, the gene annotation obtained was evaluated by trained gene predictors SNAP and AUGUSTUS. The new gene models were re-used in the next round of MAKER2 to improve the annotation and create a weighted consensus of the gene structures. Repeat sequences were annotated by both Repbase and a custom repeat library. The Repbase library (Jurka, 2000) was downloaded from <https://www.girinst.org/server/RepBase/>, and the custom repeat library was constructed on each genome sequence by using RepeatModeler (version 2.0.1; Flynn et al., 2020). These two libraries were concatenated and provided to RepeatMasker (Tarailo-Graovac and Chen, 2009) as implemented in MAKER2, to identify repetitive elements. Subsequently, the annotation completeness was evaluated with BUSCO (Simão et al., 2015). Finally, the density of genes, exons and repeats were calculated from GFF annotation files thanks to a home-made script.

### 2.3.5. Functional annotation

Gene functions were assigned according to the best alignment of predicted protein sequences using BlastP (default values: E-value 1E-03) to the Uniprot database (including the SWISS-PROT and TrEMBL databases). We used InterProScan program (Jones et al., 2014) to assign conserved protein motifs (PFAM, InterPro). An additional assignment of predicted proteins to specific COG (Clusters of Orthologous Groups) was performed independently using the “COG assignment” Galaxy wrapper available in Galaxy KaruBioNet,<sup>4</sup> (Couvin et al., 2022), based on rpsblast and cdd2cog Perl script.

### 2.3.6. Pangenome analysis

To perform the pangenome analysis of *Naegleria* genus, we used a dataset of 14 *Naegleria* genomes with clinical and environmental isolates from distinct geographic location, 8 genomes of *N. fowleri* (NF\_ATCC 30894, NF\_ATCC 30863,

<sup>4</sup> [http://calamar.univ-ag.fr/c3i/galaxy\\_karubionet.html](http://calamar.univ-ag.fr/c3i/galaxy_karubionet.html)



NF\_V212, NF\_986, NF\_TY, NF\_NF1, NF\_AR12 and NF\_PA34), 5 genomes of *N. lovaniensis* (NL\_ATCC 30569, NL\_76–15–250, NL\_F9, NL\_Lova6 and NL\_Lova7) and one of *N. gruberi* (strain NEG-M-ATCC 30224; Table 1).

For this, published protein FASTA files containing predicted protein sequences were downloaded either from the AmoebaDB resource<sup>5</sup> (release 53) or from the NCBI FTP server, and were compiled together with the MAKER2 output files generated for our 6 new genomes to perform a genomic and protein comparison.

The pangenome analysis was conducted using OrthoFinder software (Emms and Kelly, 2019) with all-versus-all BLAST strategy to define the orthogroups among the 14 genomes. The resulting presence/absence matrix was analyzed with an in-house developed Perl script to extract and classify genes as core-genes (genes present in all *Naegleria* sp.) and accessory genes (genes present at least once in 1 or more but not all *Naegleria* species). In this latter category, we emphasize on species-specific genes which can be subdivided in 2 gene sets: species-core specific genes (gene shared by all strains within one *Naegleria* species) and species-specific accessory genes (genes present at least once in 1 or more strains of one *Naegleria* species). To determine whether the pangenome can be considered closed or open, we calculated the alpha parameter using the MicroPan R library (Snipen and Liland, 2015).

### 2.3.7. Synteny analysis on *Naegleria* core genome

Chromosomal synteny was estimated by connecting core-genes between two representative genomes, NF\_NF1 and NL\_Lova7 for *N. fowleri* and *N. lovaniensis*, respectively. A home-made Perl script was used to extract core-gene locations and identify (i) specific links that connect core-genes located in different chromosomes between the two species, and (ii) links that connect core-genes that physically distant more than 50kb between homologous chromosomes to highlight insertion or inversion. Syntenic regions shared between pairs of homologous chromosomes were visualized using both Circos (Krzywinski et al., 2009) and Mauve Viewer.<sup>6</sup>

### 2.3.8. Protein–protein interaction network

Schematic information on *Naegleria* biological pathways is mainly available for *N. gruberi*.<sup>7</sup> However, based on our pangenome results, several genes present in NG are absent in NF and NL (and *vice-versa*) and many *Naegleria* genes are of unknown function. Herein, in attempt to bring new insights on *Naegleria* biological pathways, we used Cytoscape v3.8.0 software platform (Su et al., 2014) combined with StringApp (Doncheva et al., 2019) plugin. STRING is a database of quality-controlled protein–protein association networks and enables researchers to construct

a functional association network of uploaded genes/proteins of an organism based on three aspects: computational prediction, from knowledge transfer between organisms, and from interactions aggregated from other (primary) databases (Szklarczyk et al., 2019). From the 13,972 genes in *Naegleria* pangenome (Supplementary Table S4), we first constructed a network consisting of 8,829 protein nodes and 44,347 edges (data not shown), and then, we selected only the connected nodes to create a Protein–Protein Interaction (PPI) Network (PPIN) with 3,970 nodes and 44,314 edges. The enrichment analysis using StringApp was performed with a high confidence score of 0.75 and based on non-redundant terms (threshold above 0.75) of Gene Ontology (GO) term, Kyoto encyclopedia of genes and genomes (KEGG) pathway data and Reactome Pathways Functional Interaction (FI) Network. This allowed us to group genes/proteins according to their biological function.

## 3. Results and discussion

### 3.1. *Naegleria* phylogenetic structure

A description of the phylogenetic relationships within the genus *Naegleria* using different methods has been previously reported (Pelandakis et al., 2000; De Jonckheere, 2002; Joseph et al., 2021). Herein, we sequenced, assembled, and annotated new genomes from *N. fowleri* and *N. lovaniensis* species, and searched for genome-wide SNPs between strains of these two species (Figure 1; Supplementary Table S1). This measure of phylogenetic diversity has proven to be useful to discriminate among closely related organisms and help resolve both short and long branches in a tree (as reviewed by Ngoot-Chin et al., 2021). The reads associated with each sample were mapped to the *N. fowleri* TY reference genome (Ali et al., 2021) and a SNP calling process was performed. A total of 1,200,000 high-quality reference-based SNPs were detected across the 65 *Naegleria* genomes analyzed. Our results show that (i) additional clades were created when we included our new *N. lovaniensis* strains and (ii) *N. lovaniensis* is more diverse than *N. fowleri*, as 773,266 SNPs were detected within intra-*N. lovaniensis* species against only 70,026 SNPs within intra-*N. fowleri*.

By restricting the SNP matrix and associated genotyping information (reduced VCF file) to *N. fowleri* strains only, we could perform a whole-genome SNP-based phylogenetic analysis for comparing the 3 new genomes (NF\_AR12, NF\_PA34, and NF\_NF1) against 52 strains of *N. fowleri* (close-to-complete genomes or reads only, Supplementary Table S1) available in online databases at the time of the analysis (Joseph et al., 2021). Figure 1 reveals a low level of SNP variation within the 55 *N. fowleri* isolates and we concluded that the classical typing of *N. fowleri* on the basis of their ITS sequence somehow reflects the genetic diversity of the species, which is apparently associated by geographical regions as previously established (De Jonckheere, 2011). Indeed, the newly sequenced isolates NF\_AR12, NF\_PA34 and the five

<sup>5</sup> <https://amoebadb.org/amoeba/app/>

<sup>6</sup> <https://github.com/PATRIC3/mauveviewer>

<sup>7</sup> Namely at <https://www.genome.jp/kegg>

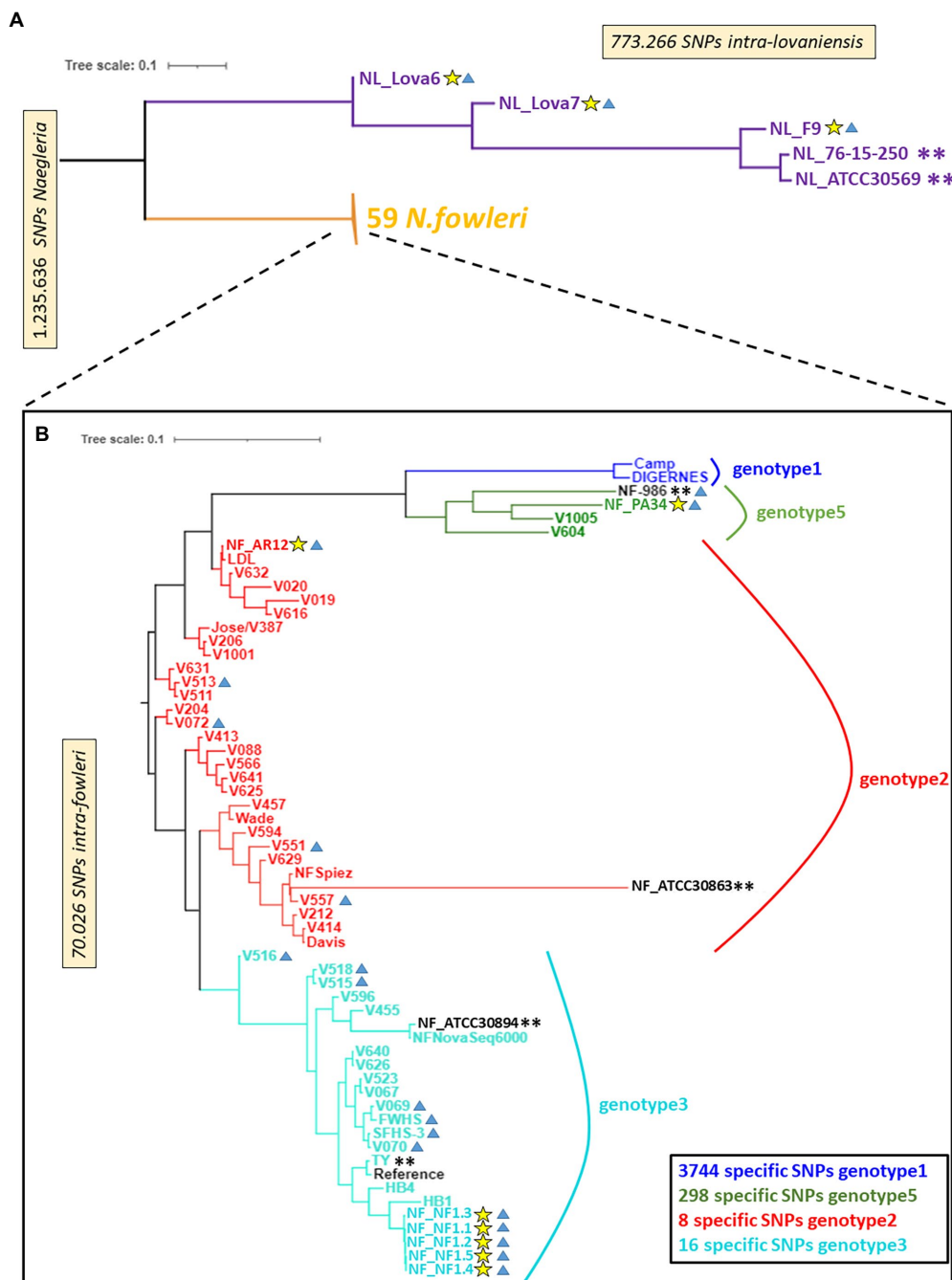


FIGURE 1

A neighbor-joining phylogenomic tree of *Naegleria fowleri* and *Naegleria lovaniensis* strains using the whole-genome SNPs. Phylogenomic trees are, respectively, based on 1,235,636 SNPs found in *Naegleria* genus (A) and 70,026 SNPs found in *N. fowleri* species (B). Yellow stars indicate strains sequenced in the present study, blue triangles indicate environmental strains, and double asterisks indicate strains for which a reference genome assembly and annotation were available at the date of writing. Bootstrap support estimates of major ancestral nodes are also shown.

biological replicates for NF\_NF1 are located in the phylogenetic clades Genotype 2, 5, and 3, according to the numbering scheme proposed by De Jonckheere (2011), respectively, as observed using the traditional mitochondrial small subunit (mtSSU) rRNA and ITS genotyping loci (Supplementary Tables S1, S2). The SNP-based phylogenetic tree however showed no clustering between clinical

and environmental isolates of *N. fowleri* strains (Figure 1; Supplementary Table S1), as recently observed by Joseph et al. (2021).

Additionally, this approach allowed us to define diagnostic SNP markers allowing to discriminate 4 genotypes of *N. fowleri*, i.e., markers whose alleles are exclusively and systematically found in all

isolates of a genotype (Figure 1). More precisely, we could identify a relatively high number of specific SNPs for genotype 1 and 5 (3,744 and 298 respectively) while the number of diagnostic SNPs identified is lower for genotypes 2 and 3 (respectively 8 and 16).

## 3.2. An overview of the newly sequenced *Naegleria fowleri* and *Naegleria lovaniensis* genomes

### 3.2.1. Genome assembly statistics and quality

Assembly statistics for the six new genomes together with the other *Naegleria* sp. whose genomes are published are presented in Table 1 and Supplementary Table S3. The six genomes have an average depth-of-coverage superior to 100X, in particular the NF\_NF1 strain which benefits from the compilation of 5 replicates. The final assemblies of the new *N. fowleri* genome consist of 500, 656, and 534 scaffolds (all anchored in 37 chromosomes) with a N50 size of 125,650, 81,421 and 112,144 bp, respectively for NF\_NF1, NF\_AR12 and NF\_PA34. Regarding the new *N. lovaniensis* genomes, we obtained for NL\_F9, NL\_Lova6 and NL\_Lova7, 754, 1959 and 2,384 (all anchored in 37 chromosomes) with N50 values of 78,479, 26,705 and 17,708 bp, respectively. Comparison between the genome size and GC content of *N. fowleri* strains NF\_ATCC 30894, NF\_ATCC 30863, NF\_V212, NF\_986 and NF\_TY and the new genomes NF\_NF1, NF\_AR12 and NF\_PA34 show relative conservation of genome statistics. Regarding *N. lovaniensis* strain NL\_ATCC 30569 and NL\_76–15–250 compared to the new isolates NL\_F9, NL\_Lova6 and NL\_Lova7, we observed that they share a similar GC content but the genome sizes for the new *N. lovaniensis* strains are smaller. As previously observed, *N. gruberi* present a slightly larger genome (40 Mb), with a 35% GC content (Table 1).

To evaluate the quality and the completeness of our assemblies, the percentage of Benchmarking Universal Single-Copy Orthologs (BUSCOs) was calculated and compared to previously sequenced *Naegleria* species (Table 1). The comparison shows globally similar numbers of complete BUSCOs within the *N. fowleri* strains, while more fragmented and missing BUSCOs could be identified in the new *N. fowleri* genomes (Table 1). Regarding the new *N. lovaniensis* genomes, the numbers of complete and fragmented BUSCOs are slightly higher than those obtained for *N. lovaniensis* NL\_ATCC 30569 and NL\_76–15–250. On the other hand, *N. lovaniensis* NL\_F9, NL\_Lova6 and NL\_Lova7 present less missing BUSCOs.

### 3.2.2. Content and organization of the genomes

To identify protein coding genes in the newly assembled *Naegleria* genomes, we performed gene prediction analyses using MAKER2 by providing evidence from transcriptomic datasets collected for each of species. Genomic features collected from the new genomes are presented in Table 1. MAKER2 gene annotation revealed that *N. fowleri* NF\_NF1 and NF\_AR12 have approximately the same number of genes as *N. fowleri* strain TY

( $N=9,405$ ), while the number of genes predicted for NF\_PA34 ( $N=11,036$ ) is close to those predicted for the *N. fowleri* strains ATCC 30863 and strain 986 ( $N=11,499$  and  $11,599$ , respectively). For *N. lovaniensis*, even though complete BUSCO levels are higher, the 3 new genomes present a significantly lower number of predicted genes, but the average length of the genes is higher ( $\sim 3,000$  bp). The repeat content is shown to be variable within *N. fowleri* strains and appears to be lower in *N. lovaniensis* new genomes (Table 1).

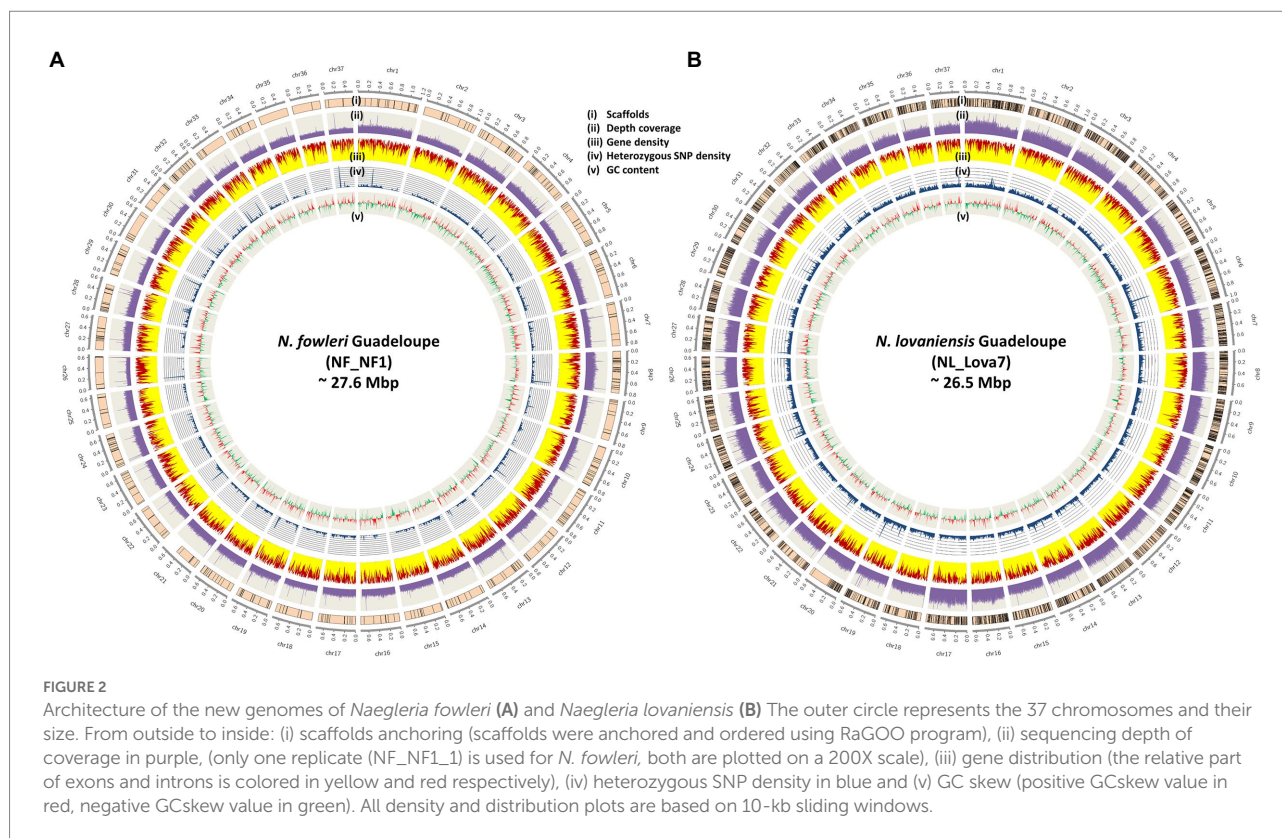
The architecture of the new genomes for *N. fowleri* and *N. lovaniensis* isolated in Guadeloupe is graphically represented in Figures 2A,B, respectively. Characteristics such as scaffolds boundaries after anchoring, sequencing coverage depth, gene density (with distribution of exons and introns), heterozygous SNPs and GC content were integrated into the Circos representations. The figures show that the 2 genomes are dense in gene and exon content, with a homogenous distribution among the 37 chromosomes. In addition, we could observe variations between chromosomes in the coverage depth level, suggesting potential indirect effect of ploidy during the mapping process.

### 3.2.3. Ploidy, aneuploidy, and loss of heterozygosity in *Naegleria*

Ploidy shifts, aneuploidy phenomena and loss of heterozygosity (LOH) have been observed in several eukaryotes (such as yeast, fungi, plants and in the parasitic amoeba *Entamoeba histolytica*; Kawano-Sugaya et al., 2020) and they have proven to be potent modulators of cell behavior, adaptation to the environment and pathogenesis (Bennett et al., 2014). The first evidence in ploidy and gene recombination in *Naegleria* was reported in 1986 using electrophoretic variation (Cariou and Pernin, 1987). In 1989, electrophoretic karyotyping showed that the number of chromosomes and their size can vary between species and even between strains of the same species (De Jonckheere, 1989).

Herein, to assess the genomic plasticity of *Naegleria* species, we collected high probability whole genome SNPs from *N. fowleri* NF\_NF1, NF\_AR12 and NF\_PA34 strains and *N. lovaniensis* NL\_Lova6, NL\_Lova7, and NL\_F9 strains. We made use of the B-Allele Frequency (BAF) information, which is a normalized measure of the allelic intensity ratio of two alleles (A and B), as an indicator measure of ploidy. For the three isolates of each species, BAF measures were either reported as a distribution curve over the whole genome (number of SNPs holding BAF values) or directly plotted physically along sequences as a Circos graphical representation of the *N. fowleri* chromosomes (Figures 3A,C, respectively) or *N. lovaniensis* chromosomes (Figures 3B,D, respectively). For *N. fowleri* NF\_NF1, NF\_AR12 and NF\_PA34 strains, we observed a peak in heterozygosity globally centered on 50% (Figure 3A), [which is consistent with the assumption that the *Naegleria* genome is diploid (Fritz-Laylin et al., 2010)], with NF\_AR12 strain presenting the highest number of heterozygous positions. When analyzing the B-allele frequency (Figure 3C), we observed the *N. fowleri* strains are mainly diploid, but that





trisomy phenomenon (aneuploidy with an additional chromosome) can be hypothesized visible on chr8 for NF\_AR12 and chr32 for NF\_PA34. This abnormality can be slightly visible also on the distributions with a slight increase to 33 and 66%. Aneuploidy is less pronounced for NF\_NF1 strain, but we observed that on chr7 or chr28, the allelic ratio seems more toward 33% than toward 50%, and on the chr9 where there are slightly 2 levels of allele ratio.

For *N. lovaniensis* strains, the allele ratio fluctuates; for NL\_Lova6 and NL\_Lova7, we showed a major peak of allele ratios at 50%, indicating that these 2 strains are diploid with just a few triploid chromosomes observed occasionally in chr15 and chr28 in NL\_Lova6, but for NL\_F9, 3 peaks are observed around 33%, 50%, and 66%, suggesting that NL\_F9 might be triploid on a larger number of chromosomes, reflecting several aneuploidy events (Figure 3B). Environmental conditions (such as *in vitro* culture conditions) can influence ploidy levels, as previously observed for diploid organisms such as *Saccharomyces cerevisiae* and *Candida* species (Gerstein et al., 2017). The strain NL\_F9 was isolated in the 1970 and was probably more subjected to adaptive conditions, leading to an accumulation of SNP and higher variation in ploidy compared to the other strains. This increased ploidy is well observable on the Circos (Figure 3D, blue color) and it manifests notably well among others on chromosomes 5, 7, 9, 10, 11, 19, 20, 22, 25, 33.

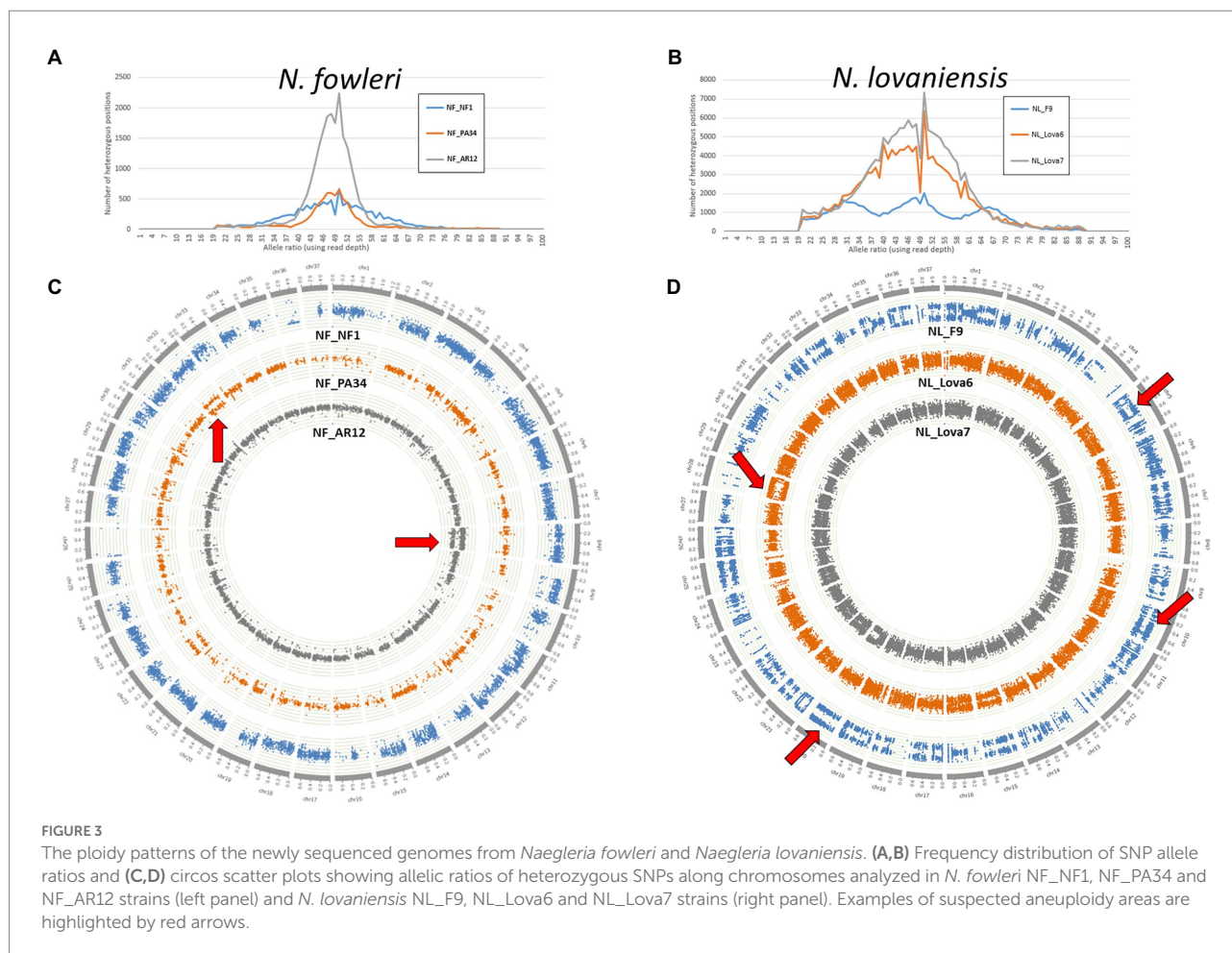
In all strains from both species, we observed several regions of loss-of-heterozygosity (LOH), which is translated by a

segmental or total loss of heterozygous SNPs. While LOH is observed in few *N. fowleri* chromosomes (chr26 for NF\_NF1, chr9 for NF\_PA34, chr11 for NF\_AR12; Figure 3C), it is particularly widespread in the NL\_F9 genome (chr4, chr13, chr23, chr28; Figure 3D).

*Naegleria* is mainly a heterozygous diploid that reproduces primarily *via* mitotic division as reviewed by De Jonckheere (2002). If the two alleles provide a differential benefit under a given stress, cells that retain the more beneficial allele after LOH may exhibit a growth advantage compared to the cells that do not undergo LOH. Extra chromosomes can arise rapidly and be lost rapidly, even within a single mitotic division. These genetic variations represent a rapid solution for adaptation to stress (Bennett et al., 2014; Peter et al., 2018).

### 3.3. *Naegleria* pangenome content

As a first step to genome functional annotation and comparative genomics, similarity searches and clustering from the 14 analyzed genomes were performed using pairwise BlastP and Orthofinder. We then analyzed two main components of the pangenome: the core genome (genes conserved across all observed genomes from a species or a genus) and accessory genome (gene(s) found at least in one strain, but not in all strains). To compare the possible advantage of using species versus genus pangenome analysis, we construct the intra-species pangenome



for *N. fowleri* ( $n=8$ ) and *N. lovaniensis* ( $n=5$ ), and the *Naegleria* genus pangenome based on 14 assembled and independently annotated isolates from (i) three different species (one for *N. gruberi*, five for *N. lovaniensis* and height for *N. fowleri*), (ii) different origin (clinical and environmental, with different abilities to grow at temperatures above 37°C and with pathogenic and non-pathogenic traits in human) and (iii) from distinct geographical regions (United States, Europe, Australia, and the Caribbean).

### 3.3.1. *Naegleria fowleri* and *Naegleria lovaniensis* species-specific pangenomes

Genome wide statistics shows that *N. fowleri* (Figure 4A) and *N. lovaniensis* (Figure 4B) pangenomes can comprise up to 12,308 and 12,207 genes, respectively, 6,531 and 5,855 being core genes for each species. The remaining genes constitute the accessory genome, being 5,777 for *N. fowleri* and 6,352 for *N. lovaniensis*. Interestingly, Figures 4A,B reveal that two *N. fowleri* and two *N. lovaniensis* strains have unique genes; indeed, 183 genes were detected only in *N. fowleri* strain NF\_ATCC 30863, 137 in *N. fowleri* strain NF\_V212, 545 in *N. lovaniensis* strain NL\_ATCC 30569 and 41 in *N. lovaniensis* strain NL\_76–15–250.

The maximum proportions of genes not shared between isolates of a single species reach a maximum 10.6% of the genes for NF (for 1,006 genes, absence in Ty only), and 11.7% of the genes for NL (for 1,116 genes, found in 2 strains among 5). This rather high proportion has already been shown in other comparative genomics analyzes in other protists (Majda et al., 2019).

The Core/Pangenome ratio of *N. fowleri* and *N. lovaniensis* correspond to 53% for and 48% of the pangenome, respectively, indicating a large potential for both *Naegleria* species to adapt to their environment.

### 3.3.2. *Naegleria* genus pangenome

Figure 4C shows that the *Naegleria* pan-genome is composed of 13,943 genes, and that the different isolates share 3,563 genes. These gene subset corresponds to the *Naegleria* core genome and provide evidence for conserved biological features among the several strains from the three species *N. gruberi*, *N. lovaniensis* and *N. fowleri*, suggesting that these genes are involved in vital role for *Naegleria* survival. The other 10,380 annotated genes correspond to the accessory genome and can be related to the evolution of a trait, speciation, or niche/host adaptation. A detailed analysis of the accessory genome allows us to detect genes exclusively present



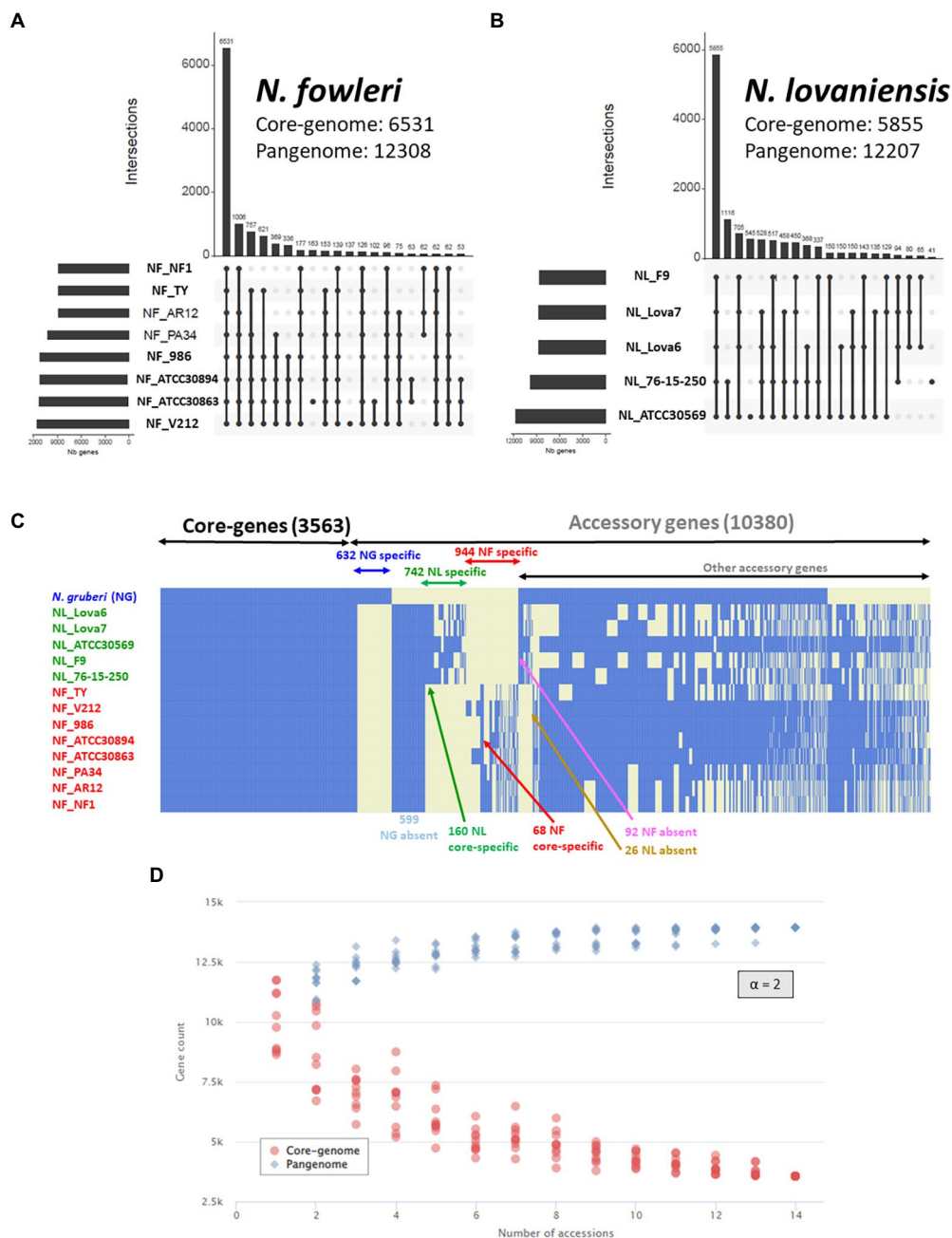


FIGURE 4

*Naegleria* pangenome analysis using OrthoFinder and visualized as UpSet and heatmap plots. UpSet plots show the intersections of the set of orthogroups from height genomes of *N. fowleri* (A) and five genomes of *N. lovaniensis* (B) species. Each vertical bar corresponds to a combination of gene sharing between strains. For each bar, black dots represent presence of the strain in the orthogroup while light gray dots denote its absence. Only the first 20 most abundant combinations are shown. The numbers of gene families (clusters/orthogroups) are indicated for each strain and strain intersection. (C) Gene presence/absence matrix for 14 strains of the three studied *Naegleria* species. The heatmap shows the presence (blue) or absence (light yellow) of all 13,943 orthogroups. Each row in the matrix corresponds to a strain/genome and each column represents an orthogroup. This representation has been conceived to visually separate *Naegleria* core-genes, species-specific genes and other accessory genes. (D) Gene accumulation curves showing how the *Naegleria* pangenome (blue) and core-genome (blue) vary as genomes are added in random order to the analysis. The power law alpha parameter shown inside the plot equals 2, which is indicative of a closed pangenome.

or absent in certain species (Figure 4C). For instance, we found (i) 599 genes absent in *N. gruberi*, while present in isolates from *N. lovaniensis* and *N. fowleri* and (ii) 92 genes absent in *N. fowleri* while present in both non-pathogenic *N. gruberi* and *N. lovaniensis*

strains. We also looked at species-specific gene lists within accessory, regrouping 944 and 742 genes for *N. fowleri* and *N. lovaniensis*, respectively. Among these, 160 and 64 genes exclusively present in all strains of the *N. lovaniensis* and *N. fowleri*,

respectively; these genes were identified as core-specific genes (i.e., species-specific and belonging to the core genome of the species).

The Core/Pangenome ratio of the *Naegleria* genus correspond to 25% of the pangenome. Compared to species-specific pangenome, our results show that the *Naegleria* core genome becomes smaller when diversity increases among the organisms. This clearly indicates that *Naegleria* community is complex and can adapt to varied niches. Additionally, the modeling of the *Naegleria* pangenome expansion show that the number of core genes (Figure 4D, red dots) and the pangenome size (Figure 4D, blue dots) stabilized after the addition of the 13 genomes, presenting an alpha parameter of 2. This demonstrates that *Naegleria* pangenome is closed (or very close to completion) and its size will not likely increase with subsequent isolates.

### 3.3.3. Functional annotation of the *Naegleria* pangenome

To understand the functional roles of the genes that constitute the core and pan-genome, we used the COGs functional classification. An enrichment analysis of COG categories assigned to the genes was performed by calculating the odds-ratio values (between a particular list of genes to be compared with the rest of the genes) and associated statistics Fisher test to define enrichment if the odds-ratio is significantly superior to 1 (Figure 5).

We first compared the COG annotations assigned to the genes between the core and accessory genes in *Naegleria* sp. sequenced strains (Figure 5A; Supplementary Table S4). The *Naegleria* core genome is mainly enriched ( $p < 0.05$ ) in protein families related to “Information storage and processing” [4 out of 5 COG categories: COG-A (RNA processing and modification), COG-B (Chromatin structure and dynamics), COG-K (Transcription) and COG-L (Replication, recombination and repair)] and “Metabolism” [5 out of 8 COG Categories: COG-C (Energy production and conversion), COG-E (Amino acid transport and metabolism), COG-G (Carbohydrate transport and metabolism) and COG-Q (Secondary metabolites biosynthesis, transport, and catabolism)] and “Cellular processing and signaling” [only 2 out of 9 COG Categories: COG-V (Defense mechanisms) and COG-Z (Cytoskeleton)]. The conservation of these shared genes among *Naegleria* species can be correlated with their biological importance in amoebae growth and survival. On the other hand, the COG functional categories of “Cellular processing and signaling” [COG-D (Cell cycle control, cell division, chromosome partitioning), COG-M (cell wall/membrane/envelope biogenesis), COG-T (Signal transduction mechanisms)], “Information storage and processing” COG-J (Translation, ribosomal structure and biogenesis) and “Metabolism” COG-F (nucleotide transport and metabolism), COG-H (Coenzyme transport and metabolism), and COG-I (Lipid transport and metabolism) are more concentrated in *Naegleria* accessory genome (Fisher *t*-test,  $p < 0.05$ ; Figure 5A; Supplementary Table S4). Functional enrichment was not statistically significant, but *Naegleria* accessory genomes clearly showed higher proportion of genes in

categories COG-N (Cell motility) and COG Y (Nuclear structure) compared to the core genome (Figure 5A). This indicates that pathways related to cell communication, ability to adapt to ecological conditions (potential niche or host-specific adaptations), genetic material processing and the metabolism of lipids and inorganic ions depend on the *Naegleria* species and/or the strain. Finally, genes within COG-S (unknown function), COG-R (general function prediction only) categories, were abundant across the pan-genome and had higher proportions in accessory genes.

To ascertain whether pathogenesis was associated with a specific functional category, we also examined the number of genes in each COG category for species-specific genes detected in pathogenic *N. fowleri* and non-pathogenic *N. lovaniensis* and *N. gruberi* (Figure 5B; Supplementary Table S4). We noticed that genes in the categories “Cellular processing and signaling” [COG-O (Post-translational modification, protein turnover, and chaperones) and COG-V (Defense mechanisms)] were remarkably enriched in *N. fowleri* strains ( $p < 0.05$ ). Functional enrichment was not statistically significant (certainly due to the low number of genes), but still *N. fowleri* genomes clearly showed higher proportion of genes in categories COG-N (Cell motility), COG-Z (Cytoskeleton), COG-A (RNA processing and modification) and COG-B (Chromatin structure and dynamics; Figure 5B). Interestingly, our results show that non-pathogenic *N. lovaniensis* and *N. gruberi* have a similar profile of statistically relevant overexpressed proteins in COG categories T (Signal transduction mechanisms), COG-K (Transcription), COG-L (Replication, recombination and repair), and COGs R and S (poorly characterized proteins). *Naegleria lovaniensis* species-specific genes are enriched in proteins COG-J (Translation, ribosomal structure and biogenesis). Therefore, *N. fowleri* genomes shared more genes related to communication and gene control, probably allowing amoebae to respond to environmental changes more readily, while *N. lovaniensis* and *N. gruberi* genomes shared more genes involved in information storage and processing.

### 3.3.4. Synteny between *Naegleria fowleri* and *Naegleria lovaniensis* core genomes

After establishing *Naegleria* core genome, conserved regions in terms of synteny were identified and visualized with Circos for both *N. lovaniensis* and *N. fowleri*; *N. gruberi* was not included in this analysis as it is more distant from the two other species. We observe in Figure 6A that gene synteny along the 37 chromosomes is highly conserved, with few microsyntenic breaks. Gray lines connecting core-genes with no change in gene order are in the vast majority ( $n = 4,151$ ), while red lines ( $n = 37$ ) highlighting regions with order changes on the same chromosome are relatively rare. For some of these cases (chr2, chr5, chr11, chr12, chr28) a zoom-in of chromosome alignment between *N. fowleri* and *N. lovaniensis* is displayed as a Mauve alignment to focus on and localize the disruption of gene order conservation (Figure 6B). Finally green lines ( $n = 88$ ) materialize order change on different chromosomes. All together, these results showed a high

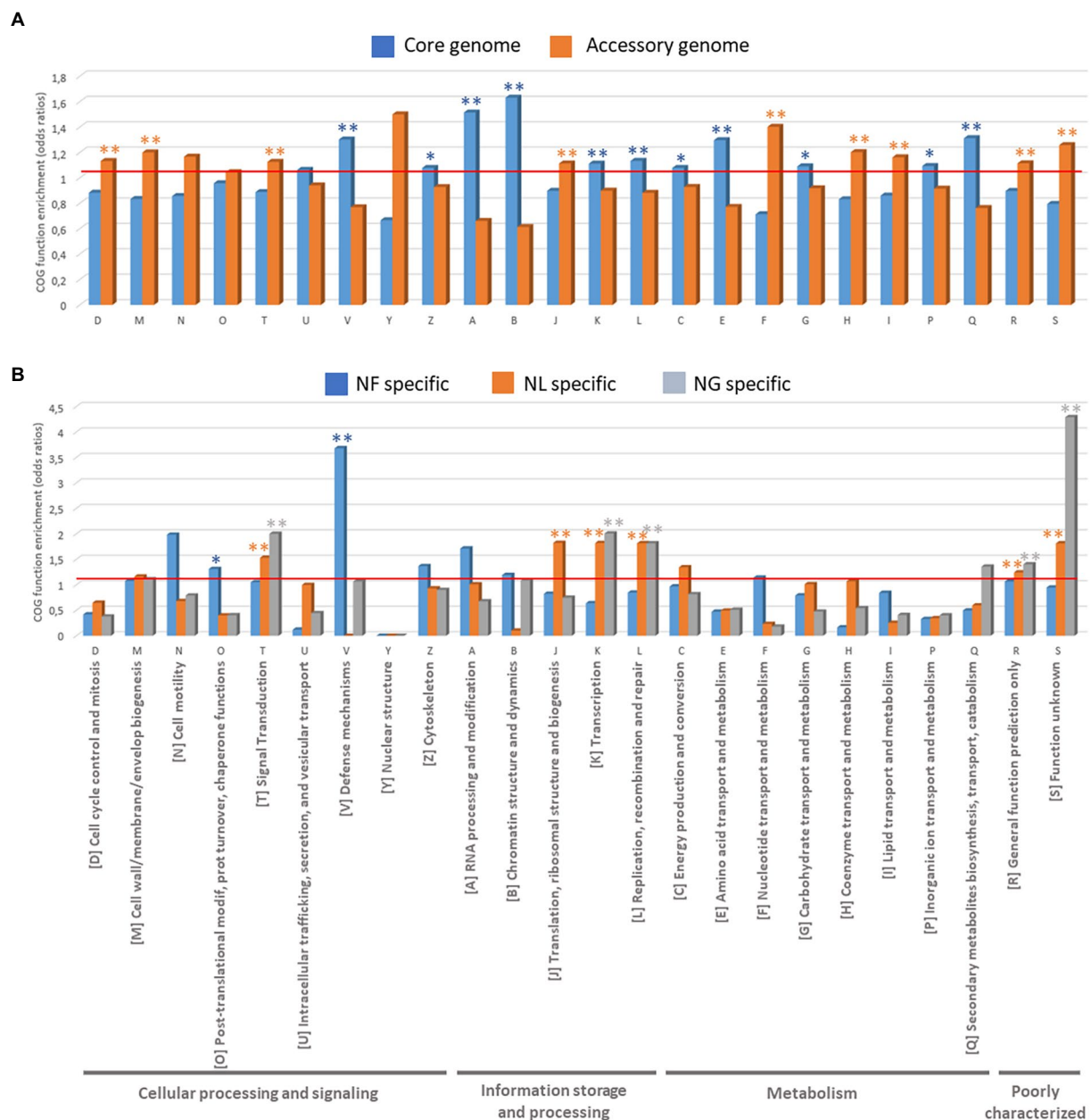


**FIGURE 5**  
Functional analyses of *Naegleria* pangenome based on COG function enrichment (odd ratios). **(A)** COGs present in *Naegleria* core and accessory genomes and **(B)** COGs specifically detected in *N. fowleri* (NF), *N. lovaniensis* (NL) and *N. gruberi* (NG) strains.

conservation of gene sequences and synteny between *N. lovaniensis* and *N. fowleri*.

### 3.3.5. *Naegleria* genes present sequence similarities with major organism groups

As a geographically widespread microorganism feeding on algae, bacteria, yeasts, and viruses in the soil and water, and with the possibility of harboring bacteria, *Naegleria* encounters a rich and diverse supply of foreign DNA, providing a large opportunity for gene exchange and acquisition (Bertelli and Greub, 2012; Sibbald et al., 2020). Herein, the functional annotation of *Naegleria*

genes allowed to identify thousands of genes showing similarities with sequences from diverse kingdoms such as Animalia (including Metazoa and *Homo sapiens*), Plantae, other amoebae, Bacteria/Monera, Fungi, viruses, and other eukaryotes (Supplementary Table S4).

The social amoeba *Dictyostelium* proteins were also found to be more similar to Plants, Metazoa and Fungi (Eichinger et al., 2005). *Naegleria* genomes are known to present key features of eukaryotic origin and 2.7% of *N. gruberi* genes are homologous to bacteria (Fritz-Laylin et al., 2011; Clarke et al., 2013). This corresponds to a notably high number of laterally acquired



bacterial genes compared to the parasitic *Entamoeba histolytica* or the social *Dictyostelium discoideum* (Clarke et al., 2013). In protists, fungi, plants, animals and even amoebae such as *Acanthamoeba*, *Dictyostelium* and *Naegleria*, lateral (or horizontal) gene transfer (LGT) has been considered a key process of genome evolution (Eichinger et al., 2005; Keeling and Palmer, 2008; Fritz-Laylin et al., 2010; Clarke et al., 2013; McCarthy and Fitzpatrick, 2019). Many of the LGT candidates across all of the *Naegleria* strains analyzed in this work have many predicted metabolic functions (Supplementary Table S4), suggesting that LGT in *Naegleria* might be driven by the selective pressure of new ecological niches.

Interestingly, we also noticed that *Naegleria* genes share similarities with human genes (Supplementary Table S4). Human orthologues have previously been found in the social amoeba *Dictyostelium discoideum* (Eichinger et al., 2005); and due to the strong protein homology, this amoeba is currently being used as a model to study genes related to human degenerative diseases (Haver and Scaglione, 2021). To assess if *Naegleria* could be used to investigate the functions of genes related to human disease, we performed a filtering of significant matches from Blast

similarity searches between *Naegleria* and *Homo sapiens* protein sequences, using a stringent threshold E-value < 10E-20 and protein similarity extending over 65% (Table 2) with sequence coverage above 80%. Surprisingly, despite the lack of a nervous system, *Naegleria*'s genome encodes genes that cause brain and neurodegenerative diseases (Table 2), including the gene *RAB7a* (also identified in *Dictyostelium*). We also found one gene related to eye disease (which would be more related to *Acanthamoeba* species). Although orthologues of human genes implicated in disease were identified in eukaryotes (including *Dictyostelium* and yeast), *Naegleria* could provide a potentially valuable vehicle for studying their functions in a system which is experimentally tractable and intermediate in complexity between the yeasts and the higher multicellular eukaryotes *Dictyostelium*.

### 3.4. *Naegleria* biology and ecology

*Naegleria* face many complex challenges in their surrounding environment. They must compete with other microorganisms for limited nutrient resources, while defending themselves against

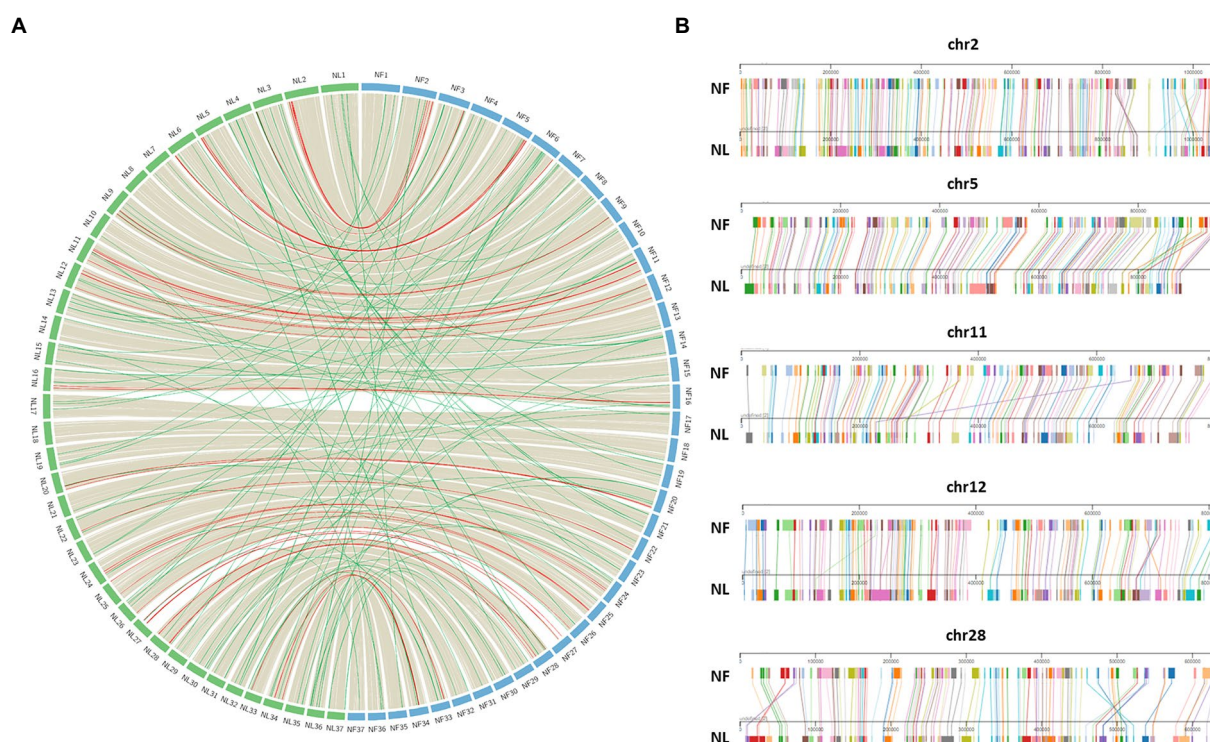


FIGURE 6

Synteny between *Naegleria fowleri* and *Naegleria lovaniensis* using core-genes. (A) In the circo plot, protein coding genes of *N. fowleri* (NF\_NF1 strain, blue) can be connected with those of *N. lovaniensis* (NL\_Lova7, green) if they belong to the core-genome. Preliminary anchoring of scaffolds using a 37 pseudo-molecules reference (NF\_TY) during the assembly process, genes can be positioned onto 37 newly assembled pseudo-molecules references. Each species' chromosome is labeled with the genus species abbreviation (NF for *N. fowleri* and NL for *N. lovaniensis*). Highly conserved syntenic blocks between the genomes are colored in gray, gene order rearrangement on the same chromosome are highlighted in red while gene order rearrangement on different chromosomes are highlighted in green. (B) Focus on chromosomes that show gene order rearrangement within the same chromosome using Mauve viewer. Pairwise chromosomal synteny between gene homologs of *N. fowleri* and *N. lovaniensis* in chromosomes 2, 5, 11, 12, and 28. Each colored box corresponds to a distinct core-gene that can be connected between the two reference genomes.

TABLE 2 Comparative analyses of *Naegleria* and human protein sequences.

Disease category	Annotation*	Gene name*	<i>Homo sapiens</i> accession number (Uniprot)	BlastP alignments results			Additional information
				Query cover (%)	Identity of coverage (%)	Probability (E-value)	
Brain disease	Cell division cycle protein 48 homolog	VCP	P55072	93	75	0	<i>Naegleria</i> core genome
	Eukaryotic translation initiation factor 2 subunit 3	EIF2S3	P41091	83	78	0	<i>Naegleria</i> core genome
	Isocitrate dehydrogenase [NADP], mitochondrial	IDH2	P48735	95%	65	0	<i>Naegleria</i> accessory genome
	14-3-3 protein epsilon	14-3-3epsilon/YWHAE	P62258	83	73	5E-136	<i>Naegleria</i> core genome
Neurodegenerative disease	Ras-related protein Rab-7A	RAB7A	P51149	96	69	6E-74	<i>Naegleria</i> core genome; also detected in <i>Dictyostelium discoideum</i>
Eye disease	Pre-mRNA-processing-splicing factor 8	PRPF8	Q6P2Q9	95	75	0	<i>Naegleria</i> core genome
Autosomal recessive metabolic disorder	Glutaryl-CoA dehydrogenase, mitochondrial	GCDH	Q92947	90	72	0	<i>Naegleria</i> accessory genome
Mitosis disorder/cancer	Serine/threonine-protein phosphatase 4 catalytic subunit	PP4C	P60510	100	78	0	<i>Naegleria</i> core genome
Intellectual disability	Thioredoxin-like protein 4A	TXN4A	P83876	100	82	1E-95	<i>Naegleria</i> accessory genome

\*Based on [Supplementary Table S4](#).

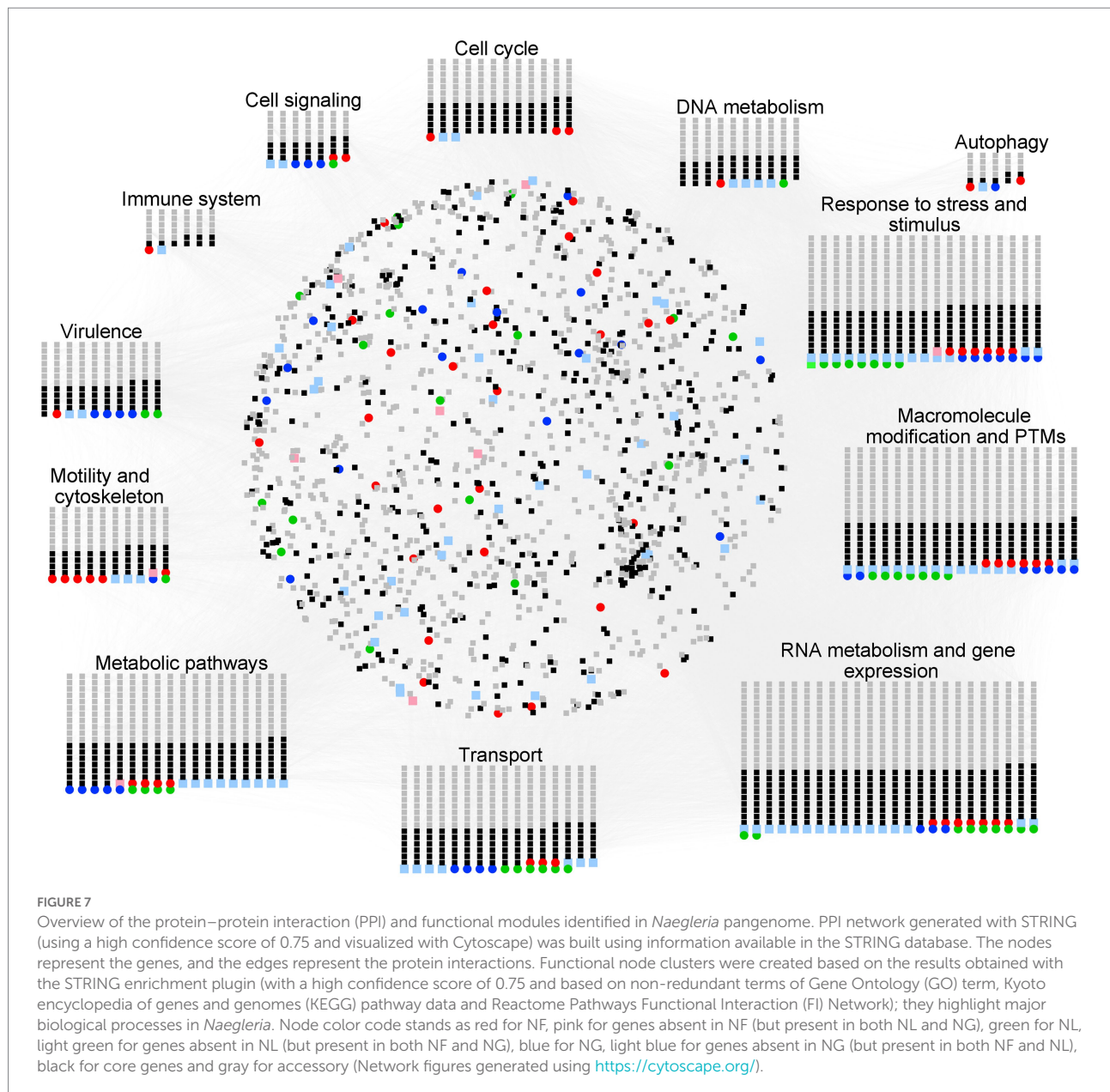
predation and toxins. The knowledge of how *Naegleria* adapt to their habitats (including during the occasional infection of the human brain) is critical for our understanding of *Naegleria* biology and pathogenesis. To move from gene content to gene context, we used Cytoscape and StringApp to construct and visualize PPI networks ([Figure 7](#)) from *Naegleria* pangenome information ([Supplementary Table S4](#)), using publicly available protein–protein–interaction information. This functional analysis allowed to infer major biological processes in *Naegleria* ([Figure 7](#)), discussed below and summarized in [Figure 8](#).

### 3.4.1. Life cycle and reproduction

*Naegleria* are known for their ability to form three types of cells: invasive trophozoites (amoeboid form) that divide by binary fission/mitosis, transient motile non-dividing flagellates, and latent double-walled cysts ([De Jonckheere, 2002](#); [Figure 8](#)). The information in differential expression of genes between the different forms of *Naegleria* is very limited. Lê and co-workers

found evidence that a Cystatin-B like protein (encoded by the gene mRNA1\_NF0117700-p1 in NF\_ATCC 30863) may play a critical role in *N. fowleri* encystation ([Lê et al., 2021](#)). We recovered Cystatin-B orthologs in *N. gruberi*, *N. fowleri* (7 out of the 8 strains analyzed) and in only *N. lovaniensis* strain ([Supplementary Table S5](#)). But our results suggest that other genes might be involved in *Naegleria* encystment, which it is not fully surprising since it has been recently shown that the encystment process is a complex phenomenon, notably for the free-living amoeba *Acanthamoeba castellanii* ([Bernard et al., 2022](#)). For instance, *A. castellanii* encystment is induced by the down-regulation of the acetyltransferase-like gene *ACA1\_384820* ([Rolland et al., 2020](#)). The *Naegleria* pangenome contains 26 N-acetyltransferase-like genes, 6 in the core and 20 in the accessory genome (3 being specific to *N. gruberi*; [Supplementary Table S4](#)) but none was found to be homologous to gene *ACA1\_384820*. We also identified the presence of 17 genes involved in “starvation” status (and possibly involved in *Naegleria*





encystment): 11 in the accessory genome, 5 in core genome, and one specific to *N. fowleri* (the gene *ULK2* coding for a Serine/threonine-protein kinase involved in autophagy in response to starvation; [Supplementary Table S4](#)). The gene coding for the transcriptional repressor *XBPI* [which is known to repress 15% of all yeast genes as cells switch to quiescence ([Miles et al., 2013](#))] was also reported and we registered the presence of 26 orthogroups encoding for adenylate cyclase, which has been involved in encystation in *Dictyostelium* ([Chen et al., 2010](#)) and *A. castellanii* ([Achar and Weisman, 1980](#)). As observed in *Saccharomyces cerevisiae* ([Yi and Huh, 2015](#)) and previously suggested by [Oppendoes et al. \(2011\)](#), *Naegleria* might take advantage of the enzymes such as UTP:glucose-1-phosphate uridylyltransferase (which plays an important role in carbohydrate metabolism) and

trehalose synthase and trehalose phosphatase to produce trehalose (a protectant against various abiotic stresses) for osmoregulation and cyst formation ([Supplementary Tables S4, S7](#)).

But other mechanisms could be involved in *Naegleria* encystment. *Dictyostelium discoideum* grows as a unicellular organism, but can switch to a multicellular development upon starvation ([Eichinger et al., 2005](#)). It has been suggested that *D. discoideum* transformation mechanism could be mediated by small non-coding RNA (ncRNA) mediated gene silencing (known as RNAi). Some genes involved in RNAi silencing was previously found in *N. gruberi* ([Fritz-Laylin et al., 2010](#)). Herein, elements of the RNAi machinery were found in all *Naegleria* species studied ( $n = 16$ , in both core and accessory genome, [Supplementary Table S4](#)). The identification of Piwi-interacting RNAs (piRNAs), a class of

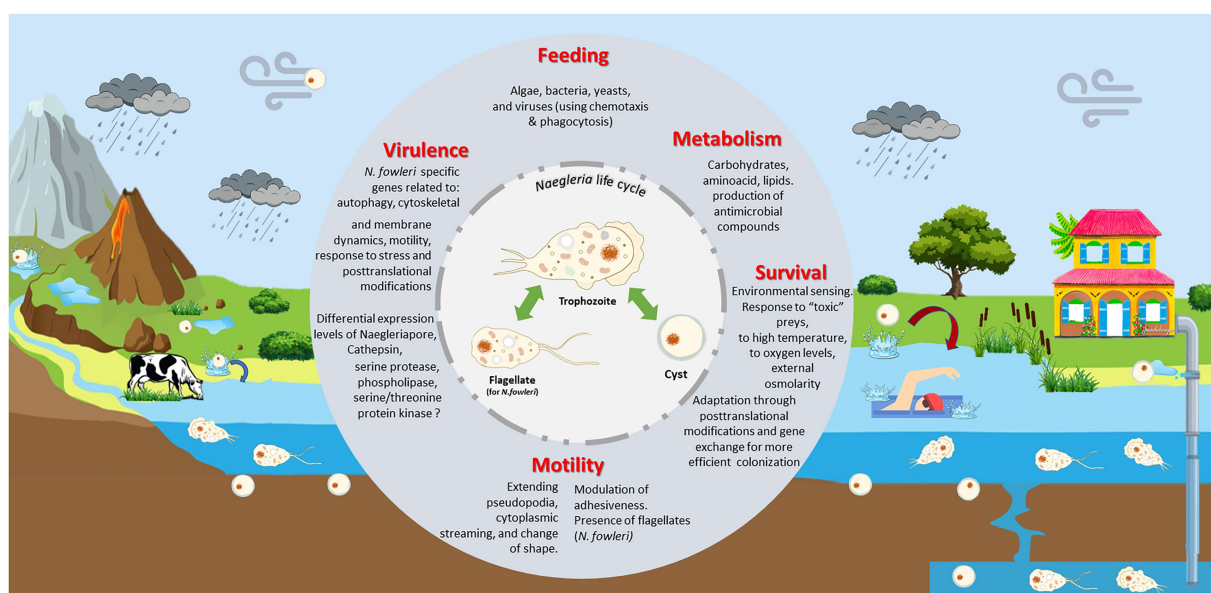


FIGURE 8

**Naegleria** biology and ecology. *Naegleria* is found worldwide in natural (such as rivers, lakes, hot springs, underground waters) and man-made (including pipes, swimming pools) aquatic environments and soil habitats. As a free-living genus, they live primarily as an amoeboid trophozoites, moving around using pseudopodia and by changing their shape. They replicate by mitosis and feed mainly on bacteria via phagocytosis, using chemotaxis as a possible hunting mechanism. Though they can obtain nutrients from the environments, they need to adapt their metabolism between feast and starvation conditions. Under nutrient deprivation, trophozoites can transform to resistant and dormant cysts; these can be transported by dust during dust storms. Several *Naegleria* species (namely *N. fowleri*) can exhibit a flagellate state, allowing to move around more rapidly searching for food or stressless situations. This incredible ability to swap between different forms must require significant biochemical and genetic modifications. *Naegleria* can use other strategies to survive to stress (oxidative and osmotic stress, high temperatures, toxic preys, and predators) namely through macromolecule modification and post-translation modifications (PTMs). Genes acquired by lateral gene transfer can also provide additional help to survive in harsh situation. Few species are pathogenic but *Naegleria fowleri* trophozoites can opportunistically infect animals and humans. If water containing *N. fowleri* enters the nose, the trophozoite can enter the nasal cavity, travel to the brain and feed on the brain, beginning with the meninges. As several virulent-associated genes (such as Cathepsin and Naegleriapore pore) were found in non-pathogenic *N. gruberi* and *N. lovaniensis* and pathogenic *N. fowleri*, this suggests that high-pathogenicity of *N. fowleri* might be linked to differential expression of these genes and/or related to *N. fowleri* specific genes involved in autophagy, motility, membrane and cytoskeleton dynamics, and even PTMs.

small RNAs that are 24–31 nucleotides in length, indicates that *Naegleria* can use gene silencing as a regulatory mechanism of gene expression. These results might encourage the use of RNAi to unravel novel aspects of *Naegleria* biology.

Despite the knowledge of the replicative ability of *Naegleria* trophozoites, little is known on the genes on *Naegleria* “sexuality.” Heterozygosity and genetic recombination found in *Naegleria gruberi* (Fritz-Laylin et al., 2010) and *N. lovaniensis* (Pernin et al., 1992) is typical of a sexual organism, and suggest some form of mating type. Meiotic and mitotic machinery was previously found in *N. gruberi* and *N. fowleri* genomes (Fritz-Laylin et al., 2010; Herman et al., 2021). Our results are in agreement with this observation as the three species studied can reproduce by mitosis ( $n=63$  genes) and they also have a complete meiosis toolkit gene (Supplementary Table S6). Indeed, we detected several genes involved in syngamy (HAP2), sister chromatid cohesion (cohesin complex, *SMC1*, *SM1A*, *DCC1*, *PDS5*, *RAD21/REC8*), formation of DNA double stranded breaks (*SPO11*, *MRE11*, and *RAD50*), homologous recombination (*DMC1*, *RAD51*, *HOP2*, and *MND1*), crossing over pathways (*MSH4-5*, *MLH1*, *MLH3*, *EXO1*, *MUS81* and *MMS4*), and gene conversion (mismatch correction, *MSH2*,

*MSH6*, *PMS1-2*; Supplementary Table S6). We did not recover the genes *GEX1* [a nuclear membrane protein involved in karyogamy, also absent in *Entamoeba* (Hofstatter et al., 2018)] and *MER3* (a DNA helicase that unwinds double-stranded DNA, previously detected by Herman et al., 2021). Although the formation of the synaptonemal complex (SC) is one of the hallmarks of meiosis, we only detected one gene (SCP-2-like) potentially involved in this process. As previously observed (Fritz-Laylin et al., 2010; Herman et al., 2021), we also noticed that some of these genes (e.g., *RAD51*, *HAP2*, *MSH6*, *SPO11*) have several paralogs and certain meiosis-specific genes are differentially present in *Naegleria* species (*N. fowleri* 986 presenting the highest number of gene paralogs namely for *HAP2*, *MSH5*, *MLH1*, *MSH6* and *MLH4*, Supplementary Table S6). This variation in sexual mechanism has been previously reported for amoebozoans (Tekle et al., 2017, 2022) and *Symbiodiniaceae* dinoflagellates (Shah et al., 2020).

### 3.4.2. Feeding and metabolism

*Naegleria* colonize environments that frequently vary in nutrient supply (carbon-, nitrogen-, phosphorus-, sulfur-sources, metal ions). To obtain nutrients such as methionine,

purine and heme, the amoebae still need to feed on various microorganisms including algae, bacteria, yeasts, and viruses (Fritz-Laylin et al., 2011). Unicellular organisms such as *Entamoeba histolytica* and *Dictyostelium discoideum* can use two complementary strategies to feed on microorganisms: chemotaxis (for detection and foraging) and phagocytosis (for recognition and digestion; Bailey et al., 1985; Xu et al., 2021). While microorganisms' detection and hunting are facilitated by chemoattractant G-protein-coupled-receptors (GPCRs), recognition and digestion require pattern-recognition receptors (PRRs), such as Toll-like receptors (TLRs) and C-type lectin receptors [as reviewed by Xu et al. (2021)]. Chemotaxis was previously observed in *N. fowleri* to bait for bacteria (Marciano-Cabral and Cline, 1987). *Naegleria fowleri* but not *N. australiensis*, *N. gruberi*, or *N. lovaniensis*, demonstrated enhanced motility when placed in proximity to mammalian cells (Cline et al., 1986). It has been also suggested that *N. fowleri* might actively use chemotaxis to reach the brain tissue (Baig, 2016). We also know that *Naegleria* uses mainly phagocytosis to digest bacteria, but the components involved in both chemotaxis and phagocytosis remain largely unknown. Herein, we detected 188 genes involved in *Naegleria* chemotaxis and phagocytic process: 71 in the *Naegleria* core genome and 117 in the accessory genome (7 being specific to *N. lovaniensis* strains, 3 to *N. gruberi* and 4 to *N. fowleri*; Supplementary Table S4). To sense microbial pathogens, TLRs proteins bind to bacterial elicitors through leucine-rich repeats (LRRs) and signal through adaptor/effector proteins which in turn, initiates the transcriptional programs that mediate specific defense responses (Chen et al., 2007). Herein, we identified 43 genes coding for TLRs with ligand-binding leucine-rich repeats (LRRs) in *Naegleria* core genome, 21 integrins (12 in accessory and 9 in core), C-type lectin (2 in the core genome) and 15 genes coding for concanavalin-type A lectin found in both core ( $n = 5$ ) and accessory ( $n = 10$ ), with one being specific to *N. lovaniensis* (OG0012291). Like human integrins, *D. discoideum* contain von Willebrand factor type A and a glycine-rich transmembrane domain and can interact with the actin-binding protein talin (Dunn et al., 2018). Herein, we found 15 genes coding for von Willebrand factor type A and interestingly only two were detected in the core genome. Among the 13 genes present in the accessory genome, 2 are specific to *N. lovaniensis* and 2 others to *N. fowleri* (Supplementary Table S4).

The phagocytotic process requires actin and cytoskeleton dynamics to accommodate the newly formed phagosome. *Naegleria gruberi* genome sequence revealed that the amoeba holds complete actin and microtubule cytoskeletons (Fritz-Laylin et al., 2010). Besides these actin-related genes, we also detected a considerable number of upstream signaling components required for cytoskeletal reorganization, such as Rho family GTPases and small GTPases. Indeed, we found that of the 25 Rho family GTPases and 111 small GTPases family detected in *Naegleria*, most of them were in the accessory, indicating that this feature is differential between the different strains or species (Supplementary Table S4). Contrary to what is observed in the

social amoeba *Dictyostelium*, Cdc42 (with a profound effect on cell polarity) is specifically present in *N. lovaniensis*. The activities of these GTPases are regulated by members of the RhoGDI family, by components of ELMO1–DOCK180 complexes and by a large number of proteins carrying RhoGEF and RhoGAP domains. Herein, we found 1 gene coding for RhoGDI (in the core genome), 6 genes with ELMO domains (mainly in the accessory genome), 2 RhoGEF (in the accessory genome) and 14 RhoGAP (Supplementary Table S4). Phosphatidylinositol phosphates are crucial players during phagosome formation phagocytic uptake and maturation (Gillooly et al., 2001). As for *Dictyostelium* (Dunn et al., 2018), *Naegleria* also possesses class I phosphatidylinositol-3-OH kinases (PI3K), which are at the crossroad of several critical signaling pathways (Supplementary Table S4). The diverse array of these regulators and the discovery of many additional actin-binding proteins suggest that there are many aspects of cytoskeletal regulation that have yet to be explored in *Naegleria*.

To breakdown several bacterial components or disrupt membrane integrity, *Naegleria* phagosome acquires a series of proteases, hydrolases, lysozymes, and antimicrobial peptides. Our results revealed the presence of 178 genes related to such pathways, with a strong homology to the genes detected in the social amoeba *Dictyostelium* (Supplementary Table S4) and with some of them being considered as virulence factors in *N. fowleri* (Herman et al., 2021). For instance, we found 19 genes coding for cathepsin proteases, including Cathepsin D (considered as a virulence factor in *N. fowleri*), a lysosomal protease involved in early phagosome steps, detected in the accessory genome. We also found that *Naegleria* is equipped with a large arsenal of lysozymes (up to 6 genes for *N. lovaniensis*, Supplementary Table S7), which suggest that each of them might be useful to kill and degrade different subsets of microorganisms. Other enzymes such as acid phosphatase, phospholipases (namely A, B, and D) and esterase [probable constituents of *Naegleria*'s phago-lysosomal system (Oppendoes et al., 2011)], chitinase, alpha and beta-amylases, alpha and beta-glucosidases, anhydro-N-acetylmuramic acid kinase and lysosomal alpha-mannosidase (that degrade bacterial peptidoglycans and glycoproteins), glucokinase, regulatory protein homolog and D-lactate dehydrogenase (involved in bacterial cell walls degradation) were also detected (Supplementary Table S7). Interestingly, the genes coding for beta-glucosidase (present in the core genome), acid phosphate (accessory genome) and lysozyme are more abundant in *N. lovaniensis*. On the other hand, the lysosomal enzyme alpha-galactosidase (involved in glycoproteins, glycolipids, and polysaccharides cleavage) was found only in some *N. fowleri* strains. Whether this relates to improved efficacy to digest bacteria or the ability to digest different bacteria genera remains to be elucidated.

As mentioned above, *Naegleria* undertake frequent transitions between feast and starvation feeding conditions, by adopting one of the three forms presented in Figure 8. All these transitions require adequate metabolic adaptations. *Naegleria*'s genomes sequencing allowed to reveal important insights into the versatility



of *Naegleria*'s metabolic capacities, including the existence of aerobic and anaerobic modes of metabolism (Fritz-Laylin et al., 2011; Opperdooes et al., 2011). Our results showed that genes involved in carbohydrate and amino acid metabolism, cholesterol and sphingolipid biosynthesis, metabolism of co-factors (Supplementary Tables S4, S7) are distributed both in *Naegleria* core and accessory genomes. Although the presence of several enzymes involved in sugar transport, pentose phosphate pathways, glycolysis/gluconeogenesis suggest that *Naegleria* utilizes a variety of monosaccharides for its carbohydrate needs (Fritz-Laylin et al., 2010; Opperdooes et al., 2011; Supplementary Table S7), the role of glycolysis in *N. fowleri* during human infection remains unresolved (Milanes et al., 2019). In fact, Bexkens et al. (2018) revealed that *N. gruberi* trophozoites would prefer to oxidize fatty acids to generate acetyl-CoA, rather than use glucose and amino acids as growth substrates (Bexkens et al., 2018). Recently, several genes involved in metabolism of both lipids and carbohydrates were shown to be upregulated in mouse-passaged *N. fowleri*, being possibly related to the amoeba pathogenesis (Herman et al., 2021). Herein, we found several orthogroups encoding for Acyl-CoA synthetase ( $n=9$ ) which could possibly explain why lipids are more use than sugars (Supplementary Table S7). We also detected several orthogroups for adenylate kinase ( $n=7$ ) and succinate dehydrogenase ( $n=4$ ; present in all *N. lovaniensis* strains) which are implicated in energy homeostasis and production. It should be noted that *N. gruberi*, *N. lovaniensis* and *N. fowleri* strains are able to grow in the absence of bacteria (i.e., in axenic culture medium), in the laboratory (Cline et al., 1983; this work). Although the reasons for this are not yet clear, we suggest that, as an analogy to what was observed in the laboratory strains of *Dictyostelium*, a mutation in the gene encoding the Ras-regulating neurofibromin (that we found in the core and accessory genomes analyzed) would result in enlarged macropinosomes, and hereby facilitate the uptake of sufficient nutrients from liquid media to support growth (Bloomfield et al., 2015).

To compete for food supply and eventually inhibit the growth of the surrounding organisms, *Naegleria* might likely rely on the production of antimicrobial compounds. The analyses performed in this work revealed the presence of gene involved in the biosynthesis of secondary metabolites and resistance to antibiotics and/or other toxic compounds (Supplementary Table S4). The high number of genes encoding efflux pumps (such as ATP-binding cassette, ABC) and polyketide synthases for producing and exporting small molecules in the *Naegleria* genomes fully supports this view. ABC transporters are known to be prevalent in the proteomes of soil microorganisms such as *Dictyostelium* (Eichinger et al., 2005) and are thought to provide resistance to xenobiotics through their ability to translocate small-molecule substrates across membranes against a substantial concentration gradient. In *Naegleria*, we found 33 ABC transporters encoded by the genome (11 in the core genome and 22 others in the accessory, with one being specific to *N. fowleri* strains). In addition to polyketide synthases ( $n=16$ , 5 in the core pangenome), the predicted *Naegleria* pangenome has O-methyl

transferases, which could increase the diversity of natural products made. Like *Dictyostelium*, *Naegleria* appears to have a large secondary metabolism, which deserves further investigation.

### 3.4.3. Motility

*Naegleria* display motility that is characteristic of human leukocytes (Fritz-Laylin et al., 2011). *Naegleria* trophozoites move slowly by extension of directional movements by means of broad, rounded anterior pseudopodia (lobopodia) while the flagellate possesses two basal bodies and flagella, providing a mechanism to locomote quickly in search of more favorable local conditions. The shape and locomotion of *Naegleria* are amazingly plastic.

Actin is also strongly associated to motility in *Naegleria* flagellate and amoeba stages (Velle and Fritz-Laylin, 2020). Herein, we found several genes coding for actin-related protein 2/3 complex subunit ( $n=5$ ), profilin ( $n=4$ ), WASP ( $n=5$ ), WAVE-complex ( $n=2$ ), formin ( $n=6$ ), and WASH-complex elements ( $n=6$ ; Supplementary Table S4), but most interestingly we noticed that Actin-1 [implicated in *N. fowleri* pathogenicity due to its role in trogocytosis via food cup formation (Sohn et al., 2010)] can be encoded by 4 (*N. lovaniensis*) to 64 genes for *N. gruberi* (Supplementary Tables S4, S5); Actin-1 can be encoded to an average of 15 genes in *N. fowleri*. The reasons for this remain unclear.

For amoeboid locomotion, the amoeba must modulate their adhesiveness to the substrate, the extracellular matrix and to other cells. To accomplish this, *Naegleria* genome encodes numerous proteins previously described as components of adherens junctions in animal Metazoa, such as  $\beta$ -catenin ( $n=1$ , absent in *N. gruberi*, Supplementary Table S4),  $\alpha$ -actinin ( $n=6$ , one being specific to *N. fowleri*, Supplementary Table S4), myosin ( $n=26$ , Supplementary Table S4), laminin (40 predicted proteins) and fibronectin. We also identified sets of genes enriched in functions specific to flagellar motility (such as dynein) in both *Naegleria* core and accessory genome. We identified 6 gene families capable of amoeboid locomotion (AMs) first detected in *N. gruberi* (Fritz-Laylin et al., 2010). Among those, only one is present in *Naegleria* core pangenome (AM46), another being specific to *N. fowleri* (AM6) and the others to accessory (Supplementary Table S4). We nevertheless noticed that *N. lovaniensis* and *N. fowleri* presented more orthogroups related to motility (namely laminin, which could represent a benefit for host tissue colonization) and in particular *N. fowleri* genomes are enriched with genes encoding proteins with leucine rich and dynein heavy chain domains (Supplementary Table S4). This higher number of genes encoding for modulation of cytoskeletal protein could be linked to *N. fowleri* pathogenesis, as previously suggest (Herman et al., 2021).

### 3.4.4. Survival

To efficiently feed, replicate and survive, *Naegleria* must be able to sense its surrounding environments (soil, water, brain), which present different physicochemical conditions, especially in pH value and oxygen partial pressure and to compete with other amoebae (including those from the same genus), fungi and

bacteria for limited resources in the different habitats. For this, *Naegleria* must have developed its gene repertoire to feed on (potentially pathogenic) microorganisms and to defend themselves against predation, toxins and environmental oxidative stress (Supplementary Table S4).

#### 3.4.4.1. Environmental sensing

*Naegleria gruberi*'s genome encodes an extensive array of intracellular signaling machinery that presumably coordinates the environmental sensing (Fritz-Laylin et al., 2010). From Supplementary Table S4, this repertoire includes G-protein-coupled receptor signaling ( $n = 37$ ) and histidine kinases ( $n = 17$ ), as well as 265 predicted protein kinases, 32 protein phosphatases, and 182 monomeric Ras-like GTPases (Supplementary Table S3). Many organisms sense their environment via membrane-bound adenylate/guanylate cyclases; *Naegleria* contains at least 81 cyclases, 6 being specific to *N. fowleri* and 4 to *N. lovaniensis*. We also detected 4 response receiver domain proteins, whereas other protists such as *T. brucei*, *Giardia*, and *Entamoeba* have none (Fritz-Laylin et al., 2010). We also found 17 sensor protein (all homologous to bacteria) genes with PAS domain and histidine kinase domain genes. Iron-sulfur (Fe-S) clusters have long been recognized as essential and versatile cofactors of proteins involved in sensing of ambient conditions, being essential for viability; however, these clusters can be degraded in the presence of copper. *Naegleria fowleri* has shown to be able to respond to limited iron availability (Arbon et al., 2020) and excess of copper (Grechnikova et al., 2020) to overcome oxidative stress. Herein, we detected genes coding for Fe-S cluster assembly, namely a cysteine desulfurase (with 5 orthogroups, and up to 5 gene encoding for the protein in *N. fowleri* 986), the iron chaperone frataxin and a NifU-like protein. To regulate copper levels, *Naegleria* uses copper-translocating ATPase, Selenium-binding protein 1-A, Globin/Protoglobin and Hemerythrin-like proteins (Grechnikova et al., 2020), detected in both core and accessory genome. Interestingly, the Globin/Protoglobin (OG0000194) and Hemerythrin-like protein (OG0000115) can be encoded by several genes in different *Naegleria* strains, which strongly suggest the importance of copper regulation for *Naegleria* survival.

#### 3.4.4.2. Response to "toxic" preys

During their hunt for food, *Naegleria* must often cope with the toxic traits of its prey. In aquatic environments, *Naegleria* can feed on cyanobacteria or eukaryotic algae which can expose them to photosynthetic oxidative stress (Uzuka et al., 2019). Herein, we found that *Naegleria* accessory genome encodes a gene for chlorophyllide-a oxygenase (CAO), which likely play a role in the degradation/detoxification of chlorophylls derived from prey during digestion. We also found other genes that could protect *Naegleria* from phototoxicity including RCC1 (Ultraviolet-B receptor UVR8 protein,  $n = 18$ ), SOQ1 ( $n = 11$ , 5 being specific to *N. lovaniensis*) and Photoactivated adenylate cyclase ( $n = 2$ ; Supplementary Table S3) homologous to *Euglena* genes and for photoresponsive behavior (Ntefidou and Häder, 2005).

It is widely recognized that some bacteria have evolved mechanisms to escape degradation within amoebae phagosomes (Dunn et al., 2018). In the social amoeba *D. discoideum*, as in other eukaryotic phagocytes, when bacteria escape from the phagosome, an alternative pathway to phagocytosis is triggered to eliminate infection in a more stringent catabolic way: autophagy (Mesquita et al., 2017). Herein, we detected at least 108 genes related to autophagy mechanism (Supplementary Table S3). These included previously considered *N. fowleri* virulence associated genes ( $n = 25$ ) such as Beclin and Serine/threonine-protein kinase.

Additionally, we found evidence that *Naegleria* genome can encode at least 194 genes related to inflammatory and subsequent adaptive immune responses which supports the facts that *Naegleria* use additional defense mechanism and secretion of intercellular signals to provide a rapid antimicrobial response. Among those, 5 are specific to *N. fowleri* and 12 to *N. lovaniensis*. The genomes of the amoebae *Acanthamoeba castellanii* and *Dictyostelium* are also known to encode a diverse repertoire of genes with predicted orthologous functions in the innate immune systems of higher organisms (Eichinger et al., 2005; Clarke et al., 2013).

#### 3.4.4.3. Response to high temperature

The vast majority of eukaryotes cannot survive prolonged exposure to temperatures above 40°C–45°C. Eukaryotic thermophiles (such as *N. fowleri* and *N. lovaniensis*) must have evolved to include several mechanisms of stabilization of enzymes or optimization of their activity, modulation of proportion of saturated fatty acids incorporated into phospholipids [so that their membrane fluidity is kept constant for the optimal functioning of membrane-localized transporters and enzymes (Arthur and Watson, 1976; Maheshwari et al., 2000)] and modulation of heat shock proteins. Herein, we found 97 genes involved in heat stress, two of them being in the core genome of *N. fowleri* (Supplementary Table S3).

#### 3.4.4.4. Response to oxygen levels

Although *Naegleria* present oxidative and non-oxidative modes of metabolism, when *N. fowleri* reaches the brain tissue it must possess an efficient antioxidant system to survive the invasion of oxygenated tissues and survive to the aerobic stress caused by the host immune response. Herein, we found 64 gene involved in oxidative stress. The amoebae *Mastigamoeba balamuthi* and *Entamoeba histolytica* share antioxidant system characteristics and their antioxidant machinery relies on the thioredoxin-based system (thioredoxin, NADPH: flavin oxidoreductase, peroxiredoxin), Fe-superoxide dismutase and rubrerythrin, and proteins (Žárský et al., 2021). *Naegleria* also encodes genes for thioredoxin ( $n = 21$ ), peroxiredoxin ( $n = 3$ ), superoxide dismutase ( $n = 4$ ) and rubrerythrin ( $n = 1$ ). These genes can either be found in the core and accessory genomes (Supplementary Table S3). As for *M. balamuthi*, *Naegleria* also possess (in the accessory genome) a homolog of the common bacterial osmotically inducible protein C (OsmC), which may



serve as a peroxidase (Žárský et al., 2021), and multiple homologs of hemerythrin ( $n=5$ , including one in the core genome) and may be involved in oxygen sensing. However, contrary to *M. balamuthi* and *E. histolytica* which lack glutathione-based pathways and catalases, we found several glutathione peroxidases that are antioxidant enzymes involved in the amoeba defense against reactive oxygen species.

### 3.4.4.5. Response to changes in osmolality

Fluctuations in external osmolality are one of the most encountered stress signals of living cells (Saran and Schaap, 2004). Eukaryotes such as yeast and *Arabidopsis* use histidine kinases to activate mitogen-activated protein (MAP) kinase pathway after osmotic up-shift; MAP kinase pathways also mediate osmotic stress responses in animals. In *D. discoideum*, osmotic up-shift reverts the histidine kinase DokA into a histidine phosphatase, which results in inactivation of the cAMP phosphodiesterase RegA. In the amoeba spore stage, osmotic up-shift activates adenylyl cyclase G, an enzyme that is structurally homologous to the *Trypanosoma* receptor adenylyl cyclases (Saran and Schaap, 2004).

Herein, we detected several genes encoding histidine kinases (as above mentioned), MAP kinases ( $n=30$ ), the 3',5'-cyclic-nucleotide phosphodiesterase regA and adenylyl cyclases ( $n=24$ , 3 are specific to *N. fowleri*; Supplementary Table S3). The presence of the genes might explain the ability of *Naegleria* to survive in various water environments.

### 3.4.4.6. Post-translational modifications

Stress responses and environmental adaptation is frequently achieved in eukaryotes through posttranslational modifications (PTMs) of signaling (Leach and Brown, 2012; Prabakaran et al., 2012; Beltrao et al., 2013). Herein, we identified for the first time, a wide repertoire of genes (at least 214 genes, 64 in core and 150 in accessory) encoding for several PTMs [such as protein SUMOylation ( $n=4$ ), ubiquitination ( $n=191$ ), neddylation ( $n=9$ ), Farnesylation ( $n=10$ ), N- and O-Mannosylation ( $n=4$ ); Supplementary Table S3]. This diverse variety of PTMs that might allow *Naegleria* to mount effective responses to adapt to their surroundings [including human brain, for *N. fowleri*, as previously suggested by Joseph et al. (2021)] and nutrient availability.

Ubiquitination is a reversible PTM that can modulate the activity of target proteins in various ways of numerous cellular processes, including cell cycle progression, gene transcription, DNA repair, and inflammation. Ubiquitination has been shown to be required for the survival of *S. cerevisiae* and *C. albicans* under starvation conditions (Leach and Brown, 2012). Herein, we detected 5 genes specific to *N. fowleri*, 11 to *N. lovaniensis* and 14 absent from *N. gruberi* but present in both *N. fowleri* and *N. lovaniensis*. We identified 14 E3 ubiquitin ligase (9 are specific to *N. lovaniensis* and 5 to *N. fowleri*). These enzymes are involved in the transfer of ubiquitin to substrate proteins, a process that determines the fate of the modified protein. The role mediated by E3 ligases is so crucial, that their activity must be tightly controlled

to ensure they solely act when necessary. The mechanisms of protein neddylation have multiple essential functions in the cell and it appears to be important for facilitating the attachment of ubiquitin E2 to the E3 ubiquitin ligase. Cullins are a key component of cullin-RING E3 ligases, which regulate the degradation, function, and subcellular trafficking of proteins. Herein, we detected 9 genes of the cullin family of proteins. Cullin proteins were also detected in *Dictyostelium* (Kim et al., 2022).

The importance of N- and O-glycosylation in pathogenic fungi has been largely attributed to their key roles in the construction and maintenance of a robust cell wall, an essential structure in fungi. Herein, we also found  $\alpha$ 1,6-mannosyltransferase and Dol-P-Man:protein O-mannosyltransferases involved in O-Mannosylation. We also found evidence of GPI-anchored proteins that are also involved in *C. albicans* cell wall biosynthesis and modeling. The implication of these enzymes in *Naegleria* biology deserves further investigation.

### 3.4.5. Virulence-associated genes

According to the initial “pangenome” concept (Tettelin et al., 2005), genes which enable the bacterial microorganisms to occupy and survive in often-hostile habitats could be considered as virulence genes. Here, we observed that many genes potentially considered as *N. fowleri* virulence associated genes (Zysset-Burri et al., 2014; Herman et al., 2021), were often found in non-pathogenic *Naegleria* strains analyzed to survive in these different habitats. These included prosaposin (termed *Naegleriapore A*), cathepsins B, C, L, Z, and F, serine protease, phospholipase B and serine/threonine-protein kinase.

Therefore, we specifically looked for candidate genes associated to virulence based on differences between *N. fowleri* with the non-pathogenic *N. gruberi* and *N. lovaniensis*. We could identify a set of genes exclusively present ( $n=946$ ) in *N. fowleri* (at least in one strain), 69 being present in all *N. fowleri* strains analyzed (Supplementary Table S4). Of these, 481 (50%) are unique to *N. fowleri*, with no clearly homologous sequence in any other organisms based on NCBI BLAST. Many of the annotated genes specific to *N. fowleri* are involved in autophagy, cytoskeletal and membrane dynamics, motility, response to stress and posttranslational modifications. Secretory products (such as glycosidase) from *N. fowleri* has been shown to play an important role in mucus degradation during the invasion process (Martínez-Castillo et al., 2017). Herein, we detected several genes coding for glycoside hydrolase (17 in core genome, 21 in accessory and 3 specific to *N. fowleri*). These enzymes could be useful to *Naegleria* to evade the mucus of the olfactory mucosa, which is part of the innate immune response (Martínez-Castillo et al., 2017). We also looked at genes specifically absent in *N. fowleri*, in particular, those potentially involved in host immune response. The absence of von Willebrand factor A domain-containing protein 3B (VWA domain-containing protein 3B) could help *N. fowleri* to escape from human immune response during infection. The presence of genes strongly homologous to human genes (Table 2) could also be useful to *N. fowleri* to go undercover in the human host.

As already discussed above, motility, proteases and lysosomal machinery have been related to *N. fowleri* pathogenesis. Recent transcriptomics experiments performed in mice suggest that up-regulation of genes involved in glutamate metabolism and ammonia transport could facilitate the spreading of *N. fowleri* in the central nervous system (Herman et al., 2021). Enzymes such as kynurenine-oxoglutarate transaminase, glutamate dehydrogenase and isocitrate dehydrogenase (involved in glutamate metabolism) and ammonium transporter were all found in the accessory genome (Supplementary Table S7) allowing the amoeba to produce brain-related neurotropic factors with impact on human mechanisms of neuroregeneration (Kim et al., 2017; Herman et al., 2021).

## 4. Conclusion

Pangenomes are becoming widely used to represent, analyze and predict the genomic diversity for populations of a single species or genus. Although the concept of the “pangenome” analysis was initially proposed in prokaryotes (Tettelin et al., 2005; Golicz et al., 2020), nowadays it is being performed in eukaryotes such as unicellular eukaryotes, fungi, plants, and animals (Aherfi et al., 2018; McCarthy and Fitzpatrick, 2019; Bayer et al., 2020; Golicz et al., 2020). In fact, pangenomics has somehow transformed eukaryote genome analyses as, regardless of their quality, eukaryote reference genomes do not and cannot contain all genetic information for a species due to genetic and genomic variation between individuals within a species or a genus (McCarthy and Fitzpatrick, 2019).

Since 2010, the number of published *Naegleria* genomes is increasing, with different levels of completeness ranging from “close-to-complete,” draft, scaffolds or reads (Fritz-Laylin et al., 2011; Liechti et al., 2018, 2019; Ali et al., 2021; Herman et al., 2021; Joseph et al., 2021). A detailed comparison of these genomes and additional functional studies using RNAseq and proteomics allowed to identify differently expressed genes potentially involved in *N. fowleri* pathogenesis (Herman et al., 2021; Joseph et al., 2021; Rodriguez-Anaya et al., 2021). Still, the understanding on how *Naegleria* can adapt to different environments, how they are phenotypically different, and why *N. fowleri* is the only pathogenic species to humans in *Naegleria* genus remains unclear.

Herein, we aimed to construct the first *Naegleria* genus pangenome, to assess the genomic repertoire of the genus and hereby open new ways to address issues related to microorganisms’ adaptation, evolution, diversity and pathogenesis (Tettelin et al., 2005; Golicz et al., 2020). For this, we presented 6 new genomes (increasing the number of genomes available for *N. fowleri* but especially for *N. lovaniensis*) and compared 14 *Naegleria* strains.

From a whole-genome SNP phylogenetic point of view, *N. lovaniensis* species displays a greater degree of variability, whereas *N. fowleri* is characterized by a phylogenetic shallowness. By defining core genomes (all genes present throughout species) and accessory genomes (strain-specific genes or genes specific to

individual groups of strains), we find strong evidence for pan-genomic structure within *Naegleria*. The analysis of the pangenome of the 3 species groups revealed how they are characterized by a closed pangenome, underlining that the gene repertoire encoded by these amoebae genus is nearly complete. A more expansive analysis of the pangenome covering more genomes (including more genomes from *N. gruberi* but also other species such as *N. australiensis* and *N. italica* known to be virulent in animals) would not substantially increase the number of genes identified in this work.

*Naegleria* inhabit a wide range of soil and aquatic environments worldwide, which represents an ideal situation for gene exchanges. The functional analyses of the *Naegleria* genomes support this idea as they revealed the existence of a large fraction of genes homologous to several kingdom such as plant, animal, archaea, to bacteria and virus. The biological significance of such degree of exchange and the high number of unique genes might rely on the fact that most of amoebae have explored many possible genetic/genomic combinations, to find the more efficient phenotype for the colonization of a given ecological niche. Interestingly, *Naegleria* share orthologous genes related to human diseases. Due to a high number of conserved features comparable to Animalia (including human) and *Dictyostelium*, *Naegleria* could be a valuable and attractive tool for the study of eukaryotic cell biology and evolution. Thermophilic *Naegleria* species could also be useful to study human disease in a system which is experimentally tractable.

Successful adaptation to different habitats must require a balance between exploiting surrounding nutrients resources, competition or symbiosis with other species, replication rate and mobility efficiency. *Naegleria* has been already considered as a versatile eukaryote due its gene repertoire (Fritz-Laylin et al., 2010, 2011). Our results reveal that genomic plasticity due to changes in ploidy and aneuploidy might be underlying its ability to adapt to several environments. An important question that will need to be answered is how *Naegleria* employs these genomic strategies as a general mechanism to adapt rapidly and flexibly to changing environmental assaults.

We observed that *Naegleria* core genomes are enriched for genes that facilitate many essential metabolic, regulatory and survival processes in both non-pathogenic (*N. gruberi* and *N. lovaniensis*) and pathogenic *N. fowleri* species. Accessory genomes are enriched for genes involved in processes like gene duplication and gain/loss events within strains, and are enriched for genes involved in molecule transport, motility, immune response and proteins modification using PTMs.

While searching for a pathogenic profile in *N. fowleri*, we found virulence factors in the *Naegleria* core genome suggesting that pathogenic and non-pathogenic lifestyles might be also a result of genes expressed differentially, as it has been shown for other taxa (Meysman et al., 2013; López-Fernández et al., 2015). The analysis of *N. fowleri* species-specific accessory genome allowed us to detect genes that could permit increased virulence. Validation of the role of these virulence factors will

require experimental confirmations. The results obtained herein suggest that drawing the line between pathogens and non-pathogenic *Naegleria* strains might be difficult, as strain-level differences in niche overlapping, ecological interactions, state of the host's immune system and environmental factors are seldom considered. Moreover, pathogenicity must be the result of a complex, multifactorial interaction, not only dependent on qualitative issues such as the presence of specific species, strains, or genes, but also on their relative abundances (Ehrlich et al., 2008) but also genomic structure.

Globally, the characterized structural and functional divergences and similarities identified here represent an important contribution toward understanding the evolution, phenotypic diversity and versatility of the poorly studied free-living amoebae of the *Naegleria* species, paving the way for further genomic and post-genomic studies.

Because of a high number of conserved features comparable to Animalia (including human), these versatile protists could be used as a non-mammalian model to study of eukaryotic cell biology features such as resistance to temperature, cell-autonomous defense mechanisms, and host-pathogen interaction. At the moment, the non-mammalian host models predominantly used belong to the genera *Acanthamoeba* and *Dictyostelium* (phylum Amoebozoa; Eichinger et al., 2005; Chen et al., 2007; Sandström et al., 2011; Dunn et al., 2018; Swart et al., 2018; Haver and Scaglione, 2021). Although they have proven to be particularly useful to study different eukaryotic mechanisms such as host-pathogen interaction, cell motility, chemotaxis, phagocytosis, and more recently autophagy and microbiome formation, one of the major drawbacks in using these amoebae is that most of them do not grow at “elevated” temperatures such as the human body temperature. As several *Naegleria* species can withstand temperatures at 37°C (and above), these free-living amoebae could be a useful alternative to study human disease in a system which is experimentally tractable.

## Data availability statement

The data presented in the study are deposited in the figshare repository [https://figshare.com/articles/dataset/NFgwada\\_genome\\_fasta/21603489](https://figshare.com/articles/dataset/NFgwada_genome_fasta/21603489) and in Genbank under BioSample accession numbers SAMN31682405, SAMN31682406, SAMN31682407, SAMN31682408, SAMN31682409 and SAMN31682410. *Naegleria* assembled chromosome sequences have been deposited on NCBI and have been assigned to accession numbers from CP113542 to CP113763. *Naegleria* ITS sequences have been deposited on NCBI and are available under accession numbers: OP867015, OP867016, OP867017 (Supplementary Table 2). Home-made scripts used for bioinformatic treatment and statistical analyses are available in a github repository accessible at [https://github.com/SouthGreenPlatform/PanExplorer\\_workflow/tree/main/Perl/Naegleria](https://github.com/SouthGreenPlatform/PanExplorer_workflow/tree/main/Perl/Naegleria).

## Author contributions

JJ, IM, and LM: sample preparation. AD, NA, VG, MG, LM, SJ, IA, and IM: data acquisition and analysis. AD and IM: conceptualization. AD, NA, MG, LM, IM, and VG: methodology. AD, NA, VG, and IM: formal analysis. AD, NA, VG, and IM: investigation. AD, NA, and IM: data curation. IM: writing—original draft preparation. AD, NA, VG, MG, LM, JJ, SJ, IA, AT, and IM: writing—review and editing. IM: supervision. IM and AT: project administration. AT: funding acquisition. All authors contributed to the article and approved the submitted version.

## Funding

This work was a part of the MALIN project funded by the European Union on the Guadeloupe Region under the European Research and Development Funds (ERDF) 2014–2020 program [2018-FED-1084]. C. Fund, Biomix Platform, C2RT, Institut Pasteur, Paris, France, supported by France Génomique (ANR-10-INBS-09-09) and IBISA.

## Conflict of interest

The authors declare that the research was conducted in the absence of any commercial or financial relationships that could be construed as a potential conflict of interest.

## Publisher's note

All claims expressed in this article are solely those of the authors and do not necessarily represent those of their affiliated organizations, or those of the publisher, the editors and the reviewers. Any product that may be evaluated in this article, or claim that may be made by its manufacturer, is not guaranteed or endorsed by the publisher.

## Author disclaimer

The findings and conclusions in this report are those of the authors, and do not necessarily represent the official positions of the Centers for Disease Control and Prevention.

## Supplementary material

The Supplementary material for this article can be found online at: <https://www.frontiersin.org/articles/10.3389/fmicb.2022.1056418/full#supplementary-material>



## References

- Achar, S., and Weisman, R. (1980). Adenylate cyclase activity during growth and encystment of *Acanthamoeba castellanii*. *Biochim. Biophys. Acta – Gen. Subj.* 629, 225–234. doi: 10.1016/0304-4165(80)90096-3
- Aherfi, S., Andreani, J., Baptiste, E., Oumessoum, A., Dornas, F. P., Andrade, A. C. D. S. P., et al. (2018). A large open pangenome and a small core genome for giant pandoraviruses. *Front. Microbiol.* 9:1486. doi: 10.3389/fmicb.2018.01486
- Ali, I. K. M., Kelley, A., Joseph, S. J., Park, S., Roy, S., Jackson, J., et al. (2021). Draft chromosome sequences of a clinical isolate of the free-living amoeba *Naegleria fowleri*. *Microbiol. Resour. Announc.* 10, e01034–e01020. doi: 10.1128/MRA.01034-20
- Alonge, M., Soyk, S., Ramakrishnan, S., Wang, X., Goodwin, S., Sedlazeck, F. J., et al. (2019). RaGOO: fast and accurate reference-guided scaffolding of draft genomes. *Genome Biol.* 20:224. doi: 10.1186/s13059-019-1829-6
- Arbon, D., Ženišková, K., Mach, J., Grechnikova, M., Malych, R., Talacko, P., et al. (2020). Adaptive iron utilization compensates for the lack of an inducible uptake system in *Naegleria fowleri* and represents a potential target for therapeutic intervention. *PLoS Negl. Trop. Dis.* 14:e0007759. Available at: doi: 10.1371/journal.pntd.0007759
- Arthur, H., and Watson, K. (1976). Thermal adaptation in yeast: growth temperatures, membrane lipid, and cytochrome composition of psychrophilic, mesophilic, and thermophilic yeasts. *J. Bacteriol.* 128, 56–68. doi: 10.1128/jb.128.1.56-68.1976
- Baig, A. M. (2016). Primary amoebic meningoencephalitis: Neurochemotaxis and neurotropic preferences of *Naegleria fowleri*. *ACS Chem. Neurosci.* 7, 1026–1029. doi: 10.1021/acschemneuro.6b00197
- Bailey, G. B., Leitch, G. J., and Day, D. B. (1985). Chemotaxis by *Entamoeba histolytica* 1. *J. Protozool.* 32, 341–346. doi: 10.1111/j.1550-7408.1985.tb03063.x
- Bayer, P. E., Golitz, A. A., Scheben, A., Batley, J., and Edwards, D. (2020). Plant pan-genomes are the new reference. *Nat. Plants* 6, 914–920. doi: 10.1038/s41477-020-0733-0
- Beltrao, P., Bork, P., Krogan, N. J., and Noort, V. (2013). Evolution and functional cross-talk of protein post-translational modifications. *Mol. Syst. Biol.* 9:714. doi: 10.1002/msb.201304521
- Bennett, R. J., Forche, A., and Berman, J. (2014). Rapid mechanisms for generating genome diversity: whole ploidy shifts, aneuploidy, and loss of heterozygosity. *Cold Spring Harb. Perspect. Med.* 4:a019604. doi: 10.1101/cshperspect.a019604
- Bernard, C., Locard-Paulet, M., Noël, C., Duchateau, M., Gai, Gianetto, Q., Moumen, B., et al. (2022). A time-resolved multi-omics atlas of *Acanthamoeba castellanii* encystment. *Nat. Commun.* 13:4104. doi: 10.1038/s41467-022-31832-0
- Bertelli, C., and Greub, G. (2012). Lateral gene exchanges shape the genomes of amoeba-resisting microorganisms. *Front. Cell. Infect. Microbiol.* 2:110. doi: 10.3389/fcimb.2012.00110
- Bexkens, M. L., Zimorski, V., Sarink, M. J., Wienk, H., Brouwers, J. F., De Jonckheere, J. F., et al. (2018). Lipids are the preferred substrate of the Protist *Naegleria gruberi*, relative of a human brain pathogen. *Cell Rep.* 25, 537–543.e3. doi: 10.1016/j.celrep.2018.09.055
- Bloomfield, G., Traynor, D., Sander, S. P., Veltman, D. M., Pachebat, J. A., and Kay, R. R. (2015). Neurofibromin controls macropinocytosis and phagocytosis in *Dictyostelium*. *eLife* 4:e04940. doi: 10.7554/eLife.04940
- Cabanettes, F., and Klopp, C. (2018). D-GENIES: dot plot large genomes in an interactive, efficient and simple way. *PeerJ* 6:e4958. doi: 10.7717/peerj.4958
- Cariou, M. L., and Pernin, P. (1987). First evidence for Diploidy and genetic recombination in free-living amoebae of the genus *Naegleria* on the basis of electrophoretic variation. *Genetics* 115, 265–270. doi: 10.1093/genetics/115.2.265
- Chen, Z., Schilde, C., and Schaap, P. (2010). Functional dissection of adenylate cyclase R, an inducer of spore encapsulation. *J. Biol. Chem.* 285, 41724–41731. doi: 10.1074/jbc.M110.156380
- Chen, G., Zhuchenko, O., and Kuspa, A. (2007). Immune-like phagocyte activity in the social amoeba. *Science* 317, 678–681. doi: 10.1126/science.1143991
- Clarke, M., Lohan, A. J., Liu, B., Lagkouvardos, I., Roy, S., Zafar, N., et al. (2013). Genome of *Acanthamoeba castellanii* highlights extensive lateral gene transfer and early evolution of tyrosine kinase signaling. *Genome Biol.* 14:R11. doi: 10.1186/gb-2013-14-2-r11
- Cline, M., Carchman, R., and Marciano-Cabral, F. (1986). Movement of *Naegleria fowleri* stimulated by mammalian cells in vitro 1. *J. Protozool.* 33, 10–13. doi: 10.1111/j.1550-7408.1986.tb05547.x
- Cline, M., Marciano-Cabral, F., and Bradley, S. G. (1983). Comparison of *Naegleria fowleri* and *Naegleria gruberi* cultivated in the same nutrient medium. *J. Protozool.* 30, 387–391. doi: 10.1111/j.1550-7408.1983.tb02936.x
- Couvin, D., Dereeper, A., Meyer, D. F., Noroy, C., Gaete, S., Bhakkan, B., et al. (2022). KaruBioNet: a network and discussion group for a better collaboration and structuring of bioinformatics in Guadeloupe (French West Indies). *Bioinforma. Adv.* 2. doi: 10.1093/bioadv/vbac010
- Danecek, P., Bonfield, J. K., Liddle, J., Marshall, J., Ohan, V., Pollard, M. O., et al. (2021). Twelve years of SAMtools and BCFtools. *Gigascience* 10:giab008. doi: 10.1093/gigascience/giab008
- De Jonckheere, J. F. (1977). Use of an axenic medium for differentiation between pathogenic and nonpathogenic *Naegleria fowleri* isolates. *Appl. Environ. Microbiol.* 33, 751–757. doi: 10.1128/aem.33.4.751-757.1977
- De Jonckheere, J. F. (1989). Variation of electrophoretic karyotypes among *Naegleria* spp. *Parasitol. Res.* 76, 55–62. doi: 10.1007/BF00931073
- De Jonckheere, J. F. (1998). Sequence variation in the ribosomal internal transcribed spacers, including the 5.8S rDNA, of *Naegleria* spp. *Protist* 149, 221–228. doi: 10.1016/S1434-4610(98)70030-6
- De Jonckheere, J. F. (2002). A century of research on the amoeboflagellate genus *Naegleria*. *Acta Protozool.* 41, 309–342.
- De Jonckheere, J. F. (2011). Origin and evolution of the worldwide distributed pathogenic amoeboflagellate *Naegleria fowleri*. *Infect. Genet. Evol.* 11, 1520–1528. doi: 10.1016/j.meegid.2011.07.023
- De Jonckheere, J. F. (2014). What do we know by now about the genus *Naegleria*? *Exp. Parasitol.* 145, S2–S9. doi: 10.1016/j.exppara.2014.07.011
- Debnath, A. (2021). Drug discovery for primary amoebic meningoencephalitis: from screen to identification of leads. *Expert Rev. Anti-Infect. Ther.* 19, 1099–1106. doi: 10.1080/14787210.2021.1882302
- Dereeper, A., Homa, F., Andres, G., Sempere, G., Sarah, G., Hueber, Y., et al. (2015). SNIPlay3: a web-based application for exploration and large scale analyses of genomic variations. *Nucleic Acids Res.* 43, W295–W300. doi: 10.1093/nar/gkv351
- Doncheva, N. T., Morris, J. H., Gorodkin, J., and Jensen, L. J. (2019). Cytoscape StringApp: network analysis and visualization of proteomics data. *J. Proteome Res.* 18, 623–632. doi: 10.1021/acs.jproteome.8b00702
- Dunn, J. D., Bosmani, C., Barisch, C., Raykov, L., Lefrançois, L. H., Cardenal-Muñoz, E., et al. (2018). Eat prey, live: *Dictyostelium discoideum* as a model for cell-autonomous defenses. *Front. Immunol.* 8:1906. doi: 10.3389/fimmu.2017.01906
- Ehrlich, G. D., Hiller, N. L., and Hu, F. (2008). What makes pathogens pathogenic. *Genome Biol.* 9:225. doi: 10.1186/gb-2008-9-6-225
- Eichinger, L., Pachebat, J. A., Glöckner, G., Rajandream, M.-A., Sucgang, R., Berriman, M., et al. (2005). The genome of the social amoeba *Dictyostelium discoideum*. *Nature* 435, 43–57. doi: 10.1038/nature03481
- Emms, D. M., and Kelly, S. (2019). OrthoFinder: phylogenetic orthology inference for comparative genomics. *Genome Biol.* 20:238. doi: 10.1186/s13059-019-1832-y
- Flynn, J. M., Hubley, R., Goubert, C., Rosen, J., Clark, A. G., Feschotte, C., et al. (2020). RepeatModeler2 for automated genomic discovery of transposable element families. *Proc. Natl. Acad. Sci. U. S. A.* 117, 9451–9457. doi: 10.1073/pnas.1921046117
- Fritz-Laylin, L. K., Ginger, M. L., Walsh, C., Dawson, S. C., and Fulton, C. (2011). The *Naegleria* genome: a free-living microbial eukaryote lends unique insights into core eukaryotic cell biology. *Res. Microbiol.* 162, 607–618. doi: 10.1016/j.resmic.2011.03.003
- Fritz-Laylin, L. K., Prochnik, S. E., Ginger, M. L., Dacks, J. B., Carpenter, M. L., Field, M. C., et al. (2010). The genome of *Naegleria gruberi* illuminates early eukaryotic versatility. *Cells* 140, 631–642. doi: 10.1016/j.cell.2010.01.032
- Gerstein, A. C., Lim, H., Berman, J., and Hickman, M. A. (2017). Ploidy tug-of-war: evolutionary and genetic environments influence the rate of ploidy drive in a human fungal pathogen. *Evolution* 71, 1025–1038. doi: 10.1111/evo.13205
- Gillooly, D. J., Simonsen, A., and Stenmark, H. (2001). Phosphoinositides and phagocytosis. *J. Cell Biol.* 155, 15–18. doi: 10.1083/jcb.200109001
- Golitz, A. A., Bayer, P. E., Bhalla, P. L., Batley, J., and Edwards, D. (2020). Pangenomics comes of age: from bacteria to plant and animal applications. *Trends Genet.* 36, 132–145. doi: 10.1016/j.tig.2019.11.006
- Grabherr, M. G., Haas, B. J., Yassour, M., Levin, J. Z., Thompson, D. A., Amit, I., et al. (2011). Full-length transcriptome assembly from RNA-Seq data without a reference genome. *Nat. Biotechnol.* 29, 644–652. doi: 10.1038/nbt.1883
- Grechnikova, M., Ženišková, K., Malych, R., Mach, J., and Sutak, R. (2020). Copper detoxification machinery of the brain-eating amoeba *Naegleria fowleri* involves copper-translocating ATPase and the antioxidant system. *Int. J. Parasitol. Drugs Drug Resist.* 14, 126–135. doi: 10.1016/j.ijiddr.2020.10.001
- Haver, H. N., and Scaglione, K. M. (2021). *Dictyostelium discoideum* as a model for investigating neurodegenerative diseases. *Front. Cell. Neurosci.* 15:759532. doi: 10.3389/fncel.2021.759532



- Herman, E. K., Greninger, A., van der Giezen, M., Ginger, M. L., Ramirez-Macias, I., Miller, H. C., et al. (2021). Genomics and transcriptomics yields a system-level view of the biology of the pathogen *Naegleria fowleri*. *BMC Biol.* 19:142. doi: 10.1186/s12915-021-01078-1
- Hoff, K. J., and Stanke, M. (2013). WebAUGUSTUS—a web service for training AUGUSTUS and predicting genes in eukaryotes. *Nucleic Acids Res.* 41, W123–W128. doi: 10.1093/nar/gkt418
- Hofstadter, P. G., Brown, M. W., and Lahr, D. J. G. (2018). Comparative genomics supports sex and meiosis in diverse Amoebozoa. *Genome Biol. Evol.* 10, 3118–3128. doi: 10.1093/gbe/evy241
- Holt, C., and Yandell, M. (2011). MAKER2: an annotation pipeline and genome-database management tool for second-generation genome projects. *BMC Bioinformatics* 12:491. doi: 10.1186/1471-2105-12-491
- Jahangeer, M., Mahmood, Z., Munir, N., Waraich, U.-E.-A., Tahir, I. M., Akram, M., et al. (2020). *Naegleria fowleri*: sources of infection, pathophysiology, diagnosis, and management; a review. *Clin. Exp. Pharmacol. Physiol.* 47, 199–212. doi: 10.1111/1440-1681.13192
- Jamerson, M., da Rocha-Azevedo, B., Cabral, G. A., and Marciano-Cabral, F. (2012). Pathogenic *Naegleria fowleri* and non-pathogenic *Naegleria lovaniensis* exhibit differential adhesion to, and invasion of, extracellular matrix proteins. *Microbiology* 158, 791–803. doi: 10.1099/mic.0.055020-0
- Jones, P., Binns, D., Chang, H.-Y., Fraser, M., Li, W., McAnulla, C., et al. (2014). InterProScan 5: genome-scale protein function classification. *Bioinformatics* 30, 1236–1240. doi: 10.1093/bioinformatics/btu031
- Joseph, S. J., Park, S., Kelley, A., Roy, S., Cope, J. R., and Ali, I. K. M. (2021). Comparative genomic and transcriptomic analysis of *naegleria fowleri* clinical and environmental isolates. *mSphere* 6, e00637–e00621. doi: 10.1128/mSphere.00637-21
- Jurka, J. (2000). Repbase update: a database and an electronic journal of repetitive elements. *Trends Genet.* 16, 418–420. doi: 10.1016/s0168-9525(00)02093-x
- Kawano-Sugaya, T., Izumiyama, S., Yanagawa, Y., Saito-Nakano, Y., Watanabe, K., Kobayashi, S., et al. (2020). Near-chromosome level genome assembly reveals ploidy diversity and plasticity in the intestinal protozoan parasite *Entamoeba histolytica*. *BMC Genomics* 21:813. doi: 10.1186/s12864-020-07167-9
- Keeling, P. J., and Palmer, J. D. (2008). Horizontal gene transfer in eukaryotic evolution. *Nat. Rev. Genet.* 9, 605–618. doi: 10.1038/nrg2386
- Kemble, S. K., Lynfield, R., DeVries, A. S., Drehner, D. M., Pomputius, W. F., Beach, M. J., et al. (2012). Fatal *Naegleria fowleri* infection acquired in minnesota: Possible expanded range of a deadly thermophilic organism. *Clin. Infect. Dis.* 54, 805–809. doi: 10.1093/cid/cir961
- Khan, N. A., Muhammad, J. S., and Siddiqui, R. (2021). Brain-eating amoebae: is killing the parasite our only option to prevent death? *Expert Rev. Anti-Infect. Ther.* 20, 1–2. doi: 10.1080/14787210.2021.1927712
- Kim, J., Lee, S., Kang, S., Kim, S.-H., Kim, J.-C., Yang, M., et al. (2017). Brain-derived neurotrophic factor and GABAergic transmission in neurodegeneration and neuroregeneration. *Neural Regen. Res.* 12, 1733–1741. doi: 10.4103/1673-5374.217353
- Kim, W. D., Mathavarajah, S., and Huber, R. J. (2022). The cellular and developmental roles of Cullins, Neddylation, and the COP9 signalosome in *Dictyostelium discoideum*. *Front. Physiol.* 13:827435. doi: 10.3389/fphys.2022.827435
- Koboldt, D. C., Zhang, Q., Larson, D. E., Shen, D., McLellan, M. D., Lin, L., et al. (2012). VarScan 2: somatic mutation and copy number alteration discovery in cancer by exome sequencing. *Genome Res.* 22, 568–576. doi: 10.1101/gr.129684.111
- Korf, I. (2004). Gene finding in novel genomes. *BMC Bioinformatics* 5:59. doi: 10.1186/1471-2105-5-59
- Krzywinski, M., Schein, J., Birol, I., Connors, J., Gascoyne, R., Horsman, D., et al. (2009). Circos: an information aesthetic for comparative genomics. *Genome Res.* 19, 1639–1645. doi: 10.1101/gr.092759.109
- Lê, H. G., Ham, A.-J., Kang, J.-M., Vö, T. C., Naw, H., Sohn, H.-J., et al. (2021). A novel cysteine protease inhibitor of *Naegleria fowleri* that is specifically expressed during encystation and at mature cysts. *Pathogens* 10:388. doi: 10.3390/pathogens10040388
- Leach, M. D., and Brown, A. J. P. (2012). Posttranslational modifications of proteins in the pathobiology of medically relevant fungi. *Eukaryot. Cell* 11, 98–108. doi: 10.1128/EC.05238-11
- Letunic, I., and Bork, P. (2021). Interactive tree of life (iTOL) v5: an online tool for phylogenetic tree display and annotation. *Nucleic Acids Res.* 49, W293–W296. doi: 10.1093/nar/gkab301
- Li, H. (2013). Aligning sequence reads, clone sequences and assembly contigs with BWA-MEM. arXiv:1303.3997.
- Li, H. (2018). Minimap2: pairwise alignment for nucleotide sequences. *Bioinformatics* 34, 3094–3100. doi: 10.1093/bioinformatics/bty191
- Liechti, N., Schürch, N., Bruggmann, R., and Wittwer, M. (2018). The genome of *Naegleria lovaniensis*, the basis for a comparative approach to unravel pathogenicity factors of the human pathogenic amoeba *N. fowleri*. *BMC Genomics* 19:654. doi: 10.1186/s12864-018-4994-1
- Liechti, N., Schürch, N., Bruggmann, R., and Wittwer, M. (2019). Nanopore sequencing improves the draft genome of the human pathogenic amoeba *Naegleria fowleri*. *Sci. Rep.* 9:16040. doi: 10.1038/s41598-019-52572-0
- López-Fernández, S., Sonego, P., Moretto, M., Pancher, M., Engelen, K., Pertot, I., et al. (2015). Whole-genome comparative analysis of virulence genes unveils similarities and differences between endophytes and other symbiotic bacteria. *Front. Microbiol.* 6:419. doi: 10.3389/fmicb.2015.00419
- Maciver, S. K., Piñero, J. E., and Lorenzo-Morales, J. (2020). Is *Naegleria fowleri* an Emerging Parasite? *Trends Parasitol.* 36, 19–28. doi: 10.1016/j.pt.2019.10.008
- Maheshwari, R., Bharadwaj, G., and Bhat, M. K. (2000). Thermophilic fungi: their physiology and enzymes. *Microbiol. Mol. Biol. Rev.* 64, 461–488. doi: 10.1128/MMBR.64.3.461-488.2000
- Majda, S., Boenigk, J., and Beisser, D. (2019). Intraspecific variation in Protists: clues for microevolution from *Poteroispumella lacustris* (Chrysophyceae). *Genome Biol. Evol.* 11, 2492–2504. doi: 10.1093/gbe/evz171
- Marciano-Cabral, F., and Cline, M. (1987). Chemotaxis by *Naegleria fowleri* for bacteria. *J. Protozool.* 34, 127–131. doi: 10.1111/j.1550-7408.1987.tb03147.x
- Martin, M. (2011). Cutadapt removes adapter sequences from high-throughput sequencing reads. *EMBnet. J.* 17 Next Gener. Seq. Data Anal. – 10.14806/ej.17.1.200. Available at: <https://journal.embnnet.org/index.php/embnnetjournal/article/view/200>
- Martínez-Castillo, M., Cárdenas-Guerra, R. E., Arroyo, R., Debnath, A., Rodríguez, M. A., Sabanero, M., et al. (2017). NF-GH, a glycosidase secreted by *Naegleria fowleri*, causes mucin degradation: an in vitro and in vivo study. *Future Microbiol.* 12, 781–799. doi: 10.2217/fmb-2016-0230
- McCarthy, C. G. P., and Fitzpatrick, D. A. (2019). Pan-genome analyses of model fungal species. *Microb. Genomics* 5:e000243. doi: 10.1099/mgen.0.000243
- Mesquita, A., Cardenal-Muñoz, E., Dominguez, E., Muñoz-Braceras, S., Nuñez-Corcuera, B., Phillips, B. A., et al. (2017). Autophagy in *Dictyostelium*: mechanisms, regulation and disease in a simple biomedical model. *Autophagy* 13, 24–40. doi: 10.1080/15548627.2016.1226737
- Meysman, P., Sánchez-Rodríguez, A., Fu, Q., Marchal, K., and Engelen, K. (2013). Expression divergence between *Escherichia coli* and *salmonella enterica* serovar typhimurium reflects their lifestyles. *Mol. Biol. Evol.* 30, 1302–1314. doi: 10.1093/molbev/mst029
- Milanes, J. E., Suryadi, J., Abendroth, J., Van Voorhis, W. C., Barrett, K. F., Dranow, D. M., et al. (2019). Enzymatic and structural characterization of the *Naegleria fowleri* Glucokinase. *Antimicrob. Agents Chemother.* 63, e02410–e02418. doi: 10.1128/AAC.02410-18
- Miles, S., Li, L., Davison, J., and Breeden, L. L. (2013). Xbp1 directs global repression of budding yeast transcription during the transition to quiescence and is important for the longevity and reversibility of the quiescent state. *PLoS Genet.* 9:e1003854. Available at: doi: 10.1371/journal.pgen.1003854
- Moseman, E. A. (2020). Battling brain-eating amoeba: enigmas surrounding immunity to *Naegleria fowleri*. *PLoS Pathog.* 16:e1008406. Available at: doi: 10.1371/journal.ppat.1008406
- Moussa, M., De Jonckheere, J. F., Guerlotti, J., Richard, V., Bastaraud, A., Romana, M., et al. (2013). Survey of *Naegleria fowleri* in geothermal recreational waters of Guadeloupe (French West Indies). *PLoS One* 8:e54414. doi: 10.1371/journal.pone.0054414
- Moussa, M., Marcelino, I., Richard, V., Guerlotti, J., and Talarmin, A. (2020). An optimized Most Probable Number (MPN) Method to assess the number of thermophilic free-living amoebae (FLA) in water samples. *Pathogens* 9:409. doi: 10.3390/pathogens9050409
- Ngoot-Chin, T., Zulkifli, M. A., van de Weg, E., Zaki, N. M., Serdari, N. M., Mustaffa, S., et al. (2021). Detection of ploidy and chromosomal aberrations in commercial oil palm using high-throughput SNP markers. *Planta* 253:63. doi: 10.1007/s00425-021-03567-7
- Nicolas, M., De Jonckheere, J. F., Pernin, P., Bataille, H., Le Bris, V., and Herrmann-Storck, C. (2010). Diagnostic moléculaire d'une méningoencéphalite amibienne primitive à l'occasion d'un cas fatal en Guadeloupe. *Bull. la Société Pathol. Exot.* 103, 14–18. doi: 10.1007/s13149-009-0028-1
- Ntefidou, M., and Häder, D.-P. (2005). Photoactivated adenyl cyclase (PAC) genes in the flagellate *Euglena gracilis* mutant strains. *Photochem. Photobiol. Sci.* 4, 732–739. doi: 10.1039/b502002f
- Oppendoes, F. R., De Jonckheere, J. F., and Tielens, A. G. M. (2011). *Naegleria gruberi* metabolism. *Int. J. Parasitol.* 41, 915–924. doi: 10.1016/j.ijpara.2011.04.004
- Pelandakis, M., Serre, S., and Pernin, P. (2000). Analysis of the 5.8S rRNA gene and the internal transcribed spacers in *Naegleria* spp. and in *N. fowleri*. *J. Eukaryot. Microbiol.* 47, 116–121. doi: 10.1111/j.1550-7408.2000.tb00020.x

- Pernin, P., Ataya, A., and Cariou, M. L. (1992). Genetic structure of natural populations of the free-living amoeba, *Naegleria lovaniensis*. Evidence for sexual reproduction. *Heredity (Edinb)*. 68, 173–181. doi: 10.1038/hdy.1992.26
- Peter, J., De Chiara, M., Friedrich, A., Yue, J.-X., Pflieger, D., Bergström, A., et al. (2018). Genome evolution across 1,011 *Saccharomyces cerevisiae* isolates. *Nature* 556, 339–344. doi: 10.1038/s41586-018-0030-5
- Prabakaran, S., Lippens, G., Steen, H., and Gunawardena, J. (2012). Post-translational modification: nature's escape from genetic imprisonment and the basis for dynamic information encoding. *WIREs Syst. Biol. Med.* 4, 565–583. doi: 10.1002/wsbm.1185
- Prijbelski, A., Antipov, D., Meleshko, D., Lapidus, A., and Korobeynikov, A. (2020). Using SPAdes De Novo Assembler. *Curr. Protoc. Bioinforma.* 70:e102. doi: 10.1002/cpbi.102
- Rodriguez-Anaya, L. Z., Félix-Sastré, Á. J., Lares-Villa, F., Lares-Jiménez, L. F., and Gonzalez-Galaviz, J. R. (2021). Application of the omics sciences to the study of *Naegleria fowleri*, *Acanthamoeba* spp., and *Balamuthia mandrillaris*: current status and future projections. *Parasite* 28, 28:36. doi: 10.1051/parasite/2021033
- Rolland, S., Mengue, L., Noël, C., Crapart, S., Mercier, A., Aucher, W., et al. (2020). Encystment induces Down-regulation of an acetyltransferase-like gene in *Acanthamoeba castellanii*. *Pathogens* 9:321. doi: 10.3390/pathogens9050321
- Sandström, G., Saeed, A., and Abd, H. (2011). *Acanthamoeba*-bacteria: a model to study host interaction with human pathogens. *Curr. Drug Targets* 12, 936–941. doi: 10.2174/138945011795677845
- Saran, S., and Schaap, P. (2004). Adenylyl cyclase G is activated by an intramolecular Osmosensor. *Mol. Biol. Cell* 15, 1479–1486. doi: 10.1091/mbc.e03-08-0622
- Sarink, M. J., van der Meijs, N. L., Denzer, K., Koenderman, L., Tielens, A. G. M., and van Hellemond, J. J. (2022). Three encephalitis-causing amoebae and their distinct interactions with the host. *Trends Parasitol.* 38, 230–245. doi: 10.1016/j.pt.2021.10.004
- Shah, S., Chen, Y., Bhattacharya, D., and Chan, C. X. (2020). Sex in Symbiodiniaceae dinoflagellates: genomic evidence for independent loss of the canonical synaptonemal complex. *Sci. Rep.* 10:9792. doi: 10.1038/s41598-020-66429-4
- Sibbald, S. J., Eme, L., Archibald, J. M., and Roger, A. J. (2020). Lateral gene transfer mechanisms and Pan-genomes in eukaryotes. *Trends Parasitol.* 36, 927–941. doi: 10.1016/j.pt.2020.07.014
- Siddiqui, R., Ali, I. K. M., Cope, J. R., and Khan, N. A. (2016). Biology and pathogenesis of *Naegleria fowleri*. *Acta Trop.* 164, 375–394. doi: 10.1016/j.actatropica.2016.09.009
- Simão, F. A., Waterhouse, R. M., Ioannidis, P., Kriventseva, E. V., and Zdobnov, E. M. (2015). BUSCO: assessing genome assembly and annotation completeness with single-copy orthologs. *Bioinformatics* 31, 3210–3212. doi: 10.1093/bioinformatics/btv351
- Snipen, L., and Liland, K. H. (2015). Micropan: an R-package for microbial pan-genomics. *BMC Bioinformatics* 16:79. doi: 10.1186/s12859-015-0517-0
- Sohn, H. J., Kim, J. H., Shin, M. H., Song, K. J., and Shin, H. J. (2010). The Nf-actin gene is an important factor for food-cup formation and cytotoxicity of pathogenic *Naegleria fowleri*. *Parasitol. Res.* 106, 917–924. doi: 10.1007/s00436-010-1760-y
- Su, G., Morris, J. H., Demchak, B., and Bader, G. D. (2014). Biological network exploration with Cytoscape 3. *Curr. Protoc. Bioinforma.* 47, 8.13.1–8.13.24. doi: 10.1002/0471250953.bi0813s47
- Swart, A. L., Harrison, C. F., Eichinger, L., Steinert, M., and Hilbi, H. (2018). *Acanthamoeba* and *Dictyostelium* as cellular models for legionella infection. *Front. Cell. Infect. Microbiol.* 8:61. doi: 10.3389/fcimb.2018.00061
- Szklarczyk, D., Gable, A. L., Lyon, D., Junge, A., Wyder, S., Huerta-Cepas, J., et al. (2019). STRING v11: protein-protein association networks with increased coverage, supporting functional discovery in genome-wide experimental datasets. *Nucleic Acids Res.* 47, D607–D613. doi: 10.1093/nar/gky1131
- Tarailo-Graovac, M., and Chen, N. (2009). Using RepeatMasker to identify repetitive elements in genomic sequences. *Curr. Protoc. Bioinforma.* 25:4.10.1-4.10.14. doi: 10.1002/0471250953.bi0410s25
- Tekle, Y. I., Wang, F., Tran, H., Hayes, T. D., and Ryan, J. F. (2022). The draft genome of *Cochliopodium minus* reveals a complete meiosis toolkit and provides insight into the evolution of sexual mechanisms in Amoebozoa. *Sci. Rep.* 12:9841. doi: 10.1038/s41598-022-14131-y
- Tekle, Y. I., Wood, F. C., Katz, L. A., Cerón-Romero, M. A., and Gorf, L. A. (2017). Amoebozoans are secretly but ancestrally sexual: evidence for sex genes and potential novel crossover pathways in diverse groups of amoebae. *Genome Biol. Evol.* 9, evx002–evx387. doi: 10.1093/gbe/evx002
- Tettelin, H., Massignani, V., Cieslewicz, M. J., Donati, C., Medini, D., Ward, N. L., et al. (2005). Genome analysis of multiple pathogenic isolates of *Streptococcus agalactiae*: implications for the microbial pan-genome. *Proc. Natl. Acad. Sci.* 102, 13950–13955. doi: 10.1073/pnas.0506758102
- Trabelsi, H., Dendana, F., Sellami, A., Sellami, H., Cheikhrouhou, F., Neji, S., et al. (2012). Pathogenic free-living amoebae: epidemiology and clinical review. *Pathol. Biol.* 60, 399–405. doi: 10.1016/j.patbio.2012.03.002
- Uzuka, A., Kobayashi, Y., Onuma, R., Hirooka, S., Kanasaki, Y., Yoshikawa, H., et al. (2019). Responses of unicellular predators to cope with the phototoxicity of photosynthetic prey. *Nat. Commun.* 10:5606. doi: 10.1038/s41467-019-13568-6
- Velle, K. B., and Fritz-Laylin, L. K. (2020). Conserved actin machinery drives microtubule-independent motility and phagocytosis in *Naegleria*. *J. Cell Biol.* 219:e202007158. doi: 10.1083/jcb.202007158
- Wang, K., Singh, D., Zeng, Z., Coleman, S. J., Huang, Y., Savich, G. L., et al. (2010). MapSplice: accurate mapping of RNA-seq reads for splice junction discovery. *Nucleic Acids Res.* 38:e178. doi: 10.1093/nar/gkq622
- Xu, X., Pan, M., and Jin, T. (2021). How phagocytes acquired the capability of hunting and removing pathogens from a human body: lessons learned from chemotaxis and phagocytosis of *Dictyostelium discoideum* (review). *Front. Cell Dev. Biol.* 9:724940. doi: 10.3389/fcell.2021.724940
- Yi, D.-G., and Huh, W.-K. (2015). UDP-glucose pyrophosphorylase Ugp1 is involved in oxidative stress response and long-term survival during stationary phase in *Saccharomyces cerevisiae*. *Biochem. Biophys. Res. Commun.* 467, 657–663. doi: 10.1016/j.bbrc.2015.10.090
- Žárský, V., Klimeš, V., Pačes, J., Vlček, Č., Hradilová, M., Beneš, V., et al. (2021). The *Mastigamoeba balamuthi* genome and the nature of the free-living ancestor of Entamoeba. *Mol. Biol. Evol.* 38, 2240–2259. doi: 10.1093/molbev/msab020
- Zysset-Burri, D. C., Müller, N., Beuret, C., Heller, M., Schürch, N., Gottstein, B., et al. (2014). Genome-wide identification of pathogenicity factors of the free-living amoeba *Naegleria fowleri*. *BMC Genomics* 15:496. doi: 10.1186/1471-2164-15-496



## OPEN ACCESS

## EDITED BY

Christopher A. Rice,  
Purdue University, United States

## REVIEWED BY

Bharath Kanakapura Sundararaj,  
Boston University, United States  
Vincent Delafont,  
University of Poitiers, France  
Wayne Heaselgrave,  
University of Wolverhampton, United Kingdom

## \*CORRESPONDENCE

Mingguang Li  
✉ mgl1800@jimu.edu.cn

## SPECIALTY SECTION

This article was submitted to  
Infectious Agents and Disease,  
a section of the journal  
Frontiers in Microbiology

RECEIVED 18 January 2023

ACCEPTED 21 March 2023

PUBLISHED 05 April 2023

## CITATION

Wang Y, Jiang L, Zhao Y, Ju X, Wang L, Jin L,  
Fine RD and Li M (2023) Biological  
characteristics and pathogenicity  
of *Acanthamoeba*.  
*Front. Microbiol.* 14:1147077.  
doi: 10.3389/fmicb.2023.1147077

## COPYRIGHT

© 2023 Wang, Jiang, Zhao, Ju, Wang, Jin, Fine  
and Li. This is an open-access article  
distributed under the terms of the [Creative  
Commons Attribution License \(CC BY\)](#). The  
use, distribution or reproduction in other  
forums is permitted, provided the original  
author(s) and the copyright owner(s) are  
credited and that the original publication in this  
journal is cited, in accordance with accepted  
academic practice. No use, distribution or  
reproduction is permitted which does not  
comply with these terms.

# Biological characteristics and pathogenicity of *Acanthamoeba*

Yuehua Wang<sup>1</sup>, Linzhe Jiang<sup>2</sup>, Yitong Zhao<sup>1</sup>, Xiaohong Ju<sup>1</sup>,  
Le Wang<sup>3</sup>, Liang Jin<sup>3</sup>, Ryan D. Fine<sup>4</sup> and Mingguang Li<sup>1\*</sup>

<sup>1</sup>College of Laboratory Medicine, Jilin Medical University, Jilin City, China, <sup>2</sup>General Surgery, Jilin People's Hospital, Jilin City, China, <sup>3</sup>Department of Laboratory Medicine, Jilin Hospital of Integrated Chinese and Western Medicine, Jilin City, China, <sup>4</sup>Center for Human Genetics and Genomics, New York University Grossman School of Medicine, New York City, NY, United States

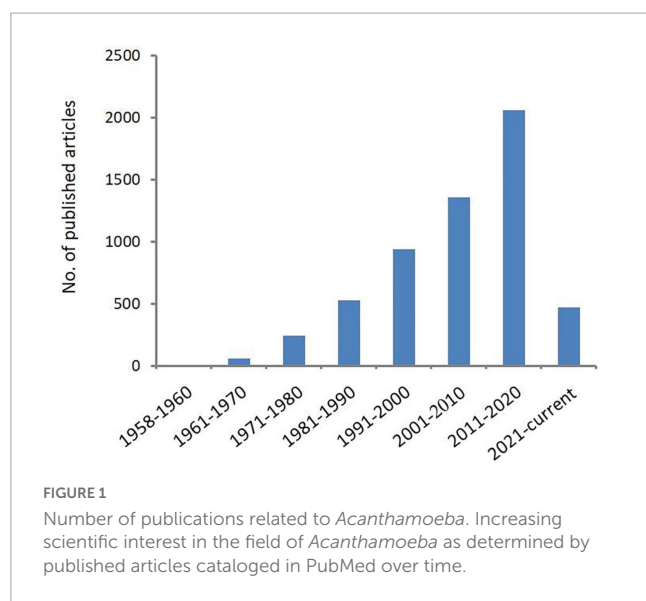
*Acanthamoeba* is an opportunistic protozoa, which exists widely in nature and is mainly distributed in soil and water. *Acanthamoeba* usually exists in two forms, trophozoites and cysts. The trophozoite stage is one of growth and reproduction while the cyst stage is characterized by cellular quiescence, commonly resulting in human infection, and the lack of effective monotherapy after initial infection leads to chronic disease. *Acanthamoeba* can infect several human body tissues such as the skin, cornea, conjunctiva, respiratory tract, and reproductive tract, especially when the tissue barriers are damaged. Furthermore, serious infections can cause *Acanthamoeba* keratitis, granulomatous amoebic encephalitis, skin, and lung infections. With an increasing number of *Acanthamoeba* infections in recent years, the pathogenicity of *Acanthamoeba* is becoming more relevant to mainstream clinical care. This review article will describe the etiological characteristics of *Acanthamoeba* infection in detail from the aspects of biological characteristic, classification, disease, and pathogenic mechanism in order to provide scientific basis for the diagnosis, treatment, and prevention of *Acanthamoeba* infection.

## KEYWORDS

*Acanthamoeba*, biological characteristics, classification, disease, pathogenesis

## 1. Introduction

*Acanthamoeba* is an opportunistic protozoa that is widely distributed in the natural environment, such as sea water, swimming pools, tap water, natural thermal water, soil, dust, and even the nasal mucosa of healthy individuals (Rivera et al., 1989, 1991; Michel et al., 1994; Tawfeek et al., 2016; Lass et al., 2017; Carnt et al., 2020; Wopereis et al., 2020). Pathogenic species can cause serious blindness in humans, arising from *Acanthamoeba* keratitis (AK) and rare granulomatous amoebic encephalitis (GAE) as well as skin and lung infections. Cases of AK and GAE were first reported by Fowler and Carter (1965) and by Naginton et al. (1974), respectively. The epidemiological investigation shows that the number of *Acanthamoeba* infection is increasing year by year, especially those with AK infection. In the United States, a study examining AK at thirteen ophthalmology centers and laboratories found that over the course of 2004–2007, a precipitous increase in AK cases had occurred: 22 cases were diagnosed in 1999, 43 cases were diagnosed in 2003, and 170 cases were diagnosed in 2007 (Yoder et al., 2012). In the UK, the numbers of AK cases diagnosed annually at the Moorfields Eye Hospital in London from 2011 to 2014 (range of 36–65 cases/year) were



approximately two-to-three times higher than in 2004–2010 (range of 15–23 cases per year) (Carnt et al., 2018). In Australia, a study from the quaternary referral center in Sydney found that over the period from 2002 to 2016, the average annual number of cases was 50% higher post-2007 relative to pre-2007, and the highest numbers of cases were reported in 2007 and 2014 (Höhlhumer et al., 2020). Studies found that wearing corneal contact lenses is the main risk factor for infection (Lindsay et al., 2007; Carnt and Stapleton, 2016; Dos Santos et al., 2018). With the increase of *Acanthamoeba* infection especially AK infection in recent years, scholars have begun expending extensive effort in characterizing and classifying the *Acanthamoeba* genus, as shown in Figure 1. This article summarizes the breadth of this work in order to provide scientific basis for the diagnosis, treatment, and prevention of *Acanthamoeba* infection.

## 2. Biological characteristics

### 2.1. Life history of *Acanthamoeba*

In general, the life cycle of *Acanthamoeba* consists of two stages, trophozoite and cyst (Marciano-Cabral and Cabral, 2003; Siddiqui and Khan, 2012; Siddiqui et al., 2012), except for *Acanthamoeba* pyriformis, which is recognized to include facultative sporocarp fruiting in its life cycle (Tice et al., 2016). The trophozoite stage dominates when the growth conditions are suitable, such as abundant food supply, neutral pH, appropriate temperature (i.e., 30°C) and osmolarity between 50 and 80 mOsmol (Siddiqui et al., 2012). The cell cycle of *Acanthamoeba* consists of growth and replication, which is carried out through mitosis under optimal living conditions (Band et al., 1970; Byers et al., 1991; Quinet et al., 2020). In axenic cultures, *Acanthamoeba* exhibits a typical exponential growth phase, followed by a period of reduced growth rate, and finally stationary phase during which no further increase in cell density occurs (Band and Mohrlok, 1973; Stevens and Pachler, 1973). Studies have revealed that the majority of *Acanthamoeba* cells in stationary phase culture

develop into quiescent cysts in response to adverse conditions such as lack of food, hyper- or hypo-osmolarity, extremes in temperature and pH, high cell densities, and chemicals (Neff and Neff, 1969; Band and Mohrlok, 1973; Weisman, 1976; Stohr et al., 1987; Sriram et al., 2008). The trophozoites of *Acanthamoeba* mainly feed on bacteria, algae, yeast, or small organic particles via phagocytosis or pinocytosis and form many food vacuoles in the cytoplasm (Bowers, 1977; Bowers and Olszewski, 1983; Marciano-Cabral and Cabral, 2003). Pinocytosis is considered to be non-specific endocytosis (Bowers and Olszewski, 1972), while phagocytosis is considered to be receptor-dependent endocytosis (Alsam et al., 2005a). Once *Acanthamoeba* cells enter stationary phase, phagocytic activity ceases, while pinocytic activity is halved. The reduced pinocytic activity remains sensitive to respiratory inhibitors. The unequal responses of phagocytosis and pinocytosis to the onset of stationary-phase growth suggest that they are independent processes subject to different controls (Chambers and Thompson, 1976).

During the stationary phase shift, cysts begin to form with minimal metabolic activity (Siddiqui and Khan, 2012). Early in encystation, large numbers of vacuoles are observed in the encysting cells and many lysosomes and peroxisomes are present in the mature cysts (Müller, 1969; Müller and Moller, 1969; Siddiqui et al., 2012). Bowers and Olszewski (1983) showed that *Acanthamoeba* have the ability to distinguish vacuoles containing digestible and indigestible particles. For example, when cells were allowed to phagocytose yeast to capacity, endocytosis stopped and subsequent presentation of particles (either yeast or beads) did not result in further uptake. By contrast, when cells were allowed to phagocytose plastic beads to capacity and a second dose of particles was presented (either yeast or beads), the cells exocytosed the internal particles and took up the new ones. Therefore, the fate of vacuoles containing yeast and vacuoles containing plastic beads in encystation is different (Bowers and Olszewski, 1983). The digestive vacuoles disappear during later stages of encystation and their contents are discharged. This phenomenon explains the weakening of phagocytic activity and pinocytic activity in this period. Cysts are highly tolerant to the extreme environmental conditions, which allows *Acanthamoeba* to spread in the environment and/or carry these pathogens into host species, which is described later in the text.

### 2.2. The morphological structure of *Acanthamoeba*

#### 2.2.1. Trophozoite

The trophozoite varies in size from 25 to 40 µm in diameter (Marciano-Cabral and Cabral, 2003) and has a long oval or irregular shape. The cytoplasmic boundary of trophozoite is unclear and the endoplasm is granular, which emits several acicular or spinous pseudopods extending to the whole surface of the cell (Figure 2A). The pseudopods give the trophozoite a characteristic appearance and participate in the feeding and movement of *Acanthamoeba*. Pseudopods in *Acanthamoeba* have a peculiar form. The term “acanth” is a Greek word meaning “spike” to indicate the presence of spine-like structures (also known as acanthopods) on the surface of the amoeba (Preston and King, 1984; Preston et al., 2001;



Marciano-Cabral and Cabral, 2003). Pseudopods are responsible for adhesion to the surface of contact lenses, increasing the chance of *Acanthamoeba* infection in the cornea (John et al., 1989; Omaña-Molina et al., 2014). The trophozoite is typically uninucleate with a nucleus that is approximately one sixth the size of the cell body, but multinucleated individuals can be seen in laboratory cultures when grown with constant agitation (Byers and James, 1967). To some extent, this phenomenon reflects the real living condition of *Acanthamoeba* in nature because the existence of *Acanthamoeba* can often be found in an aquatic environment. Any flux perturbations, such as water currents or waves, might detach amoebae from their substrate and suspend them in the water in a non-adherent state, which creates conditions for the formation of multinucleation. This process will help amoebae to colonize new environmental niches that are difficult to reach using an adherent state. When adhesion is restored, multinucleated amoebae generate a higher progeny population compared to uninucleate mother cells. This process is beneficial from the point of view of continual population reproduction (Quinet et al., 2020). The nuclear envelope is separated by a distance of about 350 Å with numerous nuclear pores (Bowers and Korn, 1968). Chromatin is located on the inner surface of the nuclear envelope. The nucleolus is perhaps the most striking feature appearing large and dense and surrounded by a unique zona pellucida (Pussard and Pons, 1977). In the trophozoite stage, *Acanthamoeba* does not differ greatly at the internal structural level from a mammalian cell. It also contains various cell organelles such as mitochondria, ribosomes, centrosome, Golgi apparatus, and vacuoles (Bowers and Korn, 1968; Figure 2B). Vacuoles are conspicuous elements in trophozoite. They exist mainly in two separate systems: one is the contractile vacuole, involved in cellular osmotic regulation (Kitching, 1967) and the other is the digestive vacuole involved in the decomposition of intake particles (Kitching, 1956). Contractile vacuoles are periodically expelled and then refilled in a specific manner, ranging in size from 0.1 µm in diameter to larger than the nucleus. Multiple small vacuoles fuse together to form large vacuoles, which are morphologically akin to digestive vacuoles (Bowers and Korn, 1968). The contractile vacuole can be distinguished from a digestive vacuole by the absence of flocculent content when examined by electron microscopy (Bowers and Korn, 1968). In addition to contractile vacuoles and digestive vacuoles, other types of vacuoles can also be observed in the cytoplasm such as lysosomes and a large number of glycogen-containing vacuoles (Bowers and Korn, 1973; Siddiqui and Khan, 2012).

### 2.2.2. Cyst

There can be a lot of variability in cyst shape, most cysts are round and the diameter is about 13–20 µm (Bowers and Korn, 1969). Unlike trophozoites, the cyst has a double-layer cell wall, which gives cysts strong resistance to many harsh environmental conditions (Figure 2C). The outer layer consists of a laminar fibrous layer also known as an ectocyst, while the inner layer is made up of fine fibers also known as an endocyst. The ectocyst is the first to be synthesized in the encysting cells and appears as an amorphous discontinuous layer just outside the plasma membrane (Bowers and Korn, 1969). The ectocyst terminates in a loose fibrous layer and the entire ectocyst is 0.3–0.5 µm in thickness. The endocyst differs from the ectocyst in texture and appears finely granular. The fibrils of both the ectocyst and the endocyst appear

to be less than 50 Å in diameter. When the cysts are fully mature, a space of about 0.1 µm is formed between the endocyst and the plasma membrane (Bowers and Korn, 1969).

The cyst wall of cyst forming protozoa is generally composed of chitin, while *Acanthamoeba* is an exception and includes both chitin and cellulose (Linder et al., 2002; Derda et al., 2009). Cellulose becomes the main component of the endocyst, accounting for about one third of the cyst wall (Tomlinson and Jones, 1962). However, it is not clear where chitin exists in ectocyst or endocyst. Cellulose is basically a straight chain polymer of β-1, 4 linked D-glucose units which are arranged in alternate orientation with respect to one another (Béguin and Aubert, 1994; Lakhundi et al., 2015). It is with no coiling and rod-like conformation that provokes spontaneous crystallization of the molecule (Schwarz, 2001). An exceptional feature of cellulose that is also relatively unusual in the polysaccharide world is its crystalline structure (Brown and Saxena, 2000; Lynd et al., 2002). Approximately 30 individual molecules of cellulose are assembled into larger units called elementary fibrils (protofibrils), which in turn are packed into larger units called microfibrils (Brown and Saxena, 2000; Lynd et al., 2002). The chains in the microfibrils are held together by hydrogen bonds giving them a high tensile strength. It is this inter- and intrachain hydrogen bonding between multiple parallel layers of cellulose that results in the formation of tightly packed microfibrils. The microfibrils then associate into crystalline cellulose fibers. The organization of individual microfibrils in crystalline cellulose is such that the component molecules are packed tightly enough to prevent penetration by enzymes. In addition, cellulose also contains various irregularities such as twists or voids, surface micropores, large pits and capillaries etc., increasing the total surface area much larger than that of an ideally smooth fiber of the same dimensions (Blouin et al., 1970; Cowling, 1975; Fan et al., 1980; Lynd et al., 2002). Overall, cellulose imparts high tensile strength to the wall it is contained in, serving as a structural component. It is an extracellular polysaccharide and is a part of the cell wall in plants, algae, bacteria, slime mold *Dictyostelium* and other protists such as the *Acanthamoeba* cyst wall (Schramm and Hestrin, 1954; Cook and Colvin, 1980; Williams and Cannon, 1989; Bishop et al., 2002). Given the structure of cellulose, it practically makes it impossible for an enzyme to clasp cellulose into a substrate site. Hence there is only a single enzyme to hydrolyze cellulose. This, together with its association with other polymers, makes cellulose containing material withstand harsh conditions making it hardy and resistant to degradation, hence its role as a structural and protective barrier.

The change of environmental factors is an important link in the transformation of trophozoites into cysts. Cyst formation occurs under adverse environmental conditions such as glucose deficiency, dryness, extreme temperature, and non-neutral pH environments (Bowers and Korn, 1969; Chagla and Griffiths, 1974; Byers et al., 1980). Even more notable is the durability of cysts with one study noting that cysts can grow after 21 years even in a completely dry environment while another conversely showed cysts surviving in water at 4°C for more than 24 years (Mazur et al., 1995; Sriram et al., 2008). Cysts have been shown to be resistant to fungicides, chlorinating agents, and antibiotics (De Jonckheere and van de Voorde, 1976; Khunkitti et al., 1998; Turner et al., 2000; Lloyd et al., 2001). However, chloroquine effectively inactivated the cells in a

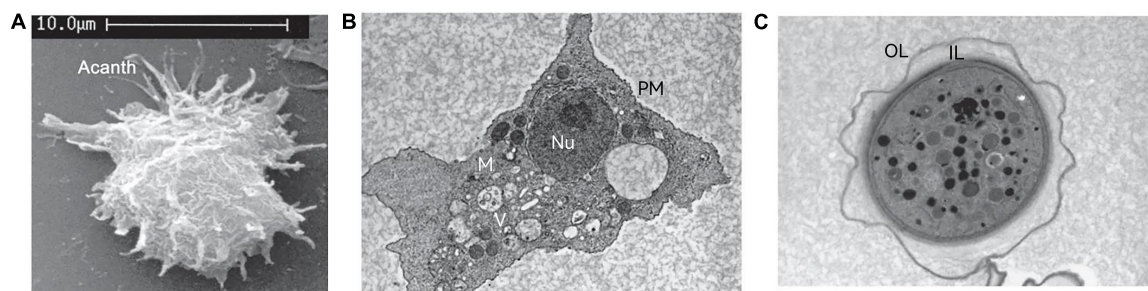


FIGURE 2

The structure of *Acanthamoeba*. (A) Scanning electron micrograph of an *Acanthamoeba* trophozoite showing many spinous pseudopods around the whole surface of the cell. Acanth, acanthopod. (B) Transmission electron micrograph of the trophozoite stage of *Acanthamoeba*. Nu, nucleus; V, vacuoles; M, mitochondria; PM, plasma membrane. (C) Transmission electron micrograph of an *Acanthamoeba* cyst. OL, outer layer; IL, inner layer. These pictures are from the work of Siddiqui et al. (2012).

dose-dependent manner during encystation (Jha et al., 2014). This result indicates that there is a potential target of chloroquine in the process of encystation, while also suggesting the importance of timing for the treatment of *Acanthamoeba* infection.

The viability and virulence of 17 *Acanthamoeba* isolates after they have been stored in water at 4°C for a period of 24 years was determined, and 3 of them were found inactivated. The remaining 14 isolates after inoculation on non-nutrient agar (NNA) gave rise to new subculture. Due to the low number of viable cysts (0–5%) measured by eosin exclusion, most of the cells entered the trophozoite stage. These results revealed the resistance and viability of *Acanthamoeba* in long term storage (Mazur et al., 1995). Separate groups of mice were inoculated intranasally with 10 subcultures characterized by varying primary virulence. In 8 groups, the mice were successfully infectious (at varying degree), and some of the mice succumbed to disease, indicating that even after 24 years, some of strains still keep very high virulence. Interestingly, however, some of the examined isolates completely lost their virulence only after 8 years of cultivation. On the basis of these results, we can assume in the environment that the period of viability for a cyst may be at least 25 years, and, more importantly, some of them still maintain high virulence (Mazur et al., 1995). It is this durability of cysts to the external environment and drugs that makes the treatment of *Acanthamoeba* infection particularly difficult. However, a 0.02% polyhexamethyl biguanide (PHMB) solution can be used as a first line of defense topical therapy for AK (Schuster and Visvesvara, 2004; Oldenburg et al., 2011; Carrijo-Carvalho et al., 2017) and is recommended by the leading national public health organizations in the USA (Centers for Disease Control and Prevention, 2020). A recent phase I study of human subjects has shown general tolerance to higher concentrations of PHMB, which makes it possible to treat deep stromal invasion of AK (Papa et al., 2022). PHMB 0.08% monotherapy is being further explored in a phase III randomized control trial for AK (ClinicalTrials.gov/NCT03274895, National Library of Medicine, 2020).

## 2.2.3. Encystation

### 2.2.3.1. Cellulose and encystation

Encystation is an essential biological process for survival of cyst forming protozoa (Eichinger, 2001). In the process, *Acanthamoeba*

undergoes drastic changes in gene expression to adapt to the new environment (Moon et al., 2009b, 2011b; Bernard et al., 2022). The most prominent characterization is the formation of cyst wall, which serves as a shelter under stressful external conditions (Marciano-Cabral and Cabral, 2003; Turner et al., 2004). The cyst wall contains at least 2 major products that are not detected in the trophozoite stage; cellulose (Tomlinson and Jones, 1962) and an acid-insoluble protein-containing material (Neff and Neff, 1969).

As described above, cellulose constitutes a major component of the *Acanthamoeba* defense system during encystation. The precursor of cellulose is glucose that is incorporated into the cell wall as  $\beta$  (1, 4)-glucans (Weisman, 1976). *Acanthamoeba* stores glucose in the form of glycogen in the active growth stage and degrades it to form glucose during the process of encystation before final conversion into cellulose (Weisman et al., 1970; Potter and Weisman, 1971; Stewart and Weisman, 1974). It has been demonstrated that glycogen is the most rapidly degraded macromolecule during the initial phase of *Acanthamoeba* encystation (Bowers and Korn, 1969; Weisman et al., 1970). Glycogen is broken down into glucose via glycogen phosphorylase (Lorenzo-Morales et al., 2008; Moon and Kong, 2012). This was demonstrated by gene silencing of glycogen phosphorylase, which prevented *Acanthamoeba* from forming a double-layered cyst wall (Lorenzo-Morales et al., 2008). There has been some debate about cellulose existing only in the endocyst (Tomlinson and Jones, 1962). However, a recent study by Garajová et al. (2019) revealed cellulose fibers through several electron microscopy methods and observed cellulose in the outer layer. *Acanthamoeba* transfected with siRNA of glycogen phosphorylase can still form outer layer of cyst wall during encystation, which may be due to the differences in the mechanisms that provide glucose for the synthesis of polysaccharides in the inner and outer cyst wall layers. It may also be attributed to the fact that the lack of cellulose is not enough to hinder the formation of the basic structure of outer layer because the main components of the ectocyst are proteins (Barrett and Alexander, 1977; Dudley et al., 2009). However, no matter what, the fact that glycogen phosphatase is required for cyst wall assembly, mainly the cell wall inner layer, has been demonstrated (Lorenzo-Morales et al., 2008). The gene expression level of glycogen phosphorylase also gradually increases during cyst formation and has been shown to reach a maximum at day 3

(10.3 times) (Moon and Kong, 2012). After glycogen breakdown, glucose is then converted to cellulose by the enzyme cellulose synthase (Delmer and Amor, 1995). Targeting cellulose synthase by siRNA has been shown to significantly inhibit the formation of mature cysts (Aqeel et al., 2013; Moon et al., 2014). The sturdy nature of *Acanthamoeba* cysts is attributed, in part, to cellulose (Potter and Weisman, 1972), but other polysaccharides (such as xylose, galactose, and mannose) may also be involved (Dudley et al., 2009). The analysis of cyst walls of *Acanthamoeba castellanii*, using gas chromatography/mass spectrometry (GC/MS) revealed that xylose (in addition to  $\beta$ -1, 4-glucan-forming cellulose) was another important component of the cyst wall (Dudley et al., 2009). Xylose isomerase is involved in the intracellular transformation of xylose. Xylose isomerase, also known as glucose isomerase, catalyzes the reversible isomerization of xylose into xylulose and glucose into fructose (Lee et al., 1990). An siRNA against xylose isomerase and its exogenous inhibitor, sorbitol, blocked *A. castellanii* encystation, suggesting that xylose isomerase plays an important role in amoebae differentiation (Aqeel et al., 2013). Aqeel et al. (2013) proposed that xylose biosynthesis could replace cellulose biosynthesis, resulting in hemicellulose entering the cyst wall and forming immature cysts. However, Moon et al. (2014) showed that cellulose synthetase and xylose isomerase were expressed independently in encysting *Acanthamoeba*, and that one cannot replace each other. Therefore, how xylose isomerase interferes with cyst wall formation leading to reduced encystation in *A. castellanii* needs to be further studied.

### 2.2.3.2. Autophagy and encystation

Autophagy is a degradative pathway necessary for the clearance of damaged or superfluous proteins and organelles and the recycling of intracellular constituents as well as providing energy during periods of unfavorable environments such as under nutrient-limiting conditions (Huang and Klionsky, 2002; Xie and Klionsky, 2007). Autophagy starts with the formation of a double-layered membrane, called a phagophore, which recruits proteins and lipids into a presumed membrane structure known as the pre-autophagosomal structure (PAS) through a series of reactions involving autophagy (Atg) proteins (Kim et al., 2002; Suzuki et al., 2002). The phagophore is enlarged and then forms an autophagosome that encloses the cytosolic components and organelles including mitochondria and endosomes (Ishihara et al., 2001; Reggiori et al., 2005). Thereafter, mature autophagosomes fuse with lysosomes and their contents are degraded (Nakatogawa, 2020).

The formation of autophagosome involves two ubiquitin like conjugation systems (UBL); Atg8 and Atg12 systems (Ohsumi and Mizushima, 2004). In the Atg8 conjugation system, Atg8 is cleaved at the C-terminal end by a cysteine protease, Atg4, producing Atg8<sup>Gly-116</sup> (Kirisako et al., 2000). It is then transferred to Atg3, an E2-like enzyme, after being activated by Atg7, an E1-like enzyme (Ichimura et al., 2000, 2004). Finally, Atg3 conjugates Atg8 with phosphatidylethanolamine (PE) (Ichimura et al., 2000), anchoring Atg8 to the autophagosome membrane. In the Atg12 conjugation system, the C-terminal glycine residue of Atg12 is activated by Atg7, an E1-like enzyme, transferred to Atg10, an E2-like enzyme, and conjugated to Atg5 covalently (Geng and Klionsky, 2008). The Atg12-Atg5 conjugate which has E3-like activity promotes the elongation of the autophagosomal membrane

by forming a multimeric complex with Atg16 (Hanada et al., 2007; Yang and Klionsky, 2009). Later studies have found that Atg12-Atg5 conjugates directly activate E2 enzyme activity of Atg3 to promote conjugation of Atg8 to phosphatidylethanolamine (Sakoh-Nakatogawa et al., 2013), indicating that two UBL systems are not completely independent in mediating autophagy.

The Atg8 and Atg12 UBL systems are well conserved in *A. castellanii* (Moon et al., 2011a; Song et al., 2012). The mediation of Atg8 and Atg12 systems in the autophagy process during encystation has been identified and autophagy proteins including Atg3, Atg8, Atg8b (isoform of Atg8), Atg12 and Atg16 have been characterized (Moon et al., 2009a, 2011a, 2013; Song et al., 2012; Kim et al., 2015). The mRNA expression level of Atg8, Atg8b, and Atg16 are highly induced during encystation (Moon et al., 2009a, 2013; Song et al., 2012). However, the transcriptional level of Atg3 and Atg12 did not change markedly in both trophozoites and cysts (Moon et al., 2011a; Kim et al., 2015). Therefore, it can be speculated that Atg3 and Atg12 proteins are used in the form of recycling during encystation. The discrepancy on gene expression does not cast their role in encystation into doubt since siRNA against the respective genes inhibited cyst formation effectively. Atg3, which is uniformly distributed in trophozoite cells, aggregates around the autophagosomal membrane in encystation and shows an activity for Atg8 lipidation (Moon et al., 2009a). As mentioned above, ATG8 is one of the ubiquitin-like proteins required for autophagosome formation. PE conjugated ATG8 is tightly bound to the autophagosome membrane and participates in autophagy (Moon et al., 2009a). Complete inhibition of encystation was not achieved in *Acanthamoeba* transfected with siRNA against Atg8, which suggests that an Atg8 isoform such as Atg8b exists (Moon et al., 2013). Both Atg8 and Atg8b were highly expressed during encystation, probably because they were needed to enable the establishment of autophagy rapidly. Atg12 together with Atg16 constituted another UBL system related to autophagy (Song et al., 2012) and the knockdown of Atg12 or Atg16 showed ultrastructural changes of the cyst. The main features of Atg12-knockdown cells are the absence of maturation of cyst wall, decrease in autophagic structures, and vacuolization (Kim et al., 2015). The ultrastructural characteristics of Atg16-knockdown cells showed that many mitochondria were still undigested and these cells are prevented from forming mature cysts, which supports the view that autophagy is necessary for the effective degradation of mitochondria during encystation in *Acanthamoeba* (Song et al., 2012).

Proteases from various protozoan parasites have been characterized at the molecular and cellular levels (Klemba and Goldberg, 2002). Comparative microarray analysis of trophozoite and cyst showed high expression of cysteine in the cyst stage (282-fold change) (Moon et al., 2011b), suggesting a pivotal role of this protease in the cyst formation. Because of its high expression in cysts, people named the gene cyst specific cysteine protease (CSCP). During encystation, CSCP showed colocalization with LysoTracker, an autophagosome marker. *Acanthamoeba* transfected with siRNA against CSCP was unable to form mature cysts and the undigested mitochondria in vacuole-like structures were observed in CSCP siRNA treated cells (Moon et al., 2012b). Mitochondria are a major target of autophagy in *Acanthamoeba*, as compared with trophozoites, the number of mitochondria left in mature cysts is significantly reduced (Moon et al., 2012b).



To degrade a large number of mitochondria, various types of autophagy may be needed. As mentioned above, Atg16, as an important component of Atg 12 UBL system, together with CSCP involved in the degradation of mitochondria during encystation. Further studies need to clarify the possible interaction between these two proteins in this regulatory process.

The encystation of *Acanthamoeba* was inhibited by the serine protease inhibitor phenylmethanesulfonyl fluoride, indicating that serine protease was also involved in encystation (Moon et al., 2008b). To confirm the role of encystation-mediating serine protease (EMSP) during encystation of *Acanthamoeba*, a gene silencing assay was performed and showed that the formation of mature cysts was almost completely inhibited in EMSP siRNA-transfected cells. Additionally, both gene and protein expression of EMSP are highly induced during encystation (Moon et al., 2008b). However, the increased gene level of EMSP during encystation was not revealed by comparative microarray analysis of trophozoite and cyst (Moon et al., 2011b). This may be due to the inconsistency of sample collection timing in the process of encystation or the use of different strains, *A. healyi* instead of *A. castellanii*. The protein turnover during *Acanthamoeba* encystation has also been studied by two-dimensional gel electrophoresis (2DE). The results showed that protein degradation mainly occurred early in the process and these changes could be significantly inhibited specifically by cysteine protease inhibitors. The conclusion is that the encystation process in *A. castellanii* is of a bipartite nature consisting of an initial phase of protein degradation by a cysteine protease and the late stage accompanied by the expression of cyst-specific gene expression (Leitsch et al., 2010).

### 2.2.3.3. Other factors of encystation

A cDNA fragment containing a member of the sirtuin family of proteins was found in a comparative microarray analysis of trophozoites and cysts (Moon et al., 2011b). Sirtuins are a silent-information regulator 2 (SIR2)-like family of protein deacetylases that require nicotinamide adenine dinucleotide (NAD<sup>+</sup>) as a cofactor in the deacetylation reaction (Sauve et al., 2001). The Sir2 homolog of *A. castellanii* (AcSir2) contains the YEATS domain which recognizes and binds acetylated lysine followed by a Sir2 catalytic domain. Nuclear extracts of AcSir2-overexpressing cells also exhibit NAD<sup>+</sup> dependent deacetylase activity (Joo et al., 2020). The overexpression of AcSir2 converted cells into mature cysts more rapidly while the encystation of *A. castellanii* was suppressed by treatment with salermide, a sirtuin inhibitor. The transcription of cellulose synthase was induced in AcSir2 overexpressing cells while the transcription was completely abolished in salermide-treated cells (Joo et al., 2020), which indicated that cellulose synthesis may serve as a potential target of Sir2. The same group also found that AcSir2 promotes encystation by increasing the expression of cyst-specific cysteine protease (CSCP). Sirtinol, another Sir2 inhibitor, suppresses CSCP transcription, suggesting that the undegraded organelles and large molecules remained in sirtinol-treated cells during encystation (Joo et al., 2022). In *Saccharomyces cerevisiae*, SIR2 levels increase during calorie restriction (Lin et al., 2000), and sirtuin overexpression is known to extend the lifespan by silencing HML and HMR loci and inhibiting the formation of extrachromosomal rDNA circles (Sinclair and Guarente, 1997; Kaeberlein et al., 1999). Therefore, it was proposed that Sirtuins may be involved in all cell survival events related

to metabolic reduction caused by nutritional deficiency, including *Acanthamoeba* encystation.

Bernard et al. (2022) studied the regulation of transcription, protein and phosphoprotein level in the early stage of *Acanthamoeba* encystation by a time-resolved multi-omics analysis. The global analysis of three omics approaches showed that the quantity of transcripts and phosphorylation sites were modified as early as 1 h after triggering encystation while the change of proteome was more gradual and occurred 8 h later. Interestingly, 1 h after induction of encystation, a decrease of phosphorylated sites was observed and accompanied by a global increased phosphatase activity (Bernard et al., 2022). *A. castellanii* is predicted to encode the largest number of protein kinases among amoebozoans (Clarke et al., 2013). However, only few signal pathways, such as PKC, Ras, and cyclic AMP (cAMP) have been proposed to be involved in encystation (Raizada and Krishna Murti, 1972; Fouque et al., 2012; Moon et al., 2012a), and there is no clear link between signals and cellular response. During encystation, these kinases may be involved in the regulation of phosphorylation at a specific site that is currently undefined. Bernard et al. (2022) also explained the transcriptomic and proteomic data at the initial stage of encystation. Their hypothesis is that the early regulation of transcription is achieved by the repression of transcription factors through phosphorylation. Some of these factors like GSK3 are highly promiscuous with a broad array of known substrates, regulate many transcription factors such as Fos/Jun AP-1 or p53 (Beurel et al., 2015). Lectins are an important part of cyst wall and three sets of these proteins have been identified as the most abundant in *A. castellanii*, which are named as the Jonah, Luke, and Leo families (Magistrado-Coxen et al., 2019). 23 out of 31 lectins described by Magistrado-Coxen et al. (2019) were present in transcriptomic data and 16 were significantly differentially expressed. However, none of them were significantly regulated at the protein level. This may be due to timing because their expression peak may be later than 8 h after induction of encystation (Magistrado-Coxen et al., 2019; Bernard et al., 2022). Part of the transcriptomic data in the multi-omics analysis (Bernard et al., 2022) may come from epigenetic regulation in the early stage of encystation. Epigenetics is associated to many cellular processes such as gene and microRNA expression, DNA-protein interactions, suppression of transposable element mobility, cellular differentiation, embryogenesis, etc. (Portela and Esteller, 2010). *A. castellanii* transfected with siRNA against Protein Arginine Methyltransferase 5 (AcPRMT5) failed to form mature cysts (Moon et al., 2016). DNA methylation is also involved in the control of CSCP expression during encystation (Moon et al., 2017).

In addition, several genes related to *Acanthamoeba* encystation have been identified from encystation-related gene profiles, such as cyst specific protein 21, Na P-type ATPase, subtilisin-like serine proteinase genes, proteasome and heat shock protein, genes like cullin 4, ubiquitin-conjugating enzymes, suggesting their potential roles in the process of cyst formation (Moon et al., 2007, 2008a).

## 2.3. Classification of *Acanthamoeba*

### 2.3.1. Traditional classification

Pussard and Pons (1977) classified *Acanthamoeba* cysts into three categories (I-III) according to their size and morphological



characteristics. This was the most appropriate classification method at that time, but has been replaced by modern advances in DNA sequencing. However, at least 30 species of *Acanthamoeba* with clear names have been classified in this manner (Table 1).

**Group I:** This group includes five clearly named *Acanthamoeba* listed in Table 1. The average diameter of cysts of this group is greater than or equal to 18  $\mu\text{m}$ . The morphological defining features are that the internal cyst wall is separated from the external wall, the outer cyst wall is slightly wrinkled or smooth, and the internal cyst is often star-shaped (Kong, 2009).

**Group II:** This group has relatively smaller cysts with an average diameter of less than 18  $\mu\text{m}$ . The outer cyst wall is folded or wavy, and the inner cyst wall is various in shape, which is wavy, round or oval, as well as star-shaped, triangular or tetragonal. The inner wall and outer wall of the cyst are obviously separated and some are closely connected. This group is the most widely isolated *Acanthamoeba*, and most pathogenic *Acanthamoeba* belong to this group (Kong, 2009; Corsaro, 2020). So far, there are 17 species of *Acanthamoeba* which have been clearly named in this group listed in Table 1.

**Group III:** At present, eight species have been clearly named in this group. This group *Acanthamoeba* cysts are also small and the average diameter is less than 18  $\mu\text{m}$ . The inner wall is round or slightly angular while the outer wall is thin and close to the inner wall, so the outer wall is sometimes difficult to observe (Kong, 2009; de Lacerda and Lira, 2021).

The morphology of *Acanthamoeba* cysts depends upon growth medium used to culture them (Stratford and Griffiths, 1978), while the *Acanthamoeba* cysts in the same group are similar, sometimes there is only a temporary difference between the two kinds of *Acanthamoeba* cysts, therefore, the morphological distinction is subjective and a more scientific classification method with clinical application value was needed.

### 2.3.2. 18S ribosomal RNA (18S rRNA) gene sequence typing

Gast et al. (1996) began classifying *Acanthamoeba* according to 18S rRNA sequencing. The analysis of full-length 18S rRNA of *Acanthamoeba* is a fast and reliable identification method which is now used extensively to identify *Acanthamoeba* isolates (Maciver et al., 2013). However, the 18S-based genotyping was rendered easier and more rapid by targeting smaller regions of the gene, such as the 464 bp long *Acanthamoeba*-specific amplicon (ASA.S1) which contains the diagnostic fragment 3 (DF3) (Taher et al., 2018). The DF3 region is a 280 bp long single highly variable region within the ASA.S1 region, which is widely used for genotyping studies since it provides equivalent results as that of ASA.S1 (Booton et al., 2002). Each genotype exhibits at least 5% sequence divergence as the typing standard (Khan, 2006). Using this technology, Maghsood et al. (2005) proposed to subdivide T2 into further two groups, i.e., T2a and T2b. T4 is further subdivided into seven groups, T4A, T4B, T4C, T4D, T4E, T4F, and T4G (Corsaro, 2020; Putaporntip et al., 2021). Indeed, DNA sequencing helps to differentiate pathogenic and non-pathogenic isolates within a genotype (Khan, 2006). Currently, most of the diagnostic and epidemiological investigations are indeed carried out with this fragment. Albeit rarely misidentifications may occur, and moreover, reliability of short fragments remains to be discussed especially for phylogenetic

analyses and identify new genotypes. Therefore, the full-length gene sequences are strongly recommended (Corsaro and Venditti, 2011; Corsaro et al., 2015).

Based on this method, all *Acanthamoeba* isolates found to date have been divided into 23 genotypes (T1-T23) (Corsaro et al., 2015, 2017; Taher et al., 2018; Corsaro, 2021; Putaporntip et al., 2021). Studies have shown that *Acanthamoeba* genotypes are related to pathogenicity (Walochnik et al., 2000), and the diseases and pathological characteristics caused by different genotypes are unique (Corsaro, 2021). *Acanthamoeba* isolated from patients with the most severe clinical *Acanthamoeba* infections belong to the T4 genotype (Booton et al., 2005; Maciver et al., 2013; Walochnik et al., 2015) followed by the T3 genotype (Booton et al., 2002; Walochnik et al., 2015). There are also reports of *Acanthamoeba* keratitis (AK) caused by T2, T5, T6, T10, T11, T12 and T15 genotypes (Maghsood et al., 2005; Di Cave et al., 2009; Nuprasert et al., 2010; Lorenzo-Morales et al., 2011; Roshni Prithiviraj et al., 2020; Otero-Ruiz et al., 2022) and GAE caused by T1, T2, T5, T10, T12, and T18 (Khan, 2006; Lackner et al., 2010; Qvarnstrom et al., 2013; Duggal et al., 2017; Matsui et al., 2018; Otero-Ruiz et al., 2022). It is difficult to classify the rarer species of *Acanthamoeba*. At present, gene sequencing and morphological classification are often used simultaneously (Walochnik et al., 2000; Kong, 2009). In terms of distribution, the T4 genotype was the most prevalent worldwide, followed by T3, T15, T11, and T5. Furthermore, the T4 genotype contains a higher number of species (Diehl et al., 2021). The currently known *Acanthamoeba* genotypes and corresponding diseases are summarized in Table 2. Meanwhile, phylogenetic relationship with 49 various genotypes or subtypes of *Acanthamoeba* T1-T23 based on “complete” 18S rRNA gene sequence has been shown in Figure 3.

## 3. *Acanthamoeba* related diseases

### 3.1. Disease type

#### 3.1.1. *Acanthamoeba* keratitis

*Acanthamoeba* keratitis (AK) is the most common disease caused by *Acanthamoeba* (Stehr-Green et al., 1989; Ibrahim et al., 2007; Jiang et al., 2015). The incidence of AK correlates significantly with corneal trauma, exposure to sewage, and wearing of contact lenses (CLs) (Moore et al., 1985; Maycock and Jayaswal, 2016; Hassan et al., 2019). Wearing CLs can cause slight abrasion on the cornea, which destroys the integrity of corneal epithelium and increases the chance of invasion of pathogenic microorganisms (Ibrahim et al., 2009). *Acanthamoeba* adhesion to the surface of contact lenses is one of the essential first steps in the pathogenesis of AK (Lee et al., 2016) and it was found that the adhesion rate of trophozoites to CL material was higher than that of cysts (Kilvington, 1993). Even when exposed to a minimally contaminated solution or environment for a few seconds, trophozoites immediately show adherence to CLs (John et al., 1989; Heidemann et al., 1990). Later, silicone hydrogel lenses became popular, accounting for 30% of new lenses in 2005 (Morgan et al., 2006). However, the first generation of silicon hydrogel lenses were found to be highly sticky to trophozoites (Beattie et al., 2003). To overcome this issue, second generation silicon hydrogel lenses

TABLE 1 The traditional classification of *Acanthamoeba*.

Classification	Species	Genotypes	ATCC #	References
Group I	<i>A. astronyxis</i>	T7	30137	Ray and Hayes, 1954
	<i>A. tubiashi</i>	T8	30867	Lewis and Sawyer, 1979
	<i>A. comandoni</i>	T9	30135	Pussard, 1964b
	<i>A. byersii</i>	T18	PRA-411	Qvarnstrom et al., 2013
	<i>A. echinulate</i>	T4	50239	Pussard and Pons, 1977
Group II	<i>A. castellanii</i>	T4	50374 = 30011	Douglas, 1930
	<i>A. polyphaga</i>	T4	30871	Page, 1967
	<i>A. triangularis</i>	T4	50254	Pussard and Pons, 1977
	<i>A. rhyodes</i>	T4	30973	Singh and Das, 1970
	<i>A. lugdunensis</i>	T4	50240	Pussard and Pons, 1977
	<i>A. quina</i>	T4	50241	Pussard and Pons, 1977
	<i>A. mauritaniensis</i>	T4	50253	Pussard and Pons, 1977
	<i>A. diuionensis</i>	T4	50238	Pussard and Pons, 1977
	<i>A. paradiuionensis</i>	T4	50251	Pussard and Pons, 1977
	<i>A. griffinii</i>	T3	30731	Sawyer, 1971
	<i>A. pearcei</i>	T3	50435	Nerad et al., 1995
	<i>A. stevensoni</i>	T11	50388	Sawyer et al., 1993
	<i>A. hatchetti</i>	T11	30730	Sawyer et al., 1977
	<i>A. micheli</i>	T9	–	Corsaro et al., 2015
	<i>A. pyriformis</i>	T21	–	Tice et al., 2016
	<i>A. terricola</i>	T4	30134	Pussard, 1964a
	<i>A. gigantean</i>	–	50670	Schmoller, 1964
Group III	<i>A. healyi</i>	T12	30866	Moura et al., 1992
	<i>A. culbertsoni</i>	T10	30171	Singh and Das, 1970
	<i>A. lenticulata</i>	T5	30841	Rivera et al., 1987
	<i>A. pustulosa</i>	T2	50252	Pussard and Pons, 1977
	<i>A. palestinesis</i>	T2	30870	Reich, 1935
	<i>A. royreba</i>	T4	30884	Willaert et al., 1978
	<i>A. sohi</i>	–	–	Im and Shin, 2003
	<i>A. jacobsi</i>	T15	30732	Sawyer and Nerad, 1992; Hewett et al., 2003

have been developed and trophozoite attachment rates for this generation of lenses were much lower than for the first generation and not statistically different from those of conventional hydrogel lenses (Beattie et al., 2006). Recently, Campolo et al. (2022) found that some contact lens materials are more conducive to cyst formation than the natural environment with encystation occurring within as little as 4 h of incubation. They hypothesized that aggregation of cysts directly obstructs multi-purpose solutions from disinfecting *Acanthamoeba*, which further indicates that contact lens materials may need to be reevaluated in the future as infection incidence increases (Campolo et al., 2022). The adhesion of trophozoites and cysts to the surface of CLs depends on the structure of both. Pseudopods of trophozoites play an important role in adhesion (John et al., 1989; Omaña-Molina et al., 2014), but cysts do not have pseudopod structure. Instead, adhesion occurs through adhesive substances in the ectocyst (Kilvington, 1993). Infection by *Acanthamoeba* starts on the epithelium and progresses

slowly into the stroma (Marciano-Cabral and Cabral, 2003). In most cases, AK is unilateral, however, evidence also suggests that it can affect both eyes (Voyatzis and McElvanney, 2007; Lee and Gotay, 2010). Symptoms of AK include conjunctival hyperemia, edema, tearing, foreign body sensation, blurred vision, decreased visual acuity, photophobia, and severe ocular pain (Kaiserman et al., 2012; Lorenzo-Morales et al., 2013, 2015). When treatment is inadequate, AK can cause corneal perforation and melting (Lorenzo-Morales et al., 2015). The process of AK infection is complex and requires both host and pathogen factors discussed later in the text.

Poor CL hygiene habits are also risk factors to induce AK (Ahearn and Gabriel, 1997; Cope et al., 2015). Studies have shown that *Acanthamoeba* exist in tap water (Carnt et al., 2020); therefore, rinsing and cleaning lenses with tap water before putting them in the storage case may cause contamination of lenses and cause infection (Nau and Dhaliwal, 2018). Repeated use of lens

TABLE 2 Known *Acanthamoeba* genotypes and associations with human diseases.

<i>Acanthamoeba</i> genotypes	Human diseases		
T1	–	GAE	
T2	AK	GAE	–
T3	AK	–	–
T4	AK	GAE	–
T5	AK	GAE	–
T6	AK	–	–
T7	AK (rare)	–	–
T8	AK	–	–
T9	AK (rare)	–	–
T10	AK	GAE	–
T11	AK	–	–
T12	–	GAE	–
T13	AK	–	–
T14	–	–	–
T15	AK	–	–
T16	AK (rare)	–	AP
T17	–	–	–
T18	–	GAE	–
T19	–	–	–
T20	–	–	–
T21	–	–	–
T22	–	–	–
T23	–	–	–

disinfectant by “topping off” old solution with new disinfectant should be avoided (Tu and Joslin, 2010). Additionally, the use of expired solution (Abjani et al., 2016), the use of self-made saline solution, and chlorine-based disinfection can increase the risk of disease (Schaumberg et al., 1998; Seal et al., 1999; Radford et al., 2002). In general, the long-term use of the same CL storage case and insufficient drying after cleaning are a breeding ground for bacteria, protozoa, and fungi which themselves are a food source of trophozoites (Kuzman et al., 2014; Zimmerman et al., 2017; Mirsayafiov et al., 2018; Tan et al., 2018). Bad habits also include rubbing the eyes while wearing CLs, leading to corneal damage and promoting the invasion of *Acanthamoeba* (Taher et al., 2018). Other risk factors include sleeping with contact lenses that can lead to corneal hypoxia, edema, thinning in the center of the cornea (Ibrahim et al., 2009), and superficial punctate keratitis (Taher et al., 2018).

The symbiotic relationship of bacteria and *Acanthamoeba* (Rayamajhee et al., 2022) may increase corneal damage after *Acanthamoeba* infection. The ability of bacteria to survive as an amoebal endosymbiont was first reported in 1975 (Proca-Ciobanu et al., 1975), while the role of *Acanthamoeba* as a host of pathogenic microorganisms was reported in 1978 (Prasad and Gupta, 1978). Spores of *Bacillus anthracis* (Ames strain) can germinate in the amoeba phage, and the number of spores can

increase 50-fold after 72 h (Dey et al., 2012). *A. castellanii* can also host *Legionella* (Swart et al., 2018; Nomura et al., 2022), *Vibrio cholerae*, *Francisella tularensis* (Abd et al., 2003) and the causative agent of Johne’s disease, *Mycobacterium avium* subsp. *paratuberculosis* (MAP) (Phillips et al., 2020). These bacteria have been referred to as amoeba-resistant bacteria. *A. castellanii* releases undigested *V. cholerae* in expelled food vacuoles (EFVs) in the form of free spherical pellets (1–5  $\mu$ m size) (Espinoza-Vergara et al., 2020). If given the right amount of nutrients or cultured at 37°C, hundreds of bacteria can escape from EFV (Rayamajhee et al., 2022). Therefore, the difficulty of treatment can increase dramatically in opportune situations.

### 3.1.2. Granulomatous amoebic encephalitis

Granulomatous amoebic encephalitis (GAE) caused by *Acanthamoeba* infection is a rare central nervous system disease that is highly fatal with mortality rate greater than 90% despite its low occurrence worldwide (Kot et al., 2018; Kalra et al., 2020). GAE is a subacute or chronic granulomatous encephalitis characterized by neck ankylosis, headache, and fever. Other progressive neurological symptoms include altered mental state, seizures, confusion, hallucination, focal neurologic signs, diplopia, cranial nerve palsies, ataxia, high grade flaccid paralysis of right lower limb, lethargy, stiff neck, and personality changes (Coven et al., 2017; Ghadage et al., 2017; Geith et al., 2018). GAE is a progressive disease leading to death within 1–2 months of symptom onset due to increased intracranial pressure (Duggal et al., 2017). It occurs especially in immunocompromised individuals including those infected with human immunodeficiency virus (HIV) or acquired immunodeficiency syndrome (AIDS), organ transplant recipients, patients with diabetes, systemic lupus erythematosus (SLE), those undergoing cancer treatment as well as immunocompetent individuals (Lalitha et al., 1985; Gonzalez et al., 1986; Carter et al., 2004; Vernon et al., 2005; Duarte et al., 2006; Sütçü et al., 2018). The pathogenesis of GAE is not fully understood. *Acanthamoeba* may enter through various routes including lower respiratory tract or breaks in the skin resulting in hematogenous dissemination to the brain (Duggal et al., 2017). Although there is no clinical evidence, *Acanthamoeba* is likely to enter the central nervous system through the blood-brain barrier and cause infection. It is worth noting that the olfactory epithelium may be another pathway for *Acanthamoeba* to enter the central nervous system (Kalra et al., 2020). GAE cases are often under diagnosed and hence strong clinical suspicion along with laboratory technical expertise is required for early diagnosis and therapeutic intervention (Parija et al., 2015).

### 3.1.3. Other diseases

*Acanthamoeba* can also cause a skin disorder known as cutaneous acanthamoebiasis (CA) and pulmonary infection, *Acanthamoeba* pneumonia (AP), but both conditions are rare. The first case of cutaneous *Acanthamoeba* infection in an AIDS patient was reported in 1986 (Gonzalez et al., 1986). Eighteen patients with AIDS and cutaneous acanthamoebiasis have been reported in the literature to date (Torno et al., 2000). A recent article of *Acanthamoeba* infections identified a number of symptoms, including fever, headache, dizziness, nausea, altered mental status, seizures, and facial palsies prior to cutaneous manifestations

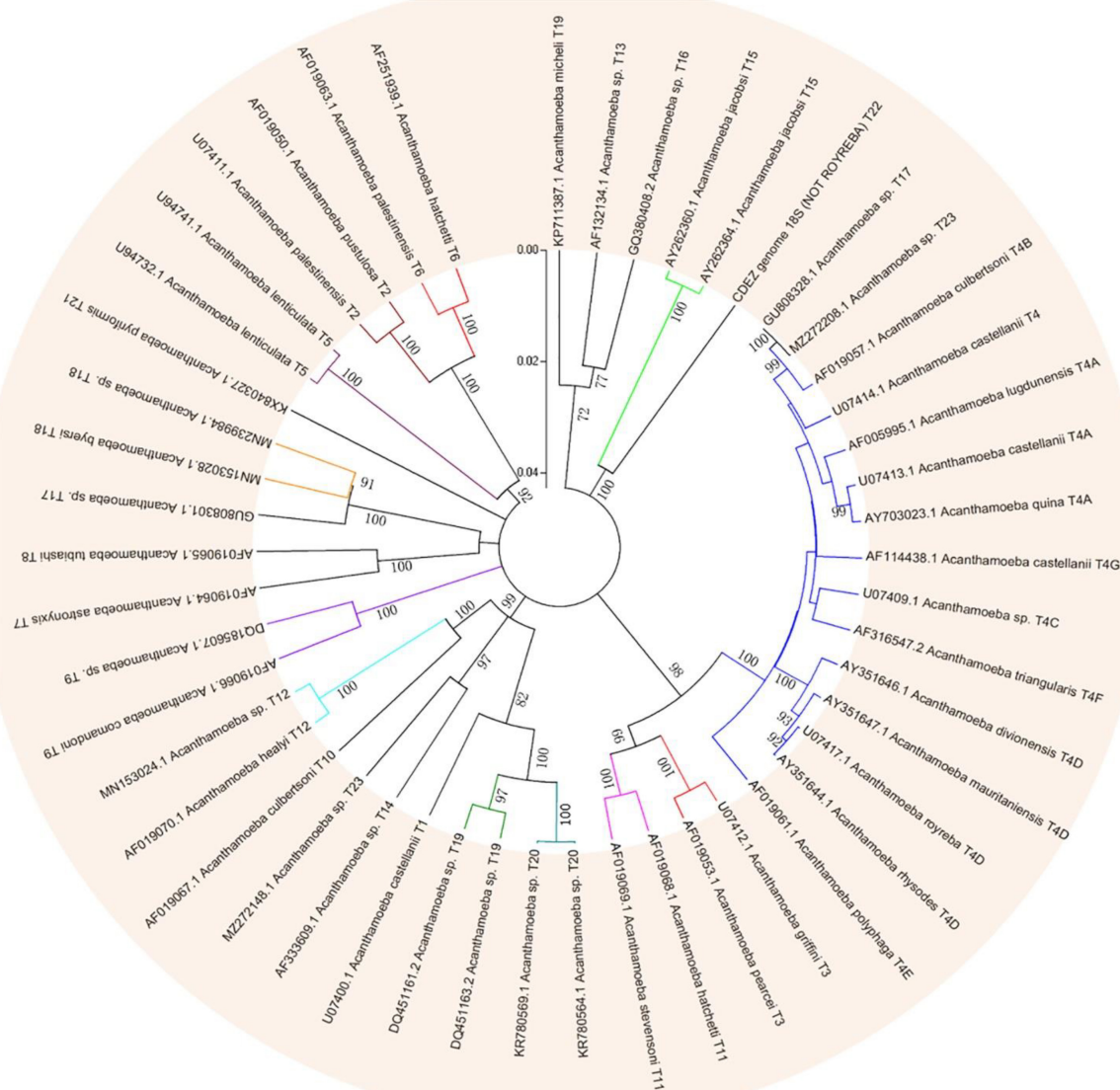


FIGURE 3

Phylogenetic relationship of 49 various genotypes or subtypes of *Acanthamoeba* T1-T23 based on "complete" 18S rRNA gene sequence. The tree was constructed using the Neighbor-Joining algorithm in MEGA 4.

(Zhang and Cheng, 2021). Lesions frequently occur on the face and extremities and exhibit heterogeneous morphology, ranging from papules, pustules, nodules, ulcers, eschars, or abscesses (Murakawa et al., 1995). However, diagnosing cutaneous acanthamoebiasis is challenging given its variable clinical presentation and lack of pathognomonic findings (Kutner et al., 2018).

*Acanthamoeba* pneumonia occurs mostly in patients with a low immune response (Visvesvara et al., 1983; Kaul et al., 2008). So far, 19 case reports of *Acanthamoeba* pneumonia (AP) or disseminated acanthamoebiasis with lung infection have been published. Most patients came from the USA, but there were also cases from Poland, Austria, France, Korea, Japan, and India. None of the patients survived (Kot et al., 2021). In patients with AP, a decrease in body weight and respiratory efficiency was observed, and in the radiological examination, interstitial changes

with visible pulmonary edema were observed (Im and Kim, 1998; Kot et al., 2021).

### 3.2. Pathogenic mechanism

Among the diseases caused by *Acanthamoeba*, the pathogenic mechanism of the rare GAE, CA, and pulmonary infection is not apparent and critically understudied compared to the relatively common AK infection. Once *Acanthamoeba* adheres to the target cells, intracellular signal transduction is quickly activated and a series of cascade effects are triggered including phagocytosis of target cells, secretion of protease, and induction of apoptosis, which will cause direct pathological damage to the host. These are further explored in-depth below.



### 3.2.1. Adhesion

The ability of *Acanthamoeba* to bind to epithelial cells is the basis of infection. At present, it is believed that there are two main factors involved in this process, one is acanthopod, the other is surface adhesion. These two factors are very important with adhesion ability of *Acanthamoeba* and directly correlate to the pathogenicity of different isolates. Studies in recent years have found that the total number of acanthopods is closely related to the adhesion rate. Pathogenic *Acanthamoeba* has more than one hundred acanthopods per cell, whereas non-pathogenic *Acanthamoeba* has no more than twenty acanthopods per cell (Lorenzo-Morales et al., 2013).

Current consensus is that the adhesion of pathogenic *Acanthamoeba* to corneal epithelial cells is mainly mediated by adhesins, including mannose-binding protein (MBP) and laminin-binding protein (LBP) (Huth et al., 2017; Corsaro, 2022). MBP is expressed by *Acanthamoeba* protozoa which is composed of several 130 kDa subunits distributed on the surface of *Acanthamoeba* and can be isolated and extracted by mannose affinity column chromatography (Garate et al., 2006a,b). *Acanthamoeba* MBP is a transmembrane protein encoded by a gene containing six exons and five introns and has a typical cell surface receptor function (Garate et al., 2004). As an exogenous lectin, it is generally bound to specific mannose-containing glycoproteins through the carbohydrate recognition domain (CRD) (Garate et al., 2006a). MBP binds to two glycoproteins of corneal epithelial cells, which are purified mannose protein and mannose bovine serum albumin (isolated and identified from primary cell cultures of rabbit corneal epithelium) (Yang et al., 1997). This is further demonstrated by studies showing that binding can be inhibited by exogenous  $\alpha$ -mannose competitively (Rocha-Azevedo et al., 2010; Kim et al., 2012), while galactose bovine albumin and other non-competitive sugars could not inhibit MBP binding, indicating that mannose's inhibitory effect was achieved by competing with MBP for sugar binding sites (Rocha-Azevedo et al., 2010). The binding of *Acanthamoeba* and mannose-containing glycoproteins leads to an increase of serine protease secretion, which is the decisive factor in host cell injury (Rocha-Azevedo et al., 2010; Lorenzo-Morales et al., 2013). MBP-mediated adhesion of *Acanthamoeba* to host cells depends on the level of MBP expression on the surface of *Acanthamoeba* and the number of mannose-containing glycoproteins synthesized by host cells. The study found that the damaged cornea can expose more mannose-rich glycoproteins, the number of *Acanthamoeba* attached to its surface is higher than healthy corneas. In addition, compared with non-pathogenic *Acanthamoeba*, pathogenic strains showed higher MBP expression levels (Yoo and Jung, 2012; Huth et al., 2017). Currently two types of MBP (MBP1 and MBP2) have been found (Corsaro, 2022). MBP1 is a conventional membrane protein with a signal peptide at the N-terminus and a transmembrane domain located at the C-terminus. The extracellular portion contains a Cys-rich repetitive motif (CXCXC) and a domain of unknown function (DUF 4114), while two NPLF motifs involved in intracellular signaling are located in the intracytoplasmic region (Garate et al., 2004). MBP1 appears to be specific only to *Acanthamoeba* species of groups 2 and 3, with different gene structure and amino acid sequence depending on the genotype, while shorter MBP-like sequences could be identified in the group 1 species (*A. astronyxis*

T7 and *A. byersi* T18), as well as in T4 and T2 genotypes. The resulting protein, labeled MBP2, covers the N-terminal part containing DUF 4114 but lacks the Cys-rich repetitive elements (usually only a single CXCXC motif is present), as well as the intracytoplasmic domain (Corsaro, 2022). MBP2 has a signal peptide at the N-terminal followed by a transmembrane motif, although a second short transmembrane motif is predicted at the C-terminus for group 1 species (Corsaro, 2022). *In silico* alignment of two kinds of MBP (L8GXW7, 360 aa; Q6J288, 833 aa) demonstrated 19.4% identity (94 similar positions). Both proteins also share a domain of unknown function (DUF4114), sharing 61.6% identity (L8GXW7, 164–256 aa and Q6J288, 156–254 aa; 61 identical positions) (Gonçalves et al., 2019). MBP1 sequences from different genotypes are variable, with identity/similarity values < 60/75%. Moreover, values between MBP1 and MBP2 are even lower (between 25 and 35%), the most conserved region being the DUF4114 domain (approximately 65% of identical sites) (Corsaro, 2022).

In addition to MBP, another important *Acanthamoeba* adhesin is the laminin-binding protein (LBP), which allows further progression of infected tissues (Rocha-Azevedo et al., 2009), as laminin is a major glycoprotein of the extracellular matrix separating epithelia from other tissues. The molecular weight is predicted to be 28.2 kDa (Hong et al., 2004; Omaña-Molina et al., 2017) and 55 kDa in *A. culbertsoni* (Rocha-Azevedo et al., 2009, 2010). *Acanthamoeba* LBP belongs to the family of non-integrin 37/67-kDa laminin receptors (37/67LR), also involved as receptors for viruses and other pathogens as well as in other cellular processes such as motility and differentiation (DiGiacomo and Meruelo, 2016). LBP homologs are present in all organisms including prokaryotes as this adhesin derives from a 40S ribosomal protein which evolved the ability to bind laminin (Ardini et al., 1998). Overall, LBPs have a short transmembrane domain at the N-terminal, three recognition domains for laminin on the extracellular C-terminal domain, comprising a palindromic LMWWML motif located in the peptide G (Castronovo et al., 1991), a direct binding region (DBR), and TEDWS motif repeats. LBP sequences are highly conserved with identity/similarity values > 80/90% for those of group 2 and 3 species and around 60/70% between these and those of group 1 species (Corsaro, 2022). It is generally believed that the adhesion of *Acanthamoeba* to the cornea is a crucial prerequisite for the subsequent inflammatory response and the degree of adhesion is directly proportional to the strength of the host's inflammatory response (Wang and Zhu, 2010). LBP participates in the initial phase where infiltration is limited to the corneal epithelium, particularly in the intercellular space (Gu et al., 2022). Therefore, the selectivity of *Acanthamoeba* for the host cornea also determines the differences in the specificity of AK in different hosts. A similar view has been established in the pathogenic mechanism of other protozoa such as the binding and lysis of *Entamoeba histolytic* to host cells being mediated by galactose adhesion protein (Guzmán-Téllez et al., 2020). Studies shows that expression levels of both MBP and LBP vary between *Acanthamoeba* strains and correlate with pathogenicity (Garate et al., 2006b; Ng et al., 2017). They were found in either low or non-existent quantities in non-pathogenic *Acanthamoeba* (Rocha-Azevedo et al., 2009; Singh et al., 2012; Huth et al., 2017; Corsaro, 2022).

### 3.2.2. Phagocytosis

Phagocytosis plays an essential role in the pathogenesis of *Acanthamoeba* infection. Phagocytosis is an actin-dependent process that drives cytoskeleton rearrangement. Cytochalasin D (a toxin that blocks actin polymerization) inhibits *Acanthamoeba*-mediated host cell death, confirming that actin-mediated cytoskeleton rearrangement plays an important role in *Acanthamoeba* phagocytosis (Taylor et al., 1995; Niederkorn et al., 1999; Alsam et al., 2005a). In order to study the relationship between cellular signal transduction pathway and phagocytosis, phagocytosis assays have been performed in the presence of protein tyrosine kinase inhibitor, genistein and a protein tyrosine phosphatase inhibitor, sodium orthovanadate. *Acanthamoeba* uptake of *Escherichia coli* is significantly reduced in the presence of genistein. In contrast, sodium orthovanadate increases bacterial uptake by *Acanthamoeba* (Alsam et al., 2005a). Rho GTPases are the key regulators of the actin cytoskeleton in all eukaryotic cells and link external signals to cytoskeleton (Mackay and Hall, 1998). This process involves three major pathways including RhoA, Rac1, and Cdc42 (Mackay and Hall, 1998). The Rho kinase inhibitor, Y27632, which partially blocks RhoA pathway, reduced bacterial uptake (Alsam et al., 2005a). These results suggested that the signal transduction pathway may regulate phagocytosis through mediating actin polymerization. Some evidence suggests that phosphatidylinositol 3-kinase (PI3K) may play important roles in regulating actin dependent-processes (Wymann and Pirola, 1998). For example, studies have shown that PI3K controls Rho-mediated changes in actin cytoskeleton in fibroblasts (Reif et al., 1996; Cantrell, 2001). When studying the phagocytosis of *Acanthamoeba*, it was found that LY294002, a specific inhibitor of PI3K, could significantly reduce the phagocytosis of *E. coli* (Alsam et al., 2005a). Interestingly, studies have also shown that the involvement of PI3K in Rac1-dependent lamellipodia formation (Wennström et al., 1994) and Cdc42-dependent cytoskeletal changes (Jiménez et al., 2000), suggesting that other GTPases such as Cdc42 and Rac1 are also involved in the phagocytosis of *Acanthamoeba*.

In addition, there is a unique actin-rich sucking structure (amoebostomes) on the surface of *Acanthamoeba*, also known as the food cup structure, which is a temporary structure that mediates phagocytosis of bacteria, yeasts, or cells (Pettit et al., 1996; Marciano-Cabral and Cabral, 2003). The mechanism involved in these goblet structures is called “trogocytosis,” which is the process whereby sections of host cells are ripped off by the amoeba (Nakada-Tsukui and Nozaki, 2021). Trogocytosis can be regarded as a special type of phagocytosis. The initial discovery of cell nibbling is from unicellular eukaryotes (Nakada-Tsukui and Nozaki, 2021). Culbertson (1970, 1971) described trogocytosis-like events in two species, *Naegleria fowleri* HB-1 and *Hartmannella Acanthamoeba* A-1. When these amoebae were inoculated into guinea pigs, pathological examination showed that amoeba in thrombi internalized erythrocytes only halfway (i.e., trogocytosis) (Culbertson, 1971). Later, trogocytosis of a mouse embryonic cell by *N. fowleri* was also confirmed (Brown, 1979). Petti found that trophozoites of 4 species of *Acanthamoeba* were cytopathic for cultured rat B 103 neuroblastoma cells and this process is achieved by destroying nerve cells through the food cup (Pettit et al., 1996). The same process can be observed in the pathogenesis of other protozoa such as *N. fowleri* (Tiewcharoen et al., 2008) and

*E. histolytica* (Miller et al., 2019). In the study of *E. histolytica*, it was found that there was pronounced actin polymerization within the amoebae at the site of human cell contact and ingested fragments were surrounded by polymerized actin, which indicates that trogocytosis is related to actin rearrangement (Ralston et al., 2014). Further studies found that Gal/GalNAc lectin, EhC2PK, and PI3K signaling were also involved in the amoebic trogocytosis-mediated human cell killing (Ralston et al., 2014; Miller et al., 2019).

In recent years, some additional proteins that play a role in *Acanthamoeba* phagocytosis have been reported. For example, *Acanthamoeba* SBDS (Shwachman-Bodian-Diamond Syndrome)-related proteins are highly expressed during phagocytosis, which may be related to cytoskeleton-related phagocytosis and cystogenesis (Wang et al., 2021). Studies have shown that *Acanthamoeba* secreted extracellular M20/M25/M40 superfamily aminopeptidase plays an important role in the *Acanthamoeba* pathogenesis (Huang et al., 2017). *Acanthamoeba* Type-I metacaspase (Ac MCP) is a caspase-like protein which is expressed during the encystations of *A. castellanii*. When vectors containing Ac MCP (pDneo2a-GFP-Ac MCP) were electro-transfected into wild type *Dictyostelium discoideum* cells, they showed a significant increase in the fluid phase internalization and phagocytosis rate compared to the control cells (Saheb et al., 2015). Therefore, metacaspase is proposed as a candidate drug target against infections caused by *A. castellanii*. Finally, *A. castellanii* Rab7 (Ac Rab7), which is involved in endosomal delivery after phagocytosis and dominates energy production and cell growth, may be an important target in some species (Hong et al., 2022).

It has also been reported that mannose inhibits *Acanthamoeba* phagocytosis, which suggests that *Acanthamoeba* phagocytosis is a receptor-dependent process and *Acanthamoeba* adhesin (or MBP) is involved in phagocytosis (Allen and Dawidowicz, 1990). Further study of other molecular pathways and the interaction between various intracellular signaling pathways will help the field to understand the phagocytosis of *Acanthamoeba* and provide a basis for clinical treatment. *Acanthamoeba*-mediated host signaling pathways as well as self-signaling pathways are shown in Figure 4.

### 3.2.3. Apoptosis of host cells

In addition to directly causing cell death, *Acanthamoeba* can induce programmed cell death, such as apoptosis. After *Acanthamoeba* infection, cell membrane rupture, condensation of nucleoplasm, and degradation of DNA can be seen, eventually forming apoptotic bodies (Khan, 2006; Lorenzo-Morales et al., 2013). Based on current research, there are at least three pathways related to apoptosis. First, Ecto-ATPase driven cell apoptosis. Ecto-ATPases hydrolyze extracellular ATP and other nucleoside triphosphates and the resulting ADP has a toxic effect on host cells. It has been shown that the ADP released binds to the P2y2 purinergic receptor on the host cell, resulting in the increase of intracellular calcium and the activation of caspase-3, which eventually leads to cell apoptosis (Mattana et al., 2002). Suramin, a P2 receptor antagonist, inhibits *Acanthamoeba*-mediated host cell apoptosis, indicating that extracellular ATP enzymes play an essential role in the pathogenesis of *Acanthamoeba* (Mattana et al., 2002). Compared with weakly pathogenic isolates, clinical isolates of *Acanthamoeba* show higher extracellular ATP activity (Sissons et al., 2004a). Several Ecto-ATPases with estimated molecular

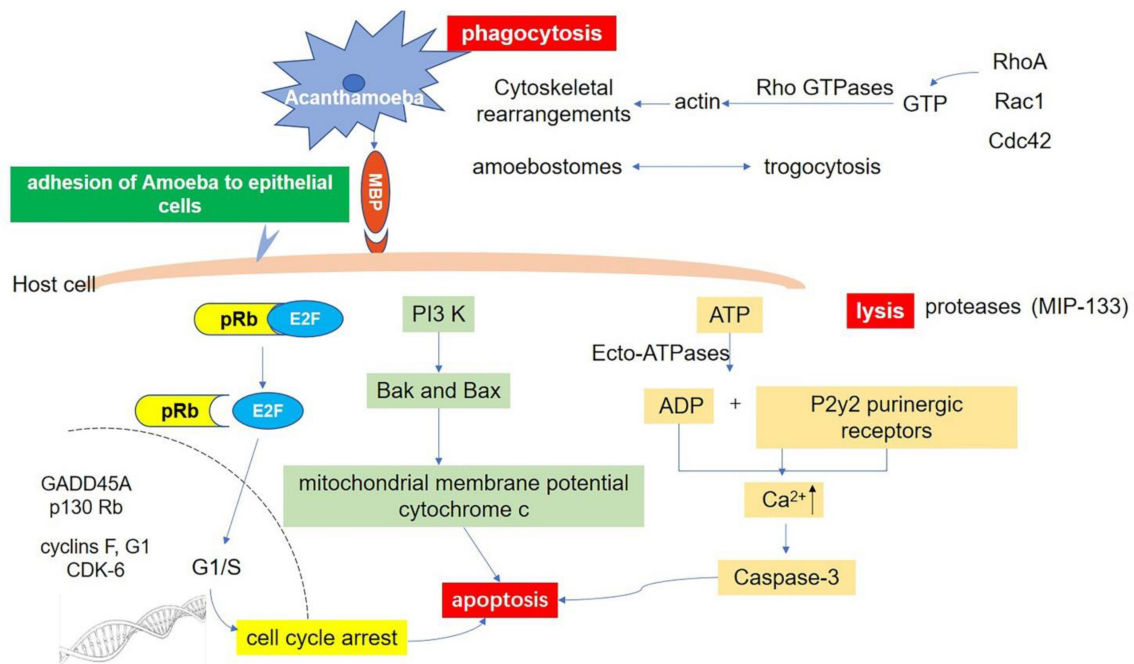


FIGURE 4

Host-Parasite interaction molecular signaling pathways. Adhesion through spinous pseudopodia and adhesin (such as MBP) is the basis for *Acanthamoeba* to establish infection. Once adhesion is completed, the intracellular signal transduction process is activated and further triggers cascade effects such as phagocytosis of target cells, secretion of protease, and apoptosis, resulting in direct pathological damage. Phagocytosis: There are three fully studied pathways involved in this process. The RhoA pathway, which leads to stress fiber formation; Rac1 activation, which triggers plate foot formation; and Cdc42 activation, which promotes filamentous foot formation. Apoptosis: There are at least three pathways related to apoptosis after infection of *Acanthamoeba*. Ecto-ATPases driven cell apoptosis; Interference with the expression of important genes that regulate cell cycle; and the phosphatidylinositol 3-kinase (PI3K) mediated apoptosis pathway. Lysis: *Acanthamoeba* secretes a variety of proteases involved in cell lysis. A serine protease (MIP133) has been identified as a key component in the pathogenesis of *Acanthamoeba*.

weights of 62, 100, 218, 272, and exceeding 300 kDa are described in *Acanthamoeba* (Sissons et al., 2004a). However, further studies are needed to clarify their function in *Acanthamoeba* biology and their pathogenicity to the host. Secondly, *Acanthamoeba* causes cell cycle arrest by affecting the expression of GADD45A, p130Rb, E, G1 protein, and cyclin-dependent kinase 6. The dephosphorylation of retinoblastoma protein (pRb) further supports this theory (Sissons et al., 2004b). Unphosphorylated pRb binds to the E2F transcription factor during the cell cycle, which inhibits E2F entry into the nucleus. When phosphorylated by CDKs, the conformational change of pRb leads to the dissociation of the pRb-E2F complex. The released E2F enters the nucleus and initiates the synthesis of DNA (Dyson, 1998; Harbour and Dean, 2000; Stevaux and Dyson, 2002). Recent studies have found that *Acanthamoeba* can induce cell cycle arrest of host cells by inhibiting this process in human corneal epithelial cells and brain microvascular endothelial cells (Sissons et al., 2004b). Third, *Acanthamoeba*-mediated apoptosis of host cells depends on the activation of phosphatidylinositol 3-kinase (PI3K) (Sissons et al., 2005). This conclusion was confirmed by using LY294002 to inhibit the activity of PI3K specifically and to express the mutant form of PI3K regulatory subunit P110 in host cells (Sissons et al., 2005). Traditionally, it has been known that PI3K plays an important role in regulating cell survival pathways. For example, Thyrell et al. (2004) have shown that  $\alpha$ -interferon (IFN $\alpha$ ) can induce PI3K-mediated apoptosis in myeloma cells without Akt phosphorylation. Further studies have shown that PI3K can mediate apoptosis by

activating the downstream pre-apoptotic molecules Bak and Bax, inducing the loss of mitochondrial membrane potential and the release of cytochrome c (Mattana et al., 2002; Chusattayanond et al., 2010). A similar mechanism may exist in the process of host cell apoptosis mediated by *Acanthamoeba*.

### 3.2.4. Lysis

When *Acanthamoeba* adheres to the host cells, it secretes a variety of proteases that create pores in host membranes, resulting in the lysis of cells and tissues (Lorenzo-Morales et al., 2013). Pathogenic *Acanthamoeba* shows higher extracellular protease activity. Protease-mediated lysing plays an important role in the pathogenesis of various protozoa, such as amoeba, trichomonas, leishmania, trypanosoma, and malaria parasites, and is directly involved in cell and tissue invasion and damage (Serrano-Luna Jde et al., 2006). It was found that *Acanthamoeba* mainly produce three types of proteases: serine proteases, cysteine proteases, and metalloproteinases (Khan, 2006). Serine proteases are the most abundant and present in almost all *Acanthamoeba* genotypes (Serrano-Luna Jde et al., 2006; Cirelli et al., 2020). Several serine proteases with molecular weights ranging from 20 to 200 kDa have been identified. They not only have collagen degradation activity, but also can degrade plasminogen activator, fibrinogen, IgG, IgA, albumin, hemoglobin, protease inhibitor, and interleukin-1 (Na et al., 2001, 2002). A serine protease called MIP133 has been identified as a key component in the pathogenesis of *Acanthamoeba*. MIP133 serine protease can induce the lysing of



corneal cells, iris ciliary body cells, retinal pigment epithelial cells, corneal epithelial cells, and corneal endothelial cells as well as induce apoptosis of macrophage-like cells (Lorenzo-Morales et al., 2015). The direct damage of serine protease in *Acanthamoeba* infection can be observed by injecting *Acanthamoeba* into the corneal stroma. This damage can be inhibited by the serine protease inhibitor phenylmethanesulfonyl fluoride (Na et al., 2001, 2002). In addition, siRNA targeting the catalytic domain of serine proteases reduced protease activity and host cytotoxicity mediated by *Acanthamoeba* (Lorenzo-Morales et al., 2005). The protease activity of pathogenic isolates, especially serine proteases, is significantly higher than that of non-pathogenic isolates, which is consistent with their cytotoxic effect on host cells.

Cysteine proteases with different molecular weights are detected in *Acanthamoeba* cell lysate and culture supernatant. These enzymes are thought to be involved in cell degradation (Hadas and Mazur, 1993; Mitro et al., 1994; Alfieri et al., 2000; Leitsch et al., 2010; Moon et al., 2012b; Ramírez-Rico et al., 2015). For example, two L-cysteine proteases, AcCP and AhCP, were identified in *Culbertson* and *Healyi Acanthamoeba* (Yun et al., 1999; Hong et al., 2002, 2018). Recombinant AcCP showed enzyme activity under acidic conditions and is the most suitable for pH4.0. Recombinant enzymes can effectively hydrolyze human proteins, including hemoglobin, albumin, immunoglobulin A and G, and fibronectin under acidic conditions (Ramírez-Rico et al., 2015; Hong et al., 2018; Cirelli et al., 2020). In addition, cysteine proteases with molecular weights of 43, 65, 70, and 130 kDa have also been reported (Khan, 2006). Although the histolytic role of cysteine proteases in the pathogenesis of parasitic pathogens has been identified (Singh et al., 2004; Jimenez-Sandoval et al., 2017), the studies on cysteine proteases in *Acanthamoeba* are limited.

In addition to serine and cysteine proteases, there is evidence of metalloproteinase activity in *Acanthamoeba* (Łanocha-Arendarczyk et al., 2018). Metalloproteinases usually play an important role in cell differentiation and migration, regulation of growth factor activity, angiogenesis, and inflammation (Sternlicht and Werb, 2001; Parks et al., 2004). An extracellular metalloprotease of 150 kDa was identified from the T1 genotype isolate of *Acanthamoeba* (Alsam et al., 2005b; Sissons et al., 2006). This metalloprotease exhibits extracellular matrix lytic properties for collagen I and III (the main components of the extracellular collagen matrix), elastin (the elastic fibers of the extracellular matrix), and plasminogen (involved in the extracellular matrix proteolysis). These, as well as casein, gelatin, and hemoglobin are degraded (Sissons et al., 2006). The specific mechanism needs to be further studied.

Phospholipases are known to cleave phospholipids, suggesting their possible involvement in the host cell plasma membrane disruption leading to host cell penetration and lysis. Matin and Jung (2011) tested the phospholipase activity and cytotoxicity of three different *Acanthamoeba* strains including an encephalitis isolate (T1 genotype), a keratitis isolate (T4 genotype), and an environmental isolate (T7 genotype) *in vitro*. The results show that all strains exhibited phospholipase A(2) [PLA(2)] and phospholipase D (PLD) activities. Moreover, *Acanthamoeba* isolates exhibited higher PLD activities compared with the PLA(2). Interestingly, the encephalitis isolates of *Acanthamoeba* exhibited higher phospholipase activities as compared with the keratitis isolates, but the environmental isolates exhibited the

highest phospholipase activities, suggesting possible differences in phospholipases in *Acanthamoeba* belonging to different genotypes (Matin and Jung, 2011). The result supporting this inference is that compound 48/80 partially blocked the encephalitis isolate-mediated cytotoxicity, i.e., 49% cell death in the presence of the inhibitor compared with 73% in the absence of the inhibitor, while it had no effect on the keratitis isolate cytotoxicity and the environmental isolate exhibited minimal cytotoxicity even in the absence of inhibitors (Matin and Jung, 2011).

Although phospholipase inhibitors do not clearly block the cytotoxicity mediated by *Acanthamoeba* alone, this does not rule out that they are involved in *Acanthamoeba* pathogenesis. *Acanthamoeba* pathogenesis is a process involved in many factors, including adhesion, phagocytosis, apoptosis, proteolytic enzyme, extracellular ATPase and so on as showing in Figure 4. The inhibition of a single factor may not be sufficient to kill host cells. In support of this notion, previous studies have shown that inhibition of *Acanthamoeba* binding to host cells is not adequate to block host cell cytotoxicity (Leher et al., 1998). It is also possible that cytotoxicity is a delayed event and that phospholipases are involved in the early events. Studies have shown that phospholipases involved in interference with the intracellular signaling pathways. Phospholipases generate lipids and lipid-derived products that act as mediators and second messengers, which may act as the modulators of signal transduction pathways (Dennis et al., 1991; Serhan et al., 1996). Studies have shown that lysophospholipids, a by-product of PLA2 and phospholipase B (PLB), can induce the activation of protein kinase C, which has diverse function in host cell signal transduction pathways (Oishi et al., 1988). Phospholipase C of *Clostridium perfringens* induces expression of IL-8 synthesis in endothelial cells (Bryant and Stevens, 1996; Bunting et al., 1997). These studies suggest that *Acanthamoeba* phospholipase may play a role in causing host cell damage or affecting other cellular functions such as inducing inflammation. In addition, studies on the pathogenicity of other species mediated by phospholipase have also been reported, such as the potential to prevent *Candida* infection by targeting phospholipase with synthetic compounds (Hänel et al., 1995). Future studies are needed to identify and characterize *Acanthamoeba* phospholipases, which should help determine their potential role for therapeutic interventions and in differentiation of *Acanthamoeba* isolates belonging to different genotypes.

*Acanthamoeba* species also show neuraminidase activity (Pellegrin et al., 1991). *Acanthamoeba* can release sialic acid after invading human cells, so the neuraminidase may be related to its colonization and play an important role in damaging the corneal epithelium rich in sialic acid (Pellegrin et al., 1991). In immunofluorescence, immunoblotting, and enzyme-linked immunosorbent assays, the neuraminidase antibody of *Trypanosoma cruzi* cross-reacted with *Acanthamoeba*, indicating that *Acanthamoeba* does have neuraminidase activity (Pellegrin et al., 1992). Although the role of *Acanthamoeba* neuraminidase in the pathogenesis of keratitis is unclear, the fact that cell damage can occur without direct contact (Visvesvara and Balamuth, 1975) suggests that the release of parasite products is involved in the mechanism of tissue injury. Neuraminidase-induced cleavage of sialic acid from glycoproteins and gangliosides of cerebral tissue may lead to the onset of granulomatous amoebic encephalitis. Such an effect of neuraminidase was suggested in primary amoebic



meningoencephalitis caused by *N. fowleri*, also a free living amoeba (Eisen and Franson, 1987). It is generally accepted that the ability of microorganisms to produce disseminated infections is related to their capacity to destroy colonized tissues. Neuraminidase may be related to the components and enzymes of several other amoebae, such as phospholipase A, sphingomyelinase, elastase, collagenase, and a cytolytic and granule-associated cytotoxic activity. The synergistic effect of these factors may participate in the destruction, mucosal surface penetration, and dissemination of *Acanthamoeba* (Ferrante and Bates, 1988; He et al., 1990).

### 3.2.5. Immune escape

The immune escape ability of *Acanthamoeba* is also an important component of its pathogenicity. Compared with uninfected individuals, the levels of IgA and IgG in tears of AK patients are lower (Carnt and Stapleton, 2016; Neelam and Niederkorn, 2017), which may be related to the fact that its secreted serine protease can destroy IgA and IgG antibodies in human tears (Kong et al., 2000; Marciano-Cabral and Cabral, 2003; Foulks, 2007). This reduction of antibodies allows *Acanthamoeba* to evade the human immune response and survive long-term in the host. Continuous low-level turnover of complement components within the eye has been recognized for many years (Sohn et al., 2000) and is known to be a major contributor to the immune privilege status of the eye (Niederkorn, 2007). For example, the major component of immune privilege, termed anterior chamber-associated immune deviation (ACAID), has been shown to be complement-dependent (Sohn et al., 2003). The complement cascade has a well-established role in the maintenance of a healthy cornea (Mondino et al., 1996). Although membrane-bound complement regulators such as CD46, CD55, and CD59 are expressed throughout the various layers of the cornea, there is a disproportionately high level of expression in the corneal epithelium (Bora et al., 1993). This may be due to the fact that the corneal surface is often exposed to various pathogens, resulting in the continuous activation of the complement system. Some bacteria produce phospholipases and other enzymes that can remove CD55 and CD59 from the surface of corneal epithelium (Cocuzzi et al., 2000), causing complement regulation disorders, which aggravate bacterial keratitis and even lead to loss of vision (Tang et al., 2009). By comparing the results of systematic analysis of *Acanthamoeba* isolates, Huang's group identified a new secretory protein, M28 aminopeptidase (M28AP). The molecular functions and characteristics of M28AP protein were studied by using anti-M28AP antibody and M28AP mutant produced by CRISPR/Cas9 system. The results showed that M28AP was involved in the degradation of human complement, such as C3b and iC3b, suggesting it played a vital role in pathology (Huang et al., 2019). The study also found that *Acanthamoeba* is usually associated with biofilms distributed throughout the environment. It has been confirmed that biofilms can promote protozoan infection (Schaumberg et al., 1998). The biofilm provides a protective niche for *Acanthamoeba*, which is conducive to immune escape, thereby enhancing invasiveness (Marciano-Cabral and Cabral, 2003; Lorenzo-Morales et al., 2015; Hasby Saad and Khalil, 2018) and thought to even provide nutrition for *Acanthamoeba* (Khan, 2006).

## 4. Conclusion

In conclusion, *Acanthamoeba*, is an opportunistic pathogenic protozoa widely existing in nature that can cause various diseases such as AK, GAE, and CA, as well as lung infections. Although its incidence is currently low, resulting infection is serious and treatment options are lacking due to understudied complex pathogenic mechanisms. An in-depth understanding of the biological characteristics and pathogenicity of *Acanthamoeba* can provide help for clinical diagnosis, effective treatment, and control of *Acanthamoeba* infection to provide a theoretical basis for the development of new drugs and vaccines against *Acanthamoeba*.

Although the widely used classification method based on 18S rRNA sequence is not as reliable as full-sequence gene analysis, it provides a rapid, simple and relatively accurate method for the study of genetic diversity of *Acanthamoeba*, which can assist in the differential diagnosis of pathogens in *Acanthamoeba* spp. The identification of *Acanthamoeba* from other cyst forming protozoa can be performed by a method based on the coupling of cellulose binding protein to fluorescent dyes. The main component of cyst wall is chitin, however, *Acanthamoeba* is an exception since its cyst wall contains cellulose (Garajová et al., 2019). Specific cytochemical differentiation between cellulose and chitin by microscopy has not been possible due to the similarity of the constituent  $\beta$ -1, 4-linked hexose backbones of these molecules. Therefore, it is necessary to develop new methods to distinguish cellulose from chitin in order to identify the source of infection. Derda et al. (2009) developed a novel immunocytochemical method for identification of *Acanthamoeba* spp. Cellulose-binding protein consisting of two cellulose-binding domains (CBDs) from *Trichoderma reesei* cellulase coupled to fluorescent dyes. No staining reaction was observed with the chitin-containing cyst walls of *Giardia intestinalis*, *Entamoeba dispar*, or *Pneumocystis carinii*. Thus, the recombinant CBD can be used as a marker to distinguish between cellulose and chitin (Derda et al., 2009). However, in later studies, cellulose was also identified as a cyst wall component of *Balamuthia mandrillaris*, which is closely related to amoeba (Siddiqui et al., 2009). Even so, it still helps to narrow the scope of differential diagnosis.

Current studies have found that *Acanthamoeba* produces a variety of proteases in the process of infecting the host, which may be an avenue for therapy. Still, the exact molecular mechanism is unclear. Future research should further explore the feasibility of protease inhibitors as therapeutic treatments. The cyst transformation function of *Acanthamoeba* increases the pathogenicity and increases the difficulty of clinical treatment. Therefore, the screening of *Acanthamoeba* cyst formation inhibitors may also prove fruitful for clinical treatment of *Acanthamoeba*. Finally, the unique morphological structure of cysts gives *Acanthamoeba* a remarkable ability to adapt to the environment and may provide another target for clinical treatment.

## Author contributions

YW and ML wrote the original draft. YZ, XJ, LW, and LJ contributed to collecting the data. YW

and LZJ contributed to curating the data into figures. RF contributed to revising the manuscript. ML conceived the idea and supervised the work. All authors read and agreed to the final version of the manuscript.

## Funding

This work was supported by the Science and Technology Research and Planning Projects of Jilin Provincial Department of Education (Nos. JJKH20220472KJ and JJKH20210489KJ), the Jilin Provincial Health Science and Technology Capacity Enhancement Project (No. 2021JC045), and the Innovation and Entrepreneurship Training Program for College Students in Jilin Province (No. 202213706006).

## References

- Abd, H., Johansson, T., Golovliov, I., Sandström, G., and Forsman, M. (2003). Survival and growth of *Francisella tularensis* in *Acanthamoeba castellanii*. *Appl. Environ. Microbiol.* 69, 600–606. doi: 10.1128/aem.69.1.600-606.2003
- Abjani, F., Khan, N. A., Yousuf, F. A., and Siddiqui, R. (2016). Targeting cyst wall is an effective strategy in improving the efficacy of marketed contact lens disinfecting solutions against *Acanthamoeba castellanii* cysts. *Cont. Lens Anterior Eye* 39, 239–243. doi: 10.1016/j.clae.2015.11.004
- Ahearn, D. G., and Gabriel, M. M. (1997). Contact lenses, disinfectants, and *Acanthamoeba* keratitis. *Adv. Appl. Microbiol.* 43, 35–56. doi: 10.1016/s0065-2164(08)70222-3
- Alfieri, S. C., Correia, C. E., Motegi, S. A., and Pral, E. M. (2000). Proteinase activities in total extracts and in medium conditioned by *Acanthamoeba polyphaga* trophozoites. *J. Parasitol.* 86, 220–227.
- Allen, P. G., and Dawidowicz, E. A. (1990). Phagocytosis in *Acanthamoeba*: I. A mannose receptor is responsible for the binding and phagocytosis of yeast. *J. Cell Physiol.* 145, 508–513. doi: 10.1002/jcp.1041450317
- Alsam, S., Sissons, J., Dudley, R., and Khan, N. A. (2005a). Mechanisms associated with *Acanthamoeba castellanii* (T4) phagocytosis. *Parasitol. Res.* 96, 402–409. doi: 10.1007/s00436-005-1401-z
- Alsam, S., Sissons, J., Jayasekera, S., and Khan, N. A. (2005b). Extracellular proteases of *Acanthamoeba castellanii* (encephalitis isolate belonging to T1 genotype) contribute to increased permeability in an in vitro model of the human blood-brain barrier. *J. Infect.* 51, 150–156. doi: 10.1016/j.jinf.2004.09.001
- Aqeel, Y., Siddiqui, R., and Khan, N. A. (2013). Silencing of xylose isomerase and cellulose synthase by siRNA inhibits encystation in *Acanthamoeba castellanii*. *Parasitol. Res.* 112, 1221–1227. doi: 10.1007/s00436-012-3254-6
- Ardini, E., Pesole, G., Tagliabue, E., Magnifico, A., Castronovo, V., Sobel, M. E., et al. (1998). The 67-kDa laminin receptor originated from a ribosomal protein that acquired a dual function during evolution. *Mol. Biol. Evol.* 15, 1017–1025. doi: 10.1093/oxfordjournals.molbev.a026000
- Band, R. N., and Mohrlök, S. (1973). The cell cycle and induced amitosis in *Acanthamoeba*. *J. Protozool.* 20, 654–657. doi: 10.1111/j.1550-7408.1973.tb03592.x
- Band, R. N., Mohrlök, S., and Rubin, R. W. (1970). Separate induction of amitotic and mitotic division in *Acanthamoeba rhysodes*. *Nature* 227, 379–381. doi: 10.1038/227379b0
- Barrett, R. A., and Alexander, M. (1977). Resistance of cysts of amoebae to microbial decomposition. *Appl. Environ. Microbiol.* 33, 670–674. doi: 10.1128/aem.33.3.670-674.1977
- Beattie, T. K., Tomlinson, A., and McFadyen, A. K. (2006). Attachment of *Acanthamoeba* to first- and second-generation silicone hydrogel contact lenses. *Ophthalmology* 113, 117–125. doi: 10.1016/j.ophtha.2005.10.018
- Beattie, T. K., Tomlinson, A., McFadyen, A. K., Seal, D. V., and Grimason, A. M. (2003). Enhanced attachment of *Acanthamoeba* to extended-wear silicone hydrogel contact lenses: A new risk factor for infection? *Ophthalmology* 110, 765–771. doi: 10.1016/s0161-6420(02)01971-1
- Béguin, P., and Aubert, J. P. (1994). The biological degradation of cellulose. *FEMS Microbiol. Rev.* 13, 25–58. doi: 10.1111/j.1574-6976.1994.tb00033.x
- Bernard, C., Locard-Paulet, M., Noël, C., Duchateau, M., Gai Gianetto, Q., Moumen, B., et al. (2022). A time-resolved multi-omics atlas of *Acanthamoeba castellanii* encystment. *Nat. Commun.* 13:4104. doi: 10.1038/s41467-022-31832-0
- Beurel, E., Grieco, S. F., and Jope, R. S. (2015). Glycogen synthase kinase-3 (GSK3): Regulation, actions, and diseases. *Pharmacol. Ther.* 148, 114–131. doi: 10.1016/j.pharmthera.2014.11.016
- Bishop, J. D., Moon, B. C., Harrow, F., Ratner, D., Gomer, R. H., Dottin, R. P., et al. (2002). A second UDP-glucose pyrophosphorylase is required for differentiation and development in *Dictyostelium discoideum*. *J. Biol. Chem.* 277, 32430–32437. doi: 10.1074/jbc.M204245200
- Blouin, F. A., Martin, L. F., and Rowland, S. P. (1970). Gel permeation properties of cellulose. III. Measurement of pore structure of unmodified and of mercerized cottons in fibrous form. *Text Res. J.* 40, 809–813.
- Booton, G. C., Kelly, D. J., Chu, Y. W., Seal, D. V., Houang, E., Lam, D. S., et al. (2002). 18S ribosomal DNA typing and tracking of *Acanthamoeba* species isolates from corneal scrape specimens, contact lenses, lens cases, and home water supplies of *Acanthamoeba* keratitis patients in Hong Kong. *J. Clin. Microbiol.* 40, 1621–1625. doi: 10.1128/jcm.40.5.1621-1625.2002
- Booton, G. C., Visvesvara, G. S., Byers, T. J., Kelly, D. J., and Fuerst, P. A. (2005). Identification and distribution of *Acanthamoeba* species genotypes associated with nonkeratitis infections. *J. Clin. Microbiol.* 43, 1689–1693. doi: 10.1128/jcm.43.4.1689-1693.2005
- Bora, N. S., Gobleman, C. L., Atkinson, J. P., Pepose, J. S., and Kaplan, H. J. (1993). Differential expression of the complement regulatory proteins in the human eye. *Invest. Ophthalmol. Vis. Sci.* 34, 3579–3584.
- Bowers, B. (1977). Comparison of pinocytosis and phagocytosis in *Acanthamoeba castellanii*. *Exp. Cell Res.* 110, 409–417. doi: 10.1016/0014-4827(77)90307-x
- Bowers, B., and Korn, E. D. (1968). The fine structure of *Acanthamoeba castellanii*. I. The trophozoite. *J. Cell Biol.* 39, 95–111. doi: 10.1083/jcb.39.1.95
- Bowers, B., and Korn, E. D. (1969). The fine structure of *Acanthamoeba castellanii* (Neff strain). II. Encystment. *J. Cell Biol.* 41, 786–805. doi: 10.1083/jcb.41.3.786
- Bowers, B., and Korn, E. D. (1973). Cytochemical identification of phosphatase activity in the contractile vacuole of *Acanthamoeba castellanii*. *J. Cell Biol.* 59, 784–791. doi: 10.1083/jcb.59.3.784
- Bowers, B., and Olszewski, T. E. (1972). Pinocytosis in *Acanthamoeba castellanii*. Kinetics and morphology. *J. Cell Biol.* 53, 681–694. doi: 10.1083/jcb.53.3.681
- Bowers, B., and Olszewski, T. E. (1983). *Acanthamoeba* discriminates internally between digestible and indigestible particles. *J. Cell Biol.* 97, 317–322. doi: 10.1083/jcb.97.2.317
- Brown, R. M., and Saxena, I. M. (2000). Cellulose biosynthesis: A model for understanding the assembly of biopolymers. *Plant Physiol. Biochem.* 38, 57–67.
- Brown, T. (1979). Observations by immunofluorescence microscopy and electron microscopy on the cytopathogenicity of *Naegleria fowleri* in mouse embryo-cell cultures. *J. Med. Microbiol.* 12, 363–371. doi: 10.1099/00222615-12-3-363
- Bryant, A. E., and Stevens, D. L. (1996). Phospholipase C and perfringolysin O from *Clostridium perfringens* upregulate endothelial cell-leukocyte adherence molecule 1

## Conflict of interest

The authors declare that the research was conducted in the absence of any commercial or financial relationships that could be construed as a potential conflict of interest.

## Publisher's note

All claims expressed in this article are solely those of the authors and do not necessarily represent those of their affiliated organizations, or those of the publisher, the editors and the reviewers. Any product that may be evaluated in this article, or claim that may be made by its manufacturer, is not guaranteed or endorsed by the publisher.

- and intercellular leukocyte adhesion molecule 1 expression and induce interleukin-8 synthesis in cultured human umbilical vein endothelial cells. *Infect. Immun.* 64, 358–362. doi: 10.1128/iai.64.1.358-362.1996
- Bunting, M., Lorient, D. E., Bryant, A. E., Zimmerman, G. A., McIntyre, T. M., Stevens, D. L., et al. (1997). Alpha toxin from *Clostridium perfringens* induces proinflammatory changes in endothelial cells. *J. Clin. Invest.* 100, 565–574. doi: 10.1172/jci119566
- Byers, T. J., Akins, R. A., Maynard, B. J., Lefken, R. A., and Martin, S. M. (1980). Rapid growth of *Acanthamoeba* in defined media; induction of encystment by glucose-acetate starvation. *J. Protozool.* 27, 216–219. doi: 10.1111/j.1550-7408.1980.tb04684.x
- Byers, T. J., and James, T. E. (1967). The influence of culture, agitation and aging on the growth and reproduction of *Acanthamoeba* sp. *Neff. J. Cell Biol.* 35:19A.
- Byers, T. J., Kim, B. G., King, L. E., and Hugo, E. R. (1991). Molecular aspects of the cell cycle and encystment of *Acanthamoeba*. *Rev. Infect. Dis.* 13(Suppl. 5), S373–S384. doi: 10.1093/clind/13.supplement\_5.5373
- Campolo, A., Pifer, R., Walters, R., Thomas, M., Miller, E., Harris, V., et al. (2022). *Acanthamoeba* spp. aggregate and encyst on contact lens material increasing resistance to disinfection. *Front. Microbiol.* 13:1089092. doi: 10.3389/fmicb.2022.1089092
- Cantrell, D. A. (2001). Phosphoinositide 3-kinase signalling pathways. *J. Cell Sci.* 114(Pt 8), 1439–1445. doi: 10.1242/jcs.114.8.1439
- Carnt, N. A., Subedi, D., Lim, A. W., Lee, R., Mistry, P., Badenoch, P. R., et al. (2020). Prevalence and seasonal variation of *Acanthamoeba* in domestic tap water in greater Sydney, Australia. *Clin. Exp. Optom.* 103, 782–786. doi: 10.1111/cxo.13065
- Carnt, N., and Stapleton, F. (2016). Strategies for the prevention of contact lens-related *Acanthamoeba* keratitis: A review. *Ophthalmic Physiol. Opt.* 36, 77–92. doi: 10.1111/opo.12271
- Carnt, N., Hoffman, J. M., Verma, S., Hau, S., Radford, C. F., Minassian, D. C., et al. (2018). *Acanthamoeba* keratitis: Confirmation of the UK outbreak and a prospective case-control study identifying contributing risk factors. *Br. J. Ophthalmol.* 102, 1621–1628. doi: 10.1136/bjophthalmol-2018-312544
- Carrijo-Carvalho, L. C., Sant'ana, V. P., Foronda, A. S., de Freitas, D., and de Souza Carvalho, F. R. (2017). Therapeutic agents and biocides for ocular infections by free-living amoebae of *Acanthamoeba* genus. *Surv. Ophthalmol.* 62, 203–218. doi: 10.1016/j.survophthal.2016.10.009
- Carter, W. W., Gompf, S. G., Toney, J. F., Greene, J. N., and Cutolo, E. P. (2004). Disseminated *Acanthamoeba* sinusitis in a patient with AIDS: A possible role for early antiretroviral therapy. *AIDS Read.* 14, 41–49.
- Castronovo, V., Taraboletti, G., and Sobel, M. E. (1991). Functional domains of the 67-kDa laminin receptor precursor. *J. Biol. Chem.* 266, 20440–20446.
- Centers for Disease Control and Prevention (2020). *Parasites/Acanthamoeba/Acanthamoeba keratitis fact sheet for healthcare professionals/treatment*. Atlanta, GA: Centers for Disease Control and Prevention.
- Chagla, A. H., and Griffiths, A. J. (1974). Growth and encystation of *Acanthamoeba castellanii*. *J. Gen. Microbiol.* 85, 139–145. doi: 10.1099/00221287-85-1-139
- Chambers, J. A., and Thompson, J. E. (1976). Phagocytosis and pinocytosis in *Acanthamoeba castellanii*. *J. Gen. Microbiol.* 92, 246–250. doi: 10.1099/00221287-92-2-246
- Chusattayanond, A. D., Boonsilp, S., Kasisit, J., Boonmee, A., and Warit, S. (2010). Thai *Acanthamoeba* isolate (T4) induced apoptotic death in neuroblastoma cells via the bax-mediated pathway. *Parasitol. Int.* 59, 512–516. doi: 10.1016/j.parint.2010.06.007
- Cirelli, C., Mesquita, E. I. S., Chagas, I. A. R., Furst, C., Possamai, C. O., Abrahão, J. S., et al. (2020). Extracellular protease profile of *Acanthamoeba* after prolonged axenic culture and after interaction with MDCK cells. *Parasitol. Res.* 119, 659–666. doi: 10.1007/s00436-019-06562-w
- Clarke, M., Lohan, A. J., Liu, B., Lagkouvardos, I., Roy, S., Zafar, N., et al. (2013). Genome of *Acanthamoeba castellanii* highlights extensive lateral gene transfer and early evolution of tyrosine kinase signaling. *Genome Biol.* 14:R11. doi: 10.1186/gb-2013-14-2-r11
- Cocuzzi, E., Guidubaldi, J., Bardenstein, D. S., Chen, R., Jacobs, M. R., and Medof, E. M. (2000). Release of complement regulatory proteins from ocular surface cells in infections. *Curr. Eye Res.* 21, 856–866. doi: 10.1076/ceyr.21.5.856.5539
- Cook, K. E., and Colvin, J. R. (1980). Evidence for a beneficial influence of cellulose production on growth of *Acetobacter xylinum* in liquid medium. *Curr. Microbiol.* 3, 203–205. doi: 10.1007/bf02602449
- Cope, J. R., Collier, S. A., Rao, M. M., Chalmers, R., Mitchell, G. L., Richdale, K., et al. (2015). Contact lens wearer demographics and risk behaviors for contact lens-related eye infections—United States, 2014. *MMWR Morb. Mortal Wkly. Rep.* 64, 865–870. doi: 10.15585/mmwr.mm6432a2
- Corsaro, D. (2020). Update on *Acanthamoeba* phylogeny. *Parasitol. Res.* 119, 3327–3338. doi: 10.1007/s00436-020-06843-9
- Corsaro, D. (2021). Correction to: Update on *Acanthamoeba* phylogeny. *Parasitol. Res.* 120, 1927–1928. doi: 10.1007/s00436-021-07102-1
- Corsaro, D. (2022). *Acanthamoeba* mannose and laminin binding proteins variation across species and genotypes. *Microorganisms* 10:2162. doi: 10.3390/microorganisms10112162
- Corsaro, D., and Venditti, D. (2011). More *Acanthamoeba* genotypes: Limits to use rDNA fragments to describe new genotype. *Acta Protozool.* 50, 51–56.
- Corsaro, D., Köhler, M., Montalbano Di Filippo, M., Venditti, D., Monno, R., Di Cave, D., et al. (2017). Update on *Acanthamoeba jacobsoni* genotype T15, including full-length 18S rDNA molecular phylogeny. *Parasitol. Res.* 116, 1273–1284. doi: 10.1007/s00436-017-5406-1
- Corsaro, D., Walochnik, J., Köhler, M., and Rott, M. B. (2015). *Acanthamoeba* misidentification and multiple labels: Redefining genotypes T16, T19, and T20 and proposal for *Acanthamoeba micheli* sp. nov. (genotype T19). *Parasitol. Res.* 114, 2481–2490. doi: 10.1007/s00436-015-4445-8
- Coven, S. L., Song, E., Steward, S., Pierson, C. R., Cope, J. R., Ali, I. K., et al. (2017). *Acanthamoeba* granulomatous amoebic encephalitis after pediatric hematopoietic stem cell transplant. *Pediatr. Transplant.* 21. doi: 10.1111/ptr.13060
- Cowling, E. B. (1975). Physical and chemical constraints in the hydrolysis of cellulose and lignocellulosic materials. *Biotechnol. Bioeng. Symp.* 5, 163–181.
- Culbertson, C. G. (1970). Pathogenic *Naegleria* and *Hartmannella* (*Acanthamoeba*). *Ann. N. Y. Acad. Sci.* 174, 1018–1022. doi: 10.1111/j.1749-6632.1970.tb45623.x
- Culbertson, C. G. (1971). The pathogenicity of soil amoebae. *Ann. Rev. Microbiol.* 25, 231–254. doi: 10.1146/annurev.mi.25.100171.001311
- De Jonckheere, J., and van de Voorde, H. (1976). Differences in destruction of cysts of pathogenic and nonpathogenic *Naegleria* and *Acanthamoeba* by chlorine. *Appl. Environ. Microbiol.* 31, 294–297. doi: 10.1128/aem.31.2.294-297.1976
- de Lacerda, A. G., and Lira, M. (2021). *Acanthamoeba* keratitis: A review of biology, pathophysiology and epidemiology. *Ophthalmic Physiol. Opt.* 41, 116–135. doi: 10.1111/opo.12752
- Delmer, D. P., and Amor, Y. (1995). Cellulose biosynthesis. *Plant Cell* 7, 987–1000. doi: 10.1105/tpc.7.7.987
- Dennis, E. A., Rhee, S. G., Billah, M. M., and Hannun, Y. A. (1991). Role of phospholipase in generating lipid second messengers in signal transduction. *FASEB J.* 5, 2068–2077. doi: 10.1096/fasebj.5.7.1901288
- Derda, M., Winięcka-Krusnell, J., Linder, M. B., and Linder, E. (2009). Labeled *Trichoderma reesei* cellulase as a marker for *Acanthamoeba* cyst wall cellulose in infected tissues. *Appl. Environ. Microbiol.* 75, 6827–6830. doi: 10.1128/aem.01555-09
- Dey, R., Hoffman, P. S., and Glomski, I. J. (2012). Germination and amplification of anthrax spores by soil-dwelling amoebae. *Appl. Environ. Microbiol.* 78, 8075–8081. doi: 10.1128/aem.02034-12
- Di Cave, D., Monno, R., Bottalico, P., Guerriero, S., D'Amelio, S., D'Orazi, C., et al. (2009). *Acanthamoeba* T4 and T15 genotypes associated with keratitis infections in Italy. *Eur. J. Clin. Microbiol. Infect. Dis.* 28, 607–612. doi: 10.1007/s10096-008-0682-4
- Diehl, M. L. N., Paes, J., and Rott, M. B. (2021). Genotype distribution of *Acanthamoeba* in keratitis: A systematic review. *Parasitol. Res.* 120, 3051–3063. doi: 10.1007/s00436-021-07261-1
- DiGiacomo, V., and Meruelo, D. (2016). Looking into laminin receptor: Critical discussion regarding the non-integrin 37/67-kDa laminin receptor/RPSA protein. *Biol. Rev. Camb. Philos. Soc.* 91, 288–310. doi: 10.1111/brv.12170
- Dos Santos, D. L., Kwitko, S., Marinho, D. R., de Araújo, B. S., Locatelli, C. I., and Rott, M. B. (2018). *Acanthamoeba* keratitis in Porto Alegre (southern Brazil): 28 cases and risk factors. *Parasitol. Res.* 117, 747–750. doi: 10.1007/s00436-017-5745-y
- Douglas, M. (1930). Notes on the classification of the amoeba found by Castellani in cultures of a yeast-like fungus. *J. Trop. Med. Hyg.* 33, 258–259.
- Duarte, A. G., Sattar, F., Granwehr, B., Aronson, J. F., Wang, Z., and Lick, S. (2006). Disseminated acanthamoebiasis after lung transplantation. *J. Heart Lung Transplant.* 25, 237–240. doi: 10.1016/j.healun.2005.09.006
- Dudley, R., Jarroll, E. L., and Khan, N. A. (2009). Carbohydrate analysis of *Acanthamoeba castellanii*. *Exp. Parasitol.* 122, 338–343. doi: 10.1016/j.exppara.2009.04.009
- Duggal, S., Rongpharpi, S., Duggal, A., Kumar, A., and Biswal, I. (2017). Role of *Acanthamoeba* in granulomatous encephalitis: A review. *J. Infect. Dis. Immune Ther.* 1:2.
- Dyson, N. (1998). The regulation of E2F by pRB-family proteins. *Genes Dev.* 12, 2245–2262. doi: 10.1101/gad.12.15.2245
- Eichinger, D. (2001). Encystation in parasitic protozoa. *Curr. Opin. Microbiol.* 4, 421–426. doi: 10.1016/s1369-5274(00)00229-0
- Eisen, D., and Franson, R. C. (1987). Acid-active neuraminidases in the growth media from cultures of pathogenic *Naegleria fowleri* and in sonicates of rabbit alveolar macrophages. *Biochim. Biophys. Acta* 924, 369–372. doi: 10.1016/0304-4165(87)90035-3
- Espinoza-Vergara, G., Hoque, M. M., McDougald, D., and Noorian, P. (2020). The impact of protozoan predation on the pathogenicity of *Vibrio cholerae*. *Front. Microbiol.* 11:17. doi: 10.3389/fmicb.2020.00017



- Fan, L. T., Lee, Y. H., and Beardmore, D. H. (1980). Mechanism of the enzymatic hydrolysis of cellulose: Effects of major structural features of cellulose on enzymatic hydrolysis. *Biotechnol. Bioeng.* 22, 177–199.
- Ferrante, A., and Bates, E. J. (1988). Elastase in the pathogenic free-living amoebae *Naegleria* and *Acanthamoeba* spp. *Infect. Immun.* 56, 3320–3321. doi: 10.1128/iai.56.12.3320-3321.1988
- Foulks, G. N. (2007). *Acanthamoeba* keratitis and contact lens wear: Static or increasing problem? *Eye Cont. Lens* 33(6 Pt 2), 412–414; discussion 424–425. doi: 10.1097/IJCL.0b013e318157e8be
- Fouque, E., Trouilhé, M. C., Thomas, V., Hartemann, P., Rodier, M. H., and Héchard, Y. (2012). Cellular, biochemical, and molecular changes during encystment of free-living amoebae. *Eukaryot. Cell* 11, 382–387. doi: 10.1128/ec.05301-11
- Fowler, M., and Carter, R. F. (1965). Acute pyogenic meningitis probably due to *Acanthamoeba* sp.: A preliminary report. *Br. Med. J.* 2, 740–742. doi: 10.1136/bmj.2.5464.734-a
- Garajová, M., Mrva, M., Vašková, N., Martinka, M., Melicherová, J., and Valigurová, A. (2019). Cellulose fibrils formation and organisation of cytoskeleton during encystment are essential for *Acanthamoeba* cyst wall architecture. *Sci. Rep.* 9:4466. doi: 10.1038/s41598-019-41084-6
- Garate, M., Alizadeh, H., Neelam, S., Niederkorn, J. Y., and Panjwani, N. (2006a). Oral immunization with *Acanthamoeba castellanii* mannose-binding protein ameliorates amoebic keratitis. *Infect. Immun.* 74, 7032–7034. doi: 10.1128/iai.00828-06
- Garate, M., Marchant, J., Cubillos, I., Cao, Z., Khan, N. A., and Panjwani, N. (2006b). In vitro pathogenicity of *Acanthamoeba* is associated with the expression of the mannose-binding protein. *Invest. Ophthalmol. Vis. Sci.* 47, 1056–1062. doi: 10.1167/iov.05-0477
- Garate, M., Cao, Z., Bateman, E., and Panjwani, N. (2004). Cloning and characterization of a novel mannose-binding protein of *Acanthamoeba*. *J. Biol. Chem.* 279, 29849–29856. doi: 10.1074/jbc.M402334200
- Gast, R. J., Ledee, D. R., Fuerst, P. A., and Byers, T. J. (1996). Subgenus systematics of *Acanthamoeba*: Four nuclear 18S rDNA sequence types. *J. Eukaryot. Microbiol.* 43, 498–504. doi: 10.1111/j.1550-7408.1996.tb04510.x
- Geith, S., Walochnik, J., Prantl, F., Sack, S., and Eyer, F. (2018). Lethal outcome of granulomatous acanthamoebic encephalitis in a man who was human immunodeficiency virus-positive: A case report. *J. Med. Case Rep.* 12:201. doi: 10.1186/s13256-018-1734-8
- Geng, J., and Klionsky, D. J. (2008). The Atg8 and Atg12 ubiquitin-like conjugation systems in macroautophagy. 'Protein modifications: Beyond the usual suspects' review series. *EMBO Rep.* 9, 859–864. doi: 10.1038/embor.2008.163
- Ghadage, D. P., Choure, A. C., Wankhade, A. B., and Bhore, A. V. (2017). Opportunistic free: Living amoeba now becoming a usual pathogen? *Indian J. Pathol. Microbiol.* 60, 601–603. doi: 10.4103/ijpm.ijpm\_815\_16
- Gonçalves, D. S., Ferreira, M. D. S., Gomes, K. X., Rodríguez-de la Noval, C., Liedke, S. C., da Costa, G. C. V., et al. (2019). Unravelling the interactions of the environmental host *Acanthamoeba castellanii* with fungi through the recognition by mannose-binding proteins. *Cell Microbiol.* 21:e13066. doi: 10.1111/cmi.13066
- Gonzalez, M. M., Gould, E., Dickinson, G., Martinez, A. J., Visvesvara, G., Cleary, T. J., et al. (1986). Acquired immunodeficiency syndrome associated with *Acanthamoeba* infection and other opportunistic organisms. *Arch. Pathol. Lab. Med.* 110, 749–751.
- Gu, X., Lu, X., Lin, S., Shi, X., Shen, Y., Lu, Q., et al. (2022). A comparative genomic approach to determine the virulence factors and horizontal gene transfer events of clinical *Acanthamoeba* isolates. *Microbiol. Spectr.* 10, e0002522. doi: 10.1128/spectrum.00025-22
- Guzmán-Téllez, P., Martínez-Castillo, M., Flores-Huerta, N., Rosales-Morgan, G., Pacheco-Yépez, J., la Garza, M., et al. (2020). Lectins as virulence factors in *Entamoeba histolytica* and free-living amoebae. *Future Microbiol.* 15, 919–936. doi: 10.2217/fmb-2019-0275
- Hadas, E., and Mazur, T. (1993). Proteolytic enzymes of pathogenic and non-pathogenic strains of *Acanthamoeba* spp. *Trop. Med. Parasitol.* 44, 197–200.
- Hanada, T., Noda, N. N., Satomi, Y., Ichimura, Y., Fujioka, Y., Takao, T., et al. (2007). The Atg12-Atg5 conjugate has a novel E3-like activity for protein lipidation in autophagy. *J. Biol. Chem.* 282, 37298–37302. doi: 10.1074/jbc.C700195200
- Hänel, H., Kirsch, R., Schmidts, H. L., and Kottmann, H. (1995). New systematically active antimycotics from the beta-blocker category. *Mycoses* 38, 251–264. doi: 10.1111/j.1439-0507.1995.tb00404.x
- Harbour, J. W., and Dean, D. C. (2000). Rb function in cell-cycle regulation and apoptosis. *Nat. Cell Biol.* 2, E65–E67. doi: 10.1038/35008695
- Hasby Saad, M. A., and Khalil, H. S. M. (2018). Biofilm testing of microbiota: An essential step during corneal scrap examination in Egyptian acanthamoebic keratitis cases. *Parasitol. Int.* 67, 556–564. doi: 10.1016/j.parint.2018.05.001
- Hassan, F., Bhatti, A., Desai, R., and Barua, A. (2019). Analysis from a year of increased cases of *Acanthamoeba* keratitis in a large teaching hospital in the UK. *Cont. Lens Anterior Eye* 42, 506–511. doi: 10.1016/j.clae.2019.04.009
- He, Y. G., Niederkorn, J. Y., McCulley, J. P., Stewart, G. L., Meyer, D. R., Silvary, R., et al. (1990). In vivo and in vitro collagenolytic activity of *Acanthamoeba castellanii*. *Invest. Ophthalmol. Vis. Sci.* 31, 2235–2240.
- Heidemann, D. G., Verdier, D. D., Dunn, S. P., and Stamler, J. F. (1990). *Acanthamoeba* keratitis associated with disposable contact lenses. *Am. J. Ophthalmol.* 110, 630–634. doi: 10.1016/s0002-9394(14)77059-x
- Hewett, M. K., Robinson, B. S., Monis, P. T., and Saint, C. P. (2003). Identification of a new *Acanthamoeba* 18S rRNA gene sequence type, corresponding to the species *Acanthamoeba jacobsoni* Sawyer, Nerad and Visvesvara, 1992 (Lobosea: Acanthamoebidae). *Acta Protozool.* 42, 325–329.
- Höllhumer, R., Keay, L., and Watson, S. L. (2020). *Acanthamoeba* keratitis in Australia: Demographics, associated factors, presentation and outcomes: A 15-year case review. *Eye* 34, 725–732. doi: 10.1038/s41433-019-0589-6
- Hong, Y. C., Hwang, M. Y., Yun, H. C., Yu, H. S., Kong, H. H., Yong, T. S., et al. (2002). Isolation and characterization of a cDNA encoding a mammalian cathepsin L-like cysteine proteinase from *Acanthamoeba healyi*. *Korean J. Parasitol.* 40, 17–24. doi: 10.3347/kjp.2002.40.1.17
- Hong, Y. C., Lee, W. M., Kong, H. H., Jeong, H. J., and Chung, D. I. (2004). Molecular cloning and characterization of a cDNA encoding a laminin-binding protein (AhLBP) from *Acanthamoeba healyi*. *Exp. Parasitol.* 106, 95–102. doi: 10.1016/j.exppara.2004.01.011
- Hong, Y., Kang, J. M., Joo, S. Y., Song, S. M., Lé, H. G., Thái, T. L., et al. (2018). Molecular and biochemical properties of a cysteine protease of *Acanthamoeba castellanii*. *Korean J. Parasitol.* 56, 409–418. doi: 10.3347/kjp.2018.56.5.409
- Hong, Z. B., Huang, J. M., Tsai, C. M., and Lin, W. C. (2022). Potential role of *Acanthamoeba* Rab7. *Exp. Parasitol.* 239:108312. doi: 10.1016/j.exppara.2022.108312
- Huang, J. M., Chang, Y. T., Shih, M. H., Lin, W. C., and Huang, F. C. (2019). Identification and characterization of a secreted M28 aminopeptidase protein in *Acanthamoeba*. *Parasitol. Res.* 118, 1865–1874. doi: 10.1007/s00436-019-06332-8
- Huang, J. M., Liao, C. C., Kuo, C. C., Chen, L. R., Huang, L. L. H., Shin, J. W., et al. (2017). Pathogenic *Acanthamoeba castellanii* secretes the extracellular aminopeptidase M20/M25/M40 family protein to target cells for phagocytosis by disruption. *Molecules* 22:2263. doi: 10.3390/molecules22122263
- Huang, W. P., and Klionsky, D. J. (2002). Autophagy in yeast: A review of the molecular machinery. *Cell Struct. Funct.* 27, 409–420. doi: 10.1247/csf.27.409
- Huth, S., Reverey, J. F., Leippe, M., and Selhuber-Unkel, C. (2017). Adhesion forces and mechanics in mannose-mediated *Acanthamoeba* interactions. *PLoS One* 12:e0176207. doi: 10.1371/journal.pone.0176207
- Ibrahim, Y. W., Boase, D. L., and Cree, I. A. (2007). Factors affecting the epidemiology of *Acanthamoeba* keratitis. *Ophthalmic Epidemiol.* 14, 53–60. doi: 10.1080/09286580600920281
- Ibrahim, Y. W., Boase, D. L., and Cree, I. A. (2009). How could contact lens wearers be at risk of *Acanthamoeba* infection? A review. *J. Optom.* 2, 60–66.
- Ichimura, Y., Imamura, Y., Emoto, K., Umeda, M., Noda, T., and Ohsumi, Y. (2004). In vivo and in vitro reconstitution of Atg8 conjugation essential for autophagy. *J. Biol. Chem.* 279, 40584–40592. doi: 10.1074/jbc.M405860200
- Ichimura, Y., Kirisako, T., Takao, T., Satomi, Y., Shimonishi, Y., Ishihara, N., et al. (2000). A ubiquitin-like system mediates protein lipidation. *Nature* 408, 488–492. doi: 10.1038/35044114
- Im, K. I., and Shin, H. J. (2003). *Acanthamoeba sohi*, n. sp., a pathogenic Korean isolate YM-4 from a freshwater fish. *Korean J. Parasitol.* 41, 181–188. doi: 10.3347/kjp.2003.41.4.181
- Im, K., and Kim, D. S. (1998). Acanthamoebiasis in Korea: Two new cases with clinical cases review. *Yonsei Med. J.* 39, 478–484. doi: 10.3349/ymj.1998.39.5.478
- Ishihara, N., Hamasaki, M., Yokota, S., Suzuki, K., Kamada, Y., Kihara, A., et al. (2001). Autophagosome requires specific early Sec proteins for its formation and NSF/SNARE for vacuolar fusion. *Mol. Biol. Cell* 12, 3690–3702. doi: 10.1091/mbc.12.11.3690
- Jha, B. K., Jung, H. J., Seo, I., Kim, H. A., Suh, S. I., Suh, M. H., et al. (2014). Chloroquine has a cytotoxic effect on *Acanthamoeba* encystation through modulation of autophagy. *Antimicrob. Agents Chemother.* 58, 6235–6241. doi: 10.1128/aac.03164-14
- Jiang, C., Sun, X., Wang, Z., and Zhang, Y. (2015). *Acanthamoeba* keratitis: Clinical characteristics and management. *Ocul. Surf.* 13, 164–168. doi: 10.1016/j.jtos.2015.01.002
- Jiménez, C., Portela, R. A., Mellado, M., Rodríguez-Frade, J. M., Collard, J., Serrano, A., et al. (2000). Role of the PI3K regulatory subunit in the control of actin organization and cell migration. *J. Cell Biol.* 151, 249–262. doi: 10.1083/jcb.151.2.249
- Jimenez-Sandoval, P., Lopez-Castillo, L. M., Traviña-Arenas, C. H., and Brieba, L. G. (2017). Cysteine proteases inhibitors with immunoglobulin-like fold in protozoan parasites and their role in pathogenesis. *Curr. Protein Pept. Sci.* 18, 1035–1042. doi: 10.2174/1389203717666160813163837
- John, T., Desai, D., and Sahm, D. (1989). Adherence of *Acanthamoeba castellanii* cysts and trophozoites to unworn soft contact lenses. *Am. J. Ophthalmol.* 108, 658–664. doi: 10.1016/0002-9394(89)90857-x



- Joo, S. Y., Aung, J. M., Shin, M., Moon, E. K., Kong, H. H., Goo, Y. K., et al. (2020). The role of the *Acanthamoeba castellanii* Sir2-like protein in the growth and encystation of *Acanthamoeba*. *Parasit. Vectors* 13:368. doi: 10.1186/s13071-020-04237-5
- Joo, S. Y., Aung, J. M., Shin, M., Moon, E. K., Kong, H. H., Goo, Y. K., et al. (2022). Sirtinol suppresses trophozoites proliferation and encystation of *Acanthamoeba* via inhibition of sirtuin family protein. *Korean J. Parasitol.* 60, 1–6. doi: 10.3347/kjp.2022.60.1.1
- Kaeberlein, M., McVey, M., and Guarente, L. (1999). The SIR2/3/4 complex and SIR2 alone promote longevity in *Saccharomyces cerevisiae* by two different mechanisms. *Genes Dev.* 13, 2570–2580. doi: 10.1101/gad.13.19.2570
- Kaiserman, I., Bahar, I., McAllum, P., Srinivasan, S., Elbaz, U., Slomovic, A. R., et al. (2012). Prognostic factors in *Acanthamoeba* keratitis. *Can. J. Ophthalmol.* 47, 312–317. doi: 10.1016/j.cjco.2012.03.040
- Kalra, S. K., Sharma, P., Shyam, K., Tejan, N., and Ghoshal, U. (2020). *Acanthamoeba* and its pathogenic role in granulomatous amebic encephalitis. *Exp. Parasitol.* 208:107788. doi: 10.1016/j.exppara.2019.107788
- Kaul, D. R., Lowe, L., Visvesvara, G. S., Farmen, S., Khaled, Y. A., and Yanik, G. A. (2008). *Acanthamoeba* infection in a patient with chronic graft-versus-host disease occurring during treatment with voriconazole. *Transpl. Infect. Dis.* 10, 437–441. doi: 10.1111/j.1399-3062.2008.00335.x
- Khan, N. A. (2006). *Acanthamoeba*: Biology and increasing importance in human health. *FEMS Microbiol. Rev.* 30, 564–595. doi: 10.1111/j.1574-6976.2006.00023.x
- Khunkitti, W., Lloyd, D., Furr, J. R., and Russell, A. D. (1998). *Acanthamoeba castellanii*: Growth, encystment, excystment and biocide susceptibility. *J. Infect.* 36, 43–48. doi: 10.1016/s0163-4453(98)90354-7
- Kilvington, S. (1993). *Acanthamoeba* trophozoite and cyst adherence to four types of soft contact lens and removal by cleaning agents. *Eye* 7(Pt 4), 535–538. doi: 10.1038/eye.1993.116
- Kim, J. H., Matin, A., Shin, H. J., Park, H., Yoo, K. T., Yuan, X. Z., et al. (2012). Functional roles of mannose-binding protein in the adhesion, cytotoxicity and phagocytosis of *Acanthamoeba castellanii*. *Exp. Parasitol.* 132, 287–292. doi: 10.1016/j.exppara.2012.08.007
- Kim, J., Huang, W. P., Stromhaug, P. E., and Klionsky, D. J. (2002). Convergence of multiple autophagy and cytoplasm to vacuole targeting components to a perivacuolar membrane compartment prior to de novo vesicle formation. *J. Biol. Chem.* 277, 763–773. doi: 10.1074/jbc.M109134200
- Kim, S. H., Moon, E. K., Hong, Y., Chung, D. I., and Kong, H. H. (2015). Autophagy protein 12 plays an essential role in *Acanthamoeba* encystation. *Exp. Parasitol.* 159, 46–52. doi: 10.1016/j.exppara.2015.08.013
- Kirisako, T., Ichimura, Y., Okada, H., Kabeya, Y., Mizushima, N., Yoshimori, T., et al. (2000). The reversible modification regulates the membrane-binding state of Apg8/Aut7 essential for autophagy and the cytoplasm to vacuole targeting pathway. *J. Cell Biol.* 151, 263–276. doi: 10.1083/jcb.151.2.263
- Kitching, J. A. (1956). *Food vacuoles. Protoplasmatologia III D 3b(1)*. Bristol: Springer-Verlag.
- Kitching, J. A. (1967). “Contractile vacuoles, ionic regulation, and excretion,” in *Research in protozoology*, ed. T. T. Chen (New York, NY: Pergamon Press, Inc).
- Klemba, M., and Goldberg, D. E. (2002). Biological roles of proteases in parasitic protozoa. *Annu. Rev. Biochem.* 71, 275–305. doi: 10.1146/annurev.biochem.71.090501.145453
- Kong, H. H. (2009). Molecular phylogeny of *Acanthamoeba*. *Korean J. Parasitol.* 47 Suppl(Suppl.), S21–S28. doi: 10.3347/kjp.2009.47.S21
- Kong, H. H., Kim, T. H., and Chung, D. I. (2000). Purification and characterization of a secretory serine proteinase of *Acanthamoeba healyi* isolated from GAE. *J. Parasitol.* 86, 12–17.
- Kot, K., Łanocha-Arendarczyk, N. A., and Kosik-Bogacka, D. I. (2018). Amoebas from the genus *Acanthamoeba* and their pathogenic properties. *Ann. Parasitol.* 64, 299–308. doi: 10.17420/ap6404.164
- Kot, K., Łanocha-Arendarczyk, N., and Kosik-Bogacka, D. (2021). Immunopathogenicity of *Acanthamoeba* spp. in the brain and lungs. *Int. J. Mol. Sci.* 22:1261. doi: 10.3390/ijms22031261
- Kutner, A., Aldrich, M., Patel, S., Kang, J. J., Amin, B., Mann, R., et al. (2018). *Acanthamoeba* endophthalmitis during treatment for cutaneous disease in a renal transplant patient. *Transpl. Infect. Dis.* 20:e12843. doi: 10.1111/tid.12843
- Kuzman, T., Kutija, M. B., Juri, J., Jandroković, S., Skegro, I., Olujić, S. M., et al. (2014). Lens wearers non-compliance – Is there an association with lens case contamination? *Cont. Lens Anterior Eye* 37, 99–105. doi: 10.1016/j.clae.2013.08.004
- Lackner, P., Beer, R., Broessner, G., Helbok, R., Pfausler, B., Brenneis, C., et al. (2010). Acute granulomatous *Acanthamoeba* encephalitis in an immunocompetent patient. *Neurocrit. Care* 12, 91–94. doi: 10.1007/s12028-009-9291-z
- Lakhundi, S., Siddiqui, R., and Khan, N. A. (2015). Cellulose degradation: A therapeutic strategy in the improved treatment of *Acanthamoeba* infections. *Parasit. Vectors* 8:23. doi: 10.1186/s13071-015-0642-7
- Lalitha, M. K., Anandi, V., Srivastava, A., Thomas, K., Cherian, A. M., and Chandhi, S. M. (1985). Isolation of *Acanthamoeba culbertsoni* from a patient with meningitis. *J. Clin. Microbiol.* 21, 666–667. doi: 10.1128/jcm.21.4.666-667.1985
- Łanocha-Arendarczyk, N., Baranowska-Bosiacka, I., Gutowska, I., Kolas-Wolosiuk, A., Kot, K., Łanocha, A., et al. (2018). The activity of matrix metalloproteinases (MMP-2, MMP-9) and their tissue inhibitors (TIMP-1, TIMP-3) in the cerebral cortex and hippocampus in experimental acanthamoebiasis. *Int. J. Mol. Sci.* 19:4128. doi: 10.3390/ijms19124128
- Lass, A., Guerrero, M., Li, X., Karanis, G., Ma, L., and Karanis, P. (2017). Detection of *Acanthamoeba* spp. in water samples collected from natural water reservoirs, sewages, and pharmaceutical factory drains using LAMP and PCR in China. *Sci. Total Environ.* 584–585, 489–494. doi: 10.1016/j.scitotenv.2017.01.046
- Lee, C. Y., Bagdasarian, M., Meng, M. H., and Zeikus, J. G. (1990). Catalytic mechanism of xylose (glucose) isomerase from *Clostridium thermosulfurogenes*. Characterization of the structural gene and function of active site histidine. *J. Biol. Chem.* 265, 19082–19090.
- Lee, G. H., Lee, J. E., Park, M. K., and Yu, H. S. (2016). Adhesion of *Acanthamoeba* on silicone hydrogel contact lenses. *Cornea* 35, 663–668. doi: 10.1097/ico.0000000000000788
- Lee, W. B., and Gotay, A. (2010). Bilateral *Acanthamoeba* keratitis in synergeyes contact lens wear: Clinical and confocal microscopy findings. *Eye Cont. Lens* 36, 164–169. doi: 10.1097/ICL.0b013e3181db3508
- Leher, H., Silvany, R., Alizadeh, H., Huang, J., and Niederkorn, J. Y. (1998). Mannose induces the release of cytopathic factors from *Acanthamoeba castellanii*. *Infect. Immun.* 66, 5–10. doi: 10.1128/iai.66.1.5-10.1998
- Leitsch, D., Köhler, M., Marchetti-Deschmann, M., Deutsch, A., Allmaier, G., Duchêne, M., et al. (2010). Major role for cysteine proteases during the early phase of *Acanthamoeba castellanii* encystment. *Eukaryot. Cell* 9, 611–618. doi: 10.1128/ec.00300-09
- Lewis, E. J., and Sawyer, T. K. (1979). *Acanthamoeba tubisahi* n. sp., a new species of fresh water amoebida (Acanthamoebidae). *Trans. Amer. Microbiol. Soc.* 98, 543–549.
- Lin, S. J., Defossez, P. A., and Guarente, L. (2000). Requirement of NAD and SIR2 for life-span extension by calorie restriction in *Saccharomyces cerevisiae*. *Science* 289, 2126–2128. doi: 10.1126/science.289.5487.2126
- Linder, M., Winička-Krusnell, J., and Linder, E. (2002). Use of recombinant cellulose-binding domains of *Trichoderma reesei* cellulase as a selective immunocytochemical marker for cellulose in protozoa. *Appl. Environ. Microbiol.* 68, 2503–2508. doi: 10.1128/aem.68.5.2503-2508.2002
- Lindsay, R. G., Watters, G., Johnson, R., Ormonde, S. E., and Snibson, G. R. (2007). *Acanthamoeba* keratitis and contact lens wear. *Clin. Exp. Optom.* 90, 351–360. doi: 10.1111/j.1444-0938.2007.00172.x
- Lloyd, D., Turner, N. A., Khunkitti, W., Hann, A. C., Furr, J. R., and Russell, A. D. (2001). Encystation in *Acanthamoeba castellanii*: Development of biocide resistance. *J. Eukaryot. Microbiol.* 48, 11–16. doi: 10.1111/j.1550-7408.2001.tb00410.x
- Lorenzo-Morales, J., Khan, N. A., and Walochnik, J. (2015). An update on *Acanthamoeba* keratitis: Diagnosis, pathogenesis and treatment. *Parasite* 22:10. doi: 10.1051/parasite/2015010
- Lorenzo-Morales, J., Kliescikova, J., Martinez-Carretero, E., De Pablos, L. M., Profotova, B., Nohynkova, E., et al. (2008). Glycogen phosphorylase in *Acanthamoeba* spp.: Determining the role of the enzyme during the encystment process using RNA interference. *Eukaryot. Cell* 7, 509–517. doi: 10.1128/ec.00316-07
- Lorenzo-Morales, J., Martín-Navarro, C. M., López-Arencibia, A., Arnalich-Montiel, F., Piñero, J. E., and Valladares, B. (2013). *Acanthamoeba* keratitis: An emerging disease gathering importance worldwide? *Trends Parasitol.* 29, 181–187. doi: 10.1016/j.pt.2013.01.006
- Lorenzo-Morales, J., Morcillo-Laiz, R., Martín-Navarro, C. M., López-Vélez, R., López-Arencibia, A., Arnalich-Montiel, F., et al. (2011). *Acanthamoeba* keratitis due to genotype T11 in a rigid gas permeable contact lens wearer in Spain. *Cont. Lens Anterior Eye* 34, 83–86. doi: 10.1016/j.clae.2010.10.007
- Lorenzo-Morales, J., Ortega-Rivas, A., Foronda, P., Abreu-Acosta, N., Ballart, D., Martínez, E., et al. (2005). RNA interference (RNAi) for the silencing of extracellular serine proteases genes in *Acanthamoeba*: Molecular analysis and effect on pathogenicity. *Mol. Biochem. Parasitol.* 144, 10–15. doi: 10.1016/j.molbiopara.2005.07.001
- Lynd, L. R., Weimer, P. J., van Zyl, W. H., and Pretorius, I. S. (2002). Microbial cellulose utilization: Fundamentals and biotechnology. *Microbiol. Mol. Biol. Rev.* 66, 506–577, table of contents. doi: 10.1128/mmbr.66.3.506-577.2002
- Maciver, S. K., Asif, M., Simmen, M. W., and Lorenzo-Morales, J. (2013). A systematic analysis of *Acanthamoeba* genotype frequency correlated with source and pathogenicity: T4 is confirmed as a pathogen-rich genotype. *Eur. J. Protistol.* 49, 217–221. doi: 10.1016/j.ejop.2012.11.004
- Mackay, D. J., and Hall, A. (1998). Rho GTPases. *J. Biol. Chem.* 273, 20685–20688. doi: 10.1074/jbc.273.33.20685
- Maghsood, A. H., Sissons, J., Rezaian, M., Nolder, D., Warhurst, D., and Khan, N. A. (2005). *Acanthamoeba* genotype T4 from the UK and Iran and isolation of

- the T2 genotype from clinical isolates. *J. Med. Microbiol.* 54(Pt 8), 755–759. doi: 10.1099/jmm.0.45970-0
- Magistrado-Coxen, P., Aqeel, Y., Lopez, A., Haserick, J. R., Urbanowicz, B. R., Costello, C. E., et al. (2019). The most abundant cyst wall proteins of *Acanthamoeba castellanii* are lectins that bind cellulose and localize to distinct structures in developing and mature cyst walls. *PLoS Negl. Trop. Dis.* 13:e0007352. doi: 10.1371/journal.pntd.0007352
- Marciano-Cabral, F., and Cabral, G. (2003). *Acanthamoeba* spp. as agents of disease in humans. *Clin. Microbiol. Rev.* 16, 273–307. doi: 10.1128/cmr.16.2.273-307.2003
- Matin, A., and Jung, S. Y. (2011). Phospholipase activities in clinical and environmental isolates of *Acanthamoeba*. *Korean J. Parasitol.* 49, 1–8. doi: 10.3347/kjp.2011.49.1.1
- Matsui, T., Maeda, T., Kusakabe, S., Arita, H., Yagita, K., Morii, E., et al. (2018). A case report of granulomatous amoebic encephalitis by group 1 *Acanthamoeba* genotype T18 diagnosed by the combination of morphological examination and genetic analysis. *Diagn. Pathol.* 13:27. doi: 10.1186/s13000-018-0706-z
- Mattana, A., Cappai, V., Alberti, L., Serra, C., Fiori, P. L., and Cappuccinelli, P. (2002). ADP and other metabolites released from *Acanthamoeba castellanii* lead to human monocytic cell death through apoptosis and stimulate the secretion of proinflammatory cytokines. *Infect. Immun.* 70, 4424–4432. doi: 10.1128/iai.70.8.4424-4432.2002
- Maycock, N. J., and Jayaswal, R. (2016). Update on *Acanthamoeba* keratitis: Diagnosis, treatment, and outcomes. *Cornea* 35, 713–720. doi: 10.1097/ico.0000000000000804
- Mazur, T., Hadaš, E., and Iwanicka, I. (1995). The duration of the cyst stage and the viability and virulence of *Acanthamoeba* isolates. *Trop. Med. Parasitol.* 46, 106–108.
- Michel, R., Hauröder-Philippczyk, B., Müller, K., and Weishaar, I. (1994). *Acanthamoeba* from human nasal mucosa infected with an obligate intracellular parasite. *Eur. J. Protistol.* 30, 104–110.
- Miller, H. W., Suleiman, R. L., and Ralston, K. S. (2019). Trophocytosis by *Entamoeba histolytica* mediates acquisition and display of human cell membrane proteins and evasion of lysis by human serum. *mBio* 10:e00068-19. doi: 10.1128/mBio.00068-19
- Mirsayafov, D. S., Albert, T. G., Shmakov, A. N., and Asitinskaya, P. V. (2018). Tap water and risk of *Acanthamoeba* keratitis in rigid gas-permeable lens wearers: Sacred cow or culprit? *Eye Cont. Lens* 44, 132–136. doi: 10.1097/icl.0000000000000450
- Mitro, K., Bhagavathiammai, A., Zhou, O. M., Bobbett, G., McKerrow, J. H., Chokshi, R., et al. (1994). Partial characterization of the proteolytic secretions of *Acanthamoeba polyphaga*. *Exp. Parasitol.* 78, 377–385. doi: 10.1006/expr.1994.1041
- Mondino, B. J., Chou, H. J., and Sumner, H. L. (1996). Generation of complement membrane attack complex in normal human corneas. *Invest. Ophthalmol. Vis. Sci.* 37, 1576–1581.
- Moon, E. K., and Kong, H. H. (2012). Short-cut pathway to synthesize cellulose of encysting *Acanthamoeba*. *Korean J. Parasitol.* 50, 361–364. doi: 10.3347/kjp.2012.50.4.361
- Moon, E. K., Chung, D. I., Hong, Y. C., and Kong, H. H. (2008b). Characterization of a serine proteinase mediating encystation of *Acanthamoeba*. *Eukaryot. Cell* 7, 1513–1517. doi: 10.1128/ec.00068-08
- Moon, E. K., Chung, D. I., Hong, Y. C., Ahn, T. I., and Kong, H. H. (2008a). *Acanthamoeba castellanii*: Gene profile of encystation by ESTs analysis and KOG assignment. *Exp. Parasitol.* 119, 111–116. doi: 10.1016/j.exppara.2008.01.001
- Moon, E. K., Chung, D. I., Hong, Y. C., and Kong, H. H. (2007). Differentially expressed genes of *Acanthamoeba castellanii* during encystation. *Korean J. Parasitol.* 45, 283–285. doi: 10.3347/kjp.2007.45.4.283
- Moon, E. K., Kim, J. O., Xuan, Y. H., Yun, Y. S., Kang, S. W., Lee, Y. S., et al. (2009b). Construction of EST database for comparative gene studies of *Acanthamoeba*. *Korean J. Parasitol.* 47, 103–107. doi: 10.3347/kjp.2009.47.2.103
- Moon, E. K., Chung, D. I., Hong, Y. C., and Kong, H. H. (2009a). Autophagy protein 8 mediating autophagosome in encysting *Acanthamoeba*. *Mol. Biochem. Parasitol.* 168, 43–48. doi: 10.1016/j.molbiopara.2009.06.005
- Moon, E. K., Xuan, Y. H., Chung, D. I., Hong, Y., and Kong, H. H. (2011b). Microarray analysis of differentially expressed genes between cysts and trophozoites of *Acanthamoeba castellanii*. *Korean J. Parasitol.* 49, 341–347. doi: 10.3347/kjp.2011.49.4.341
- Moon, E. K., Chung, D. I., Hong, Y., and Kong, H. H. (2011a). Atg3-mediated lipidation of Atg8 is involved in encystation of *Acanthamoeba*. *Korean J. Parasitol.* 49, 103–108. doi: 10.3347/kjp.2011.49.2.103
- Moon, E. K., Hong, Y., Chung, D. I., and Kong, H. H. (2012b). Cysteine protease involving in autophagosomal degradation of mitochondria during encystation of *Acanthamoeba*. *Mol. Biochem. Parasitol.* 185, 121–126. doi: 10.1016/j.molbiopara.2012.07.008
- Moon, E. K., Chung, D. I., Hong, Y., and Kong, H. H. (2012a). Protein kinase C signaling molecules regulate encystation of *Acanthamoeba*. *Exp. Parasitol.* 132, 524–529. doi: 10.1016/j.exppara.2012.07.008
- Moon, E. K., Hong, Y., Chung, D. I., and Kong, H. H. (2013). Identification of atg8 isoform in encysting *Acanthamoeba*. *Korean J. Parasitol.* 51, 497–502. doi: 10.3347/kjp.2013.51.5.497
- Moon, E. K., Hong, Y., Chung, D. I., Goo, Y. K., and Kong, H. H. (2014). Down-regulation of cellulose synthase inhibits the formation of endocysts in *Acanthamoeba*. *Korean J. Parasitol.* 52, 131–135. doi: 10.3347/kjp.2014.52.2.131
- Moon, E. K., Hong, Y., Chung, D. I., Goo, Y. K., and Kong, H. H. (2016). Identification of protein arginine methyltransferase 5 as a regulator for encystation of *Acanthamoeba*. *Korean J. Parasitol.* 54, 133–138. doi: 10.3347/kjp.2016.54.2.133
- Moon, E. K., Hong, Y., Lee, H. A., Quan, F. S., and Kong, H. H. (2017). DNA methylation of gene expression in *Acanthamoeba castellanii* encystation. *Korean J. Parasitol.* 55, 115–120. doi: 10.3347/kjp.2017.55.2.115
- Moore, M. B., McCulley, J. P., Luckenbach, M., Gelender, H., Newton, C., McDonald, M. B., et al. (1985). *Acanthamoeba* keratitis associated with soft contact lenses. *Am. J. Ophthalmol.* 100, 396–403. doi: 10.1016/0002-9394(85)90500-8
- Morgan, P. B., Efron, N., Woods, C. A., Jones, D., Pesinova, A., Grein, H., et al. (2006). International contact lens prescribing in 2005. *Cont. Lens Spect.* 21, 35–39.
- Moura, H., Wallace, S., and Visvesvara, G. S. (1992). *Acanthamoeba* *healyi* n. sp. and the isoenzyme and immunoblot profiles of *Acanthamoeba* spp., groups 1 and 3. *J. Protozool.* 39, 573–583. doi: 10.1111/j.1550-7408.1992.tb04853.x
- Müller, M. (1969). Lysosomal hydrolases in *Acanthamoeba* sp. *J. Protozool.* 16, 428–431. doi: 10.1111/j.1550-7408.1969.tb02294.x
- Müller, M., and Moller, K. M. (1969). Urate oxidase and its association with peroxisomes in *Acanthamoeba* sp. *Eur. J. Biochem.* 9, 424–430. doi: 10.1111/j.1432-1033.1969.tb00626.x
- Murakawa, G. J., McCalmont, T., Altman, J., Telang, G. H., Hoffman, M. D., Kantor, G. R., et al. (1995). Disseminated acanthamebiasis in patients with AIDS. A report of five cases and a review of the literature. *Arch. Dermatol.* 131, 1291–1296.
- Na, B. K., Cho, J. H., Song, C. Y., and Kim, T. S. (2002). Degradation of immunoglobulins, protease inhibitors and interleukin-1 by a secretory proteinase of *Acanthamoeba castellanii*. *Korean J. Parasitol.* 40, 93–99. doi: 10.3347/kjp.2002.40.2.93
- Na, B. K., Kim, J. C., and Song, C. Y. (2001). Characterization and pathogenic role of proteinase from *Acanthamoeba castellanii*. *Microb. Pathog.* 30, 39–48. doi: 10.1006/mpat.2000.0403
- Naginton, J., Watson, P. G., Playfair, T. J., McGill, J., Jones, B. R., and Steele, A. D. (1974). Amoebic infection of the eye. *Lancet* 2, 1537–1540. doi: 10.1016/s0140-6736(74)90285-2
- Nakada-Tsukui, K., and Nozaki, T. (2021). Trophocytosis in unicellular eukaryotes. *Cells* 10:2975. doi: 10.3390/cells10112975
- Nakatogawa, H. (2020). Mechanisms governing autophagosome biogenesis. *Nat. Rev. Mol. Cell Biol.* 21, 439–458. doi: 10.1038/s41580-020-0241-0
- National Library of Medicine (2020). *Polyhexamethylene Biguanide (PHMB) ophthalmic solution in subjects affected by Acanthamoeba keratitis*. Bethesda, MD: National Library of Medicine.
- Nau, A., and Dhaliwal, D. K. (2018). Exposure to tap water puts a contact lens wearer at greater risk of exposure to *Acanthamoeba*. *Eye Cont. Lens* 44:136. doi: 10.1097/icl.0000000000000453
- Neelam, S., and Niederkorn, J. Y. (2017). Pathobiology and immunobiology of *Acanthamoeba* keratitis: Insights from animal models. *Yale J. Biol. Med.* 90, 261–268.
- Neff, R. J., and Neff, R. H. (1969). The biochemistry of amoebic encystment. *Symp. Soc. Exp. Biol.* 23, 51–81.
- Nerad, T. A., Sawyer, T. K., Lewis, E. J., and McLaughlin, S. M. (1995). *Acanthamoeba pearcei* n. sp. (Protozoa: Amoebozoa) from sewage contaminated sediments. *J. Eukaryot. Microbiol.* 42, 702–705. doi: 10.1111/j.1550-7408.1995.tb01619.x
- Ng, S. L., Nordin, A., Abd Ghafar, N., Suboh, Y., Ab Rahim, N., and Chua, K. H. (2017). *Acanthamoeba*-mediated cytopathic effect correlates with MBP and AhLBP mRNA expression. *Parasit. Vectors* 10:625. doi: 10.1186/s13071-017-2547-0
- Niederkorn, J. Y. (2007). The induction of anterior chamber-associated immune deviation. *Chem. Immunol. Allergy* 92, 27–35. doi: 10.1159/000099251
- Niederkorn, J. Y., Alizadeh, H., Leher, H., and McCulley, J. P. (1999). The pathogenesis of *Acanthamoeba* keratitis. *Microbes Infect.* 1, 437–443. doi: 10.1016/s1286-4579(99)80047-1
- Nomura, H., Suda, N., Kawano, Y., Isshiki, Y., Sakuda, K., Sakuma, K., et al. (2022). Effects of oakmoss components on extra- and intracellular *Legionella pneumophila* and its host *Acanthamoeba castellanii*. *Biocontrol Sci.* 27, 21–29. doi: 10.4265/bio.27.21
- Nuprasert, W., Putaporntip, C., Pariyakanok, L., and Jongwutiwes, S. (2010). Identification of a novel t17 genotype of *Acanthamoeba* from environmental isolates and t10 genotype causing keratitis in Thailand. *J. Clin. Microbiol.* 48, 4636–4640. doi: 10.1128/jcm.01090-10
- Ohsumi, Y., and Mizushima, N. (2004). Two ubiquitin-like conjugation systems essential for autophagy. *Semin. Cell Dev. Biol.* 15, 231–236. doi: 10.1016/j.semcdb.2003.12.004

- Oishi, K., Raynor, R. L., Charp, P. A., and Kuo, J. F. (1988). Regulation of protein kinase C by lysophospholipids. Potential role in signal transduction. *J. Biol. Chem.* 263, 6865–6871.
- Oldenburg, C. E., Acharya, N. R., Tu, E. Y., Zegans, M. E., Mannis, M. J., Gaynor, B. D., et al. (2011). Practice patterns and opinions in the treatment of *Acanthamoeba* keratitis. *Cornea* 30, 1363–1368. doi: 10.1097/ICO.0b013e31820f7763
- Omaña-Molina, M. A., González-Robles, A., Salazar-Villatoro, L., Bernal-Escobar, A., Durán-Díaz, A., Méndez-Cruz, A. R., et al. (2014). Silicone hydrogel contact lenses surface promote *Acanthamoeba castellanii* trophozoites adherence: Qualitative and quantitative analysis. *Eye Cont. Lens* 40, 132–139. doi: 10.1097/icl.000000000000024
- Omaña-Molina, M., Hernandez-Martinez, D., Sanchez-Rocha, R., Cardenas-Lemus, U., Salinas-Lara, C., Mendez-Cruz, A. R., et al. (2017). In vivo CNS infection model of *Acanthamoeba* genotype T4: The early stages of infection lack presence of host inflammatory response and are a slow and contact-dependent process. *Parasitol. Res.* 116, 725–733. doi: 10.1007/s00436-016-5338-1
- Otero-Ruiz, A., Gonzalez-Zuñiga, L. D., Rodriguez-Anaya, L. Z., Lares-Jiménez, L. F., Gonzalez-Galaviz, J. R., and Lares-Villa, F. (2022). Distribution and current state of molecular genetic characterization in pathogenic free-living amoebae. *Pathogens* 11:1199. doi: 10.3390/pathogens11101199
- Page, F. C. (1967). Re-definition of the genus *Acanthamoeba* with descriptions of three species. *J. Protozool.* 14, 709–724. doi: 10.1111/j.1550-7408.1967.tb02066.x
- Papa, V., van der Meulen, I., Rottey, S., Sallet, G., Overweel, J., Asero, N., et al. (2022). Safety and tolerability of topical polyhexamethylene biguanide: A randomised clinical trial in healthy adult volunteers. *Br. J. Ophthalmol.* 106, 190–196. doi: 10.1136/bjophthalmol-2020-317848
- Parija, S. C., Dinoop, K., and Venugopal, H. (2015). Management of granulomatous amebic encephalitis: Laboratory diagnosis and treatment. *Trop. Parasitol.* 5, 23–28. doi: 10.4103/2229-5070.149889
- Parks, W. C., Wilson, C. L., and López-Boado, Y. S. (2004). Matrix metalloproteinases as modulators of inflammation and innate immunity. *Nat. Rev. Immunol.* 4, 617–629. doi: 10.1038/nri1418
- Pellegrin, J. L., Ortega-Barria, E., Barza, M., Baum, J., and Pereira, M. E. (1991). Neuraminidase activity in *Acanthamoeba* species trophozoites and cysts. *Invest. Ophthalmol. Vis. Sci.* 32, 3061–3066.
- Pellegrin, J. L., Ortega-Barria, E., Prioli, R. P., Meijia, J. S., and Pereira, M. E. (1992). The neuraminidases of *Trypanosoma cruzi* and *Acanthamoeba castellanii* are immunologically related. *Trop. Med. Parasitol.* 43, 33–37.
- Pettit, D. A., Williamson, J., Cabral, G. A., and Marciano-Cabral, F. (1996). In vitro destruction of nerve cell cultures by *Acanthamoeba* spp.: A transmission and scanning electron microscopy study. *J. Parasitol.* 82, 769–777.
- Phillips, I. L., Everman, J. L., Bermudez, L. E., and Danelishvili, L. (2020). *Acanthamoeba castellanii* as a screening tool for *Mycobacterium avium* subspecies paratuberculosis virulence factors with relevance in macrophage infection. *Microorganisms* 8:1571. doi: 10.3390/microorganisms8101571
- Portela, A., and Esteller, M. (2010). Epigenetic modifications and human disease. *Nat. Biotechnol.* 28, 1057–1068. doi: 10.1038/nbt.1685
- Potter, J. L., and Weisman, R. A. (1971). Differentiation in *Acanthamoeba*: Beta-glucan synthesis during encystment. *Biochim. Biophys. Acta* 237, 65–74. doi: 10.1016/0304-4165(71)90030-4
- Potter, J. L., and Weisman, R. A. (1972). Correlation of cellulose synthesis in vivo and in vitro during the encystment of *Acanthamoeba*. *Dev. Biol.* 28, 472–477. doi: 10.1016/0012-1606(72)90030-9
- Prasad, B. K., and Gupta, S. (1978). Preliminary report on the engulment and retention of mycobacteria by trophozoites of exenically grown *Acanthamoeba castellanii* Douglas, 1930. *Curr. Sci.* 47, 245–247.
- Preston, T. M., and King, C. A. (1984). Amoeboid locomotion of *Acanthamoeba castellanii* with special reference to cell-substratum interactions. *J. Gen. Microbiol.* 130, 2317–2323. doi: 10.1099/00221287-130-9-2317
- Preston, T. M., Richards, H., and Wotton, R. S. (2001). Locomotion and feeding of *Acanthamoeba* at the water-air interface of ponds. *FEMS Microbiol. Lett.* 194, 143–147. doi: 10.1111/j.1574-6968.2001.tb09459.x
- Proca-Ciobanu, M., Lupascu, G. H., Petrovici, A., and Ionescu, M. D. (1975). Electron microscopic study of a pathogenic *Acanthamoeba castellanii* strain: The presence of bacterial endosymbionts. *Int. J. Parasitol.* 5, 49–56. doi: 10.1016/0020-7519(75)90097-1
- Pussard, M. (1964b). *Acanthamoeba comandoni* n. sp., comparaison avec *A. terricola*. *Rev. Ecol. Biol. Sol.* 1, 587–610.
- Pussard, M. (1964a). Cytologie d'une amibe terricola: *Acanthamoeba terricola* n. sp. *Ann. Sci. Nat. Zool.* 6, 565–600.
- Pussard, M., and Pons, R. (1977). Morphologie de la paroi kystique et taxonomie du genre *Acanthamoeba* (Protozoa, Amoebozoa). *Protistologica* 13, 557–598.
- Putaporntip, C., Kuamsab, N., Nuprasert, W., Rojrung, R., Pattanawong, U., Tia, T., et al. (2021). Analysis of *Acanthamoeba* genotypes from public freshwater sources in Thailand reveals a new genotype, T23 *Acanthamoeba bangkokensis* sp. nov. *Sci. Rep.* 11:17290. doi: 10.1038/s41598-021-96690-0
- Quinet, T., Samba-Louaka, A., Héchard, Y., Van Doninck, K., and Van der Henst, C. (2020). Delayed cytokinesis generates multinuclearity and potential advantages in the amoeba *Acanthamoeba castellanii* Neff strain. *Sci. Rep.* 10:12109. doi: 10.1038/s41598-020-68694-9
- Qvarnstrom, Y., Nerad, T. A., and Visvesvara, G. S. (2013). Characterization of a new pathogenic *Acanthamoeba* species, *A. byersi* n. sp., isolated from a human with fatal amoebic encephalitis. *J. Eukaryot. Microbiol.* 60, 626–633. doi: 10.1111/jeu.12069
- Radford, C. F., Minassian, D. C., and Dart, J. K. (2002). *Acanthamoeba* keratitis in England and Wales: Incidence, outcome, and risk factors. *Br. J. Ophthalmol.* 86, 536–542. doi: 10.1136/bjo.86.5.536
- Raizada, M. K., and Krishna Murti, C. R. (1972). Transformation of trophic *Hartmannella culbertsoni* into viable cysts of cyclic 3',5'-adenosine monophosphate. *J. Cell Biol.* 52, 743–748. doi: 10.1083/jcb.52.3.743
- Ralston, K. S., Solga, M. D., Mackey-Lawrence, N. M., Bhattacharya, A., and Petri, W. A. Jr. (2014). Trophocytosis by *Entamoeba histolytica* contributes to cell killing and tissue invasion. *Nature* 508, 526–530. doi: 10.1038/nature13242
- Ramírez-Rico, G., Martínez-Castillo, M., de la Garza, M., Shibayama, M., and Serrano-Luna, J. (2015). *Acanthamoeba castellanii* proteases are capable of degrading iron-binding proteins as a possible mechanism of pathogenicity. *J. Eukaryot. Microbiol.* 62, 614–622. doi: 10.1111/jeu.12215
- Ray, D. L., and Hayes, R. E. (1954). *Hartmannella astronyxis*: A new species of free-living amoeba. *J. Morph.* 95, 159–187.
- Rayamajhee, B., Willcox, M. D. P., Henriquez, F. L., Petsoglou, C., Subedi, D., and Carnt, N. (2022). *Acanthamoeba*, an environmental phagocyte enhancing survival and transmission of human pathogens. *Trends Parasitol.* 38, 975–990. doi: 10.1016/j.pt.2022.08.007
- Reggiori, F., Shintani, T., Nair, U., and Klionsky, D. J. (2005). Atg9 cycles between mitochondria and the pre-autophagosomal structure in yeasts. *Autophagy* 1, 101–109. doi: 10.4161/auto.1.2.1840
- Reich, M. (1935). Studien über die bodenprotozoen Palastinas. *Arch. Protistenk.* 79, 76–98.
- Reif, K., Nobes, C. D., Thomas, G., Hall, A., and Cantrell, D. A. (1996). Phosphatidylinositol 3-kinase signals activate a selective subset of Rac/Rho-dependent effector pathways. *Curr. Biol.* 6, 1445–1455. doi: 10.1016/s0960-9822(96)00749-x
- Rivera, F., Lares, F., Gallegos, E., Ramirez, E., Bonilla, P., Calderon, A., et al. (1989). Pathogenic amoebae in natural thermal waters of three resorts of Hidalgo, Mexico. *Environ. Res.* 50, 289–295. doi: 10.1016/s0013-9351(89)80010-6
- Rivera, F., Lares, F., Ramirez, E., Bonilla, P., Rodriguez, S., Labastida, A., et al. (1991). Pathogenic *Acanthamoeba* isolated during an atmospheric survey in Mexico city. *Rev. Infect. Dis.* 13(Suppl. 5), S388–S389. doi: 10.1093/clind/13.supplement\_5.s388
- Rivera, F., Roy-Ocotla, G., Rosas, I., Ramirez, E., Bonilla, P., and Lares, F. (1987). Amoebae isolated from the atmosphere of Mexico city and environs. *Environ. Res.* 42, 149–154. doi: 10.1016/s0013-9351(87)80016-6
- Rocha-Azevedo, B. D., Jamerson, M., Cabral, G. A., Silva-Filho, F. C., and Marciano-Cabral, F. (2009). *Acanthamoeba* interaction with extracellular matrix glycoproteins: Biological and biochemical characterization and role in cytotoxicity and invasiveness. *J. Eukaryot. Microbiol.* 56, 270–278. doi: 10.1111/j.1550-7408.2009.00399.x
- Rocha-Azevedo, B., Jamerson, M., Cabral, G. A., and Marciano-Cabral, F. (2010). *Acanthamoeba culbertsoni*: Analysis of amoebic adhesion and invasion on extracellular matrix components collagen I and laminin-1. *Exp. Parasitol.* 126, 79–84. doi: 10.1016/j.exppara.2009.08.004
- Roshni Prithiviraj, S., Rajapandian, S. G. K., Gnanam, H., Gunasekaran, R., Mariappan, P., Sankalp Singh, S., et al. (2020). Clinical presentations, genotypic diversity and phylogenetic analysis of *Acanthamoeba* species causing keratitis. *J. Med. Microbiol.* 69, 87–95. doi: 10.1099/jmm.0.001121
- Saheb, E., Trzyna, W., Maringer, K., and Bush, J. (2015). Abnormalities of endocytosis, phagocytosis, and development process in *Dictyostelium* cells that over-express *Acanthamoeba castellanii* metacaspase protein. *Iran. J. Parasitol.* 10, 213–229.
- Sakoh-Nakatogawa, M., Matoba, K., Asai, E., Kirisako, H., Ishii, J., Noda, N. N., et al. (2013). Atg12-Atg5 conjugate enhances E2 activity of Atg3 by rearranging its catalytic site. *Nat. Struct. Mol. Biol.* 20, 433–439. doi: 10.1038/nsmb.2527
- Sauve, A. A., Celic, I., Avalos, J., Deng, H., Boeke, J. D., and Schramm, V. L. (2001). Chemistry of gene silencing: The mechanism of NAD<sup>+</sup>-dependent deacetylation reactions. *Biochemistry* 40, 15456–15463. doi: 10.1021/bi011858j
- Sawyer, T. K. (1971). *Acanthamoeba griffini*: A new species of marine amoeba. *J. Protozool.* 18, 650–654.
- Sawyer, T. K., and Nerad, T. A. (1992). *Acanthamoeba jacobsoni* sp. n. (Protozoa: Acanthamoebidae) from sewage contaminated ocean sediments. *J. Helminthol. Soc. Wash.* 59, 223–226.
- Sawyer, T. K., Nerad, T. A., Lewis, E. J., and McLaughlin, A. M. (1993). *Acanthamoeba stevensoni* N. Sp. (Protozoa: Amoebozoa) from sewage-contaminated shellfish beds in Raritan Bay, New York. *J. Eukaryot. Microbiol.* 40, 742–746.
- Sawyer, T. K., Visvesvara, G. S., and Harke, B. A. (1977). Pathogenic amoebas from brackish and ocean sediments, with a description of *Acanthamoeba hatchetti*, n. sp. *Science* 196, 1324–1325. doi: 10.1126/science.867031



- Schaumberg, D. A., Snow, K. K., and Dana, M. R. (1998). The epidemic of *Acanthamoeba* keratitis: Where do we stand? *Cornea* 17, 3–10. doi: 10.1097/00003226-199801000-00001
- Schmoller, H. (1964). [Description of some cultivated amoebae of marine origin]. *J. Protozool.* 11, 497–502.
- Schramm, M., and Hestrin, S. (1954). Factors affecting production of cellulose at the air/liquid interface of a culture of *Acetobacter xylinum*. *J. Gen. Microbiol.* 11, 123–129. doi: 10.1099/00221287-11-1-123
- Schuster, F. L., and Visvesvara, G. S. (2004). Opportunistic amoebae: Challenges in prophylaxis and treatment. *Drug Resist. Updat.* 7, 41–51. doi: 10.1016/j.drug.2004.01.002
- Schwarz, W. H. (2001). The cellulosome and cellulose degradation by anaerobic bacteria. *Appl. Microbiol. Biotechnol.* 56, 634–649. doi: 10.1007/s002530100710
- Seal, D. V., Kirkness, C. M., Bennett, H. G., and Peterson, M. (1999). *Acanthamoeba* keratitis in Scotland: Risk factors for contact lens wearers. *Cont. Lens Anterior Eye* 22, 58–68. doi: 10.1016/s1367-0484(99)80004-6
- Serhan, C. N., Haeggström, J. Z., and Leslie, C. C. (1996). Lipid mediator networks in cell signaling: Update and impact of cytokines. *FASEB J.* 10, 1147–1158. doi: 10.1096/fasebj.10.10.8751717
- Serrano-Luna Jde, J., Cervantes-Sandoval, I., Calderón, J., Navarro-García, F., Tsutsumi, V., and Shibayama, M. (2006). Protease activities of *Acanthamoeba polyphaga* and *Acanthamoeba castellanii*. *Can. J. Microbiol.* 52, 16–23. doi: 10.1139/w05-114
- Siddiqui, R., and Khan, N. A. (2012). Biology and pathogenesis of *Acanthamoeba*. *Parasit. Vectors* 5:6. doi: 10.1186/1756-3305-5-6
- Siddiqui, R., Dudley, R., and Khan, N. A. (2012). *Acanthamoeba* differentiation: A two-faced drama of Dr. Jekyll and Mr. Hyde. *Parasitology* 139, 826–834. doi: 10.1017/s0031182012000042
- Siddiqui, R., Khan, N. A., and Jarroll, E. L. (2009). The cyst wall carbohydrate composition of *Balamuthia mandrillaris*. *Parasitol. Res.* 104, 1439–1443. doi: 10.1007/s00436-009-1346-8
- Sinclair, D. A., and Guarente, L. (1997). Extrachromosomal rDNA circles—a cause of aging in yeast. *Cell* 91, 1033–1042. doi: 10.1016/s0092-8674(00)80493-6
- Singh, B. N., and Das, S. R. (1970). Studies on pathogenic and non-pathogenic small free-living amoebae and the bearing of nuclear division on the classification of the order amoebida. *Philos. Trans. R. Soc. Lond. B Biol. Sci.* 259, 435–476. doi: 10.1098/rstb.1970.0063
- Singh, B., Fleury, C., Jalalvand, F., and Riesbeck, K. (2012). Human pathogens utilize host extracellular matrix proteins laminin and collagen for adhesion and invasion of the host. *FEMS Microbiol. Rev.* 36, 1122–1180. doi: 10.1111/j.1574-6976.2012.00340.x
- Singh, D., Naik, S. R., and Naik, S. (2004). Role of cysteine proteinase of *Entamoeba histolytica* in target cell death. *Parasitology* 129(Pt 2), 127–135. doi: 10.1017/s0031182004005451
- Sissons, J., Alsam, S., Goldsworthy, G., Lightfoot, M., Jarroll, E. L., and Khan, N. A. (2006). Identification and properties of proteases from an *Acanthamoeba* isolate capable of producing granulomatous encephalitis. *BMC Microbiol.* 6:42. doi: 10.1186/1471-2180-6-42
- Sissons, J., Alsam, S., Jayasekera, S., and Khan, N. A. (2004a). Ecto-ATPases of clinical and non-clinical isolates of *Acanthamoeba*. *Microb. Pathog.* 37, 231–239. doi: 10.1016/j.micpath.2004.01.004
- Sissons, J., Alsam, S., Jayasekera, S., Kim, K. S., Stins, M., and Khan, N. A. (2004b). *Acanthamoeba* induces cell-cycle arrest in host cells. *J. Med. Microbiol.* 53(Pt 8), 711–717. doi: 10.1099/jmm.0.45604-0
- Sissons, J., Kim, K. S., Stins, M., Jayasekera, S., Alsam, S., and Khan, N. A. (2005). *Acanthamoeba castellanii* induces host cell death via a phosphatidylinositol 3-kinase-dependent mechanism. *Infect. Immun.* 73, 2704–2708. doi: 10.1128/iai.73.5.2704-2708.2005
- Sohn, J. H., Bora, P. S., Suk, H. J., Molina, H., Kaplan, H. J., and Bora, N. S. (2003). Tolerance is dependent on complement C3 fragment iC3b binding to antigen-presenting cells. *Nat. Med.* 9, 206–212. doi: 10.1038/nm814
- Sohn, J. H., Kaplan, H. J., Suk, H. J., Bora, P. S., and Bora, N. S. (2000). Chronic low level complement activation within the eye is controlled by intraocular complement regulatory proteins. *Invest. Ophthalmol. Vis. Sci.* 41, 3492–3502.
- Song, S. M., Han, B. I., Moon, E. K., Lee, Y. R., Yu, H. S., Jha, B. K., et al. (2012). Autophagy protein 16-mediated autophagy is required for the encystation of *Acanthamoeba castellanii*. *Mol. Biochem. Parasitol.* 183, 158–165. doi: 10.1016/j.molbiopara.2012.02.013
- Sriram, R., Shoff, M., Booton, G., Fuerst, P., and Visvesvara, G. S. (2008). Survival of *Acanthamoeba* cysts after desiccation for more than 20 years. *J. Clin. Microbiol.* 46, 4045–4048. doi: 10.1128/jcm.01903-08
- Stehr-Green, J. K., Bailey, T. M., and Visvesvara, G. S. (1989). The epidemiology of *Acanthamoeba* keratitis in the United States. *Am. J. Ophthalmol.* 107, 331–336. doi: 10.1016/0002-9394(89)90654-5
- Sternlicht, M. D., and Werb, Z. (2001). How matrix metalloproteinases regulate cell behavior. *Annu. Rev. Cell Dev. Biol.* 17, 463–516. doi: 10.1146/annurev.cellbio.17.1.463
- Stevaux, O., and Dyson, N. J. (2002). A revised picture of the E2F transcriptional network and RB function. *Curr. Opin. Cell Biol.* 14, 684–691. doi: 10.1016/s0955-0674(02)00388-5
- Stevens, A. R., and Pachler, P. F. (1973). RNA synthesis and turnover during density-inhibited growth and encystment of *Acanthamoeba castellanii*. *J. Cell Biol.* 57, 525–537. doi: 10.1083/jcb.57.2.525
- Stewart, J. R., and Weisman, R. A. (1974). A chemical and autoradiographic study of cellulose synthesis during the encystment of *Acanthamoeba castellanii*. *Arch. Biochem. Biophys.* 161, 488–498. doi: 10.1016/0003-9861(74)90331-2
- Stohr, M., Bommert, K., Schulze, I., and Jantzen, H. (1987). The cell cycle and its relationship to development in *Acanthamoeba castellanii*. *J. Cell Sci.* 88, 579–589.
- Stratford, M., and Griffiths, A. (1978). Variation in the properties and morphology of cysts of *Acanthamoeba castellanii*. *J. Gen. Microbiol.* 108, 33–37.
- Sütçü, M., Aktürk, H., Gülümser-Şişko, S., Acar, M., Erol, O. B., Somer, A., et al. (2018). Granulomatous amebic encephalitis caused by *Acanthamoeba* in an immunocompetent child. *Turk. J. Pediatr.* 60, 340–343. doi: 10.24953/turkjped.2018.03.019
- Suzuki, K., Kamada, Y., and Ohsumi, Y. (2002). Studies of cargo delivery to the vacuole mediated by autophagosomes in *Saccharomyces cerevisiae*. *Dev. Cell* 3, 815–824. doi: 10.1016/s1534-5807(02)00359-3
- Swart, A. L., Harrison, C. F., Eichinger, L., Steinert, M., and Hilbi, H. (2018). *Acanthamoeba* and *Dictyostelium* as cellular models for legionella infection. *Front. Cell. Infect. Microbiol.* 8:61. doi: 10.3389/fcimb.2018.00061
- Taher, E. E., Méabed, E. M. H., Abdallah, I., and Abdel Wahed, W. Y. (2018). *Acanthamoeba* keratitis in noncompliant soft contact lenses users: Genotyping and risk factors, a study from Cairo, Egypt. *J. Infect. Public Health* 11, 377–383. doi: 10.1016/j.jiph.2017.09.013
- Tan, E. M., Starr, M. R., Henry, M. R., and Pritt, B. S. (2018). The brief case: A “fresh” pair of contact lenses. *J. Clin. Microbiol.* 56:e00790-17. doi: 10.1128/jcm.00790-17
- Tang, A., Marquart, M. E., Fratkin, J. D., McCormick, C. C., Caballero, A. R., Gatlin, H. P., et al. (2009). Properties of PASP: A *Pseudomonas* protease capable of mediating corneal erosions. *Invest. Ophthalmol. Vis. Sci.* 50, 3794–3801. doi: 10.1167/iovs.08-3107
- Tawfeek, G. M., Bishara, S. A., Sarhan, R. M., ElShabrawi, T., and ElSaady Khayyal, A. (2016). Genotypic, physiological, and biochemical characterization of potentially pathogenic *Acanthamoeba* isolated from the environment in Cairo, Egypt. *Parasitol. Res.* 115, 1871–1881. doi: 10.1007/s00436-016-4927-3
- Taylor, W. M., Pidherney, M. S., Alizadeh, H., and Niederkorn, J. Y. (1995). In vitro characterization of *Acanthamoeba castellanii* cytopathic effect. *J. Parasitol.* 81, 603–609.
- Thyrell, L., Hjortberg, L., Arulampalam, V., Panaretakis, T., Uhles, S., Dagnell, M., et al. (2004). Interferon alpha-induced apoptosis in tumor cells is mediated through the phosphoinositide 3-kinase/mammalian target of rapamycin signaling pathway. *J. Biol. Chem.* 279, 24152–24162. doi: 10.1074/jbc.M312219200
- Tice, A. K., Shadwick, L. L., Fiore-Donno, A. M., Geisen, S., Kang, S., Schuler, G. A., et al. (2016). Expansion of the molecular and morphological diversity of *Acanthamoebidae* (Centramoebida, Amoebozoa) and identification of a novel life cycle type within the group. *Biol. Direct.* 11:69. doi: 10.1186/s13062-016-0171-0
- Tiewcharoen, S., Rababert, J., Chetanachan, P., Junnu, V., Worawiroungwong, D., and Malainual, N. (2008). Scanning electron microscopic study of human neuroblastoma cells affected with *Naegleria fowleri* Thai strains. *Parasitol. Res.* 103, 1119–1123. doi: 10.1007/s00436-008-1103-4
- Tomlinson, G., and Jones, E. A. (1962). Isolation of cellulose from the cyst wall of a soil amoeba. *Biochim. Biophys. Acta* 63, 194–200. doi: 10.1016/0006-3002(62)90353-0
- Torno, M. S. Jr., Babapour, R., Gurevitch, A., and Witt, M. D. (2000). Cutaneous *Acanthamoeba* infection in AIDS. *J. Am. Acad. Dermatol.* 42(2 Pt 2), 351–354. doi: 10.1016/s0190-9622(00)90110-5
- Tu, E. Y., and Joslin, C. E. (2010). Recent outbreaks of atypical contact lens-related keratitis: What have we learned? *Am. J. Ophthalmol.* 150, 602–608.e602. doi: 10.1016/j.ajo.2010.06.045
- Turner, N. A., Harris, J., Russell, A. D., and Lloyd, D. (2000). Microbial differentiation and changes in susceptibility to antimicrobial agents. *J. Appl. Microbiol.* 89, 751–759. doi: 10.1046/j.1365-2672.2000.01176.x
- Turner, N. A., Russell, A. D., Furr, J. R., and Lloyd, D. (2004). Resistance, biguanide sorption and biguanide-induced pentose leakage during encystment of *Acanthamoeba castellanii*. *J. Appl. Microbiol.* 96, 1287–1295. doi: 10.1111/j.1365-2672.2004.02260.x
- Vernon, S. E., Acar, B. C., Pham, S. M., and Fertel, D. (2005). *Acanthamoeba* infection in lung transplantation: Report of a case and review of the literature. *Transpl. Infect. Dis.* 7, 154–157. doi: 10.1111/j.1399-3062.2005.00113.x
- Visvesvara, G. S., and Balamuth, W. (1975). Comparative studies on related free-living and pathogenic amebae with special reference to *Acanthamoeba*. *J. Protozool.* 22, 245–256. doi: 10.1111/j.1550-7408.1975.tb05860.x
- Visvesvara, G. S., Mirra, S. S., Brandt, F. H., Moss, D. M., Mathews, H. M., and Martinez, A. J. (1983). Isolation of two strains of *Acanthamoeba castellanii* from



- human tissue and their pathogenicity and isoenzyme profiles. *J. Clin. Microbiol.* 18, 1405–1412. doi: 10.1128/jcm.18.6.1405-1412.1983
- Voyatzis, G., and McElvanney, A. (2007). Bilateral *Acanthamoeba* keratitis in an experienced two-weekly disposable contact lens wearer. *Eye Cont. Lens* 33, 201–202. doi: 10.1097/01.icl.0000252567.06446.7b
- Walochnik, J., Obwallner, A., and Aspöck, H. (2000). Correlations between morphological, molecular biological, and physiological characteristics in clinical and nonclinical isolates of *Acanthamoeba* spp. *Appl. Environ. Microbiol.* 66, 4408–4413. doi: 10.1128/aem.66.10.4408-4413.2000
- Walochnik, J., Scheikl, U., and Haller-Schober, E. M. (2015). Twenty years of *Acanthamoeba* diagnostics in Austria. *J. Eukaryot. Microbiol.* 62, 3–11. doi: 10.1111/jeu.12149
- Wang, P., and Zhu, J. X. (2010). Research progress on the pathogenesis of *Acanthamoeba* keratitis. *Int. J. Ophthalmol.* 10, 885–887.
- Wang, Y. J., Lin, W. C., and He, M. S. (2021). The *Acanthamoeba* SBDS, a cytoskeleton-associated gene, is highly expressed during phagocytosis and encystation. *J. Microbiol. Immunol. Infect.* 54, 482–489. doi: 10.1016/j.jmii.2019.11.003
- Weisman, R. A. (1976). Differentiation in *Acanthamoeba castellanii*. *Annu. Rev. Microbiol.* 30, 189–219. doi: 10.1146/annurev.mi.30.100176.001201
- Weisman, R. A., Spiegel, R. S., and McCauley, J. G. (1970). Differentiation in *Acanthamoeba*: Glycogen levels and glycogen synthetase activity during encystment. *Biochim. Biophys. Acta.* 201, 45–53. doi: 10.1016/0304-4165(70)90008-5
- Wennström, S., Hawkins, P., Cooke, F., Hara, K., Yonezawa, K., Kasuga, M., et al. (1994). Activation of phosphoinositide 3-kinase is required for PDGF-stimulated membrane ruffling. *Curr. Biol.* 4, 385–393. doi: 10.1016/s0960-9822(00)00087-7
- Willaert, E., Stevens, A. R., and Tyndall, R. L. (1978). *Acanthamoeba royreba* sp. n. from a human tumor cell culture. *J. Protozool.* 25, 1–14. doi: 10.1111/j.1550-7408.1978.tb03854.x
- Williams, W. S., and Cannon, R. E. (1989). Alternative environmental roles for cellulose produced by *Acetobacter xylinum*. *Appl. Environ. Microbiol.* 55, 2448–2452. doi: 10.1128/aem.55.10.2448-2452.1989
- Wopereis, D. B., Bazzo, M. L., de Macedo, J. P., Casara, F., Golfeto, L., Venancio, E., et al. (2020). Free-living amoebae and their relationship to air quality in hospital environments: Characterization of *Acanthamoeba* spp. obtained from air-conditioning systems. *Parasitology* 147, 782–790. doi: 10.1017/s0031182020000487
- Wymann, M. P., and Pirola, L. (1998). Structure and function of phosphoinositide 3-kinases. *Biochim. Biophys. Acta* 1436, 127–150. doi: 10.1016/s0005-2760(98)00139-8
- Xie, Z., and Klionsky, D. J. (2007). Autophagosome formation: Core machinery and adaptations. *Nat. Cell Biol.* 9, 1102–1109. doi: 10.1038/ncb1007-1102
- Yang, Z., and Klionsky, D. J. (2009). An overview of the molecular mechanism of autophagy. *Curr. Top. Microbiol. Immunol.* 335, 1–32. doi: 10.1007/978-3-642-00302-8\_1
- Yang, Z., Cao, Z., and Panjwani, N. (1997). Pathogenesis of *Acanthamoeba* keratitis: Carbohydrate-mediated host-parasite interactions. *Infect. Immun.* 65, 439–445. doi: 10.1128/iai.65.2.439-445.1997
- Yoder, J. S., Verani, J., Heidman, N., Hoppe-Bauer, J., Alfonso, E. C., Miller, D., et al. (2012). *Acanthamoeba* keratitis: The persistence of cases following a multistate outbreak. *Ophthalmic Epidemiol.* 19, 221–225. doi: 10.3109/09286586.2012.681336
- Yoo, K. T., and Jung, S. Y. (2012). Effects of mannose on pathogenesis of *Acanthamoeba castellanii*. *Korean J. Parasitol.* 50, 365–369. doi: 10.3347/kjp.2012.50.4.365
- Yun, H. C., Kim, K. Y., Park, S. Y., Park, S. K., Park, H., Hwang, U. W., et al. (1999). Cloning of a cysteine proteinase gene from *Acanthamoeba culbertsoni*. *Mol. Cells* 9, 491–496.
- Zhang, H., and Cheng, X. (2021). Various brain-eating amoebae: The protozoa, the pathogenesis, and the disease. *Front. Med.* 15, 842–866. doi: 10.1007/s11684-021-0865-2
- Zimmerman, A. B., Richdale, K., Mitchell, G. L., Kinoshita, B. T., Lam, D. Y., Wagner, H., et al. (2017). Water exposure is a common risk behavior among soft and gas-permeable contact lens wearers. *Cornea* 36, 995–1001. doi: 10.1097/ico.0000000000001204



## OPEN ACCESS

## EDITED BY

Ascel Samba-Louaka,  
University of Poitiers, France

## REVIEWED BY

Ashraf R. Zayed,  
An-Najah National University, Palestine  
Sébastien Pomel,  
Université Paris-Sud, France  
Christopher A. Rice,  
Purdue University, United States

## \*CORRESPONDENCE

Julia Walochnik  
✉ julia.walochnik@meduniwien.ac.at

RECEIVED 27 February 2023

ACCEPTED 03 April 2023

PUBLISHED 25 April 2023

## CITATION

Loufouma Mbouaka A, Lesiak-Markowicz I,  
Herederó-Bermejo I, Mazumdar R,  
Walochnik J and Martín-Pérez T (2023)  
Assessing *Acanthamoeba* cytotoxicity:  
comparison of common cell viability assays.  
*Front. Microbiol.* 14:1175469.  
doi: 10.3389/fmicb.2023.1175469

## COPYRIGHT

© 2023 Loufouma Mbouaka,  
Lesiak-Markowicz, Herederó-Bermejo,  
Mazumdar, Walochnik and Martín-Pérez. This is  
an open-access article distributed under the  
terms of the [Creative Commons Attribution  
License \(CC BY\)](https://creativecommons.org/licenses/by/4.0/). The use, distribution or  
reproduction in other forums is permitted,  
provided the original author(s) and the  
copyright owner(s) are credited and that the  
original publication in this journal is cited, in  
accordance with accepted academic practice.  
No use, distribution or reproduction is  
permitted which does not comply with  
these terms.

# Assessing *Acanthamoeba* cytotoxicity: comparison of common cell viability assays

Alvie Loufouma Mbouaka<sup>1</sup>, Iwona Lesiak-Markowicz<sup>1</sup>,  
Irene Herederó-Bermejo<sup>2</sup>, Rounik Mazumdar<sup>3</sup>,  
Julia Walochnik<sup>1\*</sup> and Tania Martín-Pérez<sup>1</sup>

<sup>1</sup>Center for Pathophysiology, Infectiology and Immunology, Institute of Specific Prophylaxis and Tropical Medicine, Medical University of Vienna, Vienna, Austria, <sup>2</sup>Department of Biomedicine and Biotechnology, Faculty of Pharmacy, University of Alcalá, Madrid, Spain, <sup>3</sup>Max Perutz Labs Vienna, Department of Medical Biochemistry, Medical University of Vienna, Vienna, Austria

**Background:** *In vitro* models for studying interactions between *Acanthamoeba* and host cells are crucial for understanding the pathomechanism of *Acanthamoeba* and assessing differences between strains and cell types. The virulence of *Acanthamoeba* strains is usually assessed and monitored by using cell cytotoxicity assays. The aim of the present study was to evaluate and compare the most widely used cytotoxicity assays for their suitability to assess *Acanthamoeba* cytopathogenicity.

**Methods:** The viability of human corneal epithelial cells (HCECs) after co-culture with *Acanthamoeba* was evaluated in phase contrast microscopy.

**Results:** It was shown that *Acanthamoeba* is unable to considerably reduce the tetrazolium salt and the NanoLuc<sup>®</sup> Luciferase prosubstrate to formazan and the luciferase substrate, respectively. This incapacity helped to generate a cell density-dependent signal allowing to accurately quantify *Acanthamoeba* cytotoxicity. The lactate dehydrogenase (LDH) assay led to an underestimation of the cytotoxic effect of *Acanthamoeba* on HCECs since their co-incubation negatively affected the lactate dehydrogenase activity.

**Discussion:** Our findings demonstrate that cell-based assays using the aqueous soluble tetrazolium-formazan, and the NanoLuc<sup>®</sup> Luciferase prosubstrate products, in contrast to LDH, are excellent markers to monitor the interaction of *Acanthamoeba* with human cell lines and to determine and quantify effectively the cytotoxic effect induced by the amoebae. Furthermore, our data indicate that protease activity may have an impact on the outcome and thus the reliability of these tests.

## KEYWORDS

*Acanthamoeba*, human corneal epithelial cells, pathogenesis, amoeba-host cell interaction, viability, cytotoxicity

## 1. Introduction

*Acanthamoeba* spp. are ubiquitous free-living amoebae occurring worldwide in water environments and soil, but they can also be isolated from dust and the air. They are facultative pathogens and can cause different diseases, importantly, the so-called *Acanthamoeba* keratitis (AK), a severe infection of the cornea, most commonly observed in contact lens wearers. The incidence of AK has increased within the past decades, which

may be attributed to the increasing number of contact lens users, but also to advances in diagnostics (Chawla et al., 2014; Randag et al., 2019; List et al., 2021). *Acanthamoeba* spp. may also cause granulomatous amoebic encephalitis, a fatal disease of the central nervous system, and other disseminating infections, mainly in immunocompromised individuals (Morrison et al., 2016). Treating these infections is challenging, as no specific drugs are currently available (Siddiqui et al., 2014; Lorenzo-Morales et al., 2015; Loufouma Mbouaka et al., 2021).

The pathomechanism of these amoebae still remains incompletely understood, despite significant progress made in recent years (Clarke and Niederkorn, 2006; Khan, 2006; Walochnik and Duchêne, 2016). Adhesion to the host cells is mediated by a mannose-binding protein (MBP) and other adhesion proteins, triggering the release of proteases, mainly of the serine and metalloprotease type. The immune reaction of the host is characterized by neutrophil migration and macrophage activation resulting in the release of proinflammatory cytokines such as tumor necrosis factor alpha (TNF- $\alpha$ ), interleukin-1 $\beta$  (IL-1 $\beta$ ), and interleukin-6 (IL-6). In AK, secretory IgA antibodies in the tears can prevent binding of the *Acanthamoeba* trophozoites (Mattana et al., 2002; Garate et al., 2004; Walochnik and Duchêne, 2016). However, only a comparably small percentage of environmental *Acanthamoeba* isolates are able to lyse human cells and cytopathogenicity is known to decline during long-term axenic culture – but can also be enhanced by mouse passage or serial passage over human cell lines (Mazur and Hadaś, 1994; Koehsler et al., 2009). Cell viability and cytotoxicity assays are useful tools to determine the cytotoxic effects of *Acanthamoeba* on human cells because they measure *in vitro* modifications at the cellular and metabolic levels by detecting structural changes such as loss of membrane integrity or physiological and biochemical responses associated with non-viable and viable cells, respectively (Riss et al., 2004). They are typically used in drug discovery screening to assess the effect of a compound on cell proliferation (Riss et al., 2004). However, depending on the research aims and owing to the limitations of these assays, their use may be challenging. Recently, it was demonstrated that some of these assays, when used to study and evaluate host–pathogen interactions, may interfere with the pathogen and lead to an inaccurate estimation of pathogen cytotoxicity and their effects on host cells during and after co-culture (Van den Bossche et al., 2020). Thus, it is crucial to identify or develop and validate reliable methods and models to study such interactions and to avoid any interference with the culture medium or the pathogen in co-culture.

The present study aimed to evaluate and compare the most widely used cell viability assays for their usefulness to assess the cytotoxicity of *Acanthamoeba* spp. on human corneal epithelial cells (HCECs) during co-culture. Cell morphology, viability and integrity were evaluated by phase contrast microscopy.

## 2. Materials and methods

### 2.1. *Acanthamoeba* strains

The non-pathogenic environmental isolate strain *Acanthamoeba castellanii* Neff (ATCC 50373) and two pathogenic

isolates from patients with keratitis, strains 1BU and strain SIN20, isolated in 1998 and 2020, respectively, all belonging to the T4 genotype group, were used in this study. The strains were maintained on non-nutrient agar plates coated with *Escherichia coli*. Prior to the experiments, all strains were sub-cultured and grown axenically at 34°C in peptone, yeast extract, and glucose (PYG) medium containing 10 g proteose peptone, 10 g yeast extract, 5 g NaCl, 5 g glucose, 0.7 g Na<sub>2</sub>HPO<sub>4</sub>, and 0.7 g KH<sub>2</sub>PO<sub>4</sub> per liter.

### 2.2. Human corneal epithelial cells (HCECs)

Cells and media components were purchased from Innoprot (Derio, Bizkaia, Spain). Immortalized human corneal epithelial cells (HCECs; P10871-IM) were sub-cultured in corneal epithelial cell medium (CEpiCM, P60189) containing the 5% fetal bovine serum (FBS), 1% epithelial cell growth supplement (ECGS) and 1% penicillin/streptomycin at 37°C and 5% CO<sub>2</sub>. T75 flasks and 96-well plates were coated with a thin layer of type I collagen (P8188) to enhance cell attachment and proliferation. Prior to the assays, different concentrations of HCECs were assessed to determine the optimal concentration for the subsequent experiments.

### 2.3. *Acanthamoeba*–HCEC co-culture

At least three independent experiments were performed in triplicates. Before the assays,  $1 \times 10^4$  HCECs per well were seeded in a 96-well plate and incubated overnight. Then, the medium was replaced with a serum-free medium, and cells were maintained at 34°C and 5% CO<sub>2</sub> during the co-culture to mimic the conditions of the human eye. Amoebae were added into the wells at different ratios or multiplicity of infection (MOI 1, MOI 2, and MOI 3; see Table 1) and incubated for 2, 4, 6, and 8 h. Wells containing only the HCECs were considered as positive controls, with a percentage of viability close to 100% for the following assays.

### 2.4. Cell viability and cytotoxicity assays

#### 2.4.1. Lactate dehydrogenase assay

Lactate dehydrogenase (LDH) assay is a colorimetric method used to assess cytotoxicity and quantify cell viability. The damage to the plasma membrane allows the release of LDH from the intracellular environment into the cell culture medium and can be quantified using a coupled enzymatic reaction. The LDH activity was determined using the CyQUANT™ LDH Cytotoxicity Assay

TABLE 1 Multiplicity of infection (MOI) used for cytotoxicity assays.

MOI	Number of amoeba*	Number of HCEC*
1	$1.0 \times 10^4$	$1.0 \times 10^4$
2	$2.0 \times 10^4$	$1.0 \times 10^4$
3	$3.0 \times 10^4$	$1.0 \times 10^4$

\*The total volume of the experimental serum-free medium per well containing either amoeba alone, in co-culture with HCECs or HCECs alone was 100  $\mu$ L.

Kit (Thermo Fisher Scientific, Eugene, OR, USA), and strictly following the manufacturers' instructions (Thermo Fisher, 2019). Simultaneously, the LDH positive control was established by adding the same volume of lysis buffer to samples containing only HCECs or *Acanthamoeba* alone. The plate was incubated at room temperature and protected from light for 30 min. Then, the absorbance was measured at 490 nm using a microplate absorbance spectrophotometer (Anthos Labtec Instruments HT2, Salzburg, Austria). The percentage of cytotoxicity was determined following the formula provided with the LDH assay kit and then converted to relative cell viability.

#### 2.4.2. MTS assay

The MTS assay is a colorimetric method used to assess cell viability. Viable cells reduce the yellow tetrazolium compound [3-(4,5-dimethylthiazol-2-yl)-5-(3-carboxymethoxyphenyl)-2-(4-sulfophenyl)-2H-tetrazolium, inner salt; MTS] to soluble formazan, which is purple. CellTiter 96<sup>®</sup> AQueous One Solution Reagent (Promega, Madison, WI, USA) was added to each sample (20  $\mu$ l per well) in a 96-well plate, and the plate was incubated at 34°C and 5% CO<sub>2</sub>. After 1 h incubation, absorbance at 490 nm was determined using a spectrophotometer (Tecan, Spark 10M, Switzerland).

#### 2.4.3. RealTime-Glo<sup>TM</sup> MT Cell Viability assay

The RealTime-Glo<sup>TM</sup> MT Cell Viability assay (Promega, Madison, WI, USA) is a bioluminescence assay used to assess cell viability in real time. Metabolically active cells reduce the NanoLuc<sup>®</sup> luciferase prosubstrate to the luciferase substrate, thus producing a luminescence signal, which correlates with the number of viable cells. During this assay, an opaque-walled tissue culture plate was used. The 2X RealTime-Glo<sup>TM</sup> reagent was prepared with serum-free CEpiCM, and 50  $\mu$ l was added into each well containing HCECs, followed by inoculation with an equal volume of serum-free medium containing amoebae in suspension at different MOIs. The plate was placed in a cell culture incubator at 34°C and 5% CO<sub>2</sub>, and cell viability was measured every 2 h. The viability was assessed in real time over 8 h, using a plate-reading luminometer (Tecan, Spark 10M, Switzerland).

### 2.5. Microscopy

All cells were analyzed by phase contrast microscopy and trypan blue staining. Trypan blue facilitates the determination of the cell number and percentage of viability within a cell population (Riss et al., 2004; Strober, 2015). A  $\mu$ -slide 8-well chamber (Ibidi, Martinsried, Germany) coated with collagen I was used for microscopic observation and analysis. HCECs (5  $\times$  10<sup>3</sup> per well) were seeded in the chamber and incubated overnight. After approximately 16 h, the medium was replaced with a serum-free medium, and amoebae were added at different MOI as previously described; the plates were incubated for different time periods (2, 4, 6, 8, and 24 h). For phase contrast microscopy and microphotography, a Nikon Eclipse TE200 microscope with NIS-Elements version 4.00.07 software (Optoteam, Vienna, Austria) was used.

### 2.6. Statistical analysis

Data was analyzed through two-way ANOVA with Dunnett's multiple comparisons test using GraphPad Prism version 7.0 for Windows (GraphPad Software Inc, San Diego, CA, USA).

## 3. Results

### 3.1. Growth of *Acanthamoeba* under various conditions

To ensure cell integrity, *Acanthamoeba* SIN20 and 1BU were monitored under various conditions, using CEpiCM with serum, serum-free CEpiCM, and PYG medium. Under these conditions, in serum-containing and serum-free CEpiCM, the number of amoebae on both strains remained constant over time for up to 24 h (Figure 1). Under all conditions, no dead cells were observed during the experiments. In PYG medium, the number of amoebae slightly increased after 8 h of incubation, followed by a significant increase after 12 h (Figure 1). Therefore, the time point of 8 h was selected as the maximal duration for all cytotoxicity assays, also to maintain the defined MOI ratio.

### 3.2. *Acanthamoeba* cell density affected lactate dehydrogenase production

The effect of the cell density of the *Acanthamoeba* strains Neff, SIN20, and 1BU and of the HCECs on LDH activity was assessed using a defined volume of LDH lysis buffer. As shown in Figure 2, the cell density affected the linearity of LDH activity. This effect was more pronounced with HCECs (Figure 2A) than with *Acanthamoeba* strains (Figures 2B–E). This finding may be attributed to the fact that, owing to their larger size, mammalian cells can release more LDH into the extracellular environment than amoebae. In contrast, the incubation time and type of *Acanthamoeba* strain in serum-free medium did not affect LDH release.

### 3.3. *Acanthamoeba* produced low signals in presence of tetrazolium salt and NanoLuc<sup>®</sup> luciferase prosubstrate

Similarly, the effect of cell number on absorbance at 490 nm and bioluminescence was evaluated using the MTS and RealTime-Glo<sup>TM</sup> MT Cell Viability assays, respectively, (Figures 3, 4). In contrast to the observations made in the LDH assay, *Acanthamoeba* did not increase the linear response between cell density and absorbance at 490 nm and bioluminescence, respectively, suggesting the inability of *Acanthamoeba* to considerably reduce the tetrazolium salt and NanoLuc<sup>®</sup> luciferase prosubstrate, respectively, and to produce a strong signal. However, a strong signal was observed with HCECs (Figures 3A, 4A). No differences in linearity were observed between the different *Acanthamoeba* strains used in this study.



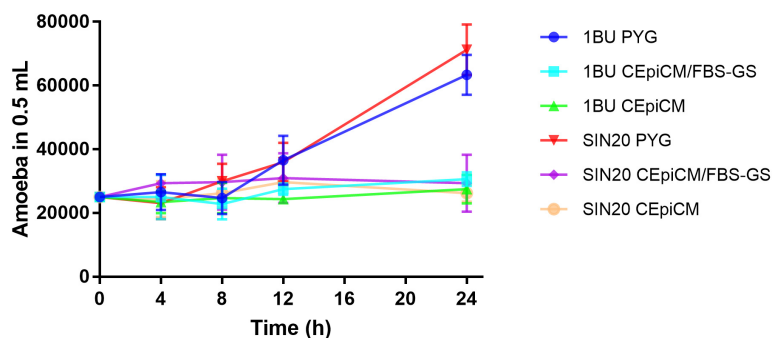


FIGURE 1

Growth curves of *Acanthamoeba* strains 1BU and SIN20 under various conditions over time at 34°C with 5% CO<sub>2</sub> atmosphere. The numbers of amoebae were determined by cell counting with a hemocytometer.

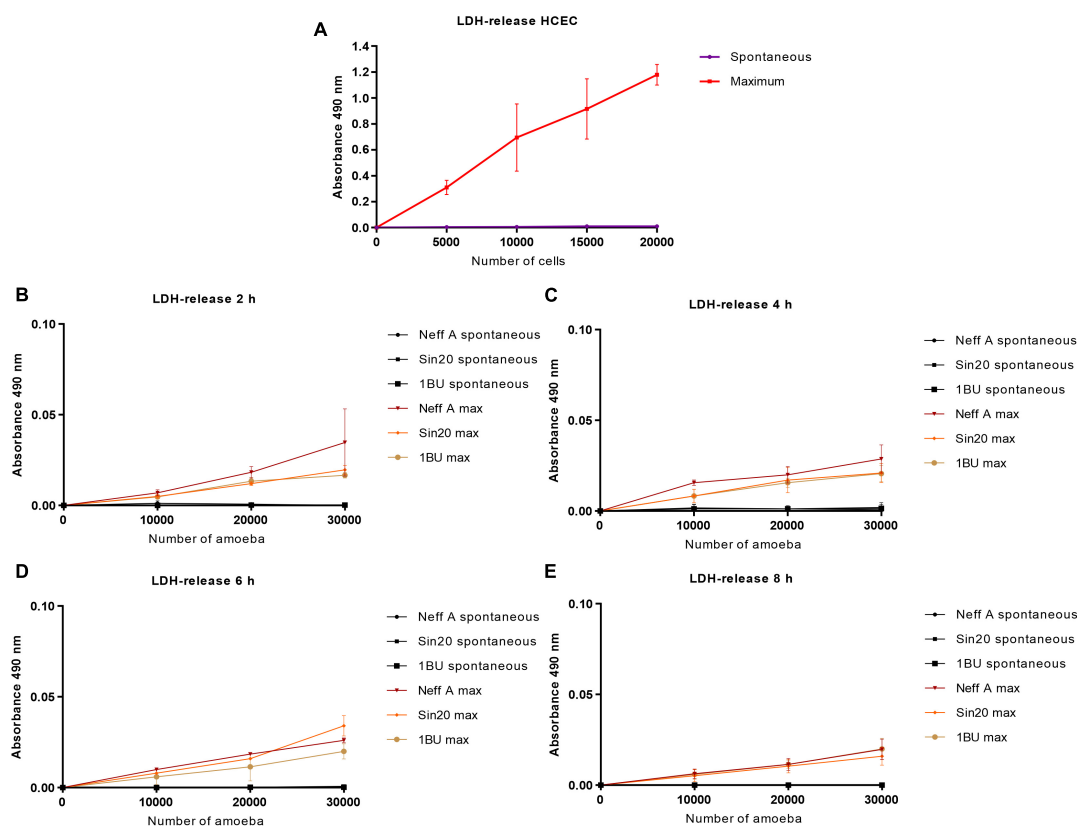


FIGURE 2

Effect of HCEC (A) and amoeba (B–E) densities on absorbance at 490 nm by using the LDH release assay, at different times. The background absorbance obtained with the media alone without cells was subtracted from all data. “Maximum” corresponds to the quantity of LDH released into the cell culture medium by lysed or damaged cells, and “Spontaneous” represents the quantity released by living or non-lysed cells.

### 3.4. Cytotoxic effects of *Acanthamoeba* on human corneal epithelial cells during co-culture

Subsequently, the cytotoxic effects of *Acanthamoeba* on HCECs and the effects on their viability at various incubation periods (2, 4, 6, and 8 h) and different MOIs (MOI 1, MOI 2, and MOI 3; see Table 1) were evaluated using the cytotoxicity assays. All assays were performed according to the manufacturer’s instructions,

and wells containing only serum-free medium were used as controls to account for culture medium background absorbance and luminescence.

As shown in Figure 5A, in the LDH assay to evaluate *Acanthamoeba*-induced cytotoxicity in HCECs, no significant differences were observed in the viability of HCECs inoculated with the environmental Neff and pathogenic 1BU strains and incubated for different periods. HCECs co-cultured with the SIN20 strain showed a slight difference in the viability of the mammalian cells at MOI 2 and MOI 3 after 8 h incubation, which refers to minor

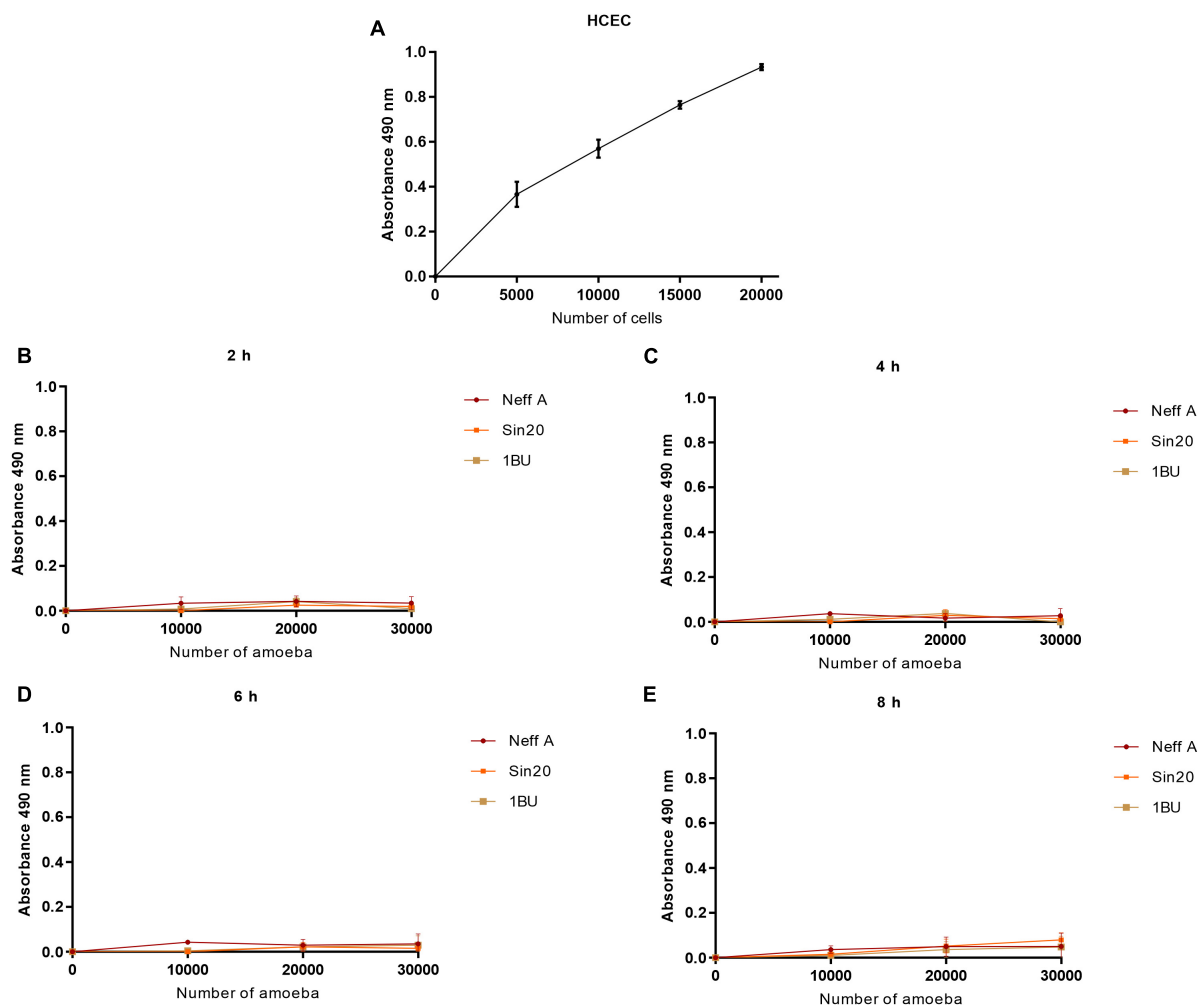


FIGURE 3

Effect of HCEC (A) and amoeba (B–E) densities on absorbance at 490 nm by using the MTS assay, at different times. The background absorbance obtained with the media alone without cells was subtracted from all data.

cytotoxic effects of this strain, but no significant differences were observed at other MOIs and incubation times.

The MTS and RealTime-Glo<sup>TM</sup> Cell Viability assays were used to assess the effect of *Acanthamoeba* on the viability of HCECs in co-culture. Both pathogenic strains showed a considerable effect on the viability of HCECs in both assays, except at MOI 1 and MOI 2 after 2 h incubation in the MTS assay (Figures 5B, C). The percentage of viability of HCECs in contact with pathogenic strains 1BU and SIN20 was markedly reduced after 4, 6, and 8 h of incubation in the MTS assay and at all incubation periods in the RealTime-Glo<sup>TM</sup> Cell Viability assay (except for 1BU at MOI 1 and 4 h incubation). No significant differences were observed in the viability of HCECs in contact with the non-pathogenic Neff strain in both assays.

### 3.5. Microscopic examination and consistency with cytotoxicity assays

The monolayer integrity of HCECs after inoculation with *Acanthamoeba* and incubation was assessed on the basis of cell

detachment by phase contrast microscopy, and microphotographs were taken (Figure 6 and Supplementary material). Under all conditions, the microscopic estimation was consistent with the results obtained with the MTS and RealTime-Glo<sup>TM</sup> MT Cell Viability assays, but not with the LDH assay. The presence of cell aggregates was observed after 2 h of co-culture, and was more pronounced after 8 h of co-culture, especially at MOI 2 and MOI 3 (Figure 6). Moreover, microscopic observations after 24 h showed total or at least significant destruction of the HCEC monolayer at MOI 2 and MOI 3, while at MOI 1, numerous HCECs were still intact in co-culture (Figure 6). Owing to the difficulty in distinguishing between non-viable HCECs and non-viable *Acanthamoeba* SIN20, cell death could not be determined by cell counting using trypan blue staining.

### 3.6. Monitoring *Acanthamoeba* cytotoxicity

After inoculation and co-culture of *Acanthamoeba* with HCECs, significant differences in results were observed between

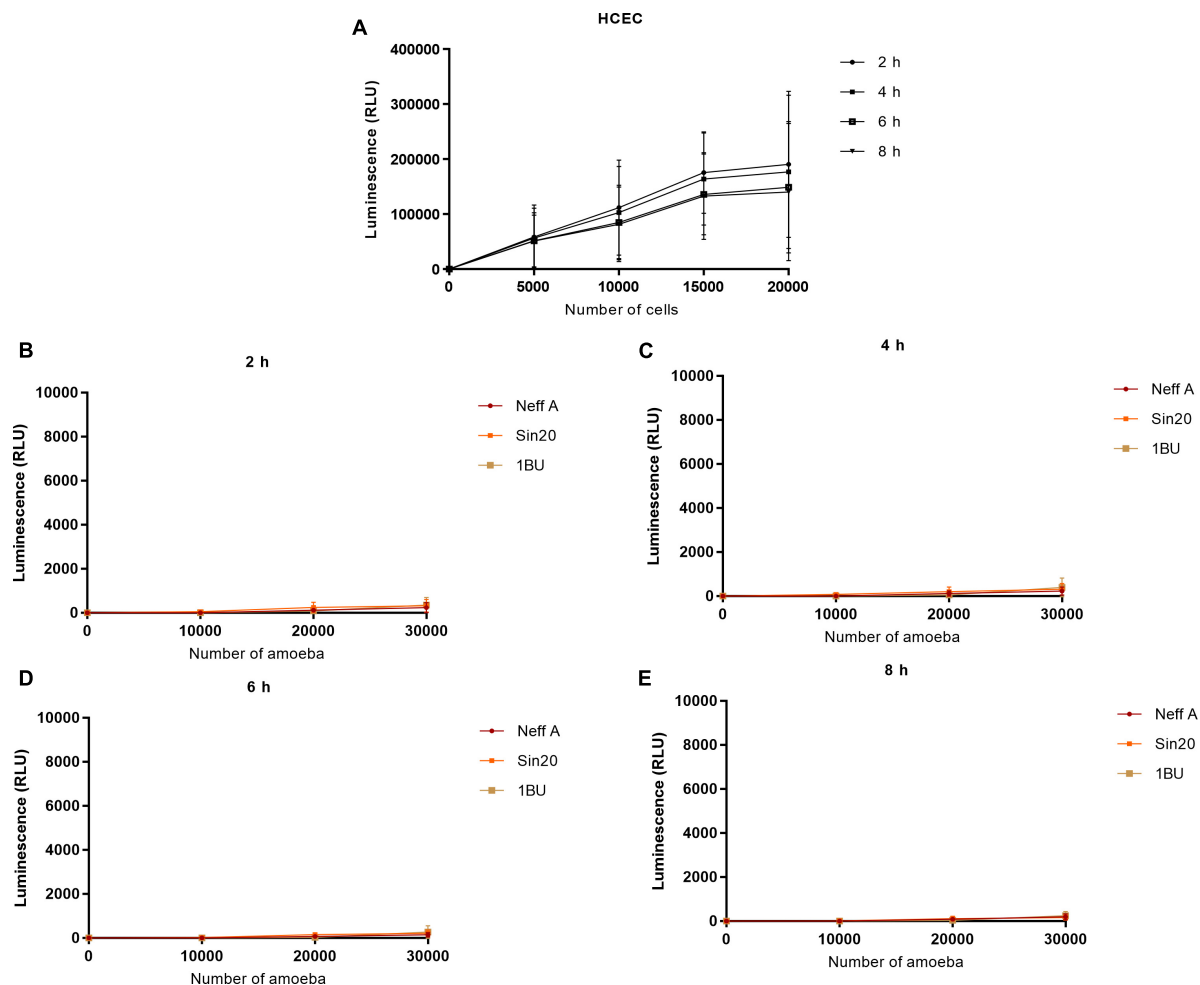


FIGURE 4

Effect of HCEC (A) and amoeba (B–E) densities on the luminescence signal by using the RealTime-Glo™ MT Cell Viability assay. The background absorbance obtained with the media alone without cells was subtracted from all data.

conventional LDH assay and other methods used in this study (Figure 5). Results of the MTS and RealTime-Glo™ MT Cell Viability assays, which were consistent with the microscopic observations of cell detachment, showed that the viability of HCECs was substantially affected by the presence of pathogenic *Acanthamoeba* strains, whereas almost no difference was observed with the LDH assay.

## 4. Discussion

Three different cytotoxicity assays, namely the LDH, MTS and RealTime-Glo™ MT Cell Viability assays, were compared in terms of their sensitivity in detecting and measuring *Acanthamoeba* cytotoxicity on human corneal epithelial cells (HCECs), in combination with microscopic examination. It was shown that pathogenic *A. castellanii* significantly reduced HCECs viability in a dose-dependent manner starting from 2 h of co-culture at varying ratios, and this effect could be monitored reliably with the MTS and RealTime-Glo™ MT Cell Viability assays, well corresponding with the observation of cell detachment and destruction.

Various methods to monitor and evaluate *in vitro* cell viability and cytotoxicity are available, such as colorimetric and luminescence assays and microscopic examination in combination with staining and cell counting. The methods compared in the present study, except for the rather new RealTime-Glo™ MT Cell Viability method, have been extensively used during recent years to evaluate the cytotoxicity of novel antimicrobial agents against protozoan parasites such as *Leishmania*, *Toxoplasma gondii*, *Naegleria fowleri* or also *Acanthamoeba* (Ganguly et al., 2006; Jin et al., 2009; Jha et al., 2015; López-Arencibia et al., 2015; Colon et al., 2019). The LDH assay is typically used to identify host cells that have lost membrane integrity and are considered dead on the basis of LDH release into the cell culture medium; in contrast, the MTS and RealTime-Glo™ MT Cell Viability assays use compounds that are metabolized and reduced by viable mammalian cells.

In this study, we first evaluated whether the number of amoebae (0–30,000 per well) and HCECs (0–20,000 per well) influenced the signal obtained with the LDH, MTS, and RealTime-Glo™ MT Cell Viability assays (Figures 2–4). Although HCECs produced a strong signal in all assays, this was not observed with the amoebae. While the LDH assay showed a cell density-dependent

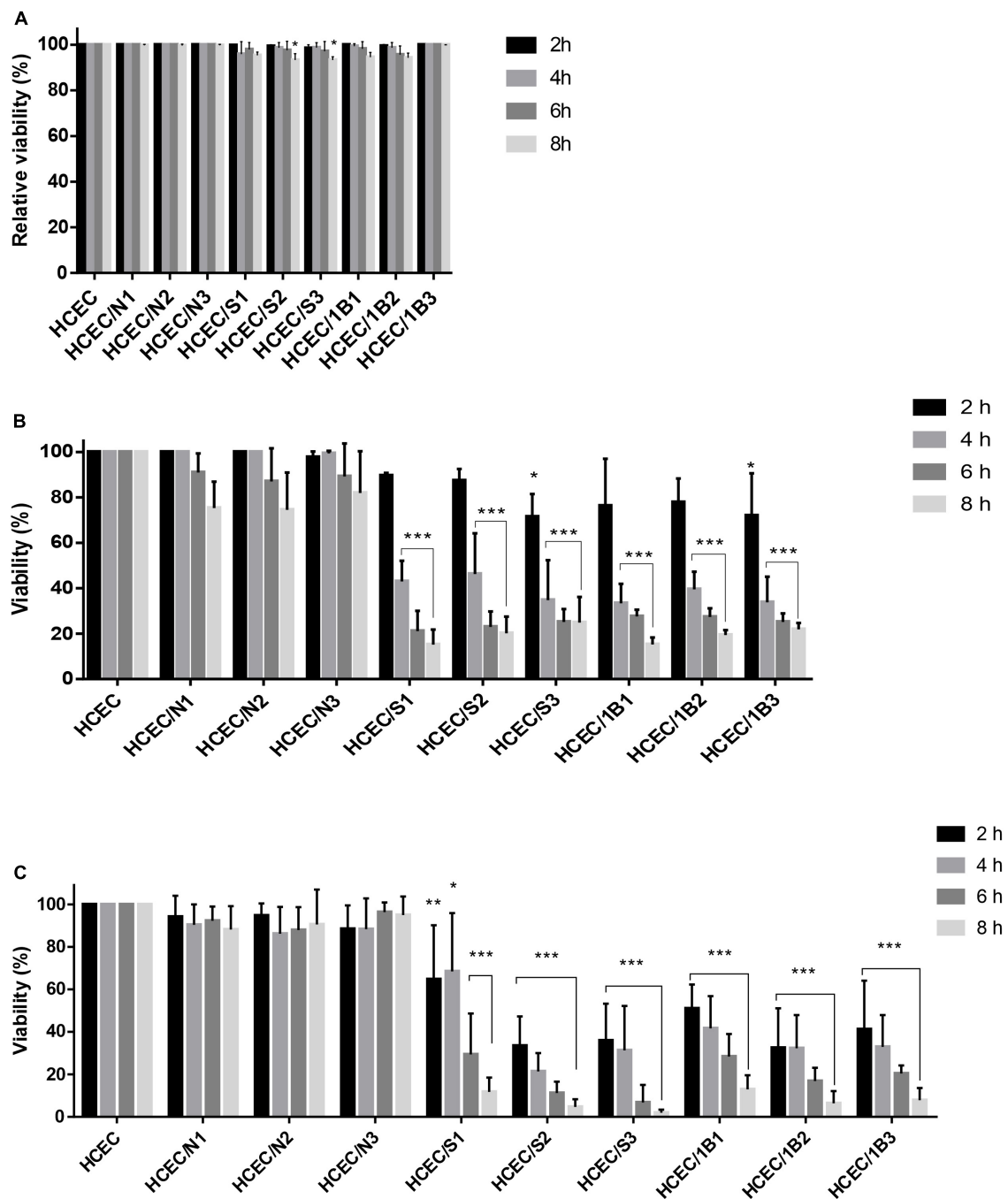


FIGURE 5

LDH release (A), MTS (B) and NanoLuc® Luciferase prosubstrate assays (C). Percentage of the viability of HCEC alone and after co-culture with *Acanthamoeba* strains Neff A (N), SIN20 (S) and 1BU (B) for different time periods (2, 4, 6, and 8 h), and MOIs (MOI 1: N1, S1, and B1; MOI 2: N2, S2, and B2; MOI 3: N3, S3, and B3). Values represent the means of three independent experiments, each in triplicate. Data were plotted after the correction of the media background. Statistical analysis was performed through two-way ANOVA with Dunnett's multiple comparisons test (\* $P < 0.01$ , \*\* $P < 0.001$ , and \*\*\* $P < 0.0001$ ).

signal also for the amoebae, the MTS and RealTime-Glo™ MT Cell Viability assays showed very weak signals for various concentrations of amoebae and incubation periods, indicating that the amoebae poorly metabolized the substrates. The MTS results are consistent with a previous study, in which the density of *Acanthamoeba castellanii* also did not affect the tetrazolium salt reduction and produced a weak signal (Heredero-Bermejo et al.,

2013). No differences in the activity of LDH released and reduction of tetrazolium salt and NanoLuc® luciferase prosubstrate were observed between the *Acanthamoeba* strains investigated.

Subsequently, the cytotoxic effects of the different *Acanthamoeba* strains on HCECs were assessed using the above-mentioned tests. Interestingly, there was a striking discrepancy between the cytotoxicity results obtained with the LDH assay and



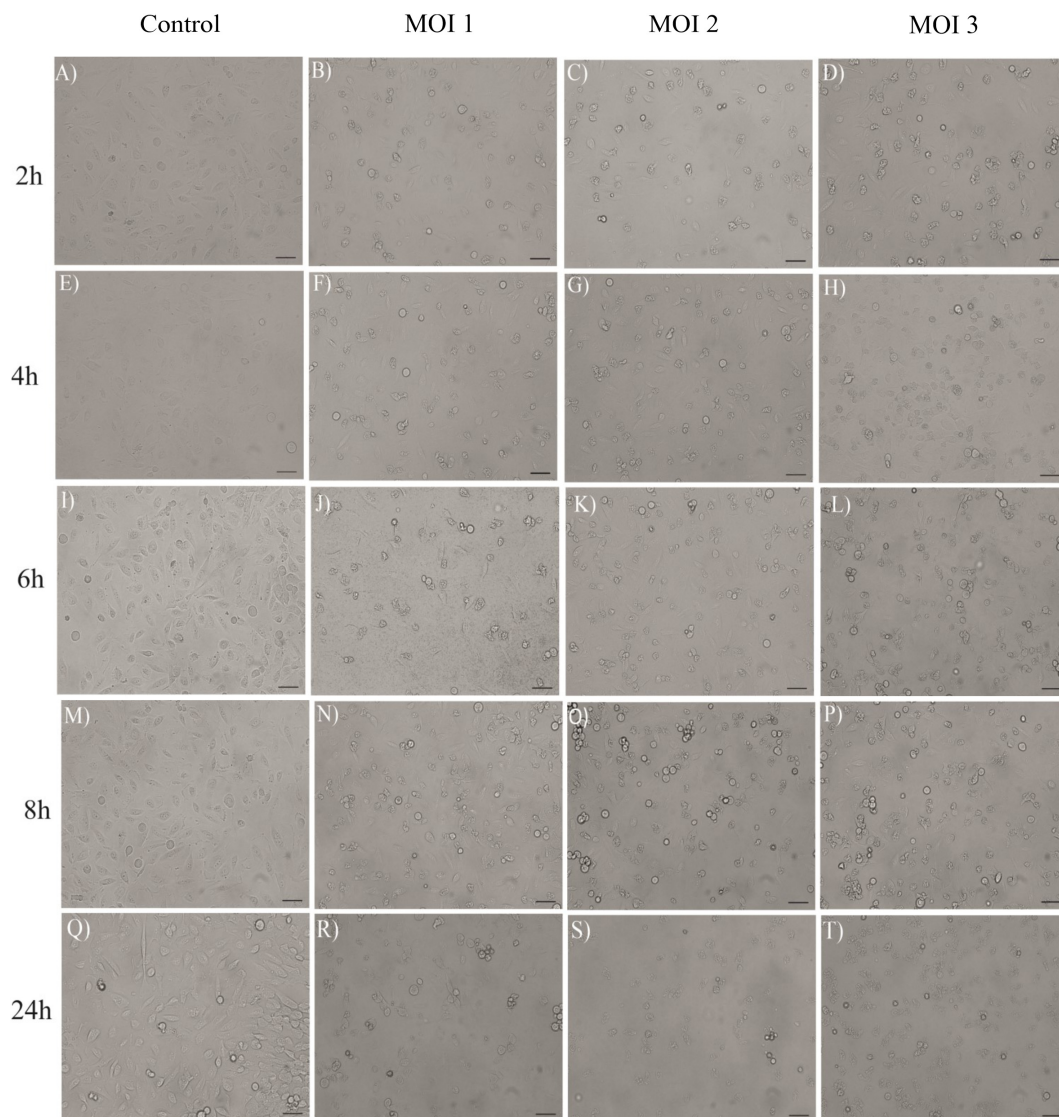


FIGURE 6

Effect of *Acanthamoeba* strain SIN20 after co-culture with HCECs, at MOI 1 (B,F,J, N,R), MOI 2 (C,G,K,O,S) and MOI 3 (D,H,L,P,T) and at different times (2, 4, 6, 8, and 24 h). Panels (A,E,I,M,Q) represent the HCEC alone without co-culture. Scale bar = 50  $\mu$ m. See [Supplementary material](#) for the amoeba controls.

the results obtained with the two other assays as well as with the microscopic examination of cell detachment. While generally, the cytotoxicity measured with the LDH assay was similar to that reported for *A. castellanii* on HCECs in a previous study (Sohn et al., 2019), we found that the LDH assay underestimated the proportion of dead cells and overestimated the proportion of living cells and thus was not reliable to determine the cytotoxic effect of *Acanthamoeba* on HCECs. However, the LDH assay has also been used to evaluate the activity of potentially anti-amoebic agents, because this enzyme is released into the culture medium when the cell membrane integrity is affected (Sissons et al., 2005; Lorenzo-Morales et al., 2010; Anwar et al., 2018; Shi et al., 2020; Akbar et al., 2022). The results obtained in the current study corroborate the suitability of the LDH assay for evaluating *Acanthamoeba* viability, but not when *Acanthamoeba* is co-cultured with other cells. We assume that proteases produced

by the pathogenic *Acanthamoeba* strains acted on the LDH released by the HCECs and thereby led to inaccurate results. A similar effect was reported for pathogenic bacteria in a recent study, where proteases produced by the bacteria during host-pathogen co-culture interacted with the LDH and thus lead to an underestimation of bacterial cytotoxicity (Van den Bossche et al., 2020). However, further studies will be necessary to confirm this hypothesis. In contrast to the LDH assay, the MTS and RealTime-Glo™ MT Cell Viability assays provided reliable and comparable results for *Acanthamoeba* cytotoxicity. The RealTime-Glo™ MT Cell Viability assay was more sensitive in determining the cytotoxic effect of *Acanthamoeba*; the lowest percentage of cell viability detected with the RealTime-Glo™ MT Cell Viability assay and MTS assay was approximately 2% with the SIN20 strain and 15% with the 1BU strain, respectively. Good

correlation in significant findings in both pathogenic strains was observed between the two assays, especially after 4 h of co-culture with HCECs ( $p < 0.0001$ ).

The ability of *Acanthamoeba* to establish contact with and adhere to host cells and induce apoptosis is crucial for their pathogenicity, but varies dramatically between strains. We used *Acanthamoeba* strains belonging to the genotype T4, since it is the most frequently genotype isolated from keratitis and non-keratitis diseases cases (Maciver et al., 2013; Walochnik et al., 2015; Castro-Artavia et al., 2017). Strains 1BU and SIN20 are AK-causing clinical isolates, isolated from patients with severe keratitis, while the Neff strain (ATCC 50373) is a non-virulent environmental isolate; and this is in line with the variations in the results obtained between 1BU and SIN20, on one hand, and Neff strains, on the other hand.

Usually, the presence of proteases and the production of extracellular vesicles are used to determine the pathogenicity of *Acanthamoeba* isolates (Khan et al., 2000; Walochnik and Duchêne, 2016; Moreira et al., 2020). The MTS and RealTime-Glo<sup>TM</sup> MT Cell Viability assays can be applied as valuable screening tools to assess directly the pathogenicity of *Acanthamoeba* isolates from environmental and clinical sources, in co-culture with mammalian cell lines.

In conclusion, the present study demonstrates the importance of choosing the most suitable method in accordance with the research purpose to meaningfully quantify cell viability and cytotoxicity *in vitro*. While the LDH assay, in contrast to the MTS and the RealTime-Glo<sup>TM</sup> MT Cell Viability assays, is suitable to determine *Acanthamoeba* viability in axenic culture, it is unsuitable to determine the cytotoxic effect of *Acanthamoeba* on host cells. However, the tetrazolium- and luciferase prosubstrate-based assays, although and because unsuitable to evaluate *Acanthamoeba* viability, were found to sensitively and reliably assess the cytotoxic effects of *Acanthamoeba* on human cells *in vitro*. To the best of our knowledge, this is the first report of a potential interference between proteases produced by *Acanthamoeba* with the LDH assay during *Acanthamoeba*-host cell co-culture leading to an underestimation of the cytotoxic effect.

## Data availability statement

The original contributions presented in this study are included in the article/**Supplementary material**, further inquiries can be directed to the corresponding author.

## References

- Akbar, N., El-Gamal, M., Saeed, B., Oh, C., Abdel-Maksoud, M., Khan, N., et al. (2022). Antiamoebic activity of imidazothiazole derivatives against opportunistic pathogen *Acanthamoeba castellanii*. *Antibiotics* 11, 1–11.
- Anwar, A., Siddiqui, R., Hussain, M., Ahmed, D., Shah, M., and Khan, N. (2018). Silver nanoparticle conjugation affects antiacanthamoebic activities of amphotericin B, nystatin, and fluconazole. *Parasitol. Res.* 117, 265–271. doi: 10.1007/s00436-017-5701-x
- Castro-Artavia, E., Retana-Moreira, L., Lorenzo-Morales, J., and Abrahams-Sandí, E. (2017). Potentially pathogenic *Acanthamoeba* genotype T4 isolated from dental units and emergency combination showers. *Mem. Inst. Oswaldo Cruz.* 112, 817–821. doi: 10.1590/0074-02760170147
- Chawla, A., Armstrong, M., and Carley, F. (2014). *Acanthamoeba keratitis*-an increasing incidence. *Contact Lens. Anterior. Eye.* 37:120. doi: 10.1016/j.clae.2013.09.002
- Clarke, D., and Niederkorn, J. (2006). The pathophysiology of *Acanthamoeba keratitis*. *Trends Parasitol.* 22, 175–180.
- Colon, B., Rice, C., Guy, R., and Kyle, D. (2019). Phenotypic screens reveal posaconazole as a rapidly acting amebicidal combination partner for treatment of

## Author contributions

JW, ALM, and TM-P designed the study. ALM, IL-M, IH-B, RM, and TM-P collected and analyzed the data. ALM, IL-M, TM-P, and JW wrote the manuscript. All authors discussed the data, read, edited, and approved the current version of the manuscript.

## Funding

This research was supported by a grant from the Austrian Science Fund (P 35259).

## Acknowledgments

We thank the members of the unit Molecular Parasitology at the Institute of Specific Prophylaxis and Tropical Medicine of the Medical University of Vienna for their technical support.

## Conflict of interest

The authors declare that the research was conducted in the absence of any commercial or financial relationships that could be construed as a potential conflict of interest.

## Publisher's note

All claims expressed in this article are solely those of the authors and do not necessarily represent those of their affiliated organizations, or those of the publisher, the editors and the reviewers. Any product that may be evaluated in this article, or claim that may be made by its manufacturer, is not guaranteed or endorsed by the publisher.

## Supplementary material

The Supplementary Material for this article can be found online at: <https://www.frontiersin.org/articles/10.3389/fmicb.2023.1175469/full#supplementary-material>

- primary amoebic meningoencephalitis. *J. Infect. Dis.* 219, 1095–1103. doi: 10.1093/infdis/jiy622
- Ganguly, S., Bandyopadhyay, S., Sarkar, A., and Chatterjee, M. (2006). Development of a semi-automated colorimetric assay for screening anti-leishmanial agents. *J. Microbiol. Methods* 66, 79–86. doi: 10.1016/j.mimet.2005.10.011
- Garate, M., Cao, Z., Bateman, E., and Panjwani, N. (2004). Cloning and characterization of a novel mannose-binding protein of *Acanthamoeba*. *J. Biol. Chem.* 279, 29849–29856. doi: 10.1074/jbc.M402334200
- Heredero-Bermejo, I., Copa-Patiño, J., Soliveri, J., Gómez, R., De La Mata, F., and Pérez-Serrano, J. (2013). In vitro comparative assessment of different viability assays in *Acanthamoeba castellanii* and *Acanthamoeba polyphaga* trophozoites. *Parasitol. Res.* 112, 4087–4095. doi: 10.1007/s00436-013-3599-5
- Jha, B., Jung, H., Seo, I., Suh, S., Suh, M., and Baek, W. (2015). Juglone induces cell death of *Acanthamoeba* through increased production of reactive oxygen species. *Exp. Parasitol.* 159, 100–106. doi: 10.1016/j.exppara.2015.09.005
- Jin, C., Kaewintajuk, K., Jiang, J., Jeong, W., Kamata, M., Kim, H., et al. (2009). Toxoplasma gondii: a simple high-throughput assay for drug screening in vitro. *Exp. Parasitol.* 121, 132–136.
- Khan, N. (2006). *Acanthamoeba*: biology and increasing importance in human health. *FEMS Microbiol. Rev.* 30, 564–595.
- Khan, N., Jarroll, E., Panjwani, N., Cao, Z., and Paget, T. (2000). Proteases as markers for differentiation of pathogenic and nonpathogenic species of *Acanthamoeba*. *J. Clin. Microbiol.* 38, 2858–2861. doi: 10.1128/JCM.38.8.2858-2861.2000
- Koehsler, M., Leitsch, D., Duchêne, M., Nagl, M., and Walochnik, J. (2009). *Acanthamoeba castellanii*: growth on human cell layers reactivates attenuated properties after prolonged axenic culture. *FEMS Microbiol. Lett.* 299, 121–127. doi: 10.1111/j.1574-6968.2009.01680.x
- List, W., Glatz, W., Riedl, R., Mossboeck, G., Steinwender, G., and Wedrich, A. (2021). Evaluation of *Acanthamoeba keratitis* cases in a tertiary medical care centre over 21 years. *Sci. Rep.* 11, 1–10. doi: 10.1038/s41598-020-80222-3
- López-Arencibia, A., García-Velázquez, D., Martín-Navarro, C., Sifaoui, I., Reyes-Battle, M., Lorenzo-Morales, J., et al. (2015). In vitro activities of hexazatrinenaphthyls against *Leishmania* spp. *Antimicrob. Agents Chemother.* 59, 2867–2874.
- Lorenzo-Morales, J., Khan, N. A., and Walochnik, J. (2015). *An update on Acanthamoeba keratitis: Diagnosis, pathogenesis and treatment*. *Parasite*, Vol. 22. Paris, 10. doi: 10.1051/parasite/2015010
- Lorenzo-Morales, J., Martín-Navarro, C., López-Arencibia, A., Santana-Morales, M., Afonso-Lehmann, R., Maciver, S., et al. (2010). Therapeutic potential of a combination of two gene-specific small interfering RNAs against clinical strains of *Acanthamoeba*. *Antimicrob. Agents Chemother.* 54, 5151–5155. doi: 10.1128/AAC.00329-10
- Loufouma Mbouaka, A., Leitsch, D., Koehsler, M., and Walochnik, J. (2021). Antimicrobial effect of auranofoin against *Acanthamoeba* spp. *Int. J. Antimicrob. Agents.* 58:106425.
- Maciver, S., Asif, M., Simmen, M., and Lorenzo-Morales, J. (2013). A systematic analysis of *Acanthamoeba* genotype frequency correlated with source and pathogenicity: T4 is confirmed as a pathogen-rich genotype. *Eur. J. Protistol.* 49, 217–221. doi: 10.1016/j.ejop.2012.11.004
- Mattana, A., Cappai, V., Alberti, L., Serra, C., Fiori, P., and Cappuccinelli, P. (2002). ADP and other metabolites released from *Acanthamoeba castellanii* lead to human monocytic cell death through apoptosis and stimulate the secretion of proinflammatory cytokines. *Infect. Immun.* 70, 4424–4432. doi: 10.1128/IAI.70.8.4424-4432.2002
- Mazur, T., and Hadaś, E. (1994). The effect of the passages of *Acanthamoeba* strains through mice tissue on their virulence and its biochemical markers. *Parasitol. Res.* 80, 431–434. doi: 10.1007/BF00932382
- Moreira, L., Ramírez, D., Linares, F., Ledezma, A., Garro, A., Osuna, A., et al. (2020). Isolation of *Acanthamoeba* t5 from water: characterization of its pathogenic potential, including the production of extracellular vesicles. *Pathogens* 9:144. doi: 10.3390/pathogens9020144
- Morrison, A., Morris, R., Shannon, A., Lauer, S., Guarnier, J., and Kraft, C. (2016). Disseminated *Acanthamoeba* infection presenting with cutaneous lesions in an immunocompromised patient: a case report, review of histomorphologic findings, and potential diagnostic pitfalls. *Am. J. Clin. Pathol.* 145, 266–270. doi: 10.1093/ajcp/aqv081
- Randag, A., Van Rooij, J., Van Goor, A., Verkerk, S., Wisse, R., Saelens, I., et al. (2019). The rising incidence of *Acanthamoeba keratitis*: a 7-year nationwide survey and clinical assessment of risk factors and functional outcomes. *PLoS One* 14:e0222092. doi: 10.1371/journal.pone.0222092
- Riss, T., Moravec, R., Niles, A., Duellman, S., Benink, H., Worzella, T., et al. (2004). Cell viability assays. *Assay Guid. Man.* 1–25. Available online at: <http://www.ncbi.nlm.nih.gov/pubmed/23805433> (accessed October 2022).
- Shi, L., Muthukumar, V., Stachon, T., Latta, L., Elhawry, M., Gunaratnam, G., et al. (2020). The effect of anti-amoebic agents and Ce6-PDT on *Acanthamoeba castellanii* trophozoites and cysts, in vitro. *Transl. Vis. Sci. Technol.* 9, 1–15. doi: 10.1167/tvst.9.12.29
- Siddiqui, R., Chaudhry, T., Lakhundi, S., Ahmad, K., and Khan, N. (2014). Failure of chemotherapy in the first reported cases of *Acanthamoeba keratitis* in Pakistan. *Pathog. Glob. Health.* 108, 49–52. doi: 10.1179/2047773213Y.0000000124
- Sissons, J., Kwang, S., Stins, M., Jayasekera, S., Alsam, S., and Khan, N. (2005). *Acanthamoeba castellanii* induces host cell death via a phosphatidylinositol 3-kinase-dependent mechanism. *Infect. Immun.* 73, 2704–2708. doi: 10.1128/IAI.73.5.2704-2708.2005
- Sohn, H., Seo, G., Lee, J., Ham, A., Oh, Y., Kang, H., et al. (2019). Cytopathic change and inflammatory response of human corneal epithelial cells induced by *Acanthamoeba castellanii* trophozoites and cysts. *Korean J. Parasitol.* 57, 217–223. doi: 10.3347/kjp.2019.57.3.217
- Strober, W. (2015). Trypan blue exclusion test of cell viability. *Curr Protoc Immunol* 111, A3.B.1–A3.B.3.
- Thermo Fisher (2019). *CyQUANT™ LDH Cytotoxicity Assay Kit Product Information Sheet. Catalog Numbers C20300 and C20301*. <https://www.thermofisher.com/order/catalog/product/C20300> (accessed October 2022).
- Van den Bossche, S., Vandeplassche, E., Ostyn, L., Coenye, T., and Crabbé, A. (2020). Bacterial interference with lactate dehydrogenase assay leads to an underestimation of cytotoxicity. *Front. Cell Infect. Microbiol.* 10:494. doi: 10.3389/fcimb.2020.0494
- Walochnik, J., and Duchêne, M. (eds). (2016). *Molecular parasitology: Protozoan parasites and their molecules*, Vol. IX. Vienna: Springer Publishing, 1–547.
- Walochnik, J., Scheikl, U., and Haller-Schober, E. (2015). Twenty years of *Acanthamoeba* diagnostics in Austria. *J. Eukaryot. Microbiol.* 62, 3–11. doi: 10.1111/jeu.12149



## OPEN ACCESS

## EDITED BY

Ascel Samba-Louaka,  
University of Poitiers, France

## REVIEWED BY

Bharath Kanakapura Sundararaj,  
Boston University, United States  
Julia Walochnik,  
Medical University of Vienna, Austria

## \*CORRESPONDENCE

Stephen Kwok-Wing Tsui  
✉ kwtsui@cuhk.edu.hk  
Patsharaporn T. Sarasombath  
✉ p.tehasintana@gmail.com;  
✉ patsharaporn.tec@mahidol.ac.th

<sup>†</sup>These authors have contributed equally to this work and share first authorship

RECEIVED 10 February 2023

ACCEPTED 06 April 2023

PUBLISHED 05 May 2023

## CITATION

Law CT-Y, Nivesvivat T, Xiong Q, Kulkeaw K, Shi L, Ruenchit P, Suwanpakdee D, Suwanpakdee P, Tongkrajang N, Sarasombath PT and Tsui SK-W (2023) Mitochondrial genome diversity of *Balamuthia mandrillaris* revealed by a fatal case of granulomatous amoebic encephalitis. *Front. Microbiol.* 14:1162963. doi: 10.3389/fmicb.2023.1162963

## COPYRIGHT

© 2023 Law, Nivesvivat, Xiong, Kulkeaw, Shi, Ruenchit, Suwanpakdee, Suwanpakdee, Tongkrajang, Sarasombath and Tsui. This is an open-access article distributed under the terms of the [Creative Commons Attribution License \(CC BY\)](https://creativecommons.org/licenses/by/4.0/). The use, distribution or reproduction in other forums is permitted, provided the original author(s) and the copyright owner(s) are credited and that the original publication in this journal is cited, in accordance with accepted academic practice. No use, distribution or reproduction is permitted which does not comply with these terms.

# Mitochondrial genome diversity of *Balamuthia mandrillaris* revealed by a fatal case of granulomatous amoebic encephalitis

Cherie Tsz-Yiu Law<sup>1,2†</sup>, Thirapa Nivesvivat<sup>3†</sup>, Qing Xiong<sup>1,2†</sup>, Kasem Kulkeaw<sup>4†</sup>, Ling Shi<sup>1,2</sup>, Pichet Ruenchit<sup>4</sup>, Detchvijitr Suwanpakdee<sup>3</sup>, Piradee Suwanpakdee<sup>5</sup>, Nongnat Tongkrajang<sup>4</sup>, Patsharaporn T. Sarasombath<sup>4\*</sup> and Stephen Kwok-Wing Tsui<sup>1,2\*</sup>

<sup>1</sup>School of Biomedical Sciences, The Chinese University of Hong Kong, Shatin, Hong Kong SAR, China,

<sup>2</sup>Hong Kong Bioinformatics Centre, The Chinese University of Hong Kong, Shatin, Hong Kong SAR, China, <sup>3</sup>Infectious Disease Unit, Department of Pediatrics, Phramongkutklao Hospital, Bangkok, Thailand, <sup>4</sup>Siriraj Integrative Center for Neglected Parasitic Diseases, Department of Parasitology, Faculty of Medicine Siriraj Hospital, Mahidol University, Bangkok, Thailand, <sup>5</sup>Neurology Division, Department of Pediatrics, Phramongkutklao Hospital, Bangkok, Thailand

**Introduction:** *Balamuthia (B.) mandrillaris* is a free-living amoeba that can cause rare yet fatal granulomatous amoebic encephalitis (GAE). However, efficacious treatment for GAE is currently unavailable, especially when genomic studies on *B. mandrillaris* are limited.

**Methods:** In this study, *B. mandrillaris* strain KM-20 was isolated from the brain tissue of a GAE patient, and its mitochondrial genome was *de novo* assembled using high-coverage Nanopore long reads and Illumina short reads.

**Results and Discussion:** Phylogenetic and comparative analyses revealed a range of diversification in the mitochondrial genome of KM-20 and nine other *B. mandrillaris* strains. According to the mitochondrial genome alignment, one of the most variable regions was observed in the ribosomal protein S3 (*rps3*), which was caused by an array of novel protein tandem repeats. The repeating units in the *rps3* protein tandem region present significant copy number variations (CNVs) among *B. mandrillaris* strains and suggest KM-20 as the most divergent strain for its highly variable sequence and highest copy number in *rps3*. Moreover, mitochondrial heteroplasmy was observed in strain V039, and two genotypes of *rps3* are caused by the CNVs in the tandem repeats. Taken together, the copy number and sequence variations of the protein tandem repeats enable *rps3* to be a perfect target for clinical genotyping assay for *B. mandrillaris*. The mitochondrial genome diversity of *B. mandrillaris* paves the way to investigate the phylogeny and diversification of pathogenic amoebae.

## KEYWORDS

granulomatous amoebic encephalitis, *Balamuthia mandrillaris*, mitochondrial genome, free-living amoeba, ribosomal protein S3, neglected diseases, genotyping



## 1. Background

*Balamuthia mandrillaris* is one of the free-living amoeba species that can cause brain infections in humans besides *Acanthamoeba* spp., *Naegleria fowleri*, and *Sappinia* spp. (Visvesvara et al., 2007; Visvesvara, 2013, 2014). *B. mandrillaris* can enter the human body through the skin via wound or inhalation, and the infection causes a cutaneous lesion or brain infection called GAE, with up to 95% mortality rate (Matin et al., 2008; Siddiqui and Khan, 2008; Visvesvara, 2013, 2014; Vollmer and Glaser, 2016). This species was first identified from the brain of a pregnant mandrill baboon at the San Diego Wildlife Park in 1986, and the first human brain infection was reported in 1990 (Visvesvara et al., 1990). Since then, more than 200 cases of *Balamuthia* encephalitis have been reported worldwide (Intalapaporn et al., 2004; Cope et al., 2019; Wang et al., 2020). Due to the rarity and non-specific presentations of GAE, the diagnosis is usually delayed and often made postmortem (Schuster et al., 2009).

Unlike other free-living amoebae, which can be cultured on agar overlaid with bacteria, this organism needs to be grown on mammalian cell monolayer cultures such as monkey kidney cells, human lung fibroblasts, and human neuroblastoma cells (Schuster, 2002). Thus, the diagnosis of *B. mandrillaris* infection mainly relies on other laboratory methods including serology and genotyping based on the molecular marker in mitochondrial DNA (da Rocha-Azevedo et al., 2009). Currently, only two complete genomes of *B. mandrillaris* are available, both of which were obtained from patients in the United States (Detering et al., 2015; Greninger et al., 2015). The genome sizes of the two assemblies are 44.3 and 67.6 Mbp, respectively (Detering et al., 2015; Greninger et al., 2015). A total of nine mitochondrial genomes of *B. mandrillaris* are available, but none of them were isolated from Asia (Detering et al., 2015; Greninger et al., 2015). A previous study compared the mitochondrial genome of seven *B. mandrillaris* strains isolated from patients and the environment in the United States (Greninger et al., 2015). In addition to the various lengths of mitochondrial DNA sequences, the phylogenetic tree shows three distinct lineages (Greninger et al., 2015).

Mitochondrial genomes are increasingly used for phylogenetic and epidemiological analyses. In addition, several antiprotozoal drugs including pentamidine exert their functions by interfering with mitochondrial metabolism (de Souza et al., 2009). Mitochondrial genome analysis of *B. mandrillaris* may provide further insights into the diversity within species and shed light on the functions of mitochondrial genes, which could serve as potential drug targets.

Using both Nanopore long-read and Illumina short-read sequencing data, we *de novo* assembled the mitochondrial genome of the *B. mandrillaris* strain isolated from Asia named strain KM-20. Phylogenetic and comparative analyses of KM-20 and nine other strains were performed to investigate the mitochondrial genome diversity among strains. Notably, a previous study has reported the difference in the mitochondrial *rps3* gene, but the authors suggested that the difference is due to a putative intron or intergenic region (Greninger et al., 2015). In this study, our results demonstrated that the diversity of the *rps3* length is attributed to an array of protein tandem repeats, and the number of repeating units is different among *B. mandrillaris* strains.

## 2. Materials and methods

### 2.1. *Balamuthia mandrillaris* culture and DNA extraction

*Balamuthia mandrillaris* strain KM-20 was obtained by inoculating the left frontoparietal brain tissue of the GAE patient reported here in a monolayer of human lung carcinoma A549 cells in Dulbecco's modified Eagle medium plus 10% fetal bovine serum at 37°C with 5% CO<sub>2</sub>, following the protocol as previously described (Schuster et al., 2009). The amoeba was first observed in the culture 4 weeks after inoculation and was maintained in a culture with A549 cells at 37°C with 5% CO<sub>2</sub> (Schuster, 2002). *B. mandrillaris* strains V039 (50209) and V416 (PRA-290) were obtained from ATCC (Manassas, VA, United States) and maintained in culture media containing human neuroblastoma SH-SY5Y cells at 37°C with 5% CO<sub>2</sub>. DNA extractions of the amoeba were performed using a QIAmp DNA Mini Kit (Qiagen, Hilden, Germany), following the manufacturer's protocol for isolating DNA from cell cultures.

### 2.2. DNA sequencing, assembly, and annotation

*Balamuthia mandrillaris* KM-20 genomic DNA was sequenced using Oxford Nanopore GridION Mk1 with a Ligation Sequencing Kit (SQK-LSK109) on an R9.4.1 MinION flow cell and an Illumina NovaSeq 6,000 sequencing system. The mitochondrial genome of *B. mandrillaris* strains 2046, V039, BeN, GAM-19, OK1, RP5, SAM, V188, and V451 (Table 1) was downloaded and used as a reference to map against the raw reads of KM-20 using Minimap2 (v2.20) to identify the mitochondrial DNA sequences of KM-20 (Li, 2018). The identified sequences were assembled into a single contig using Flye (v2.8.3) and subsequently polished by Illumina data using Pilon (v1.24) (Walker et al., 2014; Kolmogorov et al., 2019). The mitochondrial genome of KM-20 was visualized in Proksee (Stothard and Wishart, 2005; Grant and Stothard, 2008). The coding genes, introns, and novel open reading frames were identified by MITOS WebServer and GeSeq (v2.03) (Bernt et al., 2013; Tillich et al., 2017). The transfer RNA (tRNA) annotation was performed by GeSeq with ARAGORN (v1.2.38), and the rRNA subunit genes were checked by RNaseq (Laslett and Canback, 2004; Lang et al., 2007). The coverage of the mitochondrial genome of *B. mandrillaris* KM-20 was obtained by mapping the nanopore raw reads to the assembled mitochondrial genome by Minimap2 (v2.20), and the mapping coverage was obtained using SAMtools (v1.5) (Li, 2018; Danecek et al., 2021). The *B. mandrillaris* KM-20 mitochondrial genome has been deposited in the National Center for Biotechnology Information (NCBI) under the accession number OM994889.

### 2.3. Comparative mitochondrial genome analysis

Concatenated sequence data of cytochrome oxidase subunit 1 (*cox1*), cytochrome oxidase subunit 3 (*cox3*), cytochrome b (*cob*), ATP synthase F0 subunit 6 (*atp6*), ATP synthase subunit alpha (*atpa*), NADH dehydrogenase subunit 1 (*nad1*), NADH

TABLE 1 *Balamuthia mandrillaris* strains used in this study.

Strain	Accession no.	Location	Source	Sequencing technology	References
KM-20	OM994889	Thailand	4-year-old girl, cultured on A549 feeder cells	Oxford Nanopore, Illumina	Current study
2046	KP888565	California	26-year-old man, survivor, cultured on Vero cells	Illumina	<a href="#">Vollmer and Glaser (2016)</a> and <a href="#">Greninger et al. (2015)</a>
CDC-V039	CM003363	California	3-year, 10-month-old pregnant mandrill from the San Diego Zoo Wild Animal Park, axenic culture	PacBio	<a href="#">Visvesvara et al. (1990)</a> and <a href="#">Detering et al. (2015)</a>
V039*	KT175741	California	3-year, 10-month-old pregnant mandrill from the San Diego Zoo Wild Animal Park, cultured on Vero cells	Illumina	<a href="#">Visvesvara et al. (1990)</a> and <a href="#">Greninger et al. (2015)</a>
V451	KT030670	New York	6-year-old girl, cultured on Vero cells	Illumina	<a href="#">Greninger et al. (2015)</a>
GAM-19	KT175739	–	V188-frozen stock	Illumina	<a href="#">Greninger et al. (2015)</a>
RP5	KT030672	California	Environmental sample, cultured on Vero cells	Illumina	<a href="#">Greninger et al. (2015)</a> and <a href="#">Schuster et al. (2003)</a>
SAM	KT030673	California	3-year-old girl, isolated from brain	Illumina	<a href="#">Greninger et al. (2015)</a> and <a href="#">Bakardjiev et al. (2003)</a>
V188	KT175738	Georgia	59-year-old man, isolated from brain/skin lesion, cultured on Vero cells	Illumina	<a href="#">Greninger et al. (2015)</a> ; <a href="#">Gordon et al. (1992)</a>
V416*	AF477015	Australia	10-year-old girl, isolated from brain	–	<a href="#">Booton et al. (2003)</a>
OK1	KT030671	California	Environmental sample, cultured on Vero cells	Illumina	<a href="#">Dunnebacke et al. (2004)</a>
BeN	NC_027736	–	–	Illumina	Alexander LG (Unpublished)

The accession number, location, and source of the strains used in this study are presented in the table.

\*Obtained from ATCC.

dehydrogenase subunit 2 (*nad2*), NADH dehydrogenase subunit 3 (*nad3*), NADH dehydrogenase subunit 4 (*nad4*), NADH dehydrogenase subunit 5 (*nad5*), NADH dehydrogenase subunit 6 (*nad6*), NADH dehydrogenase subunit 7 (*nad7*), and NADH dehydrogenase subunit 9 (*nad9*) of 10 strains of *B. mandrillaris* were aligned with MAFFT (v7.487) ([Kuraku et al., 2013](#)). The same set of genes in a concatenated sequence of *A. castellanii* (GenBank Accession number: U12386.1) was chosen as the outgroup. The alignment was imported into MEGA-X (v10.2.6) to perform phylogenetic analysis, and a maximum likelihood phylogenetic tree was computed using a JTT matrix-based model, with a bootstrap value of 1,000 ([Jones et al., 1992](#); [Kumar et al., 2018](#)). The phylogenetic data were subsequently visualized using the Interactive Tree of Life (iTOL) (v5) ([Letunic and Bork, 2021](#)). The phylogenetic relationship and the mitochondrial sequences of 10 strains of *B. mandrillaris* were imported to AliTV for comparison and

visualization ([Ankenbrand et al., 2017](#)). Regions with a low link identity were further aligned and examined by Clustal Omega (v1.2.4) ([Sievers et al., 2011](#)).

The *rps3* protein tandem repeat sequences of all *B. mandrillaris* strains were extracted to perform a phylogenetic analysis using MEGA-X (v10.2.6) ([Kumar et al., 2018](#)). A parent tree with all protein tandem repeat sequences was constructed by the maximum likelihood method and JTT matrix-based model with a bootstrap value of 1,000 ([Jones et al., 1992](#); [Kumar et al., 2018](#)). A subtree of the protein tandem repeats was constructed by removing the most conserved branch of repeating units and the fourth repeating unit of KM-20 *rps3* from the parent tree. The remaining sequences were, then, used to construct a phylogenetic subtree by the maximum likelihood method and JTT matrix-based model and a bootstrap value of 1,000 ([Jones et al., 1992](#)). The phylogenetic data were visualized using iTOL (v5) ([Letunic and Bork, 2021](#)).

### 3. Results

#### 3.1. De novo assembly and annotation

The brain debridement of the GAE patient was sent for culture on A549 cell lines. Genomic DNA of *B. mandrillaris* KM-20 was extracted from the culture and sequenced to obtain a total of 7.66 Gb data using Oxford Nanopore long-read sequencing technology and 23Gb data using the Illumina NovaSeq 6,000 system. A circular mitochondrial genome of the *B. mandrillaris* KM-20 was *de novo* assembled in size of 42,630 bp and 35.34% GC content (Figure 1A). A total of 33 protein-coding, two rRNA, and 13 tRNA genes were annotated and located in the plus strand of the mitochondrial genome of *B. mandrillaris* KM-20 (Figure 1A). The protein-coding genes were classified into five groups, namely, ribosomal protein, NADH dehydrogenase, ATP synthase, cytochrome c oxidase, and cytochrome b.

According to a previous report, the mitochondrial genome size of *B. mandrillaris* strains ranges from 39,996 bp to 42,823 bp (Supplementary Table S2) (Greninger et al., 2015). The mitochondrial *cox1* gene of KM-20 is interrupted by a LAGLIDADG endonuclease-containing group IB intron (Supplementary Figure S2), which was also observed in four other strains, namely, 2046, SAM, RP5, and OK1 (Greninger et al., 2015). The length of LAGLIDADG endonuclease in these five strains ranges from 281 to 283 amino acids. For other strains, including, V451, V188, BeN, and GAM-19, the LAGLIDADG endonuclease is in the 23S rRNA gene, instead of the *cox1* gene (Greninger et al., 2015). V039 is the only strain that has no LAGLIDADG endonuclease inserted in protein-coding genes (Greninger et al., 2015).

#### 3.2. Comparative analysis of *Balamuthia mandrillaris* strains

The phylogenetic analysis of *B. mandrillaris* mitochondrial genomes divided 10 strains into two clades and suggested KM-20 as the most distant strain (Figure 1B). In agreement with a previous study (Greninger et al., 2015), the four California strains (RP5, SAM, 2046, and OK1) formed a highly conserved cluster in the phylogenetic tree.

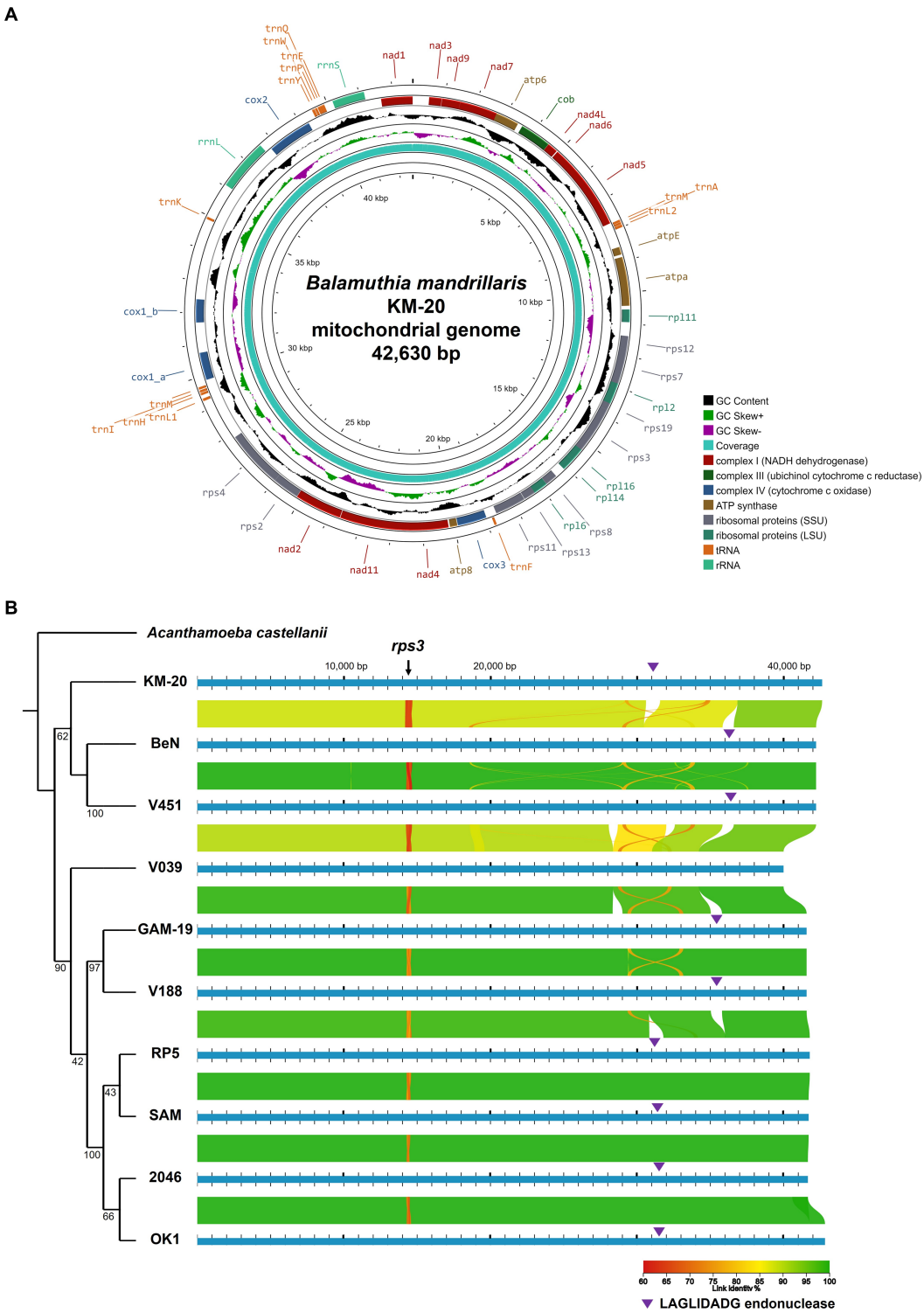
To perform a global mitochondrial genes comparison, the coding genes of 10 *B. mandrillaris* strains were compared in a matrix of pairwise identity percentage using KM-20 as a reference, and *rps3* was the only mitochondrial gene that has a percentage identity lower than 85% (Supplementary Figure S3). To further investigate the genomic diversity of *B. mandrillaris*, the mitochondrial genomic architectures of 10 strains were visualized by AliTV, and the result revealed a generally conserved gene synteny (Figure 1B) (Stajich et al., 2002; Harris, 2007; Ankenbrand et al., 2017). A break in synteny indicated in the purple triangle was observed in *cox1* and 23S rRNA, which corresponds to the introns that contain LAGLIDADG endonuclease. Other mapping gaps were caused by sequences missing in strain V039 and are not intron after manual checking. A region with only 70% link identity at approximately 14,500 bp was identified in the mitochondrial genome, and the variable position was confirmed to be the *rps3* gene. Interestingly, multiple sequence alignment of *rps3* protein sequences of 10 *B. mandrillaris* strains revealed that the variation could

be attributed to an array of protein tandem repeats (Supplementary Figure S4). The tandem repeat unit in *rps3* is named the R unit, and each R unit is composed of 17 amino acid residues, most of which started with four consensus amino acids, namely, arginine (R), proline (P), tryptophan (W), and leucine (L) (Supplementary Figure S4). KM-20 has seven R units, which is the highest number among all strains; V451 and BeN have six; GAM-19, V188, V039, RP5, and OK1 have five; SAM and 2046 have four and three R units, respectively. Despite the amino acid sequence within each R unit being conserved, the nucleotide sequences are highly degenerated and can be differentiated from each other. The identified repeats, therefore, are not due to sequencing error or collapse (Supplementary Figure S5). The length of the protein tandem repeat region in *rps3* ranges from 51 to 121 amino acid residues. The CNVs of the R units account for the difference in *rps3* length, which makes *rps3* a promising target for strain identification and genotyping of *B. mandrillaris* (Greninger et al., 2015).

The distribution of R units in *rps3* was illustrated with colors according to their phylogenetic relationship (Figure 2). A parent phylogenetic tree was constructed with all R units in 10 *B. mandrillaris* strains (Supplementary Figure S6). The last R units of all strains form a highly conserved branch in the parent phylogenetic tree and are colored in gray (Supplementary Figure S6). To better explore the R unit divergence, the gray-colored R units together with the most distant R4 unit of KM-20 were removed to construct a high-quality phylogenetic subtree (Figure 2B). The R units in 10 *B. mandrillaris* strains can be divided into nine main clades (Figure 2B).

A consensus sequence motif was generated to identify the conserved amino acid residues in different clusters by WebLogo (Figure 3) (Schneider and Stephens, 1990; Crooks et al., 2004). The R units of KM-20 are highly variable (Figure 3A), while the R units of the California strains (RP5, SAM, 2046, and OK1) are significantly conserved and start with RPWL amino acid residues (Figure 3B). The consensus sequences of the gray-colored R units in Figure 2A and overall R units from all strains are RPWLMSTWKNWKPGYAD and RPWL-G-RK--Y-EK--, respectively (Figures 3C,D). Positions 2–5 are populated by hydrophobic amino acids, which are colored in black (Figures 3A–D). The R units of all strains start with RPWL except R2, R3, and R4 of KM-20 and R5 of V451 and BeN, but the substituting amino acid residues, such as alanine, isoleucine, phenylalanine, and methionine, are also hydrophobic in nature, suggesting an N-terminal hydrophobic region is important for R units.

The general structure of *rps3* was predicted to have four transmembrane helices and three cytosolic domains by InterPro88.0 (Jones et al., 2014; Blum et al., 2021) (Supplementary Figure S7). The R units and the C-terminal domain of *rps3* are predicted to be in the cytosolic compartments (Supplementary Figure S7). The protein tandem repeats in *rps3* were identified as an intrinsically disordered region (IDR) by IUPred3 (Figure 3E) (Erdős et al., 2021). IDRs have no well-defined three-dimensional structures but are dynamically disordered and can fluctuate rapidly through different conformations (Wright and Dyson, 2015). The disordered region is in position 145–253 and overlaps with the repeating R units of KM-20, which are in position 167–293. Further structural and molecular analysis may assist in understanding the function of this highly variable region of *rps3*.





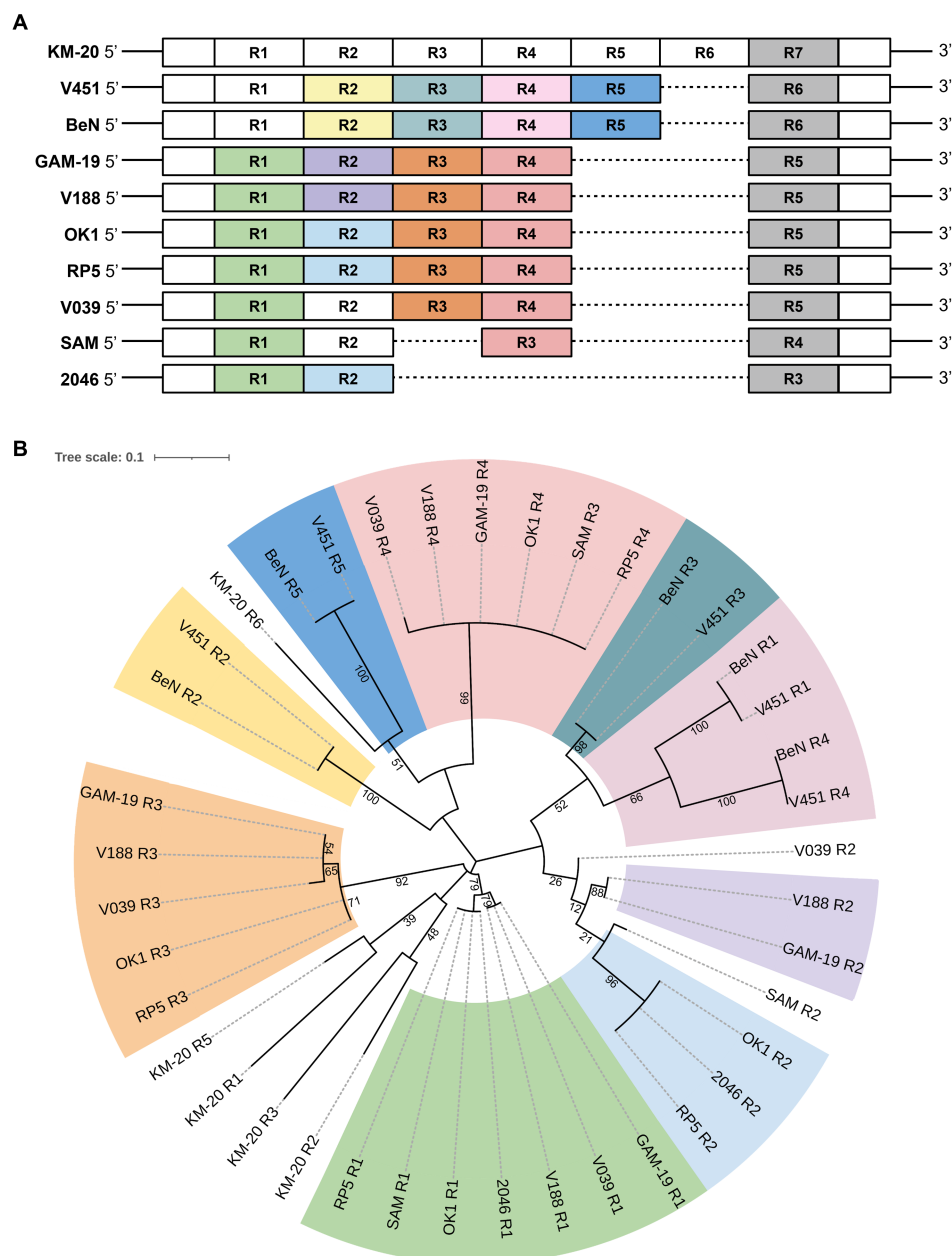


FIGURE 2

Distribution of the protein tandem repeats in *rps3* with their phylogenetic relationship matching the colors. **(A)** Distribution of protein tandem repeats in *rps3*. Sequence segments are not drawn to scale. KM-20 has seven R units; V451 and BeN have six; GAM-19, V188, V039, RP5, and OK1 strain have five; SAM strain has four, and the 2046 strain has three R units in *rps3*. **(B)** Phylogenetic analysis of *rps3* R units. The subtree of *rps3* R units shows nine main clades. R units that are not phylogenetically clustered with other repeating units are shaded in white, such as all R units of KM-20, R2 of SAM, and R2 of V039.

## 4. Discussion

*Balamuthia mandrillaris* is one of the free-living amoebae that occasionally cause GAE in humans and animals (Visvesvara et al., 2007; Visvesvara, 2013; Visvesvara, 2014), which is often life-threatening with limited treatment options (Cope et al., 2019). Owing to the restricted number of documented cases worldwide, establishing a conclusive link between genotype variation and clinical manifestation poses a challenge. It is speculated that variations in the genotypes of *B. mandrillaris* may account for the

dissimilar clinical presentations of its infection across diverse regions of the world. Retrospective reports from China and Peru demonstrated that the main clinical manifestations of *B. mandrillaris* infection are cutaneous lesions, which precede neurological involvement that develops several years later. In contrast, reported cases from the US presented solely with neurological symptoms, without any preceding skin lesion (Bravo and Seas, 2012; Wang et al., 2020), which is similar to the clinical presentation of our current case. Thus, the dissimilarity in disease aggressiveness and clinical manifestations could potentially stem in part from the genetic

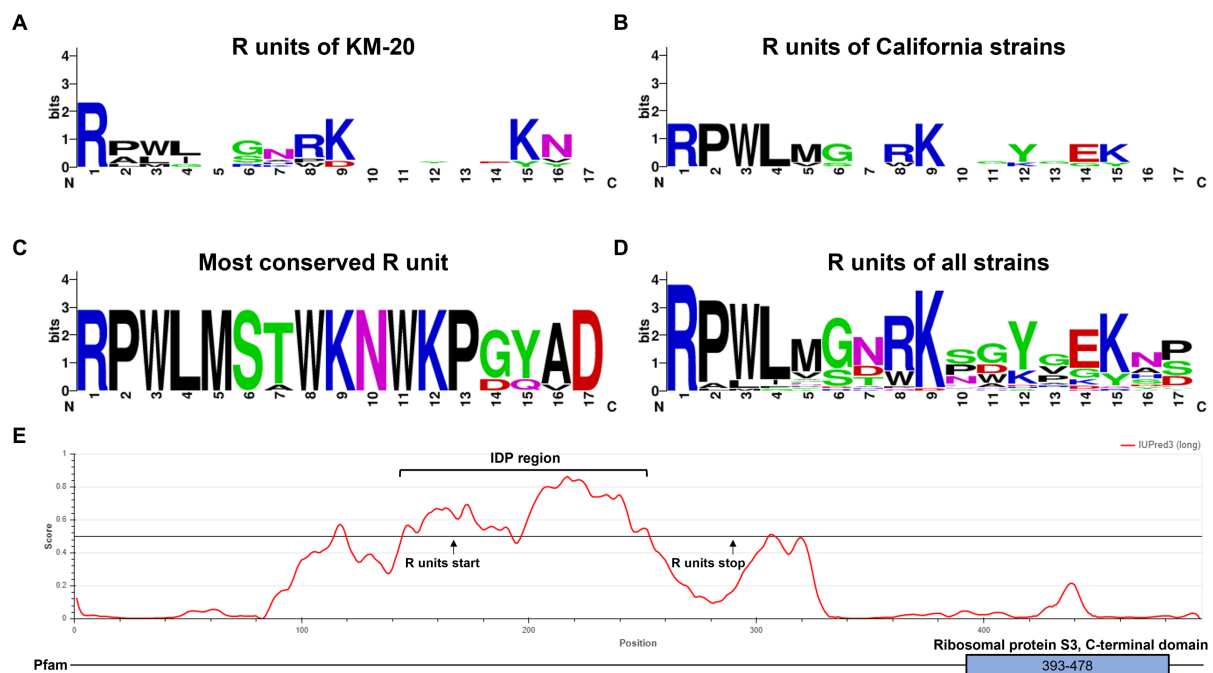


FIGURE 3

Tandem repeat consensus amino acid sequence of *B. mandrillaris* rps3. (A) Tandem repeat consensus amino acid sequence of KM-20 rps3. (B) Tandem repeat consensus amino acid sequence of California strains (RP5, 2046, SAM, and OK1 strain) rps3. (C) Tandem repeat consensus amino acid sequence of the most conserved R units, which are the sequences nearest to the C-terminal of rps3. (D) Tandem repeat consensus amino acid sequence of R units in 10 *B. mandrillaris* strains. The consensus sequence for each repeat is RPWL-G-RK--Y-EK---. The WebLogo consists of stacks of letters as follows: one stack for each position in the sequence. The overall height of the stack shows the sequence conservation at that position, which is measured in bits, while the height of the symbols within the stack represents the relative frequency of each amino acid at that position. Amino acids are colored according to their chemical properties as follows: polar amino acids are colored in green; basic are in blue; acidic are in red, and hydrophobic amino acids are in black. (E) Intrinsically disordered protein region was identified in the tandemly repeated region of KM-20 rps3. The functional ribosomal protein S3 is identified in the C-terminal domain.

variability within the species. Unfortunately, mitochondrial genome sequences of the cases reported in Peru and China, apart from those in the US, are unavailable for comparison with the current case. To comprehend the genetic variation that could be associated with clinical manifestations, the mitochondrial genome of *B. mandrillaris* strain KM-20 was *de novo* assembled and annotated in this study. To our knowledge, this study reports the first complete mitochondrial genome of *B. mandrillaris* clinical isolate obtained from Asia, as others were sequenced from samples isolated in the US. By comparing the mitochondria of KM-20 with other strains collected from the non-Asian area, we found the mitochondrial genome diversity can be attributed to the LAGALIDADG-containing intron in either *cox1* or 23S rRNA and a novel array of protein tandem repeats in *rps3*, which raises questions about the functional roles of this region within mitochondria and cells. In addition to clinical genotyping, the CNVs and domain architecture of the *rps3* tandem repeat can also infer the phylogenetic relationship among strains. The close phylogenetic relationship of the last R units among strains suggested that they could be the most ancient R unit (Supplementary Figure S6). *Cox1* gene has been widely used for species identification, phylogeography, and phylogenetic inference studies; however, the efficacy of using other mitochondrial genes has become less explored (Luo et al., 2011). The variable region in *rps3* can provide additional information on the phylogenetic relationship among strains, such as the copy number and divergence of the R units in *rps3*.

The mitochondrial features of *B. mandrillaris* among strains are generally conserved in terms of gene synteny and coding sequence, except for the presence of LAGLIDADG-containing endonuclease in either *cox1* or 23S rRNA, and the CNVs of protein tandem repeats in *rps3*. LAGLIDADG is a homing endonuclease occasionally included in the Group I self-splicing introns, which can cleave an intronless allele, resulting in the insertion of an intron and endonuclease into the previous intronless allele (Heidel and Glöckner, 2008). Group I introns are commonly found in fungi and protist nuclear rRNA genes as well as in organellar genomes, yet other organisms usually have no Group I introns in the genome (Haugen et al., 2007). Electrophoretic mobility shift assay and DNA cleavage assays can be further performed to identify the target sites of the LAGLIDADG-containing endonuclease (Grindl et al., 1998).

It is known that *rps3* plays a critical role in ribosome biogenesis and DNA repair in humans (Kim et al., 2013). Under stress conditions that promote DNA damage in which the cellular reactive oxygen species level increase, *rps3* accumulates in the mitochondria to repair damaged DNA (Kim et al., 2013). The analysis of ribosomal protein genes is currently lacking since metazoan mitochondrial genomes do not carry ribosomal protein genes (Gray et al., 1998; Heidel and Glöckner, 2008). The function of the *rps3* gene and the implication of CNV in the *rps3* tandem region in *B. mandrillaris* are currently unknown. Alterations in ribosomal genes in other species are shown to be related to adaptation and survival (Finken et al., 1993; Chittum and Champney, 1994). For example, amino acid changes in *rps12* in

*Mycobacterium tuberculosis* are adaptive for streptomycin resistance (Finken et al., 1993). Mutation in the ribosomal protein gene sequence in *Escherichia coli* is related to erythromycin resistance (Chittum and Champney, 1994). The function of CNVs in *rps3* tandem repeats will be interesting to further investigate.

The *rps3* protein sequence of KM-20 was searched in the NCBI non-redundant (NR) database using BLASTp on 26 September 2022. The result showed a significant match to the C-terminal domain of *rps3* with an e-value of 1.88e-05 (Supplementary Figure S8a), confirming the gene annotation. The percentage identities of the *rps3* protein sequence of KM-20 to humans, *Saccharomyces cerevisiae*, *Dictyostelium discoideum*, and *A. castellanii* were calculated by Clustal Omega (v1.2.4), which are 19.69%, 17.28%, 18.37%, and 30.53%, respectively. The C-terminal region of *rps3* of all *B. mandrillaris* strains constituted 113 amino acid residues and shared pairwise identities in the range of 99.12% to 100%, suggesting high conservation of *rps3* C-terminal within the species. In contrast, high variation was observed in the *rps3* sequence between *B. mandrillaris* and other species, including *A. castellanii*. Surprisingly, the *rps3* of *B. mandrillaris* is more similar to bacteria than to other amoebae, as the top BLASTp matches of KM-20 *rps3* are sequences of bacteria such as *Candidatus Caldesamantes*, *Caldiserica* bacteria, and *Metallibacterium scheffleri* (e-value: 4e-06, 5e-06, and 7e-06, respectively) (Supplementary Figure S8b). However, the *rps3* protein sequence of humans, mice, *Drosophila melanogaster*, *S. cerevisiae*, and *D. discoideum* is relatively conserved, with pairwise amino acid residues identities in the range of 59.15% to 99.59%. It is speculated that the origin of the *rps3* gene in *B. mandrillaris* is different from other amoeba species. Further investigations can be performed to investigate the evolutionary origin of *rps3* in amoeba species.

Amoebae inhabit a wide range of ecological niches and rapid adaptation to new environments is advantageous to their survival. Varying the number of tandemly arrayed repeating units can increase the genomic sequence diversity and may enable the organisms to adapt to new environments relatively quicker and undergo more rapid and error-prone evolution than non-repeat-containing proteins (Marcotte et al., 1999; Jernigan and Bordenstein, 2015). All 10 strains of *B. mandrillaris* contain an array of protein tandem repeats in the *rps3* gene, which is not found in other amoebae, including *A. castellanii* and *N. fowleri*, raising questions about the function of the protein tandem repeats in *B. mandrillaris* exclusively. Although unicellular organisms can have significant deviations from typical animal mitochondrial genomes (Lavrov and Pett, 2016), a CNV in the mitochondrial coding region with substantial size variation among strains has not been reported in amoeba before. The conserved specific residues within each R unit may be critical for the structure or function, despite the precise number of repeats and the amino acid sequence may vary among strains (Javadi and Itzhaki, 2013).

A total of two genotypes of *rps3* were observed in strain V039, and the genetic difference lies in a 102 bp insertion in *rps3* which accounts for two extra R units (Detering et al., 2015; Greninger et al., 2015) (Supplementary Figure S9a). Both samples of V039 were isolated from the brain of a pregnant baboon that died from meningoencephalitis at the San Diego Zoo Wild Animal Park in 1990 but was subsequently cultured in different culture media (Detering et al., 2015; Greninger et al., 2015). The mitochondrial genome of the axenic cultivated CDC-V039 has a size of 39,894 bp while the other published

mitochondrial genome of V039 was cultured on Vero cells and has a size of 39,996 bp (Detering et al., 2015; Greninger et al., 2015) (Supplementary Figure S9b). Multiple sequence alignment has confirmed that the axenic CDC-V039 has three R units, whereas the Vero cell-cultured V039 has five, suggesting the possibility of mitochondrial heteroplasmy in *B. mandrillaris*. To verify whether the mitochondrial heteroplasmy of *B. mandrillaris* can be observed under certain conditions, we examined whether the change in culture media or temperature would induce mitochondrial heteroplasmy. However, we did not observe any evidence of mitochondrial heteroplasmy in the *rps3* gene of three *B. mandrillaris* strains including KM-20, V039, and V416 under various culture temperatures and culture medium conditions (Supplementary Figure S10).

## 5. Conclusion

In this study, we *de novo* assembled and annotated the complete mitochondrial genome of *B. mandrillaris* KM-20 using long-read and short-read sequencing data. Our comparative results explored the mitochondrial genome diversity among *B. mandrillaris* strains and revealed that one of the mitochondrial variations arises from an array of protein tandem repeats in the *rps3* gene, which has not been reported in other amoebae before. The copy number and sequence variations of the protein tandem repeats enable *rps3* to be a promising gene target for genotyping *B. mandrillaris* and can provide additional phylogenetic information. Collectively, this comparative mitochondrial genome analysis paves the way to investigate the evolution and genetic diversity of *B. mandrillaris* and other pathogenic amoebae.

## Data availability statement

The datasets presented in this study can be found in online repositories. The names of the repository/repositories and accession number(s) can be found in the article/Supplementary material.

## Ethics statement

The studies involving human participants were reviewed and approved by Siriraj Institutional Review Board of research involving human subjects (SIRB) (COA no. Si 806/2020). Risk Management Taskforce, Mahidol University, Thailand with approval no. SI2020-035. Written informed consent to participate in this study was provided by the participants' legal guardian/next of kin. Written informed consent was obtained from the minor(s)' legal guardian/next of kin for the publication of any potentially identifiable images or data included in this article.

## Author contributions

CL, TN, QX, KK, and PTS contributed to the conception and design of the study. TN, DS, and PS provided clinical data. CL, PTS, KK, LS, PR, and NT were responsible for the laboratory study. CL, TN, and PTS wrote the first draft of the manuscript. CL, QX, PTS, KK, and ST finalized the manuscript. All authors contributed to the article and approved the submitted version.

## Funding

This study was supported by grants from the General Research Fund from Research Grants Council (Reference numbers: 464710, 475113, 14119219, 14119420, and 14175617), Health and Medical Research Fund from Food and Health Bureau (Reference numbers: 06171016 and 07181266), and Theme-based Research Scheme project from the Research Grants Council (Reference number: T11-712/19N) in Hong Kong. This study was also supported by a grant from the Faculty of Medicine Siriraj Hospital, Mahidol University (Grant number R016433002) and was carried out under the Siriraj Integrative Center for Neglected Parasitic Diseases, Faculty of Medicine Siriraj Hospital, Mahidol University. KK, PR, and PTS also received Chalermphrakiat grants from the Faculty of Medicine Siriraj Hospital, Mahidol University.

## Acknowledgments

The authors would like to thank Mathee Ongsiriporn for the brain imaging analysis, and Punpob Lertlaituan for his assistance with the amoeba culture.

## References

- Ankenbrand, M. J., Hohlfeld, S., Hackl, T., and Forster, F. (2017). AliTV—interactive visualization of whole genome comparisons. *PeerJ Comput. Sci.* 3:e116. doi: 10.7717/peerj-cs.116
- Bakardjiev, A., Azimi, P. H., Ashouri, N., Ascher, D. P., Janner, D., Schuster, F. L., et al. (2003). Amebic encephalitis caused by *Balamuthia mandrillaris*: report of four cases. *Pediatr. Infect. Dis. J.* 22, 447–452. doi: 10.1097/01.inf.0000066540.18671.f8
- Bernt, M., Donath, A., Jühling, F., Externbrink, F., Florentz, C., Fritzsche, G., et al. (2013). MITOS: improved de novo metazoan mitochondrial genome annotation. *Mol. Phylogenet. Evol.* 69, 313–319. doi: 10.1016/j.ympev.2012.08.023
- Blum, M., Chang, H., Chuguransky, S., Grego, T., Kandasamy, S., Mitchell, A., et al. (2021). The InterPro protein families and domains database: 20 years on. *Nucleic Acids Res.* 49, D344–D354. doi: 10.1093/nar/gkaa977
- Boon, G. C., Carmichael, J. R., Visvesvara, G. S., Byers, T. J., and Fuerst, P. A. (2003). Identification of *Balamuthia mandrillaris* by PCR assay using the mitochondrial 16S rRNA Gene as a target. *J. Clin. Microbiol.* 41, 453–455. doi: 10.1128/JCM.41.1.453-455.2003
- Bravo, F. G., and Seas, C. (2012). *Balamuthia Mandrillaris* amoebic encephalitis: an emerging parasitic infection. *Curr. Infect. Dis. Rep.* 14, 391–396. doi: 10.1007/s11908-012-0266-4
- Chittum, H. S., and Champney, W. S. (1994). Ribosomal protein gene sequence changes in erythromycin-resistant mutants of *Escherichia coli*. *J. Bacteriol.* 176, 6192–6198. doi: 10.1128/jb.176.20.6192-6198.1994
- Cope, J. R., Landa, J., Nethercut, H., Collier, S. A., Glaser, C., Moser, M., et al. (2019). The epidemiology and clinical features of *Balamuthia mandrillaris* disease in the United States, 1974–2016. *Clin. Infect. Dis.* 68, 1815–1822. doi: 10.1093/cid/ciy813
- Crooks, G. E., Hon, G., Chandonia, J., and Brenner, S. E. (2004). WebLogo: a sequence logo generator. *Genome Res.* 14, 1188–1190. doi: 10.1101/gr.849004
- da Rocha-Azevedo, B., Tanowitz, H. B., and Marciano-Cabral, F. (2009). Diagnosis of infections caused by pathogenic free-living amoebae. *Interdiscip. Perspect. Infect. Dis.* 2009, 251406–251414. doi: 10.1155/2009/251406
- Danecek, P., Bonfield, J. K., Liddle, J., Marshall, J., Ohan, V., Pollard, M. O., et al. (2021). Twelve years of SAMtools and BCFtools. *Gigascience* 10:giab008. doi: 10.1093/gigascience/giab008
- de Souza, W., Attias, M., and Rodrigues, J. C. F. (2009). Particularities of mitochondrial structure in parasitic protists (Apicomplexa and Kinetoplastida). *Int. J. Biochem. Cell Biol.* 41, 2069–2080. doi: 10.1016/j.biocel.2009.04.007
- Detering, H., Aebischer, T., Dabrowski, P. W., Radonić, A., Nitsche, A., Renard, B. Y., et al. (2015). First draft genome sequence of *Balamuthia mandrillaris*, the causative agent of amoebic encephalitis. *Genome Announc.* 3, e01013–e0101315. doi: 10.1128/genomeA.01013-15
- Dunnebacke, T. H., Schuster, F. L., Yagi, S., and Boon, G. C. (2004). *Balamuthia mandrillaris* from soil samples. *Microbiology (Society for General Microbiology)* 150, 2837–2842. doi: 10.1099/mic.0.27218-0
- Erdős, G., Pajkos, M., and Dosztányi, Z. (2021). IUPred3: prediction of protein disorder enhanced with unambiguous experimental annotation and visualization of evolutionary conservation. *Nucleic Acids Res.* 49, W297–W303. doi: 10.1093/nar/gkab408
- Finken, M., Kirschner, P., Meier, A., Wrede, A., and Böttger, E. C. (1993). Molecular basis of streptomycin resistance in *Mycobacterium tuberculosis*: alterations of the ribosomal protein S12 gene and point mutations within a functional 16S ribosomal RNA pseudoknot. *Mol. Microbiol.* 9, 1239–1246. doi: 10.1111/j.1365-2958.1993.tb01253.x
- Gordon, S. M., Steinberg, J. P., DuPuis, M. H., Kozarsky, P. E., Nickerson, J. F., and Visvesvara, G. S. (1992). Culture isolation of *Acanthamoeba* species and *Leptomyxid* Amoebas from patients with amebic meningoencephalitis, including two patients with AIDS. *Clin. Infect. Dis.* 15, 1024–1030. doi: 10.1093/clind/15.6.1024
- Grant, J. R., and Stothard, P. (2008). CGView server: a comparative genomics tool for circular genomes. *Nucleic Acids Res.* 36, W181–W184. doi: 10.1093/nar/gkn179
- Gray, M. W., Lang, B. F., Cedergren, R., Golding, G. B., Lemieux, C., Sankoff, D., et al. (1998). Genome structure and gene content in protist mitochondrial DNAs. *Nucleic Acids Res.* 26, 865–878. doi: 10.1093/nar/26.4.865
- Greninger, A. L., Messacar, K., Dunnebacke, T., Naccache, S. N., Federman, S., Bouquet, J., et al. (2015). Clinical metagenomic identification of *Balamuthia mandrillaris* encephalitis and assembly of the draft genome: the continuing case for reference genome sequencing. *Genome Med.* 7:113. doi: 10.1186/s13073-015-0235-2
- Grindl, W., Wende, W., Pingoud, V., and Pingoud, A. (1998). The protein splicing domain of the homing endonuclease PI-SceI is responsible for specific DNA binding. *Nucleic Acids Res.* 26, 1857–1862. doi: 10.1093/nar/26.8.1857
- Harris, R. S. (2007). *Improved pairwise alignment of genomic DNA*. State College, PA: The Pennsylvania State University.
- Haugen, P., Bhattacharya, D., Palmer, J. D., Turner, S., Lewis, L. A., and Pryer, K. M. (2007). Cyanobacterial ribosomal RNA genes with multiple, endonuclease-encoding group I introns. *BMC Evol. Biol.* 7:159. doi: 10.1186/1471-2148-7-159
- Heidel, A. J., and Glöckner, G. (2008). Mitochondrial genome evolution in the social amoebae. *Mol. Biol. Evol.* 25, 1440–1450. doi: 10.1093/molbev/msn088
- Intalapaporn, P., Suankratay, C., Shuangshoti, S., Phantumchinda, K., Keelawat, S., and Wilde, H. (2004). *Balamuthia Mandrillaris* meningoencephalitis: the first case in Southeast Asia. *Am. J. Trop. Med. Hyg.* 70, 666–669. doi: 10.4269/ajtmh.2004.70.666
- Javadi, Y., and Itzhaki, L. S. (2013). Tandem-repeat proteins: regularity plus modularity equals design-ability. *Curr. Opin. Struct. Biol.* 23, 622–631. doi: 10.1016/j.sbi.2013.06.011
- Jernigan, K. K., and Bordenstein, S. R. (2015). Tandem-repeat protein domains across the tree of life. *PeerJ (San Francisco, CA)* 3:e732. doi: 10.7717/peerj.732
- Jones, P., Binns, D., Chang, H., Fraser, M., Li, W., McAnulla, C., et al. (2014). InterProScan 5: genome-scale protein function classification. *Bioinformatics* 30, 1236–1240. doi: 10.1093/bioinformatics/btu031

## Conflict of interest

The authors declare that the research was conducted in the absence of any commercial or financial relationships that could be construed as a potential conflict of interest.

## Publisher's note

All claims expressed in this article are solely those of the authors and do not necessarily represent those of their affiliated organizations, or those of the publisher, the editors and the reviewers. Any product that may be evaluated in this article, or claim that may be made by its manufacturer, is not guaranteed or endorsed by the publisher.

## Supplementary material

The Supplementary material for this article can be found online at: <https://www.frontiersin.org/articles/10.3389/fmicb.2023.1162963/full#supplementary-material>



- Jones, D. T., Taylor, W. R., and Thornton, J. M. (1992). The rapid generation of mutation data matrices from protein sequences. *Bioinformatics* 8, 275–282. doi: 10.1093/bioinformatics/8.3.275
- Kim, Y., Kim, H. D., and Kim, J. (2013). Cytoplasmic ribosomal protein S3 (rpS3) plays a pivotal role in mitochondrial DNA damage surveillance. *Biochim. Biophys. Acta Mol. Cell Res.* 1833, 2943–2952. doi: 10.1016/j.bbamcr.2013.07.015
- Kolmogorov, M., Yuan, J., Lin, Y., and Pevzner, P. A. (2019). Assembly of long, error-prone reads using repeat graphs. *Nat. Biotechnol.* 37, 540–546. doi: 10.1038/s41587-019-0072-8
- Kumar, S., Stecher, G., Li, M., Knyaz, C., and Tamura, K. (2018). MEGA X: molecular evolutionary genetics analysis across computing platforms. *Mol. Biol. Evol.* 35, 1547–1549. doi: 10.1093/molbev/msy096
- Kuraku, S., Zmasek, C. M., Nishimura, O., and Katoh, K. (2013). aLeaves facilitates on-demand exploration of metazoan gene family trees on MAFFT sequence alignment server with enhanced interactivity. *Nucleic Acids Res.* 41, W22–W28. doi: 10.1093/nar/gkt389
- Lang, B. F., Laforest, M., and Burger, G. (2007). Mitochondrial introns: a critical view. *Trends Genet.* 23, 119–125. doi: 10.1016/j.tig.2007.01.006
- Laslett, D., and Canback, B. (2004). ARAGORN, a program to detect tRNA genes and tmRNA genes in nucleotide sequences. *Nucleic Acids Res.* 32, 11–16. doi: 10.1093/nar/gkh152
- Lavrov, D. V., and Pett, W. (2016). Animal mitochondrial DNA as we do not know it: mt-genome organization and evolution in nonbilaterian lineages. *Genome Biol. Evol.* 8, 2896–2913. doi: 10.1093/gbe/evw195
- Letunic, I., and Bork, P. (2021). Interactive tree of life (iTOL) v5: an online tool for phylogenetic tree display and annotation. *Nucleic Acids Res.* 49, W293–W296. doi: 10.1093/nar/gkab301
- Li, H. (2018). Minimap2: pairwise alignment for nucleotide sequences. *Bioinformatics* 34, 3094–3100. doi: 10.1093/bioinformatics/bty191
- Luo, A., Zhang, A., Ho, S. Y., Xu, W., Zhang, Y., Shi, W., et al. (2011). Potential efficacy of mitochondrial genes for animal DNA barcoding: a case study using eutherian mammals. *BMC Genom.* 12:84. doi: 10.1186/1471-2164-12-84
- Marcotte, E. M., Pellegrini, M., Yeates, T. O., and Eisenberg, D. (1999). A census of protein repeats. *J. Mol. Biol.* 293, 151–160. doi: 10.1006/jmbi.1999.3136
- Matin, A., Siddiqui, R., Jayasekera, S., and Khan, N. A. (2008). Increasing importance of *Balamuthia mandrillaris*. *Clin. Microbiol. Rev.* 21, 435–448. doi: 10.1128/CMR.00056-07
- Schneider, T. D., and Stephens, R. M. (1990). Sequence logos: a new way to display consensus sequences. *Nucleic Acids Res.* 18, 6097–6100. doi: 10.1093/nar/18.20.6097
- Schuster, F. L. (2002). Cultivation of pathogenic and opportunistic free-living Amebas. *Clin. Microbiol. Rev.* 15, 342–354. doi: 10.1128/CMR.15.3.342-354.2002
- Schuster, F. L., Dunnebacke, T. H., Martinez, A. J., Visvesvara, G. S., Booton, G. C., Yagi, S., et al. (2003). Environmental isolation of *Balamuthia mandrillaris* associated with a case of amebic encephalitis. *J. Clin. Microbiol.* 41, 3175–3180. doi: 10.1128/JCM.41.7.3175-3180.2003
- Schuster, F. L., Yagi, S., Gavali, S., Michelson, D., Raghavan, R., Blomquist, I., et al. (2009). Under the radar: *Balamuthia amebic encephalitis*. *Clin. Infect. Dis.* 48, 879–887. doi: 10.1086/597260
- Siddiqui, R., and Khan, N. A. (2008). *Balamuthia amebic encephalitis*: an emerging disease with fatal consequences. *Microb. Pathog.* 44, 89–97. doi: 10.1016/j.micpath.2007.06.008
- Sievers, F., Wilm, A., Dineen, D., Gibson, T. J., Karplus, K., Li, W., et al. (2011). Fast, scalable generation of high-quality protein multiple sequence alignments using Clustal omega. *Mol. Syst. Biol.* 7:539. doi: 10.1038/msb.2011.75
- Stajich, J. E., Block, D., Boulez, K., Brenner, S. E., Chervitz, S. A., Dagdigian, C., et al. (2002). The Bioperl toolkit: Perl modules for the life sciences. *Genome Res.* 12, 1611–1618. doi: 10.1101/gr.361602
- Stothard, P., and Wishart, D. S. (2005). Circular genome visualization and exploration using CGView. *Bioinformatics* 21, 537–539. doi: 10.1093/bioinformatics/bti054
- Tillich, M., Lehwark, P., Pellizzer, T., Ulbricht-Jones, E. S., Fischer, A., Bock, R., et al. (2017). GeSeq—versatile and accurate annotation of organelle genomes. *Nucleic Acids Res.* 45, W6–W11. doi: 10.1093/nar/gkx391
- Visvesvara, G. S. (2013). Infections with free-living amebae. *Handb. Clin. Neurol.* 153–168. doi: 10.1016/b978-0-444-53490-3.00010-8
- Visvesvara, G. S. (2014). “Pathogenic and opportunistic free-living amoebae: agents of human and animal disease” in *Anonymous Manson's tropical diseases*. eds. J. Farrar, P. Hotez, T. Junghanss, G. Kang, D. Lalloo and N. White 23rd ed., (essay, Elsevier Saunders), 683–691.
- Visvesvara, G. S., Martinez, A. J., Schuster, F. L., Leitch, G. J., Wallace, S. V., Sawyer, T. K., et al. (1990). Leptomyxid ameba, a new agent of amebic meningoencephalitis in humans and animals. *J. Clin. Microbiol.* 28, 2750–2756. doi: 10.1128/JCM.28.12.2750-2756.1990
- Visvesvara, G. S., Moura, H., and Schuster, F. L. (2007). Pathogenic and opportunistic free-living amoebae: *Acanthamoeba* spp., *Balamuthia mandrillaris*, *Naegleria fowleri*, and *Sappinia diploidea*. *FEMS Immunol. Med. Microbiol.* 50, 1–26. doi: 10.1111/j.1574-695X.2007.00232.x
- Vollmer, M. E., and Glaser, C. (2016). A *Balamuthia* survivor. *JMM Case Rep.* 3:e005031. doi: 10.1099/jmmcr.0.005031
- Walker, B. J., Abeel, T., Shea, T., Priest, M., Abouelliel, A., Sakthikumar, S., et al. (2014). Pilon: an integrated tool for comprehensive microbial variant detection and genome assembly improvement. *PLoS One* 9:e112963. doi: 10.1371/journal.pone.0112963
- Wang, L., Cheng, W., Li, B., Jian, Z., Qi, X., Sun, D., et al. (2020). *Balamuthia mandrillaris* infection in China: a retrospective report of 28 cases. *Emerg. Microbes Infect.* 9, 2348–2357. doi: 10.1080/22221751.2020.1835447
- Wright, P. E., and Dyson, H. J. (2015). Intrinsically disordered proteins in cellular signalling and regulation. *Nat. Rev. Mol. Cell Biol.* 16, 18–29. doi: 10.1038/nrm3920



## OPEN ACCESS

## EDITED BY

Nigel Yarett,  
Pace University, United States

## REVIEWED BY

Binod Rayamajhee,  
University of New South Wales, Australia  
Sutherland Kester Maciver,  
University of Edinburgh, United Kingdom  
Samuel Arnold,  
University of Washington, United States  
Wayne Heaselgrave,  
University of Wolverhampton, United Kingdom

## \*CORRESPONDENCE

Lori Ferrins  
✉ l.ferrins@northeastern.edu  
Christopher A. Rice  
✉ carice@purdue.edu

## †PRESENT ADDRESS

Christopher A. Rice,  
Purdue Institute for Drug Discovery (PIDD),  
Purdue University, West Lafayette,  
IN, United States; Purdue Institute of  
Inflammation, Immunology and Infectious  
Disease (PI4D), Purdue University, West  
Lafayette, IN, United States

## SPECIALTY SECTION

This article was submitted to  
Infectious Agents and Disease,  
a section of the journal  
Frontiers in Microbiology

RECEIVED 21 January 2023

ACCEPTED 29 March 2023

PUBLISHED 10 May 2023

## CITATION

Ferrins L, Buskes MJ, Kapteyn MM, Engels HN,  
Enos SE, Lu C, Klug DM, Singh B, Quotadamo A,  
Bachovchin K, Tear WF, Spaulding AE, Forbes KC,  
Bag S, Rivers M, LeBlanc C, Burchfield E,  
Armand JR, Diaz-Gonzalez R, Ceballos-Perez G,  
García-Hernández R, Pérez-Moreno G,  
Bosch-Navarrete C, Gómez-Liñán C,  
Ruiz-Pérez LM, Gamarro F,  
González-Pacanowska D, Navarro M,  
Mensa-Wilmot K, Pollastri MP, Kyle DE and  
Rice CA (2023) Identification of novel anti-  
amoebic pharmacophores from kinase  
inhibitor chemotypes.  
*Front. Microbiol.* 14:1149145.  
doi: 10.3389/fmicb.2023.1149145

## COPYRIGHT

© 2023 Ferrins, Buskes, Kapteyn, Engels, Enos,  
Lu, Klug, Singh, Quotadamo, Bachovchin, Tear,  
Spaulding, Forbes, Bag, Rivers, LeBlanc,  
Burchfield, Armand, Diaz-Gonzalez, Ceballos-  
Perez, García-Hernández, Pérez-Moreno,  
Bosch-Navarrete, Gómez-Liñán, Ruiz-Pérez,  
Gamarro, González-Pacanowska, Navarro,  
Mensa-Wilmot, Pollastri, Kyle and Rice. This is an  
open-access article distributed under the terms  
of the [Creative Commons Attribution License](#)  
(CC BY). The use, distribution or reproduction in  
other forums is permitted, provided the original  
author(s) and the copyright owner(s) are credited  
and that the original publication in this journal is  
cited, in accordance with accepted academic  
practice. No use, distribution or reproduction is  
permitted which does not comply with these  
terms.

# Identification of novel anti-amoebic pharmacophores from kinase inhibitor chemotypes

Lori Ferrins<sup>1\*</sup>, Melissa J. Buskes<sup>1</sup>, Madison M. Kapteyn<sup>2</sup>,  
Hannah N. Engels<sup>2</sup>, Suzanne E. Enos<sup>2,3</sup>, Chenyang Lu<sup>4</sup>,  
Dana M. Klug<sup>1</sup>, Baljinder Singh<sup>1</sup>, Antonio Quotadamo<sup>1,5</sup>,  
Kelly Bachovchin<sup>1</sup>, Westley F. Tear<sup>1</sup>, Andrew E. Spaulding<sup>1</sup>,  
Katherine C. Forbes<sup>1</sup>, Seema Bag<sup>1</sup>, Mitch Rivers<sup>1</sup>,  
Catherine LeBlanc<sup>1</sup>, Erin Burchfield<sup>1</sup>, Jeremy R. Armand<sup>1</sup>,  
Rosario Diaz-Gonzalez<sup>6</sup>, Gloria Ceballos-Perez<sup>6</sup>,  
Raquel García-Hernández<sup>6</sup>, Guiomar Pérez-Moreno<sup>6</sup>,  
Cristina Bosch-Navarrete<sup>6</sup>, Claudia Gómez-Liñán<sup>6</sup>,  
Luis Miguel Ruiz-Pérez<sup>6</sup>, Francisco Gamarro<sup>6</sup>,  
Dolores González-Pacanowska<sup>6</sup>, Miguel Navarro<sup>6</sup>,  
Kojo Mensa-Wilmot<sup>7</sup>, Michael P. Pollastri<sup>1</sup>, Dennis E. Kyle<sup>2</sup> and  
Christopher A. Rice<sup>2,3,4,\*†</sup>

<sup>1</sup>Department of Chemistry and Chemical Biology, Northeastern University, Boston, MA, United States,

<sup>2</sup>Center for Tropical and Emerging Global Diseases, University of Georgia, Athens, GA, United States,

<sup>3</sup>Department of Pharmaceutical and Biomedical Sciences, College of Pharmacy, University of Georgia,  
Athens, GA, United States, <sup>4</sup>Department of Comparative Pathobiology, College of Veterinary Medicine,  
Purdue University, West Lafayette, IN, United States, <sup>5</sup>Clinical and Experimental Medicine PhD Program,  
University of Modena and Reggio Emilia, Modena, Italy, <sup>6</sup>Instituto de Parasitología y Biomedicina

"López-Neyra" Consejo Superior de Investigaciones Científicas (CSIC), Granada, Spain, <sup>7</sup>Department of  
Molecular and Cellular Biology, Kennesaw State University, Kennesaw, GA, United States

*Acanthamoeba* species, *Naegleria fowleri*, and *Balamuthia mandrillaris* are opportunistic pathogens that cause a range of brain, skin, eye, and disseminated diseases in humans and animals. These pathogenic free-living amoebae (pFLA) are commonly misdiagnosed and have sub-optimal treatment regimens which contribute to the extremely high mortality rates (>90%) when they infect the central nervous system. To address the unmet medical need for effective therapeutics, we screened kinase inhibitor chemotypes against three pFLA using phenotypic drug assays involving CellTiter-Glo 2.0. Herein, we report the activity of the compounds against the trophozoite stage of each of the three amoebae, ranging from nanomolar to low micromolar potency. The most potent compounds that were identified from this screening effort were: **2d** (*A. castellanii* EC<sub>50</sub>: 0.92±0.3μM; and *N. fowleri* EC<sub>50</sub>: 0.43±0.13μM), **1c** and **2b** (*N. fowleri* EC<sub>50</sub>S: <0.63μM, and 0.3±0.21μM), and **4b** and **7b** (*B. mandrillaris* EC<sub>50</sub>S: 1.0±0.12μM, and 1.4±0.17μM, respectively). With several of these pharmacophores already possessing blood-brain barrier (BBB) permeability properties, or are predicted to penetrate the BBB, these hits present novel starting points for optimization as future treatments for pFLA-caused diseases.

## KEYWORDS

pathogenic free-living amoeba, *Acanthamoeba* species, *Naegleria fowleri*, *Balamuthia mandrillaris*, kinase inhibitors, cross-screening, hit-identification

## Introduction

Free-living amoebas are ubiquitously found in various natural and man-made sources. Many are of no significant medical importance, but some are opportunistic pathogens of humans and animals. *Acanthamoeba* was the first potential pathogenic free-living amoebae (pFLA) described by Castellani (1930). Since then, the genus of *Acanthamoeba* has been divided into 23 genotypes (T1–T23), based on the 18S rRNA gene sequences (Diehl et al., 2021; Putaporntip et al., 2021). Of these, the most common genotype belongs to the T4 clade which has multiple species and thousands of isolates associated, these are found to cause the majority of the cases of *Acanthamoeba* keratitis (Diehl et al., 2021). Although T4 is the most prevalent genotype worldwide, T1, T3, T4, T10, and T12 have all been found to cause granulomatous *Acanthamoeba* encephalitis (GAE; Megha et al., 2018). *Acanthamoeba* can enter the body by various means, it is thought to initially infect the skin (cutaneous lesions) or respiratory tract before entering the blood circulatory system. Through hematogenous dissemination it can reach other organs and becomes a major problem when it reaches the blood–brain barrier where it can break down and enter the brain causing GAE (Marciano-Cabral and Cabral, 2003). The vast variation of genotypes, species, and clinical isolates of *Acanthamoeba* pose a significant problem with drug susceptibility variation and for treatment of the diseases that they cause. To further complicate amoeba infections and resolution of AK disease, amoebae can harbor other human pathogens where they can exchange genetic material increasing pathogenicity of both amoeba (host) and symbiont (Rayamajhee et al., 2022). Assessing the microbiome during an active infection, may provide insight into a tailored drug therapy which resolves the disease quicker without secondary infection caused by such symbiont. Further work needs to be researched to determine if specific symbionts and amoeba infections cause for concern for amoeba specific drug sensitivities and resistant profiles since we are now seeing more clinical failures and blindness with AK disease.

In 1965, *Naegleria* was first described as causing meningoencephalitis in four patients in Adelaide, Australia by Fowler and Carter (1965). Based on the 5.8S rDNA and the internal transcribed spacers (ITS; one or two) gene sequences, the genus of *Naegleria* has been identified to contain 47 different species unevenly distributed around the world (De Jonckheere, 2014). Of these 47, three have been found to cause disease in animals and one of these three, *N. fowleri* is the only species to cause the brain-eating disease in humans, primary amoebic meningoencephalitis (PAM). *Naegleria* pathology starts with contaminated water going up the nose through nasal ablation, sinus rinsing, or jumping/sliding into contaminated water sources. In the sinuses, the trophozoites are thought to use the olfactory nerve to cross the cribriform plate into the olfactory bulbs and frontal lobes of the brain where it causes major pathology (Grace et al., 2015). One of the most recent deaths in the United States from PAM came in 2021 after a child fell ill following a swim in a private pond in North Carolina (North Carolina Department of Health and Human Services, 2021).

*Balamuthia mandrillaris* is currently the only pathogenic species within the *Balamuthia* genus; it was described by Dr. G. S. Visvesvara in 1986 presenting similar encephalitis as *Acanthamoeba* GAE in a pregnant mandrill (*Mandrillus sphinx*) in San Diego Zoo Wild Animal Park, United States (Visvesvara et al., 1990). Although one study suggested *B. mandrillaris* uses a similar invasion pathway to *N. fowleri*

(Kiderlen and Laube, 2004), this is not typically presented in human infection (Cope et al., 2018). Similar to *Acanthamoeba*, *B. mandrillaris* trophozoites and the persistent cyst stage, are both found in multiple infected tissues. Furthermore, in support of hematogenous dissemination, *B. mandrillaris* are typically found in clusters of patients brains close to blood vessels (Recavarren-Arce et al., 1999). Granulomatous *Acanthamoeba* Encephalitis (GAE) and *Balamuthia* Amoebic Encephalitis (BAE) are indistinguishable by diagnostic light microscopy. Recently, Next-Generation Sequencing (NGS) has proven to be a cost effective, unbiased, and quick method in the diagnosis of unknown diseases and several pFLA infections (Wang et al., 2018; Yang et al., 2019; Holmggaard et al., 2021). China has one of the fastest-growing genomics markets worldwide; it is not surprising that this is enabling earlier diagnosis of these neglected diseases. Although earlier diagnoses does not translate to curing these patients; it does open the therapeutic treatment window.

For these pFLA infections, therapeutic approaches include a multi-drug cocktail of amphotericin B and pentamidine, azoles (fluconazole, itraconazole, or posaconazole), macrolides (azithromycin), and other anti-bacterials and anti-fungals (Schuster et al., 2006; Visvesvara, 2010; Cope, 2013). Even with multi-drug cocktail treatments, CNS-involved infections are almost always fatal. The current inability to kill the trophozoites quickly, or in the case of *Acanthamoeba* and *Balamuthia* infections to inactivate the double-walled resistant cyst stage that have been found in all host infected tissues, e.g., skin, lungs, eyes, or brains, highlight the lack of effective treatments and the urgent need for developing new therapeutics against these pathogens. Given that prolonged therapy is often required, there are concerns for emergence of drug resistance (Siddiqui and Khan, 2012). Clearly, there is an unmet medical need to discover new drugs that are potent against pFLAs, are less toxic, and can cross the blood–brain barrier (BBB).

We have phenotypically screened compounds that were originally synthesized for ongoing human African trypanosomiasis and Leishmaniasis neglected tropical disease drug discovery programs (Diaz et al., 2014; Bachovchin et al., 2019) that yielded benzoxazepinoindazoles (Klug et al., 2019), pyrazolopyridazines (Tear et al., 2020), substituted azaindoles (Klug et al., 2021), and aminopurines (Singh et al., 2020). The imidazopyridines (Akao et al., 2021) were identified by the Drugs for Neglected Diseases initiative (DNDi) via the Neglected Tropical Disease (NTD) Drug Discovery Booster project (Drugs for Neglected Diseases Initiative, 2015).

The compounds were screened against *A. castellanii*, *N. fowleri*, and *B. mandrillaris* logarithmic phase trophozoites. Compounds with an  $EC_{50} < 10 \mu\text{M}$  were classed as hits, while those between 10 and 20  $\mu\text{M}$  were considered moderately potent, and compounds  $> 20 \mu\text{M}$  were considered inactive (summarized in the Supporting Information). Of the compounds tested, seven met the hit criteria for *A. castellanii*, and an additional five were moderately potent. Against *N. fowleri*, 31 compounds met the potency criteria to be classed as a hit, and an additional 14 compounds had moderately potent activity. There were 26 hit compounds identified against *B. mandrillaris*, and another 10 compounds exhibited moderately potent activity. Compounds that yielded no activity against any of the pFLA are summarized in the Supplementary Table S1. Given the need for new hits that are potent against these pFLA, and that have demonstrated BBB exposure, this dataset provides a strong starting point for medicinal chemistry optimization.

## Materials and methods

### Maintenance of amoebae

Pathogenic *Acanthamoeba castellanii* T4 isolate (ATCC 50370) used in these studies was isolated from the eye of a keratitis patient in New York, NY, United States in 1978. This isolate was purchased from American Type Culture Collection (ATCC). Trophozoites were routinely grown axenically at 27°C in Protease Peptone-Glucose Media (PG) in non-vented 75 cm<sup>2</sup> tissue culture flasks (Olympus), until the cells were 80–90% confluent. For sub-culturing, cells were mechanically harvested to detach the cells from the culture flasks. The cells were collected by centrifugation at 3,214 RCF at 4°C. Complete PG media is prepared by the addition of 100 U/mL penicillin, and 100 µg/mL streptomycin antibiotics.

Pathogenic *Naegleria fowleri* (ATCC 30215), a clinical isolate obtained from a 9-year old boy in Adelaide, Australia, who died of PAM in 1969 was previously purchased from ATCC. Trophozoites were routinely grown axenically at 34°C, 5% CO<sub>2</sub>, in Nelson's complete medium (NCM) in non-vented 75 cm<sup>2</sup> tissue culture flasks (Olympus), until the cells were 80–90% confluent. For sub-culturing, cells were placed on ice to detach the cells from the culture flasks. The cells were collected by centrifugation at 3,214 RCF at 4°C. Complete NCM media is prepared by the addition of 10% fetal bovine serum (FBS) and 100 U/mL penicillin, and 100 µg/mL streptomycin antibiotics.

Pathogenic *Balamuthia mandrillaris* (CDC:V039; ATCC 50209), a GAE isolate, isolated from a pregnant mandrill that died at the San Diego Zoo in 1986 was donated by Dr. Luis Fernando Lares-Jiménez ITSON University, Mexico. Trophozoites were routinely grown axenically in BMI media at 37°C, 5% CO<sub>2</sub> in vented 75 cm<sup>2</sup> tissue culture flasks (Olympus), until the cells were 80–90% confluent. For sub-culturing, 0.25% Trypsin-EDTA (Gibco) cell detachment reagent was used to detach the cells from the culture flasks. The cells were collected by centrifugation at 3,214 RCF at 4°C. Complete BMI media is prepared by the addition of 10% FBS and 100 U/mL penicillin, and 100 µg/mL streptomycin antibiotics.

### Compound preparation

All compounds were synthesized at Northeastern University (NEU) and had purity >95% as determined by LCMS analysis, compound identity was confirmed using <sup>1</sup>H Nuclear Magnetic Resonance (NMR). The specific instruments used to fully characterize each compound are reported in the relevant reference listed in the tables, or in the Supporting Information. Compounds were supplied as powder stocks, which were reconstituted to a 20 mM stock concentration in DMSO and diluted in each amoeba's representative neat media for standardized susceptibility screening from 20 µM.

### In vitro CellTiter-Glo trophocidal assay

The trophocidal activity of compounds was assessed using the CellTiter-Glo 2.0 luminescent viability assay (Promega, Madison, WI), as previously described (Rice et al., 2015, 2020a,b,c). Trophozoites were routinely cultured as described above and only logarithmic trophozoites were used. In brief, *A. castellanii*, *N. fowleri*, or

*B. mandrillaris* trophozoites cultured in their corresponding complete media were seeded at 1,440, 3,000, or 16,000 cells/well into white 96-well plates (Costar 3370), respectively.

All compounds were assessed in 2-fold serial dilutions from 20 to 0.625 µM. Control wells were supplemented with 0.2% DMSO, as the negative control, or 12.5 µM of chlorhexidine as the positive control. All assays were incubated at each of the parasites' representative growth temperatures, described above, for 72 h. At the 72-h time point, 25 µL of CellTiter-Glo 2.0 reagent was added to all wells of the 96-well plates by hand. The plates were protected from light and contents were mixed using an orbital shaker at 300 rpm at room temperature for 2 min to induce cell lysis. After shaking, the plates were equilibrated at room temperature for 10 min to stabilize the luminescent signal. The ATP luminescent signal (relative light units; RLUs) were measured at 490 nm with a SpectraMax I3X plate reader (Molecular Devices, Sunnyvale, CA, United States). The concentration of a drug that gives half-maximal response (EC<sub>50</sub>) were generated using total ATP RLUs where controls were calculated as the average of replicates using the Levenberg–Marquardt algorithm, using DMSO as the normalization control, as defined in CDD Vault (Burlingame, CA, United States). Values reported are from a minimum of three biological replicates with standard deviation.

### Cytotoxicity screening of reconfirmed compounds

#### Human fetal lung fibroblast (MRC5) cell assay

Intermediate plates were made as described, adding 95 µL of DMEM complete media to 5 µL of compound per well setting a 5% DMSO amount. Log-phase MRC5 cells were removed from a T-75 TC flask using TrypLE® Express (Thermo®) and dispersed by gentle pipetting. Cell density was adjusted to working concentration in prewarmed DMEM medium: 25,000 cells in 90 µL of culture were plated in 96-well transparent Nunclon plates and allowed to settle for 24 h at 37°C and 5% CO<sub>2</sub>. After settling incubation, 10 µL of freshly made intermediate plate were added per well: final maximal concentration for compounds was 50 µM in 0.5% DMSO per well. Plates were incubated for 48 h at 37°C and 5% CO<sub>2</sub>. At 4 h prior to fluorescence measurement, 20 µL of 500 µM resazurin solution was added. Fluorescence was read in an Infinite F200 plate reader (Tecan®) at 550 nm (excitation filter) and 590 nm (emission filter), as previously described (Isoet et al., 2009).

A four-parameter equation was used to fit the dose–response curves and determination of EC<sub>50</sub> by SigmaPlot® 13.0 software. Assays were performed in duplicate at least twice for positive compounds, to achieve a minimal *n* = 2 per dose response.

#### Rat skeletal muscle cell line (L6) cell assay

One hundred microliters (100 µL) per well of culture medium containing the compounds and controls were added to L6 cells previously cultured (4 × 10<sup>3</sup> L6 cells per well). After 72 h at 37°C the medium was exchanged, and the viable cell number was determined by resazurin (Sigma–Aldrich) reduction. 20 µL of resazurin (1.1 mg/ml) was added to each well and incubated in the dark for 2 h at 37°C. Cell viability was estimated by using the same method as described above in the MRC5 cytotoxicity section, as previously described (Isoet et al., 2009).



## Results and discussion

### *Acanthamoeba castellanii*

The preliminary data for the benzoxazepinoindazole series, although limited, shows promising biological potency. Strong structure–activity relationships (SAR) dependent on *N*-alkylation was observed where alkylation of the aminopyrimidine **1c** was tolerated but not on the benzoxazepinoindazole core (**1e**; EC<sub>50</sub>: >20 μM). As part of our NTD optimization program, **1e** was tested at 10 mg/kg, Intraperitoneal injection (I.P.), in a pharmacokinetic (PK) model and was found to have a blood/brain ratio of 2.4 at 0.5 h and 2.1 at 4 h (Klug et al., 2019). Truncation to **1d**, with a methyl group on the indazole nitrogen, led to retention of potency against *A. castellanii*. Further analogs are needed to explore the SAR of this related chemotype which has demonstrated improved absorption, distribution, metabolism and elimination (ADME) properties, and *in vivo* exposure, though it showed decreased BBB penetration. The limited initial screen has provided promising leads meeting the hit criteria. Aqueous solubility will need to be addressed in a hit-to-lead optimization campaign.

The two most potent compounds identified against *A. castellanii* came from the pyrazolopyridazines, with **2b** being a low micromolar inhibitor and **2d** demonstrating sub-micromolar potency, though there is potent inhibition against skeletal muscle myoblast, L6 (ATCC CRL-1458), cells for both (< 0.62 μM). The aminopyrimidine of the pyrazolopyridazines is a known hinge binding motif in human kinases and the limited modifications that were tested [replacement with an aniline (**2g**), 4-methyl aminopyrimidine (**2e**), or 2-pyridyl (**2f**) led to a loss of potency]. Compound **2b** was tested at 10 mg/kg, I.P., in a PK study and had a blood/brain ratio of 1.1 at 0.5 and 4 h (Tear et al., 2020). However, *in vivo* toxicity was observed and will be a focus of a hit-to-lead optimization campaign.

Two of the imidazopyridines tested had potency <10 μM (**3a** and **3b**) against *A. castellanii* and there is valuable SAR that can be derived from the screening set. Incorporation of the pyrazole in place of the pyridine was well tolerated and led to a moderately potent inhibitor (cf. **3b** and **3c**). Further, the free amine (**3a**) demonstrated improved activity versus the aliphatic (**3d**) and aromatic (**3e**)—NH derivatives. While no data is available on the BBB exposure of these compounds, the calculated Blood–Brain Barrier (BBB) Score (Gupta et al., 2019) for this series indicates potential exposure.

Azadinoles are another common motif in kinase inhibitor drug discovery. While two of the compounds tested demonstrated moderate potency versus *A. castellanii* (**4a** and **4b**) and the series had predicted brain penetration, when a related compound (**4c**) was progressed to PK there was negligible brain exposure; resolving this issue would need to be a focus of a subsequent hit-to-lead optimization campaign (Klug et al., 2021). There is some preliminary SAR that is apparent with the series, replacement of the tetrahydropyran with the piperidine (**4c**) was not tolerated and could indicate that the presence of a hydrogen bond donor at this position is unfavorable. Additionally, it is apparent that substituting the azaindole with a 4-methyl (**4b**) was well tolerated, as was introduction of the additional heteroatom (**4a**).

### *Naegleria fowleri*

The benzoxazepinoindazoles yielded the most potent hit for *N. fowleri* (**1c** EC<sub>50</sub>: <0.63 μM) which demonstrated >10-fold selectivity

versus THP-1 (see Supplementary Table S1 for full data set) and MRC5 cells. Alkylation of the indazole nitrogen was unfavorable (**1e** and **1d**) though the loss of potency for **1d** may be impacted by the removal of the northern aromatic ring and further analogs are needed. The aminopyrazine motif that is present in **1a–c** leads to potent activity against *N. fowleri* and the alkylation of the amine in **1c** is well tolerated.

Modifications to the aminopyrazine of the pyrazolopyridazines led to the identification of **2f** which had potent *N. fowleri* activity (EC<sub>50</sub>: 1.0 μM) and no activity against MRC5 or L6 cells at 50 μM. This compound is significant as it demonstrates that alteration to the reported hinge binding region (Tavares et al., 2004; Stevens et al., 2008) and removal of one of the hydrogen bond acceptors, is tolerated, and may afford an opportunity to obtain selectivity versus human kinases. Also tolerated was replacement of the benzonitrile with the cyclohexylamine (**2p**), or 3-aminopyridine (**2b**), and substitution of the 2-position of the pyrazolopyridazine with an isopropyl (**2n**) or alkyl ether (**2l**). While these compounds were all low micromolar versus *N. fowleri*, variable levels of toxicity were observed particularly for **2p**, **2b**, and **2d**, notably, when **2b** and **2d** (L6 CC<sub>50</sub>: <0.62 μM) was advanced into PK studies (dosed I.P. at 10 mg/kg) acute toxicity was seen. Given the selectivity of **2f** this serves as an excellent starting point for further optimization.

Of the imidazopyridines there were three moderately potent, or better, inhibitors of *N. fowleri*. Compound **3e** was the most potent compound with a BBB Score (5.1) that predicts BBB penetration. However, replacement of the aniline portion with aliphatic amines led to a complete loss of potency (**3f** and **3d**). Truncation of the aniline to the free amine was reasonably well tolerated (**3a**; EC<sub>50</sub>: 15 μM). Derivatization to the amide was unfavorable (**3k**, **3l**, and **3h**). Modification to the pyridine region was also trialed and pyrimidines (**3i** and **3j**), methylpyridine (**3c**) and 3-pyridine (**3g**) all led to a loss of potency. Though replacement with the *N*-methylpyrazole was reasonably well tolerated (**3b**).

Of the five 2,4-disubstituted azaindoles tested, four were found to be potent against *N. fowleri* with only the amide **5e** being inactive. No modifications to the pyrazole were made, though secondary (**5d**) and tertiary (**5a** and **5c**) amines were both tolerated, as was removal of the benzylic methylene (**5b**). Of the seven 3,5-disubstituted azaindoles tested, only one was active (**4d**) and any replacement of the pyrazole led to a complete loss of potency (**4f** and **4e**). Additionally, the benzonitrile at the 3-position appears to be unfavorable for potency when comparing **4d** with **4e**.

The preliminary data for the aminopurines, although limited, shows moderate biological potency against *N. fowleri*, though valuable SAR data has been gleaned. Alkylation of the purine -NH (**6c**) led to a loss of activity, as did elongation (replacement with the ethylpyrrolidine; **6d**), increased bulk (4,4-difluoropiperidine; **6e**) or incorporation of heteroatoms (replaced with morpholine) into the aliphatic amine, and replacement of the thiophene with either 4-fluoroaniline or *N*-methylpyrazole amine. While we have PK data on compounds in this series, brain exposure levels were not measured and need to be assessed as part of any optimization campaign.

Only one of the lapatinib derivatives (**7a**) tested had moderate potency against *N. fowleri*. Replacement of the aryl ether with the aminopyrazine led to a complete loss of activity and, given the lipophilicity of the aryl ether the lipophilic ligand efficiency (LLE) is poor (1.40). Additional analogs with improved aqueous solubility

need to be tested to confirm the activity of this series and improve our analysis.

There were 19 carbazoles tested with most of the modifications in the pendant amine. In general, the secondary amines were preferred with **8c** being more potent than **8f**. Though, the piperidine derivative (**8d**) opposed this trend and was equipotent with **8c**. There may also be a shape and steric component to the secondary amines with **8a** showing optimal activity ( $EC_{50}$ : 5.1  $\mu$ M; LLE: 1.9) versus the cyclopentane (**8k**; LLE: 1.95) and cycloheptane (**8h**; LLE: 1.1). Two compounds from this series have previously been advanced into PK studies and **8c** was found to have excellent exposure in the brain and, at 40 mg/kg per os (P.O.; oral administration), it had a brain:blood ratio at 1 h of 5.1 (male) and 4.1 (female); and at 4 h it was 3.6 (male) and 5.2 (female; Singh et al., 2023). Further SAR scoping with a focus on reducing the lipophilicity and maintaining the potency is underway.

## Balamuthia mandrillaris

Alkylation of the indazole -NH for the **benzoxazepinoindazoles** led to a compound with moderate potency against *B. mandrillaris* (**1e**;  $EC_{50}$ :  $14 \pm 0.29 \mu$ M). Additionally, the pyrimidine regioisomers appear to have an impact on the activity of the compounds (cf. **1a** and **1b**). Preliminary SAR suggests that the 2-pyridyl-5-amino motif may be driving the potency against *B. mandrillaris*. Finally, the truncated analog **1d** demonstrated improved potency ( $EC_{50}$ :  $9.49 \pm 0.23 \mu$ M) particularly when compared to **1e** (which retains the same aminopyrazine motif).

Differential SAR was observed for the pyrazolopyridazines with the *m*-benzonitrile not well tolerated against *B. mandrillaris* (cf. **2c**), though this trend is complicated due to a lack of match pairs. Removal of either nitrogen in the pyrimidine led to a loss of activity (**2g** and **2f**) which is largely consistent with the SAR observed across the other pFLA. Replacement of the aniline with the 4-aminocyclohexanol was generally not well tolerated (**2k**), though activity could be recovered via substitution of the 6-methoxy (cf. **2s** and **2u**) which led to potent activity against *B. mandrillaris*.

For the 2,4-disubstituted azaindoles, one compound demonstrated potent activity against *B. mandrillaris* (**5e**), however, this also had high L6 toxicity which would prevent their progression forward. Moving to the 3,5-disubstituted azaindoles led to the identification of **4b** which demonstrated potent activity and was not toxic against MRC5 cells. However, **4b** has a moderate predicted BBB penetration from the BBB Score (3.2). As opposed to the SAR that was observed for *N. fowleri* the benzonitrile substituent is preferred (**4e**, **4a**, and **4b**). Replacement of the methyl on the pyrazole is tolerated with the tetrahydropyran (**4a** and **4b**), but not the piperidine (**4c**, Table 1) suggesting that a basic nitrogen may not be tolerated.

Only one of the lapatinib derivatives (**7b**) tested was active against *B. mandrillaris*, and it showed potent inhibition. Compound **7b** is structurally related to several analogs in the data set and its activity could be driven by either a change in the lipophilicity (though this would be negligible when compared to the other bridged piperazines, or spirocycles), or due to the change in vector. Further analogs are required to try and understand the specifics of the observed SAR.

The SAR for the carbazoles largely tracks with that observed for *N. fowleri* with **8c** being the most active compound against *B. mandrillaris* ( $EC_{50}$ : 2.4  $\mu$ M). Though there are some notable

differences; for example, the homomorpholine (**8j**) was well tolerated ( $EC_{50}$ : 3.3  $\mu$ M), and the (R)-methylmorpholine derivative (**8l**) showed moderate inhibition ( $EC_{50}$ : 12  $\mu$ M) which could be due to the configuration of the methyl group.

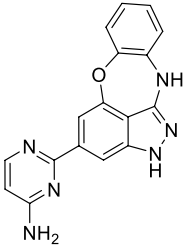
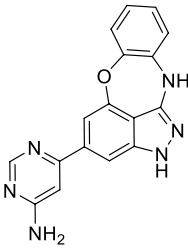
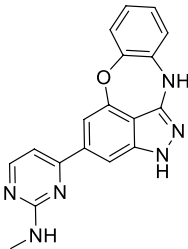
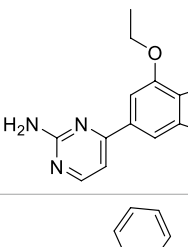
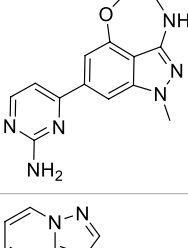
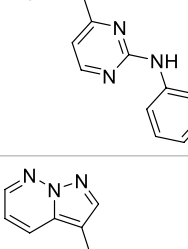
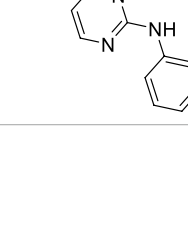
## Current anti-amoebic remedies, and the drug discovery landscape

No standardized treatment regimens or FDA compounds are approved for *Acanthamoeba* CNS infections with the recommended treatments being empirically based on previous reports of the very limited number of patients that have survived GAE. As is true with other free-living amoeba infections, therapeutic approaches include the use of a multi-drug cocktail of antimicrobials (amphotericin B and pentamidine), azoles (fluconazole or itraconazole), macrolides (azithromycin), and, recently, miltefosine (Schuster et al., 2006; Visvesvara, 2010; Cope, 2013). Even with the laborious use of multi-drug cocktail-based treatments, CNS-involved infections are almost always fatal possibly due to the likelihood of inducing encystation. The current inability to kill the double-walled resistant cyst stage that have been found in all host infected tissues, e.g., skin, lungs, eye(s), or brain, and emphasizes the lack of effective treatments and the urgent need for developing new therapeutics against this pathogen. Besides from 5-fluorocytosine being rigorously tested in *in vivo* models of *Acanthamoeba* GAE in 1974 (Stevens and O'dell, 1974) there has not been any dedicated efforts in this space. We have previously identified repurposed drugs with a demonstrated potential for therapeutic use but many of these are not known to cross the BBB and will require significant optimization (Rice et al., 2020a). Therefore, compounds **1a**, and **1c** from the benzoxazepinoindazole series, **2b**, **2c**, and **2d** from the pyrazolopyridazine series, and **3a** and **3b** from the imidazopyridine series would suggest utility and further development of these pharmacophores against *Acanthamoeba*.

Of the CDC recommended multi-drug combination therapeutics suggested for *Naegleria fowleri* CNS disease, PAM, only amphotericin B, posaconazole, and azithromycin displayed great nanomolar activity (Colon et al., 2018). Fluconazole and miltefosine both display micromolar activity (Troth and Kyle, 2021). We note that several CYP51 inhibitors have previously been reported with low nanomolar-to-micromolar activity against *N. fowleri*, and acceptable cLogP values, though there is no measure of BBB penetration potential (Debnath et al., 2017). Separately, compounds which were predicted to have BBB penetration properties through *in vivo* models such as, posaconazole, ketoconazole, corifungin, rokitamycin, and roxithromycin have demonstrated varying level of curative effects for PAM resolution (Debnath et al., 2012; Debnath, 2021). Though there has not been any reported follow up on these compounds and the addition of compounds that will likely have a different mechanism of action would be advantageous. Therefore, compounds with  $EC_{50} \leq 14 \mu$ M (better than fluconazole) will be prioritized for hit-to-lead optimization. This would include the benzoxazepinoindazoles (**1a**, **1b**, and **1c**), pyrazolopyridazines (**2a-d**, **2f**, **2h**, **2j**, **2k**, **2l**, **2n-q**, and **2s**), 3-5-substituted azaindoles (**4d**), 2,4-substituted azaindoles (**5a-d**), and carbazoles (**8a-d**, **8g**, **8h**, and **8j-k**) from this study.

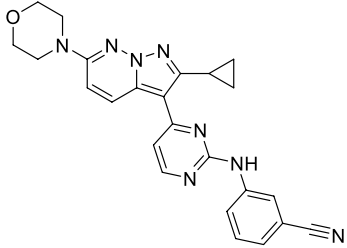
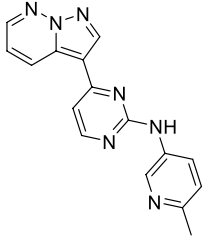
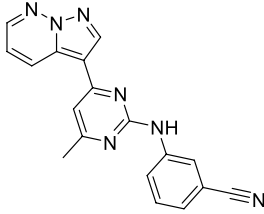
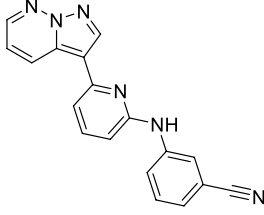
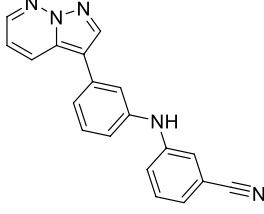
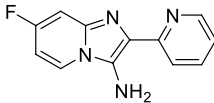
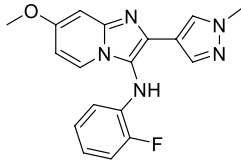
Currently, no effective treatments for infections caused by *B. mandrillaris* have been identified, instead a cocktail of drugs has been recommended by the CDC based on previous reports of

TABLE 1 Active compounds against *Acanthamoeba castellanii*, n=3.

Class	ID	Structure	<i>Acanthamoeba castellanii</i>	MRC5	L6 CC <sub>50</sub>
			EC <sub>50</sub> (μM)±SD	CC <sub>50</sub> (μM)±SD	(μM)±SD
Benzoxazepinoindazoles (Klug et al., 2019)	1a		3.8±0.46	> 50	32±2.5
	1b		12±8.2	> 50	1.0±0.14
	1c		3.3±0.31	> 50	6.3±0.55
	1d		12±8.3	> 50	> 17±0.05
	1e		> 20	> 50	> 50
Pyrazolopyridazines (Tear et al., 2020)	2a		13±6.9	> 50	3.2±0.08
	2b		1.5±0.12	> 50	< 0.62

(Continued)

TABLE 1 (Continued)

Class	ID	Structure	<i>Acanthamoeba castellanii</i>	MRC5	L6 CC <sub>50</sub>
			EC <sub>50</sub> (μM)±SD	CC <sub>50</sub> (μM)±SD	(μM)±SD
	2c		5.9±0.17	> 50	22±2.1
	2d		0.92±0.3	> 50	< 0.62
	2e		> 20	> 50	> 50
	2f		> 20	> 50	> 50
	2g		> 20	19±1.0	28±1.1
Imidazopyridines (Dichiara et al., 2022)	3a		6.94±0.11	nt	nt
	3b		4.33±0.57	nt	nt

(Continued)



TABLE 1 (Continued)

Class	ID	Structure	<i>Acanthamoeba castellanii</i>	MRC5	L6 CC <sub>50</sub>
			EC <sub>50</sub> (μM)±SD	CC <sub>50</sub> (μM)±SD	(μM)±SD
	3c		> 20	nt	nt
	3d		> 20	nt	nt
	3e		> 20	nt	nt
3-5-substituted azaindoles (Klug et al., 2021)	4a		11±9.0	> 50	2.8±0.92
	4b		11±2.3	> 50	11±1.5
	4c		> 20	13±2.4	9.0±0.78
Reference Drugs	Azithromycin		0.26±0.14		
	Chlorhexidine		11±3.5		
	Pentamidine		4.2±0.08		

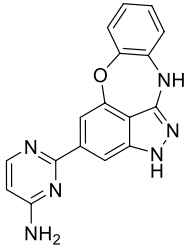
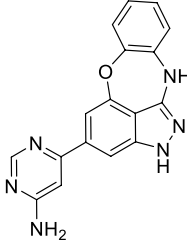
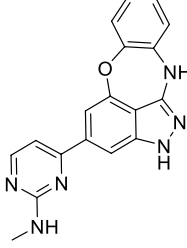
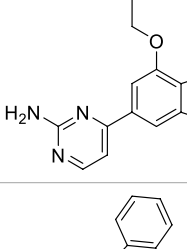
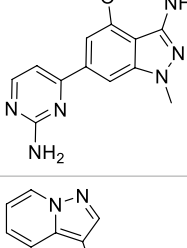
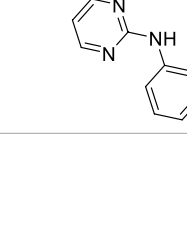
nt, not tested.

successful therapeutic intervention (Centers for Disease Control and Prevention, 2021). We have previously tested all compounds within the CDC's suggested treatment regimen (Phan et al., 2020). Of these active therapeutics, only pentamidine, flucytosine, and chlorpromazine are known to cross the BBB yet CNS-involved infections are almost always fatal, emphasizing the lack of effective treatments and the urgent need for developing new therapeutic approaches. We define any compound with  $\geq 2\times$  better activity than pentamidine ( $EC_{50} = 18.35\ \mu\text{M}$ ) would warrant further exploration, therefore, the benzoxazepinoindazoles (1b, 1c, and 1d), pyrazolopyridazines (2a, 2b, 2c, 2h, 2j, 2p, and 2u), 3-5-substituted azaindoles (4a-b, and 4e), 2,4-substituted azaindoles (5b and 5e),

4-aminoquinolines (7b), and carbazoles (8a, 8c, 8h-k) will be prioritized against *B. mandrillaris* in our future hit-to-lead optimization.

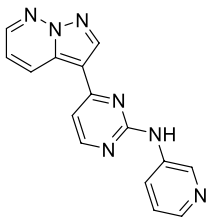
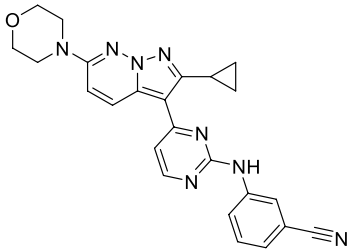
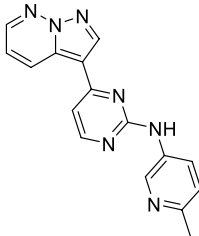
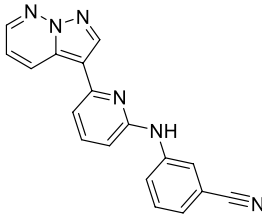
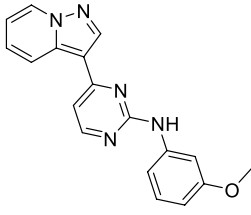
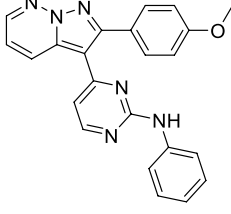
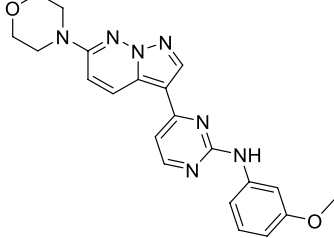
With a dearth of ongoing drug discovery efforts for anti-amoebics we believe that the described results (Tables 1–3) represent a significant contribution to this community. These compounds demonstrate superior activity in comparison to currently used anti-amoebic therapies. This, coupled with predicted, or measured BBB exposure in mice, establish this data set as highly unique. Hit-to-lead optimization efforts are underway for several of these chemotypes against the respected pathogenic free-living amoebae and we will report the results of this in future communications.

TABLE 2 Active compounds against *Naegleria fowleri*,  $n=3$ .

Class	ID	Structure	<i>Naegleria fowleri</i>	MRC5 CC <sub>50</sub>	L6 CC <sub>50</sub>
			EC <sub>50</sub> (μM)±SD	(μM)±SD	(μM)±SD
Benzoxazepinoindazoles (Klug et al., 2019)	1a		8.5 ± 0.34	> 50	32 ± 2.5
	1b		3.9 ± 0.62	> 50	1.0 ± 0.14
	1c		< 0.63	> 50	6.3 ± 0.55
	1d		> 20	> 50	> 17 ± 0.05
	1e		> 20	> 50	> 50
Pyrazolopyridazines (Tear et al., 2020)	2a		0.94 ± 0.17	> 50	3.2 ± 0.08

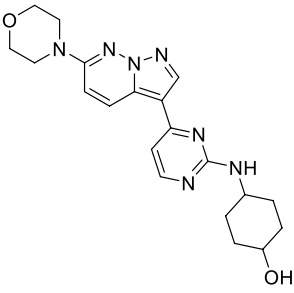
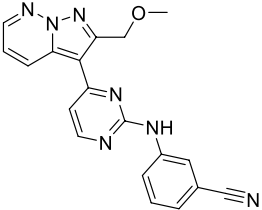
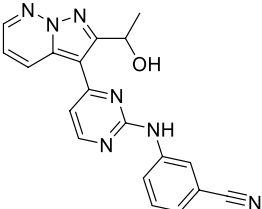
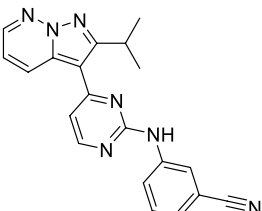
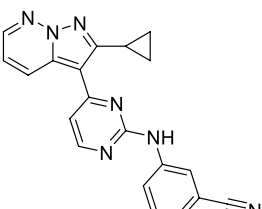
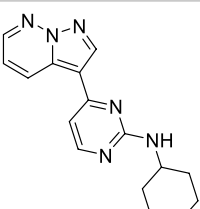
(Continued)

TABLE 2 (Continued)

Class	ID	Structure	<i>Naegleria fowleri</i>	MRC5 CC <sub>50</sub>	L6 CC <sub>50</sub>
			EC <sub>50</sub> (μM)±SD	(μM)±SD	(μM)±SD
	2b		0.3±0.21	> 50	< 0.62
	2c		3.5±0.7	> 50	22±2.1
	2d		0.43±0.13	> 50	< 0.62
	2f		1.0±0.01	> 50	> 50
	2h		1.3±0.26	> 50	4.2±0.89
	2i		17±3.5	> 50	48±9.4
	2j		0.98±0.13	> 50	4.1±0.94

(Continued)

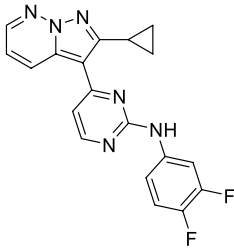
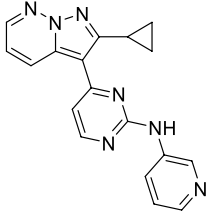
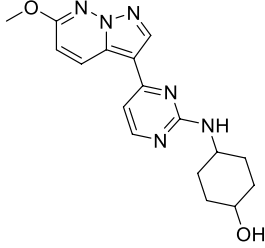
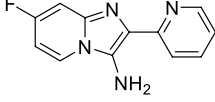
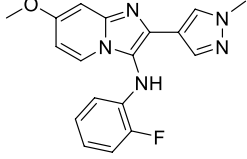
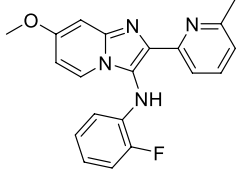
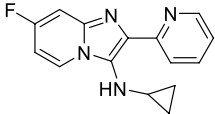
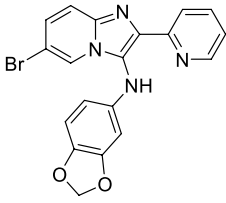
TABLE 2 (Continued)

Class	ID	Structure	<i>Naegleria fowleri</i>	MRC5 CC <sub>50</sub>	L6 CC <sub>50</sub>
			EC <sub>50</sub> (μM)±SD	(μM)±SD	(μM)±SD
	2k		7.5±2.5	> 50	9.9±1.7
	2l		1.1±0.16	> 50	14.2±1.1
	2m		17±0.76	> 50	nt
	2n		1.3±0.33	33±2.0	19±1.1
	2o		9.6±6.6	> 50	14±0.75
	2p		1.4±0.76	> 50	5.5±1.1

(Continued)

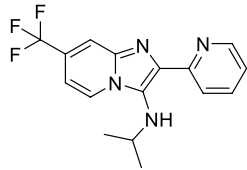
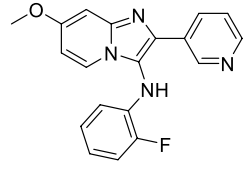
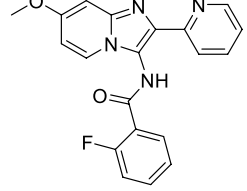
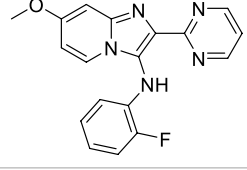
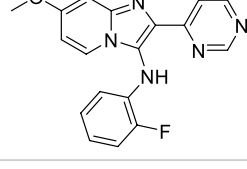
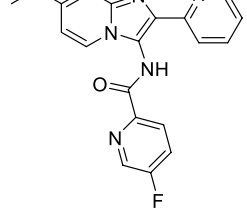
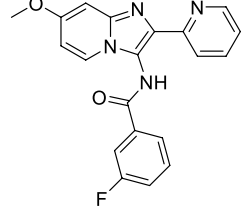
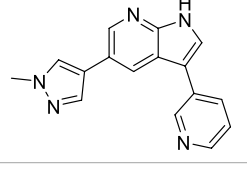


TABLE 2 (Continued)

Class	ID	Structure	<i>Naegleria fowleri</i>	MRC5 CC <sub>50</sub>	L6 CC <sub>50</sub>
			EC <sub>50</sub> (μM)±SD	(μM)±SD	(μM)±SD
	2q		12±7.8	> 50	50±0
	2r		16±3.7	> 50	31±2.1
	2s		2.3±1.0	> 50	30.5±1.3
Imidazopyridines (Dichiara et al., 2022)	3a		15±4.7	nt	nt
	3b		13±6.7	nt	nt
	3c		> 20	nt	nt
	3d		> 20	nt	nt
	3e		> 20	nt	nt

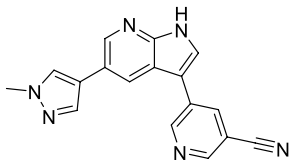
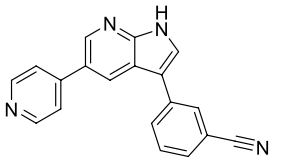
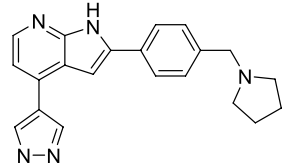
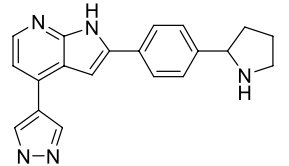
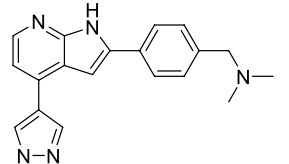
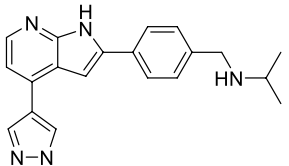
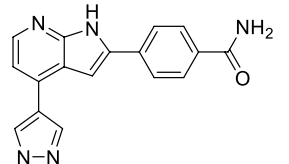
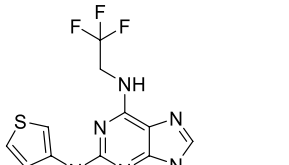
(Continued)

TABLE 2 (Continued)

Class	ID	Structure	<i>Naegleria fowleri</i>	MRC5 CC <sub>50</sub>	L6 CC <sub>50</sub>
			EC <sub>50</sub> (μM)±SD	(μM)±SD	(μM)±SD
	3f		> 20	nt	nt
	3g		> 20	nt	nt
	3h		> 20	nt	nt
	3i		> 20	nt	nt
	3j		> 20	nt	nt
	3k		> 20	nt	nt
	3l		> 20	nt	nt
3-5-substituted azaindoles (Klug et al., 2021)	4d		8.4±0.71	> 50	17±2.0

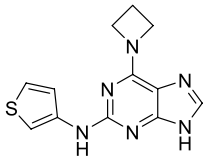
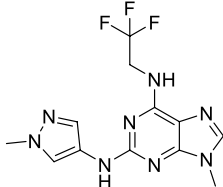
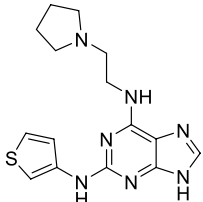
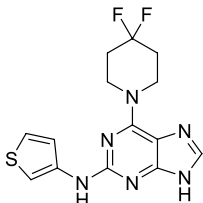
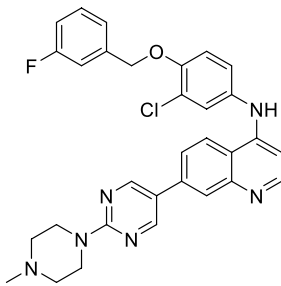
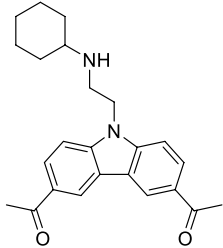
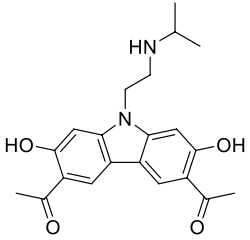
(Continued)

TABLE 2 (Continued)

Class	ID	Structure	<i>Naegleria fowleri</i>	MRC5 CC <sub>50</sub>	L6 CC <sub>50</sub>
			EC <sub>50</sub> (μM)±SD	(μM)±SD	(μM)±SD
	4e		> 20	> 50	17 ± 2.0
	4f		> 20	> 50	> 50
2,4-Disubstituted azaindoles	5a		4.0 ± 0.36	16 ± 1.4	< 0.62
	5b		7.4 ± 0.25	5.7 ± 0.45	< 0.62
	5c (Diaz et al., 2014)		5.6 ± 0.29	11 ± 0.90	< 0.62
	5d		5.4 ± 0.21	1.3 ± 0.05	< 0.62
	5e		> 20	> 5.5 ± 0.00	nt
Aminopurines (Singh et al., 2020)	6a (Diaz et al., 2014)		11 ± 0.60	50 ± 0.00	nt

(Continued)

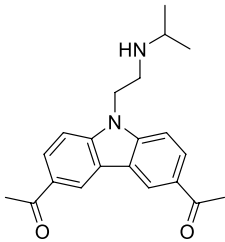
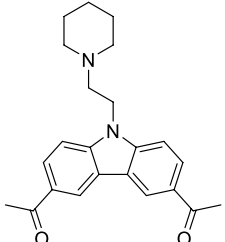
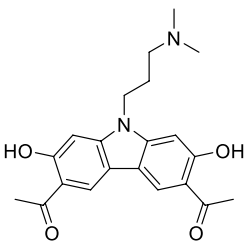
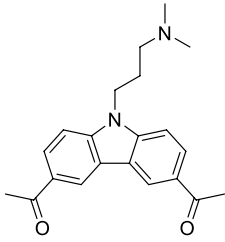
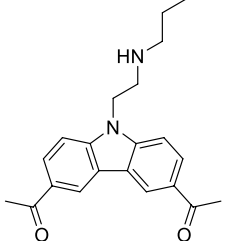
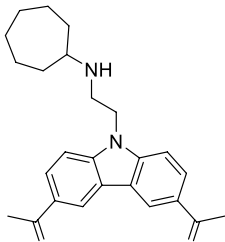
TABLE 2 (Continued)

Class	ID	Structure	<i>Naegleria fowleri</i>	MRC5 CC <sub>50</sub>	L6 CC <sub>50</sub>
			EC <sub>50</sub> (μM)±SD	(μM)±SD	(μM)±SD
	6b		14 ± 5.7	> 50	nt
	6c		> 20	> 50	> 50
	6d		> 20	> 50	> 50
	6e		> 20	> 50	> 50
4-Aminoquinolines (Mehta et al., 2018)	7a		16 ± 4.1	nt	nt
Carbazoles (Singh et al., 2023)	8a		5.1 ± 0.06	nt	nt
	8b		8.8 ± 0.71	nt	nt

(Continued)

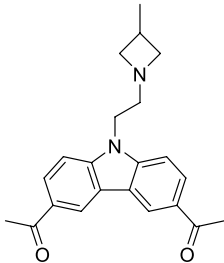
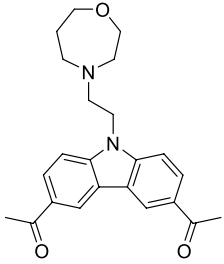
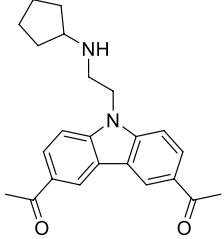
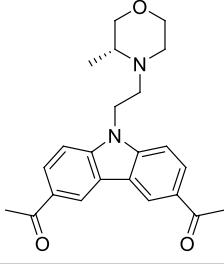


TABLE 2 (Continued)

Class	ID	Structure	<i>Naegleria fowleri</i>	MRC5 CC <sub>50</sub>	L6 CC <sub>50</sub>
			EC <sub>50</sub> (μM) ± SD	(μM) ± SD	(μM) ± SD
	8c		4.8 ± 0.09	nt	nt
	8d		4.3 ± 0.22	nt	nt
	8e		17 ± 0.65	nt	nt
	8f		17 ± 0.2	nt	nt
	8g		9.6 ± 0.05	nt	nt
	8h		13 ± 2.6	nt	nt

(Continued)

TABLE 2 (Continued)

Class	ID	Structure	<i>Naegleria fowleri</i>	MRC5 CC <sub>50</sub>	L6 CC <sub>50</sub>
			EC <sub>50</sub> (μM) ± SD	(μM) ± SD	(μM) ± SD
	8i		18 ± 0.45	nt	nt
	8j		10 ± 1.4	nt	nt
	8k		9.0 ± 0.01	nt	nt
	8l		16 ± 2.6	nt	nt
Reference Drugs	Azithromycin		0.02 ± 0.01		
	Chlorhexidine		5.8 ± 0.22		
	Pentamidine		> 50		

nt, not tested.

## Conclusion

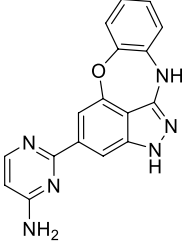
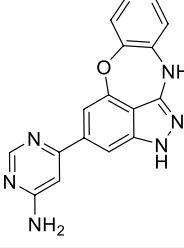
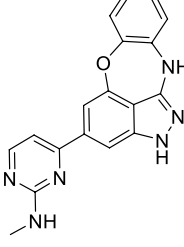
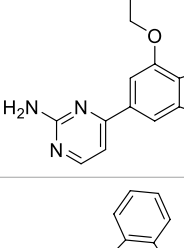
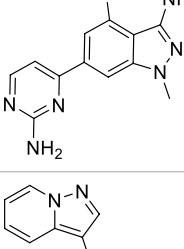
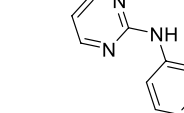
This work represents a significant screening campaign against three pFLA from which we have identified several new chemical series with sub-to-low-micromolar potency. Many of the compounds discovered and described here have better potency and selectivity profiles than the suggested multi-drug cocktail treatment regimen against *A. castellanii*, *N. fowleri*, or *B. mandrillaris* from the U.S. Centers for Disease Control and Prevention (CDC). These pharmacophores are currently being further optimized using medicinal chemistry to develop

compounds with greater potency for these pFLA, selectivity, and higher brain exposure. The results of these studies will be reported in due course.

## Data availability statement

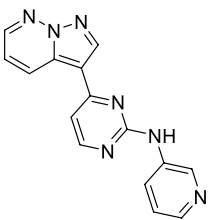
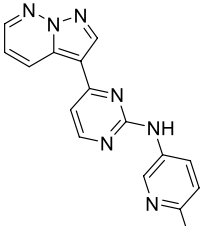
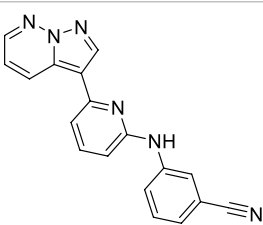
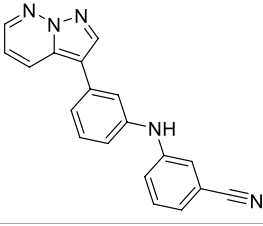
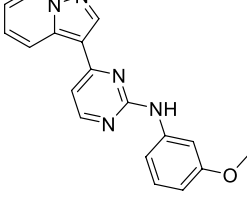
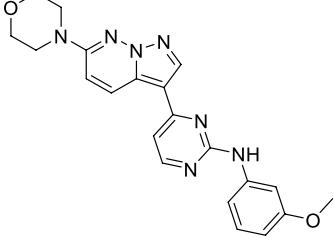
The datasets presented in this study can be found in online repositories. The names of the repository/repositories and accession number(s) can be found in the article/[Supplementary material](#).

TABLE 3 Active compounds against *Balamuthia mandrillaris*,  $n=3$ .

Class	ID	Structure	<i>Balamuthia mandrillaris</i>	MRC5 CC <sub>50</sub>	L6 CC <sub>50</sub>
			EC <sub>50</sub> (μM) ± SD	(μM) ± SD	(μM) ± SD
Benzoxazepinoindazoles (Klug et al., 2019)	1a		17 ± 3.0	> 50	32 ± 2.5
	1b		1.8 ± 0.46	> 50	1.0 ± 0.14
	1c		1.9 ± 1.3	> 50	6.3 ± 0.55
	1d		9.5 ± 0.23	> 50	> 17 ± 0.05
	1e		14 ± 0.29	> 50	> 50
Pyrazolopyridazines (Tear et al., 2020)	2a		4.2 ± 0.6	> 50	3.2 ± 0.08

(Continued)

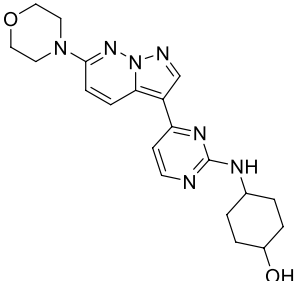
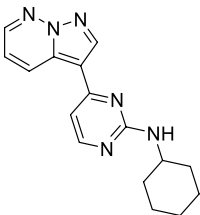
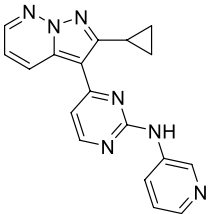
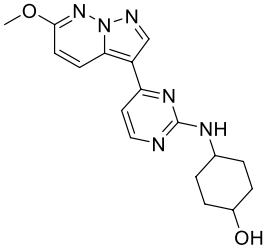
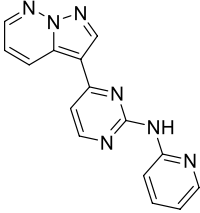
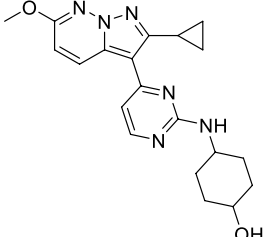
TABLE 3 (Continued)

Class	ID	Structure	<i>Balamuthia mandrillaris</i>	MRC5 CC <sub>50</sub>	L6 CC <sub>50</sub>
			EC <sub>50</sub> (μM) ± SD	(μM) ± SD	(μM) ± SD
	2b		5.0 ± 0.1	> 50	< 0.62
	2d		1.6 ± 0.1	> 50	< 0.62
	2f		> 20	> 50	> 50
	2g		> 20	19 ± 1.0	28 ± 1.1
	2h		3.3 ± 0.97	> 50	nt
	2j		4.9 ± 1.6	> 50	4.1 ± 0.94

(Continued)

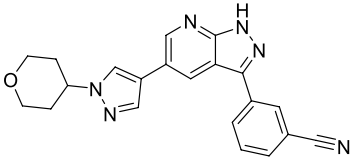
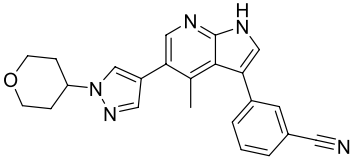
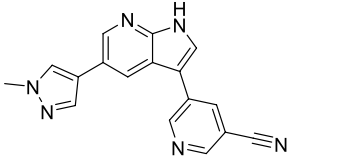
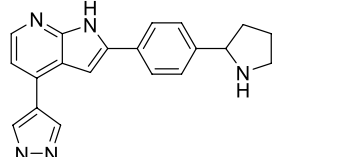
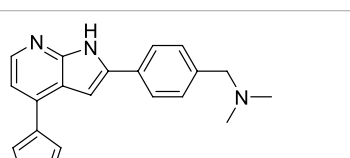
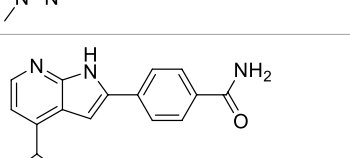
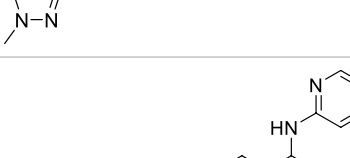
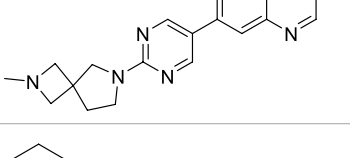


TABLE 3 (Continued)

Class	ID	Structure	<i>Balamuthia mandrillaris</i>	MRC5 CC <sub>50</sub>	L6 CC <sub>50</sub>
			EC <sub>50</sub> (μM)±SD	(μM)±SD	(μM)±SD
	2k		> 20	> 50	9.9±1.7
	2p		7.5±3.1	> 50	5.5±1.1
	2r		13±7.5	> 50	31±2.1
	2s		11±4.2	> 50	31±1.3
	2t		10±2.8	> 50	3.7±0.46
	2u		9.4±3.4	> 50	> 50

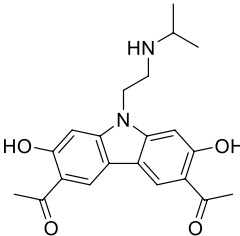
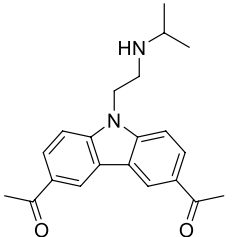
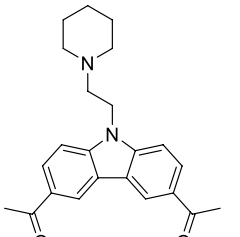
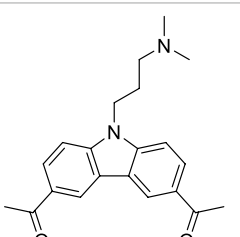
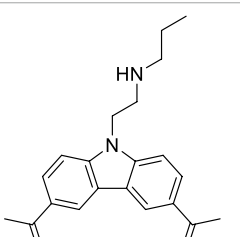
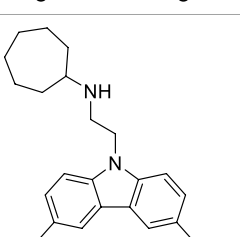
(Continued)

TABLE 3 (Continued)

Class	ID	Structure	<i>Balamuthia mandrillaris</i>	MRC5 CC <sub>50</sub>	L6 CC <sub>50</sub>
			EC <sub>50</sub> (μM) ± SD	(μM) ± SD	(μM) ± SD
3-5-substituted azaindoles (Klug et al., 2021)	4a		3.3 ± 0.62	> 50	2.8 ± 0.92
	4b		1.0 ± 0.12	> 50	11 ± 1.5
	4e		8.3 ± 1.3	> 50	17 ± 2.0
2,4-substituted azaindoles	5b		7.25 ± 0.7	5.7 ± 0.45	< 0.62
	5c (Diaz et al., 2014)		12 ± 0.09	11 ± 0.90	< 0.62
	5e		1.8 ± 0.24	> 5.5 ± 0.00	nt
4-Aminoquinolines (Bachovchin et al., 2019)	7b		1.4 ± 0.17	nt	nt
Carbazoles (Singh et al., 2023)	8a		6.8 ± 0.1	nt	nt

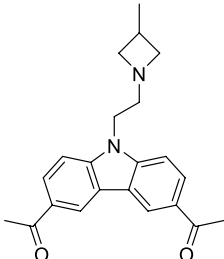
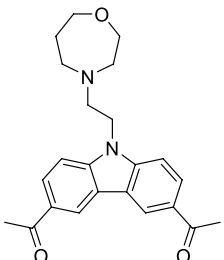
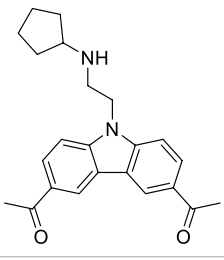
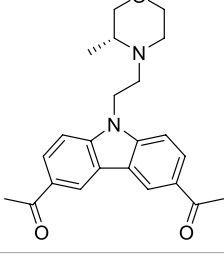
(Continued)

TABLE 3 (Continued)

Class	ID	Structure	<i>Balamuthia mandrillaris</i>	MRC5 CC <sub>50</sub>	L6 CC <sub>50</sub>
			EC <sub>50</sub> (μM) ± SD	(μM) ± SD	(μM) ± SD
	8b		11 ± 0.35	nt	nt
	8c		2.4 ± 0.17	nt	nt
	8d		12 ± 0.26	nt	nt
	8f		19 ± 1.1	nt	nt
	8g		12 ± 0.07	nt	nt
	8h		7.3 ± 0.38	nt	nt

(Continued)

TABLE 3 (Continued)

Class	ID	Structure	<i>Balamuthia mandrillaris</i>	MRC5 CC <sub>50</sub>	L6 CC <sub>50</sub>
			EC <sub>50</sub> (μM)±SD	(μM)±SD	(μM)±SD
	8i		7.3 ± 0.28	nt	nt
	8j		3.3 ± 0.24	nt	nt
	8k		7.4 ± 0.36	nt	nt
	8l		13 ± 0.35	nt	nt
Reference Drugs	Azithromycin		>20		
	Chlorhexidine		1.6 ± 0.17		
	Pentamidine		18.35 ± 1.47		

nt, not tested.

Author contributions

CR, MB, and LF: conceptualization. LF, MB, MK, HE, SE, CLu, DKl, BS, AQ, KB, WT, AS, KF, SB, MR, CLe, EB, JA, RD-G, GC-P, GP-M, CB-N, CG-L, DG-P, MN, and CR: methodology. CR, DKy, MP, and LF: validation and supervision. LF and CR: formal analysis and writing – original draft preparation. DKy, MP, and LF: resources and funding acquisition. LF, MB, DKl, BS, KB, WT, SB, MK, HE, SE, CLu, CB-N, and CR: data curation. LF, MB, MK, HE, SE, CLu, DKl, BS, AQ, KB, WT, AS, KF, SB, MR, CLe, EB, JA, RD-G, GC-P, RG-H, GP-M, CB-N, CG-L, LR-P, FG, DG-P, MN, KM-W, MP, DKy, and CR: writing – review and editing. All authors contributed to the article and approved the submitted version.

Funding

This study was supported by the Georgia Research Alliance (DKy). Additional funding was received from the National Institute of Allergy and Infectious Diseases (MP and MN, R01AI114685; MP, 1R21AI127594 and R01AI124046; and CC, R21AI126296; <https://www.niaid.nih.gov/>), the Spanish Ministerio de Economía, Industria y Competitividad (MN, SAF2015-71444-P; DG-P, SAF2016-79957-R; <http://www.mineco.gob.es>), Subdirección General de Redes y Centros de Investigación Cooperativa-Red de Investigación Cooperativa en Enfermedades Tropicales [RICET, <https://www.ricet.es/>; M.N.,



RD16/0027/0019; DG-P, the MCIN/AEI/10.13039/501100011033 (PID2019-109623RB-I00), the MCIN/AEI/10.13039/501100011033, and FEDER Una manera de hacer Europa (2016-79957-R)], and RTI2018-097210-B-I00 (MINCIU-FEDER) to FG. An ACS MEDI Predoctoral Fellowship for DKl is gratefully acknowledged, as is support from the National Science Foundation for KF (CHE-1262734). This project has been co-funded by the Tres Cantos Open Lab Foundation projects TC-007 and TC-164.

## Acknowledgments

We thank AstraZeneca, Charles River Laboratories, and GlaxoSmithKline for the provision of the *in vitro* ADME and physicochemical properties data. We would also like to thank the Drugs for Neglected Diseases initiative (DNDi) for their in kind, standard, host cell cytotoxicity screening. CR would like to acknowledge and thank Purdue University for a grant labeled as Purdue Libraries Open Access Fund, to publish our work within this open access journal.

## References

- Akao, Y., Canan, S., Cao, Y., Condroski, K., Engkvist, O., Itono, S., et al. (2021). Collaborative virtual screening to elaborate an imidazo[1,2-a]pyridine hit series for visceral leishmaniasis. *Rsc Med. Chem.* 12, 384–393. doi: 10.1039/D0MD00353K
- Bachovchin, K. A., Sharma, A., Bag, S., Klug, D. M., Schneider, K. M., Singh, B., et al. (2019). Improvement of aqueous solubility of Lapatinib-derived analogues: identification of a Quinolinimine Lead for human African trypanosomiasis drug development. *J. Med. Chem.* 62, 665–687. doi: 10.1021/acs.jmedchem.8b01365
- Castellani, A. (1930). An amoeba found in cultures of a yeast. *J. Trop. Med. Hyg.* 30:160.
- Centers for Disease Control and Prevention (2021). Parasites—Balamuthia mandrillaris—granulomatous amebic encephalitis (Gae) [online]. Available at: <https://www.cdc.gov/parasites/balamuthia/treatment-hcp.html> (Accessed September 13 2021).
- Colon, B. L., Rice, C. A., Guy, R. K., and Kyle, D. E. (2018). Phenotypic screens reveal Posaconazole as a rapidly acting Amebicidal combination partner for treatment of primary amoebic meningoencephalitis. *J. Infect. Dis.* 219, 1095–1103. doi: 10.1093/infdis/jiy622
- Cope, J. R. (2013). Investigational drug available directly from Cdc for the treatment of infections with free-living amebae. *Morbidity Mortal. Weekly Rep.* 62:666. Available at: <https://www.cdc.gov/mmwr/preview/mmwrhtml/mm6233a4.htm>
- Cope, J. R., Landa, J., Nethercut, H., Collier, S. A., Glaser, C., Moser, M., et al. (2018). The epidemiology and clinical features of Balamuthia mandrillaris disease in the United States, 1974–2016. *Clin. Infect. Dis.* 68, 1815–1822. doi: 10.1093/cid/ciy813
- De Jonckheere, J. F. (2014). What do we know by now about the genus Naegleria? *Exp. Parasitol.* 145, S2–S9. doi: 10.1016/j.exppara.2014.07.011
- Debnath, A. (2021). Drug discovery for primary amebic meningoencephalitis: from screen to identification of leads. *Expert Rev. Anti-Infect. Ther.* 19, 1099–1106. doi: 10.1080/14787210.2021.1882302
- Debnath, A., Calvet, C. M., Jennings, G., Zhou, W., Aksenov, A., Luth, M. R., et al. (2017). Cyp51 is an essential drug target for the treatment of primary amoebic meningoencephalitis (pam). *PLoS Negl. Trop. Dis.* 11:e0006104. doi: 10.1371/journal.pntd.0006104
- Debnath, A., Tunac, J. B., Galindo-Gómez, S., Silva-Olivares, A., Shibayama, M., and Mckerrow, J. H. (2012). Corifungin, a new drug Lead against Naegleria, identified from a high-throughput screen. *Antimicrob. Agents Chemother.* 56, 5450–5457. doi: 10.1128/AAC.00643-12
- Diaz, R., Luengo-Arratta, S. A., Seixas, J. D., Amata, E., Devine, W., Cordon-Obras, C., et al. (2014). Identification and characterization of hundreds of potent and selective inhibitors of Trypanosoma brucei growth from a kinase-targeted library screening campaign. *PLoS Negl. Trop. Dis.* 8:e3253. doi: 10.1371/journal.pntd.0003253
- Dichiara, M., Simpson, Q. J., Quotadamo, A., Jalani, H. B., Huang, A. X., Millard, C. C., et al. (2022). Structure-property optimization of a series of imidazopyridines for visceral leishmaniasis.
- Diehl, M. L. N., Paes, J., and Rott, M. B. (2021). Genotype distribution of Acanthamoeba in keratitis: a systematic review. *Parasitol. Res.* 120, 3051–3063. doi: 10.1007/s00436-021-07261-1
- Drugs for Neglected Diseases Initiative (2015). Ntd drug discovery booster [online]. Available at: <https://www.dndi.org/diseases-projects/open-innovation/drug-discovery-booster/> (Accessed May 25 2020).
- Fowler, M., and Carter, R. F. (1965). Acute pyogenic meningitis probably due to Acanthamoeba sp.: a preliminary report. *Br. Med. J.* 2, 734–742. doi: 10.1136/bmj.2.5464.734-a
- Grace, E., Asbill, S., and Virga, K. (2015). Naegleria fowleri: pathogenesis, diagnosis, and treatment options. *Antimicrob. Agents Chemother.* 59, 6677–6681. doi: 10.1128/AAC.01293-15
- Gupta, M., Lee, H. J., Barden, C. J., and Weaver, D. F. (2019). The blood–brain barrier (Bbb) score. *J. Med. Chem.* 62, 9824–9836. doi: 10.1021/acs.jmedchem.9b01220
- Holmgard, D. B., Barnadas, C., Mirbarati, S. H., Andersen, L. O. B., Nielsen, H. V., Stensvold, C. R., et al. (2021). Detection and identification of Acanthamoeba and other nonviral causes of infectious keratitis in corneal scrapings by real-time Pcr and next-generation sequencing-based 16S-18S gene analysis. *J. Clin. Microbiol.* 59, e02224–e02220. doi: 10.1128/JCM.02224-20
- Ioset, J. R., Brun, R., Wenzler, T., Kaiser, M., and Yardley, V. (2009). Drug screening for kinetoplastids diseases: a training manual for screening in neglected diseases. The Pan-Asian Screening Network. 1–74
- Kiderlen, A. F., and Laube, U. (2004). Balamuthia mandrillaris, an opportunistic agent of granulomatous amebic encephalitis, infects the brain via the olfactory nerve pathway. *Parasitol. Res.* 94, 49–52. doi: 10.1007/s00436-004-1163-z
- Klug, D. M., Mavrogiannaki, E. M., Forbes, K. C., Silva, L., Diaz-Gonzalez, R., Pérez-Moreno, G., et al. (2021). Lead optimization of 3,5-Disubstituted-7-Azaindoles for the treatment of human African trypanosomiasis. *J. Med. Chem.* 64, 9404–9430. doi: 10.1021/acs.jmedchem.1c00674
- Klug, D. M., Tschiegg, L., Diaz, R., Rojas-Barros, D., Perez-Moreno, G., Ceballos, G., et al. (2019). Hit-to-Lead optimization of Benzoxazepinoindazoles as human African trypanosomiasis therapeutics. *J. Med. Chem.* 63, 2527–2546. doi: 10.1021/acs.jmedchem.9b01506
- Marciano-Cabral, F., and Cabral, G. (2003). Acanthamoeba spp. as agents of disease in humans. *Clin. Microbiol. Rev.* 16, 273–307. doi: 10.1128/CMR.16.2.273-307.2003
- Megha, K., Sehgal, R., and Khurana, S. (2018). Genotyping of Acanthamoeba spp. isolated from patients with granulomatous amebic encephalitis. *Indian J. Med. Res.* 148, 456–459. doi: 10.4103/ijmr.IJMR\_1564\_17
- Mehta, N., Ferrins, L., Leed, S. E., Sciotti, R. J., and Pollastri, M. P. (2018). Optimization of physicochemical properties for 4-Anilinoquinoline inhibitors of plasmodium falciparum proliferation. *ACS Infect. Dis.* 4, 577–591. doi: 10.1021/acsinfecdis.7b00212

## Conflict of interest

The authors declare that the research was conducted in the absence of any commercial or financial relationships that could be construed as a potential conflict of interest.

## Publisher's note

All claims expressed in this article are solely those of the authors and do not necessarily represent those of their affiliated organizations, or those of the publisher, the editors and the reviewers. Any product that may be evaluated in this article, or claim that may be made by its manufacturer, is not guaranteed or endorsed by the publisher.

## Supplementary material

The Supplementary material for this article can be found online at: <https://www.frontiersin.org/articles/10.3389/fmicb.2023.1149145/full#supplementary-material>

- North Carolina Department of Health and Human Services (2021). Rare brain infection, Pediatric Death Linked to Swim in a Private Pond in Central Nc.
- Phan, I. Q., Rice, C. A., Craig, J., Noorai, R. E., McDonald, J., Subramanian, S., et al. (2020). The transcriptome of *Balamuthia mandrillaris* trophozoites for structure-based drug design. *bioRxiv* [Preprint]. doi: 10.1038/s41598-021-99903-8
- Putaporntip, C., Kuamsab, N., Nuprasert, W., Rojrung, R., Pattanawong, U., Tia, T., et al. (2021). Analysis of Acanthamoeba genotypes from public freshwater sources in Thailand reveals a new genotype, T23 Acanthamoeba bangkokensis sp. nov. *Sci. Rep.* 11:17290. doi: 10.1038/s41598-021-96690-0
- Rayamajhee, B., Willcox, M. D. P., Henriquez, F. L., Petsoglou, C., Subedi, D., and Carnt, N. (2022). Acanthamoeba, an environmental phagocyte enhancing survival and transmission of human pathogens. *Trends Parasitol.* 38, 975–990. doi: 10.1016/j.pt.2022.08.007
- Recavarren-Arce, S., Velarde, C., Gotuzzo, E., and Cabrera, J. (1999). Amoeba angeitic lesions of the central nervous system in Balamuthia mandrillaris amoebiasis. *Hum. Pathol.* 30, 269–273. doi: 10.1016/S0046-8177(99)90004-7
- Rice, C. A., Colon, B. L., Alp, M., Göker, H., Boykin, D. W., and Kyle, D. E. (2015). Bis-Benzimidazole hits against Naegleria fowleri discovered with new high-throughput screens. *Antimicrob. Agents Chemother.* 59, 2037–2044. doi: 10.1128/AAC.05122-14
- Rice, C. A., Colon, B. L., Chen, E., Hull, M. V., and Kyle, D. E. (2020a). Discovery of repurposing drug candidates for the treatment of diseases caused by pathogenic free-living amoebae. *PLoS Negl. Trop. Dis.* 14:e0008353. doi: 10.1371/journal.pntd.0008353
- Rice, C. A., Lares-Jiménez, L. F., Lares-Villa, F., and Kyle, D. E. (2020b). In vitro screening of the open-source Medicines for Malaria Venture malaria and pathogen boxes to discover novel compounds with activity against Balamuthia mandrillaris. *Antimicrob. Agents Chemother.* 64, e02233–e02219. doi: 10.1128/AAC.02233-19
- Rice, C. A., Troth, E. V., Russell, A. C., and Kyle, D. E. (2020c). Discovery of anti-amoebic inhibitors from screening the mmv pandemic response box on Balamuthia mandrillaris, Naegleria fowleri, and Acanthamoeba castellanii. *Pathogens* 9:476. doi: 10.3390/pathogens9060476
- Schuster, F. L., Guglielmo, B. J., and Visvesvara, G. S. (2006). In-vitro activity of Miltefosine and Voriconazole on clinical isolates of free-living Amebas: Balamuthia mandrillaris, Acanthamoeba spp., and Naegleria fowleri. *J. Eukaryot. Microbiol.* 53, 121–126. doi: 10.1111/j.1550-7408.2005.00082.x
- Siddiqui, R., and Khan, N. A. (2012). Biology and pathogenesis of Acanthamoeba. *Parasit. Vectors* 5:6. doi: 10.1186/1756-3305-5-6
- Singh, B., Diaz-Gonzalez, R., Ceballos-Perez, G., Rojas-Barros, D. I., Gunaganti, N., Gillingwater, K., et al. (2020). Medicinal chemistry optimization of a Diaminopurine Chemotype: toward a Lead for Trypanosoma brucei inhibitors. *J. Med. Chem.* 63, 9912–9927. doi: 10.1021/acs.jmedchem.0c01017
- Singh, B., Sharma, A., Gunaganti, N., Rivers, M., Gadekar, P. K., Greene, B., et al. (2023). Chemical optimization of Cbl0137 for human African trypanosomiasis Lead drug discovery. *J. Med. Chem.* 66, 1972–1989. doi: 10.1021/acs.jmedchem.2c01767
- Stevens, A. R., and O'dell, W. D. (1974). In vitro and in vivo activity of 5-Fluorocytosine on Acanthamoeba. *Antimicrob. Agents Chemother.* 6, 282–289. doi: 10.1128/AAC.6.3.282
- Stevens, K. L., Reno, M. J., Alberti, J. B., Price, D. J., Kane-Carson, L. S., Knick, V. B., et al. (2008). Synthesis and evaluation of pyrazolo[1,5-b]pyridazines as selective cyclin dependent kinase inhibitors. *Bioorg. Med. Chem. Lett.* 18, 5758–5762. doi: 10.1016/j.bmcl.2008.09.069
- Tavares, F. X., Boucheron, J. A., Dickerson, S. H., Griffin, R. J., Preugschat, F., Thomson, S. A., et al. (2004). N-Phenyl-4-pyrazolo[1,5-b]pyridazin-3-ylpyrimidin-2- amines as potent and selective inhibitors of glycogen synthase kinase 3 with good cellular efficacy. *J. Med. Chem.* 47, 4716–4730. doi: 10.1021/jm040063i
- Tear, W. F., Bag, S., Diaz-Gonzalez, R., Ceballos-Pérez, G., Rojas-Barros, D. I., Cordon-Obras, C., et al. (2020). Selectivity and physicochemical optimization of repurposed Pyrazolo[1,5-b]pyridazines for the treatment of human African trypanosomiasis. *J. Med. Chem.* 63, 756–783. doi: 10.1021/acs.jmedchem.9b01741
- Troth, E. V., and Kyle, D. E. (2021). EdU incorporation to assess cell proliferation and drug susceptibility in Naegleria fowleri. *Antimicrob. Agents Chemother.* 65, e00017–e00021. doi: 10.1128/AAC.00017-21
- Visvesvara, G. S. (2010). Amebic meningoencephalitis and keratitis: challenges in diagnosis and treatment\*. *Curr. Opin. Infect. Dis.* 23, 590–594. doi: 10.1097/QCO.0b013e32833ed78b
- Visvesvara, G. S., Martinez, A. J., Schuster, F. L., Leitch, G. J., Wallace, S. V., Sawyer, T. K., et al. (1990). Leptomyxid ameba, a new agent of amebic meningoencephalitis in humans and animals. *J. Clin. Microbiol.* 28, 2750–2756. doi: 10.1128/jcm.28.12.2750-2756.1990
- Wang, Q., Li, J., Ji, J., Yang, L., Chen, L., Zhou, R., et al. (2018). A case of Naegleria fowleri related primary amoebic meningoencephalitis in China diagnosed by next-generation sequencing. *BMC Infect. Dis.* 18:349. doi: 10.1186/s12879-018-3261-z
- Yang, Y., Hu, X., Min, L., Dong, X., and Guan, Y. (2019). Balamuthia mandrillaris-related primary amoebic encephalitis in China diagnosed by next generation sequencing and a review of the literature. *Lab. Med.* 51, e20–e26. doi: 10.1093/labmed/lmz079



## OPEN ACCESS

APPROVED BY  
Frontiers Editorial Office,  
Frontiers Media SA, Switzerland

## \*CORRESPONDENCE

Lori Ferrins  
✉ l.ferrins@northeastern.edu  
Christopher A. Rice  
✉ carice@purdue.edu

## †PRESENT ADDRESS

Christopher A. Rice,  
Purdue Institute for Drug Discovery (PIDD),  
Purdue University, West Lafayette, IN,  
United States; Purdue Institute of Inflammation,  
Immunology and Infectious Disease (PI4D),  
Purdue University, West Lafayette, IN,  
United States

RECEIVED 29 September 2023

ACCEPTED 02 October 2023

PUBLISHED 25 October 2023

## CITATION

Ferrins L, Buskes MJ, Kapteyn MM, Engels HN,  
Enos SE, Lu C, Klug DM, Singh B, Quotadamo A,  
Bachovchin K, Tear WF, Spaulding AE,  
Forbes KC, Bag S, Rivers M, LeBlanc C,  
Burchfield E, Armand JR, Diaz-Gonzalez R,  
Ceballos-Perez G, Garcia-Hernández R,  
Pérez-Moreno G, Bosch-Navarrete C,  
Gómez-Liñán C, Ruiz-Pérez LM, Gamarro F,  
González-Pacanowska D, Navarro M,  
Mensa-Wilmot K, Pollastri MP, Kyle DE and  
Rice CA (2023) Corrigendum: Identification of  
novel anti-amoebic pharmacophores from  
kinase inhibitor chemotypes.  
*Front. Microbiol.* 14:1304196.  
doi: 10.3389/fmicb.2023.1304196

## COPYRIGHT

© 2023 Ferrins, Buskes, Kapteyn, Engels, Enos,  
Lu, Klug, Singh, Quotadamo, Bachovchin, Tear,  
Spaulding, Forbes, Bag, Rivers, LeBlanc,  
Burchfield, Armand, Diaz-Gonzalez,  
Ceballos-Perez, Garcia-Hernández,  
Pérez-Moreno, Bosch-Navarrete,  
Gómez-Liñán, Ruiz-Pérez, Gamarro,  
González-Pacanowska, Navarro,  
Mensa-Wilmot, Pollastri, Kyle and Rice. This is  
an open-access article distributed under the  
terms of the [Creative Commons Attribution  
License \(CC BY\)](https://creativecommons.org/licenses/by/4.0/). The use, distribution or  
reproduction in other forums is permitted,  
provided the original author(s) and the  
copyright owner(s) are credited and that the  
original publication in this journal is cited, in  
accordance with accepted academic practice.  
No use, distribution or reproduction is  
permitted which does not comply with these  
terms.

# Corrigendum: Identification of novel anti-amoebic pharmacophores from kinase inhibitor chemotypes

Lori Ferrins<sup>1\*</sup>, Melissa J. Buskes<sup>1</sup>, Madison M. Kapteyn<sup>2</sup>,  
Hannah N. Engels<sup>2</sup>, Suzanne E. Enos<sup>2,3</sup>, Chenyang Lu<sup>4</sup>,  
Dana M. Klug<sup>1</sup>, Baljinder Singh<sup>1</sup>, Antonio Quotadamo<sup>1,5</sup>,  
Kelly Bachovchin<sup>1</sup>, Westley F. Tear<sup>1</sup>, Andrew E. Spaulding<sup>1</sup>,  
Katherine C. Forbes<sup>1</sup>, Seema Bag<sup>1</sup>, Mitch Rivers<sup>1</sup>,  
Catherine LeBlanc<sup>1</sup>, Erin Burchfield<sup>1</sup>, Jeremy R. Armand<sup>1</sup>,  
Rosario Diaz-Gonzalez<sup>6</sup>, Gloria Ceballos-Perez<sup>6</sup>,  
Raquel García-Hernández<sup>6</sup>, Guiomar Pérez-Moreno<sup>6</sup>,  
Cristina Bosch-Navarrete<sup>6</sup>, Claudia Gómez-Liñán<sup>6</sup>,  
Luis Miguel Ruiz-Pérez<sup>6</sup>, Francisco Gamarro<sup>6</sup>,  
Dolores González-Pacanowska<sup>6</sup>, Miguel Navarro<sup>6</sup>,  
Kojo Mensa-Wilmot<sup>7</sup>, Michael P. Pollastri<sup>1</sup>, Dennis E. Kyle<sup>2</sup> and  
Christopher A. Rice<sup>2,3,4\*†</sup>

<sup>1</sup>Department of Chemistry and Chemical Biology, Northeastern University, Boston, MA, United States,

<sup>2</sup>Center for Tropical and Emerging Global Diseases, University of Georgia, Athens, GA, United States,

<sup>3</sup>Department of Pharmaceutical and Biomedical Sciences, College of Pharmacy, University of Georgia,

Athens, GA, United States, <sup>4</sup>Department of Comparative Pathobiology, College of Veterinary Medicine,

Purdue University, West Lafayette, IN, United States, <sup>5</sup>Clinical and Experimental Medicine PhD Program,

University of Modena and Reggio Emilia, Modena, Italy, <sup>6</sup>Instituto de Parasitología y Biomedicina

"López-Neyra" Consejo Superior de Investigaciones Científicas (CSIC), Granada, Spain, <sup>7</sup>Department of

Molecular and Cellular Biology, Kennesaw State University, Kennesaw, GA, United States

## KEYWORDS

pathogenic free-living amoeba, *Acanthamoeba* species, *Naegleria fowleri*, *Balamuthia mandrillaris*, kinase inhibitors, cross-screening, hit-identification

## A corrigendum on

## Identification of novel anti-amoebic pharmacophores from kinase inhibitor chemotypes

by Ferrins, L., Buskes, M. J., Kapteyn, M. M., Engels, H. N., Enos, S. E., Lu, C., Klug, D. M., Singh, B., Quotadamo, A., Bachovchin, K., Tear, W. F., Spaulding, A. E., Forbes, K. C., Bag, S., Rivers, M., LeBlanc, C., Burchfield, E., Armand, J. R., Diaz-Gonzalez, R., Ceballos-Perez, G., Garcia-Hernández, R., Pérez-Moreno, G., Bosch-Navarrete, C., Gómez-Liñán, C., Ruiz-Pérez, L. M., Gamarro, F., González-Pacanowska, D., Navarro, M., Mensa-Wilmot, K., Pollastri, M. P., Kyle, D. E., and Rice, C. A. (2023). *Front. Microbiol.* 14, 1149145. doi: 10.3389/fmicb.2023.1149145

In the published article, there was an error in the author list, and author "Claudia Gómez-Liñán" was erroneously excluded. The corrected author list appears below.

Lori Ferrins<sup>1\*</sup>, Melissa J. Buskes<sup>1</sup>, Madison M. Kapteyn<sup>2</sup>, Hannah N. Engels<sup>2</sup>, Suzanne E. Enos<sup>2,3</sup>, Chenyang Lu<sup>4</sup>, Dana M. Klug<sup>1</sup>, Baljinder Singh<sup>1</sup>, Antonio Quotadamo<sup>1,5</sup>,

Kelly Bachovchin<sup>1</sup>, Westley F. Tear<sup>1</sup>, Andrew E. Spaulding<sup>1</sup>, Katherine C. Forbes<sup>1</sup>, Seema Bag<sup>1</sup>, Mitch Rivers<sup>1</sup>, Catherine LeBlanc<sup>1</sup>, Erin Burchfield<sup>1</sup>, Jeremy R. Armand<sup>1</sup>, Rosario Diaz-Gonzalez<sup>6</sup>, Gloria Ceballos-Perez<sup>6</sup>, Raquel García-Hernández<sup>6</sup>, Guiomar Pérez-Moreno<sup>6</sup>, Cristina Bosch-Navarrete<sup>6</sup>, Claudia Gómez-Liñán<sup>6</sup>, Luis Miguel Ruiz-Pérez<sup>6</sup>, Francisco Gamarro<sup>6</sup>, Dolores González-Pacanowska<sup>6</sup>, Miguel Navarro<sup>6</sup>, Kojo Mensa-Wilmot<sup>7</sup>, Michael P. Pollastri<sup>1</sup>, Dennis E. Kyle<sup>2</sup> and Christopher A. Rice<sup>2,3,4\*†</sup>

In the original article there was also an error in the **Author Contribution** section.

The correct author contributions section appears below:

## Author contributions

CR, MB, and LF: conceptualization. LF, MB, MK, HE, SE, CLu, DKL, BS, AQ, KB, WT, AS, KF, SB, MR, CLe, EB, JA, RD-G, GC-P, GP-M, CB-N, CG-L, DG-P, MN, and CR: methodology. CR, DKy, MP, and LF: validation and supervision. LF and CR: formal

analysis and writing—original draft preparation. DKy, MP, and LF: resources and funding acquisition. LF, MB, DKL, BS, KB, WT, SB, MK, HE, SE, CLu, CB-N, and CR: data curation. LF, MB, MK, HE, SE, CLu, DKL, BS, AQ, KB, WT, AS, KF, SB, MR, CLe, EB, JA, RD-G, GC-P, RG-H, GP-M, CB-N, CG-L, LR-P, FG, DG-P, MN, KM-W, MP, DKy, and CR: writing—review and editing. All authors contributed to the article and approved the submitted version.

The authors apologize for this error and state that this does not change the scientific conclusions of the article in any way. The original article has been updated.

## Publisher's note

All claims expressed in this article are solely those of the authors and do not necessarily represent those of their affiliated organizations, or those of the publisher, the editors and the reviewers. Any product that may be evaluated in this article, or claim that may be made by its manufacturer, is not guaranteed or endorsed by the publisher.





## OPEN ACCESS

## EDITED BY

Carlos Robello,  
Universidad de la República, Uruguay

## REVIEWED BY

John Frean,  
National Institute of Communicable Diseases  
(NICD), South Africa  
Sébastien Pomel,  
Université Paris-Sud, France

## \*CORRESPONDENCE

Kasem Kulkeaw  
✉ kasem.kuk@mahidol.edu

RECEIVED 21 March 2023

ACCEPTED 14 August 2023

PUBLISHED 05 September 2023

## CITATION

Whangviboonkij N, Pengsart W, Chen Z, Han S,  
Park S and Kulkeaw K (2023) Phenotypic assay  
for cytotoxicity assessment of *Balamuthia*  
*mandrillaris* against human neurospheroids.  
*Front. Microbiol.* 14:1190530.  
doi: 10.3389/fmicb.2023.1190530

## COPYRIGHT

© 2023 Whangviboonkij, Pengsart, Chen, Han,  
Park and Kulkeaw. This is an open-access  
article distributed under the terms of the  
[Creative Commons Attribution License \(CC BY\)](https://creativecommons.org/licenses/by/4.0/).  
The use, distribution or reproduction in other  
forums is permitted, provided the original  
author(s) and the copyright owner(s) are  
credited and that the original publication in this  
journal is cited, in accordance with accepted  
academic practice. No use, distribution or  
reproduction is permitted which does not  
comply with these terms.

# Phenotypic assay for cytotoxicity assessment of *Balamuthia mandrillaris* against human neurospheroids

Narisara Whangviboonkij<sup>1</sup>, Worakamol Pengsart<sup>1</sup>,  
Zhenzhong Chen<sup>2</sup>, Seokgyu Han<sup>2</sup>, Sungsu Park<sup>2,3,4</sup> and  
Kasem Kulkeaw<sup>1\*</sup>

<sup>1</sup>Siriraj Integrative Center for Neglected Parasitic Diseases, Department of Parasitology, Faculty of Medicine Siriraj Hospital, Mahidol University, Bangkok, Thailand, <sup>2</sup>School of Mechanical Engineering, Sungkyunkwan University, Suwon, Republic of Korea, <sup>3</sup>Department of Biomedical Engineering, Sungkyunkwan University, Suwon, Republic of Korea, <sup>4</sup>Institute of Quantum Biophysics, Sungkyunkwan University, Suwon, Republic of Korea

**Introduction:** The phenotypic screening of drugs against *Balamuthia mandrillaris*, a neuropathogenic amoeba, involves two simultaneous phases: an initial step to test amoebicidal activity followed by an assay for cytotoxicity to host cells. The emergence of three-dimensional (3D) cell cultures has provided a more physiologically relevant model than traditional 2D cell culture for studying the pathogenicity of *B. mandrillaris*. However, the measurement of ATP, a critical indicator of cell viability, is complicated by the overgrowth of *B. mandrillaris* in coculture with host cells during drug screening, making it challenging to differentiate between amoebicidal activity and drug toxicity to human cells.

**Methods:** To address this limitation, we introduce a novel assay that utilizes three-dimensional hanging spheroid plates (3DHSPs) to evaluate both activities simultaneously on a single platform.

**Results and discussion:** Our study showed that the incubation of neurospheroids with clinically isolated *B. mandrillaris* trophozoites resulted in a loss of neurospheroid integrity, while the ATP levels in the neurospheroids decreased over time, indicating decreased host cell viability. Conversely, ATP levels in isolated trophozoites increased, indicating active parasite metabolism. Our findings suggest that the 3DHSP-based assay can serve as an endpoint for the phenotypic screening of drugs against *B. mandrillaris*, providing a more efficient and accurate approach for evaluating both parasite cytotoxicity and viability.

## KEYWORDS

granulomatous amoebic encephalitis, *Balamuthia mandrillaris*, neurospheroid, cytotoxicity, drug discovery, neglected disease, tropical disease

## 1. Introduction

Some protozoan species naturally reside in the environment, while some are amphizoic and capable of adapting to survive in the human body (Haston and Cope, 2023). *Balamuthia mandrillaris* is an environment-dwelling amoeba that causes lethal brain damage, termed granulomatous amoebic encephalitis (GAE). Metabolically active trophozoites of *B. mandrillaris* can be isolated from soil and freshwater (Gompf and Garcia, 2019). Thus, two routes of

transmission are proposed: direct exposure to soil and water via skin ulcers or inhalation via the olfactory epithelium in the nose (Kiderlen and Laube, 2004; Piper et al., 2018; Gompf and Garcia, 2019) or the respiratory tract (Schuster and Visvesvara, 2004a). According to the report in 2019, more than 200 cases of GAE have been estimated (Gompf and Garcia, 2019). Although *Balamuthia*-GAE is extremely rare, the disease is highly fatal (Schuster and Visvesvara, 2004b). More than a 95% mortality rate is documented worldwide. Regardless of immune competency, everyone is at risk of being infected by *B. mandrillaris* (Wu et al., 2020; Xu et al., 2022). Hence, environment-derived *B. mandrillaris* infections have challenged our efforts to prevent this highly lethal disease.

The poor prognosis of GAE is multifactorial. Differential diagnosis of GAE from other inflamed brains is difficult. GAE has symptoms similar to those of viral or bacterial encephalitis, which are more common. Moreover, a definitive diagnosis is based on observation of the trophozoites in the histological section of the inflamed brain under a microscope (Peng et al., 2022; Liu et al., 2023). The sensitivity of the microscopic diagnosis depends on the site of the brain biopsy, the number of trophozoites, and the skill of the examiner. Other laboratory procedures may support definitive diagnosis, including time-consuming *in vitro* culture and/or high-sensitivity detection of trophozoite DNA (Wu et al., 2020; Yang et al., 2020). However, the lack of a sensitive diagnosis makes GAE more dangerous (Schuster and Visvesvara, 2004b). A definitive diagnosis is often made after death by autopsy of brain tissue. Importantly, there is no specific drug targeting *B. mandrillaris*. Current treatments for GAE rely primarily on trial combinations of antimicrobial and antifungal drugs, resulting in variations in clinical outcomes (Doyle et al., 2011; Cuoco et al., 2022). Thus, the development of more effective drugs remains a topic of intensive research (Phan et al., 2021; Ferrins et al., 2023).

Three-dimensional (3D) cell cultures have emerged as useful models for the study of pathogenicity owing to their similarity to cell and tissue physiology compared to conventional 2D cell culture. Several cancer cell lines are capable of forming spherical cell aggregates, known as spheroids (Kapalczyńska et al., 2018). Additional physiological relevance of spheroids has been recognized, including cell functions (Lagies et al., 2020) and drug response (Mittler et al., 2017). Previously, our group developed a chemiluminescence assay for assessing the cytotoxicity of *B. mandrillaris* against the human neurospheroid, a 3D cell clump (Pengsart and Kulkeaw, 2022). However, the measurement of ATP, a critical indicator of cell viability, is complicated by the overgrowth of *B. mandrillaris* in coculture with host cells during drug screening, making it challenging to differentiate between amoebicidal activity and drug toxicity to human cells. We previously reported the use of a three-dimensional hanging spheroid plate (3DHSP) to facilitate the formation of spheroids and the separation of unbound and dead cells during cytotoxicity assays using chimeric antigen receptor (CAR) T cells and demonstrated the direct measurement of cytotoxic effects of CAR T cells on spheroids using optical imaging without the need for live and dead fluorescent staining of the cells (Chen et al., 2022). This study adapts the 3D neurospheroid plate by which the growing trophozoites were separated before measuring the ATP level. Thus, it is applicable for screening amoebicidal activity and cytotoxicity in the same setting. This dual phenotypic assay allows the identification of drugs that ameliorate the severity of disease and drugs that are safe in a single step.

## 2. Materials and methods

### 2.1. Culture of a clinical isolate of *Balamuthia mandrillaris* trophozoites

*Balamuthia mandrillaris* trophozoites were isolated from biopsied brain tissue of a human subject who gave consent to participate (COA no. Si806/2020). The experiments involving *B. mandrillaris* trophozoites were approved by the Siriraj Institutional Review Board (COA. no. 146/2022). The detailed protocol was explained in Pengsart et al. (2022). Briefly, small pieces of the biopsied brain were digested with pepsin. After passing through a sterile gauze bandage, the small cell clumps were mixed with DMEM supplemented with 10% heat-inactivated fetal bovine serum (FBS, HyClone, Utah) and subjected to coculture with a monolayer of human lung carcinoma A549 cells (as feeders). The culture medium was renewed every 2–3 days. The floating cells were transferred to a new lot of feeder cells every week. Any cells with a morphology distinct from that of the A549 cells were observed for slow movement of the projecting cytoplasm. Moreover, a small area of the feeder cell-free appearance could indicate the presence of trophozoites. For regular maintenance, *B. mandrillaris* trophozoites were cultured with A549 cells. Prior to studying neurospheroid damage, trophozoites were plated onto a monolayer of human SH-SY5Y cells for 2–3 passages. When the monolayer of SH-SY5Y cells was removed from more than 80% of the surface area, the trophozoites were transferred to a new monolayer of 80–90% confluent SH-SY5Y cells. For human cell-free culture, the trophozoites were maintained in the feeder-free culture (Law et al., 2023). BM-3 medium was used and consisted of peptone (16.4 mM), yeast extract (4 mg/mL), yeast RNA (1 mg/mL), liver digest (10 mg/mL), glucose (5.5 mM), hemin (3 µM), taurine (0.4 mM), 1xMEM vitamin mixture, 1xlipid mixture, and 10% newborn calf serum.

### 2.2. Culture of human lung carcinoma A549 and neuroblastoma SH-SY5Y cells

Human neuroblastoma SH-SY5Y cells were obtained from the American Type Culture Collection (ATCC® No. CRL-2266TM), while human lung carcinoma A549 cells were kindly provided by Prof. Wanpen Chaicumpa. Both cell types were maintained following the ATCC's instructions. For the SH-SY5Y cells, a 1:1 ratio of ATCC-formulated Eagle's minimum essential medium (EMEM) (ATCC, Utah) and F12 medium (Gibco, Gaithersburg, MD) was prepared. The complete medium of the human neuroblastoma SH-SY5Y cells is EMEM-F12 medium supplemented with 10% heat-inactivated FBS (HyClone, Utah), herein called complete EMEM-F12 medium. For the A549 cells, 10% FBS-supplemented DMEM was used. Cells were incubated at 37°C in a humidified atmosphere containing 5% CO<sub>2</sub> and subcultured every 2–3 days or when the cell density reached 60–80% confluence. Cells were detached from the polystyrene well using 0.25% trypsin in 0.5 mM EDTA solution (STEMCELL Technologies, Vancouver, Canada). Viable and nonviable cells were identified using Trypan blue and counted using a hemocytometer under a light microscope. Human neuroblastoma SH-SY5Y cells were subcultured at a 1:10 ratio per well of a 6-well plate.

## 2.3. Formation of human neurospheroids in 3DHSP

The 3DHSP is a 24-well plate consisting of two layers. The upper layer forms hanging drops, and the lower layer consists of a spheroid retaining well and a waste well connected by channels with a height of 40  $\mu\text{m}$  (Figure 1A). The upper layer was printed using a 3D printer (Cubicon, Seongnam, Korea) with acrylonitrile butadiene styrene (ABS) filaments. The lower layer was made of polydimethylsiloxane (PDMS) (Dow Corning Co., Midland, MI, United States) (Chen et al., 2022). Human neuroblastoma SH-SY5Y cells were collected from the 2D culture well using cell dissociation buffer (Life Technology, New York). Viable cells were prepared at  $1.7 \times 10^4$  cells per 25  $\mu\text{L}$  of complete EMEM-F12. Then, the cell suspension was filled into a small channel on the upper layer of the 3DHSP. The complete EMEM-F12 was placed into the waste well to prevent evaporation of the hanging drop. The plate was placed in a reservoir containing sterile distilled water and covered with a lid to prevent evaporation of the culture medium in the hanging drop.

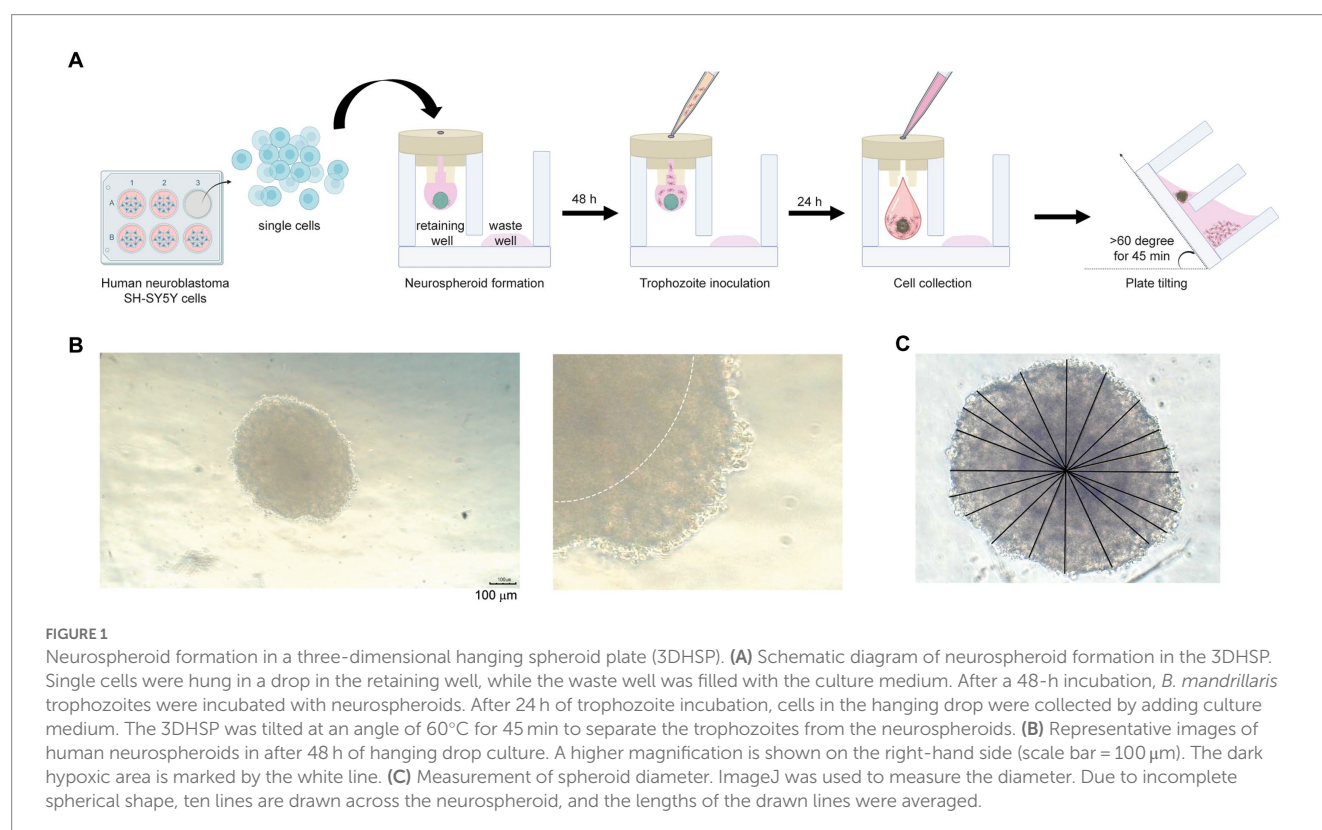
## 2.4. Culture of *Balamuthia mandrillaris* with human neurospheroids

After 2 days of hanging drop incubation, 1,000 trophozoites in 10  $\mu\text{L}$  were filled into the same small channel, allowing the coculture of trophozoites with human cells in a hanging drop. For analysis of human cell viability, 100  $\mu\text{L}$  of complete EMEM-F12 medium was added to the hanging drop at 24 h post-coculture to push the cell

mixture into the retaining well. The 3DHSP plate was tilted for 45 or 90 min to allow the single cells to pass through a 40  $\mu\text{m}$ -diameter hole. The neurospheroids in the retaining well and the separated cells in the waste well were subjected to analysis of size, morphology, and viability. To measure the diameter of the nonspherical neurospheroid, lines were drawn from the perimeter of the spheroid, passed through the center, and ended at the opposite perimeter. Lengths of the lines were measured using ImageJ software and calculated for a diameter mean.

## 2.5. Fluorescence labeling of human neurospheroids

Human neuroblastoma SH-SY5Y cells were cultured in 2D, and single cells were prepared, followed by incubation with 2.5  $\mu\text{M}$  CellTracker™ Green CMFDA (5-chloromethylfluorescein diacetate, Invitrogen, OR) and 1:1600 diluted DiD (Invitrogen, OR) to label proteins and lipids, respectively. The labeled cells were subjected to neurospheroid formation as mentioned above. After 48 h of hanging drop culture, *B. mandrillaris* trophozoites were added to the hanging drop and incubated for 24 h. The drops were pushed into the lower plate by adding 100  $\mu\text{L}$  of culture medium. The lower plate was tilted at an angle of more than 60° for 45 min at room temperature to separate the cell debris and trophozoites into the waste well. For visualization, neurospheroids and cell debris were transferred into ultralow attachment (SPL Life Sciences, South Korea) and flat-bottom plates (Thermo Fisher Scientific, United States), respectively, for confocal imaging (Nikon Eclipse Ti, Nikon, Japan).



## 2.6. Efficiency of trophozoite removal from human neurospheroids

To examine the separation of the trophozoites from the neurospheroid after 3DHSP tilting, the presence of trophozoites adhering to the neurospheroid in the retaining well and those in the waste well was measured using quantitative PCR. Genomic DNA was isolated using a QIAamp DNA Mini Kit (QIAGEN, Hilden, Germany) following the manufacturer's instructions. The primer set used for the amplification of 16S rRNA gene of the *B. mandrillaris* included a forward primer (5'-TAACCTGCTAAATAGTCATGCCAAT-3') and a reverse primer (5'-CAAACCTCCCTCGGCTAATCA-3') (Wu et al., 2020). The thermal cycles for each transcript were as follows: initial denaturation at 95°C for 1 min, followed by 40 cycles of DNA denaturation at 95°C for 15 s, primer annealing at 60°C for 30 s, and DNA strand extension at 60°C for 5 s. Given the same volume of DNA extracts, the level of *B. mandrillaris* DNA was directly compared among samples using the cycle threshold (Ct). Delta cycle threshold ( $\Delta Ct$ ) was calculated following the formula:  $\Delta Ct = [Ct \text{ of the trophozoite DNA in the waste well} - Ct \text{ of the trophozoite DNA in the retaining well}]$  (Rao et al., 2013). The DNA obtained from an untilted plate was set as a positive control because all trophozoites remained. Then, the  $2^{-\Delta Ct}$  was calculated and displayed as a relative expression compared to the positive control (the untilted plate).

## 2.7. Cell viability

Intracellular ATP was used as a readout indicating the metabolically active stage of viable cells. The CellTiter-Glo® 3D Cell Viability Assay (Promega, United States) was deployed for direct detection of the intracellular level of ATP. ATPs can change luciferin to a luminescence-emitting oxyluciferin. Briefly, the neurospheroids and the separated trophozoites were transferred to a low attachment round-bottom well of the 96-well plate (SPL Life Sciences, South Korea) and a Nunclon Delta Surface 96-well plate (Thermo Fisher Scientific, MA), respectively, followed by adding the CellTiter-Glo® solution. The luminescence signal was measured by using a BioTek Synergy H1 Hybrid Multi-Mode plate reader. After removing the background luminescence of the culture medium, the data were displayed as relative light units (RLUs). Changes in the RLUs of each sample were related to the RLUs of control neurospheroids that were free from *B. mandrillaris* trophozoites.

## 2.8. Statistical analysis

Differences between two independent samples were calculated using the Mann-Whitney test. Student's *t* test was used to examine the difference in the means of relative DNA and ATP levels and the RLUs of ATP levels. Multiple comparisons of the spheroid diameter of more than two groups were assessed by using one-way ANOVA with Bonferroni correction. A statistically significant difference was dependent on a *p* value: less than 0.05 indicated that a given value of each sample was different, while more than 0.05 implied a probability that a given value was the same among samples.

## 3. Results

### 3.1. Formation of human neurospheroids in the 3DHSP

First, the number of cells was optimized to form a spheroid in a hanging drop. Various numbers of human SH-SY5Y cells were hung as a drop in the upper part of the 3DHSP (Supplementary Figure S1A). To capture images of spheroid-forming cells, culture medium needs to be added to push the cell clump into a well of the lower part, or a stereomicroscope needs to be used to capture the cells in the hanging drop. Thus, early-forming spheroids could not be imaged due to fragmentation. Finally, we determined that the optimal number of human SH-SY5Y cells was  $6.8 \times 10^5$  cells/mL (Supplementary Figure S1A). At 48 h post cell hanging, the neurospheroid was opaque with central dark zones, and clearly seen edges were observed (dotted line in the right panel, Figure 1B). Given an incomplete spherical shape, several straight lines were drawn from side to side through the center (Figure 1C). The average diameter of the 48-h neurospheroids was  $438.4 \pm 18 \mu\text{m}$  ( $n = 6$ ) (Figure 1B). Thus, the human neuroblastoma SH-SY5Y cells could proliferate and form spherical shapes in a hanging drop of the 3DHSP. Notably, sterile distilled water or culture medium was added underneath the hanging drop in the lower part of the plate. Due to proximity to the solution below, some SH-SY5Y cells migrated to adhere to the surface of the lower plate (Supplementary Figure S1B). Thus, the original protocol was modified by placing the 3DHSP in a humidified chamber without the liquid fill in the lower part. Instead, the culture medium was filled in the waste well, preventing the evaporation of liquid from the hanging drop.

### 3.2. Separation of cell debris from the human neurospheroid using 3DHSP

An advantage of the 3DHSP is the ability to remove cell debris, as demonstrated previously (Chen et al., 2022). To assess the efficiency of trophozoite separation from neurospheroids, the cells in the retaining and waste wells after plate tilting were visualized. Human neuroblastoma SH-SY5Y cells were labeled with two fluorophores: CMFDA for protein and DiD for lipid (Figure 2A). Following cell labeling, the fluorescence intensity remained detectable for up to 48 h (Figures 2B,C). CMFDA and DiD had different patterns. CMFDA-bound protein was dispersed, while DiD-bound lipids appeared as globules of various sizes. Without plate tilting, the neurospheroids were retained in the chamber. No cell debris was observed in the waste chamber (lower panels, Figure 2B). In contrast, the 60 degree-tilted 3DHSP allowed cell debris to be moved into the waste well (lower panels, Figure 2C). The cell debris observed in the waste well still showed CMFDA and DiD fluorescence. Without fluorescent labeling, it was difficult to observe cell debris using the phase contrast view of the inverted microscope. The representative image shows 47 fluorescent particles per waste well following the 60-degree-tilted 3DHSP while there was no fluorescent particle detected in the waste well without plate tilting.



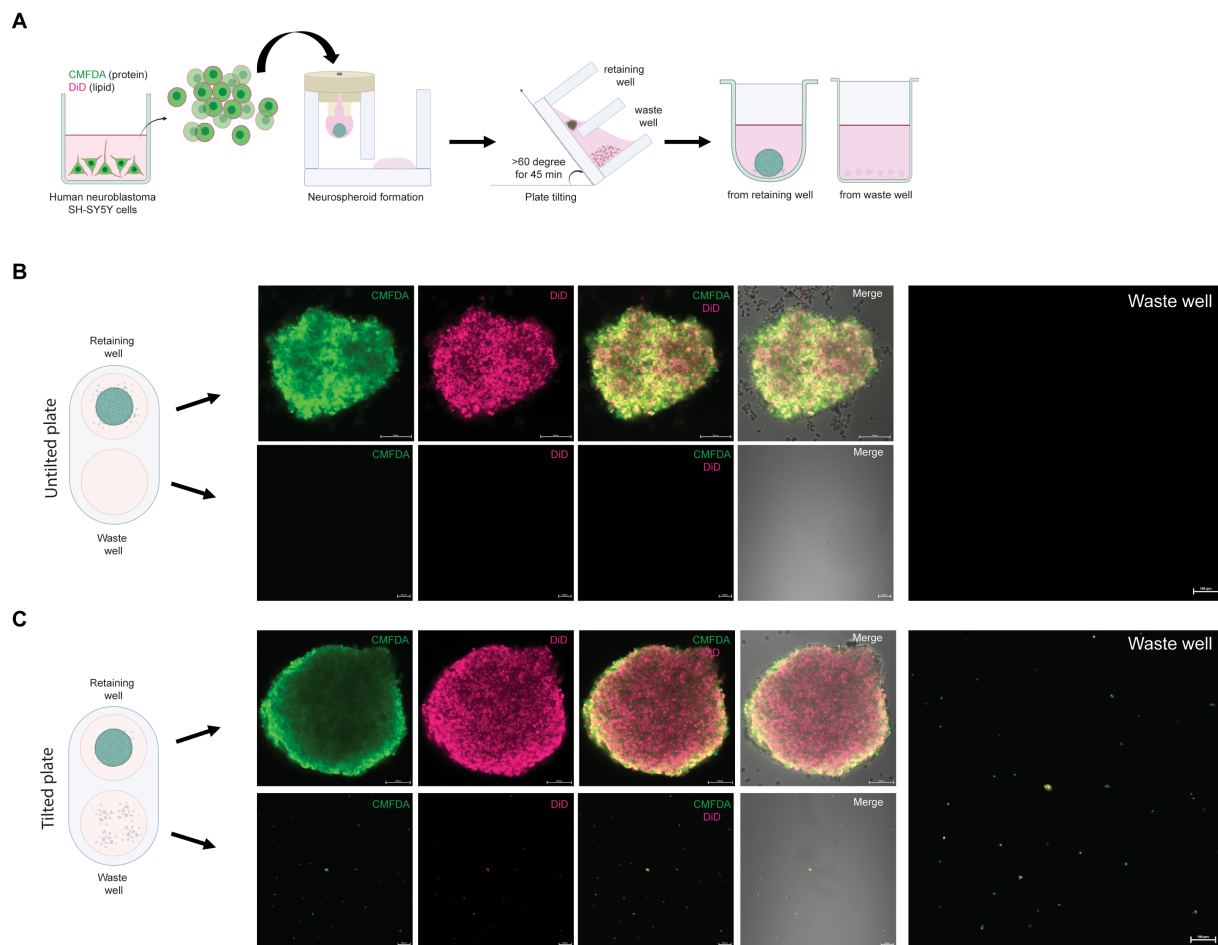


FIGURE 2

Removal of single SH-SY5Y cells from the neurospheroid. (A) Illustration of the method for forming fluorescent neurospheroids. Human neuroblastoma SH-SY5Y cells were incubated with protein-binding CMFDA and lipid-binding DiI in the 2D cell culture well. After cell labeling, single SH-SY5Y cells were subjected to neurospheroid formation in the 3DHSP. After plate tilting, the neurospheroids and the cells in the waste well were transferred to a round or flat bottom-containing plate, respectively. The fluorescence-labeled neurospheroids and cells were imaged under a confocal microscope. (B) Confocal microscopic images of SH-SY5Y neurospheroids in the retaining well (upper panel, scale bar = 100 μm) and waste well (lower panel, scale bar = 100 μm) of the untilted plate. Images of CMFDA- and DiI-labeled neurospheroid are merged with the differential interference contrast (Merge). A higher magnification of the CMFDA- and DiI-visualizing waste well is shown on the right-hand side (scale bar = 100 μm). (C) Confocal microscopic images of SH-SY5Y neurospheroids in the retaining well (upper panel, scale bar = 100 μm) and the waste well (lower panel, scale bar = 100 μm) after tilting for 90 min. Images of CMFDA- and DiI-labeled neurospheroid are merged with the differential interference contrast (Merge). A higher magnification of the CMFDA- and DiI-visualizing waste well is shown on the right-hand side (scale bar = 100 μm).

### 3.3. Loss of neurospheroid integrity in coculture with *Balamuthia mandrillaris*

To apply an optical measurement for examining neurospheroid integrity, the diameter of neurospheroids was measured after the settling of spheroids in the retaining well (Figure 3A). Since the trophozoites could be cultured with or without a monolayer of human neuroblastoma SH-SY5Y cells, we examined both types of trophozoites regarding their effects on neurospheroid integrity (Supplementary Figure S2A). The trophozoites were collected after the monolayer of human neuroblastoma SH-SY5Y cells disappeared. After 48 h of coculture with the neurospheroids, some trophozoites adhered to the neurospheroids, while some did not (Figure 3B). Different morphologies of the trophozoites were observed to relate to the source of the trophozoites. Some trophozoites obtained from the monolayered SH-SY5Y cells scattered as single cells, while some

adhered to the neurospheroid (Supplementary Figure S2B). In contrast, most of the trophozoites obtained from the feeder-free culture (BM-3 medium) formed clumps proximal to the neurospheroid (Supplementary Figure S2C). Without plate tilting, the sizes of the neurospheroids cocultured with the feeder-derived trophozoites were not different from those of the noninfected neurospheroids (red bar in the untilted plate in Figure 3D). In contrast, the BM3-derived trophozoites significantly reduced the size of the neurospheroid (teal bars, Figure 3D). Following plate tilting, the cell debris and trophozoites were separated into the waste well (Figure 3C). The size of the neurospheroids cocultured with feeder-derived trophozoites was significantly decreased (red bar in tilted plate, Figure 3D). When cocultured with trophozoites from BM-3 medium, the neurospheroids were significantly smaller than the control neurospheroids in both tilted and untilted plates (teal bars, Figure 3D). In summary, a size-based assay allows the assessment of

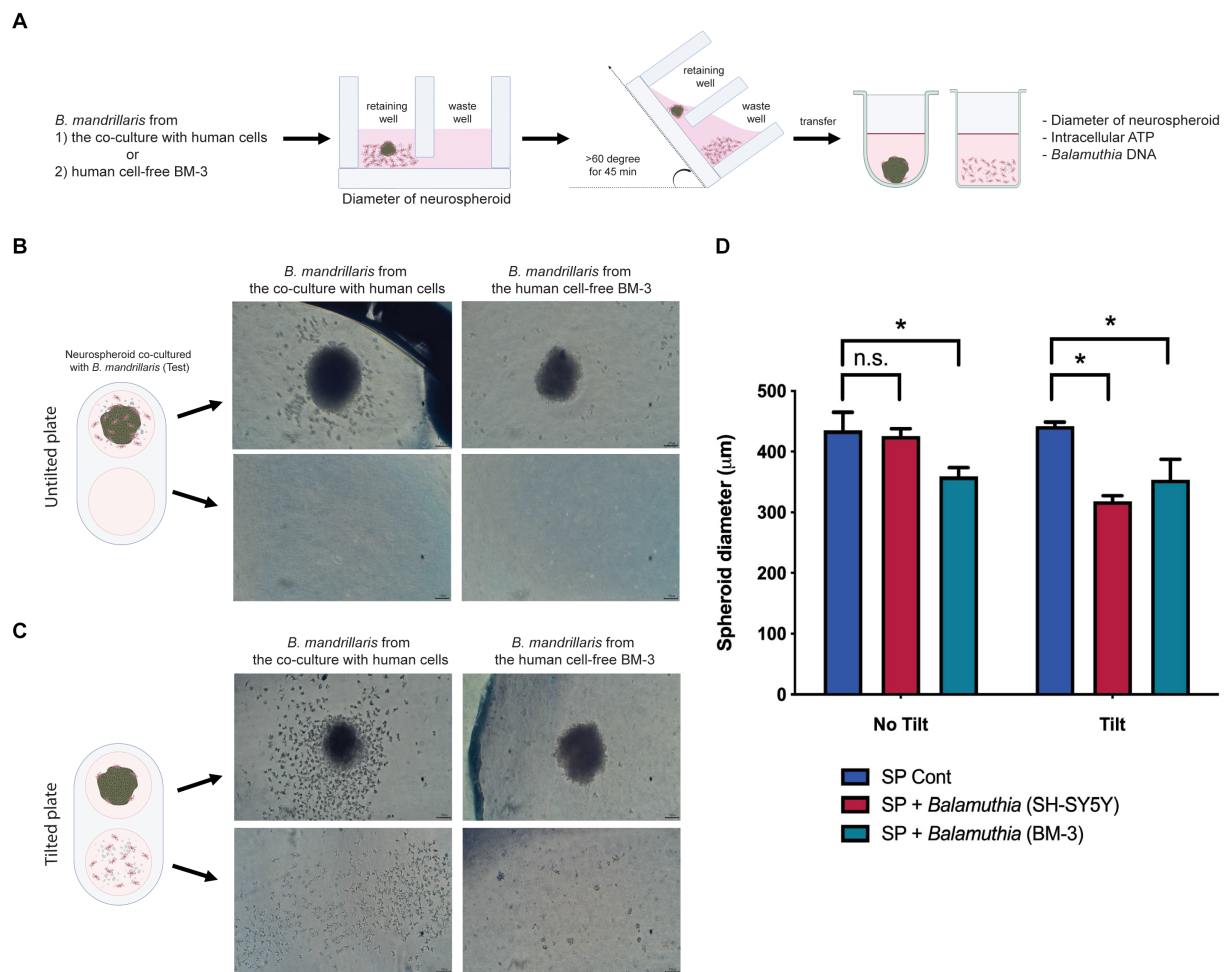


FIGURE 3

The effects of *B. mandrillaris* trophozoites on the integrity of neurospheroids. (A) Schematic diagram illustrating the assessment of the cytotoxicity of trophozoites against neurospheroids. The trophozoites were obtained from two sources: the coculture with human SH-SY5Y cells and the human cell-free BM-3 culture. Following 3DHSP tilting, the neurospheroids and cells in the waste well were transferred into a new round bottom and flat bottom plate for measuring the intracellular ATP and neurospheroid size. (B) Illustration of neurospheroids cultured with and without *B. mandrillaris* trophozoites in the hanging drops of the untilted plate. The spherical shape of the neurospheroid in the drop observed under a stereomicroscope. Scale bar, 100 μm. (C) Illustration of the neurospheroid and *B. mandrillaris* trophozoites in the retaining well and the waste well after plate tilting. (D) Sizes of the neurospheroids in the retaining wells were calculated from the untilted and tilted plates. Due to asymmetry, several lines of diameter were drawn and subjected to the calculation of spheroid diameter using ImageJ (left panel). The bar graph is the diameter of the neurospheroid (right panel). The *B. mandrillaris* trophozoites used in the coculture with neurospheroid (SP) were from the culture with human neuroblastoma cells (SH-SY5Y) or the feeder-free culture (BM-3).

neurospheroid damage in coculture with trophozoites. The culture method used to prepare trophozoites affects this size-based assay.

### 3.4. Decrease in intracellular ATP in coculture with *Balamuthia mandrillaris*

After plate tilting, the neurospheroids in the retaining well and the cells in the waste well were transferred into new round bottom and flat bottom plates, respectively (Figure 3A). To examine the survivability of human neurospheroids in coculture with *B. mandrillaris* trophozoites, intracellular ATPs of cells were measured in the retaining well, while those of the trophozoites were measured in the waste well after tilting the 3DHSP for 45 and 90 min (left and right panel, Figure 4A). In the absence of trophozoites, the 3DHSP-derived

neurospheroids remained intact in the retaining wells, as indicated by the ATP level (teal dots in control groups in left and right panel, Figure 4A). Nevertheless, the 3DHSP enabled the removal of cell debris, as shown by detectable ATP in the waste well, albeit at the lowest level (dark purple dots, Figure 4A). After coculture with trophozoites and 45-min plate tilting, the levels of intracellular ATPs in neurospheroids were significantly lower by 6-fold than those in noninfected neurospheroids (teal dots in the test groups, Figure 4A). Due to the presence of the trophozoites in the waste wells, the ATP levels increased after plate tilting (dark purple dots, Figure 4A), suggesting a separation of active trophozoites from the neurospheroids. There was no difference in ATP levels between the remaining and waste wells when the 3DHSP was tilted for 45 min; however, a longer tilting time allowed more trophozoites to be separated from the neurospheroids when cocultured with the SH-SY5Y-derived

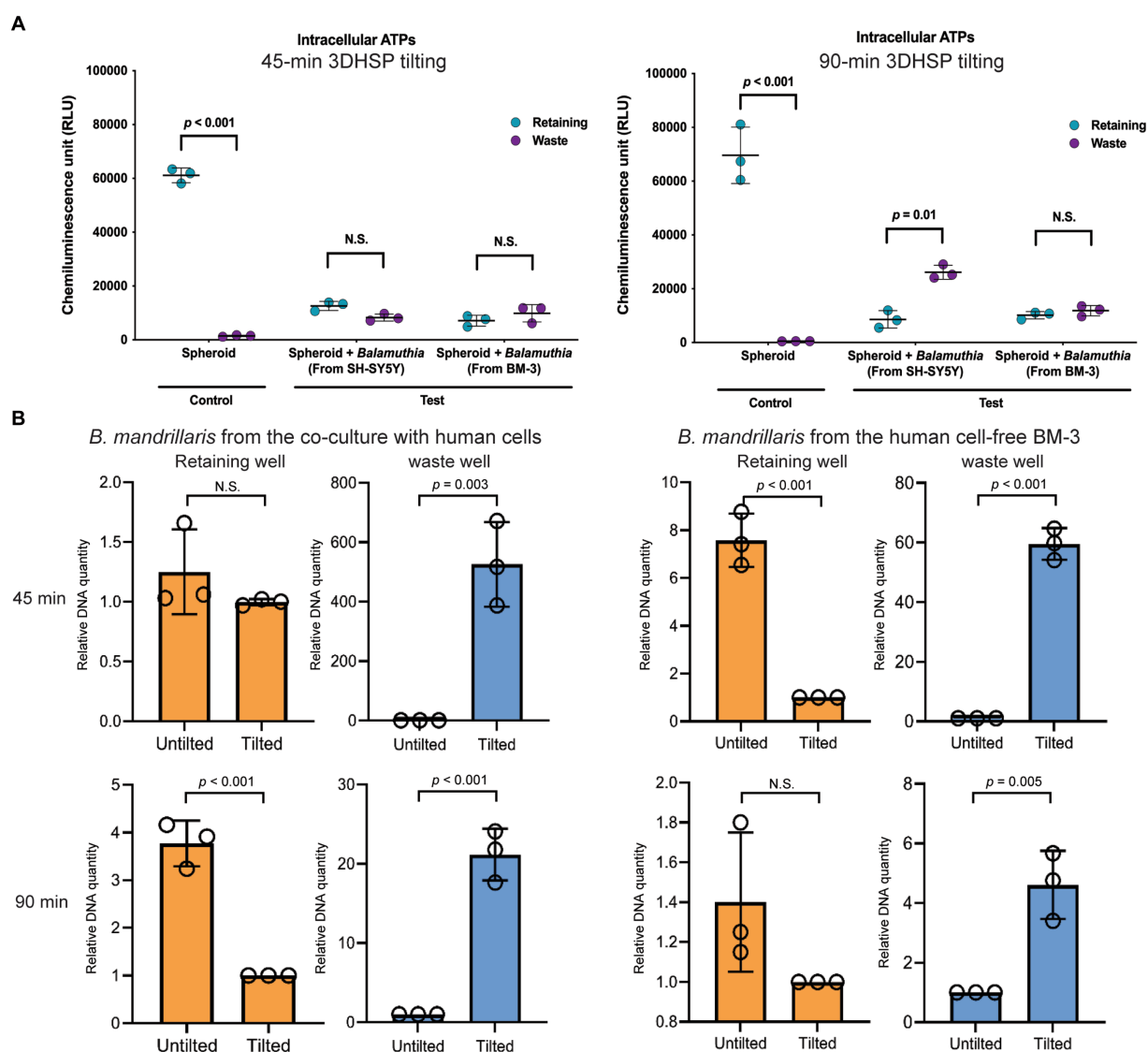


FIGURE 4

The effects of *B. mandrillaris* trophozoites on the survival of neurospheroids. (A) The level of intracellular ATP produced by the neurospheroid in the retaining wells and the *B. mandrillaris* trophozoites in the waste wells. The control group consisted of human neurospheroids without trophozoites, while the test groups consisted of human neurospheroids cocultured with trophozoites. The 3DHSPs were tilted for 45 and 90 min (left and right panels, respectively). Each colored dot represents three biological replicates. (B) PCR data show the relative DNA quantity of *B. mandrillaris* DNA remaining in the retaining and waste wells before and after 3DHSP tilting for 45 and 90 min (upper and lower panel, respectively). Trophozoites were obtained from a culture with human neuroblastoma SH-SY5Y cells (left panel) and a feeder-free BM-3 medium (right panel). Circles represent triplicate wells of the quantitative PCR.

*B. mandrillaris* (right panel, Figure 4A). However, the intracellular ATP level does not discriminate trophozoites, small cell clumps or single cells. To confirm the separation of the trophozoites, PCR was performed to detect the DNA of trophozoites in a relative quantitative manner. As shown in Figure 4B, the DNA of the trophozoites in the retaining well was not changed after 45 min of tilting (orange bars in upper panel, Figure 4B). In contrast, longer 3DHSP tilting (90 min) allowed greater removal of the trophozoites from the neurospheroids (orange bars in lower panel,  $p < 0.001$ , Figure 4B). Plate tilting significantly increased the number of trophozoites in the waste wells as well (blue bars in the upper and lower panel, Figure 4B). Moreover, the use of trophozoites obtained from feeder-free culture (right panel, Figure 4B) allowed higher efficiency in the separation of the trophozoites from the neurospheroid after 45-min 3DHSP tilting

(orange bars in the upper right panel, Figure 4B). In all experiments, the number of trophozoites in the waste well significantly increased following plate tilting (blue bars in all panel, Figure 4B). Regardless of the source of the trophozoites, the 90-min 3DHSP tilting removed the trophozoites from the neurospheroid (blue bars in all panel, Figure 4B), confirming the microscopic imaging (Figure 3C) and ATP detection in the waste wells.

### 3.5. Cytophagy of the *Balamuthia mandrillaris* trophozoites

To demonstrate the use of 3DHSP for elucidating the mechanisms of trophozoite survival, we observed host cell ingestion by trophozoites.

Proteins and lipids of human neuroblastoma cells were labeled with the fluorophores CMFDA and DiD, respectively. A 90-min tilting was performed to obtain more trophozoites in the waste cells. Regardless of the sources, the trophozoites scattered throughout the retaining well (arrowheads in Figures 5A,B). Most of the trophozoites in the waste well were positive for CMFDA and DiD (Figure 5C), indicating human cell ingestion. After plate tilting, the trophozoites in the waste wells were observed under a laser confocal microscope. The SH-SY5Y-derived trophozoites had more elongated cytoplasm, while the feeder-free trophozoites were rounder with short protrusions of cytoplasm (DIC images, Figure 5C). Human lipid and protein were observed in the cytoplasm of the trophozoites in a distinct pattern. The SH-SY5Y-derived trophozoites had dispersed granules containing human protein and lipids (arrowheads in upper panel in Figure 5C). In contrast, larger vacuoles were observed in the trophozoites obtained from the feeder-free culture. These vacuole-like structures contained both human lipids and proteins (arrowheads in upper panel in Figure 5C). These results imply that the amoebae obtained the energy source from a human neurospheroid in a different way.

## 4. Discussion

Forming the neurospheroid in a hanging drop of the 3DHSP allows assessment of the cytotoxicity of *B. mandrillaris* trophozoites,

a clinical isolate of the parasitic amoeba. The 3DHSP offers advantages for host–parasite interaction in a context relevant to the 3D organizing cells in a given tissue. In the hanging drop, the *B. mandrillaris* trophozoites decreased the viability of human cells in the neurospheroid. The 3DHSP is capable of separating the amoebic trophozoites from the neurospheroid, allowing accurate measurement of host and parasite survivability. Following separation, it is also feasible to study the mechanism of host cell ingestion of the amoeba. Although the separation efficiency of trophozoites and amoebas needs further improvement, the dual phenotype platform is likely applicable for screening a lead compound that has low cytotoxic and amoebicidal effects in a single plate.

Several strains of *B. mandrillaris* have been isolated from patients and from the environment across continents. *B. mandrillaris* trophozoites can be maintained in a standard laboratory as a routine procedure, allowing the study of their pathogenicity (Greninger et al., 2015). Here, the *B. mandrillaris* strain was isolated from the third case of *Balamuthia* amoebic encephalitis in Thailand (Intalaporn et al., 2004; Krasaelap et al., 2013) and used as a representative virulent strain (Law et al., 2023). We have been able to grow this amoeba strain in feeder-free conditions using BM-3 medium in addition to coculture with human lung carcinoma A549 and neuroblastoma SH-SY5Y cells (Pengsaart et al., 2022). Regardless of the culture conditions, the *B. mandrillaris* trophozoites exert a cytotoxic effect on the human neurospheroid.

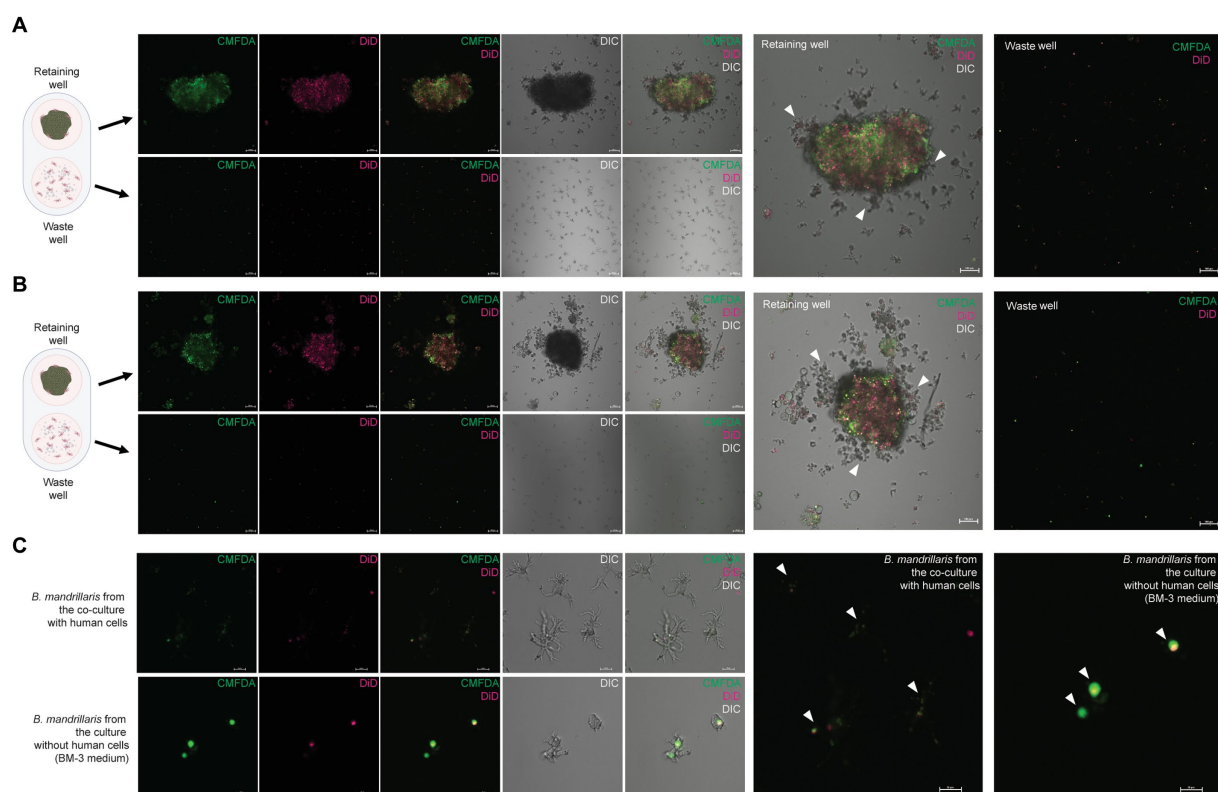


FIGURE 5

Cytophagy of the *B. mandrillaris* trophozoites in the 3DHSP. (A) Representative images of human neurospheroids cocultured with *B. mandrillaris* trophozoites obtained from culture with human neuroblastoma SH-SY5Y cells. Scale bars, 100 µm. (B) Representative images of human neurospheroids cocultured with *B. mandrillaris* trophozoites obtained from the feeder-free culture (BM-3 medium). Scale bars, 100 µm. (C) Zoomed-in images of *B. mandrillaris* trophozoites. The upper panels are representative images of the trophozoites obtained from (A), while the lower panels are images of the trophozoites obtained from (B). Microscopic images were captured in differential interference contrast (DIC) and fluorescence modes. The 3DHSP was tilted for 90 min. Scale bars, 20 µm. CMFDA, the protein-binding fluorophore, and DiD, the lipid-binding fluorophore.



A decrease of neurospheroid size was observed in the presence of *B. mandrillaris* originating from BM-3 medium in both tilted and non-tilted plates. However, the size of neurospheroid cocultured with *B. mandrillaris* originating from human feeder cells decreased only in the tilted plates. This difference is likely due to rapid damage of neurospheroid caused by the trophozoite derived from the BM-3 medium. Moreover, there was discrepancy in the data of DNA detection and ATP measurement in this study. In Figure 4B, a factor of difference of 600 was observed at 45 min in the waste well in the tilted plated in comparison to the non-tilted plate. This difference is much higher than in the other conditions, especially, at 90 min in the same condition, where only a factor of difference of 20 was observed. This difference between 45 min and 90 min for spheroids incubated with *B. mandrillaris* originating from human cells was not in agreement with the ATP results in Figure 4A. This discrepancy issue might be due to sensitivity and nature of the parameter detected. The amount of DNA represents dead and alive cells (Cangelosi and Meschke, 2014) while ATP levels are dependent on metabolic activity of cells (Chan et al., 2013).

However, there is a noticeable question regarding which culture to use. The trophozoites harvested from the coculture with human SH-SY5Y neuroblastoma cells cannot be used until the monolayer of human cells is removed from the culture dish. Moreover, the trophozoites obtained from coculture with human SH-SY5Y cells tend to form cell clumps in the hanging drop of the 3DHSP, limiting the separation of trophozoites from the neurospheroid. Thus, optimizing the tilting time of the 3DHSP is recommended. In contrast, our results showed that the BM-3-derived trophozoites could be separated from the neurospheroid at a higher efficiency in the 3DHSP. No cell clump was observed when culturing the BM-3-derived trophozoites in the hanging drop on the 3DHSP. Due to the ease of cell preparation, the feeder-free culture in BM-3 is suitable for coculture with neurospheroids. Nevertheless, BM-3 medium contains many nutrients and is not commercially available (Schuster and Visvesvara, 1996). Thus, the use of BM-3 medium is limited. The reason underlying the clump of the trophozoites remains unknown. It is likely that trophozoites tend to form clumps when lacking nutrient sources or in response to changes in the microenvironment. However, this opens a question that needs to be further elucidated since this cell clump might also be a mechanism of drug resistance, as observed in quorum sensing of bacteria (Donabedian, 2003; Bassler and Losick, 2006).

Physiologically relevant models are essential for validating the therapeutic effect of lead pharmaceutical substances. It is also feasible to use immunodeficient and immunocompetent mice to study the pathogenesis of granulomatous encephalitis (Janitschke et al., 1996) and the route of infection (Kiderlen and Laube, 2004). However, the use of animal models in drug screening is time-consuming and expensive and is possible only in laboratories with standard animal care. The culture of brain tissue or neurons may recapitulate *in vivo* conditions. A drug screening study used human brain tissue explants to indicate the therapeutic effect of nitroxoline (Laurie et al., 2018), leading to successful treatment of *Balamuthia* amoebic encephalitis in a human patient (Spottiswoode et al., 2023). Thus, a greater degree of physiological relevance allows higher similarity between *in vitro* and *in vivo* assays. Nevertheless, the *in vitro* culture of human brain tissue faces several concerns, such as tissue shortage, limited number of cells, and difficulty in culture and expansion. Cancer cell lines are more convenient for culture and expansion, supporting high-throughput drug screening. Human neuroblastoma SH-SY5Y cells originate from

immature neurons (Biedler et al., 1978; Gilany et al., 2008). However, *in vitro* models of human neuroblastoma SH-SY5Y cells are applicable for elucidating the mechanisms of neuron dysfunction (Elyasi et al., 2020). Therefore, the use of neuroblastoma cells reduces the need for primary neurons and is more suitable for drug screening. After drug screening in the cancer cell-based platform, the use of brain tissue explants or cerebral organoids is more relevant to the brain and can be used as a secondary screening phase without animal models.

Several cell culture platforms allow the generation of spheroids, including the embedding of cells in semisolid medium. A limit of the semisolid platform is the physical barrier against trophozoite penetration. Thus, a liquid drop allows cell contact without the physical barrier. Similar to other spheroid models, 3DHSP-derived neurospheroids have a hypoxic core (Anada et al., 2012; Leek et al., 2016). The advantage of hanging drop-based spheroid formation is the lack of dependence on a scaffold. Nevertheless, it remains difficult to capture images of a spheroid in a drop using an inverted microscope. Moreover, the drop is prone to evaporation, requiring a humid environment. Due to the tight adherence of trophozoites to the neurospheroid, it was difficult to separate the trophozoites from the neurospheroid. Moreover, there were trophozoites surrounding the neurospheroid without cell contact after the 3DHSP was tilted. The sizes of trophozoites in the retaining well and the waste well were similar, implying that the trophozoites could be drained out from the retaining well. The presence of trophozoites in the retaining well might suggest a need to increase the flow but not the pore size.

Originally designed to assess the cytotoxic effect of CAR T cells against cancer spheroids (Chen et al., 2022), the 3DHSP is unsuitable for separating trophozoites from neurospheroids due to cell-to-cell interaction (Pongsart et al., 2022; Pongsart and Kulkeaw, 2022); however, it may be useful in a drug screen for assessing both cytotoxic and amoebic effects by adjusting the size of the neurospheroids and using the ATP of trophozoites as a readout, despite the low separation efficiency, thereby reducing interexperimental variation (Iversen et al., 2006; Larsson et al., 2020). However, improvements are needed for the use of 3DHSPs with fluorescence- or chemiluminescence-based plate readers for ATP measurement and high-content imaging for measuring the size of the neurospheroids.

## Data availability statement

The original contributions presented in the study are included in the article/Supplementary material, further inquiries can be directed to the corresponding author.

## Ethics statement

*Balamuthia mandrillaris* trophozoites were isolated from biopsied brain tissue of a human subject who gave written informed consent to participate (COA no. Si806/2020). The experiments involving *B. mandrillaris* trophozoites were approved by the Siriraj Institutional Review Board (COA. no. 146/2022). Ethical approval was not required for the studies on human cells obtained from commercially available cell lines in accordance with the local legislation and institutional requirements because only commercially available established cell lines were used.

## Author contributions

NW, WP, and KK: conceptualization. NW, WP, ZC, and SH: methodology. NW and WP: writing—original draft preparation and visualization. KK, ZC, and SP: writing—review and editing. KK and SP: supervision. KK: funding acquisition. All authors have read and approved the published version of the manuscript.

## Funding

The research project was supported by the Siriraj Research Fund, Grant no. (IO)R016433023, Faculty of Medicine Siriraj Hospital, Mahidol University and Industrial Strategic Technology Development for the program-development of disease models based on a 3D microenvironmental platform mimicking multiple organs and evaluation of drug efficacy (grant no. 20008413) funded by the Ministry of Trade, Industry and Energy (MOTIE, Korea). KK is supported by a grant for Mid-career Talented Researchers provided by the National Research Council of Thailand and Mahidol University (Grant no. R016541029).

## Acknowledgments

The authors would like to thank all staff at the Department of Parasitology, Faculty of Medicine Siriraj Hospital, for technical support. The human lung carcinoma A549 cell line was kindly

provided by Wanpen Chaicumpa, the Head of Center of Excellence on Therapeutic Proteins and Antibody Engineering, Department of Parasitology, Faculty of Medicine Siriraj Hospital, Mahidol University. All illustrations were created with [BioRender.com](https://www.biorender.com).

## Conflict of interest

The authors declare that the research was conducted in the absence of any commercial or financial relationships that could be construed as a potential conflict of interest.

## Publisher's note

All claims expressed in this article are solely those of the authors and do not necessarily represent those of their affiliated organizations, or those of the publisher, the editors and the reviewers. Any product that may be evaluated in this article, or claim that may be made by its manufacturer, is not guaranteed or endorsed by the publisher.

## Supplementary material

The Supplementary material for this article can be found online at: <https://www.frontiersin.org/articles/10.3389/fmicb.2023.1190530/full#supplementary-material>.

## References

- Anada, T., Fukuda, J., Sai, Y., and Suzuki, O. (2012). An oxygen-permeable spheroid culture system for the prevention of central hypoxia and necrosis of spheroids. *Biomaterials* 33, 8430–8441. doi: 10.1016/j.biomaterials.2012.08.040
- Bassler, B. L., and Losick, R. (2006). Bacterially speaking. *Cells* 125, 237–246. doi: 10.1016/j.cell.2006.04.001
- Biedler, J. L., Roffler-Tarlov, S., Schachner, M., and Freedman, L. S. (1978). Multiple neurotransmitter synthesis by human neuroblastoma cell lines and clones. *Cancer Res.* 38, 3751–3757.
- Cangelosi, G. A., and Meschke, J. S. (2014). Dead or alive: molecular assessment of microbial viability. *Appl. Environ. Microbiol.* 80, 5884–5891. doi: 10.1128/AEM.01763-14
- Chan, G. K., Kleinheinz, T. L., Peterson, D., and Moffat, J. G. (2013). A simple high-content cell cycle assay reveals frequent discrepancies between cell number and ATP and MTS proliferation assays. *PLoS One* 8:e63583. doi: 10.1371/journal.pone.0063583
- Chen, Z., Han, S., Sanny, A., Chan, D. L., van Noort, D., Lim, W., et al. (2022). 3D hanging spheroid plate for high-throughput CAR T cell cytotoxicity assay. *J. Nanobiotechnol.* 20:30. doi: 10.1186/s12951-021-01213-8
- Cuoco, J. A., Klein, B. J., LeBel, D. P., Faulhaber, J., Apfel, L. S., and Witcher, M. R. (2022). Successful treatment of a Balamuthia mandrillaris cerebral abscess in a pediatric patient with complete surgical resection and antimicrobial therapy. *Pediatr. Infect. Dis. J.* 41, e54–e57. doi: 10.1097/INF.00000000000003418
- Donabedian, H. (2003). Quorum sensing and its relevance to infectious diseases. *J. Infect.* 46, 207–214. doi: 10.1053/jinf.2002.1120
- Doyle, J. S., Campbell, E., Fuller, A., Spelman, D. W., Cameron, R., Malham, G., et al. (2011). Balamuthia mandrillaris brain abscess successfully treated with complete resection and prolonged combination antimicrobial therapy. *J. Neurosurg.* 114, 458–462. doi: 10.3171/2010.10.JNS10677
- Elyasi, L., Jahanshahi, M., Jamei, S. B., Hamid Abadi, H. G., Nikmahzar, E., Khalili, M., et al. (2020). 6-OHDA mediated neurotoxicity in SH-SY5Y cellular model of Parkinson disease suppressed by pretreatment with hesperidin through activating L-type calcium channels. *J. Basic Clin. Physiol. Pharmacol.* 32, 11–17. doi: 10.1515/jbcp-2019-0270
- Ferrins, L., Buskes, M. J., Kapteyn, M. M., Engels, H. N., Enos, S. E., Lu, C., et al. (2023). Identification of novel anti-amoebic pharmacophores from kinase inhibitor chemotypes. *Front. Microbiol.* 14:1149145. doi: 10.3389/fmicb.2023.1149145
- Gilany, K., Van Elzen, R., Mous, K., Coen, E., Van Dongen, W., Vandamme, S., et al. (2008). The proteome of the human neuroblastoma cell line SH-SY5Y: an enlarged proteome. *Biochim. Biophys. Acta* 1784, 983–985. doi: 10.1016/j.bbapap.2008.03.003
- Gompf, S. G., and Garcia, C. (2019). Lethal encounters: the evolving spectrum of amoebic meningoencephalitis. *IDCases* 15:e00524. doi: 10.1016/j.idcr.2019.e00524
- Greninger, A. L., Messacar, K., Dunnebacke, T., Naccache, S. N., Federman, S., Bouquet, J., et al. (2015). Clinical metagenomic identification of Balamuthia mandrillaris encephalitis and assembly of the draft genome: the continuing case for reference genome sequencing. *Genome Med.* 7:113. doi: 10.1186/s13073-015-0235-2
- Haston, J. C., and Cope, J. R. (2023). Amebic encephalitis and meningoencephalitis: an update on epidemiology, diagnostic methods, and treatment. *Curr. Opin. Infect. Dis.* 36, 186–191. doi: 10.1097/QCO.0000000000000923
- Intalapaporn, P., Suankratay, C., Shuangshoti, S., Phantumchinda, K., Keelawat, S., and Wilde, H. (2004). Balamuthia mandrillaris meningoencephalitis: the first case in Southeast Asia. *Am. J. Trop. Med. Hyg.* 70, 666–669. doi: 10.4269/ajtmh.2004.70.666
- Iversen, P. W., Eastwood, B. J., Sittampalam, G. S., and Cox, K. L. (2006). A comparison of assay performance measures in screening assays: signal window, Z' factor, and assay variability ratio. *J. Biomol. Screen.* 11, 247–252. doi: 10.1177/1087057105285610
- Janitschke, K., Martinez, A. J., Visvesvara, G. S., and Schuster, F. (1996). Animal model Balamuthia mandrillaris CNS infection: contrast and comparison in immunodeficient and immunocompetent mice: a murine model of granulomatous amebic encephalitis. *J. Neuropathol. Exp. Neurol.* 55, 815–821. doi: 10.1097/00005072-199607000-00006
- Kapalczyńska, M., Kolenda, T., Przybyla, W., Zajackowska, M., Teresiak, A., Filas, V., et al. (2018). 2D and 3D cell cultures—a comparison of different types of cancer cell cultures. *Arch. Med. Sci.* 14, 910–919. doi: 10.5114/aoms.2016.63743
- Kiderlen, A. F., and Laube, U. (2004). Balamuthia mandrillaris, an opportunistic agent of granulomatous amebic encephalitis, infects the brain via the olfactory nerve pathway. *Parasitol. Res.* 94, 49–52. doi: 10.1007/s00436-004-1163-z
- Krasaelap, A., Prechawit, S., Chansaenroj, J., Punyahotra, P., Puthanakit, T., Chomtho, K., et al. (2013). Fatal Balamuthia amebic encephalitis in a healthy child: a case report with review of survival cases. *Korean J. Parasitol.* 51, 335–341. doi: 10.3347/kjp.2013.51.3.335
- Lagies, S., Schlimpert, M., Neumann, S., Waldin, A., Kammerer, B., Borner, C., et al. (2020). Cells grown in three-dimensional spheroids mirror in vivo metabolic response of epithelial cells. *Commun. Biol.* 3:246. doi: 10.1038/s42003-020-0973-6
- Larsson, P., Engqvist, H., Biermann, J., Werner Ronnerman, E., Forsell-Aronsson, E., Kovacs, A., et al. (2020). Optimization of cell viability assays to improve replicability and reproducibility of cancer drug sensitivity screens. *Sci. Rep.* 10:5798. doi: 10.1038/s41598-020-62848-5

- Laurie, M. T., White, C. V., Retallack, H., Wu, W., Moser, M. S., Sakanari, J. A., et al. (2018). Functional assessment of 2,177 U.S. and international drugs identifies the quinoline nitroxoline as a potent amoebicidal agent against the pathogen *Balamuthia mandrillaris*. *MBio* 9:e02051. doi: 10.1128/mBio.02051-18
- Law, C. T., Nivesvivat, T., Xiong, Q., Kulkeaw, K., Shi, L., Ruenchit, P., et al. (2023). Mitochondrial genome diversity of *Balamuthia mandrillaris* revealed by a fatal case of granulomatous amoebic encephalitis. *Front. Microbiol.* 14:1162963. doi: 10.3389/fmicb.2023.1162963
- Leek, R., Grimes, D. R., Harris, A. L., and McIntyre, A. (2016). Methods: using three-dimensional culture (spheroids) as an in vitro model of tumour hypoxia. *Adv. Exp. Med. Biol.* 899, 167–196. doi: 10.1007/978-3-319-26666-4\_10
- Liu, J., Zhang, W., Wu, S., Zeng, T., Luo, F., Jiang, Q., et al. (2023). A clinical case report of *Balamuthia* granulomatous amoebic encephalitis in a non-immunocompromised patient and literature review. *BMC Infect. Dis.* 23:245. doi: 10.1186/s12879-023-08228-6
- Mittler, F., Obeid, P., Rulina, A. V., Haguët, V., Gidrol, X., and Balakirev, M. Y. (2017). High-content monitoring of drug effects in a 3D spheroid model. *Front. Oncol.* 7:293. doi: 10.3389/fonc.2017.00293
- Peng, L., Zhou, Q., Wu, Y., Cao, X., Lv, Z., Su, M., et al. (2022). A patient with granulomatous amoebic encephalitis caused by *Balamuthia mandrillaris* survived with two excisions and medication. *BMC Infect. Dis.* 22:54. doi: 10.1186/s12879-021-07020-8
- Pengsart, W., and Kulkeaw, K. (2022). An optical and chemiluminescence assay for assessing the cytotoxicity of *Balamuthia mandrillaris* against human neurospheroids. *Bioengineering (Basel)* 9:330. doi: 10.3390/bioengineering9070330
- Pengsart, W., Tongkrajang, N., Whangviboonkij, N., Sarasombath, P. T., and Kulkeaw, K. (2022). *Balamuthia mandrillaris* trophozoites ingest human neuronal cells via a trogocytosis-independent mechanism. *Parasit. Vectors* 15:232. doi: 10.1186/s13071-022-05306-7
- Phan, I. Q., Rice, C. A., Craig, J., Noorai, R. E., McDonald, J. R., Subramanian, S., et al. (2021). The transcriptome of *Balamuthia mandrillaris* trophozoites for structure-guided drug design. *Sci. Rep.* 11:21664. doi: 10.1038/s41598-021-99903-8
- Piper, K. J., Foster, H., Susanto, D., Maree, C. L., Thornton, S. D., and Cobbs, C. S. (2018). Fatal *Balamuthia mandrillaris* brain infection associated with improper nasal lavage. *Int. J. Infect. Dis.* 77, 18–22. doi: 10.1016/j.ijid.2018.09.013
- Rao, X., Huang, X., Zhou, Z., and Lin, X. (2013). An improvement of the  $2^{-\Delta\Delta CT}$  method for quantitative real-time polymerase chain reaction data analysis. *Biostat. Bioinform. Biomath.* 3, 71–85.
- Schuster, F. L., and Visvesvara, G. S. (1996). Axenic growth and drug sensitivity studies of *Balamuthia mandrillaris*, an agent of amebic meningoencephalitis in humans and other animals. *J. Clin. Microbiol.* 34, 385–388. doi: 10.1128/jcm.34.2.385-388.1996
- Schuster, F. L., and Visvesvara, G. S. (2004a). Free-living amoebae as opportunistic and non-opportunistic pathogens of humans and animals. *Int. J. Parasitol.* 34, 1001–1027. doi: 10.1016/j.ijpara.2004.06.004
- Schuster, F. L., and Visvesvara, G. S. (2004b). Opportunistic amoebae: challenges in prophylaxis and treatment. *Drug Resist. Updat.* 7, 41–51. doi: 10.1016/j.drug.2004.01.002
- Spottiswoode, N., Pet, D., Kim, A., Gruenberg, K., Shah, M., Ramachandran, A., et al. (2023). Successful treatment of *Balamuthia mandrillaris* granulomatous amoebic encephalitis with nitroxoline. *Emerg. Infect. Dis.* 29, 197–201. doi: 10.3201/eid2901.221531
- Wu, X., Yan, G., Han, S., Ye, Y., Cheng, X., Gong, H., et al. (2020). Diagnosing *Balamuthia mandrillaris* encephalitis via next-generation sequencing in a 13-year-old girl. *Emerg. Microbes Infect.* 9, 1379–1387. doi: 10.1080/22221751.2020.1775130
- Xu, C., Wu, X., Tan, M., Wang, D., Wang, S., and Wu, Y. (2022). Subacute *Balamuthia mandrillaris* encephalitis in an immunocompetent patient diagnosed by next-generation sequencing. *J. Int. Med. Res.* 50:3000605221093217. doi: 10.1177/03000605221093217
- Yang, Y., Hu, X., Min, L., Dong, X., and Guan, Y. (2020). *Balamuthia mandrillaris*-related primary amoebic encephalitis in China diagnosed by next generation sequencing and a review of the literature. *Lab. Med.* 51, e20–e26. doi: 10.1093/labmed/lmz079



## OPEN ACCESS

## EDITED BY

Ascel Samba-Louaka,  
University of Poitiers, France

## REVIEWED BY

Marcel I. Ramirez,  
Oswaldo Cruz Foundation, Brazil  
Patricia Talamás-Rohana,  
National Polytechnic Institute of Mexico  
(CINVESTAV), Mexico  
E. Ashley Moseman,  
Duke University, United States

## \*CORRESPONDENCE

Dennis E. Kyle  
✉ dennis.kyle@uga.edu

RECEIVED 20 July 2023

ACCEPTED 08 September 2023

PUBLISHED 27 September 2023

## CITATION

Russell AC, Bush P, Grigorean G and  
Kyle DE (2023) Characterization of the  
extracellular vesicles, ultrastructural  
morphology, and intercellular interactions of  
multiple clinical isolates of the brain-eating  
amoeba, *Naegleria fowleri*.  
*Front. Microbiol.* 14:1264348.  
doi: 10.3389/fmicb.2023.1264348

## COPYRIGHT

© 2023 Russell, Bush, Grigorean and Kyle. This  
is an open-access article distributed under the  
terms of the [Creative Commons Attribution  
License \(CC BY\)](#). The use, distribution or  
reproduction in other forums is permitted,  
provided the original author(s) and the  
copyright owner(s) are credited and that the  
original publication in this journal is cited, in  
accordance with accepted academic practice.  
No use, distribution or reproduction is  
permitted which does not comply with these  
terms.

# Characterization of the extracellular vesicles, ultrastructural morphology, and intercellular interactions of multiple clinical isolates of the brain-eating amoeba, *Naegleria fowleri*

A. Cassiopeia Russell<sup>1,2</sup>, Peter Bush<sup>3</sup>, Gabriela Grigorean<sup>4</sup> and  
Dennis E. Kyle<sup>1,2,5\*</sup>

<sup>1</sup>Center for Tropical and Emerging Global Diseases, University of Georgia, Athens, GA, United States,  
<sup>2</sup>Department of Infectious Diseases, University of Georgia, Athens, GA, United States, <sup>3</sup>School of Dental  
Medicine, University at Buffalo, Buffalo, NY, United States, <sup>4</sup>Proteomics Core Facility, University of  
California, Davis, Davis, CA, United States, <sup>5</sup>Department of Cellular Biology, University of Georgia,  
Athens, GA, United States

**Introduction:** As global temperatures rise to unprecedented historic levels, so too do the latitudes of habitable niches for the pathogenic free-living amoeba, *Naegleria fowleri*. This opportunistic parasite causes a rare, but >97% fatal, neurological infection called primary amoebic meningoencephalitis. Despite its lethality, this parasite remains one of the most neglected and understudied parasitic protozoans.

**Methods:** To better understand amoeboid intercellular communication, we elucidate the structure, proteome, and potential secretion mechanisms of amoeba-derived extracellular vesicles (EVs), which are membrane-bound communication apparatuses that relay messages and can be used as biomarkers for diagnostics in various diseases.

**Results and Discussion:** Herein we propose that *N. fowleri* secretes EVs in clusters from the plasma membrane, from multivesicular bodies, and via beading of thin filaments extruding from the membrane. Uptake assays demonstrate that EVs are taken up by other amoebae and mammalian cells, and we observed a real-time increase in metabolic activity for mammalian cells exposed to EVs from amoebae. Proteomic analysis revealed >2,000 proteins within the *N. fowleri*-secreted EVs, providing targets for the development of diagnostics or therapeutics. Our work expands the knowledge of intercellular interactions among these amoebae and subsequently deepens the understanding of the mechanistic basis of PAM.

## KEYWORDS

*Naegleria fowleri*, extracellular vesicles, ultrastructure, intercellular interactions, parasite

## 1. Introduction

*Naegleria fowleri* is a thermophilic free-living amoeba found ubiquitously in soil, fresh, and brackish waters (Fowler and Carter, 1965; Grace et al., 2015; Siddiqui et al., 2016; Xue



et al., 2018). This amphizoic pathogen is the etiologic agent for the fulminant disease known as primary amoebic meningoencephalitis (PAM), a neurological illness that commonly affects young healthy individuals (Visvesvara et al., 2007; Capewell et al., 2015). Infections in humans occur when contaminated warm water enters the nose—usually during recreational water sports or nasal irrigation/ablutions—and the invasive trophozoite stage of the parasite binds to and colonizes the nasal epithelium (Visvesvara et al., 2007; Pugh and Levy, 2016). *N. fowleri* then travels through the nasal mucosa and along the neuro-olfactory nerves through the cribriform plate to reach the olfactory bulbs in the frontal lobes where it feeds on neurons and damages brain membranes and meninges (Barnett et al., 1996; Capewell et al., 2015; Grace et al., 2015; Siddiqui et al., 2016). Although the pathogenicity of the amoeba contributes to some of the damage, the host's profound immune response ultimately leads to death due to increased intracranial pressure and brain herniation resulting in pulmonary edema and cardiopulmonary arrest (Visvesvara et al., 2007). The incubation period of PAM ranges from 2 to 15 days with >97% of cases resulting in death approximately one week after the initial appearance of symptoms (Ma et al., 1990; Siddiqui et al., 2016). Hundreds of cases have been documented worldwide with the majority of cases being reported in countries with developed medical systems (Visvesvara et al., 2007) including the United States, Australia, and Europe, thus it can be assumed that there are many more cases globally that go undiagnosed, mistaken for bacterial or viral meningitis, and unreported in less developed tropical regions. Though a rare infection, it most likely kills thousands worldwide, but is overlooked due to lack of routinely performed post-mortem examination of inexplicable neurological deaths. In the last 20 years, a rise in the number of reported PAM cases can be attributed to increased awareness and the onset of global warming (Kemble et al., 2012) leading to the expansion of suitable climates for *N. fowleri* (Booth et al., 2015; Cope and Ali, 2016).

Various proteins have been identified that aid *N. fowleri* in the attachment to host cells, in invasion of the host central nervous system (CNS), and in obtaining nutrients from target cells (Sohn et al., 2010; Jamerson et al., 2012; Lam et al., 2017), but little is known regarding the mechanism of secretion of vesicles containing these proteins and other cargoes. Extracellular vesicles (EVs), which are membrane-bound particles shed from cells, are known to carry cargo that consists of proteins, DNA, mRNAs, and microRNAs (van Niel et al., 2018; Malkin and Bratman, 2020). These particles, known as exosomes and microvesicles, merge with recipient cells and deliver their contents, thereby altering the function of the recipient cell (Mathieu et al., 2019). Numerous pathogens and eukaryotic parasites are known to secrete EVs to mediate host responses to infection and to communicate intercellularly (Marcilla et al., 2014; Quintana et al., 2017; Gonçalves et al., 2018; Lin et al., 2019; Rai and Johnson, 2019). Additionally, recent reports show that *N. fowleri* secretes EVs (Nf-EVs) that are immunogenic, contain at least 200 proteins, and are taken up via phagocytosis by macrophages (Lertjuthaporn et al., 2022; Retana Moreira et al., 2022), but no research has been performed that explores the mechanism of EV release, or the uptake of Nf-EVs by amoebae or multiple mammalian cell lines. The uptake of secretions by multiple cell lines could be important because *N. fowleri* must traverse numerous types of cells before reaching the brain (Martinez et al., 1973). Moreover, little has been done to elucidate specific physical

structures that amoebae may exhibit when in the process of invading, interacting with, or actively feeding upon mammalian cells versus typical morphology of axenically cultured amoebae. Information about specific morphological changes as well as the mechanism by which immunogenic Nf-EVs are secreted could be vital in illuminating novel structures and downstream processes to target by drugs and potential prophylactics.

Herein, we use scanning electron microscopy (SEM) to characterize the ultrastructural morphology of five clinical isolates of *N. fowleri* in both axenic culture and when feeding on various mammalian cell lines. Isolates of *N. fowleri* are known to have differences in drug susceptibilities and growth rate (Duma and Finley, 1976; Schuster et al., 2006; Russell and Kyle, 2022), thus we selected five of varying genotypes for further characterization in this study: Nf69 (genotype IV/5), V067 (III/3), HB4 (III/3), V631 (I/2), and 6088 (II/1). Additionally, we propose the secretion of clusters of Nf-EVs from the amoebae via multivesicular bodies, plasma membrane budding and a novel secretion technique in which clusters of uroid and/or adhesive filaments attach to the substrate and either break off from the cell in an intact form, or vesicularize in a beaded manner. Furthermore, we show the uptake of Nf-EVs by various mammalian cell lines and the real-time response of three of these cell lines when taking up Nf-EVs over time. Lastly, we provide a proteomic profile of >2,000 proteins found within Nf-secreted EVs which could be used as a resource for the development of novel therapeutics and protein-based diagnostics.

## 2. Materials and methods

### 2.1. *Naegleria fowleri* cultivation

All clinical isolates were obtained as previously described in Russell and Kyle (2022). Trophozoites were cultured axenically as previously described with some changes according to desired uses. Shortly, trophozoites were grown from stocks axenically at 34°C and 5% CO<sub>2</sub> in non-vented 75-cm<sup>2</sup> tissue culture flasks (Olympus, El Cajon, CA, United States; cat#:25-208) with Nelson's complete medium (NCM) supplemented with 10% fetal bovine serum (FBS; Corning, Oneonta, NY, United States; cat#:35-016-CV) and 1,000 U/mL penicillin and 1,000 mg/mL streptomycin (penstrep; Gibco, Gaithersburg, MD, United States; cat#:15140-122) until 80–90% confluent.

### 2.2. Mammalian cell cultivation

All mammalian cells were grown in vented 75-cm<sup>2</sup> tissue culture flasks (ThermoFisher, Waltham, MA, United States; cat#:156367) at 37°C and 5% CO<sub>2</sub>. A549 cells (Human lung carcinoma cells; ATCC CCL-185) were purchased from American Type Culture Collection (ATCC) and grown in F12K media (Corning, Oneonta, NY, United States; cat#:10-025-CV) supplemented with 10% FBS and 1% penstrep. B103 cells (rat neuroblastoma cells) were purchased from AddexBio (cat#:C0005003) and were grown in DMEM (Corning, Oneonta, NY, United States; cat#:10-013-CM) supplemented with 10% FBS and 1% penstrep. HFF cells (Human foreskin fibroblasts; HFF-1

ATCC SCRC-1041) were purchased from ATCC and were cultured in DMEM supplemented with 15% FBS and 1% penstrep. Vero cells (green monkey kidney cells; E6; ATCC CRL-1586) were purchased from ATCC and were cultured in DMEM supplemented with 10% FBS and 1% penstrep. For passaging, all cell types were first washed with pre-warmed PBS to remove residual serum and then incubated with pre-warmed 0.25% Trypsin–EDTA (Gibco, Gaithersburg, MD, United States; cat#:25200-056) for 5 min at 37°C. Following incubation, flasks were lightly tapped until all cells were detached and respective pre-warmed media supplemented with FBS was added to inactivate the trypsin prior to centrifugation at 37°C for 5 min at 3,900 rpm and resuspension in respective media.

## 2.3. Preparation of samples for SEM

For imaging axenic cultures,  $5 \times 10^5$  amoebae were allowed to attach to 13 mm Thermanox coverslips (Electron Microscopy Sciences, Hatfield, PA, United States; cat#:50-949-480) in 12-well plates prior to fixation. For feeding assays,  $2.5\text{--}6 \times 10^5$  mammalian cells were seeded into plates containing coverslips and allowed to attach/grow for 18–24 h before adding  $3\text{--}6 \times 10^5$  amoebae that were allowed to feed for various timepoints prior to fixation. Media was initially gently removed from samples and replaced with 2.5% glutaraldehyde (Electron Microscopy Sciences, Hatfield, PA, United States; cat#:16220) diluted in respective base media (no FBS or antibiotics added) and incubated for 1 h at RT. This was replaced with 2.5% glutaraldehyde diluted in 0.1  $\mu\text{m}$  filtered 1X PBS (Gibco, Gaithersburg, MD, United States; cat#:10010-023) and incubated for 10 min at RT prior to being washed with PBS two times, each with a 10 min incubation period. Samples were then incubated for 5 min each with serially increasing concentrations (30, 50, 70, 90%) of molecular biology grade absolute ethanol (EtOH; Fisher BioReagents, Pittsburgh, PA; cat#:BP2818-500) diluted in 0.1  $\mu\text{m}$  filtered MilliQ H<sub>2</sub>O. This was followed by two incubation periods of 5 min each in 100% EtOH. A final incubation step of 5 min in hexamethyldisilazane (Electron Microscopy Sciences, Hatfield, PA, United States; cat#:16700) was performed, liquid was removed, and samples were allowed to air dry in fume hood for 30 min – 1 h before being mounted on carbon-conductive tape (Ted Pella, Redding, CA, United States; cat#:16084-8) on microscope slides. Samples were transported to SEM facility, carbon-coated and imaged with a Hitachi SU70 scanning electron microscope at 2 kV. For preparation of EVs for imaging, EVs were diluted in 1 mL of 0.1  $\mu\text{m}$ -filtered 1X PBS and this dilution was passed over a 13 mm 0.2  $\mu\text{m}$  Whatman Nucleopore Track Etch Membrane (Cytiva, Marlborough, MA, United States; cat#:10417001) mounted in a 13 mm Swinnex Filter Holder (MilliporeSigma, Burlington, MA, United States; cat#:SX0001300) using a 3 mL syringe. Following this step, a new syringe containing 2.5% glutaraldehyde in 0.1  $\mu\text{m}$  filtered PBS was attached and some of the contents were passed over the filter before capping and allowing to rest for 2 h at 4°C. Subsequent steps through imaging were performed in parallel with previously described samples in plates starting at 2.5% glutaraldehyde in PBS 10 min incubation step. Measurements were either performed upon pre-calibrated micrographs using the Quartz PCI SEM software (v8) or by manually calibrating to scale bars with ImageJ (v1.53k). Figures were generated using Adobe Photoshop (v23.5.2).

## 2.4. EV extraction

### 2.4.1. Conditioned media preparation

To generate conditioned media for EV extractions, amoebae were extracted from flasks containing NCM supplemented with normal FBS by placing flasks on ice for ~15 min to detach adherent cells which were collected via centrifugation at 4°C for 5 min at 4,000 rpm. The resulting supernatant was discarded, and the amoebae pellets were washed two times with 0.1  $\mu\text{m}$ -filtered 1X PBS to remove any residual FBS EVs or proteins. These washed cells were then placed into a non-vented 225-cm<sup>2</sup> tissue culture flask (Corning, Oneonta, NY, United States; cat#:431081) containing  $2 \times 0.1 \mu\text{m}$  filtered ~50 mL of Nelson's Complete Media supplemented with  $2 \times 0.2 \mu\text{m}$  filtered 10% EV-depleted FBS (Gibco, Gaithersburg, MD, United States; cat#:A2720801) and 5% penstrep and allowed to adapt to the differing conditions (with media changes as needed to remove debris/dead cells) and grow until ~80–90% confluent. This flask was then passaged to 5–10,225-cm<sup>2</sup> flasks each containing ~200 mL of NCM supplemented with 10% EV-depleted FBS and 5% penstrep and these flasks were allowed to grow for 5–15 days with daily gentle swirling/agitation to induce growth until a peak yield was reached (based on morphology/visual inspection of health of amoebae) and flasks were >90% confluent. To harvest cells and conditioned media, flasks were placed on ice for 30 min to thoroughly cool the contents, and the cell suspensions were spun at 3,900 rpm for 15 min at 4°C in 500 mL bottles (VWR, Radnor, PA, United States; cat#:525-1598). The resulting cell pellet was separated, and all pellets were combined for a final count (in duplicate) via hemocytometer for each prep. The supernatant was removed and spun for an additional 15 min at 10,000 g at 4°C to remove remaining cellular debris. The final supernatant was then sterile filtered through a 0.45  $\mu\text{m}$  filter (ThermoFisher, Waltham, MA, United States; cat#:167-0045) to remove any remaining large particles or aggregates and create amoeba-conditioned media that was stored at 4°C for no more than 48 h prior to ultracentrifugation.

### 2.4.2. Ultracentrifugation protocol

Using 70 mL polycarbonate centrifuge tubes (Beckman Coulter, Brea, CA, United States; cat#:355655), conditioned media was spun using a Ti45 fixed-angle rotor in an Optima XE-90 ultracentrifuge at ~118,000 g/39,000 rpm for 1 h 34 min with max acceleration and deceleration at 4°C. Additional spins were performed as needed by pouring off supernatant and adding remaining conditioned media until the entire volume was processed into a pellet. The resulting pellet was washed for 30 min at 4°C in 2–3 mL of ice-cold 0.1  $\mu\text{m}$  sterile-filtered 1X PBS on a shaker, followed by another spin and one final wash/spin to remove secreted proteins and other components. After the final spin, the supernatant was discarded, and the EV pellet was resuspended in 3 mL of 1X PBS by incubating at 4°C on a shaker for 45 min–1 h. The resulting EV suspension was then concentrated down to 500  $\mu\text{L}$  using a Amicon Ultra-4 3 kDa centrifugal filter unit (MilliporeSigma, Burlington, MA, United States; cat#:UFC800396) that was previously primed with 3 mL of PBS that was centrifuged out to remove particulates from the filter.

### 2.4.3. Size exclusion chromatography

Size Exclusion Chromatography was then performed on the 500  $\mu\text{L}$  concentrated suspension to clean up sample and remove secreted proteins using a qEVoriginal 70 nm column (Izon Science,

Christchurch, New Zealand) according to manufacturer protocols. In short, column was first equilibrated to room temperature and then washed with three column volumes (10 mL each) of sterile 0.1  $\mu$ m filtered 1X PBS. The concentrated 0.5 mL suspension from the ultracentrifugation protocol was then added to the column followed by 2.5 mL of PBS. The next 3–4 fractions (each consisting of 0.5 mL) were then collected depending on whether a purer EV suspension was desired or a higher yield. These fractions were pooled and transferred to another Amicon Ultra-4 3 kDa centrifugal filter and concentrated to ~100–250  $\mu$ L according to manufacturer's protocols.

#### 2.4.4. EV protein concentration measurement

Protein contents of EVs were measured using the Bio-Rad Protein Assay Kit II (BioRad, Hercules, CA, United States; cat#:5000002) according to the manufacturer's microtiter plate protocol. Briefly, 5  $\mu$ L of the 100–250  $\mu$ L EV suspension plus 5  $\mu$ L of 0.1  $\mu$ m filtered 1X PBS was added to Corning 96-well clear polystyrene microplates (MilliporeSigma, Burlington, MA, United States; cat#:CLS3370) in duplicate, and a serial dilution of the provided bovine serum albumin (BSA) was performed in triplicate with 10  $\mu$ L of each standard being added to three wells each prior to adding 200  $\mu$ L of the dye reagent solution. Absorbance was measured after a 5 min incubation at 595 nm using a SpectraMax I3X plate reader (Molecular Devices, Sunnyvale, CA, United States), and protein concentrations of samples were determined by creating a standard curve of the BSA.

#### 2.4.5. Nanoparticle tracking analysis

A NanoSight NS300 (Malvern Pananalytical, Malvern, United Kingdom) instrument equipped with a syringe pump and utilizing NTA software v3.2 was used to determine particle size and concentration according to the following protocol. While 3 mL of 0.1  $\mu$ m filtered 1X PBS was running through the machine with an infusion rate of 1,000, a 1:100 (10  $\mu$ L EVs in 990  $\mu$ L PBS) dilution was made before loading sample into the syringe pump and allowing ~300  $\mu$ L to run through the line until particles were visible under camera. In the case of a highly concentrated sample in which particles are not easily identifiable and differentiated from one another, a new dilution of 1:1000 (1  $\mu$ L of EVs in 999  $\mu$ L PBS) was created and tested. A camera level of 14 was used for 10 captures with durations of 60 s each with a syringe pump infusion rate of 100. Once captures were collected, a detection threshold of 4 to 5 was selected depending on sensitivity required to detect the majority of particles in sample frames prior to data processing.

#### 2.4.6. SDS-PAGE gel

Protein contents of EVs were visualized on SDS PAGE gels prior to sending samples for mass spectrometry to confirm concentration and expected complexity of EV proteome. To obtain protein lysates of serial dilutions of amoebae, cell pellets were subjected to three freeze–thaw cycles (–80°C to 37°C) prior to resuspending in PBS. EV and cell lysate samples were first mixed with 4x Laemmli Sample Buffer (BioRad, Hercules, CA, United States; cat#:1610747) that was pre-mixed 1:10 (v/v) with 2-mercaptoethanol according to manufacturer protocols. Samples were then vortexed for 3 s prior to incubating at 70°C for 10 min followed by another 3 s vortex. Mini-PROTEAN 4–15% TGX Stain-Free protein gels (BioRad, Hercules, CA, United States; cat#:4568085) were prepared by rinsing with diH<sub>2</sub>O prior to

submerging in SDS-PAGE running buffer and manually rinsing each well of the gel. Samples, 1  $\mu$ L of BenchMark Protein Ladder (Invitrogen, Waltham, MA, United States; cat#:10747012) or blanks (sample buffer with PBS) were loaded to each well and gel was run at 100 V first for 2–3 min followed by 200 V for 20–30 min prior to imaging with a Bio-Rad ChemiDoc Imaging System.

## 2.5. Fluorescence microscopy of nanotubes

Amoebae were grown on glass coverslips under normal culturing procedures in 6-well plates until ~70–80% confluent. For fluorescence microscopy, samples were first fixed with 4% PFA and 0.5% glutaraldehyde for 15 min followed by a wash with PBS and a subsequent incubation with 2  $\mu$ g/mL Hoescht 33342 (Invitrogen, Waltham, MA, United States; cat#:H21492) for 30 min. This was followed by another wash and a subsequent incubation step with 4  $\mu$ L of the 1,000X DMSO suspension of SPY620-actin stain (Cytoskeleton Inc., Denver, CO, United States; cat#:CY-SC505) in a 1 mL stain solution for 30–45 min. A final wash with PBS was performed prior to mounting and imaging with either the DeltaVision II (pd20621) microscope or the Carl Zeiss Elyra 7 microscope. For the DeltaVision II, we show the maximum intensity projection of z-stacks imaged with the 100X objective that were deconvolved using the SoftWorx software (settings: enhanced ratio(aggressive), 10 cycles, medium(200 nm) noise filtering). For the Zeiss Elyra 7, a z-stack of 106 slices (9.546  $\mu$ m) was obtained with the 63X objective and the Lattice SIM<sup>2</sup> reconstruction algorithm was used to reconstruct the images and generate a 3D rendering (Grating Period: 617.32 nm, Processing: 3D, Input SNR: Medium, Iterations: 16, Regularization Weight: 0.065, Processing and Output Sampling: 4, Filter: Median, Detrend: No, Sectioning: 100, Baseline: Yes).

## 2.6. R18 EV uptake assays

### 2.6.1. R18 EV labeling and excess dye removal

Octadecyl rhodamine B chloride (R18; Biotium, Fremont, CA, United States; cat#:60033) was diluted from 10 mM to 1 mM in DMSO (5  $\mu$ L in 45  $\mu$ L DMSO). EV suspensions that were split into 20  $\mu$ g aliquots and stored at –80°C until use were allowed to thaw on ice, and PBS was added to reach a volume of 1 mL. 1  $\mu$ L of 1 mM R18 was added to each tube for a final concentration of 1  $\mu$ M. In parallel, 1  $\mu$ L of 1 mM R18 was added to 999  $\mu$ L of PBS as a control which was treated the same as samples from this step forward. All sample tubes were covered in foil to protect from light and incubated at 4°C overnight. The next morning, two PD-10 desalting columns (Cytiva, Marlborough, MA, United States; cat#:17-0851-01) were equilibrated per sample with 25 mL of 0.1  $\mu$ m filtered 1X PBS. R18:vesicle solutions were passed through an equilibrated column by first adding the 1 mL suspension followed by 1.5 mL 1X PBS before eluting with 3.5 mL 1X PBS directly into a pre-washed Amicon Ultra-4 3 kDa centrifugal filter. These samples were concentrated to 1 mL before passing through a second desalting column and being concentrated to a final volume of 500  $\mu$ L (equivalent to 1  $\mu$ g of protein in 25  $\mu$ L). Dyed EVs and control samples were stored in dark at 4°C until use (within 24 h).



### 2.6.2. Deltavision high resolution imaging

$3 \times 10^5$  B103 cells were seeded onto glass coverslips in 6-well plates and allowed to attach and grow under normal growth conditions for 24 h. Media was then removed, and cells were washed once with 1 mL of pre-warmed serum-free DMEM prior to adding 2 mL of serum-free DMEM and serum starving cells for at least 1 h prior to EV treatment. All media was removed and replaced with  $\sim 500 \mu\text{L}$  of prewarmed serum-free DMEM (or enough to just coat glass coverslip) and  $25 \mu\text{L}$  (equivalent to  $1 \mu\text{g}$ ) of R18-stained EVs were added to glass coverslips for various timepoints. At end of timepoint, samples were carefully washed thrice with prewarmed PBS prior to a combined stain/fix step with 4% PFA and  $10 \mu\text{g/mL}$  Hoescht 33342. Coverslips were mounted on glass slides and sealed with clear nail polish prior to being imaged at 100X with the DeltaVision I (pd125225) Olympus IX-71 inverted microscope. Images were obtained with consistent percent transmission and exposure settings regardless of timepoint. Images were acquired as z-stacks that were deconvolved using the SoftWorx software (settings: enhanced ratio(aggressive), 10 cycles, medium(200 nm) noise filtering). The scaling for image/wavelength attributes of each channel for the maximum intensity projections were edited to the same values for every exported photo (DAPI = 82/872/1; TRITC = 51/1044/1) to reflect any changes in fluorescence intensity consistently without introducing bias.

### 2.6.3. High-content imaging of R18-stained EV uptake by mammalian cells

Cells were seeded at 10,000 cells per well for A549, 7,500 cells per well for HFF, and 5,000 cells per well for B103 and Vero into  $\mu\text{Clear}$  black Cellstar 96-well microplates (Greiner Bio-One, Kremsmünster, Austria; cat#:655090) in  $100 \mu\text{L}$  of their respective media per well. The next morning, media was removed and replaced with respective serum-free base medias to serum starve cells for 1–3 h. Cells were then treated with  $0.25 \mu\text{g}$  ( $6.25 \mu\text{L}$ ),  $0.5 \mu\text{g}$  ( $12.5 \mu\text{L}$ ) or  $1 \mu\text{g}$  ( $25 \mu\text{L}$ ) of Nf69-secreted R18-labeled EVs starting at the longest timepoints and followed by shorter timepoints prior to the final 3 washes with  $50 \mu\text{L}$  of PBS and fixation with 4% PFA for 15 min prior to a wash with PBS followed by staining with  $10 \mu\text{g/mL}$  of Hoescht for 45 min and one final wash in PBS. Plates were then sealed with Axygen sealing film (Corning, Somerville, MA, United States; cat#:PCR-SP) prior to imaging at 20X with an ImageXpress Micro Confocal system using a DAPI filter to image Hoescht-stained nuclei and a TRITC filter to image R18-labeled membranes. The MetaXpress High-Content Image Acquisition and Analysis Software (v6.7.2.290) was used to create a custom module to analyze images and enumerate fluorescence intensity at the cell population level in a non-biased manner. Cells were detected with a cell scoring mask that first identified nuclei using the DAPI channel (size range of  $2\text{--}30 \mu\text{m}$ ; intensity 1,500–15,000 above background). The nuclei were then deemed positive or negative depending on the intensity above the local background surrounding the nucleus in the TRITC channel (size range of  $5\text{--}50 \mu\text{m}$ ; intensity of 200–425 above background). The mean integrated intensity of the fluorescent values in the TRITC channel for “positive nuclei” was calculated and the summation of these values are presented in [Supplementary Figure S4](#). The exact intensity cutoffs for the above masking strategy were calibrated to each plate and cell line using unstained controls. Four technical replicate wells were used per treatment group and two independent biological replicates were performed.

### 2.6.4. Amoebae R18-stained EV uptake visualization via ImageStream

Two days before assay, V631 amoebae were harvested, counted, and seeded into microcentrifuge tubes at concentrations of 50,000 cells per tube in a total volume of 1 mL of NCM supplemented with 10% EV-depleted FBS and penstrep. Tubes were gently agitated once a day to induce growth. Nf69 EVs were stained as described earlier and each tube was treated with  $1 \mu\text{g}$  of R18-stained EVs and incubated at  $34^\circ\text{C}$  for various timepoints. At the end of a timepoint, tubes were spun down at 14,000 rpm for 2 min and the supernatant was carefully aspirated and replaced with  $500 \mu\text{L}$  of incomplete NCM. This wash process was repeated two more times prior to adding a stain/fixative mixture that consisted of 4% PFA, 0.5% glutaraldehyde and  $2 \mu\text{g/mL}$  Hoescht and incubating at RT for 45 min. Tubes were spun down at 14,000 rpm for 2 min and washed with  $500 \mu\text{L}$  of PBS prior to a final spin and resuspension in  $100 \mu\text{L}$  of PBS. The imaging flow cytometry data acquisition template was set to collect 15,000 events at 60X magnification with channel 405 set to 10 mW, channel 561 set to 200 mW and the SSC channel set to 1 mW. Flow cytometry data was analyzed and compensated using the IDEAS software (Luminex, Austin, TX, United States; v6.2.187.0). Unstained and single-color controls were used to compensate data for each replicate. Gating was first performed to select for focused cells followed by Hoescht-positive cells as a secondary gate to exclude debris. Data was exported to FCS Express 7 Plus (*De Novo Software*, Pasadena, CA; v7.12.0007) to create histogram overlays and visualize shifts in fluorescence intensity for cell populations from each timepoint.

## 2.7. RealTime-Glo EV assay

The RealTime-Glo MT Cell Viability Assay (RTG; Promega, Madison, WI; cat#:G9712) previously described by Colon et al. and Rice et al., was used to assess whether any differences in viability of Vero, A549, or B103 cells occurred in response to exposure to Nf-secreted EVs (Colon et al., 2019; Rice et al., 2020). As shown in [Supplementary Figure S5](#), we first determined the optimal seeding density of cells within 96-well plates for each mammalian cell line by performing dilution series testing (2,500 to 40,000 cells/well) at various timepoints (6 h, 12 h, 24 h and 36 h) using the CellTiter-Glo 2.0 assay as described in our previous publication (Russell and Kyle, 2022). Being that 5,000 cells fell within the linear range of the assay at all timepoints tested (except for HFFs which were excluded from this assay due to a lack of linearity), we selected this concentration and seeded cells with four technical replicates per concentration tested in a volume of  $35 \mu\text{L}$  per well. Cells were allowed to attach and then serum-starved by adding non-supplemented base media 1–2 h prior to adding EVs. The protein concentration of freshly extracted brain passaged Nf69 EVs was determined, and dilutions were made as necessary to allow a standard volume of  $15 \mu\text{L}$  to be added to each well. The same process was followed for frozen stocks that were pulled from  $-80^\circ\text{C}$  storage and thawed on ice for testing. Prior to adding EVs, the RTG substrate and enzyme were equilibrated to  $37^\circ\text{C}$  and mixed in respective base growth medias of each cell line. EVs were added to cells and  $50 \mu\text{L}$  of the 2X RTG enzyme-substrate mixture was immediately added to obtain a 1X concentration. Plates were quickly sealed and incubated in a SpectraMax i3x plate reader (Molecular Devices, Sunnyvale, CA, United States) at  $37^\circ\text{C}$  and relative



luminescence units (RLUs) were recorded every 2.5 min for 20 h. Negative/untreated controls were seeded with four replicates per cell line and included 15  $\mu$ L PBS + cells, 15  $\mu$ L media + cells, 50  $\mu$ L media only, and 50  $\mu$ L PBS only. EV only controls were included for each replicate and consisted of 1  $\mu$ g of EVs (15  $\mu$ L) in 35  $\mu$ L of PBS. Initial dilution series testing of varying EV protein concentrations exposed to B103 cells was performed (Supplementary Figure S6) prior to proceeding with 1 and 0.5  $\mu$ g. Data was analyzed and graphed using GraphPad Prism 9 (GraphPad Software, La Jolla, CA, United States; v9.5.0).

## 2.8. Proteomic characterization of EVs

### 2.8.1. Preparation of samples

Three biological replicates of 2 L EV preps for *Nf69*-conditioned media were extracted under aseptic conditions (in biosafety cabinet, with 70% EtOH sterilized equipment, etc) and concentrated to <200  $\mu$ L in PBS prior to measuring protein concentration as described above. Aliquots of 20  $\mu$ g were frozen at  $-80^{\circ}\text{C}$  and sent on dry ice for mass spectrometry analyses at UC Davis. The protein samples were subjected to proteolysis by using suspension-trap (ProtiFi) devices. S-Trap is a powerful Filter-Aided Sample Preparation (FASP) method that consists in trapping acid aggregated proteins in a quartz filter prior enzymatic proteolysis. Here, proteins were resuspended in 50  $\mu$ L of our solubilisation buffer consisting of sodium dodecyl sulphate, 50 mM triethyl ammonium bicarbonate in water, pH 7.55. Disulfide bonds were reduced with dithiothreitol and alkylated (in the dark) with iodoacetamide in 50 mM TEAB buffer. Digestion constituted of a first addition of trypsin 1:100 enzyme: protein (wt/wt) for 4 h at  $37^{\circ}\text{C}$ , followed by a boost addition of trypsin using same wt/wt ratios for overnight digestion at  $37^{\circ}\text{C}$ . Peptides were eluted from S-Trap by sequential elution buffers of 100 mM TEAB, 0.5% formic acid, and 50% acetonitrile 0.1% formic acid. The eluted tryptic peptides were dried in a vacuum centrifuge and re-constituted in 0.1% trifluoroacetic acid. A small portion of the extract is used for fluorometric peptide quantitation (ThermoFisher, Waltham, MA, United States), to confirm the amount of peptide injected into the LCMS system.

### 2.8.2. LC-MS

Liquid chromatographic peptide separation was done on an ultra-high pressure nano-flow Easy nLC (Bruker Daltonics, Billerica, MA, United States). Flow rate of buffers was 0.85  $\mu$ L/min, on a PepSep 150  $\mu$ m x 25 cm C18 column (Bruker, Billerica, MA, United States) with 1.5  $\mu$ m particle size (100 Å pores; Bruker Daltonics, Billerica, MA, United States), heated to a constant temperature of  $40^{\circ}\text{C}$ ; nanoESI via a ZDV spray emitter (Bruker Daltonics, Billerica, MA, United States). Mobile phases A and B consisted of water with 0.1% formic acid (v/v) and 80/20/0.1% ACN/water/formic acid (v/v/vol), respectively. Peptides were separated using a 35 min gradient: from 0–2 min increase buffer B to 5%, 2–5 min 5–10% B, 5–28 min 10–36% B, 28–35 min 80% B. This was followed by direct elution into the mass spectrometer. MS was performed on a hybrid trapped ion mobility spectrometry-quadrupole time of flight mass spectrometer (timsTOF Pro; Bruker Daltonics, Billerica, MA, United States) with a modified nano-electrospray ion source (CaptiveSpray; Bruker Daltonics, Billerica, MA, United States). In the experiments described

here, the mass spectrometer was operated in PASEF mode. Desolvated ions entered the vacuum region through the glass capillary and deflected into the TIMS tunnel which is electrically separated into two parts (dual TIMS). Here, the first region is operated as an ion accumulation trap that primarily stores all ions entering the mass spectrometer, while the second part performs trapped ion mobility analysis. Data-independent analysis (DIA) was performed on a nanoElute UHPLC coupled to a timsTOF Pro. The acquisition scheme used for DIA consisted of four 25 m/z precursor windows per 100 ms TIMS scan. Sixteen TIMS scans, creating 64 total windows, layered the doubly and triply charged peptides on the m/z and ion mobility plane. Precursor windows began at 400 m/z and continued to 1,200 m/z. The collision energy was ramped linearly as a function of the mobility from 63 eV at  $1/K0=1.5$  versus  $\text{cm}^{-2}$  to 17 eV at  $1/K0=0.55$  versus  $\text{cm}^{-2}$ .

### 2.8.3. Data analysis

The data-independent LCMS data was analysed with Spectronaut (Biognosys) software v16. First, the Bruker LCMS DIA files were converted into htrms files using the htrms converter (Biognosys). MS1 and MS2 data were centroided during conversion, and the other parameters were set to default. First the htrms files were analyzed with Spectronaut (version: 14.0.200601.47784, Biognosys). Then, the htrms files were subjected to quantitative data analysis via direct DIA. Here, the Spectronaut software generates a directDIA library. To generate it, calibration was set to non-linear iRT calibration with precision iRT selected. We used the protein sequence database of unreviewed *N. fowleri*, rUP000444721 and the Uniprot Crap common contaminants were used. Decoy sequences were generated and appended to the original database. A maximum of two missing cleavages were allowed, the required minimum peptide sequence length was 7 amino acids, and the peptide mass was limited to a maximum of 4,600 Da. Carbamidomethylation of cysteine residues was set as a fixed modification, and methionine oxidation and acetylation of protein N termini as variable modifications. The initial maximum mass tolerances were 70 ppm for precursor ions and 35 ppm for fragment ions. A reversed sequence library was generated/used to control the false discovery rate (FDR) at less than 1% for peptide spectrum matches and protein group identifications. Decoy database hits, proteins identified as potential contaminants, and proteins identified exclusively by one site modification were excluded from further analysis.

### 2.8.4. Functional analyses of identified proteins

The returned list of identified proteins consisted of 2,295 proteins, 2,270 of which were specific to *N. fowleri* (others included common human or bovine contaminants such as keratin, serum albumin, etc. that came from the media or the preparation process). These amoebae-specific proteins were first run through the Blast2GO (v6.0.3) pipeline (steps included: blast search, interpro classification, GO mapping, annotation, and goslim reduction) and this annotation data was associated with the protein list in Supplementary Table S2 (Conesa et al., 2005; Conesa and Gotz, 2008; Gotz et al., 2008). Because the hierarchical charts generated by Blast2GO were too complex/difficult to follow, we utilized the Panther Classification System (v17.0) to perform functional classifications and identify potential gene family enrichment (Thomas et al., 2022). Data lists were exported, and pie charts were generated in Microsoft Excel (v2212).

### 3. Results

#### 3.1. Axenically cultured clinical isolates of *Naegleria fowleri* are distinguishable by size

We utilized SEM to visualize and compare five axenically cultured clinical isolates of *N. fowleri*. When analyzing each isolate, we made morphometric observations and took measurements of structures that are labeled throughout [Figure 1](#) and summarized in [Figure 1F](#). When comparing between culturing conditions (axenic or fed over mammalian cells), we found no significant differences in the average width of each individual isolate, however we did discover statistically significant differences when comparing the overall widths among isolates as determined by one-way analysis of variance (ANOVA) [ $F(4,893)=6.983$ ;  $p < 0.0001$ ]. The average combined width of the five clinical isolates (composed of at least 3 measurements of length and/or width per amoeba  $\pm$  s.e.m.) was  $10.3 \pm 0.6 \mu\text{m}$  ( $n = 898$  amoebae measured), with *Nf69* being significantly larger than both *6088* ( $p = 0.0012$ ) and *V631* ( $p = 0.0001$ ), and *HB4* also being larger than *V631* ( $p = 0.0012$ ; *post hoc* Tukey comparisons; [Table 1](#); [Figure 1F](#)).

We took note of one structural motif known as the uroid—an organelle previously observed on the posterior end of *N. fowleri* trophozoites with trailing filaments or processes ([Carter, 1970](#); [Visvesvara et al., 2005](#)). It is referred to as an excretory organelle in limax amoebae ([Vickerman, 1962](#)), the potential location of the contractile vacuole in *N. fowleri* ([Martinez et al., 1971](#)), and a structure potentially involved in releasing vacuoles, waste, and excretory granules in *Entamoeba histolytica* ([Hopkins and Warner, 1946](#)). Our current work shows that the uroid of *N. fowleri* consists of clusters of hemispherical bulges of the membrane (rounded blebs or clusters of membranous invaginations) and was identified in all clinical isolates analyzed except for *6088*, although it was only visible in a subset of the amoebae. The size of the uroid regions (reported in [Table 1](#) and [Figure 1F](#)) seemingly correlated with the width of the isolates as evidenced by the largest isolate, *Nf69*, boasting a significantly larger uroid region compared to *V067* ( $p = 0.0081$ ), to *V631* ( $p = 0.0002$ ), and to *HB4* ( $p = 0.0109$ ) [one-way ANOVA and *post hoc* Tukey comparisons;  $F(3,132)=6.540$ ;  $p = 0.0004$ ].

Often, we observed bundles of thin filaments with occasional bulbous tips—herein referred to as uroid filaments—that extruded from the uroid region, adhered to the substrate, and were repeatedly found broken off on either the mammalian cell or the substrate surface surrounding imaged amoebae. Other filaments with occasional bulbous tips that we suggest are adhesive filaments, often extended from the membrane around the entire cell periphery. We measured the diameters of these filaments in axenic cultures and report them in [Table 1](#). Lastly, we have confirmed the observation made by Antonios et al. that no or very few organized “suckers” or food-cups/amoebastomes were identified on the trophozoite stages examined ([Antonios, 2010](#)). Contrary to some reports of one or more food cups per amoeba ([John et al., 1984](#); [Sohn et al., 2010](#)), easily identifiable food cups were rare, and only identified in a small fraction of images taken of axenically cultured amoebae as well as those cultured over mammalian cells ([Figures 1A,F](#); [Table 1](#); [Supplementary Figures S1A,D,H,J](#)).

#### 3.2. Feeding *Naegleria fowleri* produces distinct structures and induces cytopathic effects in co-cultured mammalian cells

Evidence shown by [John and John \(1994\)](#) indicates that allowing *N. fowleri* clinical or environmental isolates to feed over mammalian cells for multiple passages confers higher levels of pathogenicity, thus we reasoned that this mechanism could be leveraged in a controlled visual assay for understanding the structural differences arising from actively feeding versus growing axenically in culture. We exposed the amoebae to three different food sources: human foreskin fibroblasts (HFF), B103 rat neuroblastoma cells (B103), and Vero green monkey kidney cells. All isolates, except for *6088*, readily consumed HFF and Vero monolayers, while feeding on B103s was rare and commonly resulted in amoeboid encystation. Initial criteria for the selection of mammalian cells to monitor sub-micron level interactions among amoebae and their food allowed for the exclusion of B103s and HFFs as these both produce long/fibrous cellular connections and raise from the substrate at times when growing in a semi-confluent to confluent monolayer ([Supplementary Figures S2A,C](#)). Vero cells were selected as these produced uniformly flat monolayers with little to no visual fibrous intracellular connections or extracellular nanotube structures, thereby allowing for the least confounding identification and differentiation between amoebae and mammalian cells ([Supplementary Figures S2E,G](#)). Cytopathic effects were noted for all strains and cell lines when cultured with amoebae ([Figure 2C](#); [Supplementary Figure S2](#)) and consisted of initial apoptotic bleb formation (inset in [Figure 2C](#)) followed by rounding of the mammalian cell accompanied by partial detachment from the substrate and the formation of long thin dendritic fibrils extending from main cell body. When these thin fibrils are formed, the amoebae attach to them and cluster along them (regardless of whether they are still associated with the substrate), and a common phenomenon seen when culturing over mammalian cells are networks of floating mammalian cell connections with dense clusters of amoebae dispersed along their lengths (example in right side of [Figure 2C](#)).

Prior work on *N. fowleri* by Antonios et al., described a thin surface extension when comparing the morphology of axenically cultured amoebae versus those freshly extracted from a brain and speculated that they played a role in adherence to brain tissues ([Antonios, 2010](#)). In our study, we also noted the formation of elongated thin filopodia extending from amoebae to mammalian cells ([Figure 2Ai,ii](#)). Due to their thick nature and extension over mammalian cells, we speculate that these could provide a basis for material exchange (inset in [Figure 2Ai](#)). Additionally, in an axenically cultured *V631* prep, we noted a thick filopodial extension connecting three different trophozoites ([Figure 2E](#)) which could contribute to biofilm formation. We also observed pseudopodia with raised topographies extended onto mammalian cells, sometimes with thinner tubular structures connecting them to the main cell body ([Figure 2B](#)), but mostly with the canonical fan-shaped pseudopodia ([Figure 2Bi,ii,iii](#); [Supplementary Figures S1C,F,L](#)). We speculate that, due to the raised nature of the pseudopodia, there are likely amoebastomes or other structures facilitating material exchange being formed at the interface between the pseudopodia and the mammalian cell, but further characterization was not possible due to the limitations of SEM.

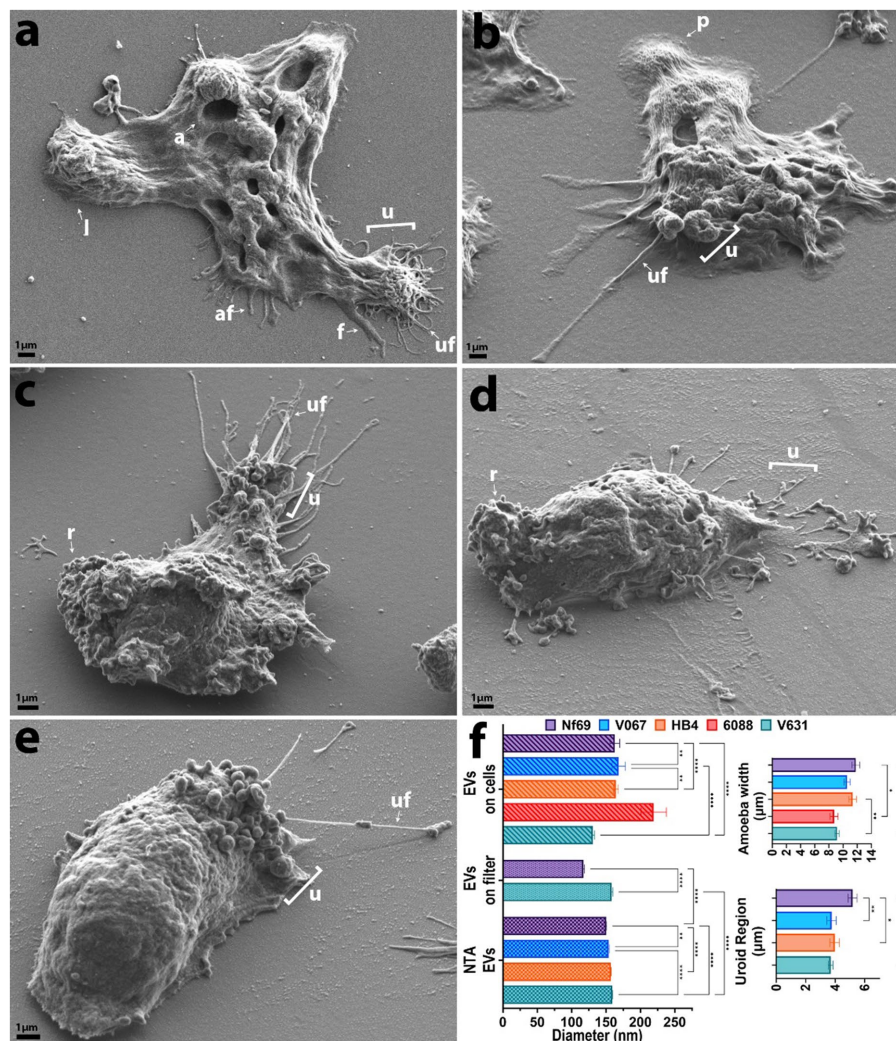


FIGURE 1

SEM micrographs of each clinical isolate in axenic culture. (A) *Nf69*, (B) *V067*, (C) *HB4*, (D) *6088*, (E) *V631*. (F) Graphical depiction of SEM measurements and EV size comparison between analysis techniques (NTA, EVs run over filter, and EVs identified on/around cells). Error bars on the charts represent the standard error of the mean. af, adhesive filament (originating from regions other than the uroid and < 300 nm); a, amoebastome; f, filopodia (>300 nm); u, uroid region; uf, uroid filaments (generally associated with uroid region and < 300 nm); p, pseudopodia; l, lobopodia; r, rough. Data shown are representative of 2 independent experiments.

Another phenomenon that we noted was the formation of thin branching filaments—sometimes emanating from the uroid region (Figures 2C,D), sometimes surrounding the entire cell periphery (Figure 2F; Supplementary Figure S1C)—that seem to be in contact with other amoebae and/or mammalian cells. We hypothesize that this could be a method of probing of the environment employed by the amoebae. We show that these thin filopodial extensions are formed via actin polymerization and can be visualized with high resolution fluorescence microscopy (Figures 3A–G; Supplementary Video S1). Moreover, we also observed the formation of thin filamentous connections from cysts to neighboring trophozoites (Supplementary Figures S1E,I). We speculate that this is either a tethering technique or a technique for intracellular signaling between cysts and/or trophozoites and the environment. The cysts exhibited the canonical rounded/oval form—sometimes with an exit pore (Supplementary Figure S1F) – and a finely reticulated membrane texture previously described by Lastovica (1974).

### 3.3. *Nf*-EVs are spherical and secreted in clusters from multiple sources

To ascertain the structure and mechanism of secretion of *Nf*-EVs, we designed an ultracentrifugation and purification technique following the Minimal Information for the Study of Extracellular Vesicles (MISEV) guidelines (Théry et al., 2018), and adapted from Bayer-Santos et al. (2013) and Szempluch et al. (2016) to extract vesicles from amoeba-conditioned media of four of the five isolates analyzed in this study. We extracted EVs from all isolates except 6088 as it was particularly sensitive to the transition from normal culture media to the EV-depleted fetal bovine serum (FBS) supplemented media. Nanoparticle tracking analysis revealed an average diameter of 152.6 nm for *Nf*-EVs across all isolates (Table 1; Figure 1F; Supplementary Figures S3A–D). Upon examination of freshly extracted *Nf69* and *V631* EV suspensions passed over a filter, we observed clusters of *Nf*-EVs with spherical morphologies



TABLE 1 Measurements of *Naegleria fowleri* amoebae and *Nf*-EVs taken with SEM and NTA (mean  $\pm$  s.e.m.).

Clinical Isolate	<i>Nf69</i>	<i>V067</i>	<i>HB4</i>	<i>6088</i>	<i>V631</i>
Width ( $\mu$ m) <i>n</i> = number of amoebae measured	11.8 $\pm$ 0.5 ( <i>n</i> = 174)	10.6 $\pm$ 0.4 ( <i>n</i> = 199)	11.37 $\pm$ 0.5 ( <i>n</i> = 208)	8.73 $\pm$ 0.6 ( <i>n</i> = 47)	9.15 $\pm$ 0.3 ( <i>n</i> = 270)
Uroid region ( $\mu$ m) <i>n</i> = number of measurements	5.18 $\pm$ 0.3 ( <i>n</i> = 27)	3.75 $\pm$ 0.3 ( <i>n</i> = 20)	3.97 $\pm$ 0.3 ( <i>n</i> = 34)	n/a	3.69 $\pm$ 0.2 ( <i>n</i> = 55)
Number of amoebastomes <i>n</i> = number of amoebae analyzed	0.24 $\pm$ 0.06 ( <i>n</i> = 104)	0.23 $\pm$ 0.13 ( <i>n</i> = 22)	0.03 $\pm$ 0.04 ( <i>n</i> = 61)	0.05 $\pm$ 0.05 ( <i>n</i> = 22)	0.35 $\pm$ 0.18 ( <i>n</i> = 26)
Filament diameter (nm) <i>n</i> = number of measurements	137.2 $\pm$ 8.0 ( <i>n</i> = 174)	172.3 $\pm$ 4.4 ( <i>n</i> = 301)	212.2 $\pm$ 4.0 ( <i>n</i> = 758)	156.7 $\pm$ 4.4 ( <i>n</i> = 369)	173.0 $\pm$ 5.0 ( <i>n</i> = 658)
EV NTA diameter (nm) <i>n</i> = number of EVs measured	150.2 $\pm$ 0.6 ( <i>n</i> = 61,130)	153.8 $\pm$ 0.7 ( <i>n</i> = 106,876)	157.2 $\pm$ 0.2 ( <i>n</i> = 75,436)	n/a	158.9 $\pm$ 0.7 ( <i>n</i> = 68,157)
EVs on filter diameter (nm) <i>n</i> = number of EVs measured	117.0 $\pm$ 1.4 ( <i>n</i> = 1,369)	n/a	n/a	n/a	158.1 $\pm$ 1.8 ( <i>n</i> = 817)
EVs on/near cells diameter (nm) <i>n</i> = number of EVs measured	162.7 $\pm$ 7.1 ( <i>n</i> = 150)	168.4 $\pm$ 9.6 ( <i>n</i> = 69)	164.2 $\pm$ 3.7 ( <i>n</i> = 496)	219.2 $\pm$ 19 ( <i>n</i> = 14)	130.9 $\pm$ 2.1 ( <i>n</i> = 342)

(Figures 4A,B). We took measurements of individual *Nf*-EVs found on the filter, including those with easily interpretable edges and excluding those associated with clusters, and present them in Table 1. Following this, we examined the SEM images of amoebae and took measurements of potential EVs being secreted from the cell membrane or from filaments around the cell that are summarized in Table 1 and Figure 1F. Our results coincide with the range of 131–172 nm reported by Lertjuthaporn et al. (2022) and 43.88–216 nm reported by Retana Moreira et al. (2022). When comparing the sizes of measured *Nf*-EVs across the 3 measurement techniques and also among the 5 isolates, we found them to be significantly different via two-way ANOVA (across measurement techniques: [ $F(2,314,849) = 15.91$ ;  $p < 0.0001$ ]; among isolates: [ $F(4,314,849) = 27.42$ ;  $p < 0.0001$ ]; Figure 1F; Supplementary Table S1). In short, among the NTA preparations, V631, HB4 and V067 EVs were significantly larger than *Nf69* EVs; V631 EVs were significantly larger than V067 EVs; and HB4 EVs were significantly larger than V067 EVs. When comparing NTA to filter measurements, *Nf69* and V631 NTA EVs were significantly larger than their counterparts measured on the filter. This could be due to clusters of EVs being detected as a single EV in NTA and our exclusion of these clusters from our manual measurements of SEM images.

To determine the potential source of the secreted EVs, we scanned our SEM images for secretions from amoebae that resembled the EVs visualized on filters and identified three probable sources (Figures 4C–G). Firstly, we observed that the uroid/adhesive filaments commonly separate into vesicles via beading or pearling (Rilla, 2021) and break off onto the substrate leaving behind clusters of material (Figures 4C,D,E,G). This source of EVs from filopodial extensions has been described for numerous types of mammalian cells (Lai et al., 2015; Mathieu et al., 2019; Rilla, 2021). To support this phenomenon in *N. fowleri*, we mined the images of *Nf*-EVs passed over filters and found an example of a filament associated with clusters of EVs in a similar manner to those that we visualized in amoebae cultures (Figure 4H). Secondly, we noted the release of clusters of EVs from the periphery of the cell membrane (Figure 4E) which could indicate emission of vesicles via multivesicular bodies (MVBs). Lastly,

we observed clusters of materials being released from regions of the plasma membrane (Supplementary Figure S1D). Upon taking measurements of the adhesive/uroid filaments, the putative vesicles formed via beading of filaments, and the clusters of putative vesicles secreted from the plasma membrane, we found that the size range overlaps with measurements that we obtained via NTA and manually on filters.

### 3.4. R18-stained *Nf*-EVs are taken up by mammalian cells and other amoebae

To determine whether *Nf*-EVs are taken up by mammalian cells, we labeled *Nf69*-EVs with the lipophilic fluorophore octa-decyl rhodamine B (R18) and performed fluorescence dequenching assays to monitor time-dependent increases in fluorescence that would be indicative of EV uptake by recipient cells. We first exposed B103 cells to *Nf69*-secreted R18-stained EVs for various timepoints and imaged the resulting cells (Figure 5). At the 5-min timepoint we noted initial dim lipid equilibration with B103 cell body membranes indicated by dim/diffuse staining through the 30-min timepoint (Figures 5E–H) compared to the R18-stained PBS control cells (Figures 5A–D). As more EVs were taken up by host cells over time, more of the R18 dye was diluted resulting in brighter fluorescent signals on the host cell membranes (Figures 5I–P). Initial punctate staining patterns occurred over the cell body, and this escalated to bright coverage of the full membrane (including the axons and dendrites) until fluorescence reached a plateau at ~6 h (Figures 5Q–T). We next quantified levels of *Nf69*-EV uptake for different cell lines at the population level (as a function of integrated fluorescence intensity) by using different concentrations of *Nf69*-EVs with B103, HFF, Vero, and A549 cells. We developed a 96-well plate assay using high-content imaging to detect host cell nuclei which were defined as Hoescht+ and then host cytosol defined as R18+/-. When quantifying the mean fluorescent intensity of double positive cells (host nuclei and cytosol), we observed a time and concentration-dependent increase in mean integrated fluorescence intensity per treatment group that plateaued at approximately 6–12 h (Supplementary Figure S4).



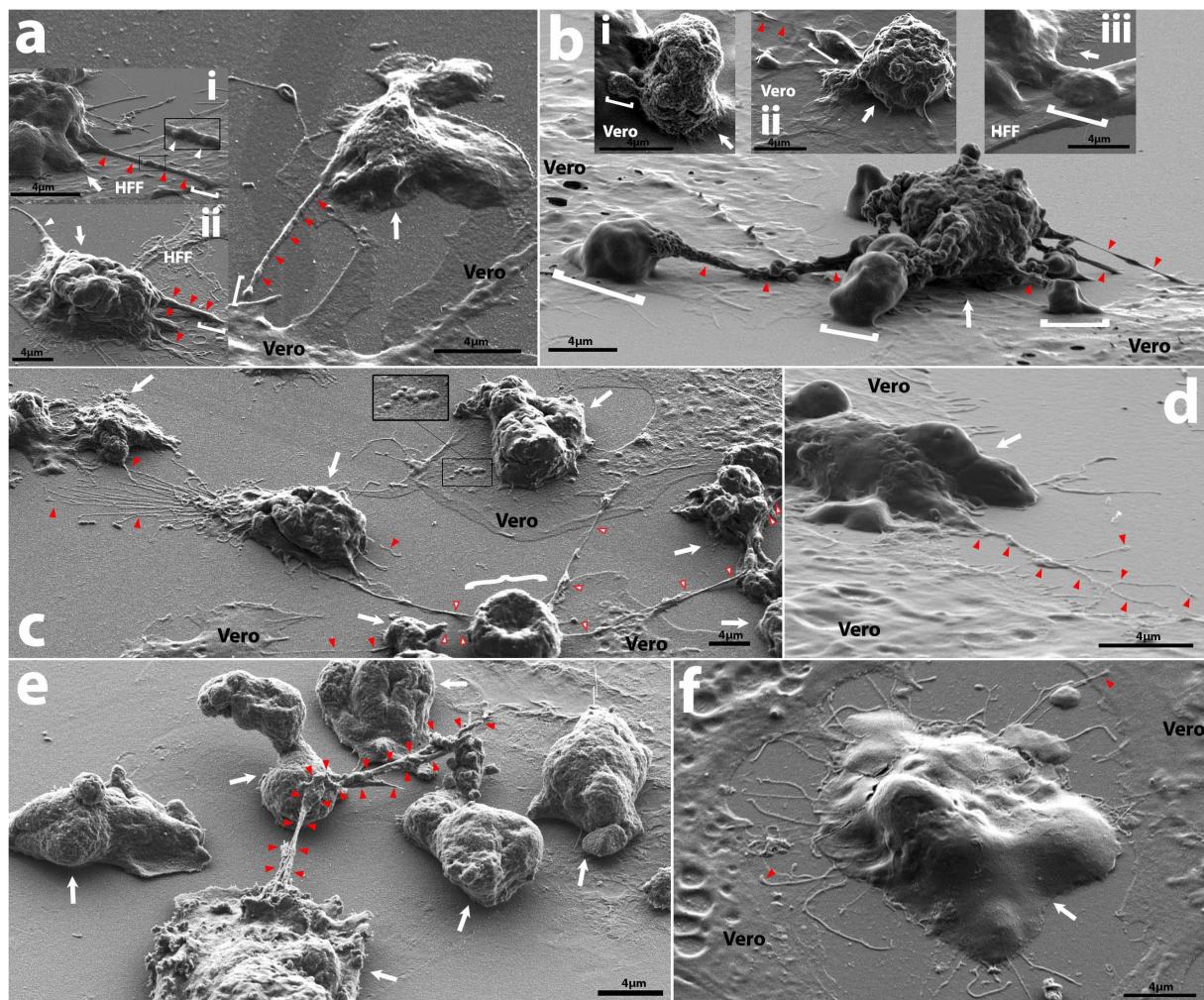


FIGURE 2

Representative SEM micrographs of intercellular interactions among amoebae and mammalian cell monolayers. **(A)** Main panel shows V067 trophozoite (white arrow) extending a filopodium of  $\sim 300$  nm in diameter (red arrowheads) a distance of  $\sim 6.3$   $\mu$ m away from the cell body to a nearby Vero, subpanel i shows a V631 trophozoite (white arrow) feeding on HFF and extending filopodia of  $\sim 300$  nm diameter a distance of  $>6.75$   $\mu$ m containing potential cargo of  $\sim 200$  nm (white arrowheads) onto HFF, while subpanel ii shows a V631 trophozoite (white arrow) feeding on HFF cell with 5.6  $\mu$ m long uroid filament extending from rear of cell (left white arrowhead) and filopodia of varying width (right red arrowheads) reaching onto HFF cell (of which the largest varies in diameter from 600 nm to 1.1  $\mu$ m and extends  $\sim 6.74$   $\mu$ m from cell), a white bracket shows contact point; **(B)** V631 trophozoite (white arrow) producing pseudopodia that act as contact points with Vero cells (white brackets) and extend from the cell body via rough tubular structures (red arrowheads), also labelled with red arrowheads are uroid/adhesive filaments, subpanel i shows a V631 trophozoite with a rough surface feeding on a Vero cell and extending a pseudopodium (white bracket), subpanel ii shows a V631 trophozoite feeding on an HFF cell with a long filament (white arrowhead) extending from a thicker filopodium (white bracket), and subpanel iii shows a V631 trophozoite extending a pseudopodium with raised topography onto an HFF; **(C)** HB4 with connections to neighboring amoeba via uroid filaments (red arrows), white curly bracket shows apoptotic Vero cell with adhesive filopodia (white arrowheads w/red outline) that amoebae on right side of photo are attached to and cluster along when feeding; inset shows apoptotic blebs forming on Vero; **(D)** Nf69 trophozoite (white arrow) on Vero cell and extending a thin, branching filament (red arrows); **(E)** axenically cultured V631 trophozoites connected via a filopodial structure ranging from 172.6 nm to 1.27  $\mu$ m a total distance of  $\sim 15.4$   $\mu$ m from the originating cell; **(F)** Nf69 trophozoite (white arrow) producing filaments around the cell perimeter that make contact with neighboring Vero cells (red arrowheads).

To determine whether EVs are taken up by other amoebae, we grew the amoebae in suspension and treated V631 with 1  $\mu$ g of Nf69-secreted R18-stained EVs for various timepoints and performed imaging flow cytometry. We used Hoescht+ gating to select for viable amoebae followed by R18+ gating to quantify fluorescence levels of each treatment population of amoebae. Similar to mammalian cells, we saw initial rapid lipid equilibration with amoeba cell membranes (Figure 6A, 5 min) and this was followed by increasing numbers of punctate staining patterns (Figure 6A, 15 min – 2 h) indicative of vacuolized EVs taken up by

the amoebae via phagocytosis with increasing levels of uptake over time (Figure 6B).

### 3.5. Exposure to Nf-EVs induces an increase in metabolic activity in mammalian cells

To determine if there are any measurable effects on cellular metabolism in real-time after treating cells with Nf69-EVs, we first

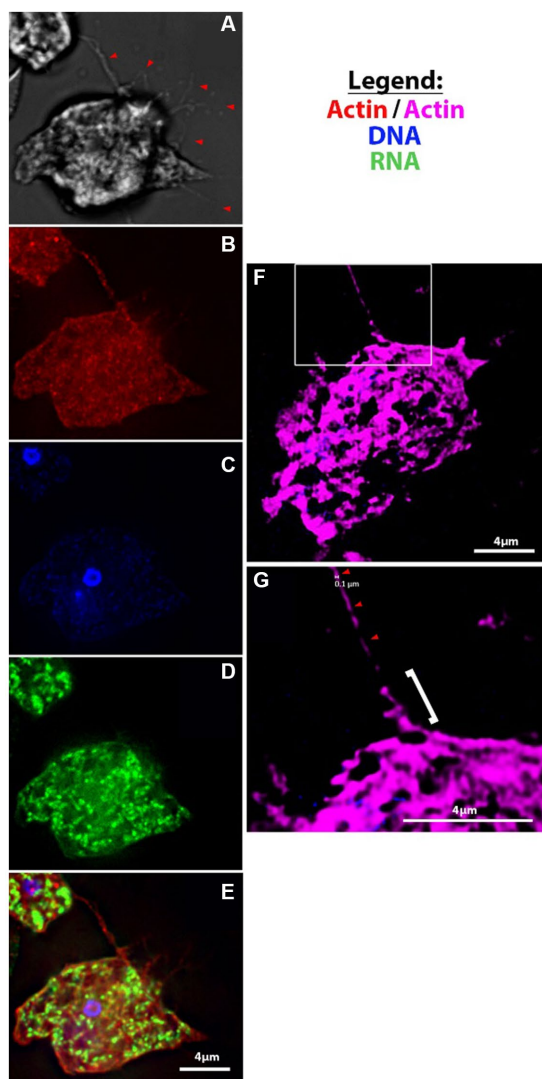


**FIGURE 3**  
Fluorescent microscopy of filopodia and filaments of amoebae. (A–E) V631 trophozoites at 100X using Deltavision II [(A) DIC, (B) Actin, (C) Hoescht, (D) 132A RNA stain, (E) merge]; (F–G) super-resolution images of actin-stained HB4 filament of ~100 nm diameter (red arrowheads) that looks to be protruding from a thicker filopodial extension from cell body (white bracket).

optimized the seeding densities of tested cells using the CellTiter-Glo 2.0 kit in 96-well plates to confirm that the luminescence readings fell within the linear range of the RealTime-Glo MT cell viability assay at various timepoints throughout the planned incubation period (Supplementary Figure S5). The RealTime-Glo MT kit allows real-time monitoring of cell viability depending on the ability of exposed cells to take up and metabolize/reduce the prosubstrate to a substrate that is exported from the cell to bind to the NanoLuc Enzyme and produce the bioluminescence (in RLU) that is measured as an output for the assay. We anticipated a decrease in cellular viability in response to *Nf*-EV uptake according to prior work showing that the EVs of another free-living amoeba, *Acanthamoeba castellanii*, induce cytotoxic effects in mammalian cells (Goncalves et al., 2018). On the contrary, we observed an increase in RLU in the treatment groups compared to control groups regardless of low versus high doses, or the cell line used (Supplementary Figure S6; Figure 7). We observed the

same phenomenon when we compared the efficacy of freshly extracted and processed EVs to those that were frozen immediately after processing and stored at  $-80^{\circ}\text{C}$  for 14 weeks prior to thawing for the assay (Supplementary Figure S7).

### 3.6. *Naegleria fowleri* EV proteome consists of a diverse range of proteins

To date, little is known about the protein composition of *Nf*-EVs. A preliminary visualization of protein contents of *Nf*69-EVs via SDS-PAGE gel is shown in Supplementary Figure S3E and the presence of at least 24 bands indicates that many different protein populations are present in the secreted EV proteome. To elucidate these proteins, we performed LC-MS/MS on two independent preparations of *Nf*69-EVs extracted from amoeba-conditioned media and identified 2,270 proteins present within both samples that represent the EV proteome (Supplementary Table S2). This represents a subset of 16.7% of the full 13,596 protein *N. fowleri* proteome (Zysset-Burri et al., 2014). These EV proteins were run through the Blast2GO suite, and the resulting annotations are also provided in Supplementary Table S2. We then compared our proteomic profile to the previously reported *N. fowleri* EV proteome and found that out of the 184 proteins reported by Retana Moreira et al. (2022), 18 proteins were specific to the non-pathogenic *Naegleria gruberi*. Of the remaining 166 *N. fowleri* specific proteins, 16 were not recapitulated in our study, resulting in an overlap of 150 proteins (highlighted in yellow in Supplementary Table S2) that are reiterated in our proteomic profile. We utilized the Panther classification system (Thomas et al., 2022) to identify enriched protein classes or functionalities. Out of the 2,270 proteins submitted to Panther, 1,876 were recognized for each of the 3 classification schemas. Graphical summaries of the Panther results are presented in Figure 8 and Supplementary Figures S9A,B with 1,430 protein class hits, 1,312 molecular function hits, and 2,109 biological process hits. The 5 categories in the Protein Class schema with the highest prevalence were: metabolite interconversion enzyme (26.6%; 380 proteins), protein-binding activity modulator (14.8%; 211 proteins), transporter (8.5%; 121 proteins), translational protein (7.8%; 112 proteins), and membrane traffic protein (6.9%; 98 proteins). The 5 categories in the Biological Process schema with the highest prevalence were: cellular process (38.3%; 808 proteins), metabolic process (22.0%; 465 proteins), localization (12.7%; 267 proteins), biological regulation (11.7%; 246 proteins), and response to stimulus (7.0%; 147 proteins). Lastly, the 5 categories in the Molecular Function schema with the highest prevalence were: catalytic activity (45%; 591 proteins), binding (31.5%; 413 proteins), transporter activity (5.9%; 77 proteins), molecular function regulator (5.4%; 71 proteins), and ATP-dependent activity (3.3%; 43 proteins). A direct comparison of PANTHER protein class hit categories for the entire *N. fowleri* proteome (Supplementary Figure S8) compared to hits for the *Nf*-EV proteome is provided in Supplementary Table S3.

## 4. Discussion

Ultrastructural analyses of pathogens have proven to play a significant role in the discovery of novel cell–cell interactions and provide insight into the mechanisms of cellular processes (de Souza and Attias, 2018; Caldas et al., 2020; Qian et al., 2022). Prior studies



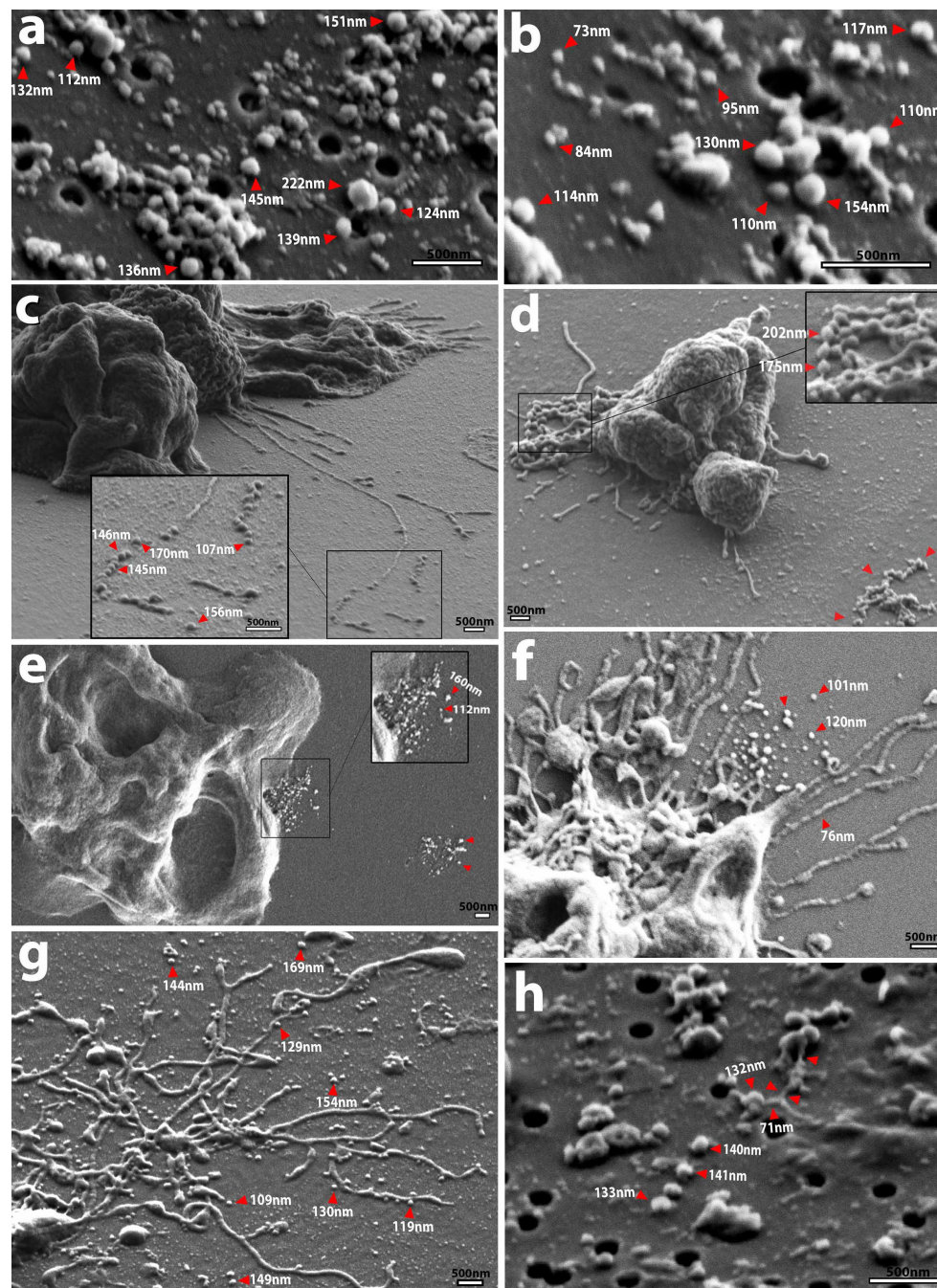


FIGURE 4

SEM micrographs showing EV shape and size as well as routes of secretion. (A,B) Spherical *Nf69* EVs and clusters of EVs with an avg. diameter of ~117 nm (smaller than the mean of ~140.6 nm obtained with NTA shown in [Supplementary Figure S3A](#)). (C) *HB4* releasing filaments that adhere to the substrate and are separating into potential EVs in a sequential beading manner. (D) Putative vesicles being formed in a “beads on a string” manner with successive fusion of thin filaments (red arrowheads) that ranged from ~175–200 nm. The cluster of secreted material on the right side of the panel (red arrowheads). (E) *Nf69* releasing clusters of EVs of various size from the periphery of the cell, potentially from a multivesicular body (MVB; red arrowheads) with another cluster on the right side of the panel (red arrowheads). (F) *Nf69* releasing a suspension of EVs from the uroid area of the cell. (G) *V631* uroid filaments surrounded by dissociated and dissociating EVs. (H) Example of filamentous connection of ~71 nm in diameter between EVs collected on filter from *V631* EV prep, supporting the hypothesis that extracted EVs come from both the amoeba cell membrane and adhesive/uroid filaments.

using high-resolution electron microscopy on parasitic protozoans have identified the mechanisms of extracellular vesicle secretion in *Trypanosoma cruzi* ([Szempluch et al., 2016](#); [Diaz Lozano et al., 2017](#); [Garrison et al., 2021](#)), monitored phenotypic effects in response to drug

treatment of *Leishmania amazonensis* ([de Macedo-Silva et al., 2013](#)), and characterized the intercellular interactions between *Trichomonas vaginalis* or *Tritrichomonas foetus* and mammalian cells ([Vilela and Benchimol, 2012](#)). Thus, we utilized this technique to perform a

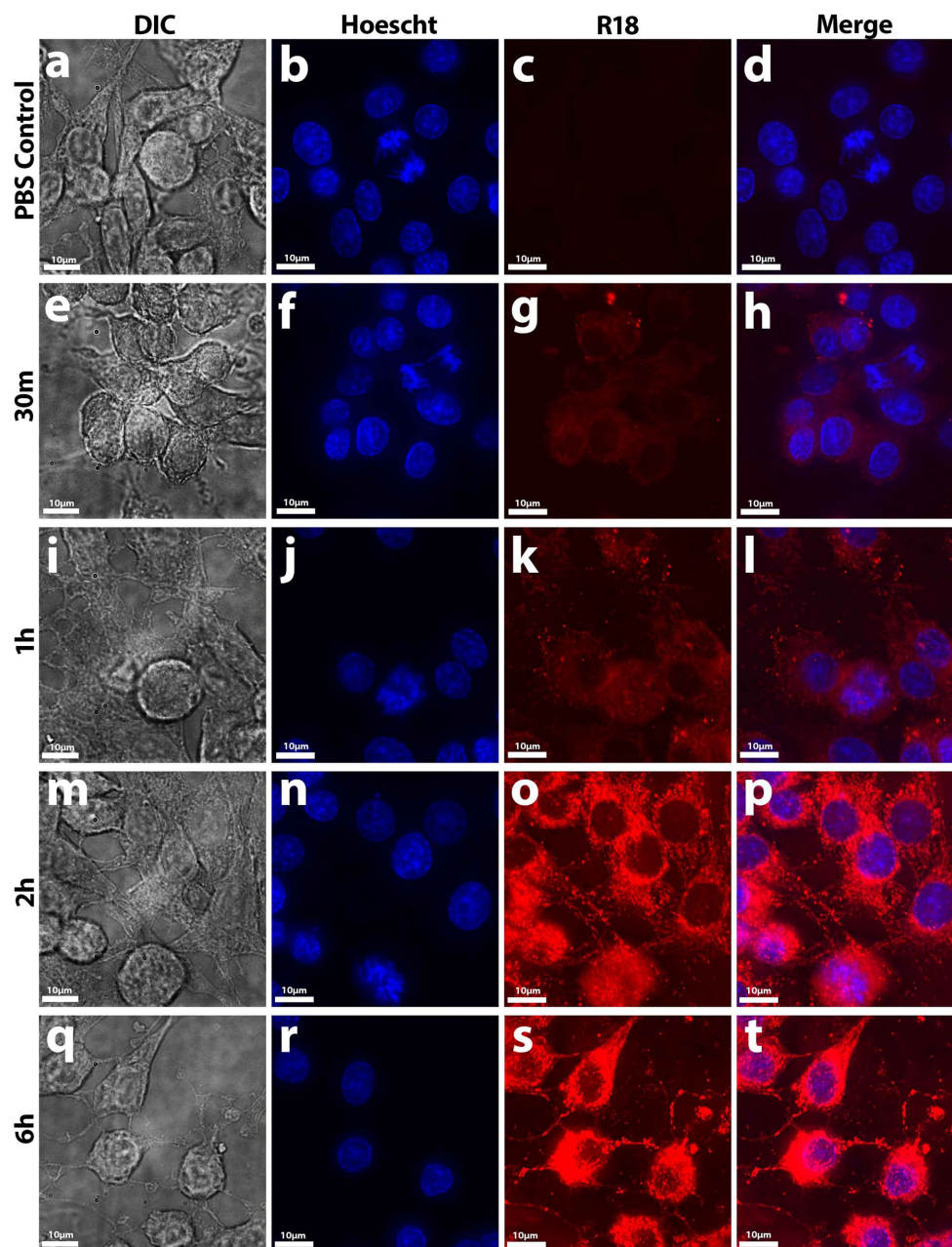


FIGURE 5

Uptake of R18-stained *Nf*-secreted EVs by B103 Rat Neuroblastoma cells. At early timepoints up to 30 min (E–H), initial diffuse lipid equilibration with outer cell membranes (mainly on the cell body) occurred in treated cells compared to control samples (A–D). At 1 h onward (I–L), punctate staining patterns in not only the cell body but also on the axons and dendrites occurred until maximal fluorescence potential was reached at 6 h (M–T). EV uptake was measured by fluorescence dequenching of R18-labeled *Nf69* EVs with mammalian cell membranes by imaging with deconvolution microscopy.

thorough characterization of multiple clinical isolates of *N. fowleri* and EVs secreted by these amoebae. EVs are known to have a central role in intercellular communication, thus EVs and their cargo have high utility when studying infectious parasites as they have been shown to play key roles in the modulation of infection processes (Twu and Johnson, 2014; de Souza and Barrias, 2020; Drurey and Maizels, 2021). Additionally, using multiple clinical isolates of an infectious organism allows one to confirm whether specific phenotypes are conserved within the species, or potentially identify differences that could be leveraged for downstream therapeutic and diagnostic development.

In the present study, we observed significant size differences between isolates of *N. fowleri*. We also observed that actively feeding amoebae are more likely to produce filopodial or pseudopodial extensions to reach their food than their axenically cultured counterparts. Furthermore, we identified elongated filamentous structures that could aid the amoebae in communication, adherence to and steering on substrates or host cells (Xue et al., 2010), or probing the environment and searching for prey. Our observations with *N. fowleri* agree with previous studies of *Naegleria gruberi* that explore the adhesive properties and the trailing dendritic loss of



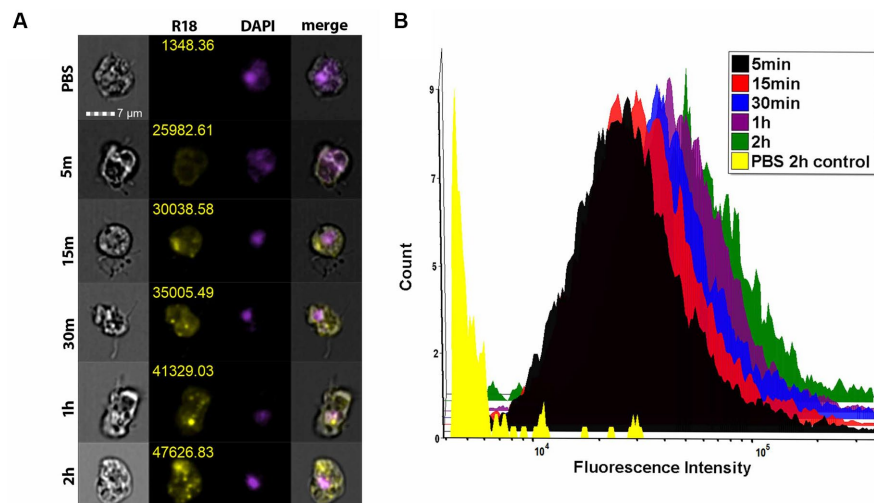


FIGURE 6

Imaging flow cytometry shows EV uptake by amoebae. (A) ImageStream flow cytometry data showing representative panels of mean fluorescence intensity for each timepoint. (B) Histogram depicting the fluorescence intensity of each of the treatment groups shows a time-dependent increase in fluorescence intensity across each treated population compared to the R18-stained PBS control.

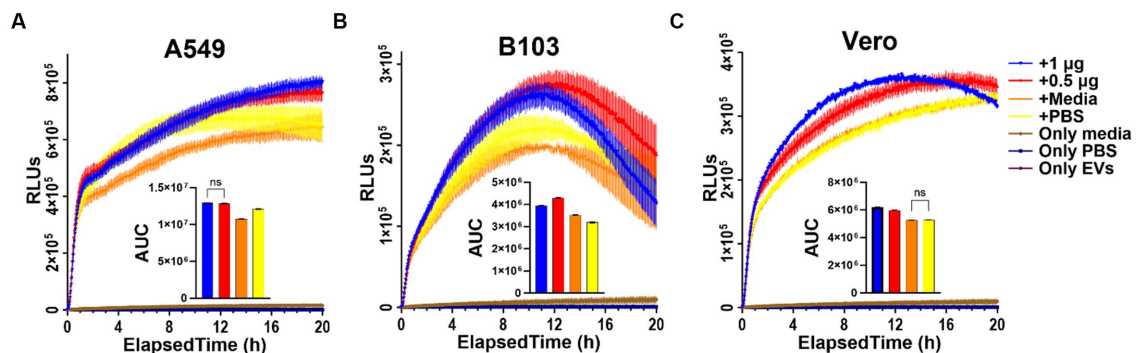


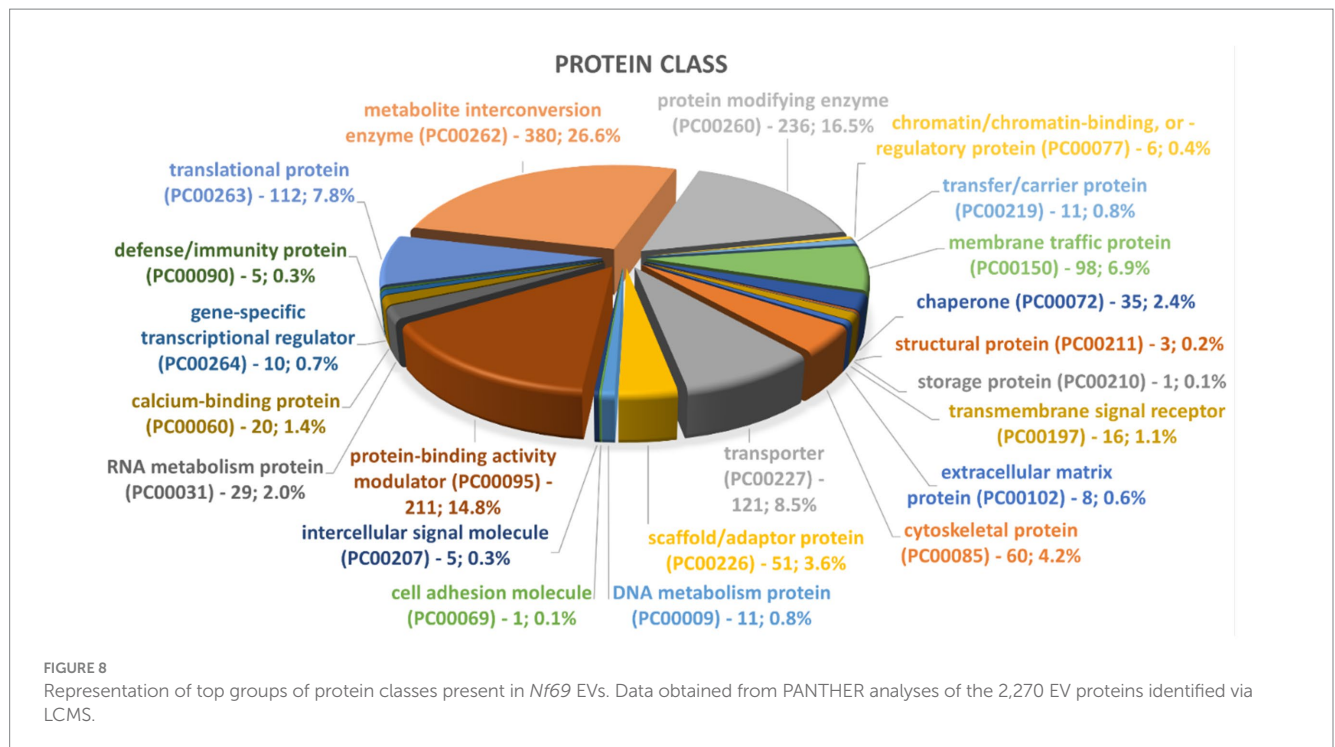
FIGURE 7

RealTime Glo results indicating increase in reducing potential in EV-treated cells. (A) A549 human lung carcinoma cells; (B) B103 Rat Neuroblastoma cells; (C) Vero green monkey kidney cells treated with freshly extracted *Nf69*-secreted EVs. AUC, area under the curve.

cellular material as related to amoeboid locomotion (Preston and King, 1978; Preston and O'dell, 1980; King et al., 1983). We hypothesize that these are formed as the amoebae initially attach or move while adhering to different types of substrates. Furthermore, when we allowed the amoebae to adhere for longer periods of time (>3 h as compared to ~45 min–1 h), we noticed a flatter phenotype with less filament production (Supplementary Figures S1E,K). The functionality of the thicker filopodial extensions remains unknown, but we speculate that they could participate in material exchange as shown in *Trichomonas vaginalis* (Salas et al., 2023) or assist the amoebae in attaching to and feeding on bacterial biofilms. Additionally, clusters of amoebae connected by filopodia (Figure 2E) could explain our observation that amoebae float in biofilms when cultures reach high confluency, exhibit density-dependent behaviors such as cluster formation, and seemingly grow/feed faster at higher densities.

Our findings also suggest that *Nf*-EVs are released individually and in clusters and are secreted via three different mechanisms. These

findings coincide with those reported for other free-living amoebae such as *A. castellanii*, which sheds vesicles from the plasma membrane (Goncalves et al., 2018), and *E. histolytica*, which sheds vesicles from MVBs and the plasma membrane (Nievas et al., 2020). Furthermore, our results with R18-stained EV uptake assays, as well as the measurement of *Nf*-EV zeta potential by Retana Moreira et al. (2022) indicate that amoebae EVs are easily taken up by numerous types of mammalian cells and other amoebae. Further experimentation utilizing plasma membrane, endosome, and lysosome markers as well as temperature controls and/or endocytosis inhibitors is warranted to provide clarification of the extent of vesicle fusion and the route of material uptake within cells. Lastly, our real-time data indicates that *Nf*-EVs induce an increase in metabolic activity in mammalian cells. We hypothesize that this could be a stress response by the mammalian cells. This metabolic response could also be explained by data from recent publications by Lertjuthaporn et al. and Moreira et al., the first showing that the EVs are immunogenic for macrophages, and the latter showing that the protein contents are immunogenic and antibodies were



raised against them (Lertjuthaporn et al., 2022; Retana Moreira et al., 2022).

Very few studies have examined *Nf*-EVs and the methods used have varied significantly. Previous studies performed upon *Nf*-EVs have several shortcomings; for example, the extraction process in one study involves two separate freeze–thaw cycles (one being at  $-20^{\circ}\text{C}$  for an undisclosed amount of time before EV extraction) prior to downstream analyses (Lertjuthaporn et al., 2022). This is problematic as prior EV studies have shown that conditioned media should be stored at  $4^{\circ}\text{C}$  for no longer than a week prior to processing and then samples should be stored at  $-80^{\circ}\text{C}$  in aliquots that are only put through one freeze–thaw cycle to prevent degradation of EV cargoes and maintain optimal quality and enzymatic activity (Lorincz et al., 2014; Bachurski et al., 2019). Secondly, a prior study on *Nf*-EVs used a PKH26 dye to perform fusion and uptake assays (Lertjuthaporn et al., 2022), and various EV publications have shown that PKH26 dyes form contaminating aggregates (Puzar Dominkus et al., 2018; Melling et al., 2022) that must be separated from dyed EVs via sucrose gradients. This additional purification step was not performed in the prior *Nf*-EV study (Lertjuthaporn et al., 2022), thus raising the question of whether *Nf*-EVs rather than PKH26 nanoparticle contaminants are being internalized by recipient cells. In this study we utilized an extraction process that provided fresh EVs to definitively show internalization of *Nf*-EVs over a broader time range, and more accurately characterize the uptake and morphology, without destruction of membrane integrity. Lastly, another study on *Nf*-EVs (Retana Moreira et al., 2022) implemented an MISEV guided extraction process to prevent degradation, but their proteomic characterization of *Nf*-EVs consists of significantly fewer proteins (184) than we found (2,270). These differences are likely due to the short period of time (5 h) that trophozoites were incubated in

media, and the lower volume of media (10 mL) used to extract EVs (Retana Moreira et al., 2022).

While SEM is powerful in deducing three-dimensional micron-level surface characteristics over a considerable area, it has limited capabilities in determining the fine microstructure of internal cellular components (Carr, 1971; de Souza and Attias, 2018). This drawback could have hindered our ability to fully explore the interaction and secretion mechanisms proposed in this study. Future studies using TEM could provide valuable mechanistic insights into the intercellular interactions and allow for definitive determination of the mechanisms of EV secretion described in this study. Being that our data has implicated the uroid structure as a key player in the secretion of materials, future functional analyses should be performed to determine whether it could assist in feeding (Chapman-Andresen, 1977) or in pathogenicity as it releases materials into the CNS that could contribute to the intense immune response associated with the disease. Despite limitations of some studies, the data on *Nf*-EVs obtained thus far warrant additional studies to establish the responses elicited by *Nf*-EVs extracted from amoebae cultured with various food sources and with differing stressors. The latter could yield significant results according to evidence that EVs secreted by *E. histolytica* contribute to parasite:parasite communication and that the amoeboid encystation process is modulated according to whether populations were exposed to EVs extracted from logarithmically growing trophozoites or encysting cells (Sharma et al., 2020). Furthermore, research exploring the effects of exposure to EVs secreted by more or less pathogenic *N. fowleri* amoebae as well as other amoebae species should be explored. Ongoing studies to characterize the RNA contents of *Nf*-EVs as well as the potential effects of EV exposure to other amoebae are being carried out in our laboratory.

## Data availability statement

The datasets presented in this study can be found in online repositories. The names of the repository/repository and accession number(s) can be found in the article/[Supplementary material](#).

## Author contributions

AR: Conceptualization, Investigation, Writing – original draft, Writing – review & editing, Data curation, Formal analysis, Methodology, Validation, Visualization. PB: Formal analysis, Investigation, Methodology, Validation, Visualization, Writing – review & editing, Resources, Supervision. GG: Investigation, Methodology, Resources, Writing – review & editing, Data curation. DK: Investigation, Resources, Writing – review & editing, Conceptualization, Funding acquisition, Project administration, Supervision, Writing – original draft.

## Funding

The author(s) declare financial support was received from the Georgia Research Alliance (D.E.K.) and the NIH (T32 AI060546, A.C.R.; R03 AI141709, D.E.K.).

## References

- Antonios, S. N. (2010). Scanning electron microscopic study of trophozoite and cyst stages of *Naegleria fowleri*. *J. Egypt. Soc. Parasitol.* 40, 271–276.
- Bachurski, D., Schuldner, M., Nguyen, P. H., Malz, A., Reiners, K. S., Grenzi, P. C., et al. (2019). Extracellular vesicle measurements with nanoparticle tracking analysis - an accuracy and repeatability comparison between NanoSight NS300 and ZetaView. *J. Extracell. Vesicles* 8:1596016. doi: 10.1080/20013078.2019.1596016
- Barnett, N. D., Kaplan, A. M., Hopkin, R. J., Saubolle, M. A., and Rudinsky, M. F. (1996). Primary amoebic meningoencephalitis with *Naegleria fowleri*: clinical review. *Pediatr. Neurol.* 15, 230–234. doi: 10.1016/S0887-8994(96)00173-7
- Bayer-Santos, E., Aguilar-Bonavides, C., Rodrigues, S. P., Cordero, E. M., Marques, A. F., Varela-Ramirez, A., et al. (2013). Proteomic analysis of *Trypanosoma cruzi* secretome: characterization of two populations of extracellular vesicles and soluble proteins. *J. Proteome Res.* 12, 883–897. doi: 10.1021/pr300947g
- Booth, P. J., Bodager, D., Slade, T. A., and Jett, S. (2015). Primary Amebic meningoencephalitis associated with hot spring exposure during international travel - Seminole County, Florida, July 2014. *MMWR Morb. Mortal. Wkly Rep.* 64:1226. doi: 10.15585/mmwr.mm6443a5
- Caldas, L. A., Carneiro, F. A., Higa, L. M., Monteiro, F. L., Da Silva, G. P., Da Costa, L. J., et al. (2020). Ultrastructural analysis of SARS-CoV-2 interactions with the host cell via high resolution scanning electron microscopy. *Sci. Rep.* 10:16099. doi: 10.1038/s41598-020-73162-5
- Capewell, L. G., Harris, A. M., Yoder, J. S., Cope, J. R., Eddy, B. A., Roy, S. L., et al. (2015). Diagnosis, clinical course, and treatment of primary amoebic meningoencephalitis in the United States, 1937–2013. *J. Pediatric Infect Dis Soc* 4, e68–e75. doi: 10.1093/jpids/piu103
- Carr, K. E. (1971). Applications of scanning electron microscopy in biology. *Int. Rev. Cytol.* 30, 183–255. doi: 10.1016/S0074-7696(08)60048-0
- Carter, R. F. (1970). Description of a naegleria sp. isolated from two cases of primary amoebic meningo-encephalitis, and of the experimental pathological changes induced by it. *J. Pathol.* 100, 217–244. doi: 10.1002/path.1711000402
- Chapman-Andresen, C. (1977). Endocytosis in freshwater amebas. *Physiol. Rev.* 57, 371–385. doi: 10.1152/physrev.1977.57.3.371
- Colon, B. L., Rice, C. A., Guy, R. K., and Kyle, D. E. (2019). Phenotypic screens reveal Posaconazole as a rapidly acting amebicidal combination partner for treatment of primary amoebic meningoencephalitis. *J. Infect. Dis.* 219, 1095–1103. doi: 10.1093/infdis/jiy622
- Conesa, A., and Gotz, S. (2008). Blast2GO: a comprehensive suite for functional analysis in plant genomics. *Int J Plant Genomics* 2008:619832, 1–12. doi: 10.1155/2008/619832
- Conesa, A., Gotz, S., Garcia-Gomez, J. M., Terol, J., Talon, M., and Robles, M. (2005). Blast2GO: a universal tool for annotation, visualization and analysis in functional genomics research. *Bioinformatics* 21, 3674–3676. doi: 10.1093/bioinformatics/bti610
- Cope, J. R., and Ali, I. K. (2016). Primary Amebic meningoencephalitis: what have we learned in the last 5 years? *Curr. Infect. Dis. Rep.* 18:31. doi: 10.1007/s11908-016-0539-4
- De Macedo-Silva, S. T., Urbina, J. A., De Souza, W., and Rodrigues, J. C. (2013). In vitro activity of the antifungal azoles itraconazole and posaconazole against leishmania amazonensis. *PLoS One* 8:e83247. doi: 10.1371/journal.pone.0083247
- De Souza, W., and Attias, M. (2018). New advances in scanning microscopy and its application to study parasitic protozoa. *Exp. Parasitol.* 190, 10–33. doi: 10.1016/j.exppara.2018.04.018
- De Souza, W., and Barrias, E. S. (2020). Membrane-bound extracellular vesicles secreted by parasitic protozoa: cellular structures involved in the communication between cells. *Parasitol. Res.* 119, 2005–2023. doi: 10.1007/s00436-020-06691-7
- Diaz Lozano, I. M., De Pablos, L. M., Longhi, S. A., Zago, M. P., Schijman, A. G., and Osuna, A. (2017). Immune complexes in chronic chagas disease patients are formed by exovesicles from *Trypanosoma cruzi* carrying the conserved MASP N-terminal region. *Sci. Rep.* 7:44451. doi: 10.1038/srep44451
- Drurey, C., and Maizels, R. M. (2021). Helminth extracellular vesicles: interactions with the host immune system. *Mol. Immunol.* 137, 124–133. doi: 10.1016/j.molimm.2021.06.017
- Duma, R. J., and Finley, R. (1976). In vitro susceptibility of pathogenic naegleria and acanthamoeba species to a variety of therapeutic agents. *Antimicrob. Agents Chemother.* 10, 370–376. doi: 10.1128/AAC.10.2.370
- Fowler, M., and Carter, R. F. (1965). Acute pyogenic meningitis probably due to acanthamoeba sp.: a preliminary report. *Br. Med. J.* 2, 740–742. doi: 10.1136/bmj.2.5464.734-a
- Garrison, P., Khan, U., Cipriano, M., Bush, P. J., McDonald, J., Sur, A., et al. (2021). Turnover of variant surface glycoprotein in *Trypanosoma brucei* is a bimodal process. *MBio* 12:e0172521. doi: 10.1128/mBio.01725-21
- Goncalves, D. S., Ferreira, M. D. S., Liedke, S. C., Gomes, K. X., De Oliveira, G. A., Leao, P. E. L., et al. (2018). Extracellular vesicles and vesicle-free secretome of the protozoa *Acanthamoeba castellanii* under homeostasis and nutritional stress and their damaging potential to host cells. *Virulence* 9, 818–836. doi: 10.1080/21505594.2018.1451184
- Gotz, S., Garcia-Gomez, J. M., Terol, J., Williams, T. D., Nagaraj, S. H., Nueda, M. J., et al. (2008). High-throughput functional annotation and data mining with the Blast2GO suite. *Nucleic Acids Res.* 36, 3420–3435. doi: 10.1093/nar/gkn176

## Conflict of interest

The authors declare that the research was conducted in the absence of any commercial or financial relationships that could be construed as a potential conflict of interest.

## Publisher's note

All claims expressed in this article are solely those of the authors and do not necessarily represent those of their affiliated organizations, or those of the publisher, the editors and the reviewers. Any product that may be evaluated in this article, or claim that may be made by its manufacturer, is not guaranteed or endorsed by the publisher.

## Supplementary material

The supplementary material for this article can be found online at: <https://www.frontiersin.org/articles/10.3389/fmicb.2023.1264348/full#supplementary-material>



- Grace, E., Asbill, S., and Virga, K. (2015). *Naegleria fowleri*: pathogenesis, diagnosis, and treatment options. *Antimicrob. Agents Chemother.* 59, 6677–6681. doi: 10.1128/AAC.01293-15
- Hopkins, D. L., and Warner, K. L. (1946). Functional cytology of *Entamoeba histolytica*. *J. Parasitol.* 32, 175–189. doi: 10.2307/3272594
- Jamerson, M., Da Rocha-Azevedo, B., Cabral, G. A., and Marciano-Cabral, F. (2012). Pathogenic *Naegleria fowleri* and non-pathogenic *Naegleria lovaniensis* exhibit differential adhesion to, and invasion of, extracellular matrix proteins. *Microbiology (Reading)* 158, 791–803. doi: 10.1099/mic.0.055020-0
- John, D. T., Cole, T. B. Jr., and Marciano-Cabral, F. M. (1984). Sucker-like structures on the pathogenic amoeba *Naegleria fowleri*. *Appl. Environ. Microbiol.* 47, 12–14. doi: 10.1128/aem.47.1.12-14.1984
- John, D. T., and John, R. A. (1994). Enhancement of virulence of *Naegleria fowleri* by growth in Vero-cell cultures. *J. Parasitol.* 80, 149–151. doi: 10.2307/3283359
- Kemble, S. K., Lynfield, R., Devries, A. S., Drehner, D. M., Pomputius, W. F. 3rd, Beach, M. J., et al. (2012). Fatal *Naegleria fowleri* infection acquired in Minnesota: possible expanded range of a deadly thermophilic organism. *Clin. Infect. Dis.* 54, 805–809. doi: 10.1093/cid/cir961
- King, C. A., Preston, T. M., and Miller, R. H. (1983). Cell-substrate interactions in amoeboid locomotion - a matched reflexion interference and transmission electron microscopy study. *Cell Biol. Int. Rep.* 7, 641–649. doi: 10.1016/0309-1651(83)90119-4
- Lai, C. P., Kim, E. Y., Badr, C. E., Weissleder, R., Mempel, T. R., Tannous, B. A., et al. (2015). Visualization and tracking of tumour extracellular vesicle delivery and RNA translation using multiplexed reporters. *Nat. Commun.* 6:7029. doi: 10.1038/ncomms8029
- Lam, C., Jamerson, M., Cabral, G., Carlesso, A. M., and Marciano-Cabral, F. (2017). Expression of matrix metalloproteinases in *Naegleria fowleri* and their role in invasion of the central nervous system. *Microbiology (Reading)* 163, 1436–1444. doi: 10.1099/mic.0.000537
- Lastovica, A. J. (1974). Scanning electron microscopy of pathogenic and non-pathogenic naegleria cysts. *Int. J. Parasitol.* 4, 139–142. doi: 10.1016/0020-7519(74)90096-4
- Lertjuthaporn, S., Somkird, J., Lekmanee, K., Atipimonpat, A., Sukapirom, K., Sawasdiopin, H., et al. (2022). Extracellular vesicles from *Naegleria fowleri* induce IL-8 response in THP-1 macrophage. *Pathogens* 11:632. doi: 10.3390/pathogens11060632
- Lin, W. C., Tsai, C. Y., Huang, J. M., Wu, S. R., Chu, L. J., and Huang, K. Y. (2019). Quantitative proteomic analysis and functional characterization of *Acanthamoeba castellanii* exosome-like vesicles. *Parasit. Vectors* 12:467. doi: 10.1186/s13071-019-3725-z
- Lorincz, A. M., Timar, C. I., Marosvari, K. A., Veres, D. S., Otrókoci, L., Kittel, A., et al. (2014). Effect of storage on physical and functional properties of extracellular vesicles derived from neutrophilic granulocytes. *J. Extracell. Vesicles* 3:25465. doi: 10.3402/jev.v3.25465
- Ma, P., Visvesvara, G. S., Martinez, A. J., Theodore, F. H., Daggett, P. M., and Sawyer, T. K. (1990). *Naegleria* and *acanthamoeba* infections: review. *Rev. Infect. Dis.* 12, 490–513. doi: 10.1093/clindis/12.3.490
- Malkin, E. Z., and Bratman, S. V. (2020). Bioactive DNA from extracellular vesicles and particles. *Cell Death Dis.* 11:584. doi: 10.1038/s41419-020-02803-4
- Marcilla, A., Martin-Jaular, L., Trelis, M., De Menezes-Neto, A., Osuna, A., Bernal, D., et al. (2014). Extracellular vesicles in parasitic diseases. *J. Extracell. Vesicles* 3:25040. doi: 10.3402/jev.v3.25040
- Martinez, J., Duma, R. J., Nelson, E. C., and Moretta, F. L. (1973). Experimental naegleria meningoencephalitis in mice. Penetration of the olfactory mucosal epithelium by naegleria and pathologic changes produced: a light and electron microscope study. *Lab. Invest.* 29, 121–133.
- Martinez, A. J., Nelson, E. C., Jones, M. M., Duma, R. J., and Rosenblum, W. I. (1971). Experimental naegleria meningoencephalitis in mice. An electron microscope study. *Lab. Invest.* 25, 465–475.
- Mathieu, M., Martin-Jaular, L., Lavieu, G., and Thery, C. (2019). Specificities of secretion and uptake of exosomes and other extracellular vesicles for cell-to-cell communication. *Nat. Cell Biol.* 21, 9–17. doi: 10.1038/s41556-018-0250-9
- Melling, G. E., Conlon, R., Pantazi, P., Dellar, E. R., Samuel, P., Baena-Lopez, L. A., et al. (2022). Confocal microscopy analysis reveals that only a small proportion of extracellular vesicles are successfully labelled with commonly utilised staining methods. *Sci. Rep.* 12:262. doi: 10.1038/s41598-021-04225-4
- Nieves, Y. R., Lizarraga, A., Salas, N., Coceres, V. M., and De Miguel, N. (2020). Extracellular vesicles released by anaerobic protozoan parasites: current situation. *Cell. Microbiol.* 22:e13257. doi: 10.1111/cmi.13257
- Preston, T. M., and King, C. A. (1978). Cell-substrate associations during the amoeboid locomotion of naegleria. *J. Gen. Microbiol.* 104, 347–351. doi: 10.1099/00221287-104-2-347
- Preston, T. M., and O'dell, D. S. (1980). The cell surface in amoeboid locomotion: behaviour of *Naegleria gruberi* on an adhesive lectin substrate. *Microbiology* 116, 515–520. doi: 10.1099/00221287-116-2-515
- Pugh, J. J., and Levy, R. A. (2016). *Naegleria fowleri*: diagnosis, pathophysiology of brain inflammation, and antimicrobial treatments. *ACS Chem. Neurosci.* 7, 1178–1179. doi: 10.1021/acscchemneuro.6b00232
- Puzar Dominkus, P., Stenovec, M., Sitar, S., Lasic, E., Zorec, R., Plemenitas, A., et al. (2018). PKH26 labeling of extracellular vesicles: characterization and cellular internalization of contaminating PKH26 nanoparticles. *Biochim. Biophys. Acta Biomembr.* 1860, 1350–1361. doi: 10.1016/j.bbamem.2018.03.013
- Qian, P., Wang, X., Guan, C., Fang, X., Cai, M., Zhong, C. Q., et al. (2022). Apical anchorage and stabilization of subpellicular microtubules by apical polar ring ensures plasmodium ookinete infection in mosquito. *Nat. Commun.* 13:7465. doi: 10.1038/s41467-022-35270-w
- Quintana, J. F., Babayan, S. A., and Buck, A. H. (2017). Small RNAs and extracellular vesicles in filarial nematodes: from nematode development to diagnostics. *Parasite Immunol.* 39:e12395. doi: 10.1111/pim.12395
- Rai, A. K., and Johnson, P. J. (2019). Trichomonas vaginalis extracellular vesicles are internalized by host cells using proteoglycans and caveolin-dependent endocytosis. *Proc. Natl. Acad. Sci. U. S. A.* 116, 21354–21360. doi: 10.1073/pnas.1912356116
- Retana Moreira, L., Steller Espinoza, M. F., Chacon Camacho, N., Cornet-Gomez, A., Saenz-Arce, G., Osuna, A., et al. (2022). Characterization of extracellular vesicles secreted by a clinical isolate of *Naegleria fowleri* and identification of immunogenic components within their protein cargo. *Biology (Basel)* 11:983. doi: 10.3390/biology11070983
- Rice, C. A., Colon, B. L., Chen, E., Hull, M. V., and Kyle, D. E. (2020). Discovery of repurposing drug candidates for the treatment of diseases caused by pathogenic free-living amoebae. *PLoS Negl. Trop. Dis.* 14:e0008353. doi: 10.1371/journal.pntd.0008353
- Rilla, K. (2021). Diverse plasma membrane protrusions act as platforms for extracellular vesicle shedding. *J. Extracell. Vesicles* 10:e12148. doi: 10.1002/jev2.12148
- Russell, A. C., and Kyle, D. E. (2022). Differential growth rates and in vitro drug susceptibility to currently used drugs for multiple isolates of *Naegleria fowleri*. *Microbiol. Spectr.* 10:e0189921. doi: 10.1128/spectrum.01899-21
- Salas, N., Blasco Pedreros, M., Dos Santos Melo, T., Maguire, V. G., Sha, J., Wohlschlegel, J. A., et al. (2023). Role of cytoneme structures and extracellular vesicles in trichomonas vaginalis parasite: parasite communication. *elife* 12:e86067. doi: 10.7554/eLife.86067
- Schuster, F. L., Guglielmo, B. J., and Visvesvara, G. S. (2006). In-vitro activity of miltefosine and voriconazole on clinical isolates of free-living amebas: *Balamuthia mandrillaris*, *acanthamoeba* spp., and *Naegleria fowleri*. *J. Eukaryot. Microbiol.* 53, 121–126. doi: 10.1111/j.1550-7408.2005.00082.x
- Sharma, M., Morgado, P., Zhang, H., Ehrenkaufer, G., Manna, D., and Singh, U. (2020). Characterization of extracellular vesicles from *Entamoeba histolytica* identifies roles in intercellular communication that regulates parasite growth and development. *Infect. Immun.* 88:e00349-20. doi: 10.1128/IAI.00349-20
- Siddiqui, R., Ali, I. K. M., Cope, J. R., and Khan, N. A. (2016). Biology and pathogenesis of *Naegleria fowleri*. *Acta Trop.* 164, 375–394. doi: 10.1016/j.actatropica.2016.09.009
- Sohn, H. J., Kim, J. H., Shin, M. H., Song, K. J., and Shin, H. J. (2010). The Nf-actin gene is an important factor for food-cup formation and cytotoxicity of pathogenic *Naegleria fowleri*. *Parasitol. Res.* 106, 917–924. doi: 10.1007/s00436-010-1760-y
- Szempruch, A. J., Sykes, S. E., Kieft, R., Dennison, L., Becker, A. C., Gartrell, A., et al. (2016). Extracellular vesicles from *Trypanosoma brucei* mediate virulence factor transfer and cause host Anemia. *Cells* 164, 246–257. doi: 10.1016/j.cell.2015.11.051
- Théry, C., Witwer, K. W., Aikawa, E., Alcaraz, M. J., Anderson, J. D., Andriantsitohaina, R., et al. (2018). Minimal information for studies of extracellular vesicles 2018 (MISEV2018): a position statement of the International Society for Extracellular Vesicles and update of the MISEV2014 guidelines. *J. Extracell. Vesicles* 7:1535750. doi: 10.1080/20013078.2018.1535750
- Thomas, P. D., Ebert, D., Muruganujan, A., Mushayahama, T., Albou, L. P., and Mi, H. (2022). PANTHER: making genome-scale phylogenetics accessible to all. *Protein Sci.* 31, 8–22. doi: 10.1002/pro.4218
- Twu, O., and Johnson, P. J. (2014). Parasite extracellular vesicles: mediators of intercellular communication. *PLoS Pathog.* 10:e1004289. doi: 10.1371/journal.ppat.1004289
- Van Niel, G., D'angelo, G., and Raposo, G. (2018). Shedding light on the cell biology of extracellular vesicles. *Nat. Rev. Mol. Cell Biol.* 19, 213–228. doi: 10.1038/nrm.2017.125
- Vickerman, K. (1962). Patterns of cellular organisation in *Limax* amoebae. An electron microscope study. *Exp. Cell Res.* 26, 497–519. doi: 10.1016/0014-4827(62)90155-6
- Vilela, R. C., and Benchimol, M. (2012). Trichomonas vaginalis and *Trichomonas foetus*: interaction with fibroblasts and muscle cells - new insights into parasite-mediated host cell cytotoxicity. *Mem. Inst. Oswaldo Cruz* 107, 720–727. doi: 10.1590/S0074-02762012000600003
- Visvesvara, G. S., De Jonckheere, J. F., Sriram, R., and Daft, B. (2005). Isolation and molecular typing of *Naegleria fowleri* from the brain of a cow that died of primary amebic meningoencephalitis. *J. Clin. Microbiol.* 43, 4203–4204. doi: 10.1128/JCM.43.8.4203-4204.2005



Visvesvara, G. S., Moura, H., and Schuster, F. L. (2007). Pathogenic and opportunistic free-living amoebae: *Acanthamoeba* spp., *Balamuthia mandrillaris*, *Naegleria fowleri*, and *Sappinia diploidea*. *FEMS Immunol. Med. Microbiol.* 50, 1–26. doi: 10.1111/j.1574-695X.2007.00232.x

Xue, F., Janzen, D. M., and Knecht, D. A. (2010). Contribution of filopodia to cell migration: a mechanical link between protrusion and contraction. *Int J Cell Biol* 2010:507821, 1–13. doi: 10.1155/2010/507821

Xue, J., Lamar, F. G., Zhang, B., Lin, S., Lamori, J. G., and Sherchan, S. P. (2018). Quantitative assessment of *Naegleria fowleri* and fecal indicator bacteria in brackish water of Lake Pontchartrain, Louisiana. *Sci. Total Environ.* 622–623, 8–16. doi: 10.1016/j.scitotenv.2017.11.308

Zysset-Burri, D. C., Müller, N., Beuret, C., Heller, M., Schürch, N., Gottstein, B., et al. (2014). Genome-wide identification of pathogenicity factors of the free-living amoeba *Naegleria fowleri*. *BMC Genomics* 15, 1–15. doi: 10.1186/1471-2164-15-496



## OPEN ACCESS

## EDITED BY

Christopher A. Rice,  
Purdue University, United States

## REVIEWED BY

Anjan Debnath,  
University of California, United States  
Antoinette Cassiopeia Russell,  
University of Colorado Anschutz Medical  
Campus, United States

## \*CORRESPONDENCE

Abdullah Nadeem  
✉ iam.abduln@outlook.com

RECEIVED 24 July 2023

ACCEPTED 29 September 2023

PUBLISHED 19 October 2023

## CITATION

Nadeem A, Malik IA, Afridi EK and Shariq F  
(2023) *Naegleria fowleri* outbreak in Pakistan:  
unveiling the crisis and path to recovery.  
*Front. Public Health* 11:1266400.  
doi: 10.3389/fpubh.2023.1266400

## COPYRIGHT

© 2023 Nadeem, Malik, Afridi and Shariq. This is  
an open-access article distributed under the  
terms of the [Creative Commons Attribution  
License \(CC BY\)](#). The use, distribution or  
reproduction in other forums is permitted,  
provided the original author(s) and the  
copyright owner(s) are credited and that the  
original publication in this journal is cited, in  
accordance with accepted academic practice.  
No use, distribution or reproduction is  
permitted which does not comply with these  
terms.

# *Naegleria fowleri* outbreak in Pakistan: unveiling the crisis and path to recovery

Abdullah Nadeem<sup>1\*</sup>, Inshal Arshad Malik<sup>2</sup>, Eesha Khan Afridi<sup>2</sup> and Fariha Shariq<sup>3</sup>

<sup>1</sup>Department of Medicine, Dow University of Health Sciences, Karachi, Pakistan, <sup>2</sup>Department of Medicine, Jinnah Sindh Medical University, Karachi, Sindh, Pakistan, <sup>3</sup>Department of Medicine, Karachi Medical and Dental College, Karachi, Sindh, Pakistan

The outbreak of *Naegleria fowleri* in Pakistan presents a significant public health concern due to its high fatality rate and limited treatment options. This review explores the impact of the outbreak on communities and the challenges faced in combating the disease. It evaluates available treatment options and highlights the need for early diagnosis and intervention. The study proposes recommendations to improve public health preparedness, including public awareness campaigns, enhanced healthcare infrastructure, and robust water surveillance systems. Collaboration between research institutions and public health organizations is emphasized to develop effective outbreak response strategies.

## KEYWORDS

*Naegleria fowleri*, primary amebic meningoencephalitis, outbreak, treatment options, public health, Pakistan

## 1. Introduction

*Naegleria fowleri* known more frequently as the “brain-eating ameba,” is a free-living ameba species belonging to the *Naegleria* genus and it is the only pathogenic species of the genus (1). It is the causative agent of Primary amebic meningoencephalitis (PAM), an infection that is rare but has a mortality rate of 95–99% (2). It is a thermophilic microorganism that flourishes at elevated temperatures of up to 46°C (115°F) and may endure even greater temperatures for brief periods of time (1, 2). As such, it is found in warm freshwater bodies and soil. Apart from that, it may also be present in swimming pools, splash pads, surf parks, or other recreational venues that are inadequately maintained and insufficiently chlorinated. Its thermophilic nature also explains why it is more likely to cause infection in the summer season (1).

The ameba can enter the nasal cavity when swimming or diving in contaminated water bodies or as is more commonly seen in Pakistan, irrigating the nose with contaminated water as part of ritual ablution. From here, it makes its way into the brain and starts devouring the brain tissue thus deriving the name “brain-eating ameba” (3).

According to a study, Pakistan had the second highest prevalence of *Naegleria* infections around the world (4). The first case of PAM in Pakistan was recorded in Karachi in October 2008. Within a decade of this, the number of cases in Pakistan had overtaken those reported in the USA in a span of 50 years (5, 6). As of 2023, *Naegleria* has claimed seven lives in

Pakistan. Of these, six deaths were reported in Karachi (four cases originating in Karachi, one in Hyderabad, and one in Quetta)<sup>1</sup> and one in Lahore.<sup>2</sup>

It has been pointed out that while Pakistan produces < 1% of the world's greenhouse emissions, it is disproportionately vulnerable to the wide-ranging effects of climate change because of its geographic location (7). One of these effects has substantialized in the form of worsening heat waves (8) that provide suitable temperatures for *N. fowleri* which is already a growing problem for the country.

Additionally, recent mortalities have raised a question about the maintenance and chlorination of recreational water bodies and tap water provided by the Karachi Water & Sewerage Board (KWSB) in the city that may be housing *N. fowleri*<sup>1</sup> (9). Moreover, the COVID-19 pandemic unveiled some significant deficiencies in Pakistan's healthcare system's ability to provide health equity (10) and the country simply cannot afford another outbreak, that too with such a high rate of mortality.

Thus, keeping all of this in mind, it is of vital importance that this infection is recognized and timely addressed to prevent further morbidity and mortality.

## 2. Understanding *Naegleria fowleri*

*N. fowleri*, belongs to the Percolozoa phylum (20) and is primarily transmitted through water, although another method of infection is through dirt or dust (11, 12).

As a free-living protist, *N. fowleri* mostly consumes bacteria, both Gram-positive and negative, along with yeast, algae, and other microorganisms. *N. fowleri* responds to bacteria by forming food cups, engaging in chemotaxis, and secreting chemokines (13, 14). While more than 40 species of *Naegleria* have been found, only *N. fowleri* causes primary amoebic meningoencephalitis (PAM), a fatal brain infection (2, 15).

### 2.1. Habitat of *Naegleria fowleri*

This thermophilic microorganism can be categorized into two groups based on its habitat, with one group inhabiting natural settings and the other being found in urban areas. Natural habitats include locations like hot springs, warm water bodies, ponds, freshwater lakes, and rivers, while urban areas may harbor *N. fowleri* in drinking water distribution systems (DWDS) within pipe wall biofilms (16). It can also be encountered in various settings such as hospitals, geothermally heated water sources, contaminated drinking water supplies, water parks, dental unit waterlines (DUWLs), and instances where nasal exposure to tap water occurs, including swimming pools in hotels and homes.

Moreover, the prevalence of *N. fowleri* tends to be higher in regions where the water temperature reaches or exceeds 28°C (17).

### 2.2. Life cycle of *Naegleria fowleri*

*N. fowleri*'s life cycle is divided into three phases: trophozoites, cysts, and flagellates (18).

The ameboid trophozoite shown in Figure 1, is the active, reproducing and feeding stage of *N. fowleri* (19). These trophozoites enter the body through the nasal tissue and travel to the brain via the olfactory nerves, resulting in a condition known as primary amoebic meningoencephalitis (PAM). Once *N. fowleri* reaches the olfactory bulbs, it elicits a significant immune response through activation of the innate immune system, including macrophages and neutrophils. Among the three stages, only the trophozoite is capable of causing infection in humans (20). When faced with certain conditions, such as a scarcity of nutrients, trophozoites can temporarily transform into a non-feeding flagellated stage. They can then revert back to the trophozoite form when favorable conditions return (18). Trophozoites of *Naegleria fowleri* primarily localize in the tissues of the central nervous system, particularly within the brain. However, flagellated forms of the organism are typically observed in cerebrospinal fluid (CSF) when the CSF is intentionally diluted for diagnostic flagellation tests. These tests are conducted to evaluate the presence and characteristics of the flagellated form, aiding in the diagnosis of *N. fowleri* infections.

The third form is a dormant spherical cyst. Notably, cysts are not detected in brain tissue (21). Trophozoites or flagellates encyst under unfavorable environmental circumstances such as lack of nutrients, overcrowding, desiccation, the buildup of waste materials, and extreme temperatures (22) (Figure 2). This enhances the chances of survival until better environmental conditions are present.

### 2.3. Transmission routes for *Naegleria fowleri*

PAM is substantially more common in immunologically healthy people, healthy children, and young adults who have recently been exposed to recreational freshwater (23). Since PAM is a waterborne illness, the majority of cases are linked to diving and swimming in under-chlorinated pools, polluted canals, spas, or engaging in recreational activities like water skiing in contaminated water sources, as well as the use of neti pots for nasal cleansing and ablution (24). When contaminated water is forced or splashed into the nasal cavity under pressure during swimming, diving, or otherwise, the amoeba colonizes the nasal cavity. After nasal inoculation, the amoeba passes through the respiratory epithelium and attaches to the olfactory mucosa. The pathogen then moves along the olfactory nerve and past the cribriform plate, which is more permeable in children and young adults, to reach the olfactory bulbs within the central nervous system (CNS) (11). Once *N. fowleri* enters the olfactory bulbs, it triggers the innate immune system, which includes neutrophils and macrophages, to produce a strong immunological response (12, 13).

1 Reemergence of Deadly Brain-Eating Amoeba Sets Off Alarms. Available from: <https://tribune.com.pk/story/2425212/reemergence-of-deadly-brain-eating-amoeba-sets-off-alarms> (accessed July 11, 2023).

2 Pakistan Man Dies From 'Brain-Eating Amoeba' After Going for a Swim. Available from: <https://www.telegraph.co.uk/global-health/science-and-disease/pakistan-amoeba-man-dies-naegleria-fowleri/> (accessed July 11, 2023).

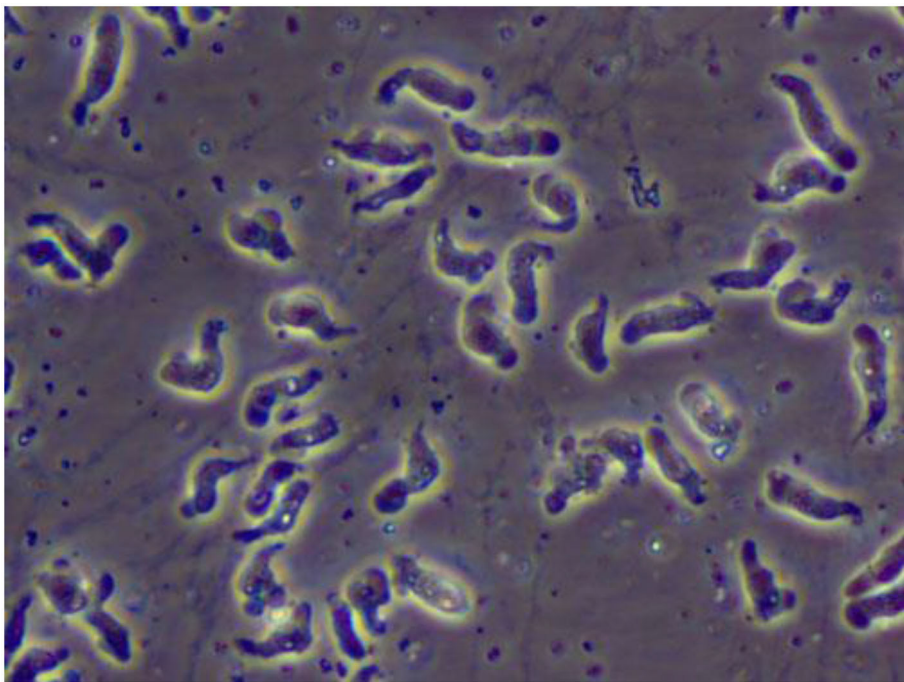
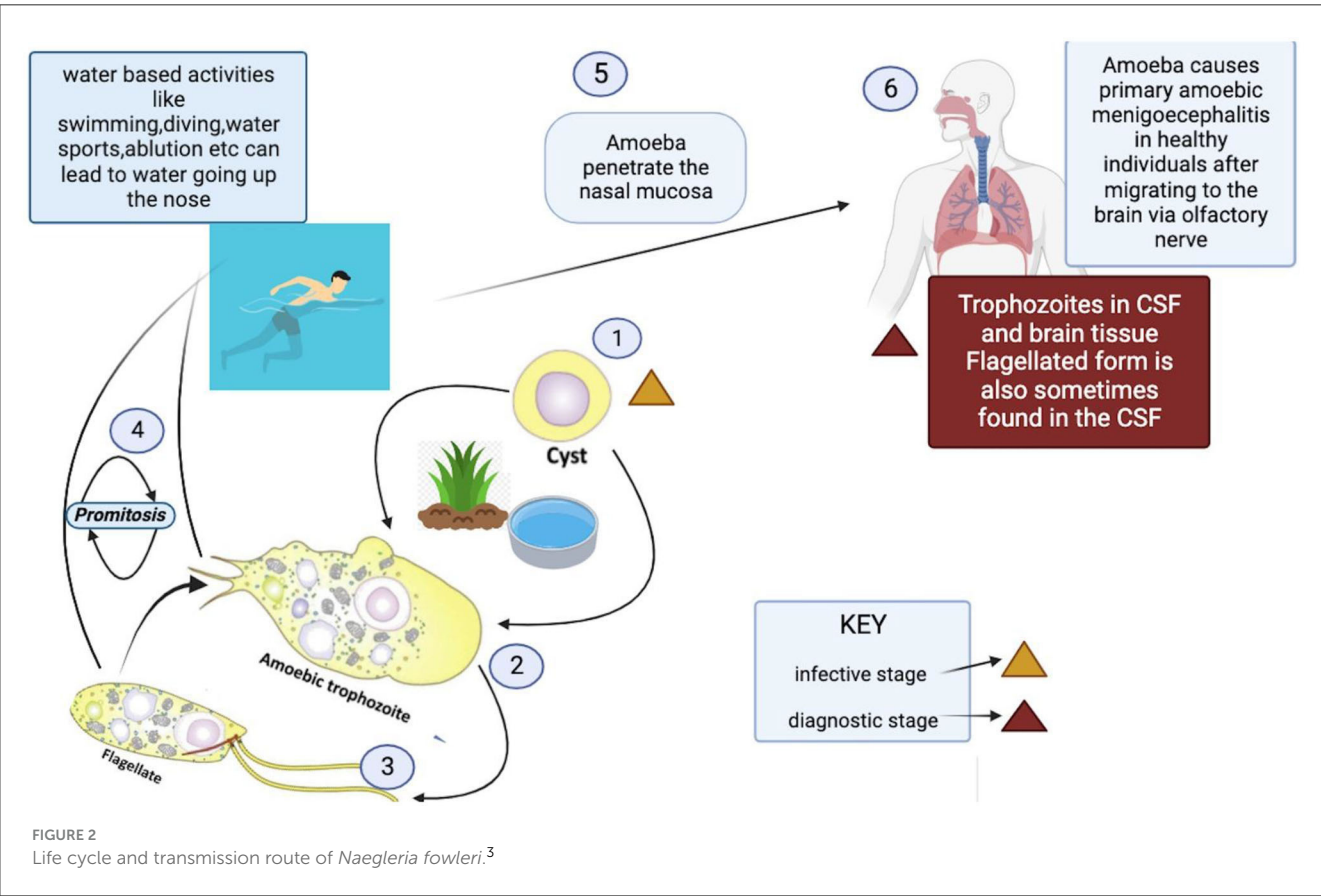


FIGURE 1  
A wet mount of *Naegleria fowleri* trophozoites cultured from a patient of primary amebic encephalitis (PAM) (from <https://www.cdc.gov/parasites/Naegleria/Naegleria-fowleri-media.html>).



3 BioRender. Available online at: <https://app.biorender.com/user/signin> (accessed July 14, 2023).



TABLE 1 Onset signs and symptoms of *Naegleria fowleri* infection (26).

Onset	Signs and Symptoms
Early	Fever Headache Nausea Vomiting Changes in smell and taste
Late	Stiff neck Fatigue Hemorrhage Confusion Changes in personality Hallucinations Seizures Coma

### 3. Clinical manifestations and signs and symptoms

PAM is characterized by symptoms that resemble those of bacterial or viral meningitis, such as fever, stiff neck, headache, vomiting, anorexia, and seizures (25). Fatigue, headaches, nausea, and vomiting are a few of the early signs of the illness. Later, more serious symptoms including confusion, neck stiffness, photophobia, seizures, and cranial nerve abnormalities start to appear (18) (Table 1). The amount of time between initial contact with the pathogenic *N. fowleri* strain and the onset of clinical symptoms can range from 2 to 3 days to as long as 7–15 days, depending on the strain's virulence and the size of the inoculums (27). Clinical signs like changes in smell perception and respiratory infections indicate involvement of the olfactory epithelium and invasion of brain tissue (28). Before showing signs of PAM, such as meningitis, patients with PAM do not exhibit any nasal irritation symptoms, such as pain, bleeding, tenderness at the bridge of the nose, sneezing, and/or prolonged rhinorrhea (25). Severe headache, fever, chills, positive Brudzinski and Kernig signs, photophobia, confusion, seizures, and potential coma are among the most typical symptoms. In a few cases, myocardial necrosis and aberrant heart rhythms have also been reported (29). The apparent correlation between elevated cerebral spinal fluid (CSF) and intracranial pressure and mortality is, arguably, the most significant finding. Patients with *N. fowleri* infections have been shown to have CSF pressures of 600 mm H<sub>2</sub>O (28). According to CSF analysis, there are several color anomalies, ranging from gray in the early stages of infection to red in the late stages of sickness because of a large increase in red blood cells (30, 31). Additional increases in trophozoites and polymorphonuclear cell densities (up to 26,000 mm<sup>3</sup>) are also observed (28, 29). In the majority of cases, primary amebic encephalitis advances quickly, resulting in hemorrhage, coma, and death (18) (Figure 3). Death usually occurs 3–7 days following the onset of these symptoms (25).

### 4. Virulence of *Naegleria fowleri*

*N. fowleri*'s pathogenicity can be attributed to two primary characteristics. First, *N. fowleri* may consume brain tissue

by a sucker-like surface structure known as a “food cup”. These feeding cups are created by the phagocytic activity of *N. fowleri*, which is mediated by Nf1 and Nfactin (32). Second, *N. fowleri* secretes a variety of cytolytic chemicals, such as neuraminidases, acid hydrolases, phospholipases, and phospholipolytic enzymes, which can damage nerves in the central nervous system (CNS). Additionally, *N. fowleri* infection triggers a strong immune response that further damages the CNS (33). Although not fully understood (32), it is believed that *N. fowleri* has also developed mechanisms that inhibit the host immune system (34).

### 5. Replication of *Naegleria fowleri*

*N. fowleri* reproduces through a process known as binary fission, a form of asexual reproduction that allows a single organism to divide and generate two identical offspring (2). Reproductive division in *N. fowleri* involves promitosis, which occurs without the breakdown of the nuclear envelope (35). During this process, the mature parent cell undergoes replication of its genetic material while simultaneously increasing in size. The DNA within the parent cell then migrates toward opposite poles, and eventually, the cell membrane undergoes division, resulting in the formation of two daughter cells that are genetically indistinguishable from each other and from the parent cell (2).

### 6. Epidemiology of *Naegleria fowleri*

*N. fowleri* may be found anywhere around the world except for Antarctica (36), but it is dominant in certain geographic areas that offer suitable conditions for its survival and growth. Statistics show that infections with *N. fowleri* have been documented in 39 different nations. However, Pakistan, Mexico, Australia, the Czech Republic, and India have been the countries most impacted, along with the United States of America (USA) (19). This is because *Naegleria* thrives in hot temperatures and may be more prevalent in certain regions of these countries with warmer temperatures and an abundance of warm freshwater bodies, such as lakes, ponds, and poorly maintained swimming pools. For instance, in the USA, they were more prevalent in the Southern states (37) that have hotter temperatures (38).

Pakistan has faced several *N. fowleri* outbreaks in the past, causing serious public health issues. In several parts of Pakistan, the temperature can rise beyond 50°C,<sup>4</sup> and the monsoon season, which is characterized by increased rainfall and stagnant water,<sup>5</sup>

4 Pakistan Records Hottest Day Ever in Turbat Area of Balochistan. Al Arabiya English. Available online at: <https://english.alarabiya.net/News/world/2017/05/29/Pakistan-records-hottest-day-ever-in-Turbat-area-of-Balochistan> (accessed September 6, 2023).

5 Pakistan - Climatology. Climate Change Knowledge Portal. Available from: <https://climateknowledgeportal.worldbank.org/country/pakistan/climate-data-historical> (accessed September 6, 2023).

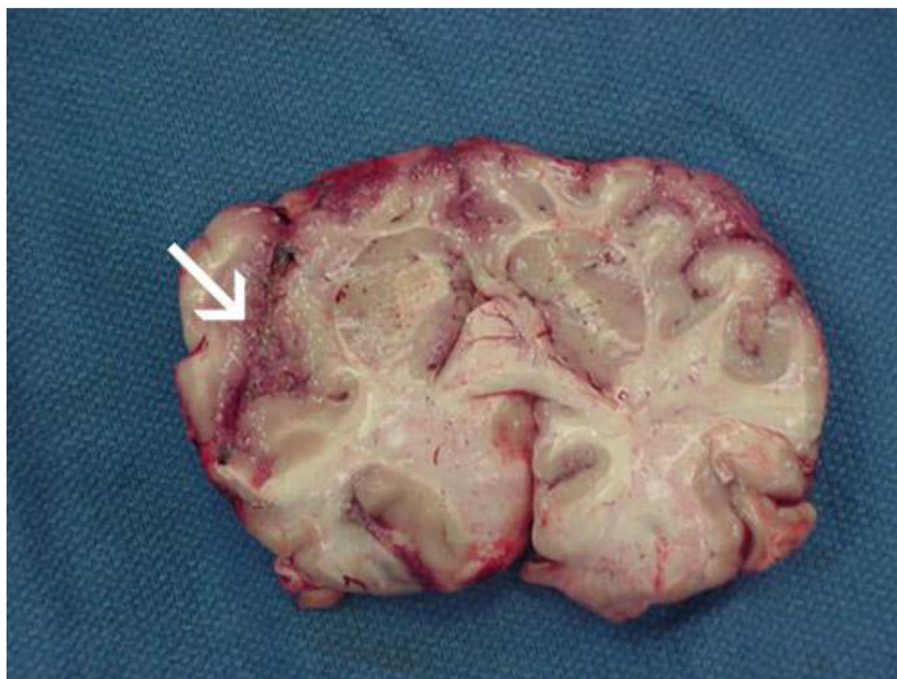


FIGURE 3

Focal hemorrhage and necrosis in frontal cortex due to *Naegleria fowleri* (from <https://www.cdc.gov/parasites/Naegleria/Naegleria-fowleri-media.html>).

also has an impact on the epidemiology of the disease there (39). A significant number of cases were reported in Karachi which has particularly scorching temperatures (40), most of them being reported between April and September when temperatures are peaking (41).

It is also noteworthy that individuals are more likely to engage in water-related activities such as swimming during the hot summer months, thereby increasing the likelihood of contracting *Naegleria*.

A study revealed that the water chlorination levels in Karachi's municipal water supply fell below the World Health Organization's recommended level of 0.5 ppm (41). Moreover, a significant number of individuals, particularly those from rural backgrounds, rely on unfiltered and non-chlorinated groundwater, which can act as a conducive breeding environment for *N. fowleri*. Pakistan is a predominantly Muslim country, and the use of groundwater and contaminated tap water for ritual ablution is a crucial factor contributing to the increase in *Naegleria* infections within the country.

## 7. Global geographic spread of infection

PAM is an uncommon but lethal disease that primarily affects young adults in wealthy nations but has also lately been documented in poorer nations, with a 95–99% fatality rate (2). After four patients died in Australia's Adelaide Children's Hospital in

1965, Fowler and Carter became the first to characterize PAM (19). An ameba invasion of their meninges, which caused significant damage and inflammation in the brain, was identified as the cause of death (42–44). PAM has since been recorded in other nations, with an estimated 400 victims globally. The total number of cases, however, is unknown and may be higher because of incorrect diagnoses or unreported cases (45–47). Except for Antarctica, 15 countries throughout the world have reported PAM cases (48, 49). These cases, which only number a few hundred, are primarily from Europe, Australia, the United States, and several Asian nations (13). Despite the stability of the reported infections in the United States each year (0–8), recent alterations in the epidemiology of PAM are quite concerning (50). In 2010, a PAM case from the northern state of Minnesota was reported for the first time. In 2011 and 2012, additional cases from Indiana, Minnesota, and Kansas were then reported, raising concerns about the infection's potential to spread across a wider geographic area due to the heat-loving, potentially climate-sensitive pathogen (51). In the United States, 142 PAM patients were recorded between 1937 and 2013. Approximately 260 cases have been reported worldwide between 1962 and 2014, according to a comprehensive study. Of these, 132 cases originated from the United States, 19 from Australia, 17 from Pakistan, 16 from the Czech Republic, 11 from India, 9 from Mexico, 9 from New Zealand, 7 from Venezuela, 5 each from Thailand and Belgium, 4 from Nigeria, 2 from the United Kingdom, and 1 case each from Namibia, Iran, Costa Rica, New Guinea, South Africa, and Madagascar. Out of the 260 documented cases (50, 52), just 11 individuals were said to have survived. The US Center for Disease Control and Prevention (CDC) reports

**TABLE 2** Reported cases and fatalities of primary amebic meningoencephalitis (PAM) in Pakistan (2008–2023) by year and gender.

Year	Number of cases and fatalities	Age group-gender	References
2008	2 cases	Age group: 30-y-old, 25-y-old Gender: all are males	(24)
2009	11 cases	Age group: from 16 to 64 y	(55)
2010	20 cases	Age group: not reported Gender: all are males	(56)
2011	13 cases	Age group: not reported Gender: all are males	(24)
2012	22 cases	Gender: all are males	(41)
2013	3 cases	Age group: from 14 to 40 y Gender: all are males	(41)
2014	14 cases	Age group: from 14 to 40 y Gender: all are males	(41)
2015	13 cases	Age group: from 16 to 56 y Gender: 10 males, 3 females	(41)
2016	5 cases	Not reported	(57)
2017	6 fatalities	Not reported	(57)
2018	7 fatalities	Not reported	(58)
2019	11 fatalities	Age group: from 21 to 45 y Gender: 10 males	(58)
2020	16 cases	Not reported	(59)
2021	1 case	Age: 19 y old	(60)
2022	5 cases	Age: 2 cases of 59 y old, 1 case of 38 y old, 1 case of 28 y old Gender: 2 males, rest not reported.	(54)
2023	5 cases	Age: 1 case of 21 y old, 1 case of 45 y old Gender: 1 female, 2 males, rest not reported.	(61)

that there were 138 PAM cases in the US between 1962 and 2015 (53). A recent rise in PAM instances has been observed in Asian nations.

## 8. *Naegleria fowleri* outbreak in Pakistan

In Karachi, Pakistan's largest city, this ameba has been a growing concern (54). The Aga Khan University Hospital in Karachi, Pakistan, reported a noticeable death rate of about 20 deaths per year caused by PAM in Pakistan (2). As shown in Table 2 and Figure 4, from 2008 onwards *N. fowleri* has consistently been associated with a variable number of cases and fatalities.

Up to October of the year 2019, fifteen fatalities were documented (58, 62). 2020 had no confirmed deaths, although there is no assurance because of a lack of data collecting and

**TABLE 3** Detection methods for *Naegleria fowleri* in clinical and environmental samples.

Detection method	Description
Direct visualization	The motile ameba can be observed under a microscope in a fresh sample of cerebrospinal fluid (CSF).
Antigen detection	Specific antibodies can be used in conjunction with immunohistochemistry (IHC) or indirect immunofluorescence (IIF) to directly stain amebic antigens in tissue.
Polymerase chain reaction (PCR)	Specific molecular tools can amplify DNA from the ameba in CSF or tissue.
Ameba culture	The ameba can be grown into culture, increasing the likelihood of detecting it by direct visualization or PCR.
Environmental detection	Water samples can be collected, concentrated, and put into culture to grow and select for <i>N. fowleri</i> .

unreported instances. In 2021, six fatalities were recorded (63). As of July 1, 2022, there have been four fatalities (64).

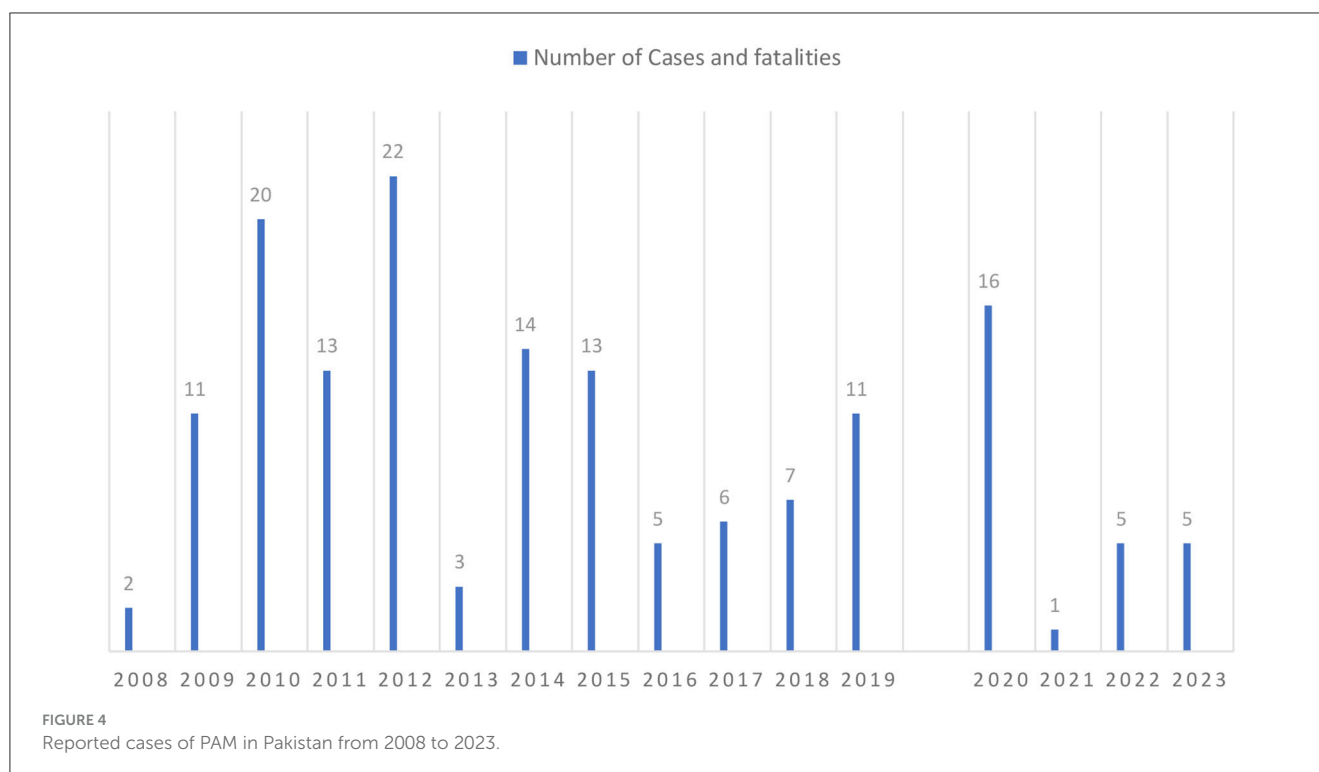
## 9. Factors contributing to the outbreak

The environment where *N. fowleri* infection is most likely to occur is characterized by warmer, polluted water. Infectious trophozoites can enter the body through the nose, cross the cribriform plate, and enter the human brain, where they can cause serious CNS damage, brain hemorrhage, and eventually death within 3–7 days. Moreover, this illness is made more deadly by delayed diagnosis and a lack of effective treatment options (2). Since the 1970s, researchers have known that *N. fowleri* and other free-living ameba multiply best between 30–42°C (65–67). When compared to cultures cultivated at the ideal 37°C, *N. fowleri* has also been proven to endure temperatures up to 45°C, however with reduced survival (66, 68). Environmental investigations have established that *Naegleria* can be found in thermal saline baths and naturally low-salinity water (68, 69). Lam et al. determined that after 48 h *N. fowleri* could survive in moderate salinity of up to 1.4%. This is roughly half as salty as ocean water and three to four times as salty as saltwater swimming pools (70).

## 10. Diagnostic modalities for *Naegleria fowleri* and primary amebic meningoencephalitis

It is difficult to treat *Naegleria* patients because of the rarity of the infection and the challenges in initial detection. Usually, the parasite is detected posthumously in the CSF samples of the victim using microscopy and advanced referral testing techniques. To form a definitive diagnosis, PAM can be confirmed in patients through investigations mentioned in Table 3 below.

Typically, cultivation and confirmation of *N. fowleri* in the cerebrospinal fluid (CSF) are required for the laboratory diagnosis of PAM. A flagellation test (FT) is also frequently



employed as an additional diagnostic method for *N. fowleri*. Due to the prevalence of some false negatives, FT must be followed by Enzyme-linked immunosorbent assay (ELISA) or another diagnostic technique [PCR, Restriction fragment length polymorphism (RFLP)] following both positive and negative results (71).

Diagnostic techniques based on ELISA typically only offer postmortem, retrospective, and late diagnoses. The genus *Naegleria*'s various restriction profiles serve as the foundation for the species-specific diagnostic technique known as RFLP. This method's advantage is its capacity to diagnose not only *N. fowleri* but also other *Naegleria* genus species. In the middle of the 1990s, a DNA probe-based detection approach was described (72). A useful alternative to microscopy and culture, molecular approaches are generally quite sensitive and may enable the discovery of microorganisms that are challenging to identify.

Most of these procedures have limitations, though, such as taking a long time (cultivation), being expensive (RFLP), only offering a late and retrospective diagnosis (ELISA), or yielding insufficient data (flagellation test). Many of these issues are resolved by PCR diagnostic techniques, which are helpful for the diagnosis of clinical and environmental specimens. One of the main benefits is that these PCR procedures take less time because it is possible to isolate DNA from the sample without prior culture. Additionally, PCR permits not only the detection of *N. fowleri* but also the distinction between other species of the *Naegleria* genus. Real-time PCR-based diagnostic techniques have the advantage of producing results quickly and allowing for real-time amplification process observation (73).

LAMP, or loop-mediated isothermal amplification, is a recent technique for amplifying DNA. LAMP is a gene amplification assay that is extremely specific, sensitive, quick, and repeatable.

LAMP has several key advantages over other approaches, including ease of use, the ability to produce many precise amplification products at a consistent temperature without the need for expensive equipment, and the ability to visually assess the outcome of an amplification response. In clinical laboratories or field studies, such a test could be a helpful diagnostic tool, particularly in countries with limited resources. LAMP has been extensively utilized to find protozoan infections. Only one study proves that LAMP can be used to detect *Naegleria* in place of conventional PCR tests. This is because only a few of the putative DNA targets of the parasite have been investigated, probably because PAM is a rare disease (74).

Furthermore, patients with *N. fowleri* infections have been seen to have CSF pressures as high as 600 mm<sup>3</sup> H<sub>2</sub>O. Due to a considerable rise in red blood cells, CSF analysis reveals a variety of color abnormalities, ranging from gray in the early stages of infection to red in the late stages. Additional increases are noted in trophozoites present in the CSF (using trichrome or Giemsa stain) and polymorphonuclear cell concentrations (as high as 26,000 mm<sup>3</sup>). The midbrain and subarachnoid space are two areas of the brain that Magnetic resonance imaging (MRI) frequently reveals to be abnormal (28, 29) in PAM.

## 11. Treatment options available

Since the discovery of primary amebic meningoencephalitis, numerous antifungal, antiprotozoal, antibacterial, and antipsychotic therapeutics have been tested against *N. fowleri*. Most of these medications were shown to be ineffective or hardly effective against *N. fowleri*, both *in vitro* and *in vivo*. Even though Amphotericin B (AmB) is still the drug of choice for treating



primary amebic meningoencephalitis, using it is usually linked to renal damage, which manifests as azotemia and hypokalaemia. AmB frequently results in anemia, and many patients also have headaches, nausea, vomiting, chills, and fever. Additionally, not all AmB-treated patients have recovered from primary amebic meningoencephalitis (75).

Azithromycin (AZM) has demonstrated *in vivo* action against experimental toxoplasmosis as well as *in vitro* activity against *Acanthamoeba* spp. By attaching to the bacterial 50S ribosomal subunit and preventing the creation and translocation of peptide bonds, AZM prevents the production of proteins by bacteria. However, the mechanisms of action of AZM in *Acanthamoeba*, *Naegleria*, and *Toxoplasma* spp. have not been determined and require further research (75).

In combination with some of these other medications, the anti-leishmanial and breast cancer medication, miltefosine (MLT), has shown some promise against free-living amebae. MLT has demonstrated amebicidal activity against *Balamuthia*, *N. fowleri*, and *Acanthamoeba* *in vitro* and in mice models. It has been used to successfully treat patients with disseminated *Acanthamoeba* infection and *Balamuthia* infection. At high doses, patients taking MLT may experience nausea, vomiting, or diarrhea. It is somewhat nephrotoxic meaning that people with compromised kidney function may need to have their dosage modified and the risk for nephrotoxicity should be weighed against the risk for PAM-related mortality. It is important to note that there is still limited data on the dose of MLT that effectively treats amebic infection (76).

Auranofin, an anti-rheumatic medication, is amebicidal against *N. fowleri*. Auranofin treatment of *N. fowleri* cultures resulted in decreased ameba numbers, increased metabolic activity, and enhanced cell permeability at biologically relevant concentrations of 0.75–3.0 g/ml. These findings imply that the inclusion of auranofin in the treatment regimen for *N. fowleri*-infected individuals experiencing PAM may be beneficial (77, 78).

Staurosporine (STS), an indolocarbazole isolated from the bacteria *Streptomyces sanyensis*, has also demonstrated high activity against *N. fowleri* trophozoites *in vitro*. It has been suggested that its amebicidal activity occurs by inhibiting the ameba's protein kinase (PK) and inducing an apoptosis-like mechanism via the mitochondrial pathway, but more studies are required to confirm the mechanism of action (19).

Another drug with potential against *N. fowleri* trophozoites is pitavastatin. This medication has shown EC50 values against five different strains that range from 0.3 to 4  $\mu$ M, demonstrating that it is more potent than miltefosine (EC50 values between 15 and 58  $\mu$ M), but less potent than AmB (EC50 values between 0.06 and 0.2  $\mu$ M). Pitavastatin decreases the development of the ameba *in vitro* by more than 60% as early as 10 h after exposure. Inhibition reaches 81% after 16 h and 96% after 24 h. Pitavastatin is an FDA-approved cholesterol-lowering drug, therefore its effects on various human cell lines have been well-studied (19, 79).

In a more recent investigation, different antibiotics and antifungals that could be used to treat PAM were evaluated using a high-throughput phenotypic screening method. The antifungal posaconazole (PCZ) stood out amongst these medications. This substance has an IC50 value of 0.24  $\mu$ M and can stop an ameba's growth in about 12 h. Although no synergy was seen, PCZ also

showed additive activity with AZM, AmB, and MLT. Additionally, sick mice who received 20 mg/kg of PCZ intravenously had a 33% survival rate; however, when PCZ and AZM were combined, the survival time was dramatically increased (80, 81).

Fluconazole, rifampin, and dexamethasone are some other drugs used in combination with amphotericin B. To kill the ameba inside the CNS, however, a minimum inhibitory concentration (MIC) of these medications must be provided, and they have demonstrated poor blood-brain barrier penetration (19).

The limited efficacy that many medications display because of their failure to successfully cross the BBB is one of the key issues associated with CNS infections. Sometimes, the solution to this issue is to deliver more of the medicine, however doing so may cause cell toxicity. Since they can increase a drug's effectiveness and enable a reduction in dosage, nanoparticles have drawn interest from the pharmaceutical sector. Studies have been conducted to understand the benefits of employing medications conjugated with nanoparticles to treat PAM because nanoparticle drug delivery methods have been shown to boost bioavailability, minimize cell toxicity, and are site-specific (19).

Recently, AmB and nystatin (NYS) coupled with silver nanoparticles (AgNp) have been shown to be more effective against *N. fowleri* than on their own. Apart from that gold nanoparticles (AuNp) are also being investigated as potential drug delivery techniques to treat PAM. In one study, AuNp was combined with curcumin to test its effectiveness against *N. fowleri* because the compound has anti-inflammatory characteristics and can reduce lipid peroxidation. At a concentration of 200  $\mu$ M, curcumin exhibited a 66% amebicidal activity against *N. fowleri* because of concentration-dependent action. The bioavailability of curcumin was greatly increased by conjugation with AuNp, and this led to a 69% amebicidal activity at a concentration of 10  $\mu$ M. The human keratinized skin cells were not cytotoxically affected by curcumin conjugated with AuNp. Additionally, the secondary plant metabolite trans-cinnamic acid, which is derived from plants, has been conjugated with AuNp. Green nanoparticles created using green chemistry have also been investigated as potential safer and more environmentally friendly medicine delivery systems. Therefore, more recently, plant-derived polysaccharides such as gum tragacanth (Gt) and gum acacia (Ga) have been used to stabilize metal nanoparticles. Hesperidin (HDN) and Naringin (NRG), two flavonoids with antioxidant and anti-inflammatory properties that may help lessen the immunopathogenic process released during PAM, were conjugated to the green nanoparticles. In comparison to the nanoparticles alone, both Ga-AgNPs-HDN and Gt-AuNPs-NRG have shown substantial amebic activity against *N. fowleri* (19).

## 12. Impact on communities

Both communicable and non-communicable disorders are already overburdening Pakistan's healthcare system. Pakistan is one of the few nations where poliovirus is still prevalent and at this point, if a *Naegleria* epidemic occurs, it would further exacerbate already existing gaps in the healthcare system (54).

Pakistan has experienced massive outbreaks of diseases like diarrhea, dengue, malaria, polio, and COVID-19 amid record floods that have harmed over 900 medical facilities and affected 33 million people. The nation has the second-highest global hepatitis C burden.<sup>6</sup> Following the floods, Pakistan has seen an increase in both malaria and dengue cases and 78% of all confirmed malaria cases in 2022 occurred in Sindh and Balochistan (82). Flood water stands still and can be a breeding ground for *Naegleria*. The hot temperature of Punjab and Sindh province of Pakistan further boost survival conditions for *N. fowleri*. The optimal temperature range for *N. fowleri* growth is up to 115°F (46°C) and it may endure greater temperatures for brief periods even though it may not be able to develop as effectively. The trophozoites and cysts may endure 122–149°F (50–65°C) for minutes to hours, with the cysts being more resilient (35). The community can face harsh consequences due to an *N. fowleri* outbreak. This is keeping in mind that the public and economy still haven't been able to move on from the damage imposed by previous outbreaks like malaria and dengue which were also due to massive floods in Pakistan.

The cases of *N. fowleri* infections that have occurred in Pakistan during the past 8 years have not been completely described by any study. Most of the data for the nation is either missing or not reported. The healthcare system in Pakistan is already overstressed. The system has a lack of employees and is underfunded. Since PAM progresses quickly, most patients have clinically deteriorated by the time the diagnosis is made. Due to the disease's rarity, the CDC reports that autopsies performed after patient deaths confirm the diagnosis in 75% of instances. After the development of clinical symptoms, the patient only has a very small window of time for therapy to be effective. Given the exceedingly high death rates associated with PAM (almost 100%), it is likely that many individuals seek medical care at a point where current treatments are useless. The available information summarized in Section 8, Table 2, and Figure 4 indicates that there have been more deaths in recent years, thus reiterating the need for action to combat the increasing trend.

### 13. Overcoming the crisis

No significant measures are being taken by the Government of Pakistan to counter the *N. fowleri* outbreak because of the rarity of the disease and absence of definitive treatment. But during 1970s and 1980s cases of *Naegleria* associated PAM came up in Australia (83). There, drinking water was distributed by overland pipes for hundreds of kilometers before it arrived at household faucets with no discernible residual disinfection. Implementing an amoeba monitoring scheme and raising disinfection residual levels was the successful Australian reaction to these PAM incidents (19); nevertheless, certain systems necessitated switching to chlorination to maintain disinfectant residual levels over extended distances

(89). The health authorities of Pakistan should adopt the methods used by the Australians with the hope of ensuring the safety of the civilians and countering this outbreak. The concerned authorities could also set up an amoeba monitoring system and an efficient chlorination system. The chlorination facility is available in Pakistan but no check and balance is implemented for its proper working. Moreover, for the first time, a PAM-associated death was linked to a U.S. treated drinking water system that had culturable *N. fowleri* in it (84). Previously, in 2011, one neti pot PAM incident occurred in the same US area of St. Bernard Parish, Louisiana and this discovery sparked an environmental assessment of the household and parish water distribution system, and the results finally revealed the presence of *N. fowleri* along with numerous undetected disinfectant residual areas (84).

Water utility and health officials decided that a temporary chlorine conversion was necessary to inactivate *N. fowleri* and reduce biofilm in the distribution systems because the St. Bernard and DeSoto Parish water utilities used chlorination to maintain a disinfectant residual in their systems. According to health officials, *N. fowleri* should not grow if a free chlorine level of 2.0 mg/L is maintained in all storage tanks for at least 60 days and a free chlorine level of 2.0 mg/L is maintained at all points in the distribution system. Each water system turned off the ammonia feed and boosted the free chlorine feed to start the chlorine conversion process after warning the public about the upcoming conversion of chlorine. Disinfectant residuals in the St. Bernard and DeSoto distribution systems met or exceeded the 1 mg/L free chlorine objective following the chlorine conversion (85). Since *N. fowleri* is vulnerable to chlorine inactivation, no *N. fowleri* was found in either system after the chlorine conversion. Conditions in the St. Bernard distribution system favored *N. fowleri* growth and persistence. The distribution system's water temperatures rose, thus allowing *N. fowleri* to flourish (86). It was challenging to keep the disinfectant residual consistent throughout the distribution system, as seen by a decline in average concentration over time. Over the course of the year, Heterotrophic Plate Count (HPC) concentrations also increased. HPC is widely regarded as a good measure of biofilm formation and is an indicator of bacterial regeneration inside a distribution system (87). Because *N. fowleri* easily forms biofilms and survives there, more residual or contact time with the disinfectant is needed to sufficiently inactivate it (85). Therefore, a rise in HPC over time suggests that *N. fowleri* may be present and that the distribution system's circumstances are conducive to biofilm formation and persistence. According to a 1984 study, the abundance of *N. fowleri* in drinking water distribution systems was inversely correlated with chlorine residual and positively correlated with water temperature and colony counts at 35°C (like HPC) (88). *N. fowleri* was both eliminated and prevented from recolonizing in bulk water and biofilm at a constant free chlorine concentration of >1 mg/L (85). The discovery of non-viable *N. fowleri* in the St. Bernard system in September suggests that the circumstances in the distribution system were suitable for containing *N. fowleri*. To find out what other elements contribute to the discovery of *N. fowleri* in drinking water distribution systems, further research is required. If such a chlorination system is recruited by the government of Pakistan then combating *N. fowleri*

6 Pakistan Faces Widespread Outbreaks of Infectious Diseases Amid Unprecedented Floods. Available online at: <https://www.news-medical.net/news/20220909/Pakistan-faces-widespread-outbreaks-of-infectious-diseases-amid-unprecedented-floods.aspx> (accessed July 14, 2023).

outbreak will be quite easy. Managers of water distribution systems should be knowledgeable about the ecology of their systems, be aware of any changes in water quality brought on by rising water temperatures, and seek to minimize any locations where biofilm formation may be an issue and have an impact on water quality (89). There aren't any biofilm monitors (such as) for water in pipelines in Pakistan but to avoid a dangerous *N. fowleri* outbreak such monitoring systems should be installed. Also, strict measures to chlorinate tap water should be adopted to eliminate any parasites existing in this supply.

The public should take extra precautions when using tap water for nose or sinus cleaning because there is no guarantee that even the most careful drinking water system can entirely eradicate *N. fowleri*. At the point of use, water used for nasal, or sinus rinses should receive additional treatment. This can include boiling the water for 1 min and letting it cool before using, filtering the water through a device with an absolute pore size of one micron or less, disinfecting the water with chlorine bleach, or using distilled or sterile water (89). Furthermore, if swimming in water bodies can at no cost be avoided then one should put nose plugs in use to prevent water entering the nose. In addition, whilst swimming one's head should be held up above the surface of water. It would be better to ensure that chlorine levels of the water body are appropriately high to keep the parasite out of it (20).

## 14. Lessons learned and recommendations

To build resilience for future outbreaks and to promote early detection of *N. fowleri* in Pakistan, both of which mitigate the potential dangers associated with this lethal amoeba, it is important that we first evaluate the gaps in preparedness and response mechanisms to *N. fowleri* in Pakistan and then work toward filling those gaps.

Pakistan is a developing country with a high percentage of people living under the poverty line (90). It has a literacy rate of only 62.3% which indicates that at present, ~60 million people are illiterate in the country.<sup>7</sup> Public awareness and education are two major areas that require attention. The existence and consequences of *N. fowleri* are still largely unknown among the general public in Pakistan.

The deficiencies in our healthcare system also need to be dealt with. These include rural-urban disparity in healthcare provision, lack of essential diagnostic and therapeutic facilities, and a low doctor-population, nurse-population, and hospital beds to population ratio in the country (10).

Third, as mentioned before, poorly maintained and chlorinated water supply systems, swimming pools, and recreational water bodies are all possible breeding grounds for *N. fowleri* and serve as sources of infection. This is a major challenge in Pakistan

where water surveillance and water standards are far from satisfactory (9).

To bridge these gaps and to safeguard public health in Pakistan it should be ensured that information on symptoms, preventive measures like the use of nose clips and water chlorination, and the value of early diagnosis and treatment, which have been shown to increase survival rates (91) is communicated widely among the people. This can be done by way of public health advertisement campaigns on social media, TV, radio, and newspapers in addition to conducting informative sessions about the disease.

The current health expenditure in Pakistan is only 2.95% of the GDP<sup>8</sup> and a greater budget needs to be allocated to healthcare to deal with the various problems associated with it. The formation of well-equipped healthcare centers and laboratories along with the training of health workers to promptly identify and formulate effective treatment regimens for *N. fowleri* patients is of vital importance. It must also be made certain that all patients, including those living in far-off rural areas, have access to appropriate medical services to help tackle the infection.

Besides that, laws should be set in place to tighten water surveillance and improve water quality in line with WHO standards,<sup>9</sup> and greater investment in water infrastructure also needs to be made.

Finally, and most importantly, cooperation and a joint, collaborative effort between the various interested parties including the public, governmental organizations, healthcare providers, and water supply authorities is imperative and will help to ensure an effective and systemized response even if an *N. fowleri* epidemic arises in the future.

## 15. Role of research and public health organizations in *Naegleria* prevention and control

Research institutions play a crucial role in providing up-to-date information necessary for a better understanding of *N. fowleri*. This knowledge contributes to the development of effective preventive measures, targeted therapies, and advancements in disease detection and diagnosis. Through studies on the prevalence and distribution of disease, research institutions can also help identify disease patterns and high-risk groups. Additionally, they can investigate water quality and contamination to identify potential sources of infection. Furthermore, research allows for the evaluation of the effectiveness of preventive measures and treatment options.

Consequently, establishing a strong link between research institutions and public health organizations is vital in creating comprehensive strategies that encompass prevention, monitoring, and rapid intervention to safeguard the public from the threat

7 Ministry of Federal Education and Professional Training. Available online at: <https://mofept.gov.pk/ProjectDetail/NjQ4ZTg2NjltOWM2NC00Y2lxLTkzMDgtMjU2OTFhMjA4NzNh> (accessed July 13, 2023).

8 Current health expenditure (% of GDP) - Pakistan. Data. Available online at: <https://data.worldbank.org/indicator/SH.XPD.CHEX.GD.ZS?locations=PK> (accessed July 13, 2023).

9 Water Sanitation and Health. Available online at: <https://www.who.int/teams/environment-climate-change-and-health/water-sanitation-and-health/water-safety-and-quality> (accessed July 13, 2023).

of *N. fowleri*. Collaboration and teamwork between these entities facilitate the pooling of resources and data. This collaborative effort leads to the formulation of policies and treatments that are firmly grounded in scientific evidence, thereby improving the overall health of the general population. Moreover, this collaborative approach aims to reduce or eliminate inequalities in healthcare, ensuring that all individuals have access to appropriate care and resources (92).

## 16. Conclusion

In conclusion, the *N. fowleri* crisis in Pakistan has exposed an alarming situation that requires urgent action and recovery initiatives. The devastating impact of this brain-eating amoeba on public health necessitates a comprehensive and well-executed action plan. Despite this, through collective efforts and an unrelenting dedication to public health, there is hope that the country can overcome this calamity. The outbreaks of *N. fowleri* in Pakistan have compounded existing healthcare burdens and environmental issues, making it imperative for the government to take proactive measures. Implementing an amoeba monitoring system and efficient water chlorination are crucial steps to prevent further spread of the amoeba.

Public awareness campaigns and education are vital to inform the population about preventive measures and the significance of early diagnosis and treatment. Collaboration between research institutions and public health organizations is crucial in formulating evidence-based policies and treatments, ensuring the safety and wellbeing of the people.

## References

1. CDC. General Information. *Naegleria fowleri*. (2023). Available online at: [https://www.cdc.gov/parasites/naegleria/general.html#anchor\\_91787](https://www.cdc.gov/parasites/naegleria/general.html#anchor_91787) (accessed July 10, 2023).
2. Jahangeer M, Mahmood Z, Munir N, Waraich Ue A, Tahir IM, Akram M, et al. *Naegleria fowleri*: sources of infection, pathophysiology, diagnosis, and management; a review. *Clin Exp Pharmacol Physiol*. (2020) 47:199–212. doi: 10.1111/1440-1681.13192
3. Sarfraz MR, Tariq H, Rehman S, Khan S. *Naegleria fowleri*—the brain-eating amoeba: an emerging threat in Pakistan. *Acta Bio-medica*. (2023) 94:e2023024. doi: 10.23750/abm.v94i2.13843
4. Aurongzeb M, Rashid Y, Naqvi SHA, Khatoon A, Haq SA, Azim MK, et al. *Naegleria fowleri* from Pakistan has type-2 genotype. *Iran J Parasitol*. (2022) 17:43–52. doi: 10.18502/ijpa.v17i1.9015
5. CDC. Case Report Data & Graphs. *Naegleria fowleri*. (2023). Available online at: <https://www.cdc.gov/parasites/naegleria/graphs.html> (accessed July 11, 2023).
6. Ali M, Jamal SB, Farhat SM. *Naegleria fowleri* in Pakistan. *Lancet Infect Dis*. (2020) 20:27–8. doi: 10.1016/S1473-3099(19)30675-9
7. United Nations Development Programme. *Environment and Climate Change*. Available online at: <https://www.undp.org/pakistan/environment-and-climate-change> (accessed July 11, 2023).
8. BBC News. *Climate Change Swells Odds of Record India, Pakistan Heatwaves*. (2022). Available online at: <https://www.bbc.com/news/science-environment-61484697> (accessed July 11, 2023).
9. DAWN.COM. *Alarmed by Naegleria Deaths, Karachi Experts Urge Govt to Supply Chlorinated Water – Pakistan*. (2023). Available online at: <https://www.dawn.com/news/1756950> (accessed July 13, 2023).
10. Shaikh BT, Ali N. Universal health coverage in Pakistan: is the health system geared up to take on the challenge? *Global Health*. (2023) 19:1–6. doi: 10.1186/s12992-023-00904-1
11. CDC. *Naegleria fowleri — Primary Amebic Meningoencephalitis (PAM) — Amebic Encephalitis*. (2023). Available online at: <https://www.cdc.gov/parasites/naegleria/index.html> (accessed July 17, 2023).
12. Maciver SK, Piñero JE, Lorenzo-Morales J. Is *Naegleria fowleri* an emerging parasite? *Trends Parasitol*. (2020) 36:19–28. doi: 10.1016/j.pt.2019.10.008
13. Siddiqui R, Ali IKM, Cope JR, Khan NA. Biology and pathogenesis of *Naegleria fowleri*. *Acta Trop*. (2016) 164:375–94. doi: 10.1016/j.actatropica.2016.09.009
14. De Jonckheere JF. Origin and evolution of the worldwide distributed pathogenic amoeboflagellate *Naegleria fowleri*. *Infect Genet Evol*. (2011) 11:1520–8. doi: 10.1016/j.meegid.2011.07.023
15. Baig AM, Khan NA. Novel chemotherapeutic strategies in the management of primary amoebic meningoencephalitis due to *Naegleria fowleri*. *CNS Neurosci Ther*. (2014) 20:289. doi: 10.1111/cns.12225
16. Miller HC, Morgan MJ, Walsh T, Wylie JT, Kaksonen AH, Puzon GJ. Preferential feeding in *Naegleria fowleri*; intracellular bacteria isolated from amoebae in operational drinking water distribution systems. *Water Res*. (2018) 141:126–34. doi: 10.1016/j.watres.2018.05.004
17. Bellini NK, Santos TM, da Silva MTA, Thiemann OH. The therapeutic strategies against *Naegleria fowleri*. *Exp Parasitol*. (2018) 187:1–11. doi: 10.1016/j.exppara.2018.02.010
18. Shibayama M, Serrano-Luna J, Cervantes-Sandoval I, Tsutsumi V. *Naegleria. Molecular Detection of Human Parasitic Pathogens* (2022). p. 109–18. Available online at: <https://www.ncbi.nlm.nih.gov/books/NBK535447/> (accessed July 21, 2023).
19. Güémez A, García E, Julian Fernández Martín J, San-Millán-Tejado B. primary amoebic meningoencephalitis by *naegleria fowleri*: pathogenesis and treatments. *Biomolecules*. (2021) 11:1320. doi: 10.3390/biom11091320
20. Grace E, Asbill S, Virga K. *Naegleria fowleri*: pathogenesis, diagnosis, and treatment options. *Antimicrob Agents Chemother*. (2015) 59:6677. doi: 10.1128/AAC.01293-15

## Author contributions

AN: Conceptualization, Writing—original draft, Writing—review and editing. IM: Writing—review and editing. EA: Writing—review and editing. FS: Writing—review and editing.

## Funding

The author(s) declare that no financial support was received for the research, authorship, and/or publication of this article.

## Conflict of interest

The authors declare that the research was conducted in the absence of any commercial or financial relationships that could be construed as a potential conflict of interest.

## Publisher's note

All claims expressed in this article are solely those of the authors and do not necessarily represent those of their affiliated organizations, or those of the publisher, the editors and the reviewers. Any product that may be evaluated in this article, or claim that may be made by its manufacturer, is not guaranteed or endorsed by the publisher.



21. Disabled World. *naegleria fowleri: A Brain Eating Amoeba*. (2014). Available online at: <https://www.disabled-world.com/health/neurology/naegleria-fowleri.php> (accessed September 6, 2023).
22. Marciano-Cabral F. Biology of *Naegleria* spp. *Microbiol Rev*. (1988) 52:114.
23. Hara T, Fukuma T. Diagnosis of the primary amoebic meningoencephalitis due to *Naegleria fowleri*. *Parasitol Int*. (2005) 54:219–21. doi: 10.1016/j.parint.2005.06.001
24. Shakoor S, Beg MA, Mahmood SF, Banda R, Sriram R, Noman F, et al. Primary amoebic meningoencephalitis caused by *Naegleria fowleri*, Karachi, Pakistan. *Emerg Infect Dis*. (2011) 17:258. doi: 10.3201/eid1702.100442
25. Yoder JS, Eddy BA, Visvesvara GS, Capewell L, Beach MJ. The epidemiology of primary amoebic meningoencephalitis in the USA, 1962–2008. *Epidemiol Infect*. (2010) 138:968–75. doi: 10.1017/S0950268809991014
26. HealthyChildren.org. *Naegleria Fowleri: How to Protect Against a Rare Brain Infection*. (2023). Available online at: <https://www.healthychildren.org/English/health-issues/conditions/infections/Pages/naegleria-fowleri-the-brain-eating-amoeba-how-to-prevent-this-rare-infection.aspx> (accessed July 16, 2023).
27. Shariq A, Afridi FI, Farooqi BJ, Ahmed S, Hussain A. Fatal primary meningoencephalitis caused by *Naegleria fowleri*. *J Coll Phys Surg Pak*. (2014) 24:523–5.
28. Visvesvara GS, Moura H, Schuster FL. Pathogenic and opportunistic free-living amoebae: *Acanthamoeba* spp, *Balamuthia mandrillaris*, *Naegleria fowleri*, and *Sappinia diploidea*. *FEMS Immunol Med Microbiol*. (2007) 50:1–26. doi: 10.1111/j.1574-695X.2007.00232.x
29. Martinez AJ, Augusto J. *Free-Living Amebas: Natural History, Prevention, Diagnosis, Pathology, and Treatment of Disease*. CRC Press (2017). Available online at: <https://www.routledge.com/Free-Living-Amebas-Natural-History-Prevention-Diagnosis-Pathology-and/Martinez/p/book/9781315893044> (accessed July 17, 2023).
30. CDC. *Primary Amebic Meningoencephalitis — Arizona, Florida, and Texas* (2007). Available online at: <https://www.cdc.gov/mmwr/preview/mmwrhtml/mm5721a1.htm> (accessed July 17, 2023).
31. Khanna V, Khanna R, Hebbar S, Shashidhar V, Mundkar S, Munim F, et al. Primary amoebic meningoencephalitis in an infant due to *Naegleria fowleri*. *Case Rep Neurol Med*. (2011) 2011:621905. doi: 10.1155/2011/782539
32. Lee J, Kang JM, Kim TI, Kim JH, Sohn HJ, Na BK, et al. Excretory and secretory proteins of *Naegleria fowleri* induce inflammatory responses in BV-2 microglial cells. *J Eukaryot Microbiol*. (2017) 64:183–92. doi: 10.1111/jeu.12350
33. Yu Z, Miller HC, Puzon GJ, Clowers BH. Development of untargeted metabolomics methods for the rapid detection of pathogenic *Naegleria fowleri*. *Environ Sci Technol*. (2017) 51:4210–9. doi: 10.1021/acs.est.6b05969
34. Marciano-Cabral F, Cabral GA. The immune response to *Naegleria fowleri* amebae and pathogenesis of infection. *FEMS Immunol Med Microbiol*. (2007) 51:243–59. doi: 10.1111/j.1574-695X.2007.00332.x
35. CDC. *Pathogen and Environment*. *Naegleria fowleri*. (2022). Available online at: <https://www.cdc.gov/parasites/naegleria/pathogen.html> (accessed July 21, 2023).
36. CDIPD. *Global Impact*. Available online at: <https://www.cdipd.org/index.php/naegleriiasis-global-impact> (accessed July 15, 2023).
37. Gharpure R, Bliton J, Goodman A, Ali IKM, Yoder J, Cope JR. Epidemiology and clinical characteristics of primary amoebic meningoencephalitis caused by *Naegleria fowleri*: a global review. *Clin Infect Dis*. (2021) 73:e19. doi: 10.1093/cid/ciaa520
38. Wisevoter. *Hottest States in the US 2023*. Available online at: <https://wisevoter.com/state-rankings/hottest-states/> (accessed July 15, 2023).
39. DAWN.COM. *Measures Ordered to Combat 'Brain-Eating' Amoeba Amid Monsoon - Newspaper*. Available online at: <https://www.dawn.com/news/1342165> (accessed July 15, 2023).
40. Mahmood K. *Naegleria fowleri in Pakistan - An Emerging Catastrophe* (2015). 7 p. Available online at: [www.archivepp.com](http://www.archivepp.com) (accessed July 21, 2023).
41. Abbas Naqvi A, Yazdani N, Ahmad R, Zehra F, Ahmad N. Epidemiology of primary amoebic meningoencephalitis-related deaths due to *Naegleria fowleri* infections from freshwater in Pakistan: An analysis of 8-year dataset. *Arch Pharm Pract*. (2023) 7.
42. Cooper AM, Aouthmany S, Shah K, Rega PP. Killer amoebas: primary amoebic meningoencephalitis in a changing climate. *J Am Acad Physician Assist*. (2019) 32:30–5. doi: 10.1097/01.JAA.0000558238.99250.4a
43. Cope JR, Ali IK. Primary amoebic meningoencephalitis: what have we learned in the last five years? *Curr Infect Dis Rep*. (2016) 18:31. doi: 10.1007/s11908-016-0539-4
44. Gompf SG, Garcia C. Lethal encounters: the evolving spectrum of amoebic meningoencephalitis. *IDCases*. (2019) 15:e00524. doi: 10.1016/j.idcr.2019.e00524
45. Król-Turmińska K, Olender A. Human infections caused by free-living amoebae. *Ann Agric Environ Med*. (2017) 24:254–60. doi: 10.5604/12321966.1233568
46. Ong TYY, Khan NA, Siddiqui R. Brain-eating amoebae: predilection sites in the brain and disease outcome. *J Clin Microbiol*. (2017) 55:1989–97. doi: 10.1128/JCM.02300-16
47. Bonilla-Lemus P, Rojas-Hernández S, Ramirez-Flores E, Castillo-Ramirez DA, Monsalvo-Reyes AC, Ramirez-Flores MA, et al. Isolation and identification of *Naegleria* species in irrigation channels for recreational use in Mexicali Valley, Mexico. *Pathogens*. (2020) 9:820. doi: 10.3390/pathogens9100820
48. Vyas IK, Jamerson M, Cabral GA, Marciano-Cabral F. Identification of peptidases in highly pathogenic vs. weakly pathogenic *Naegleria fowleri* amebae. *J Eukaryot Microbiol*. (2015) 62:51–9. doi: 10.1111/jeu.12152
49. Gupta R, Parashar MK, Kale A. *Primary Amoebic Meningoencephalitis* (2015). Available online at: [https://www.researchgate.net/publication/282820266\\_Primary\\_Amoebic\\_Meningoencephalitis](https://www.researchgate.net/publication/282820266_Primary_Amoebic_Meningoencephalitis) (accessed July 16, 2023).
50. Capewell LG, Harris AM, Yoder JS, Cope JR, Eddy BA, Roy SL, et al. Diagnosis, clinical course, and treatment of primary amoebic meningoencephalitis in the United States, 1937–2013. *J Pediatric Infect Dis Soc*. (2015) 4:e68–75. doi: 10.1093/jpids/piu103
51. Cope JR, Conrad DA, Cohen N, Cotilla M, Dasilva A, Jackson J, et al. Use of the novel therapeutic agent miltefosine for the treatment of primary amoebic meningoencephalitis: report of one fatal and one surviving case. *Clin Infect Dis*. (2016) 62:774. doi: 10.1093/cid/civ1021
52. Anser H, Khatoun H, Khan SS, Imam S, Hasan A. A review on global distribution of primary amoebic meningoencephalitis (PAM) caused by *Naegleria fowleri* - the brain eating amoeba RADS. *J Pharm Pharm Sci*. (2018) 6:95–9.
53. Chomba M, Mucheleng'anga LA, Fwoloshi S, Ngulube J, Mutengo MM. A case report: Primary amoebic meningoencephalitis in a young Zambian adult. *BMC Infect Dis*. (2017) 17:1–5. doi: 10.1186/s12879-017-2638-8
54. Tabassum S, Naeem A, Gill S, Mumtaz N, Khan MZ, Tabassum S, et al. Increasing cases of *Naegleria fowleri* during the time of COVID 19: an emerging concern of Pakistan. *Int J Surg*. (2022) 105:106881. doi: 10.1016/j.ijsu.2022.106881
55. Saleem T, Rabbani M, Jamil B. Primary amoebic meningoencephalitis: two new cases from Pakistan. *Trop Doct*. (2009) 39:242–3. doi: 10.1258/td.2009.090032
56. Siddiqui R, Khan NA. Is ritual cleansing a missing link between fatal infection and brain-eating amoebae? *Clin Infect Dis*. (2012) 54:1817–8. doi: 10.1093/cid/cis309
57. Fatal primary meningoencephalitis caused by *Naegleria fowleri*.
58. Outbreak News Today. *Karachi: 11 Naegleria fowleri Deaths in 2019 Through July According to Pakistan Media*. (2019). Available online at: <https://outbreaknewstoday.com/karachi-11-naegleria-fowleri-deaths-in-2019-through-july-according-to-pakistan-media-15269/> (accessed July 16, 2023).
59. Outbreak News Today. *Pakistan: Is the Naegleria fowleri Strain Seen in Karachi Different?* (2019). Available online at: <https://outbreaknewstoday.com/pakistan-is-the-naegleria-fowleri-strain-seen-in-karachi-different-15208/> (accessed July 16, 2023).
60. Outbreak News Today. *Karachi Sees 5th Naegleria fowleri Death of 2021*. (2020). Available online at: <https://outbreaknewstoday.com/karachi-sees-5th-naegleria-fowleri-death-of-2021/> (accessed July 16, 2023).
61. Outbreak News Today. *Brain Eating Amoeba: Cases Reported in Karachi, Pakistan and Kerala, India*. (2021). Available online at: <https://outbreaknewstoday.com/brain-eating-amoeba-cases-reported-in-karachi-pakistan-and-kerala-india-58128/> (accessed July 16, 2023).
62. Outbreak News Today. *Pakistan: 15th Naegleria fowleri Death Reported in Karachi*. (2021). Available online at: <https://outbreaknewstoday.com/pakistan-15th-naegleria-fowleri-death-reported-in-karachi-97298/> (accessed July 16, 2023).
63. DAWN.COM. *PMA Urges People to Take Precautions to Avoid 'Brain-Eating' Amoeba - Pakistan*. (2021). Available online at: <https://www.dawn.com/news/1635136> (accessed July 16, 2023).
64. Outbreak News Today. *Pakistan: Two Additional Naegleria fowleri Deaths Reported in Karachi*. (2022). Available online at: <https://outbreaknewstoday.com/pakistan-two-additional-naegleria-fowleri-deaths-reported-in-karachi-41589/> (accessed July 16, 2023).
65. Jamerson M, Remmers K, Cabral G, Marciano-Cabral F. Survey for the presence of *Naegleria fowleri* amebae in lake water used to cool reactors at a nuclear power generating plant. *Parasitol Res*. (2009) 104:969–78. doi: 10.1007/s00436-008-1275-y
66. Stevens AR, Tyndall RL, Coutant CC, Willaert E. Isolation of the etiological agent of primary amoebic meningoencephalitis from artificially heated waters. *Appl Environ Microbiol*. (1977) 34:701–5. doi: 10.1128/aem.34.6.701-705.1977
67. Zbikowska E, Walczak M, Krawiec A. Distribution of *Legionella pneumophila* bacteria and *Naegleria* and *Hartmannella* amoebae in thermal saline baths used in balneotherapy. *Parasitol Res*. (2013) 112:77–83. doi: 10.1007/s00436-012-3106-4
68. Tsvetkova N, Schild M, Panaiotov S, Kurdova-Mintcheva R, Gottstein B, Walochnik J, et al. The identification of free-living environmental isolates of amoebae from Bulgaria. *Parasitol Res*. (2004) 92:405–13. doi: 10.1007/s00436-003-1052-x
69. Ettinger MR, Webb SR, Harris SA, McIninch SP, Garman GC, Brown BL. Distribution of free-living amoebae in James River, Virginia, USA. *Parasitol Res*. (2002) 89:6–15. doi: 10.1007/s00436-002-0707-3

70. Lam C, He L, Marciano-Cabral F. The effect of different environmental conditions on the viability of *Naegleria fowleri* amoebae. *J Eukaryot Microbiol.* (2019) 66:752–6. doi: 10.1111/jeu.12719
71. Behets J, Seghi F, Declercq P, Verelst L, Duvivier L, Van Damme A, et al. Detection of *Naegleria* spp. and *Naegleria fowleri*: a comparison of flagellation tests. *ELISA PCR* (2003) 47:117–22. doi: 10.2166/wst.2003.0177
72. RSC Education. *Biosensors Based on DNA. Feature.* (2008). Available online at: <https://edu.rsc.org/feature/biosensors-based-on-dna/2020103.article> (accessed September 7, 2023).
73. Madarová L, Trnková K, Feiková S, Klement C, Obernauerová M. A real-time PCR diagnostic method for detection of *Naegleria fowleri*. *Exp Parasitol.* (2010) 126:37–41. doi: 10.1016/j.exppara.2009.11.001
74. Mahittikorn A, Mori H, Popruk S, Roobthaisong A, Sutthikornchai C, Koompapong K, et al. Development of a Rapid, Simple Method for Detecting *Naegleria fowleri* Visually in Water Samples by Loop-Mediated Isothermal Amplification (LAMP) (2015) Available online at: <http://primerexplorer.jp/elamp4.0.0/index.html> (accessed July 21, 2023).
75. Goswick SM, Brenner GM. Activities of azithromycin and amphotericin B against *Naegleria fowleri* in vitro and in a mouse model of primary amebic meningoencephalitis. *Antimicrob Agents Chemother.* (2003) 47:524–8. doi: 10.1128/AAC.47.2.524-528.2003
76. CDC. *Treatment. Naegleria fowleri.* Available online at: <https://www.cdc.gov/parasites/naegleria/treatment-hcp.html> (accessed July 21, 2023).
77. Peroutka-Bigus N, Bellaire BH. Antiparasitic activity of auranofin against pathogenic *Naegleria fowleri*. *J Eukaryot Microbiol.* (2019) 66:684–8. doi: 10.1111/jeu.12706
78. Escrig JJ, Hahn HJ, Debnath A. Activity of auranofin against multiple genotypes of *Naegleria fowleri* and its synergistic effect with amphotericin B in vitro. *ACS Chem Neurosci.* (2020) 11:2464. doi: 10.1021/acscchemneuro.0c00165
79. Debnath A, Hahn HJ, Abagyan R, Podust LM, Roy S, Ali IKM. HMG-CoA reductase inhibitors as drug leads against *Naegleria fowleri*. *ACS Chem Neurosci.* (2020) 11:3089. doi: 10.1021/acscchemneuro.0c00428
80. Colon BL, Rice CA, Guy RK, Kyle DE. Phenotypic screens reveal posaconazole as a rapidly acting amebicidal combination partner for treatment of primary amebic meningoencephalitis. *J Infect Dis.* (2019) 219:1095–103. doi: 10.1093/infdis/jiy622
81. Zhou W, Debnath A, Jennings G, Hahn HJ, Vanderloop BH, Chaudhuri M, et al. Enzymatic chokepoints and synergistic drug targets in the sterol biosynthesis pathway of *Naegleria fowleri*. *PLoS Pathog.* (2018) 14:e1007245. doi: 10.1371/journal.ppat.1007245
82. Venkatesan P. Disease outbreaks in Pakistan, Lebanon, and Syria. *Lancet Microbe.* (2023) 4:e18–9. doi: 10.1016/S2666-5247(22)00358-5
83. Dorsch MM, Cameron AS, Robinson BS. The epidemiology and control of primary amebic meningoencephalitis with particular reference to South Australia. *Trans R Soc Trop Med Hyg.* (1983) 77:372–7. doi: 10.1016/0035-9203(83)90167-0
84. Cope JR, Ratard RC, Hill VR, Sokol T, Causey JJ, Yoder JSm et al. The first association of a primary amebic meningoencephalitis death with culturable *Naegleria fowleri* in tap water from a US treated public drinking water system. *Clin Infect Dis.* (2015) 60:e36. doi: 10.1093/cid/civ017
85. Miller HC, Wylie J, Dejean G, Kaksonen AH, Sutton D, Braun K, et al. reduced efficiency of chlorine disinfection of *Naegleria fowleri* in a drinking water distribution biofilm. *Environ Sci Technol.* (2015) 49:11125–31. doi: 10.1021/acs.est.5b02947
86. Jonckheere D, Century JA. A century of research on the amoeboflagellate genus *Naegleria*. *Acta Protozool.* (2002) 41:309.
87. Bartram J, Cotruvo J, Exner M, Fricker C, Glasmacher A. Heterotrophic plate count measurement in drinking water safety management: report of an Expert Meeting Geneva, 24–25 April 2002. *Int J Food Microbiol.* (2004) 92:241–7. doi: 10.1016/j.ijfoodmicro.2003.08.005
88. Esterman A, Roder DM, Cameron AS, Robinson BS, Walters RP, Lake JA, et al. Determinants of the microbiological characteristics of South Australian swimming pools. *Appl Environ Microbiol.* (1984) 47:325. doi: 10.1128/aem.47.2.325-328.1984
89. Cope JR, Kahler AM, Causey J, Williams JG, Kihlken J, Benjamin C, et al. Response and remediation actions following the detection of *Naegleria fowleri* in two treated drinking water distribution systems, Louisiana, 2013–2014. *J Water Health.* (2019) 17:777–87. doi: 10.2166/wh.2019.239
90. Saddique R, Zeng W, Zhao P, Awan A. Understanding multidimensional poverty in pakistan: implications for regional and demographic-specific policies. *Environ Sci Pollut Res.* (2023) 1:1–16. doi: 10.1007/s11356-023-28026-6
91. CDC. *Illness and Symptoms. Naegleria fowleri.* (2023). Available online at: <https://www.cdc.gov/parasites/naegleria/illness.html> (accessed July 13, 2023).
92. Plianbangchang S. Public health and research: an overview. *J Health Res.* (2020) 35:374–8. doi: 10.1108/JHR-03-2020-0074



## OPEN ACCESS

## EDITED BY

Antonio Battisti,  
Institute of Experimental Zooprophyllactic of  
the Lazio and Tuscany Regions (IZSLT), Italy

## REVIEWED BY

Amélia M. Sarmento,  
Fernando Pessoa University, Portugal  
Elisabeth M. Liebler-Tenorio,  
Friedrich Loeffler Institute, Germany  
Alfonso Martin Cabello Vilchez,  
Peruvian University Cayetano Heredia, Peru  
Matteo Ricchi,  
Experimental Zooprophyllactic Institute of  
Lombardy and Emilia Romagna (IZSLER), Italy

## \*CORRESPONDENCE

Yann Héchard  
✉ yann.hechard@univ-poitiers.fr

RECEIVED 20 October 2023

ACCEPTED 06 December 2023

PUBLISHED 22 December 2023

## CITATION

Jessu A, Delafont V, Moyen J-L, Biet F,  
Samba-Louaka A and Héchard Y (2023)  
Characterization of *Rosculus vilicus* sp. nov., a  
rhizarian amoeba interacting with  
*Mycobacterium avium* subsp.  
*paratuberculosis*.  
*Front. Microbiol.* 14:1324985.  
doi: 10.3389/fmicb.2023.1324985

## COPYRIGHT

© 2023 Jessu, Delafont, Moyen, Biet, Samba-Louaka and Héchard. This is an open-access article distributed under the terms of the [Creative Commons Attribution License \(CC BY\)](https://creativecommons.org/licenses/by/4.0/). The use, distribution or reproduction in other forums is permitted, provided the original author(s) and the copyright owner(s) are credited and that the original publication in this journal is cited, in accordance with accepted academic practice. No use, distribution or reproduction is permitted which does not comply with these terms.

# Characterization of *Rosculus vilicus* sp. nov., a rhizarian amoeba interacting with *Mycobacterium avium* subsp. *paratuberculosis*

Amélie Jessu<sup>1,2</sup>, Vincent Delafont<sup>1</sup>, Jean-Louis Moyen<sup>2</sup>,  
Franck Biet<sup>3</sup>, Ascel Samba-Louaka<sup>1</sup> and Yann Héchard<sup>1\*</sup>

<sup>1</sup>Université de Poitiers, CNRS, EBI, Poitiers, France, <sup>2</sup>Laboratoire Départementale d'Analyse et de Recherche de la Dordogne, Coulounieix-Chamiers, France, <sup>3</sup>Institut National de Recherche pour l'Agriculture, l'Alimentation et l'Environnement, Université de Tours, UMR 1282, Infectiologie et Santé Publique, Nouzilly, France

Free-living amoebae are described as potential reservoirs for pathogenic bacteria in the environment. It has been hypothesized that this might be the case for *Mycobacterium avium* subsp. *paratuberculosis*, the bacterium responsible for paratuberculosis. In a previous work, we isolated an amoeba from a water sample in the environment of infected cattle and showed that this amoeba was associated with *Mycobacterium avium* subsp. *paratuberculosis*. While a partial 18S rRNA gene has allowed us to suggest that this amoeba was *Rosculus*-like, at that time we were not able to sub-cultivate it. In the present study, we succeeded in cultivating this strain at 20–25°C. This amoeba is among the smallest (5–7 µm) described. The sequencing of the whole genome allowed us to extract the full 18S rRNA gene and propose this strain as a new species of the *Rosculus* genus, i.e., *R. vilicus*. Of note, the mitochondrial genome is particularly large (184,954 bp). Finally, we showed that this amoeba was able to phagocyte *Mycobacterium avium* subsp. *paratuberculosis* and that the bacterium was still observed within amoebae after at least 3 days. In conclusion, we characterized a new environmental amoeba species at the cellular and genome level that was able to interact with *Mycobacterium avium* subsp. *paratuberculosis*. As a result, *R. vilicus* is a potential candidate as environmental reservoir for *Mycobacterium avium* subsp. *paratuberculosis* but further experiments are needed to test this hypothesis.

## KEYWORDS

amoeba, *Rosculus*, rhizarian, *Mycobacterium*, paratuberculosis, genome, protist, water

## 1 Introduction

Free-living amoebae (FLA) are single-celled eukaryotes, omnipresent in water and soil environments (Rodríguez-Zaragoza, 1994; Samba-Louaka et al., 2019). These protists share common morphological features, notably pseudopods that allow them to move upon surfaces and to thrive by phagocytosis. Even though they are likely to play an important role in microbial ecology due to their ability to ingest bacteria as their main food sources (Jürgens and Matz, 2002), FLA have yet to be adequately described.

FLA constitutes a highly polyphyletic group of microbial eukaryotes and can be affiliated not only to Amoebozoa, the sole supergroup exclusively represented by amoeboid microorganisms, but also to Opisthokonta, Heterolobosea and Rhizaria. Among those three large eukaryotic groups, FLA consist mostly in small clades of amoebae, featuring a varied array of cell morphologies (Bass et al., 2009; Samba-Louaka et al., 2019). Among Rhizaria, the most notorious amoebae representatives are Vampyrellids, a group of predatory amoebae found in freshwater and marine environments. They can feed on bacteria and other eukaryotic preys (Hess and Suthaus, 2022). Additionally, other lesser known rhizarian amoebae were recently described. Most notably, molecular analyses highlighted the existence of a potentially very diverse clade, the Sainouroidea. The latter encompasses several genera of small-sized amoeba, such as *Rosculus*, which can be found in cattle, snake, fish feces, freshwater and soil (Schuler et al., 2018).

While FLA ingest bacteria by phagocytosis, some bacteria can resist phagocytosis and, consequently, might more specifically be able to resist phagocytosis by the immune cells of animals. This is due to a high level of conservation between phagocytosis mechanisms of FLA and animal cells (Escoll et al., 2013). This resistance was initially described for *Legionella pneumophila*, and many similar observations were made later on, involving diverse bacteria such as *Mycobacterium* spp., including *Mycobacterium avium* subsp. *paratuberculosis* (MAP) the bacterium responsible for paratuberculosis (Drancourt, 2014; Claeys and Robinson, 2018). In addition, amoeba-resistant bacteria might become more virulent insofar as they are adapted to the phagocyte environment and express virulence genes, thereby exemplifying the concept of coincidental evolution (Primm et al., 2004; Sun et al., 2018). Consequently, interest in FLA was revived by their capacity to become reservoirs of pathogenic bacteria in the environment.

It has been hypothesized that amoebae might be environmental reservoirs of *Mycobacteria* (Salah et al., 2009). To test this, we tried to isolate amoebae from water in the environment of infected cattle and look for the association between MAP, the bacterium responsible for paratuberculosis, and indigenous amoebae (Samba-Louaka et al., 2018). One amoeba was detected and identified, via 18S rRNA partial gene sequencing, as a *Rosculus*-like amoeba belonging to the supergroup Rhizaria. However, we were not able at that time to maintain the growth of this strain.

In this work, we ultimately identified optimal conditions for growing and isolating the strain associated with MAP. We fully sequenced the genome of this amoeba and analysis of the 18S rRNA gene sequence allowed us to confirm this amoeba among the *Rosculus* genus. Finally, an interaction study was performed to test the ability of this amoeba to phagocytose MAP.

## 2 Materials and methods

### 2.1 Isolation and cultivation of amoeba

This amoeba was previously isolated from an environmental water sample from the environment of infected cattle (Samba-Louaka et al., 2018). A sample (cryotube) frozen at that time was used to obtain a pure culture by critical dilution. Then, the cultivation was maintained within PAS buffer ( $\text{Na}_3\text{C}_6\text{H}_5\text{O}_7$  1 g/L,  $\text{MgSO}_4 \cdot 7\text{H}_2\text{O}$  0.4 M,  $\text{CaCl}_2 \cdot 2\text{H}_2\text{O}$

0.05 M,  $\text{Na}_2\text{HPO}_4 \cdot 2\text{H}_2\text{O}$  0.25 M,  $\text{KH}_2\text{PO}_4$  0.25 M, pH 6.5) containing *E. coli* ( $5 \cdot 10^8$  bacteria/mL) as nutrient.

To determine the optimal growing temperatures, *Rosculus vilicus* was cultured at 20, 25, 30 or 37°C for 24 h. Cells were detached and counted after an incubation of 3, 6 and 24 h. The experiment was repeated three times.

### 2.2 DNA extraction and genome sequencing

From pure culture, DNA was extracted in order to sequence this amoeba genome with two sequencing technologies, short and long-read approaches. Briefly, lysis buffer was added directly on adherent *R. vilicus*. Then, DNA was extracted with Blood & Tissue kit (Qiagen) following the manufacturer's recommendations and quantified using the Qubit fluorometer (Thermo Fischer Scientific).

For the long-read approach, 3 µg of DNA was used for library preparation using the Oxford Nanopore Technologies ligation kit (SQK-LSK109) according to the manufacturer's protocol with the Long Fragment Buffer (LFB). The library was then loaded on a flow cell (R9.4.1) and sequenced with MinION Mk1C. Base calling was done using Guppy v6.5.7 in high-accuracy mode. Simultaneously, genomic DNA was sent to SeqCenter (Pittsburgh, PA, USA) for library preparation and short read sequencing on an Illumina NovaSeq 6000. Demultiplexing, quality control and adapter trimming were performed with BCL convert software at SeqCenter.

### 2.3 Phylogenetic and genome analysis

We strived to follow a hybrid-based approach inspired by recently published protocols (Wick et al., 2023) to assemble a high-quality draft genome. For this, initial assembly was performed using Flye v. 2.9.1 (Kolmogorov et al., 2019) with long reads only, displaying quality score (Q) > 9 after base calling. A step of self-polishing was then implemented using Medaka v 1.7.2. Illumina reads were trimmed based on Q > 30 using Cutadapt v 4.4 (Martin, 2011), and for additional polishing of contigs using Polypolish v 0.5 (Wick and Holt, 2022). The resulting, fully polished assembly was then binned using Metabat2 V 2.15 (Kang et al., 2019). Manual inspections of bins were performed to ensure proper binning of sequences. For inferring phylogeny, Barrnap v 1.2.2 was used to identify and extract gene sequences coding for ribosomal RNA.<sup>1</sup> Full-length 18S rRNA gene sequence was used to reconstruct phylogeny using IQ-TREE v 2.0.3 (Minh et al., 2020). The optimal substitution model was chosen based on the output of ModelFinder (Kalyanamoorthy et al., 2017), according to the best Bayesian information criterion score. The robustness of nodes was tested by 1,000 iterations of conventional bootstraps and 1,000 iterations of the Shimodaira–Hasegawa approximate likelihood ratio test.

Mitochondrial genome was extracted based on joint analysis of graph assemblies, contig coverage and GC content. After manual and putative identification, the supposedly mitochondrial genome was further confirmed as such using multiple dedicated annotation tools,

<sup>1</sup> <https://github.com/tseemann/barrnap>



i.e., MITOS 2 (Donath et al., 2019), Mfannot<sup>2</sup> and RNAweasel<sup>3</sup> to identify mitochondrial proteins and RNAs. The nuclear genome and mitochondrial genome data were deposited at NCBI under the BioProject ID PRJNA1029052.

## 2.4 Morphological characterization of amoeba strain

Trophozoites and cyst-like forms from *R. vilicus* were observed by microscopy (Olympus IX73 inverted microscope, 1,000x magnification) using a differential interference contrast. All sizes were measured using ImageJ (Schneider et al., 2012). The morphological comparison between trophozoite and cyst-like forms was also assessed by electron microscopy. For scanning electron microscopy (SEM), cells were cryofixed in nitrogen with VCM (Leica), sublimed and 4 nm wolfram coated in ACE 600 (Leica). Each step was performed under vacuum and samples were transferred from one station to another using VCT 500 (Leica). Samples were observed at  $-100^{\circ}\text{C}$  in scanning electron microscope Teneo VolumeScope (Thermo Fisher) to 3.5 kV and 10 kV.

For transmission electron microscopy (TEM), amoebae were fixed with 2.5% glutaraldehyde and 2% osmium tetroxide. Dehydration was carried out using different concentrations of acetone. Epon resin were used for impregnation and embedding process. After cutting with ultramicrotome UC6 (Leica), samples were contrasted with uranyl acetate and lead citrate. Samples observations were proceeded on transmission electron microscope (JEOL 1010) at 80 keV. Images were acquired with Quemesa camera (Olympus).

## 2.5 Infection experiments

To study the permissiveness of *R. vilicus* to MAP infection, an infection experiment was set up using a MAP K10-GFP strain (Li et al., 2005). *R. vilicus* ( $2.10^5$  cells) were added in each well of a 6-well plate in a 2 mL PAS buffer and incubated for 1 h at  $20^{\circ}\text{C}$ . MAP clumps were disaggregated with 3 passages in 27 gauges needle, centrifuged for 5 min at 200 g and added to *R. vilicus* at MOI 10 during 2 h at  $20^{\circ}\text{C}$ . Amikacin ( $100\mu\text{g/mL}$ ) was added for 2 h to remove extracellular mycobacteria before the washing step. Finally, the infected cells were incubated in PAS buffer added with *E. coli* ( $4.10^8$  bacteria/mL) for 3 days at  $20^{\circ}\text{C}$ . Colocalization of MAP K10-GFP with *R. vilicus* was observed under fluorescence microscope (Olympus IX51 inverted fluorescence microscope).

## 3 Results

### 3.1 *Rosculus vilicus* grows preferentially between $20^{\circ}\text{C}$ and $25^{\circ}\text{C}$

We previously isolated a *Rosculus*-like amoeba that we cultured at  $30^{\circ}\text{C}$  but we ultimately lost over subcultures,

suggesting at that time that growth conditions were not appropriate for this isolate. To determine the optimal temperature, we cultivated this amoeba at 20, 25, 30, and  $37^{\circ}\text{C}$ . As demonstrated in this study, the optimal growth temperatures ranged from  $20^{\circ}\text{C}$  to  $25^{\circ}\text{C}$ . Indeed, at  $30^{\circ}\text{C}$  the development was inhibited while at  $37^{\circ}\text{C}$ , the total number of cells decreased, suggesting cell death (Figure 1).

### 3.2 *Rosculus vilicus* shares morphological features with *Rosculus* genus

To characterize this isolate, microscopic studies were performed. Differential interferential contrast micrographs showed a monopodial lobose amoeba with a well-defined frontal hyaline area. Trophozoite cells usually displayed rapid eruptive locomotion with some lateral eruption (Figures 2A–C). An uroidal structure could be observed on some trophozoites, the opposite of that found in the hyaline area (Figures 2A–C). Average length was estimated at  $7.1\mu\text{m}$  (range of  $4.2\text{--}13.8\mu\text{m}$ ) and average width was  $4.8\mu\text{m}$  (range of  $2.7\text{--}12.1\mu\text{m}$ ). During observations, some amoebae adopted a floating form, more rounded than trophozoite ( $6.0\mu\text{m}$  average length and  $4.9\mu\text{m}$  average width), harboring a long stem, about  $18.9\mu\text{m}$  on average ( $10.2\text{--}31.4\mu\text{m}$ ) (Figures 2F,G). All amoeba cells contained a large vacuole and several granularities. Given the ability of amoebae to differentiate into cyst forms, we incubated our amoebae in an encysting buffer for 4 days. We observed rounded cells with an average width of  $4.8\mu\text{m}$  (Figures 2D,E). The observation of trophozoites and cyst-like forms under a scanning electron microscope confirmed their estimated size (Figures 3A–D). The cell surface of cyst-like forms displayed one ostiole (Figure 3D).

Transmission electron micrographs enabled us to observe the ultrastructure of both trophozoites and cyst-like forms. The cell membrane in both trophozoites and cyst-like forms consisted of a thin single membrane (Figures 4A,B). Regarding trophozoites, the cytoplasm contained a large nucleus bordered by a dense chromatin, large mitochondria with discoidal mitochondrial cristae and several vacuoles (Figure 4A). Interestingly, in encystment conditions, the

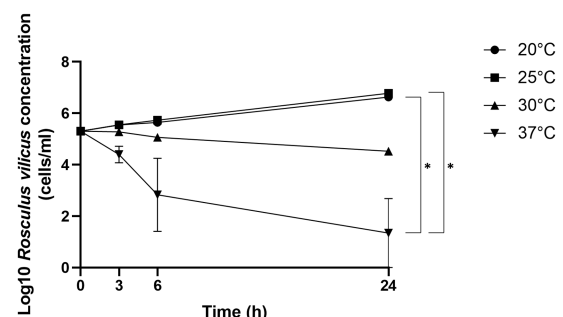


**FIGURE 1**  
*R. vilicus* optimal growth was at  $20^{\circ}\text{C}$  and  $25^{\circ}\text{C}$ . Growth comparison of *R. vilicus* was tested by counting number of cells per ml at different incubation temperatures. The results represent three independent counts, and errors bars represent the standard error of the mean ( $\pm\text{SEM}$ ). Statistical analysis was performed using Kruskal-Wallis test and uncorrected Dunn's test (\* $p < 0.05$ ).

<sup>2</sup> <https://megasun.bch.umontreal.ca/apps/mfannot/>

<sup>3</sup> <https://megasun.bch.umontreal.ca/apps/rnaweasel/>

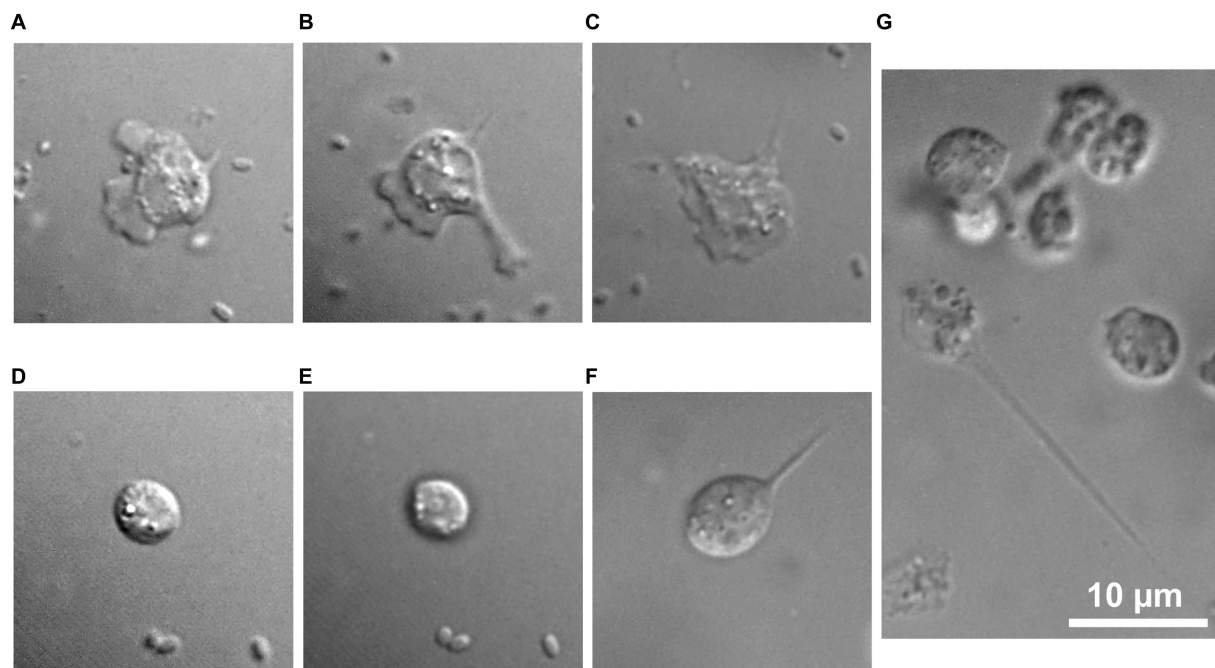


FIGURE 2

*R. vilicus* adopts different forms. Trophozoite forms (A–C), rounded cells (D,E) and floating forms with a stem (F,G). Bar length represents 10 μm.

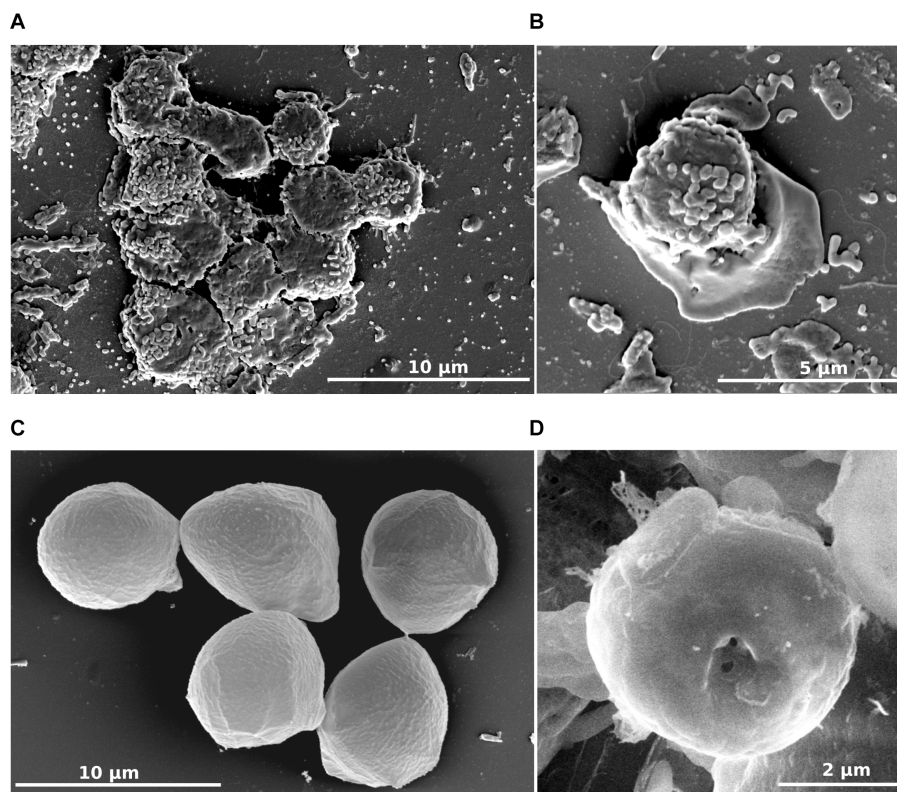
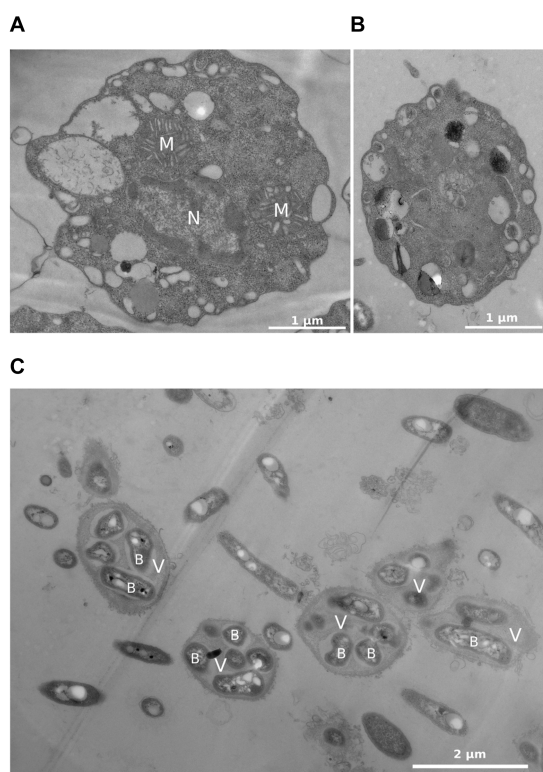


FIGURE 3

*R. vilicus* external morphology viewed by scanning electron microscopy. Trophozoite forms (A,B) and cyst-like forms (C,D).



**FIGURE 4**  
*R. vilicus* internal ultrastructure viewed by transmission electron microscopy; trophozoite form (A) cyst-like form (B) and extracellular medium observed for encystment condition containing vesicles and bacteria (C). N, nucleus; M, mitochondria; V, vesicle containing bacteria; B, bacteria.

extracellular medium contained free bacteria and numerous vesicle-like structures filled with bacteria (Figure 4C).

### 3.3 *Rosculus vilicus* is a new species with a large mitochondrial genome

As no genome was described in the *Rosculus* genus and even in the Sainouroidea clade, we decided to further characterize the isolate on this aspect. Whole genome sequencing was undertaken, using a hybrid, short and long-read sequencing approach. Based on this, the assembled genome of this isolate was predicted to be 40.8 Mb long, showing 37.7% GC enrichment (Table 1). While *E. coli* genome (used as a food source) was recovered in the sequencing data, no other bacterial genome could be retrieved. In this hybrid assembly, particular focus was given to recovery of the mitochondrial genome. One contiguous, highly covered sequence was recovered from the assembly, consisting in a 184,954 bp long sequence, with overall 24.9% GC enrichment. While it was unusually long, even when compared with other mitochondrial genomes from other related protists from the Cercozoa group (Wideman et al., 2020) we are confident that it corresponds to a *bona fide* mitochondrion. Indeed, mitochondrial genome annotation revealed gene repertoires similar to mitochondria from other cercozoans, while showing even coverage and reproducible assembly features, even with short reads only (Supplementary Figure S1).

**TABLE 1** Statistics and features of *R. vilicus* nuclear and mitochondrial genome assemblies.

	<i>Rosculus vilicus</i> nuclear genome	<i>Rosculus vilicus</i> mitochondrial genome
Total length	40,828,467	184,954
Coverage	309X (Illumina) / 300X (MinIon)	1,152X (Illumina) / 1,110X (MinIon)
GC content	37.72%	24.95%
No of contigs	69	1
Largest contig	4,194,092	184,954
N50	1,847,826	184,954
N90	622,946	184,954
L50	8	1
L90	22	1

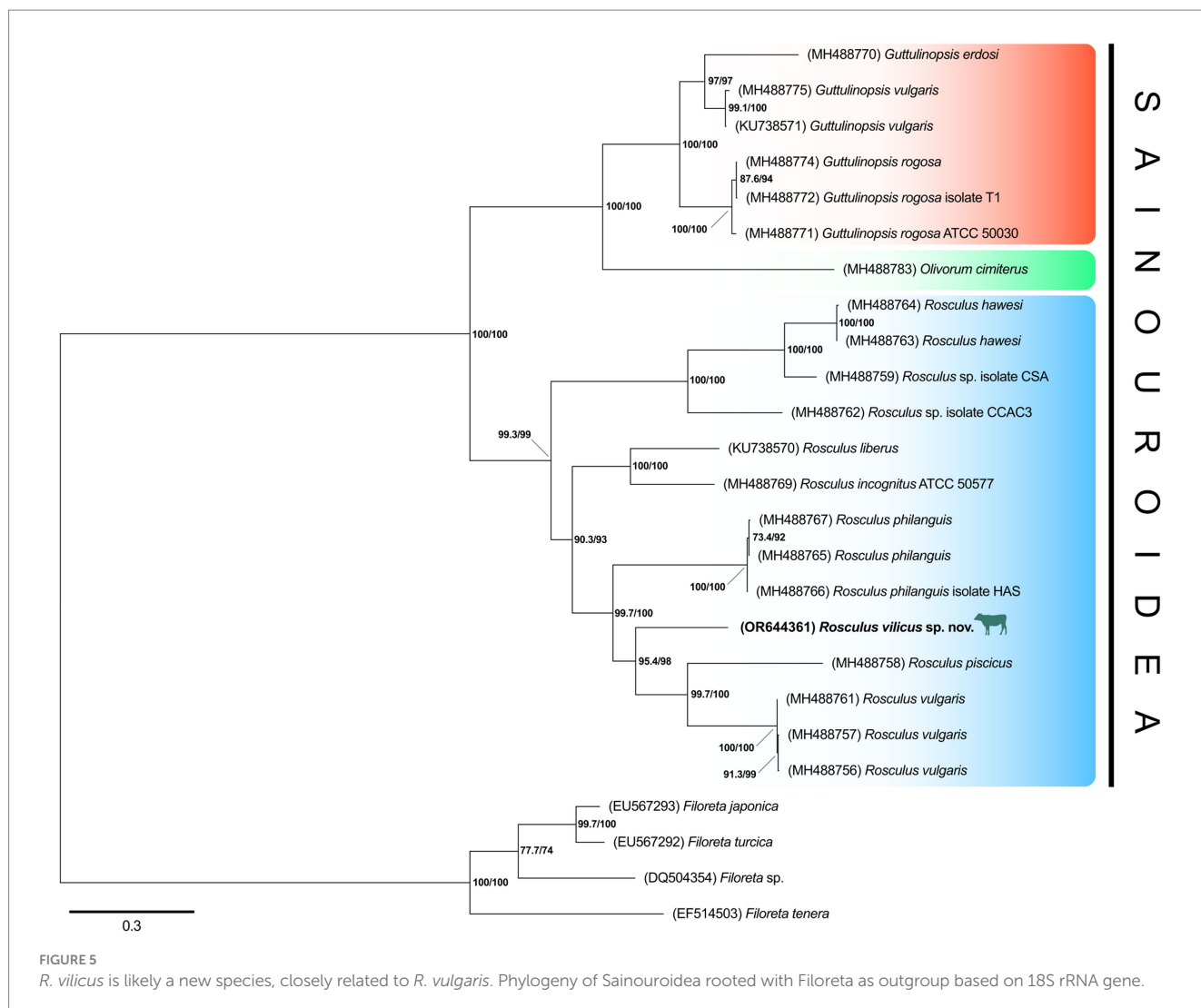
This sequencing effort brought into focus the first draft genome for the whole Sainouroidea. Because of this, however, comparative analyses of gene and genome sequences was clearly hampered, and consequently restricted to widely used marker genes. Given the resulting paucity of genomic information on this clade (and on Cercozoa in general), in order to investigate the taxonomy and phylogenetic positioning of our isolate, we focused on 18S rRNA gene sequences. The full-length 18S rRNA gene sequence (2,128 bp) used for BLASTn search showed its highest match with a sequence designated as ‘uncultured Cercozoa isolate 1’ (98.18% identity, 59% of query coverage). This sequence indeed corresponds to the previously published partial 18S rRNA gene sequence of this isolate (Samba-Louaka et al., 2018).

To confirm the belonging of this amoeba to the *Rosculus* genus, a phylogenetic tree of the 18S rRNA gene was constructed, using a set of rRNA sequences from all available Sainouroidea representatives as of June 2023. Phylogeny inferences clearly placed our isolate within the *Rosculus* genus (Figure 5). The relationship between the sequence from our isolate, compared to other known sequences of the *Rosculus* genus, justified our proposal of a new species, which we tentatively named *Rosculus vilicus* sp. nov., pertaining to the farm where the amoeba was isolated.

### 3.4 *Rosculus vilicus* interacts with MAP for at least a few days

*Rosculus vilicus* was previously isolated in association with a MAP (Samba-Louaka et al., 2018). Here, we evaluated the permissiveness of *R. vilicus* to the MAP K10 strain. An interaction experiment was carried out with the MAP K10-GFP strain to follow the fate of the bacteria by fluorescence microscopy. The result showed that *R. vilicus* co-localized with MAP K10-GFP at least 72 h post-infection (indicated by white arrows, Figures 6A–D). Some MAP K10 were localized extracellularly (Figures 6A,B). Furthermore, video-microscopy experiments highlighted *R. vilicus* moving by ameboid movement with MAP K10 following the same course (Supplementary Figures S2, S3). These results suggest an association for a period of at least 3 days between *R. vilicus* and MAP.





## 4 Discussion

It is well-known that FLA can host pathogenic and non-pathogenic bacteria, thereby playing a potential role on their persistence in the environment. However, in the environment the interactions between FLA and MAP have been very poorly investigated (Drancourt, 2014).

In a previous study, aimed at isolating FLA associated with MAP in the environment of infected cattle, we isolated a strain, which we identified at the time as being somehow related to *Rosculus*, from a drinking trough (Samba-Louaka et al., 2018). This strain was grown for a short period of time, but lost along subcultures, most likely indicating that the growth conditions were not fully adequate at that time. Here, the first challenge was to identify the conditions for optimal and perennial cultivation of this FLA. Different incubation temperatures were tested, clearly showing an optimum at 20–25°C. This result is in accordance with the cultivation conditions described for other *Rosculus* species (Schuler et al., 2018). Current knowledge on Sainouroidea, and more particularly on *Rosculus* spp., suggests that they are amphizoic (Bass et al., 2016). Members of the *Rosculus* genus were repeatedly isolated from both soil and fecal matter (Schuler et al., 2018) and sometimes even directly from rectal sampling of the animal host (Hawes, 1955). This would indicate that

*Rosculus* are not only able to grow in the environment, but also in the feces and even in the digestive system of their respective hosts. In the case of *Rosculus vilicus*, our inability to grow at 37°C may be surprising, as one may expect its ability to thrive at temperatures close to the bovine digestive system (Burfeind et al., 2010). The presence of complex bacterial consortia and oxygenation levels may play an important role in growth capabilities of this amoeba and would necessitate further characterization. Also, it is possible that *Rosculus* is present in feces but may be able to grow only in the environment when the temperature drops to 20–25°C and not in the gut at 37°C.

The morphology of *R. vilicus*, observed under light microscopy, displays features comparable to the *Rosculus* strain previously described in the literature. For example, its small size is a morphological trait found in the other *Rosculus* isolates described. In line with this, we observed that *R. vilicus* trophozoites were on average 7.1 µm long and 4.8 µm wide, while cyst-like forms were round and on average 4.8 µm in diameter. These observations correspond to the measurements of previously isolated *Rosculus* strains. Depending on the species, they are between 2.5 and 13 µm long and between 4.2 and 5.5 µm wide in their locomotive forms (Hawes, 1963; Bass et al., 2009; Týmľ and Dyková, 2018). Trophozoite forms of *Rosculus* were shown



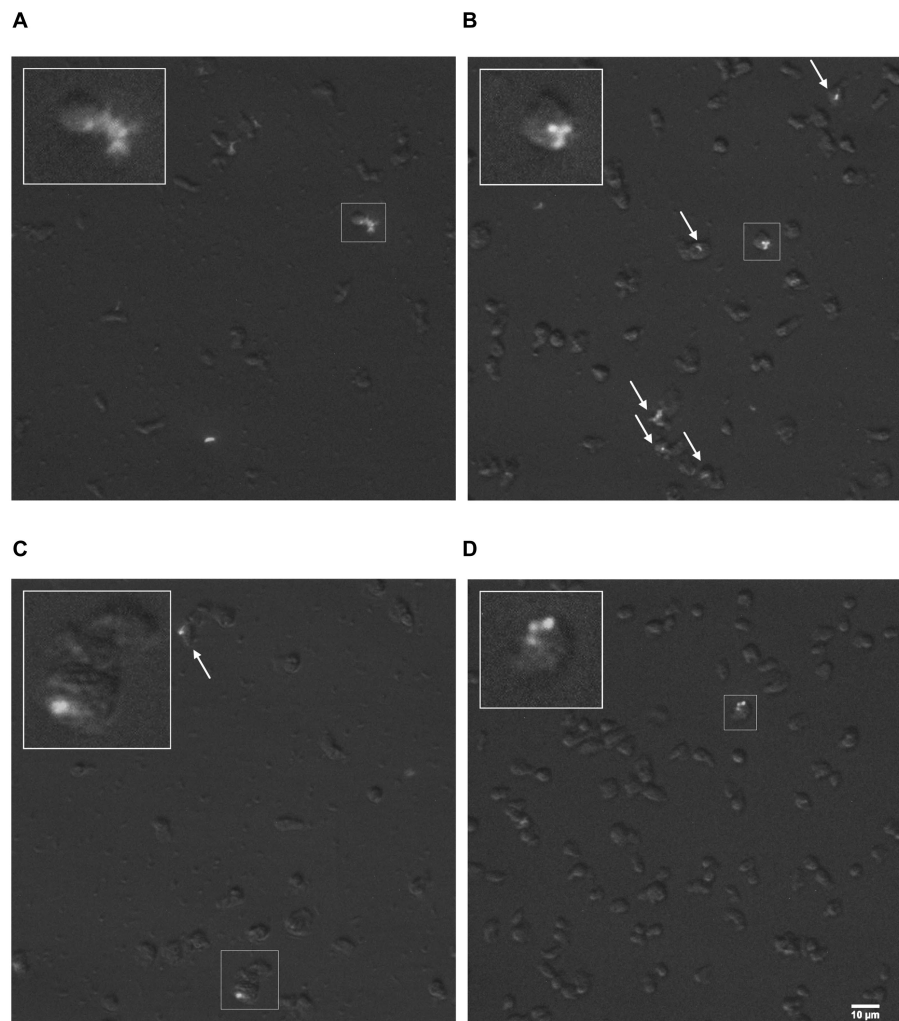


**FIGURE 6**  
*R. vilicus* co-localized with MAP K10-GFP. Micrographs with magnification x400 show *R. vilicus* in co-localization with MAP K10-GFP at 4 h (A) 24 h (B) 48 h (C) and 72 h post-infection (D). The interaction is highlighted with white arrows or framed and magnified three times.

to have a rapid eruptive locomotion with an elongate hyaline pseudopod. Endoplasm is described as crowded with vacuoles, resulting in a “sandy appearance” (Hawes, 1963; Bass et al., 2009). In our observations, similar morphological traits were noticed; rapid eruptive locomotion with one hyaline pseudopod and dense granuloplasm. No flagella were observed on *R. vilicus*, as described on the other *Rosculus* strains (Hawes, 1963; Bass et al., 2009; Týmł and Dyková, 2018). However, a new morphological trait, hitherto undescribed in *Rosculus* species, was a long stem on floating forms (Figures 3A,B). To our knowledge, it had not been described previously, and while the associated function is not obvious, we may hypothesize that adopting such a morphology may impact cell buoyancy, thereby facilitating dispersal along with the flow of liquid.

Cyst-like forms observed under light microscopy were round or oval-shaped, with refringent wall, and correspond to previously observed cystic form. Observation by TEM was more difficult because few cells were observed in our encystment conditions. The cells observed had a thin cell wall, contrary to what had been observed before, and which is generally found in amoeba encystment forms (Hawes, 1963; Bass et al., 2009; Týmł and Dyková, 2018). Despite the

lack of thick cell wall, the observation of an ostiole with SEM suggests that it is really a cyst form.

As is the case with most protist clades, genomic information on FLA is dramatically lacking. This should stimulate a systemic attempt at producing genomic data for novel protists isolates (Sibbald and Archibald, 2017). In line with this intent, we proceeded with the genomic characterization of *R. vilicus*, which has yielded the first genomic data for the Sainouroidea and adds to the (poorly) known genomic diversity of rhizarian protists. The draft genome of *R. vilicus*, assembled through a combination of long and short read data, provided an estimate of its size, which is ca. 40.8 Mbp long. This genome size is comparable with other FLA from distinct groups, such as *Acanthamoeba castellanii* (43.8 Mbp; Matthey-Doret et al., 2022), *Vermamoeba vermiformis* (39.5 Mbp; Delafont et al., 2021) or *Naegleria gruberi* (41 Mbp, Fritz-Laylin et al., 2010). Further studies providing transcriptomic data on *R. vilicus* could provide an initial annotation of this genome, a prerequisite for in-depth studies of gene repertoire. Aside from this nuclear genome, our hybrid assembly approach enabled us identify and isolate the mitochondrial genome of *R. vilicus*, which is unusually long

(185 kbp). This size estimate far exceeds the size of other mitochondrial genomes from the Cercozoa, for which recent estimates indicated sizes around 40 to 50 kbp (Wideman et al., 2020). While significantly larger than other known sequences from the same clade, mitochondrial gene repertoire of *R. vilicus* is highly comparable to that of other cercozoans and seems to once again prove that we have identified and correctly assembled this organellar genome (Supplementary Figure S1). To our knowledge, the characterization of *R. vilicus* mitochondrion represents the largest known mitochondrial genome ever described for a single-celled organism, thereby providing an interesting model for investigation of the dynamics of mitochondrial genome evolution. The novelty of this isolate should be seen as another argument in favor of the systematic implementation of genome sequencing for all novel protist isolates, as it represents a huge source of original findings.

In the process of assembling *R. vilicus* genome, we noted that no bacteria (apart from *E. coli* used as food source) was recovered. This suggests that *R. vilicus* does not live in symbiotic associations with other bacteria, as is the case for numerous other FLA (Samba-Louaka et al., 2019). However, one cannot rule out the possibility that the growth conditions we used, and more globally a switch from environmental to *in vitro* conditions, may have contributed to a loss of this association, on which we may have missed out in this study.

The strain isolated from water trough of infected cattle herds with paratuberculosis was a good candidate to verify our hypothesis that free-living amoebae could be MAP vectors. Since the first evidence the ability of mycobacteria species to survive in amoebae (Prasad and Gupta, 1978) different *Mycobacterium* species have been investigated regarding their interactions with phagocytic protozoan such as *Acanthamoeba*, *Dictyostelium* or *Tetrahymena*. Several *Mycobacterium* species were able to resist amoebal digestion, suggesting a role of amoebae in mycobacterial infections (Thomas and McDonnell, 2007). Most of these findings documented the involvement of amoebozoans and heteroloboseans representative in such interactions (Balczun and Scheid, 2017; Shi et al., 2021). However, recent work has demonstrated that numerous rhizarian FLA could also bear intracellular bacteria, thereby confirming that tight FLA-bacteria interactions indeed occur in all these taxonomic groups (Pohl et al., 2021; Solbach et al., 2021).

Few studies have related MAP association with amoebae. Among them, it was shown that incubation of MAP with *Acanthamoeba polyphaga* and *Acanthamoeba castellanii*, led to a decreasing MAP number in the first few post-internalization days, but increased after an extended period of several weeks (Mura et al., 2006; Whan et al., 2006; Phillips et al., 2020). Our results provide evidence that MAP can also persist for at least for 3 days in association with *R. vilicus*. However, it was a rare event, as only a few amoebae were associated with the MAP K10-GFP and it was not possible to distinguish if the bacteria were inside (phagocytized) or outside the amoebae. This suggests, added to previous observations using different FLA, that MAP might interact with a wide range of amoebae distantly related.

In conclusion, our study enabled to recover *R. vilicus*, a new species of *Rosculus* that grows preferentially between 20 and 25°C. Microscopic observations showed a small amoeba with morphological traits representative of the genus *Rosculus*. Whole genome sequencing added genomic data to the poorly known genomic diversity of rhizarian protists. Unexpectedly, this work highlighted the particularities mitochondrial genome size. *R. vilicus*

can interact with MAP for at least a few days. This result suggests the possible role of amoebae in the persistence of MAP and contributes new evidence about the protists range that interact with MAP in environment.

## 4.1 Description of *Rosculus vilicus* sp. nov

Description of *Rosculus vilicus* [vi.li.cus. N.L. adj.] sp. nov.

Taxonomic assignment: Eukaryota; TSAR; Rhizaria; Cercozoa; Sainouroidea; Guttulinopsidae; *Rosculus*.

Diagnosis: Cercozoan, limax-shaped amoeba. Single nucleus. Found in freshwater. Trophozoites: 4.2–13.8 µm (average: 7.1 µm) in length and 2.7–12.1 µm (average: 4.8 µm) in width. Trophozoites can adopt a more rounded floating form which typically displays a 10.2–31.4 µm stem (average: 18.9 µm). The amoebae can form a cyst-like structure when starved (average: 4.8 µm). The amoebae feed on the bacteria *Escherichia coli*.

Type strain: Isolate AJ1 (available upon request). Isolated from cattle drinking trough located in Indre et Loire department, France. The amoebae were isolated on a non-nutrient agar plate seeded with *E. coli* and routinely cultivated on PAS buffer with *E. coli* (OD 0.5) at 20°C.

Etymology: vilicus from *villa* (“country house”) + *icus*; pertaining to the farm.

The genome size of this isolate is was predicted to be 40.8 Mb long, showing 37.7% GC enrichment. This is the first genome of *Rosculus* spp. and there is no genome available in related species shown in Figure 5. The sequence was deposited at NCBI under the BioProject ID PRJNA1029052.

## Data availability statement

The data presented in this study are deposited in the NCBI database under accession numbers OR644361 and PRJNA1029052.

## Author contributions

AJ: Conceptualization, Data curation, Writing – original draft, Writing – review & editing, Formal analysis, Investigation. VD: Writing – original draft, Writing – review & editing, Conceptualization, Data curation, Methodology, Formal analysis. J-LM: Writing – review & editing, Project administration, Funding acquisition. FB: Writing – review & editing, Conceptualization, Funding acquisition. AS-L: Writing – original draft, Writing – review & editing, Conceptualization, Data curation, Methodology, Formal analysis. YH: Conceptualization, Data curation, Funding acquisition, Supervision, Writing – original draft, Writing – review & editing.

## Funding

The author(s) declare financial support was received for the research, authorship, and/or publication of this article. This work was supported by the Agence Nationale de la Recherche (ANR-22-CE35-0010, « Amitub », 01-01-2027).

## Acknowledgments

We thank Emile Bere (ImageUp, Université de Poitiers) for his assistance with microscopy experiments and Thibault Chautrand for his technical assistance. We also thank Bouziane Moumen from the Ebioinf bioinformatics platform CNRS UMR7267, EBI.

## Conflict of interest

The authors declare that the research was conducted in the absence of any commercial or financial relationships that could be construed as a potential conflict of interest.

## Publisher's note

All claims expressed in this article are solely those of the authors and do not necessarily represent those of their affiliated organizations, or those of the publisher, the editors and the reviewers. Any product that may be evaluated in this article, or claim that may be made by its manufacturer, is not guaranteed or endorsed by the publisher.

## References

- Balczun, C., and Scheid, P. L. (2017). Free-living amoebae as hosts for and vectors of intracellular microorganisms with public health significance. *Viruses* 9:65. doi: 10.3390/v9040065
- Bass, D., Chao, E. E.-Y., Nikolaev, S., Yabuki, A., Ishida, K.-I., Berney, C., et al. (2009). Phylogeny of novel naked filose and reticulose cercozoa: granofilosea cl. n. and proteomyxidea revised. *Protist* 160, 75–109. doi: 10.1016/j.protis.2008.07.002
- Bass, D., Silberman, J. D., Brown, M. W., Pearce, R. A., Tice, A. K., Jousset, A., et al. (2016). Coprophilic amoebae and flagellates, including Guttulinopsis, Rosculus and Helkesimastix, characterise a divergent and diverse rhizarian radiation and contribute to a large diversity of faecal-associated protists. *Environ. Microbiol.* 18, 1604–1619. doi: 10.1111/1462-2920.13235
- Burfeind, O., von Keyserlingk, M. A. G., Weary, D. M., Veira, D. M., and Heuwieser, W. (2010). Short communication: repeatability of measures of rectal temperature in dairy cows. *J. Dairy Sci.* 93, 624–627. doi: 10.3168/jds.2009-2689
- Claeys, T. A., and Robinson, R. T. (2018). The many lives of nontuberculous mycobacteria. *J. Bacteriol.* 200:e00739-17. doi: 10.1128/JB.00739-17
- Delafont, V., Gasque, M., and Hechard, Y. (2021). Simultaneous hybrid genome sequencing of *Vermamoeba vermiformis* and its *Dependentiae* endosymbiont *Vermiphilus pyriformis*. *bioRxiv*. doi: 10.1101/2021.04.23.440484
- Donath, A., Jühling, F., Al-Arab, M., Bernhart, S. H., Reinhardt, F., Stadler, P. F., et al. (2019). Improved annotation of protein-coding genes boundaries in metazoan mitochondrial genomes. *Nucleic Acids Res.* 47, 10543–10552. doi: 10.1093/nar/gkz833
- Drancourt, M. (2014). Looking in amoebae as a source of mycobacteria. *Microb. Pathog.* 77, 119–124. doi: 10.1016/j.micpath.2014.07.001
- Escoll, P., Rolando, M., Gomez-Valero, L., and Buchrieser, C. (2013). From amoeba to macrophages: exploring the molecular mechanisms of *Legionella pneumophila* infection in both hosts. *Curr. Top. Microbiol. Immunol.* 376, 1–34. doi: 10.1007/82\_2013\_351
- Fritz-Laylin, L. K., Prochnik, S. E., Ginger, M. L., Dacks, J. B., Carpenter, M. L., Field, M. C., et al. (2010). The genome of *Naegleria gruberi* illuminates early eukaryotic versatility. *Cells* 140, 631–642. doi: 10.1016/j.cell.2010.01.032
- Hawes, R. S. J. (1955). A *Limax-Amoeba* from the rectum of the grass snake, *Natrix natrix*, as a facultative aerobe in vitro. *Nature* 175, 779–780. doi: 10.1038/175779b0
- Hawes, R. S. (1963). On *Rosculus ithacus* gen. N., Sp. N. (protozoa, amoebina), with special reference to its mitosis and phylogenetic relations. *J. Morphol.* 113, 139–149. doi: 10.1002/jmor.1051130202
- Hess, S., and Suthaus, A. (2022). The vampyrellid amoebae (Vampyrellida, Rhizaria). *Protist* 173:125854. doi: 10.1016/j.protis.2021.125854
- Jürgens, K., and Matz, C. (2002). Predation as a shaping force for the phenotypic and genotypic composition of planktonic bacteria. *Antonie Van Leeuwenhoek* 81, 413–434. doi: 10.1023/A:1020505204959
- Kalyaanamoorthy, S., Minh, B. Q., Wong, T. K. F., von Haeseler, A., and Jermin, L. S. (2017). ModelFinder: fast model selection for accurate phylogenetic estimates. *Nat. Methods* 14, 587–589. doi: 10.1038/nmeth.4285
- Kang, D., Li, F., Kirton, E. S., Thomas, A., Egan, R. S., An, H., et al. (2019). MetaBAT 2: an adaptive binning algorithm for robust and efficient genome reconstruction from metagenome assemblies. *PeerJ* 7:e7359. doi: 10.7287/peerj.preprints.27522v1
- Kolmogorov, M., Yuan, J., Lin, Y., and Pevzner, P. A. (2019). Assembly of long, error-prone reads using repeat graphs. *Nat. Biotechnol.* 37, 540–546. doi: 10.1038/s41587-019-0072-8
- Li, L., Bannantine, J. P., Zhang, Q., Amons, A., May, B. J., Alt, D., et al. (2005). The complete genome sequence of *Mycobacterium avium* subspecies paratuberculosis. *Proc. Natl. Acad. Sci. U. S. A.* 102, 12344–12349. doi: 10.1073/pnas.0505662102
- Martin, M. (2011). Cutadapt removes adapter sequences from high-throughput sequencing reads. *EMBnet J* 17, 10–12. doi: 10.14806/ej.17.1.200
- Matthey-Doret, C., Colp, M. J., Escoll, P., Thierry, A., Moreau, P., Curtis, B., et al. (2022). Chromosome-scale assemblies of *Acanthamoeba castellanii* genomes provide insights into *Legionella pneumophila* infection-related chromatin reorganization. *Genome Res.* 32, 1698–1710. doi: 10.1101/gr.276375.121
- Minh, B. Q., Schmidt, H. A., Chernomor, O., Schrempf, D., Woodhams, M. D., von Haeseler, A., et al. (2020). IQ-TREE 2: new models and efficient methods for phylogenetic inference in the genomic era. *Mol. Biol. Evol.* 37, 1530–1534. doi: 10.1093/molbev/msaa015
- Mura, M., Bull, T. J., Evans, H., Sidi-Boumedine, K., McMinn, L., Rhodes, G., et al. (2006). Replication and long-term persistence of bovine and human strains of *Mycobacterium avium* subsp. paratuberculosis within *Acanthamoeba polyphaga*. *Appl. Environ. Microbiol.* 72, 854–859. doi: 10.1128/AEM.72.1.854-859.2006
- Phillips, I. L., Everman, J. L., Bermudez, L. E., and Danelishvili, L. (2020). *Acanthamoeba castellanii* as a screening tool for *Mycobacterium avium* subspecies paratuberculosis virulence factors with relevance in macrophage infection. *Microorganisms* 8:1571. doi: 10.3390/microorganisms8101571
- Pohl, N., Solbach, M. D., and Dumack, K. (2021). The wastewater protist *Rhogostoma minus* (Thecofilosea, Rhizaria) is abundant, widespread, and hosts *Legionellales*. *Water Res.* 203:117566. doi: 10.1016/j.watres.2021.117566
- Prasad, B. N. K., and Gupta, S. K. (1978). Preliminary report on the engulphment and retention of mycobacteria by trophozoites of exenically grown *Acanthamoeba castellanii* douglas, 1930. *Curr. Sci.* 47, 245–247.
- Pimm, T. P., Lucero, C. A., and Falkinham, J. O. 3rd (2004). Health impacts of environmental mycobacteria. *Clin. Microbiol. Rev.* 17, 98–106. doi: 10.1128/CMR.17.1.98-106.2004
- Rodríguez-Zaragoza, S. (1994). Ecology of free-living amoebae. *Crit. Rev. Microbiol.* 20, 225–241. doi: 10.3109/10408419409114556

## Supplementary material

The Supplementary material for this article can be found online at: <https://www.frontiersin.org/articles/10.3389/fmicb.2023.1324985/full#supplementary-material>

### SUPPLEMENTARY FIGURE S1

The unusually large mitochondrion of *R. vilicus* shows a gene repertoire comparable to, and phylogenetic affinities with, other cercozoans. Analyses of mitochondrial contig coverage suggests that its unusual size does not result from artefactual assembly (A). Gene and transfer RNA repertoire from *R. vilicus* almost perfectly mirror that of other cercozoans, as identified by Wideman et al. (2020). For tRNA, a red-filled square indicates an independent codon reassignment. The 'extras' category indicates the unusual codons N (auu) in A (uau) in B (B). Maximum likelihood phylogeny of the COX1 protein (332 amino acid residues) shows clear affiliation of *R. vilicus* with other cercozoans, congruent with nuclear rRNA phylogeny (C).

### SUPPLEMENTARY FIGURE S2

*R. vilicus* and MAP K10-GFP co-localize on the video taken 4 hours post-infection.

### SUPPLEMENTARY FIGURE S3

*R. vilicus* and MAP K10-GFP co-localize on the video taken 72 hours post-infection.

- Salah, I. B., Ghigo, E., and Drancourt, M. (2009). Free-living amoebae, a training field for macrophage resistance of mycobacteria. *Clin. Microbiol. Infect.* 15, 894–905. doi: 10.1111/j.1469-0691.2009.03011.x
- Samba-Louaka, A., Delafont, V., Rodier, M.-H., Cateau, E., and Héchard, Y. (2019). Free-living amoebae and squatters in the wild: ecological and molecular features. *FEMS Microbiol. Rev.* 43, 415–434. doi: 10.1093/femsre/fuz011
- Samba-Louaka, A., Robino, E., Cochard, T., Branger, M., Delafont, V., Aucher, W., et al. (2018). Environmental *Mycobacterium avium* subsp. paratuberculosis hosted by free-living amoebae. *Front. Cell. Infect. Microbiol.* 8:28. doi: 10.3389/fcimb.2018.00028
- Schneider, C. A., Rasband, W. S., and Eliceiri, K. W. (2012). NIH image to ImageJ: 25 years of image analysis. *Nat. Methods* 9, 671–675. doi: 10.1038/nmeth.2089
- Schuler, G. A., Tice, A. K., Pearce, R. A., Foreman, E., Stone, J., Gammill, S., et al. (2018). Phylogeny and classification of novel diversity in Sainouroidea (Cercozoa, Rhizaria) sheds light on a highly diverse and divergent clade. *Protist* 169, 853–874. doi: 10.1016/j.protis.2018.08.002
- Shi, Y., Queller, D. C., Tian, Y., Zhang, S., Yan, Q., He, Z., et al. (2021). The ecology and evolution of amoeba-bacterium interactions. *Appl. Environ. Microbiol.* 87:e01866-20. doi: 10.1128/AEM.01866-20
- Sibbald, S. J., and Archibald, J. M. (2017). More protist genomes needed. *Nat Ecol Evol* 1:145. doi: 10.1038/s41559-017-0145
- Solbach, M. D., Bonkowski, M., and Dumack, K. (2021). Novel endosymbionts in rhizarian amoebae imply universal infection of unrelated free-living amoebae by Legionellales. *Front. Cell. Infect. Microbiol.* 11:642216. doi: 10.3389/fcimb.2021.642216
- Sun, S., Noorian, P., and McDougald, D. (2018). Dual role of mechanisms involved in resistance to predation by protozoa and virulence to humans. *Front. Microbiol.* 9:1017. doi: 10.3389/fmicb.2018.01017
- Thomas, V., and McDonnell, G. (2007). Relationship between mycobacteria and amoebae: ecological and epidemiological concerns. *Lett. Appl. Microbiol.* 45, 349–357. doi: 10.1111/j.1472-765X.2007.02206.x
- Tyml, T., and Dyková, I. (2018). Sappinia sp. (Amoebozoa: Thecamoebida) and Rosculus sp. (SAR: Cercozoa) isolated from king penguin guano collected in the Subantarctic (South Georgia, Salisbury plain) and their coexistence in culture. *J. Eukaryot. Microbiol.* 65, 544–555. doi: 10.1111/jeu.12500
- Whan, L., Grant, I. R., and Rowe, M. T. (2006). Interaction between *Mycobacterium avium* subsp. paratuberculosis and environmental protozoa. *BMC Microbiol.* 6:63. doi: 10.1186/1471-2180-6-63
- Wick, R. R., and Holt, K. E. (2022). Polypolish: short-read polishing of long-read bacterial genome assemblies. *PLoS Comput. Biol.* 18:e1009802. doi: 10.1371/journal.pcbi.1009802
- Wick, R. R., Judd, L. M., and Holt, K. E. (2023). Assembling the perfect bacterial genome using Oxford Nanopore and Illumina sequencing. *PLoS Comput. Biol.* 19:e1010905. doi: 10.1371/journal.pcbi.1010905
- Wideman, J. G., Monier, A., Rodríguez-Martínez, R., Leonard, G., Cook, E., Poirier, C., et al. (2020). Unexpected mitochondrial genome diversity revealed by targeted single-cell genomics of heterotrophic flagellated protists. *Nat. Microbiol.* 5, 154–165. doi: 10.1038/s41564-019-0605-4





## OPEN ACCESS

## EDITED BY

Isabel Marcelino,  
Institut Pasteur de la Guadeloupe, Guadeloupe

## REVIEWED BY

Johid Malik,  
University of Nebraska Medical Center,  
United States  
Ladawan Khowawisetsut,  
Mahidol University, Thailand

## \*CORRESPONDENCE

Lisette Retana Moreira  
✉ lisette.retanamoreira@ucr.ac.cr  
Antonio Osuna  
✉ aosuna@ugr.es

<sup>†</sup>These authors share senior authorship

RECEIVED 28 November 2023

ACCEPTED 16 January 2024

PUBLISHED 05 February 2024

## CITATION

Retana Moreira L, Cornet-Gomez A, Sepulveda MR, Molina-Castro S, Alvarado-Ocampo J, Chaves Monge F, Jara Rojas M, Osuna A and Abrahams Sandi E (2024) Providing an *in vitro* depiction of microglial cells challenged with immunostimulatory extracellular vesicles of *Naegleria fowleri*. *Front. Microbiol.* 15:1346021. doi: 10.3389/fmicb.2024.1346021

## COPYRIGHT

© 2024 Retana Moreira, Cornet-Gomez, Sepulveda, Molina-Castro, Alvarado-Ocampo, Chaves Monge, Jara Rojas, Osuna and Abrahams Sandi. This is an open-access article distributed under the terms of the [Creative Commons Attribution License \(CC BY\)](https://creativecommons.org/licenses/by/4.0/). The use, distribution or reproduction in other forums is permitted, provided the original author(s) and the copyright owner(s) are credited and that the original publication in this journal is cited, in accordance with accepted academic practice. No use, distribution or reproduction is permitted which does not comply with these terms.

# Providing an *in vitro* depiction of microglial cells challenged with immunostimulatory extracellular vesicles of *Naegleria fowleri*

Lisette Retana Moreira<sup>1,2\*</sup>, Alberto Cornet-Gomez<sup>3</sup>,  
M. Rosario Sepulveda<sup>4</sup>, Silvia Molina-Castro<sup>5,6</sup>,  
Johan Alvarado-Ocampo<sup>2</sup>, Frida Chaves Monge<sup>1</sup>,  
Mariana Jara Rojas<sup>1</sup>, Antonio Osuna<sup>3\*†</sup> and  
Elizabeth Abrahams Sandi<sup>1,2†</sup>

<sup>1</sup>Departamento de Parasitología, Facultad de Microbiología, Universidad de Costa Rica, San José, Costa Rica, <sup>2</sup>Centro de Investigación en Enfermedades Tropicales (CIET), Universidad de Costa Rica, San José, Costa Rica, <sup>3</sup>Grupo de Bioquímica y Parasitología Molecular (CTS 183), Departamento de Parasitología, Campus de Fuentenueva, Instituto de Biotecnología, Universidad de Granada, Granada, Spain, <sup>4</sup>Departamento de Biología Celular, Facultad de Ciencias, Universidad de Granada, Granada, Spain, <sup>5</sup>Instituto de Investigaciones en Salud (INISA), Universidad de Costa Rica, San José, Costa Rica, <sup>6</sup>Departamento de Bioquímica, Escuela de Medicina, Universidad de Costa Rica, San José, Costa Rica

*Naegleria fowleri* is the causative agent of primary amoebic meningoencephalitis, a rapid and acute infection of the central nervous system with a fatal outcome in >97% of cases. Due to the infrequent report of cases and diagnostic gaps that hinder the possibility of recovering clinic isolates, studies related to pathogenesis of the disease are scarce. However, the secretion of cytolytic molecules has been proposed as a factor involved in the progression of the infection. Several of these molecules could be included in extracellular vesicles (EVs), making them potential virulence factors and even modulators of the immune response in this infection. In this work, we evaluated the immunomodulatory effect of EVs secreted by two clinic isolates of *Naegleria fowleri* using *in vitro* models. For this purpose, characterization analyses between EVs produced by both isolates were first performed, for subsequent gene transcription analyses post incubation of these vesicles with primary cultures from mouse cell microglia and BV-2 cells. Analyses of morphological changes induced in primary culture microglia cells by the vesicles were also included, as well as the determination of the presence of nucleic acids of *N. fowleri* in the EV fractions. Results revealed increased expression of *NOS*, proinflammatory cytokines *IL-6*, *TNF-α*, and *IL-23*, and the regulatory cytokine *IL-10* in primary cultures of microglia, as well as increased expression of *NOS* and *IL-13* in BV-2 cells. Morphologic changes from homeostatic microglia, with small cellular body and long processes to a more amoeboid morphology were also observed after the incubation of these cells with EVs. Regarding the presence of nucleic acids, specific *Naegleria fowleri* DNA that could be amplified using both conventional and qPCR was confirmed in the EV fractions. Altogether, these results confirm the immunomodulatory effects of EVs of *Naegleria fowleri* over microglial cells and suggest a potential role of these vesicles as biomarkers of primary acute meningoencephalitis.

## KEYWORDS

extracellular vesicles, trophozoites, *Naegleria fowleri*, microglia, cytokines, morphological changes, DNA

# 1 Introduction

Primary amoebic meningoencephalitis (PAM) is an infection of the central nervous system (CNS) produced by *Naegleria fowleri*, a thermophilic free-living amoeba (FLA) that can be found in different water sources and in soil. This infection is characterized by an acute and fulminant course, with initial symptoms that are undistinguishable from bacterial meningitis, a fact that complicates its diagnosis. Since the first description of the infection (Fowler and Carter, 1965), approximately 440 cases have been reported worldwide (Jahangeer et al., 2020); around one third of these cases have occurred in the United States, a country in which is suggested an underestimation of cases that could exceed 50% (Matanock et al., 2018). Due to the low number of diagnosed cases, PAM is considered a rare disease; however, mortality rates of this disease surpass 97% (CDC, 2023). The most affected population includes children and young adults and among the risk factors, aquatic activities like diving, waterskiing, surfing, swimming, exposition to hot springs, and nasal rinsing with tap water can be listed, as *N. fowleri* enters the host through the nose (Pana et al., 2023).

Since more than two decades, the study of free-living amoebae and its impact in human health has increased. In this sense, research has focused in trying to identify the mechanisms employed by these organisms to produce damage, as well as possible diagnostic and therapeutic alternatives for this type of infections. For *N. fowleri*, some virulence factors that could contribute to the pathogenesis of the infection have been identified and can be classified into contact-dependent and contact-independent. It has been also demonstrated that the adhesion of trophozoites of the amoeba to the nasal mucosa via integrin-like adhesins and fibronectin binding protein is a critical initial step during the infection process. Once the amoeba is adhered to the mucosa, the increase in its locomotion rate and the chemotactic response to components of the CNS are crucial factors for the progression of the disease (Marciano-Cabral and Cabral, 2007; Naqvi et al., 2016). Moreover, food cups employed by the amoeba for trophocytosis and the secretion of cytolytic molecules like neuraminidases, hydrolases, phospholipases and pore-forming proteins (naegleriapores A and B) participate in the invasion process and in tissue damage.

The invasion of *Naegleria fowleri* to the host induces an intense immune response, characterized by the activation of innate defense mechanisms during the early stages of the infection, including an increased secretion of mucin (MUC5AC) and the production of IL-8 and IL-1 $\beta$  by respiratory epithelial cells (Siddiqui et al., 2016). Once the amoeba reaches the brain, an intense inflammatory response is produced, characterized by tissue infiltration of eosinophils, neutrophils, and macrophages, as well as increased levels of TNF- $\alpha$ , which is considered to stimulate the adherence of neutrophils to the amoeba, triggering its destruction (Marciano-Cabral and Cabral, 2007).

It has been proposed that activated macrophages have an amoebicidal effect over *N. fowleri* by the production of reactive oxygen species (ROS) during the oxidative burst, besides nitric oxide (NO) and mediators like TNF- $\alpha$  and IL-1 (Siddiqui et al., 2016). Studies performed by other groups using microglia, the

primary immune cells in the brain, confirm the production of inflammatory cytokines after the contact with trophozoites of the amoeba, reporting robust levels of mRNAs for IL-1 $\alpha$ , IL-1 $\beta$ , IL-6, and TNF- $\alpha$  after 6 h of incubation (Marciano-Cabral et al., 2001; Marciano-Cabral and Cabral, 2007). Regarding the role of the immune response during this infection, recent investigations have focused in analyzing excretion/secretion products of the amoeba as possible modulators of this response in the host. Within the secreted products by different microorganisms and its target cells, research in extracellular vesicles (EV) has played a leading role in this and other protozoan microorganisms (Wan et al., 2022).

Initially considered as cellular waste products, the role of EVs in intercellular communication is now fully recognized, a process that is highly conserved among eukaryotic and prokaryotic cells. Moreover, the participation of EVs in inflammatory processes and the transference of genetic information has been confirmed, also demonstrating that their cargo, as well as structural molecules of the vesicles, could trigger and modulate the immune response (Islek et al., 2022). For example, in the case of *Plasmodium*, it has been reported that EVs are able to regulate the immune activity, increasing the parasite's survival inside the host and considering these vesicles key for the pathogenesis of the disease (Opadokun and Rohrbach, 2021). For extracellular protozoan parasites like *Entamoeba histolytica*, EVs have shown a role in NETosis and ROS production by neutrophils (Díaz-Godínez et al., 2022), while exosomes of *Trichomonas vaginalis* can induce IL-6 production and downregulate the expression of IL-8 (cytokine that recruits neutrophils) in cells of the vaginal epithelium; besides, it has been shown that EVs could modulate the immune response of macrophages *in vitro*, stimulating the release of NO and inducing IL-10 production (Nievas et al., 2020).

Regarding FLA, the production and characterization of EVs has been recently documented. For *Acanthamoeba*, biological and nanomechanical properties of EVs secreted by clinical and environmental isolates have been reported (de Souza Gonçalves et al., 2018; Gonçalves et al., 2019; Retana Moreira et al., 2020a), including an analysis of the immunostimulatory effect of these vesicles over the THP-1 cell line that revealed an increment in transcription levels of cytokines IL-6 and IL-12 (Lin et al., 2019). For *N. fowleri*, the isolation and characterization of EVs from two different clinic isolates was achieved in 2022, demonstrating the presence of proteins as part of their cargo, as well as the induction of the expression of costimulatory molecules and IL-8 in THP-1 macrophages (Lertjuthaporn et al., 2022; Retana Moreira et al., 2022). Taking into account that brain tissue is the target of *N. fowleri* and that the immune response contributes significantly to the damage produced during the infection with this species, the aim of the present work is to evaluate the effect of EVs secreted by two clinic isolates of *N. fowleri* using an *in vitro* model with primary cultures of mouse brain microglia and BV-2 cells, a microglial cell line derived from C57/BL6 mice. For this purpose, transcription levels of different cytokines and NOS after the incubation of these cells with EVs secreted by trophozoites of the amoeba during different time points were determined. Characterization analysis of EVs secreted by both *N. fowleri* isolates, analyses of morphological changes induced by these vesicles in primary cultures of mouse brain microglia and a

preliminary detection of nucleic acids (including bioactive DNA) of *N. fowleri* in the EV fractions were also achieved.

## 2 Materials and methods

### 2.1 Axenic culture of *Naegleria fowleri* trophozoites

Trophozoites of two clinic isolates of *Naegleria fowleri* from Costa Rica (accession numbers MT090627 and MT210902) (Retana Moreira et al., 2020b) were cultured in 75 cm<sup>2</sup> Nunc EasYFlask cell culture flasks (Thermo Fisher Scientific, Waltham, Massachusetts, United States) with 2% casein hydrolysate (Sigma Aldrich, Missouri, United States) culture medium, supplemented with 10% inactivated fetal bovine serum (Gibco, Grand Island, New York, United States) and antibiotics (penicillin/streptomycin). The flasks were incubated at 37°C, with daily observation of the cultures under an inverted microscope. For each flask, the culture medium was replaced, at least, every 2 days.

### 2.2 Animal handling and permission of the animal welfare and ethics committee

The experiments performed using animals were approved by the Ethical Committee of the University of Granada (235-CEEA-OH-2018) and by the authorities of the Regional Government of Andalucía (JJAA) (number 12/11/2017/162). The use of animals was performed according to the institutional guidelines (Spanish government regulations) (Real Decreto RD1201/05) and the guidelines of the European Union (European Directive 2010/63/EU).

### 2.3 Isolation of extracellular vesicles

Extracellular vesicles of trophozoites of each *Naegleria fowleri* isolate were obtained as previously described by Retana Moreira et al. (2022), following the Minimal Information for the Study of Extracellular Vesicles (MISEV) guidelines (Théry et al., 2018). Briefly, trophozoites were washed 3 times using sterile PBS and then,  $5 \times 10^7$  trophozoites were incubated for 5 h at 37°C in 75 cm<sup>2</sup> Nunc EasYFlask cell culture flasks (Thermo Fisher Scientific, Waltham, Massachusetts, United States) with 3.5 mL of 2% casein hydrolysate (Sigma Aldrich, Missouri, United States) culture medium without serum nor antibiotics. After this incubation, the supernatants were collected and centrifuged at  $3,500 \times g$  for 15 min at 4°C to remove possible remaining trophozoites. The resulting supernatants were collected again for extracellular vesicle purification as previously described (Retana Moreira et al., 2022), applying a protocol that includes a centrifugation step at  $16,000 \times g$  for 30 min at 4°C to remove larger vesicles, filtration of the supernatant using 0.22 µm pore filters (Sartorius, Göttingen, Germany) and ultracentrifugation steps at  $120,000 \times g$  for 150 min at 4°C in a Sorwall™ WX80 ultracentrifuge (Thermo Fisher Scientific, Waltham, Massachusetts, United States). The resulting pellets were washed two times in sterile filtered (0.22 µm pore

filter) PBS at  $120,000 \times g$  for 150 min and suspended in 100 µL sterile PBS. The viability of trophozoites after the 5 h secretion period was evaluated using the trypan blue exclusion test and the protein concentration of each sample was quantified using the Micro-BCA protein assay (Thermo Fischer Scientific, Waltham, Massachusetts, United States), following the manufacturer's instructions.

The characterization of EVs secreted by each isolate was performed using transmission electron microscopy (TEM), scanning electron microscopy (SEM) and nanoparticle tracking analysis (NTA), as described in previous works (Retana Moreira et al., 2019, 2021, 2022; Cornet-Gomez et al., 2023).

### 2.4 Transmission electron microscopy

To confirm the production of extracellular vesicles by each *Naegleria fowleri* isolate, pellets of the samples obtained after the ultracentrifugation steps were fixed in 500 µL of Karnovsky's fixative (2.5% glutaraldehyde and 2% formaldehyde in 0.1 M cacodylate buffer, 50 mg of CaCl<sub>2</sub> in 100 mL) for 2 h at 37°C. Then, the samples were dehydrated and embedded in Spurr resin (Sigma Aldrich, Missouri, United States) and ultra-thin sections were performed and stained using 1% uranyl acetate. Final examination of the samples was performed using a Carl Zeiss LIBRA 120 PLUS SMT electron microscope (Carl Zeiss, Oberkochen, Germany).

### 2.5 Scanning electron microscopy

Trophozoites of each isolate of *Naegleria fowleri* were washed 3 times using sterile PBS and  $5 \times 10^4$  trophozoites were suspended in 2% casein hydrolysate (Sigma Aldrich, Missouri, United States) culture medium and placed in 18 mm round coverslips (Fisher Scientific, New Hampshire, United States). After 5 h of incubation at 37°C, the coverslips with trophozoites were carefully fixed with 2.5% glutaraldehyde in cacodylate buffer with 0.1 M saccharose and maintained in the fixative solution for 24 h at 4°C. Then, the samples were dehydrated in a graded series of ethanol, desiccated using a critical point dryer (Leica EM CPD 300) and then evaporated with high vacuum carbon coater (Emitech K975X) as described by Díaz Lozano et al. (2017). The samples were finally carbon-coated for 3 min and analyzed using a Zeiss Supra 40VP high-resolution scanning electron microscope.

### 2.6 Nanoparticle tracking analysis

Distribution, size, and concentration of extracellular vesicles of *Naegleria fowleri* were determined by measuring the rate of Brownian motion according to the particle size, using a Nanosight NS300 (Malvern Panalytical, Worcestershire, UK). The system was equipped with a sCMOS camera and a blue 488 nm laser beam.

Before the analysis, the samples were diluted 1/100 in low-binding Eppendorf tubes with sterile-filtered (0.22 µm pore filter) PBS. Measurements were performed at 25°C. For data acquisition and

information processing, the NTA software 3.2 Dev Build 3.2.16 was employed.

## 2.7 Protein pattern and recognition of extracellular vesicles secreted by each isolate by polyclonal anti-*Naegleria fowleri* antibodies

### 2.7.1 Preparation of whole protein extracts of *Naegleria fowleri* trophozoites

Whole protein extracts of lysates of each isolate of *Naegleria fowleri* were obtained as previously described (Retana Moreira et al., 2022). Briefly,  $5 \times 10^7$  trophozoites were washed three times in sterile PBS, suspended in 500  $\mu$ L sterile PBS and submitted to sonication in a 4710 series ultrasonic homogenizer (Cole-Parmer Instrument Co., Illinois, United States) applying 3 cycles of 30 s, with a 60 s pause between cycles. Protein quantification of the whole protein extracts was also achieved using the Micro-BCA protein assay (Thermo Fischer Scientific, Waltham, Massachusetts, United States).

### 2.7.2 Electrophoretic separation of proteins using SDS-PAGE

To obtain protein profiles, samples of extracellular vesicles and whole protein extracts of each isolate of *Naegleria fowleri* were diluted 1:1 in sample buffer (Laemmli, 1970), heated for 10 min at 98°C and subsequently loaded onto 12% SDS-polyacrylamide gels. Electrophoretic runs were performed for 90 min (120 V). Once the electrophoresis was completed, silver stain was performed, following previously described protocols (Heukeshoven and Dernick, 1988).

### 2.7.3 Polyclonal antibody production

Polyclonal anti-*Naegleria fowleri* antibodies were produced after the immunization of four-week-old female Wistar rats with 40  $\mu$ g of whole protein extract of lysates of trophozoites of *Naegleria fowleri* (ATCC *N. fowleri* Carter 30808), following the methodology previously described by our group (Retana Moreira et al., 2022). Briefly, the antigen was prepared by emulsification of the amoebae lysate (prepared in sterile PSB) in complete Freund's adjuvant (Sigma, Ronkonkoma, NY, United States), using a 1:1 ratio (final volume: 500  $\mu$ L). This emulsion was administered intraperitoneally to the rats. For subsequent immunizations, the adjuvant was switched to incomplete Freund's adjuvant (Sigma-Aldrich, St. Louis, MO, United States). A total of 8 immunizations (1 per week) were performed and the antibody production was evaluated using ELISA and Western blot (WB), as described elsewhere (Towbin et al., 1979).

### 2.7.4 Western blot

The recognition of the origin of extracellular vesicles, as coming from trophozoites of *Naegleria fowleri*, was performed by Western blot, where proteins separated from lysates of trophozoites and EVs using SDS-PAGE electrophoresis were confronted to polyclonal anti-*N. fowleri* antibodies obtained as described above. Briefly, SDS-PAGE electrophoresis was performed, the separated proteins in the polyacrylamide gels were transferred to nitrocellulose membranes (60 min, 90 V) in an Enduro VE10 Vertical Gel System (Labnet International, New Jersey, United States) and, after the transference, the membranes were blocked overnight with 5% non-fat milk in PBS-0.1% Tween 20, washed four times in a solution

of PBS-0.1% Tween 20 and incubated overnight at 4°C with the polyclonal anti-*Naegleria fowleri* antibodies (1: 10,000). After the incubation, the membranes were washed and incubated for 1 h with peroxidase-conjugated goat anti-rat IgGs (1, 10,000) (Thermo Scientific, Massachusetts, United States) and, once four washing steps with PBS-0.1% Tween 20 were performed, the reaction was visualized using the Clarity ECL Western substrate (BioRad, California, United States) in a ChemiDoc Imaging system (BioRad, California, United States).

## 2.8 Cytokine expression analyses in microglial cultures

### 2.8.1 Primary culture from mouse cell microglia and BV-2 cell line culture

Primary cultures of mouse brain microglia were prepared according to Morales-Ropero et al. (2021). Briefly, newborn (1-day old) C57BL/6 mice were obtained from the animal facility service of the “Centro de Instrumentación Científica” at the University of Granada (UGR) and meninges-free cerebral cortex from the brains were dissected and collected in DMEM with 4.5 g/L D-glucose, 4 mM glutamine, 10% fetal bovine serum, 10% horse serum, 100 U/mL penicillin and 100  $\mu$ g/mL streptomycin (all reagents from GIBCO, Waltham, Massachusetts, United States). After disaggregation and homogenization, cells were seeded and incubated at 37°C with 5% CO<sub>2</sub> for 10–12 days. Then, cultures were softly shaken at 37°C for 2 h and the primary microglia-enriched supernatant was subcultured in the same medium for 2 days before the experiments. Cultures of microglia showed >95% of microglial marker Iba1-positive cells by immunocytochemistry.

BV-2 cells (AcceGen Biotechnology, Fairfield, NJ, United States) were cultured in 25 cm<sup>2</sup> Nunc EasYFlask cell culture flasks (Thermo Fisher Scientific, Waltham, Massachusetts, United States) using RPMI-1640 culture medium (Sigma Aldrich, Missouri, United States) supplemented with 10% inactivated fetal bovine serum (Gibco, Grand Island, New York, United States), 2 mM glutamine, 100 U/mL penicillin and 100  $\mu$ g/mL streptomycin (complete culture medium).

### 2.8.2 EVs-cell interactions and cytokine expression analyses

For primary microglial cultures,  $2.5 \times 10^4$  cells were seeded in in 6-well plates (Thermo Fisher Scientific, Waltham, Massachusetts, United States), using DMEM with 4.5 g/L D-glucose, 4 mM glutamine, 10% fetal bovine serum, 10% horse serum and 100 U/mL penicillin, 100  $\mu$ g/mL streptomycin (all reagents from GIBCO, Grand Island, New York, United States). After 72 h of incubation at 37°C, 50% of the culture medium in each well was removed and 25  $\mu$ g of EVs of each *N. fowleri* isolate was suspended in fresh culture medium and added to the cells. In this case, the incubations were performed for 48 h, and, after this time, the supernatants were removed and the cells were lysed and homogenized using TRIzol reagent (Thermo Fischer Scientific, Waltham, Massachusetts, United States) for RNA purification, which was performed following the manufacturer's instructions. Incubation of cells with bacterial 100 ng/mL lipopolysaccharide (LPS, serotype 0111: B4; Sigma Aldrich, Missouri, United States) and with the complete culture medium were also included as control of cell stimulation.



For BV-2 cell line,  $2.5 \times 10^5$  cells were seeded in 6-well plates (Thermo Fisher Scientific, Waltham, Massachusetts, United States) with RPMI-1640 culture medium (Sigma Aldrich, Missouri, United States) supplemented with 10% inactivated fetal bovine serum (Gibco, Grand Island, New York, United States), 2 mM glutamine and antibiotics (penicillin/streptomycin). After 24 h of incubation at 37°C, the culture medium was removed and cells were incubated with 25 µg of EVs of each *N. fowleri* isolate, suspended in complete culture medium and incubated for different time points: 4, 24 and 48 h. After each incubation time, the culture medium was removed and TRIzol reagent (Thermo Fisher Scientific, Waltham, Massachusetts, United States) was added for RNA extractions, which were performed as previously mentioned.

After RNA extractions, an incubation with DNase I, RNase-free (Thermo Fisher Scientific, Waltham, Massachusetts, United States) was performed according to the manufacturer's recommendations and, once the RNAs were purified and quantified, expression analyses of genes *IL-1β*, *IL-6*, *IL-10*, *IL-12*, *IL-13*, *IL-18*, *IL-23*, *TNF-α*, *IFN-γ*, *TGF-β* and nitric oxide synthase (NOS) were performed by qRT-PCR (primer sequences are shown in [Supplementary Table S1](#)). For this purpose, the iTaq™ universal SYBR® Green one-step universal SYBR® kit (BioRad, Hercules, CA, United States) was employed, using *gapdh* and *actin* as reference genes. The sequences of the primers employed in this analysis are listed in [Supplementary Table S1](#); primer sequences were located across exon–exon borders, avoiding any interspecifically and intraspecifically variable positions. Moreover, a calibration curve was performed according to [Gómez-Sambblas et al. \(2018\)](#) to calculate the efficiency of each pair of primers.

Reactions were performed in a CFX-96 qRT-PCR system (BioRad, Hercules, CA, United States), using a final volume of 10 µL, which included 300 nM of each primer and 50 ng of RNA per reaction. The thermal cycling conditions consisted of retrotranscription at 50°C for 10 min, followed by an enzymatic activation step and DNA denaturation at 95°C for 1 min, 40 cycles of denaturation at 95°C for 10 s and annealing and extension steps at 60°C for 30 s, followed by plate reading. At the end of the qRT-PCR reactions, a melting gradient was applied from 65°C to 95°C in 0.5°C increments. Cytokine expression results were normalized against *gapdh* and *actin*, as well as the negative control (cells in complete culture medium).

### 2.8.3 Analysis of morphological changes induced by EVs of *Naegleria fowleri* in culture primary culture from mouse cell microglia using immunofluorescence

Primary cultures of mouse brain microglia were prepared as previously described. Briefly, primary microglia ( $2.5 \times 10^4$  cells) were seeded onto 12 mm-diameter round glass coverslips coated with 0.1 mg/mL poly-D-lysine and cultured in DMEM with 4.5 g/L D-Glucose, 4 mM glutamine, 10% fetal bovine serum, 10% horse serum and 100 U/mL penicillin, 100 µg/mL streptomycin for 2 days before the experiments. Cell stimulation was induced by 100 ng/mL LPS and 25 µg of EVs of each *N. fowleri* isolate suspended in the culture medium for 24 and 48 h.

To analyze microglial cell morphology, microglial cells were fixed with 4% cold paraformaldehyde in PBS for 20 min. After a washing step using PBS, the cells were permeabilized with 0.2% Triton X-100 in PBS for 10 min, blocked with 3% bovine serum albumin in PBS for 1 h, and stained with isolectin B4 from *Griffonia simplicifolia* (GS-IB4) Alexa Fluor 488 conjugate (Thermo Fisher Scientific, Waltham,

Massachusetts, United States) diluted 1:100 in PBS for 1 h. DAPI staining was used to visualize nuclei. Coverslips were mounted in slides with FluorSave Reagent (Millipore, Burlington, Massachusetts, United States) and images were taken using a Zeiss Axiophot fluorescent microscope.

Images were analyzed by Image J software (version 1.50i, NIH). The cell morphology was studied by determination of the aspect ratio, as the ratio of width to height, of individual cells. Values of aspect ratio start at 1.0, which indicates a circle, while ascending values indicate enhanced cell ramification and elongation.

## 2.9 Determination of nucleic acids of *Naegleria fowleri* in EVs and PCR

In order to evaluate the presence of nucleic acids of *N. fowleri* in the EV fractions, samples of conditioned media (supernatants collected after the 5-h incubation period of trophozoites of the amoeba in 2% casein hydrolysate), and from the pellets obtained after the 16,000 × g (larger vesicles) and the 120,000 × g centrifugations (EV fraction, enriched in exosomes) from the EV isolation protocol were submitted to DNA extractions using phenol:chloroform:isoamyl alcohol (25:24:1) (Sigma Aldrich, Missouri, United States), following the manufacturer's instructions. For these experiments, 50 mL of conditioned media collected for EV isolation (from approximately  $7.9 \times 10^7$  trophozoites) were employed and DNA samples were finally suspended in 40 µL nuclease-free water. DNA concentration was determined using a NanoDrop 2000 spectrophotometer (Thermo Fisher Scientific, Waltham, Massachusetts, United States).

After nucleic acid quantification of the samples, amplification of the ITS region of Vahlkampfiids was performed by PCR, using the pair of primers Vahl-F and Vahl-R, as previously described. Besides, *N. fowleri* species-specific conventional and quantitative PCR (qPCR) using primers NfITS-F and NfITS-R were also performed, according to the protocols described by [Retana Moreira et al. \(2020b\)](#) and including at least 12 DNA dilutions. Negative controls (template DNA replaced with distilled water) and positive controls (DNA extracted from trophozoites of *Naegleria fowleri*) were also included.

Amplification reactions of conventional PCRs were run in a Biometra TOne thermal cycler (Labgene Scientific, Châtel-Saint-Denis, Switzerland) and visualization of PCR products was performed using 1% agarose gels with SYBR safe DNA gel stain (Invitrogen, Waltham, Massachusetts, United States). For qPCR, the StepOne Real Time PCR System (Thermo Fisher Scientific, Waltham, Massachusetts, United States) was employed.

## 3 Results

### 3.1 Characterization of extracellular vesicles secreted by two clinic isolates of *Naegleria fowleri*

#### 3.1.1 Transmission electron microscopy, scanning electron microscopy and nanoparticle tracking analyses

The production of extracellular vesicles secreted by trophozoites of two clinic isolates of *Naegleria fowleri* was confirmed by TEM and

NTA, after applying the isolation protocol described. Under our incubation conditions, amoebae produced approximately  $0.94\text{ }\mu\text{g}/\mu\text{L}$  (*N. fowleri* Guanacaste) and  $1.02\text{ }\mu\text{g}/\mu\text{L}$  (*N. fowleri* Limón) protein in extracellular vesicles and, after the 5h incubation, viability of trophozoites was not affected.

Figure 1 shows representative transmission electron microscopy images and nanoparticle tracking analysis of extracellular vesicles secreted by both isolates, after applying the isolation procedure. NTA revealed a mean hydrodynamic size of extracellular vesicles of  $216\text{ nm} \pm 83\text{ nm}$  and a mode of  $206\text{ nm}$  for *N. fowleri*, as previously described (Retana Moreira et al., 2022), while the mean size of EVs secreted by *N. fowleri* Limón was  $268 \pm 139\text{ nm}$ , with a mode of  $234\text{ nm}$ . Using the same methodology, it was also possible to determine that  $5 \times 10^7$  trophozoites of *N. fowleri* Guanacaste secreted  $4.96 \times 10^8$  particles/mL, while trophozoites of *N. fowleri* Limón secreted  $3.2 \times 10^8$  particles/mL.

Scanning electron microscopy also confirmed the secretion of extracellular vesicles by both clinic isolates of *Naegleria fowleri*, as shown in Figure 2. In these images, it is possible to observe individual vesicles and clusters of different sizes surrounding the trophozoites. Vesicles of variable sizes being released from

different regions of the plasma membrane are also observed (Figure 2).

### 3.2 Protein pattern and recognition of extracellular vesicles by polyclonal anti-*Naegleria fowleri* antibodies

The protein profile of extracellular vesicles secreted by trophozoites of both isolates of *Naegleria fowleri* after silver staining is shown in Figure 3 and Supplementary Figure S1, in which protein bands ranging from approximately  $>15\text{ kDa}$  to  $260\text{ kDa}$  were identified. In this Figure, high molecular weight bands seem to be more predominant in EVs from both isolates.

Western blot analysis using polyclonal anti-*Naegleria fowleri* antibodies confirmed the recognition of proteins of *N. fowleri* in lysates of trophozoites employed to produce the antibodies (Supplementary Figure S2), as well as the recognition of *N. fowleri* proteins in extracellular vesicles secreted by both isolates. In this sense, recognition of EV bands was observed from over  $10\text{ kDa}$  to  $175\text{ kDa}$ , as previously reported.

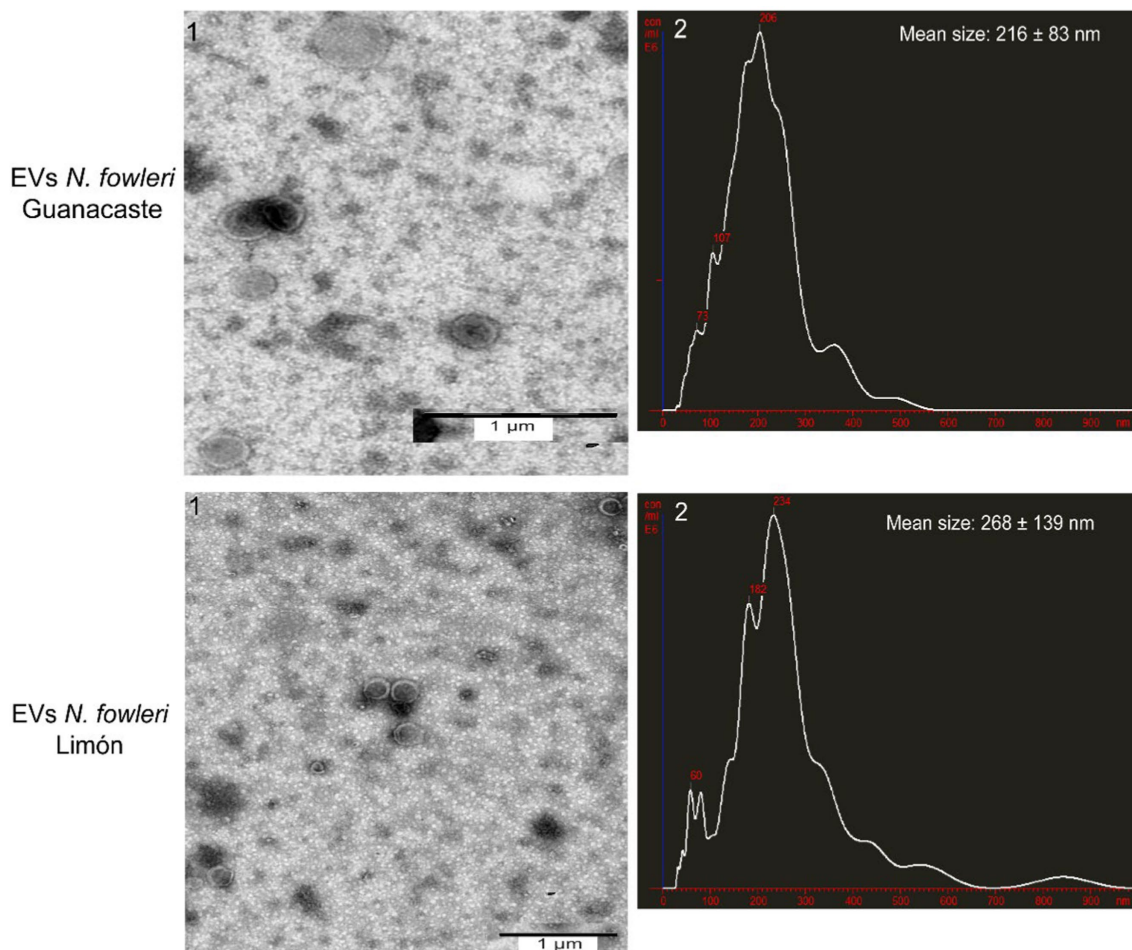


FIGURE 1

Transmission electron microscopy images and nanoparticle tracking analysis graphs of extracellular vesicles secreted by trophozoites of two clinic isolates of *Naegleria fowleri*. Typical cup shaped EVs of different diameters are produced by both isolates; hydrodynamic mean sizes of EVs obtained were  $216 \pm 83\text{ nm}$  in *N. fowleri* Guanacaste and  $268 \pm 139\text{ nm}$  in *N. fowleri* Limón.



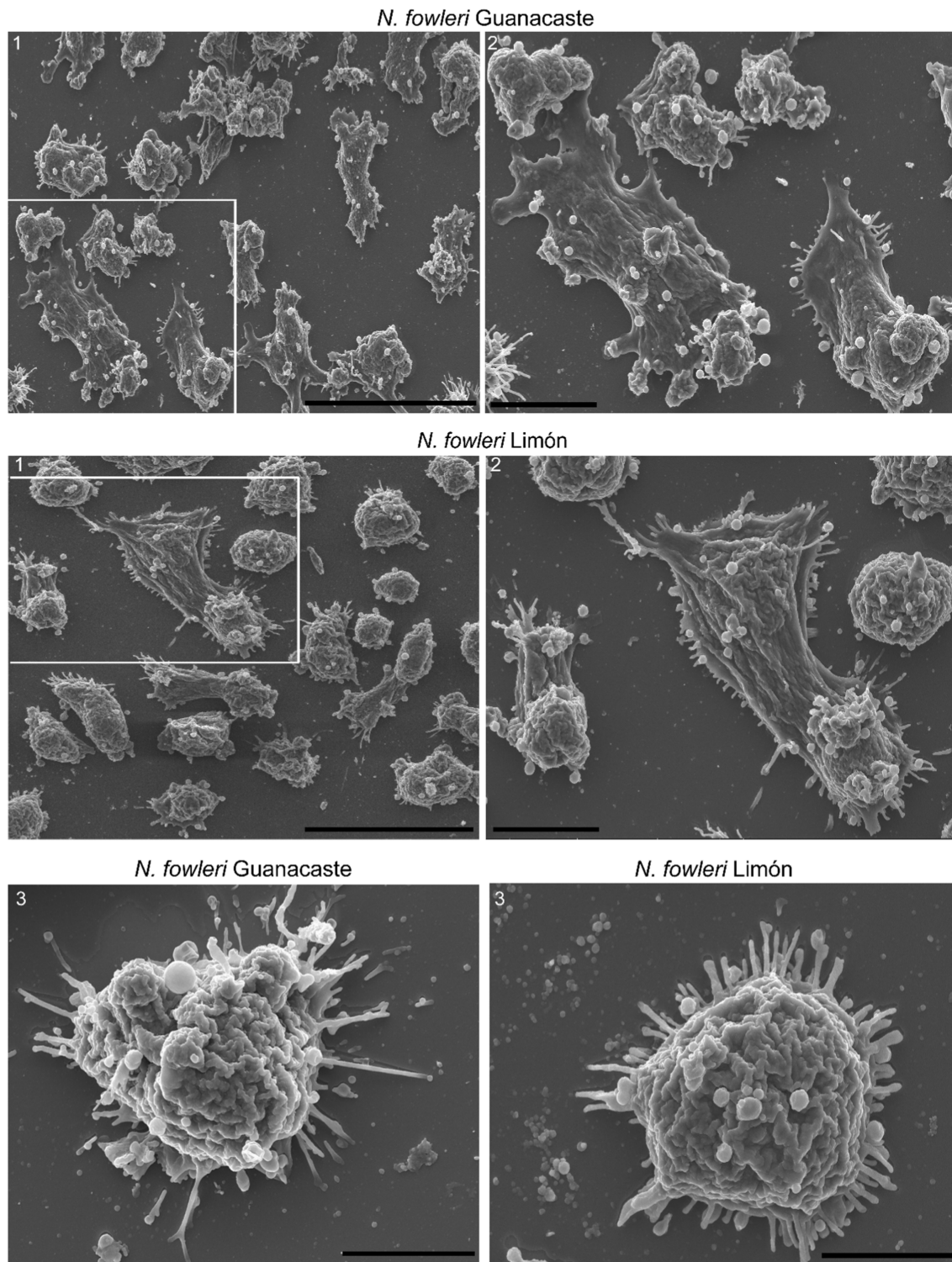


FIGURE 2

Scanning electron microscopy of trophozoites of *Naegleria fowleri* Guanacaste and *N. fowleri* Limón that confirms the secretion of extracellular vesicles. In these images, individual and grouped EVs of different sizes can be observed surrounding the trophozoites, as well as vesicles of variable sizes being released from different regions of the plasma membrane. In these Figure correspond to magnifications of 1. Scale bars: 40μm (1), 10μm (2), and 5μm (3).

### 3.3 Cytokine expression analyses

NOS and cytokine expression analyses performed after the incubation of primary cultures of mouse brain microglia with EVs of

each isolate of *N. fowleri* for 48 h are shown in [Figure 4](#). In this Figure, an upregulation of NOS and proinflammatory cytokines *IL-6*, *IL-23*, and *TNF-α* was observed, as well as the increased expression of *IL-10*, the latter a regulatory cytokine. In all cases, transcription levels of

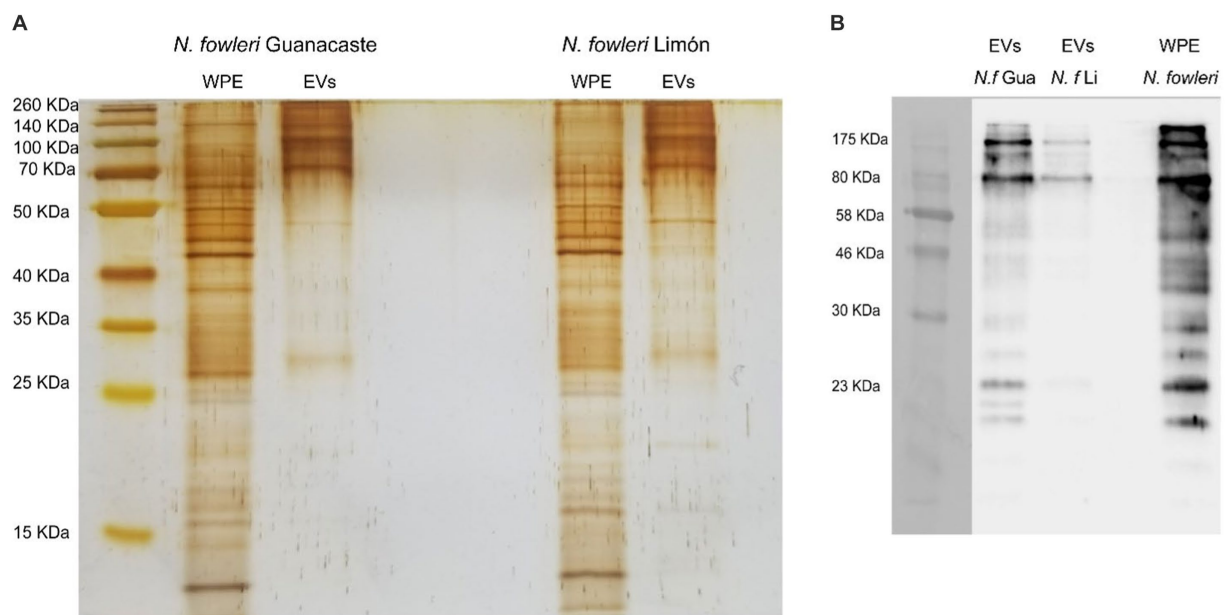


FIGURE 3

Protein profile of extracellular vesicles secreted by *Naegleria fowleri* and recognition by polyclonal anti-*Naegleria fowleri* antibodies: (A) Silver staining apparently showing similar band patterns in extracellular vesicles from isolates Guanacaste and Limón, which range from >15 kDa to 260 kDa. (B) Western blot that shows the recognition of different bands in EVs of each isolate. In this sense, bands over 70–80 kDa were highly recognized in EVs of both isolates by the polyclonal antibodies; however, recognition of more protein bands was observed in EVs secreted *N. fowleri* Guanacaste (Retana Moreira et al., 2022). For silver staining, approximately 9 µg of protein/EV sample were loaded onto the gel; for Western blot, approximately 6 µg of protein/EV sample were loaded onto the gel. WPE, whole protein extracts of trophozoites of *N. fowleri*; EVs, extracellular vesicles.

genes were significantly higher than the expression levels found in control cells, especially when the isolate *N. fowleri* Guanacaste was employed. LPS activation of cells and its cytokine expression analysis is shown in [Supplementary Figure S3](#).

For BV-2 cells, results of interleukin expression after the incubation with EVs of the two isolates of *N. fowleri* revealed a downregulation in the expression of *IL-18* and an upregulation for *IL-13* 48h after the stimuli ([Figure 5](#)). However, non-statistically significant differences were found in the expression levels of the rest of cytokines assayed with respect to control cells ([Supplementary Figure S4](#)). For NOS, transcription levels were significantly higher after 4h of incubation of cells with the EVs; moreover, these differences were not found after 24 and 48h of incubation.

### 3.4 Microglial cell morphology analysis using fluorescence microscopy

In order to perform an analysis of inflammatory phenotype of microglia, primary microglia from newborn mouse brains were incubated with EVs of the two isolates of *N. fowleri*; the bacterial endotoxin LPS-induction in primary microglia was also included ([Figure 6](#)). GS-IB4 staining showed the characteristic change in morphology from homeostatic microglia, with small cellular body and long processes in control cultures, to LPS-stimulated microglia with a more amoeboid morphology ([Figure 6A](#)), as it was determined in terms of the aspect ratio parameter ([Figure 6B](#)). However, evident changes in the morphology of cells were observed after the incubation

with EVs of each isolate of *N. fowleri*. In this sense, cells incubated with EVs from *N. fowleri* Limón exhibited a clear morphological change to a more rounded shape, more similar to that found under LPS conditions. However, the incubation with EVs isolated from *N. fowleri* Guanacaste induced changes in morphology to a lesser extent, since cells still showed long processes, but with larger lamellipodia than controls. Similar results were found between 24 and 48h of cell incubation with the stimuli.

### 3.5 Detection of DNA of *Naegleria fowleri* in EV fractions

[Figure 7](#) reveals conventional PCR results in which DNA from the EV fractions were employed. In this sense, conditioned media and samples of pellets obtained after the 16,000×g and 120,000×g centrifugation steps for EV isolation were submitted to phenol:chloroform:isoamyl alcohol DNA extractions, for further analyses of *N. fowleri* specific DNA amplification using family (Vahlkampfiid) and *N. fowleri* species-specific primers. In [Figures 7A,B](#), conditioned media (lane 1) and the pellets obtained after the 16,000×g centrifugation (lane 2) resulted negative for Vahlkampfiids and *N. fowleri* at the DNA amounts employed (700 ng) while the pellets corresponding to DNA obtained from the EV fraction resulted positive, demonstrating the presence of bioactive *N. fowleri*-specific DNA in these fractions.

To confirm this result, another species-specific PCR using primers NfITS and applying serial dilutions to the DNA extracted from the EV fraction was performed, resulting in amplification until employing a



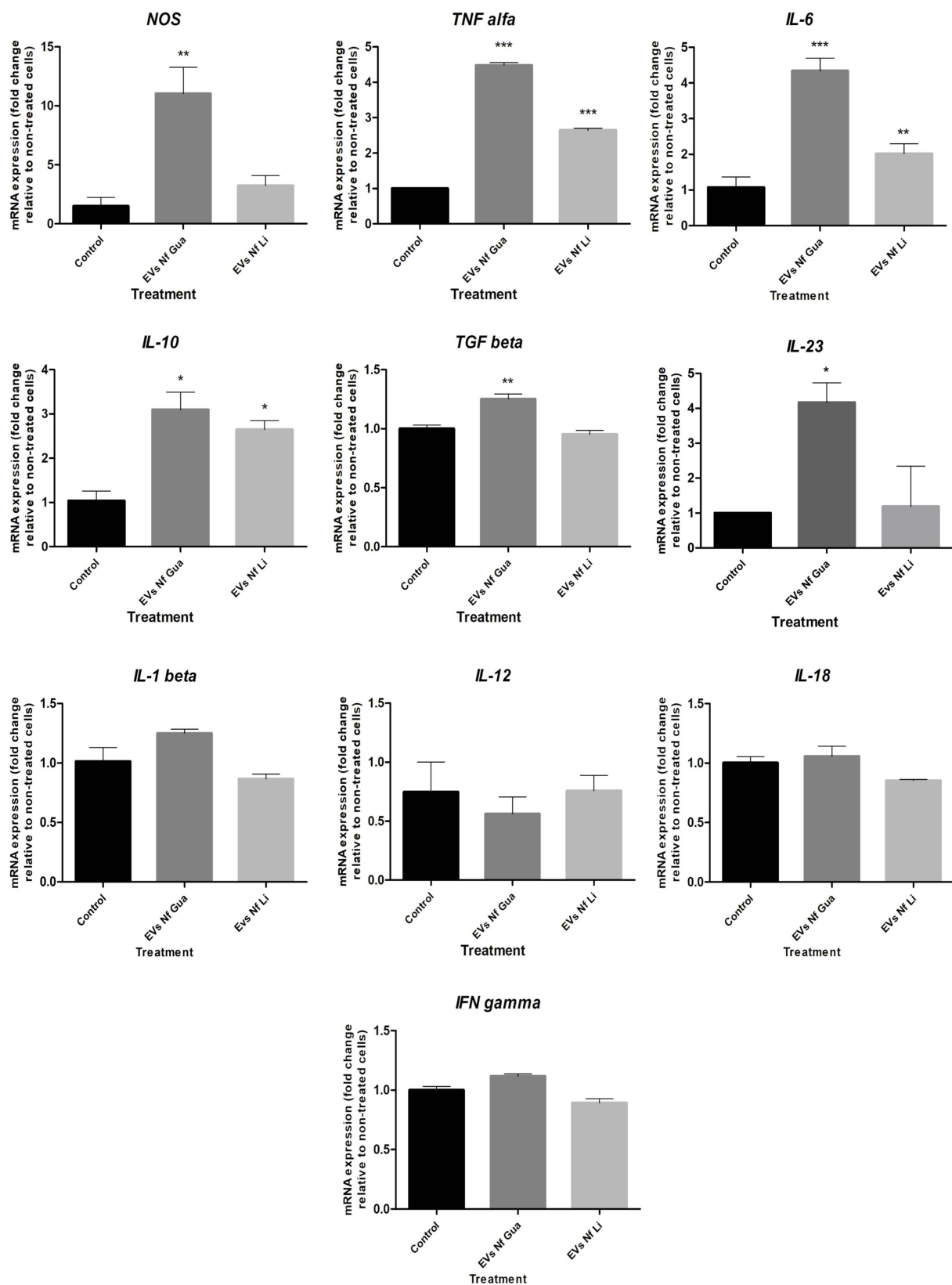


FIGURE 4  
Differential mRNA expression analyses of *NOS* and cytokines after the incubation of primary culture of mouse brain microglia with extracellular vesicles secreted by *Naegleria fowleri* Guanacaste and *N. fowleri* Limón. Primary cultures of mouse brain microglia were stimulated with extracellular vesicles (25 µg) of two clinic isolates of *N. fowleri* for 48 h and qRT-PCRs were performed to analyze the expression pattern of *NOS* and cytokines. Values are presented as the mean ± SD and one-way ANOVA with Tukey *post hoc* test was performed for multiple comparisons to the negative control without treatment. \*\*\**p* < 0.0005, \*\**p* < 0.005, \**p* < 0.05.

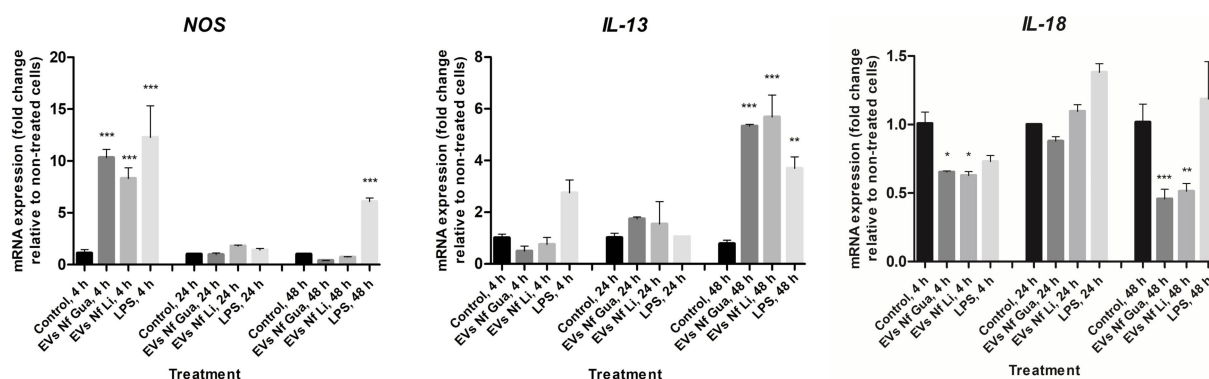


FIGURE 5

Differential mRNA expression analyses of *NOS*, *IL-13*, and *IL-18* after the incubation of BV-2 cells with extracellular vesicles secreted by *Naegleria fowleri* Guanacaste and *N. fowleri* Limón. BV-2 microglial cells were stimulated with extracellular vesicles (25 µg) of two clinic isolates of *N. fowleri* for 4, 24, and 48 h and qRT-PCRs were performed to analyze the expression pattern of *NOS* and cytokines. Values are presented as the mean ± SD and one-way ANOVA with Tukey *post hoc* test was performed for multiple comparisons to the negative control without treatment. \*\*\* $p < 0.0005$ , \*\* $p < 0.005$ , \* $p < 0.05$ .

DNA concentration of 3.125 ng, the last dilution in which the specific conventional PCR for *N. fowleri* resulted positive (Figures 7C,D). These results were confirmed with a *N. fowleri* species-specific qPCR (Retana Moreira et al., 2020a,b), in which mean CT = 30 for the dilution that contained 0.4 ng of DNA, mean CT = 31.5 for the dilution that contained 0.2 ng of DNA and mean CT = 32 for the dilution that contained 0.1 ng DNA.

## 4 Discussion

Extracellular vesicles are a heterogeneous group of vesicles delimited by a lipid bilayer and are considered part of the excretion/secretion products. These vesicles are released by almost all cell types and have a pivotal role in intercellular communication, as they have been considered “delivery trucks” that transport diverse molecules from one cell to another, inducing changes at different levels in the recipient cell (Dong et al., 2021). A role of EVs in the pathogenesis of several diseases has also been proposed by different authors, which supports their study and evaluation as potential biomarkers. In this sense, it has been demonstrated the presence of virulence factors as part of the cargo of the vesicles, related to adhesion, invasion and survival processes, as well as the modulation of the immune response they could exert (Nievas et al., 2020).

Isolated from most organisms, the study and characterization of EVs in protozoan parasites has gained considerable interest, mostly in the case of infections that lack efficient diagnostic tools and effective treatments (Dong et al., 2021; Cruz Camacho et al., 2023); primary amoebic meningoencephalitis, caused by the free-living amoeba *Naegleria fowleri*, is one of this type of infections. Primary acute meningoencephalitis is a necrotizing haemorrhagic meningoencephalitis of acute and fulminant course, with a lethality rate of 97–98% (Siddiqui et al., 2016). In this infection, the trophozoite stage of the amoeba enters the host through the nasal passage and reaches brain tissue throughout the olfactory bulb as early as 24 h post inoculation (Jarolim et al., 2000). The establishment of the amoeba in the brain induces an

intense inflammatory response that, along with the mechanic damage directly provoked by the microorganism (Cervantes-Sandoval et al., 2008; Lertjuthaporn et al., 2022), are responsible of the extensive lesions observed. Previous studies have demonstrated that excretion/secretion products, including EVs, are involved in the pathogenic processes of infections, mainly by the stimulation and modulation these products could exert over the immune response of the host (Kim et al., 2009). In this work, a characterization of the extracellular vesicles secreted by two clinic isolates of *N. fowleri* was performed, and the effect these vesicles exert over microglial cells was analyzed.

For the purpose of our analyses, EVs from trophozoites of two clinic isolates of *N. fowleri* were obtained after applying differential centrifugation, filtration and ultracentrifugation of conditioned media obtained after 5 h of incubation. Size ranges of the vesicles obtained, analyzed by NTA, revealed particles of  $216 \pm 83$  nm (EVs of *N. fowleri* Guanacaste) and  $268 \pm 139$  nm (EVs of *N. fowleri* Limón). These sizes coincide with previous studies performed by our research group (Retana Moreira et al., 2022), but result slightly higher to the sizes reported by Lertjuthaporn et al. (2022). Moreover, scanning electron microscopy images show the secretion of individual EVs, as well as EVs forming small clusters, that appear to be released through the plasma membrane of trophozoites of amoebae. With the methodologies employed for characterization of EVs in this study, it was not possible to observe statistically significant differences between the vesicles secreted by both clinical isolates.

To evaluate the presence of proteins in EVs that could be recognized by the antibodies obtained after the immunization, SDS-PAGE electrophoresis and Western blot were employed, the latter using polyclonal anti-*N. fowleri* antibodies produced in rats against a complete extract of trophozoites of *N. fowleri* (ATCC *N. fowleri* Carter 30808). Results obtained after these analyses also revealed similarities in both isolates (Figure 3), in which antibody recognition was confirmed. In these experiments, a lysate of trophozoites of *N. fowleri* was also included and the recognition of bands by the antibodies was also observed, a result that evidences that EVs of both isolates of *N. fowleri* include cytosolic and plasma membrane components of the

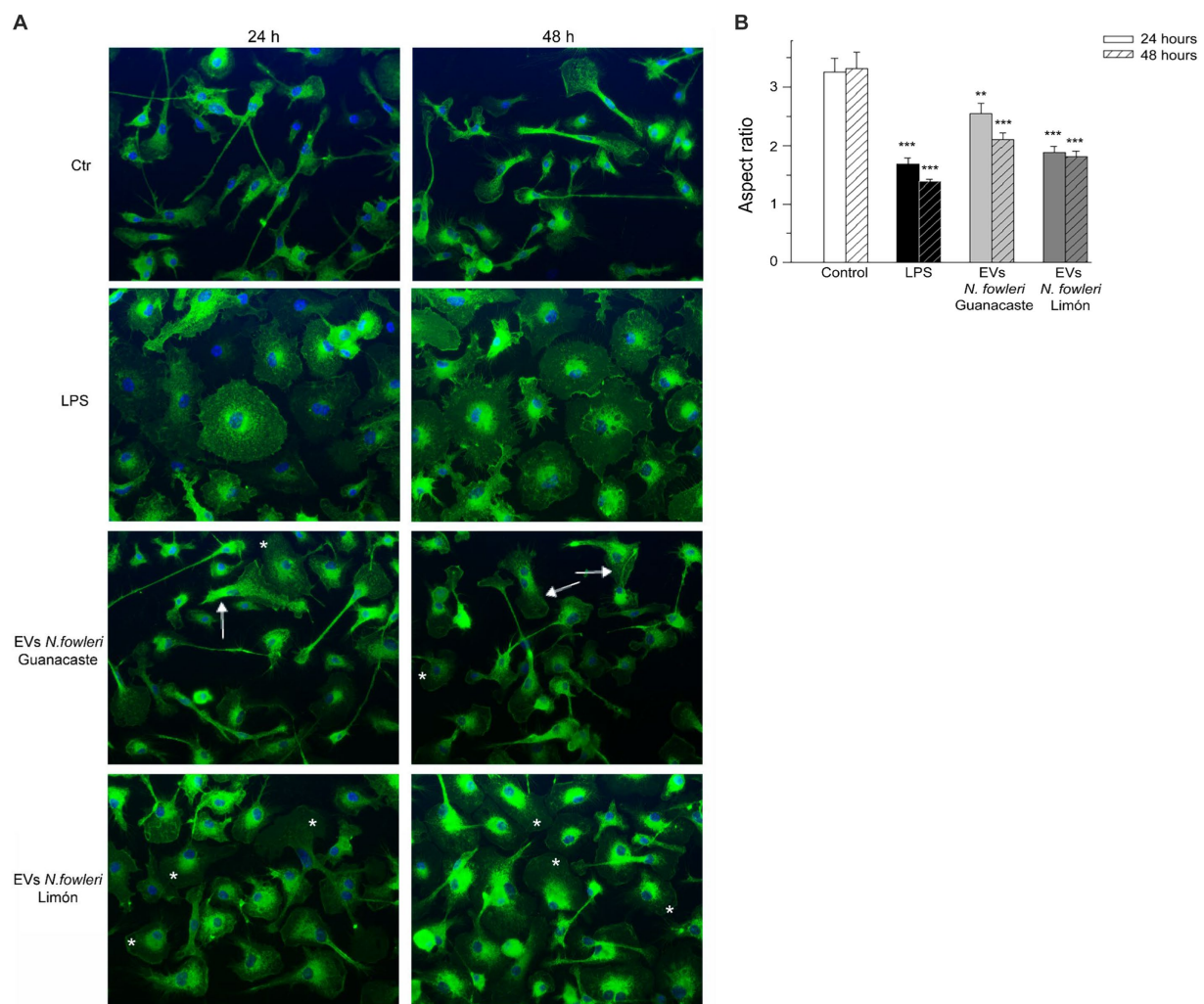


**FIGURE 6**  
Morphological changes of primary microglia from mouse brain stimulated with LPS or with extracellular vesicles secreted by two isolates of *Naegleria fowleri*. **(A)** GS-IB<sub>4</sub> Alexa Fluor 488 conjugate (green) was used to visualize microglial cell morphology and DAPI staining (blue) to visualize nuclei. Cells showed the expected change in morphology from control microglia in culture with small cellular bodies and long processes (Ctr) to LPS-stimulated microglia with amoeboid morphology (LPS). While cells incubated with EVs isolated from *N. fowleri* Guanacaste barely showed a morphological change except for lamellipodia expansion (arrows), cells incubated with EVs from *N. fowleri* Limón strongly reacted and showed processes retraction and a more amoeboid morphology (\*). Moreover, similar results were found after 24 and 48 h of incubation. Scale bar: 30  $\mu$ m. **(B)** Determination of the aspect ratio parameter in control cells, LPS-activated microglia, and cells stimulated with EVs from the two *N. fowleri* isolates. Values of aspect ratio start at 1.0, which indicates a circle, while ascending values indicate enhanced cell ramification and elongation. Data are presented as the mean  $\pm$  SEM and one-way ANOVA with Tukey *post hoc* test was performed for multiple comparisons to the negative control for each time point. \*\*\* $p < 0.0005$ , \*\* $p < 0.005$ .

trophozoites that are recognized by the antibodies obtained. More studies are necessary to identify potential significant differences between the cargo of EVs secreted by both isolates.

Regarding band components above 80 kDa, the recognition of 3 bands was clearly observed. Previous proteomic analyses performed by our research group (Retana Moreira et al., 2022) demonstrated the presence of components of the plasma membrane and cytoskeleton in these bands, as well as some virulence factors reported in infections with this and other species of parasites, that can eventually activate or modulate the immune response, such as leucine aminopeptidase and elongation factor 1- $\alpha$  (eEF1- $\alpha$ ), the latter an important factor for immunosuppression and priming of host cells for *Leishmania* invasion (Silverman and Reiner, 2011; Vyas et al., 2014; Timm et al., 2017).

Since brain tissue is the target during a *N. fowleri* infection, we decided to evaluate the possible role of EVs of *N. fowleri* in the immune modulation of microglial cells. These are highly specialized resident cells responsible of monitoring brain microenvironment, detecting and responding to any type of tissue damage, infections, or homeostatic disturbance (Nimmerjahn et al., 2005). Microglia stimulation may induce a drastic change in cellular morphology and, to evidence possible cell responses after the stimulus with EVs *N. fowleri*, we employed isolectin-B4 fluorescence staining for the observation of morphological changes in microglia. In this sense, we employed primary microglia obtained from newborn mice brain in order to have a more physiological approach compared to transformed cell lines. Results revealed a change from a ramified cell with small cellular bodies and long processes (related

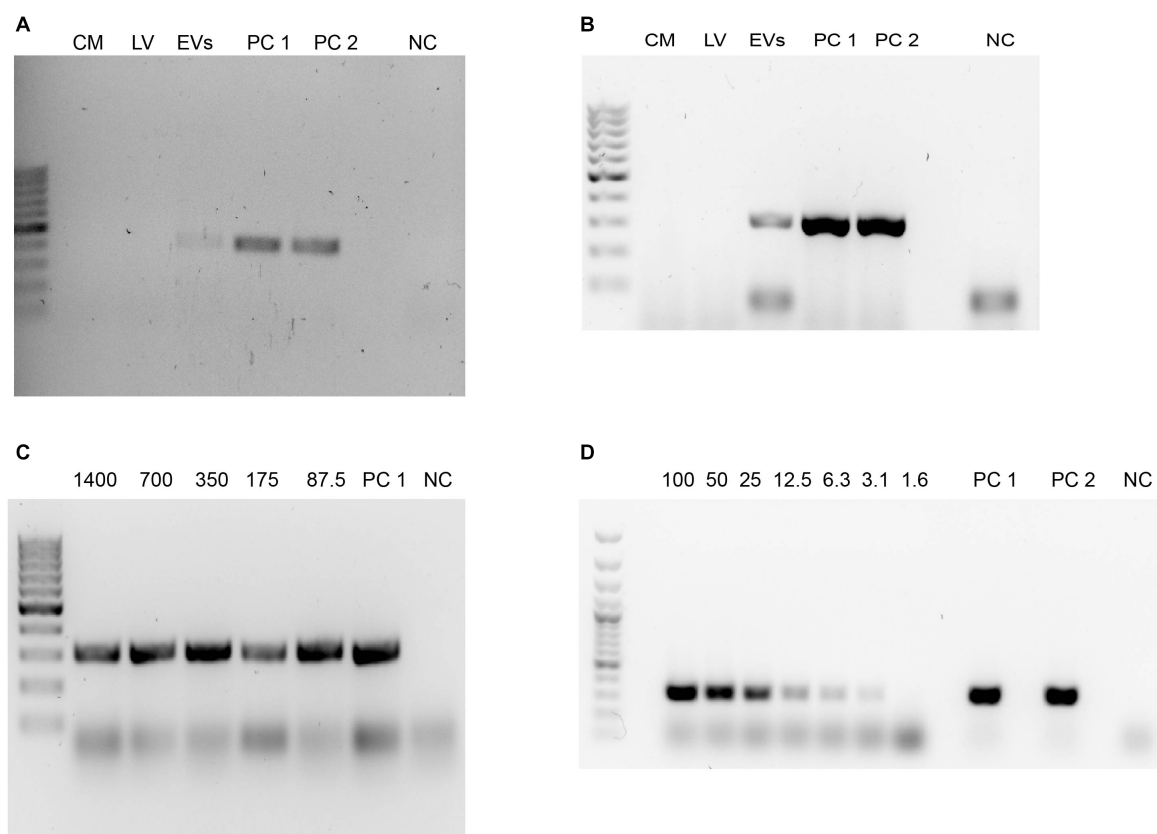


FIGURE 7

Detection of DNA from *Naegleria fowleri* in the EV fractions using phenol:chloroform:isoamyl alcohol extractions and conventional PCR. (A) Agarose gel electrophoresis after the amplification of the ITS region of *Vahlkampfiids* using Vahl-F and Vahl-R primers. (B) Agarose gel electrophoresis after the amplification of the ITS region of *N. fowleri* using NfITS-F and NfITS-R primers. For these PCRs, the same amount of DNA (700 ng) was employed in each sample. (C,D) Agarose gel electrophoresis after the amplification of the ITS region of *N. fowleri* using NfITS-F and NfITS-R primers, in which serial dilutions of the DNA obtained from the EV fraction were employed (expressed in ng). CM, conditioned media; LV, 16,000 x g pellet sample that contains larger vesicles; EVs: pellet of extracellular vesicles obtained after the 120,000 x g ultracentrifugation; PC 1: DNA from trophozoites of *N. fowleri* Guanacaste (positive control); PC 2: DNA from trophozoites of *N. fowleri* Limón (positive control); NC: negative control. GeneRuler 100 bp Plus DNA ladder (Thermo Fischer Scientific, Waltham, Massachusetts, United States) was employed as the DNA ladder.

to a homeostatic microglial state), to an amoeboid morphology more characteristic of a pro-inflammatory phenotype, including transient states that reflect functional events related to the disturbing fact (Colonna and Butovsky, 2017). In this study, when primary microglia was challenged with EVs secreted by *N. fowleri*, evident morphological changes were observed when compared to control cells, especially when EVs from *N. fowleri* Limón were employed, which confirmed the proinflammatory microglial response induced by EVs produced by amoebae.

Cell responses to EVs secreted by *N. fowleri* were also quantitatively assayed, determining changes in the expression levels of cytokines and NOS using qRT-PCR, which revealed increased levels of NOS and proinflammatory cytokines *IL-6*, *IL-23*, and *TNF- $\alpha$* , as well as increased levels of the regulatory cytokine *IL-10*. In all cases, statistically significant differences were observed when compared to control unstimulated cells, especially when EVs of the isolate Guanacaste were employed. Similar results -but registered during the first 12 h after the stimulus- were reported by other authors when rat primary microglia cells were co-cultured with trophozoites of the amoeba (Oh et al., 2005), or when excretory/secretory products were employed (Lee et al., 2011), reinforcing the idea that these cells (and the cytokines they produce after the

contact with trophozoites of *N. fowleri* or its excretory/secretory products) have a crucial role in the exacerbated inflammatory response observed during PAM. Moreover, the concomitant and very marked increase in the expression of *TNF- $\alpha$* , NOS, and *IL-6* in the primary microglial culture suggests a *N. fowleri* EV-induced polarization of the cells to a proinflammatory profile, capable of secreting destructive factors that contribute to neuronal damage. A more discrete augmentation in the regulatory cytokines *IL-10* and *TGF- $\beta$*  was also observed, and these are markers of more anti-inflammatory phenotype, the other side of the spectrum. Although it may appear as a contradiction, the plasticity of the functional polarization in microglial cells could provide some clarity. In contrast to the behavior in non-CNS sites, where macrophages tend to first acquire proinflammatory characteristics upon the harmful stimulus and then, the response evolves toward a regulatory profile, in the CNS this process is inverted (Hu et al., 2015). Moreover, and according to Saraiva and O'Garra (2010), *IL-10* could be induced in many situations in which proinflammatory cytokines are also induced, despite the pathways that induce its expression can regulate the expression of those cytokines in time. Park et al. (2007) demonstrated the endogenous production of *IL-10* by rat microglial



cells after the stimulation with LPS; interestingly, IL-10 was simultaneously produced with proinflammatory cytokines like IL-1 $\beta$ , TNF- $\alpha$  and iNOS. The authors propose that this endogenous production of IL-10 could help to control the production of inflammatory mediators in microglia in an autocrine way, resulting in neuroprotection even in the early stage of an acute inflammation of the brain. Due to the technical challenges of primary microglial culture and to minimize the number of animals used in the experiments, a kinetic evaluation of the markers' expression was not performed, nor the use of different doses of EVs was included in this study, but it would be suggested to evaluate this aspect. A further consequence of this expression profile could be the priming of CD4+ T lymphocytes for a Th17 adaptive response, a response that has not been studied during a *N. fowleri* infection, but it has been shown to amplify the inflammatory response in murine models of CNS inflammation (Rostami and Ciric, 2013). As stated by Moseman (2020), there are many open questions surrounding fundamental immunological processes during a *N. fowleri* infection, so that more studies should be carried out to clarify the contribution of the early proinflammatory response by microglial cells to the immune-mediated pathological mechanisms of PAM.

Antiparasitic effects of nitric oxide in infections caused by helminths and protozoan parasites are widely known and described; however, it has also been postulated its role in producing damage during this type of infections (Brunet, 2001; Omar and Abdelal, 2022). Regarding *N. fowleri*, the first published results related to this topic revealed that activated macrophages could destroy the amoebae by an arginase-dependent cytolytic mechanism that results in NO production (Fischer-Stenger and Marclano-Cabral, 1992). However, using an *in vitro* model, Rojas-Hernández et al. (2007) demonstrated that this amoeba was highly resistant to NO-destruction, suggesting that its production during PAM could contribute to tissue damage instead of amoeba destruction. Regarding TNF- $\alpha$ , its transcendental role in increasing the oxidative burst in neutrophils, as well as the release of lysosomal enzymes in response to the amoeba has also been reported (Ferrante et al., 1988; Michelson et al., 1990). Moreover, tentative anti-amoebic roles of IL-6 are still unclear, even suggesting that its upregulation during the infection could contribute, as a secondary effect, to the tissue damage observed in the brain during PAM (Chen and Moseman, 2023).

In this work, if we try to compare transcription levels of mRNA of cytokines evaluated after the incubation of primary cultures from mouse cell microglia and BV-2 cells with EVs of *N. fowleri* for 48 h, both similarities and differences could be found. For example, while expression levels of IL-12 and IFN- $\gamma$  were not statistically different when compared to the controls for both cell types, an upregulation of NOS, IL-6, and IL-10 was found only in primary cultures of microglia; additionally, a downregulation of IL-18 was observed only in BV-2 cells. These results, especially the differences observed, are expected when different cell types are employed, particularly if responses of primary cells are compared to responses of immortalized cell lines. While the use of a primary cell model could more accurately reflect what occurs in an infection *in vivo* with this amoeba, it is clear that the use of cell lines such as BV-2 is advantageous for the experimental work at a laboratory level, since its "immortality" allows its indefinite cultivation, facilitating the analysis and characterization of biological processes. In a recent publication, Lê et al. (2023) analyzed the immune response in BV-2

microglial cells upon incubation with EVs of *N. fowleri* (Carter NF69 strain, ATCC 30215) for 3, 6, and 9 h. In this work, besides IL-6 and TNF- $\alpha$ , increased expression levels of IL-1 $\alpha$ , IL-1 $\beta$ , IFN- $\gamma$ , MIP-1, and MIP-2 (but not IL-10) was also reported. The authors suggested that EVs of *N. fowleri* are pathogenic factors involved in contact independent pathogenic mechanisms of *N. fowleri* by inducing proinflammatory immune responses. In our study, and using the same cell line, increased expression levels of NOS (after 4 h of incubation with EVs of *N. fowleri*) and IL-13 (after 48 h of incubation with EVs of *N. fowleri*) were observed, but not increased expression of IL-1 $\beta$  or IFN- $\gamma$ , differences that could be explained due to differences in the incubation times employed and the individual characteristics of the *N. fowleri* clinical wild isolates in comparison to a reference strain.

It is also interesting to highlight the upregulation of IL-13 and the simultaneous downregulation of IL-18 expression found in our study using the BV-2 cell line. In a murine model of infection with the nematode *Nippostrongylus brasiliensis*, IL-13 was shown to inhibit the expression of IL-18, an inflammasome-activated cytokine that contributes to inflammation a cell death via pyroptosis (Chenery et al., 2021). Furthermore, IL-13 has been described as a key modulator of brain inflammation as it has been shown to induce microglial cell death to downregulate the inflammatory process and hinder neuronal damage and its blockade can increase the expression of TNF- $\alpha$  and iNOS (Shin et al., 2004), which is consistent with our findings on the kinetics of NOS and IL-13 expression. This study suggests that IL-13 expression may act as a mechanism for neuronal survival; however, in the case of *N. fowleri*, it may be insufficient to compensate for the damage induced by the initial proinflammatory response. The authors also described regulation of IL-13 secretion by other cells present in the brain's microenvironment, such as neurons, so a next step in the study of the IL-13/iNOS and IL-13/IL-18 regulation should be the study in co-culture or animal models. Altogether, the results derived from our work confirm the immunostimulatory role of EVs secreted by *N. fowleri* over microglial cells, suggesting that the strong proinflammatory response observed during primary acute meningoencephalitis could have a fundamental role in the tissue damage observed in *in vivo* infections in less than 96 h after the infection with the amoeba (Rojas-Hernández et al., 2004).

Finally, the existence of DNA in EVs is now considered a consensus in the field of EVs (Ghanam et al., 2022). In all previous works regarding the characterization of EVs secreted by *N. fowleri* (Lertjuthaporn et al., 2022; Retana Moreira et al., 2022; Lê et al., 2023; Russell et al., 2023), the presence of bioactive nucleic acids as part of the EV cargo or in the EV fractions has not been analyzed. However, in this work, we report the preliminary finding of DNA in the EV fraction that corresponds to small EVs, detectable using a phenol:chloroform extraction and *N. fowleri* species-specific PCR protocols even in a concentration of 3.125 ng for conventional PCR. DNA-containing EVs from human cells have been well studied in terms of DNA loading in vesicles and their role in homeostasis, immunomodulation and gene transference (Chang et al., 2020; Malkin and Bratman, 2020; Elzanowska et al., 2021). Moreover, the presence of DNA in EVs has also been described in EVs secreted by other protozoan organisms (Tatischeff et al., 1998; Douanne et al., 2022). In this sense, and as this is a preliminary report, there are pending assays to ascertain the location of this DNA in the vesicles, the profile of the

DNA content and its implication in host immune response and messaging with host-cells and other amoebae. Moreover, our group is currently working in applying different enzymatic treatments to the EV fractions to confirm that bioactive DNA is included within the smaller EVs, especially if it is taken into account that, at least in these preliminary experiments, bioactive *N. fowleri* DNA was not found in the larger vesicle fractions that are supposed to contain ectosomes, a type of EVs with a different cargo and formed through outward budding of the plasma membrane.

Regarding the DNA cargo in EVs secreted by trophozoites of *N. fowleri*, we suggest two prospective research opportunities: the DNA interaction with host cell machinery and its potential use as a biomarker in a clinical context. As described elsewhere, it has been shown that DNA-harboring EVs from malaria parasites could stimulate cytosolic pathogen DNA sensors in host monocytes to elicit a cytokine response (Sisquella et al., 2017). On the other hand, cancer related studies of EV-DNA in plasma and other body fluids for new liquid biopsy applications are a reality (Malkin and Bratman, 2020), and this sets a base for understanding and proposing that DNA from pathogens, included in EV fractions, could also be considered a molecular biomarker as it has been proposed in a study with chronic Chagas disease patients, in which the detection of *Trypanosoma cruzi* nuclear and kinetoplast DNA was performed in serum circulating EVs (Lozano et al., 2023). For the specific case of primary acute meningoencephalitis, a biomarker present in blood instead of cerebrospinal fluid could make the difference in timely and non-invasive diagnosis, and we suggest this could be studied as it has been found that DNA-carrying EVs could cross the intact blood–brain-barrier, being detectable in peripheral blood (García-Romero et al., 2017). Small RNAs have also been found in protozoan derived EVs (Sabatke et al., 2021), which also suggests that EV nucleic acids represent open novel approaches for parasitic diseases research.

## Data availability statement

The raw data supporting the conclusions of this article will be made available by the authors, without undue reservation.

## Ethics statement

The animal study was approved by the Ethics Committee of the University of Granada (Ethics Committee, 235- CEEA-OH-2018), as well as by the authorities of the Regional Government of the Junta de Andalucía with number 12/11/2017/162. The study was conducted in accordance with the local legislation and institutional requirements.

## Author contributions

LR: Conceptualization, Formal analysis, Funding acquisition, Investigation, Methodology, Supervision, Visualization, Writing – original draft, Writing – review & editing. AC-G: Conceptualization, Investigation, Methodology, Visualization, Writing – original draft, Writing – review & editing. MS: Conceptualization, Formal analysis, Investigation,

Methodology, Writing – original draft, Writing – review & editing. SM-C: Formal analysis, Investigation, Visualization, Writing – original draft, Writing – review & editing. JA-O: Formal analysis, Investigation, Writing – original draft, Writing – review & editing. FC: Methodology, Writing – original draft. MJ: Methodology, Writing – original draft. AO: Conceptualization, Formal analysis, Funding acquisition, Investigation, Supervision, Writing – original draft, Writing – review & editing. EA: Conceptualization, Funding acquisition, Investigation, Methodology, Supervision, Visualization, Writing – original draft, Writing – review & editing.

## Funding

The author(s) declare financial support was received for the research, authorship, and/or publication of this article. This research was funded by projects C-2600: “Secreción de vesículas extracelulares por *Naegleria fowleri* y evaluación de su potencial rol inmunomodulador en un modelo *in vitro*” and C-1061: “Caracterización de antígenos de excreción/secreción y antígenos somáticos en amebas de vida libre mediante el empleo de anticuerpos policlonales producidos en roedores”, supported by Vicerrectoría de Investigación of the University of Costa Rica.

## Acknowledgments

LR was supported by the Oficina de Asuntos Internacionales y Cooperación Externa (OAICE) of Universidad de Costa Rica and Fundación Carolina (Spain). AC-G was supported by the “Contrato de Formación de Profesorado Universitario” of the Ministry of Science, Culture and Sports (Spain). Transmission and scanning electron microscopy were performed at the “Centro de Instrumentación Científica” of the University of Granada.

## Conflict of interest

The authors declare that the research was conducted in the absence of any commercial or financial relationships that could be construed as a potential conflict of interest.

## Publisher's note

All claims expressed in this article are solely those of the authors and do not necessarily represent those of their affiliated organizations, or those of the publisher, the editors and the reviewers. Any product that may be evaluated in this article, or claim that may be made by its manufacturer, is not guaranteed or endorsed by the publisher.

## Supplementary material

The Supplementary material for this article can be found online at: <https://www.frontiersin.org/articles/10.3389/fmicb.2024.1346021/full#supplementary-material>

## References

- Brunet, L. R. (2001). Nitric oxide in parasitic infections. *Int. Immunopharmacol.* 1, 1457–1467. doi: 10.1016/s1567-5769(01)00090-x
- CDC (2023). *Naegleria fowleri* — Primary amebic meningoencephalitis (PAM) — Amebic encephalitis. Available at: [www.cdc.gov/parasites/naegleria/general.html](http://www.cdc.gov/parasites/naegleria/general.html).
- Cervantes-Sandoval, I., Serrano-Luna, J. D. J., García-Latorre, E., Tsutsumi, V., and Shibayama, M. (2008). Characterization of brain inflammation during primary amebic meningoencephalitis. *Parasitol. Int.* 57, 307–313. doi: 10.1016/j.parint.2008.01.006
- Chang, X., Fang, L., Bai, J., and Wang, Z. (2020). Characteristics and changes of DNA in extracellular vesicles. *DNA Cell Biol.* 39, 1486–1493. doi: 10.1089/dna.2019.5005
- Chen, C., and Moseman, E. A. (2023). Pro-inflammatory cytokine responses to *Naegleria fowleri* infection. *Front. Trop. Dis.* 3:1082334. doi: 10.3389/ftd.2022.1082334
- Chenery, A. L., Rosini, S., Parkinson, J. E., Ajendra, J., Herrera, J. A., Lawless, C., et al. (2021). IL-13 deficiency exacerbates lung damage and impairs epithelial-derived type 2 molecules during nematode infection. *Life Sci. Alliance* 4:e202001000. doi: 10.26508/LSA.202001000
- Colonna, M., and Butovsky, O. (2017). Microglia function in the central nervous system during health and neurodegeneration. *Annu. Rev. Immunol.* 35, 441–468. doi: 10.1146/annurev-immunol
- Cornet-Gomez, A., Retana Moreira, L., Kronenberger, T., and Osuna, A. (2023). Extracellular vesicles of trypomastigotes of *Trypanosoma cruzi* induce changes in ubiquitin-related processes, cell-signaling pathways and apoptosis. *Sci. Rep.* 13:7618. doi: 10.1038/s41598-023-34820-6
- Cruz Camacho, A., Alfandari, D., Kozela, E., and Regev-Rudzki, N. (2023). Biogenesis of extracellular vesicles in protozoan parasites: the ESCRT complex in the trafficking fast lane? *PLoS Pathog.* 19:e1011140. doi: 10.1371/journal.ppat.1011140
- de Souza Gonçalves, D., da Silva Ferreira, M., Liedke, S. C., Gomes, K. X., de Oliveira, G. A., Leão, P. E. L., et al. (2018). Extracellular vesicles and vesicle-free secretome of the protozoa *Acanthamoeba castellanii* under homeostasis and nutritional stress and their damaging potential to host cells. *Virulence* 9, 818–836. doi: 10.1080/21505594.2018.1451184
- Díaz Lozano, I. M., De Pablos, L. M., Longhi, S. A., Zago, M. P., Schijman, A. G., and Osuna, A. (2017). Immune complexes in chronic Chagas disease patients are formed by exovesicles from *Trypanosoma cruzi* carrying the conserved MASP N-terminal region. *Sci. Rep.* 7:44451. doi: 10.1038/srep44451
- Díaz-Godínez, C., Ríos-Valencia, D. G., García-Aguirre, S., Martínez-Calvillo, S., and Carrero, J. C. (2022). Immunomodulatory effect of extracellular vesicles from *Entamoeba histolytica* trophozoites: regulation of NETs and respiratory burst during confrontation with human neutrophils. *Front. Cell. Infect. Microbiol.* 12:1018314. doi: 10.3389/fcimb.2022.1018314
- Dong, G., Wagner, V., Minguez-Menendez, A., Fernandez-Prada, C., and Olivier, M. (2021). Extracellular vesicles and leishmaniasis: current knowledge and promising avenues for future development. *Mol. Immunol.* 135, 73–83. doi: 10.1016/j.molimm.2021.04.003
- Douanne, N., Dong, G., Amin, A., Bernardo, L., Blanchette, M., Langlais, D., et al. (2022). *Leishmania* parasites exchange drug-resistance genes through extracellular vesicles. *Cell Rep.* 40:111121. doi: 10.1016/j.celrep.2022.111121
- Elzanowska, J., Semira, C., and Costa-Silva, B. (2021). DNA in extracellular vesicles: biological and clinical aspects. *Mol. Oncol.* 15, 1701–1714. doi: 10.1002/1878-0261.12777
- Ferrante, A., Carter, R. F., Lopez, A. F., Rowan-Kelly, B., Hill, N. L., and Vadas, M. A. (1988). Depression of immunity to *Naegleria fowleri* in mice by selective depletion of neutrophils with a monoclonal antibody. *Infect. Immun.* 56, 2286–2291. doi: 10.1128/iai.56.9.2286-2291.1988
- Fischer-Stenger, K., and Marclano-Cabral, F. (1992). The arginine-dependent Cytolytic mechanism plays a role in destruction of *Naegleria fowleri* amoebae by activated macrophages. *Infect. Immun.* 60, 5126–5131. doi: 10.1128/iai.60.12.5126-5131.1992
- Fowler, M., and Carter, R. F. (1965). Acute pyogenic meningitis. *Br. Med. J.* 67, 739–740.
- García-Romero, N., Carrión-Navarro, J., Esteban-Rubio, S., Lázaro-Ibáñez, E., Peris-Celda, M., Alonso, M. M., et al. (2017). DNA sequences within glioma-derived extracellular vesicles can cross the intact blood-brain barrier and be detected in peripheral blood of patients. *Oncotarget* 8, 1416–1428. doi: 10.18632/oncotarget.13635
- Ghanam, J., Chetty, V. K., Barthel, L., Reinhardt, D., Hoyer, P. F., and Thakur, B. K. (2022). DNA in extracellular vesicles: from evolution to its current application in health and disease. *Cell Biosci.* 12:37. doi: 10.1186/s13578-022-00771-0
- Gómez-Samblas, M., Bernal, D., Bolado-Ortiz, A., Vilchez, S., Bolás-Fernández, F., Espino, A. M., et al. (2018). Intraperitoneal administration of the anti-IL-23 antibody prevents the establishment of intestinal nematodes in mice. *Sci. Rep.* 8:7787. doi: 10.1038/s41598-018-26194-x
- Gonçalves, D. D. S., Ferreira, M. D. S., and Guimarães, A. J. (2019). Extracellular vesicles from the protozoa *Acanthamoeba castellanii*: their role in pathogenesis, environmental adaptation and potential applications. *Bioengineering* 6:13. doi: 10.3390/bioengineering6010013
- Heukeshoven, J., and Dernick, R. (1988). Improved silver staining procedure for fast staining in PhastSystem development unit I. Staining of sodium dodecyl sulfate gels. *Electrophoresis* 9, 28–32. doi: 10.1002/elps.1150090106
- Hu, X., Leak, R. K., Shi, Y., Suenaga, J., Gao, Y., Zheng, P., et al. (2015). Microglial and macrophage polarization - new prospects for brain repair. *Nat. Rev. Neurol.* 11, 56–64. doi: 10.1038/nrneurol.2014.207
- Islek, Z., Bozkurt, B. T., Ücisik, M. K., and Sahin, F. (2022). “The role of extracellular vesicles in immunomodulation and pathogenesis of *Leishmania* and other protozoan infections,” in *Extracellular Vesicles - Role in diseases, pathogenesis and therapy*. IntechOpen. Available at: <http://dx.doi.org/10.5772/intechopen.101682>.
- Jahangeer, M., Mahmood, Z., Munir, N., Waraich, U. E. A., Tahir, I. M., Akram, M., et al. (2020). *Naegleria fowleri*: sources of infection, pathophysiology, diagnosis, and management; a review. *Clin. Exp. Pharmacol. Physiol.* 47, 199–212. doi: 10.1111/1440-1681.13192
- Jarolim, K. L., McCosh, J. K., Howard, M. J., and John, D. T. (2000). A light microscopy study of the migration of *Naegleria fowleri* from the nasal submucosa to the central nervous system during the early stage of primary amebic meningoencephalitis in mice. *J. Parasitol.* 86, 50–55. doi: 10.1645/0022-3395(2000)086[0050:almsot]2.0.co;2
- Kim, J. H., Yang, A. H., Sohn, H. J., Kim, D., Song, K. J., and Shin, H. J. (2009). Immunodominant antigens in *Naegleria fowleri* excretory-secretory proteins were potential pathogenic factors. *Parasitol. Res.* 105, 1675–1681. doi: 10.1007/s00436-009-1610-y
- Laemmli, U. K. (1970). Cleavage of structural proteins during the assembly of the head of bacteriophage. *Nature* 227, 680–685. doi: 10.1038/227680a0
- Lê, H. G., Kang, J. M., Vö, T. C., Yoo, W. G., and Na, B. K. (2023). *Naegleria fowleri* extracellular vesicles induce Proinflammatory immune responses in BV-2 microglial cells. *Int. J. Mol. Sci.* 24:13623. doi: 10.3390/ijms241713623
- Lee, Y. J., Park, C. E., Kim, J. H., Sohn, H. J., Lee, J., Jung, S. Y., et al. (2011). *Naegleria fowleri* lysate induces strong cytopathic effects and pro-inflammatory cytokine release in rat microglial cells. *Korean J. Parasitol.* 49, 285–290. doi: 10.3347/kjp.2011.49.3.285
- Lertjuthaporn, S., Somkird, J., Lekmanee, K., Atipimonpat, A., Sukapirom, K., Sawasdiopin, H., et al. (2022). Extracellular vesicles from *Naegleria fowleri* induce IL-8 response in THP-1 macrophage. *Pathogens* 11:632. doi: 10.3390/pathogens11060632
- Lin, W. C., Tsai, C. Y., Huang, J. M., Wu, S. R., Chu, L. J., and Huang, K. Y. (2019). Quantitative proteomic analysis and functional characterization of *Acanthamoeba castellanii* exosome-like vesicles. *Parasit. Vectors* 12:467. doi: 10.1186/s13071-019-3725-z
- Lozano, N., Samblas, M. G., Calabuig, E., Giménez Martí, M. J., Gómez Ruiz, M. D., Arce, J. M. S., et al. (2023). Use of sera cell free DNA (cfDNA) and exovesicle-DNA for the molecular diagnosis of chronic Chagas disease. *PLoS One* 18:e0282814. doi: 10.1371/journal.pone.0282814
- Malkin, E. Z., and Bratman, S. V. (2020). Bioactive DNA from extracellular vesicles and particles. *Cell Death Dis.* 11:584. doi: 10.1038/s41419-020-02803-4
- Marciano-Cabral, F., and Cabral, G. A. (2007). The immune response to *Naegleria fowleri* amoebae and pathogenesis of infection. *FEMS Immunol. Med. Microbiol.* 51, 243–259. doi: 10.1111/j.1574-695X.2007.00332.x
- Marciano-Cabral, F., Ludwick, C., and Cabral, G. A. (2001). The interaction of *Naegleria fowleri* amoebae with brain microglial cells. In: *Proceedings of the IXth Intern. Mtg. Biol. Path. Free-Living Amoebae*, Paris.
- Matanock, A., Mehal, J. M., Liu, L., Blau, D. M., and Cope, J. R. (2018). Estimation of underdiagnosed *Naegleria fowleri* primary amebic meningoencephalitis, United States. *Emerg. Infect. Dis.* 24, 162–164. doi: 10.3201/eid2401.170545
- Michelson, M. K., Henderson, W. R. Jr., Chi, E. Y., Fritsche, T. R., and Klebanoff, S. J. (1990). Ultrastructural studies on the effect of tumor necrosis factor on the interaction of neutrophils and *Naegleria fowleri*. *Am. J. Trop. Med. Hyg.* 42, 225–233. doi: 10.4269/ajtmh.1990.42.225
- Morales-Ropero, J. M., Arroyo-Urea, S., Neubrand, V. E., Martín-Oliva, D., Marín-Teva, J. L., Cuadros, M. A., et al. (2021). The endoplasmic reticulum Ca<sup>2+</sup>-ATPase SERCA2b is upregulated in activated microglia and its inhibition causes opposite effects on migration and phagocytosis. *Glia* 69, 842–857. doi: 10.1002/glia.23931
- Moseman, E. A. (2020). Battling brain-eating amoeba: enigmas surrounding immunity to *Naegleria fowleri*. *PLoS Pathog.* 16:e1008406. doi: 10.1371/journal.ppat.1008406
- Naqvi, A., Yazdani, N., Ahmad, R., Zehra, F., and Ahmad, N. (2016). Epidemiology of primary amebic meningoencephalitis-related deaths due to *Naegleria fowleri* infections from freshwater in Pakistan: an analysis of 8-year dataset. *Arch. Pharm. Pract.* 7:119. doi: 10.4103/2045-080x.191924
- Nievas, Y. R., Lizarraga, A., Salas, N., Cócères, V. M., and de Miguel, N. (2020). Extracellular vesicles released by anaerobic protozoan parasites: current situation. *Cell. Microbiol.* 22:e13257. doi: 10.1111/cmi.13257
- Nimmerjahn, A., Kirchhoff, F., and Helmchen, F. (2005). Resting microglial cells are highly dynamic Surveillants of brain parenchyma in vivo. *Science* 308, 1314–1318. doi: 10.1126/science.1110647
- Oh, Y.-H., Jeong, S.-R., Kim, J.-H., Song, K.-J., Kim, K., Park, S., et al. (2005). Cytopathic changes and pro-inflammatory cytokines induced by *Naegleria fowleri* trophozoites in rat microglial cells and protective effects of an anti-Nf1 antibody. *Parasite Immunol.* 27, 453–459. doi: 10.1111/j.1365-3024.2005.00799.x



- Omar, M., and Abdelal, H. O. (2022). Nitric oxide in parasitic infections: a friend or foe? *J. Parasit. Dis.* 46, 1147–1163. doi: 10.1007/s12639-022-01518-x
- Opadokun, T., and Rohrbach, P. (2021). Extracellular vesicles in malaria: an agglomeration of two decades of research. *Malar. J.* 20:442. doi: 10.1186/s12936-021-03969-8
- Pana, A., Vijayan, V., and Anilkumar, A. C. (2023). *Amebic meningoencephalitis*. Treasure Islands, FL: StatPearls Publishing. Available at: <https://www.ncbi.nlm.nih.gov/books/NBK430754/>.
- Park, K. W., Lee, H. G., Jin, B. K., and Lee, Y. B. (2007). Interleukin-10 endogenously expressed in microglia prevents lipopolysaccharide-induced neurodegeneration in the rat cerebral cortex *in vivo*. *Exp. Mol. Med.* 39, 812–819. doi: 10.1038/emmm.2007.88
- Retana Moreira, L., Prescilla-Ledezma, A., Cornet-Gomez, A., Linares, F., Jódar-Reyes, A. B., Fernandez, J., et al. (2021). Biophysical and biochemical comparison of extracellular vesicles produced by infective and non-infective stages of *Trypanosoma cruzi*. *Int. J. Mol. Sci.* 22:5183. doi: 10.3390/ijms22105183
- Retana Moreira, L., Ramírez, D. V., Linares, F., Ledezma, A. P., Garro, A. V., Osuna, A., et al. (2020a). Isolation of *Acanthamoeba* T5 from water: characterization of its pathogenic potential, including the production of extracellular vesicles. *Pathogens* 9:144. doi: 10.3390/pathogens9020144
- Retana Moreira, L., Rojas, L. Z., Murillo, M. G., Castro, S. E. M., and Sandí, E. A. (2020b). Primary amebic meningoencephalitis related to groundwater in Costa Rica: diagnostic confirmation of three cases and environmental investigation. *Pathogens* 9, 1–9. doi: 10.3390/pathogens9080629
- Retana Moreira, L., Serrano, F. R., and Osuna, A. (2019). Extracellular vesicles of *Trypanosoma cruzi* tissue-culture cell-derived trypomastigotes: induction of physiological changes in non-parasitized culture cells. *PLoS Negl. Trop. Dis.* 13:e0007163. doi: 10.1371/journal.pntd.0007163
- Retana Moreira, L., Steller Espinoza, M. F., Chacón Camacho, N., Cornet-Gomez, A., Sáenz-Arce, G., Osuna, A., et al. (2022). Characterization of extracellular vesicles secreted by a clinical isolate of *Naegleria fowleri* and identification of immunogenic components within their protein cargo. *Biology (Basel)* 11:983. doi: 10.3390/biology11070983
- Rojas-Hernández, S., Jarillo-Luna, A., Rodríguez-Monroy, M., Moreno-Fierros, L., and Campos-Rodríguez, R. (2004). Immunohistochemical characterization of the initial stages of *Naegleria fowleri* meningoencephalitis in mice. *Parasitol. Res.* 94, 31–36. doi: 10.1007/s00436-004-1177-6
- Rojas-Hernández, S., Rodríguez-Monroy, M. A., Moreno-Fierros, L., Jarillo-Luna, A., Carrasco-Yepez, M., Miliar-García, A., et al. (2007). Nitric oxide production and nitric oxide synthase immunoreactivity in *Naegleria fowleri*. *Parasitol. Res.* 101, 269–274. doi: 10.1007/s00436-007-0495-x
- Rostami, A., and Ciric, B. (2013). Role of Th17 cells in the pathogenesis of CNS inflammatory demyelination. *J. Neurol. Sci.* 333, 76–87. doi: 10.1016/j.jns.2013.03.002
- Russell, A. C., Bush, P., Grigorean, G., and Kyle, D. E. (2023). Characterization of the extracellular vesicles, ultrastructural morphology, and intercellular interactions of multiple clinical isolates of the brain-eating amoeba, *Naegleria fowleri*. *Front. Virol.* 14:1264348. doi: 10.3389/fmicb.2023.1264348
- Sabatke, B., Gavinho, B., Coceres, V., de Miguel, N., and Ramirez, M. I. (2021). Unveiling the role of EVs in anaerobic parasitic protozoa. *Mol. Immunol.* 133, 34–43. doi: 10.1016/j.molimm.2021.02.007
- Saraiva, M., and O'Garra, A. (2010). The regulation of IL-10 production by immune cells. *Nat. Rev. Immunol.* 10, 170–181. doi: 10.1038/nri2711
- Shin, W. H., Lee, D. Y., Park, K. W., Kim, S. U., Yang, M. S., Joe, E. H., et al. (2004). Microglia expressing Interleukin-13 undergo cell death and contribute to neuronal survival *in vivo*. *Glia* 46, 142–152. doi: 10.1002/glia.10357
- Siddiqui, R., Ali, I. K. M., Cope, J. R., and Khan, N. A. (2016). Biology and pathogenesis of *Naegleria fowleri*. *Acta Trop.* 164, 375–394. doi: 10.1016/j.actatropica.2016.09.009
- Silverman, J. M. A., and Reiner, N. E. (2011). *Leishmania* exosomes deliver preemptive strikes to create an environment permissive for early infection. *Front. Cell. Infect. Microbiol.* 1:26. doi: 10.3389/fcimb.2011.00026
- Sisquella, X., Ofir-Birin, Y., Pimentel, M. A., Cheng, L., Abou Karam, P., Sampaio, N. G., et al. (2017). Malaria parasite DNA-harboring vesicles activate cytosolic immune sensors. *Nat. Commun.* 8:1985. doi: 10.1038/s41467-017-02083-1
- Tatschegg, I., Bomsel, M., De Paillerets, C., Durand, H., Geny, B., Segretain, D., et al. (1998). *Dictyostelium discoideum* cells shed vesicles with associated DNA and vital stain Hoechst. *Cell. Mol. Life Sci.* 54, 476–487. doi: 10.1007/s000180050176
- Théry, C., Witwer, K. W., Aikawa, E., Jose Alcaraz, M., Anderson, J. D., Andriantsitohaina, R., et al. (2018). Journal of extracellular vesicles minimal information for studies of extracellular vesicles 2018 (MISEV 2018): a position statement of the International Society for Extracellular Vesicles and update of the MISEV 2014 guidelines. *J. Extracell. Vesicles* 7:1535750. doi: 10.1080/20013078.2018.1535750
- Timm, T., Annoscia, G., Klein, J., and Lochnit, G. (2017). The eukaryotic elongation factor 1 alpha (eEF1a) from the parasite leishmania infantum is modified with the immunomodulatory substituent phosphorylcholine (PC). *Molecules* 22:2094. doi: 10.3390/molecules22122094
- Towbin, H., Staehelin, T., and Gordon, J. (1979). Electrophoretic transfer of proteins from polyacrylamide gels to nitrocellulose sheets: procedure and some applications (ribosomal proteins/radioimmunoassay/fluorescent antibody assay/peroxidase-conjugated antibody/autoradiography). *Proc. Natl. Acad. Sci. U. S. A.* 76, 4350–4354. doi: 10.1073/pnas.76.9.4350
- Vyas, I. K., Jamerson, M., Cabral, G. A., and Marciano-Cabral, F. (2014). Identification of peptidases in highly pathogenic vs. weakly pathogenic *Naegleria fowleri* amebae. *J. Eukaryot. Microbiol.* 62, 51–59. doi: 10.1111/jeu.12152
- Wan, C., Stowell, M. H. B., and Shen, J. (2022). Progress and gaps of extracellular vesicle-mediated intercellular cargo transfer in the central nervous system. *Commun. Biol.* 5:1223. doi: 10.1038/s42003-022-04050-z



# Frontiers in Microbiology

Explores the habitable world and the potential of microbial life

The largest and most cited microbiology journal which advances our understanding of the role microbes play in addressing global challenges such as healthcare, food security, and climate change.

## Discover the latest Research Topics

[See more →](#)

### Frontiers

Avenue du Tribunal-Fédéral 34  
1005 Lausanne, Switzerland  
[frontiersin.org](https://frontiersin.org)

### Contact us

+41 (0)21 510 17 00  
[frontiersin.org/about/contact](https://frontiersin.org/about/contact)

